Automated Rendezvous and Docking of Spacecraft

Wigbert Fehse

CAMBRIDGE AEROSPACE SERIES

CAMBRIDGE

more information - www.cambridge.org/9780521824927

This page intentionally left blank

Automated Rendezvous and Docking of Spacecraft

The definitive reference for space engineers on all issues related to rendezvous and docking/berthing (RVD/B), *Automated Rendezvous and Docking of Spacecraft* answers key questions such as:

- How does the docking vehicle accurately approach the target spacecraft?
- What technology is needed aboard the spacecraft to perform automatic rendezvous and docking, and what systems are required by ground control to supervise this process?
- How can the proper functioning of all rendezvous related equipment, systems and operations be verified before launch?

The book provides an overview of the major issues governing approach and mating strategies, and system concepts for rendezvous and docking/berthing. These issues are described and explained such that aerospace engineers, students and even newcomers to the field can acquire a basic understanding of RVD/B.

Cambridge Aerospace Series 16

Editors:
MICHAEL J. RYCROFT AND WEI SHYY

1. J. M. Rolfe and K. J. Staples (eds.): *Flight Simulation*
2. P. Berlin: *The Geostationary Applications Satellite*
3. M. J. T. Smith: *Aircraft Noise*
4. N. X. Vinh: *Flight Mechanics of High-Performance Aircraft*
5. W. A. Mair and D. L. Birdsall: *Aircraft Performance*
6. M. J. Abzug and E. E. Larrabee: *Airplane Stability and Control*
7. M. J. Sidi: *Spacecraft Dynamics and Control*
8. J. D. Anderson: *A History of Aerodynamics*
9. A. M. Cruise, J. A. Bowles, C. V. Goodall, and T. J. Patrick: *Principles of Space Instrument Design*
10. G. A. Khoury and J. D. Gillett (eds.): *Airship Technology*
11. J. Fielding: *Introduction to Aircraft Design*
12. J. G. Leishman: *Principles of Helicopter Dynamics*
13. J. Katz and A. Plotkin: *Low Speed Aerodynamics, Second Edition*
14. M. J. Abzug and E. E. Larrabee: *Airplane Stability and Control, Second Edition*
15. D. H. Hodges and G. A. Pierce: *Introduction to Structural Dynamics and Aeroelasticity*

Automated Rendezvous and Docking of Spacecraft

WIGBERT FEHSE

CAMBRIDGE UNIVERSITY PRESS
Cambridge, New York, Melbourne, Madrid, Cape Town, Singapore, São Paulo

Cambridge University Press
The Edinburgh Building, Cambridge CB2 2RU, United Kingdom

Published in the United States of America by Cambridge University Press, New York

www.cambridge.org

Information on this title: www.cambridge.org/9780521824927

First published in print format 2003

ISBN-13 978-0-511-06240-7 eBook (NetLibrary)
ISBN-10 0-511-06240-0 eBook (NetLibrary)

ISBN-13 978-0-521-82492-7 hardback
ISBN-10 0-521-82492-3 hardback

For my wife Ulla, for all her love, care and patience

Contents

Preface

The material presented in this book provides a general overview of the major issues related to the development of automatic rendezvous and docking systems, without restricting the discussion to any particular project. It is intended to explain the general principles, and examples of actual developments are included only to demonstrate these general principles. Because of the large number of aspects to be discussed, the depth of discussion of each single issue will necessarily be limited and cannot go further than an introduction.

The information presented is based on the experience of the author, gained during his work with the European Space Agency (ESA), where, between 1981 and 1998, he was responsible for the development of rendezvous and docking technology. ESA has conducted a comprehensive development programme, within which it has awarded to European industry a large number of study and development activities to prepare the rendezvous and docking techniques and technology, first for the *Hermes–Columbus Free-Flyer* scenario, which was abandoned in 1992, and thereafter for the *ATV–ISS* scenario. The Automated Transfer Vehicle (ATV) is one of Europe's contributions to the International Space Station (ISS) Programme. In this context, the two largest technology development activities, among many others, were:

- the Rendezvous and Docking Pre-Development Programme for Hermes–Columbus (1989–1993),
- the ATV Rendezvous Pre-Development (1994–1998).

The design and development of the automatic rendezvous control system of the ATV, for which these two activities formed the basis, are driven to a large extent by the interfaces and requirements given by the ISS. This required extended and detailed discussions with the international partners involved. The information on techniques and technology for automated rendezvous and docking, presented in this book, relies mainly on (a) the results of the above-mentioned research and development activities prepared by European industry under ESA guidance and (b) information obtained in the course of ESA's cooperation with its international partners (NASA, RSC-Energia, NASDA) under the aegis of the International Space Station Programme.

Concerning the ESA RVD development programme, the great effort made by all the individuals at ESA and in industry, without which this book could not have been written,

is gratefully acknowledged. The industrial team involved in the European rendezvous technology development included the following companies:

- MATRA Marconi Space (Toulouse) and DASA (Bremen, Ottobrunn), now merged in the Astrium company,
- Aerospatiale, now part of EADS (Les Mureaux),
- Alenia (Turin),
- GMV (Madrid),
- Sener (Bilbao),

and many others.

A large amount of information concerning the development of automated rendezvous and docking systems by Russia, the USA and Japan was available thanks to cooperation within the International Space Station Programme. In this international cooperative effort, rendezvous and docking/berthing became one of the major operational and physical interfaces between vehicles of different space powers, requiring an openness of information transfer between the international partners which was previously unheard of.

No project such as this book can successfully be concluded without help. The author also wishes to express his gratitude to all colleagues who supported him. In particular, the author wants to thank two colleages, who contributed major inputs to the written text:

> F. Ankersen, ESA-ESTEC, contributed Appendix A on 'Motion dynamics' and supplied information for chapter 6 'The onboard rendezvous control system'. He is ESA's leading person in the control system development of all ESA rendezvous development activities.
>
> J. Sommer, Astrium Bremen, also contributed inputs to chapter 6. He was one of the key development engineers in industry for both of the above mentioned technology projects.

The author owes both these contributors a great debt of gratitude for their contributions not only to the book but also to the rendezvous development work in general.

In addition, the following colleagues and friends of the international rendezvous and docking community helped to review some of chapters and provided valuable comments and suggestions, for which the author expresses his gratitude: E. Belikov, Sener, Bilbao; Ch. Beskow, ESA-ESTEC, Noordwijk; J.-L. Gonnaud, Astrium, Toulouse; S. Mancuso, ESA-ESTEC, Noordwijk; G. Ortega, ESA-ESTEC, Noordwijk; I. Rasmussen, ESA-ESTEC, Noordwijk; V. Semyachkin, RSC Energia, Moscow; D. Wilde, Astrium, Bremen; K. Yamanaka, NASDA, Tokyo.

The European Space Agency has made this project possible by giving permission for the publication of development results. The author is grateful in particular to ESA's *Control and Data Systems Division* for providing accommodation, computer infrastructure, software and administrative support.

The manuscript was written in LaTeX and most of the figures have been prepared with the Xfig drawing program. For trajectory plots the 'Fast Interactive Rendezvous Simulation Tool' (FIRST), developed by ESA, was used; this is a trajectory analysis software, based on the commercial computer aided dynamic analysis package MATRIX$_{\text{X}}$ from Integrated Systems Inc.

Symbols

a	semi major axis of ellipse
c	velocity of light
C	spring constant
D	damping constant
e	eccentricity of orbit
ϵ	error factor
ε	angle between ecliptic and equatorial plane
f	frequency
F	force
$\mathbf{F}_i$	coordinate frame
γ	imposed force per unit of mass
i	inclination
m	mass
μ	gravitational constant of Earth
ν	true anomaly, angular position on orbit measured from perigee
$\mathbf{O}_i$	origin of coordinate frame
ϕ, Φ	phase
r	radius, orbit radius
R, r	range

t	time
T	orbital period; time
V	velocity
ΔV	velocity increment
ω, ω_o	angular frequency of orbit
ω	angular rate; argument of perigee
Ω	angle between vernal equinox and ascending node (see RAAN)

1

Introduction

1.1 Background

Rendezvous and docking or berthing (RVD/B) is a key operational technology, which is required for many missions involving more than one spacecraft. RVD/B technology and techniques are key elements in missions such as

- assembly in orbit of larger units;
- re-supply of orbital platforms and stations;
- exchange of crew in orbital stations;
- repair of spacecraft in orbit;
- retrieval, i.e. capture and return to ground, of spacecraft;
- re-joining an orbiting vehicle using a lander in the case of lunar and planetary return missions.

The first rendezvous and docking between two spacecraft took place on 16 March 1966, when Neil Armstrong and Dave Scott manually performed rendezvous in a Gemini vehicle and then docked with an unmanned Agena target vehicle. The first automatic RVD took place on 30 October 1967, when the Soviet vehicles Cosmos 186 and 188 docked. Thereafter, RVD/B operations have regularly been performed by the Russian (Soviet) and US space programmes; e.g. in the following:

- US Apollo (1968–1972) and Skylab programmes (1973–1974);
- Russian (Soviet) Salyut and Mir Space Station programmes (1971–1999) with docking of the manned Soyuz and unmanned Progress spaceships;

- US/Soviet Apollo–Soyuz docking mission (Apollo–Soyuz Test Project, ASTP, 1975);
- US Space Shuttle retrieval and servicing missions (starting in 1984 with the retrieval and repair of the Solar Max satellite);
- US Space Shuttle missions to the Russian space station Mir in the 1990s in preparation for the ISS programme;
- assembly, crew exchange and re-supply of the International Space Station (ISS) (begun in November 1998).

RVD/B technology and techniques have been studied and developed in Western Europe by the European Space Agency since the beginning of the 1980s, first as 'enabling technology' and, from the mid-1980s onwards, for the Columbus Man-Tended Free-Flyer (MTFF), which was intended to dock with the American Space Station Freedom, and for the European spaceplane Hermes, which was intended to visit the MTFF (Pairot, Fehse & Getzschmann 1992).

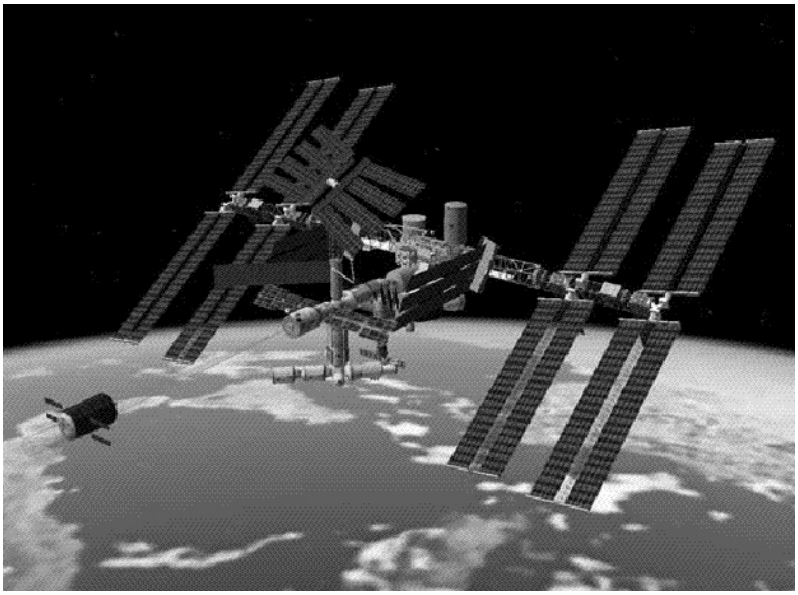

Figure 1.1. Approach of the ATV to the International Space Station (courtesy ESA).

After the cancellation of the MTFF and Hermes projects (as a result of the political changes in Europe) and after the merger of the eastern and western space station programmes into the International Space Station (ISS) Programme (NASA 1998*a*), the Automated Transfer Vehicle (ATV) has become part of the western European contribution (Cornier *et al*. 1999). The ATV will participate in the re-boost and re-supply

missions to the ISS. The total fleet of vehicles, which will perform RVD/B operations with the ISS, includes the US Space Shuttle (manned), the Russian Soyuz (manned) and Progress (unmanned) vehicles, the European ATV (unmanned) and the Japanese H-II Transfer Vehicle (HTV, unmanned; (Kawasaki *et al*. 2000)). In addition to these transport vehicles it can be expected that, in future, inspection vehicles will be attached to the ISS. If required, they will fly around the station to inspect problem areas and to identify the nature of problems (Wilde & Sytin 1999). In the far future, such vehicles may also be used for maintenance and repair tasks. RVD/B technology will be required for the departure and re-attachment of such vehicles as well as for their operational tasks.

Although the ISS will probably be the most important application of RVD/B technology and techniques for the first two decades of the twenty-first century, there have been and will be other rendezvous missions, e.g. servicing of spacecraft in orbit (Hubble Space Telescope for example), spacecraft retrieval (EURECA, SPAS for example) and lunar/planetary return missions. Rendezvous and docking operations in geo-synchronous orbit for the servicing of communication satellites have been studied in the past in some depth; however, no such mission has yet been realised.

1.2 The complexity of the rendezvous process

The rendezvous and docking/berthing process consists of a series of orbital manoeuvres and controlled trajectories, which successively bring the active vehicle (chaser) into the vicinity of, and eventually into contact with, the passive vehicle (target). The last part of the approach trajectory has to put the chaser inside the narrow boundaries of position, velocities, and attitude and angular rates required for the mating process.

- In the case of *docking*, the guidance, navigation and control (GNC) system of the chaser controls the vehicle state parameters required for entry into the docking interfaces of the target vehicle and for capture.

- In the case of *berthing*, the GNC system of the chaser delivers the vehicle at nominally zero relative velocities and angular rates to a meeting point, where a manipulator, located either on the target or chaser vehicle, grapples it, transfers it to the final position and inserts it into the interfaces of the relevant target berthing port.

The complexity of the rendezvous approach and mating process and of the systems required for its execution results from the multitude of conditions and constraints which must be fulfilled. These conditions and constraints will be discussed in detail in the relevant chapters. A few examples are given below.

Launch and phasing trajectory strategy

For the chaser to arrive in the close vicinity of the target, it must be brought into the same orbital plane and must eventually have the same orbital height, phase angle and

eccentricity parameters as the target. Due to the oblateness of the Earth, the orbital plane drifts with time and the drift rate depends on the orbital height. Therefore, the difference in plane drift of the chaser during phasing at lower altitude must be taken into account when choosing the orbital plane at launch.

After launch of the chaser, changes in the orbital parameters of the target station, e.g. due to attitude and orbit correction manoeuvres and orbital disturbances, have to be taken into account up to the final part of the orbital rendezvous, and the approach trajectories have to be updated accordingly.

Operations in the vicinity of the target station

The target station may impose safety zones, approach-trajectory corridors and hold points along the way to check out vehicle functions and other conditions. At certain points, permission to proceed by either ground or target crew may have to be received by the chaser prior to further approach. Any dynamic state (position and velocities, attitude and angular rates) of the chaser vehicle outside the nominal limits of the approach trajectory could lead to collision with the target, a situation dangerous for crew and vehicle integrity. Therefore, all approach trajectories must fulfil the following two conditions:

(a) Where possible, they should be inherently safe, which means that they should not lead to collision with the target, even in the case of loss of thrust capability or control at any point of the trajectory.

(b) If condition (a) cannot be achieved, a collision avoidance manoeuvre, valid for each point of the trajectory in question, must be available, which will move the vehicle safely out of the critical area.

Onboard system requirements and constraints

The nominal attitude of the chaser vehicle is determined by several factors, e.g. by the operational range of the sensors for attitude and trajectory control, by the range of the antennas for communication with ground and with the target station, and by the need to point solar arrays toward the Sun to obtain the necessary supply of power. Thrusters may also be arranged on the vehicle in such a way that they can produce certain forces with respect to (w.r.t.) a certain trajectory direction only at a certain vehicle attitude.

Synchronisation with Sun illumination conditions and crew work cycle

The rendezvous process has to be synchronised with the occurrence of suitable illumination conditions, i.e. the last part of the approach prior to arrival and the capture process must take place under proper illumination conditions. This is necessary in order to make monitoring of the docking or berthing process possible, either visually or by video cameras. An alternative would be artificial illumination, but this is constrained by the available electrical power. Also, the work/rest cycles of the crew in the target station may have to be taken into account. All these constraints may lead to very limited windows in the timeline where final approach and capture can take place.

Communication link constraints

In missions where at least one of the vehicles is manned, ground and/or target crew must, for safety reasons, monitor the last part of the approach and the docking. Since communication coverage, in particular to ground, is not complete, even when using two relay satellites, synchronisation with the communication windows imposes another constraint on the trajectory design. Furthermore, the data rate which can be transmitted is usually limited to a few kilobytes per second. Video transmission is very costly and, if it is available at all, would for this reason be restricted to the last few metres of approach and contact. In the major part of the approach, human operators can, therefore, monitor only key parameters of the vehicle, and human interaction with the onboard system will be restricted to simple commands, such as stop and go and collision avoidance manoevre initiation.

Effects on system and operations

The onboard system must cope with all these constraints by active control; otherwise the timeline and all events have to be pre-planned or controlled by ground. After launch, however, the nominal interaction with the spacecraft by ground is limited, as mentioned above. For unmanned vehicles this leads to the requirement of high onboard autonomy and, as a result, to highly complex onboard systems. It is not too difficult to meet each single condition and constraint addressed above. The combination of all the requirements, conditions and constraints, however, makes the automatic control of rendezvous and docking/berthing by an onboard system a very complex and challenging task.

In addition to the constraints addressed above, and to the multitude of functions required aboard chaser and target vehicles, monitoring and high level control by their respective control centres on ground, together with the infrastructure for communication and navigation in orbit and on ground, further increase the complexity of the rendezvous process. The most important functions in space and on ground required for automatic rendezvous and docking are shown schematically in figure 1.2.

Verification of proper operation and performance of all these functions alone and together in a system is the most difficult and critical task of the development of a rendezvous system and of the preparation of a rendezvous mission. It is not possible to test the various functions of the complete system in the proper environment, as this environment will only be available during the mission itself. Therefore, verification has to rely to a large extent on simulation. The validation of these simulations is an additional challenge.

Owing to the many players involved in rendezvous missions, both in orbit and on ground, and due to the fact that the sequence of operations will be relatively rapid toward the end of a rendezvous mission, operations tasks for the ground segment are more complex and challenging than for the operation of a single satellite. Proper coordination, allocation of tasks and a hierarchy of control authority have to be established between all players for the nominal mission operations and for all credible contingency cases.

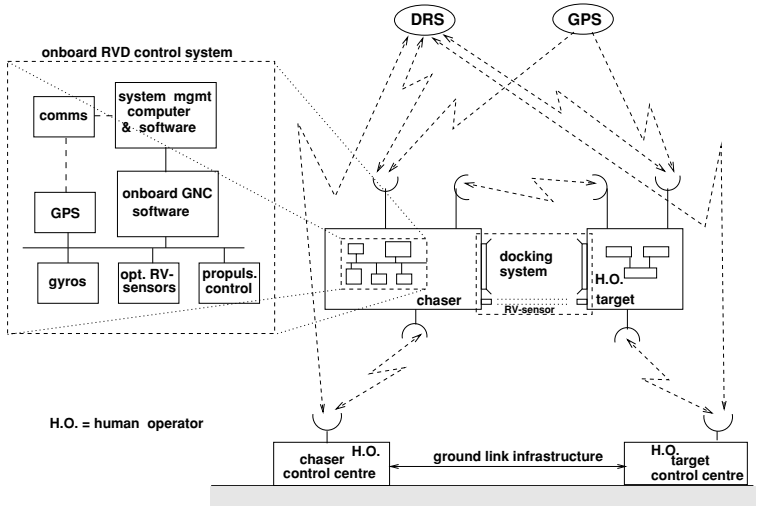

Figure 1.2. Major functions involved in the RVD process.

1.3 Objective and scope

The objective of this book is to provide a compendium for space engineers on all issues related to rendezvous and docking/berthing. The intention is to describe and explain issues in such a way that students and newcomers to the field can acquire a basic understanding of the problems and receive an overview on the major issues governing the approach and mating strategies and the system concepts for RVD/B. In particular, the book will enable spacecraft system engineers to obtain the background information on the RVD/B issues necessary for the conception of missions and vehicles.

The book is structured to provide successive answers to the following questions:

- How does the chaser reach the target spacecraft, and what manoeuvres and trajectory elements are needed to achieve this?
- What onboard functions are needed to perform RVD/B?
- What other functions in space and on ground must be available for the performance of RVD/B operations?
- How can proper functioning of all rendezvous systems and operations be assured before launch?

Chapters 2–5 are dedicated to the approach strategy, i.e. they intend to provide answers to the question: 'How does the chaser reach the target spacecraft?' In chapter 2, all phases of a rendezvous mission, including departure, are briefly described. Manoeuvre objectives, end conditions to be achieved and major issues for each phase are

discussed. Chapter 3 provides an introduction to orbit dynamics and the trajectory and manoeuvre elements used in the rendezvous approach. The properties of the various manoeuvres concerning trajectory evolution, duration and delta-V (ΔV) requirements are derived and explained. Chapter 4 deals with fault tolerance and trajectory safety requirements. In particular, it addresses the effects of external disturbances, the sensitivity to measurement and thrust errors, the protection possibilities against such errors and the implementation of collision avoidance manoeuvres. Chapter 5 looks at all the other operational issues and constraints which are driving the design of the approach strategy. Issues such as location and attitude of docking ports and berthing boxes, sensor characteristics, monitoring conditions (illumination and ground coverage) and safety zones and corridors around the target vehicle are discussed.

Chapters 6–8 discuss the onboard functions required for RVD/B, including the algorithmic functions and the equipment. In chapter 6 the guidance, navigation and control (GNC) functions of the chaser vehicle are described for automatic systems and with man-in-the-loop. This chapter discusses further the automatic mission and vehicle management (MVM) functions and basic implementation possibilities of failure detection, identification and recovery (FDIR) functions. The MVM function is responsible for the automatic switching of GNC modes and of equipment required to implement the various trajectories and manoeuvres. Chapter 7 looks into the most important sensor design principles used for rendezvous trajectory control, and provides information on their performance requirements and operational range. Chapter 8 describes the docking and berthing concepts, the problems of contact dynamics and capture, the interfaces between GNC and mating systems and the different types of docking and berthing mechanisms.

The tasks of the ground control centres and of the target crew are discussed in chapter 9. This chapter also addresses the control hierarchy for RVD missions, involving manned and unmanned vehicles, and includes a description of typical setups and constraints of a communication infrastructure between space and ground and between the control centres. Requirements and concepts for support tools, used for monitoring and interaction with chaser spacecraft by ground operators and target crew, are addressed.

Chapter 10 intends to provide an answer to the question: ‘How can proper functioning and performance of all systems and operations involved in the rendezvous and mating process be verified and validated prior to launch?’ Verification and validation are the most critical and expensive parts of any development of a RVD capability, which has to be understood not as just the final act of development, but as an integral process of it, starting with the first mission concept and continuing with the development process. In this final chapter the possibilities and limitations of mathematical modelling of spacecraft, onboard systems and environmental features are discussed, various simulators and stimulation facilities for sensors used for verification are described, and the possibilities for validation of models and simulators by means of comparison with other proven models or simulations and comparison with actual flight data are addressed.

2

The phases of a rendezvous mission

The purpose of this chapter is to give the reader a short overview of the different phases of a rendezvous approach and to describe the major issues of these phases. It is hoped that it will be easier, after familiarisation with the basic concept of a rendezvous mission, for the reader to put the information given in the subsequent chapters into their proper context. For this reason, some of the information provided in more detail in the later chapters had to be duplicated in condensed form here.

A rendezvous mission can be divided, as indicated in figure 2.1, into a number of major phases: launch, phasing, far range rendezvous, close range rendezvous and mating. During these phases, the kinematic and dynamic conditions that will eventually allow the connection of the chaser to the target spacecraft are successively established. In the following sections of this chapter an overview of the objectives, the end conditions to be achieved and the trajectory implementation possibilities of each of those phases will be given. This includes a rough order of magnitude of the major performance values which the guidance, navigation and control system of the chaser will have to achieve. For completeness, a short section on departure has been added, which addresses the issues and constraints of separation from and moving out of the vicinity of the target station. The mission phases between mating and departure and after departure are not addressed as they are both, in objective and concept, fully independent of the rendezvous mission.

2.1 Launch and orbit injection

2.1.1 The launch window

Owing to the rotation of the Earth, each point on its surface passes twice per day through any orbit plane. However, as a launch in an easterly direction produces a gain in launch

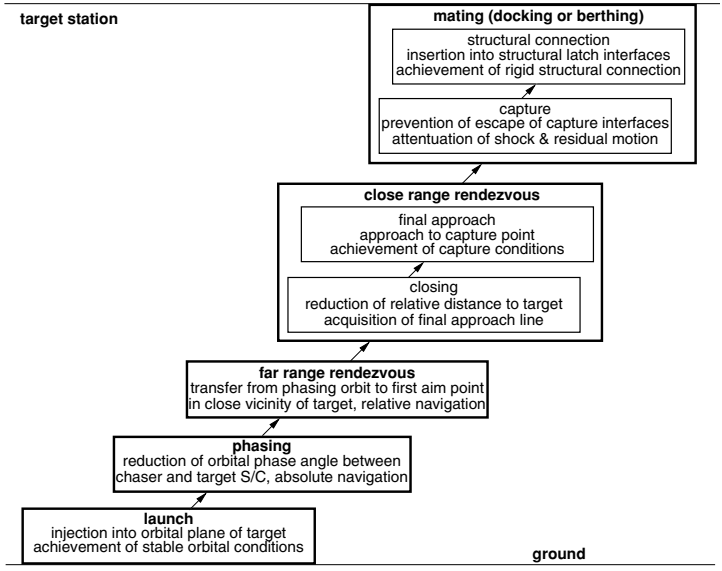

Figure 2.1. Main phases of a rendezvous mission.

velocity due to the tangential velocity component of the rotation of the Earth (≈463 m/s at the equator), and since at most launch sites only a limited sector of launch directions can be used (e.g. toward the sea), there is, practically, only one opportunity per day to launch a spacecraft into a particular orbit plane. With the Earth rotation of 15 deg/h, during every minute the launch site will move ≈0.25 deg w.r.t. the orbital plane (neglecting for the moment other drift effects). Plane differences resulting from a deviation from the nominal launch time can be most efficiently corrected by the launcher shortly after lift-off, when the relative velocities are still relatively low. A correction of the plane error in the final orbit would be much more expensive; e.g. at an orbital height of 400 km it would cost a ΔV of about 32 m/s to correct a 1 minute launch delay, see Eq. (3.20). Therefore, the size of the launch window, i.e. the margin around the time when the launch site passes through the orbital plane, will mainly be determined by the correction capabilities of the launcher.

2.1.2 Definition of orbit plane and other orbit parameters

Some brief definitions of concepts used in orbit mechanics are given here to provide the basis for the description of the rendezvous mission phases. A more detailed treatment is provided in chapter 3.

The direction in inertial space of the plane of an Earth orbit can be defined by two angles (see figures 2.2 and 2.3):

- its 'inclination' angle i, measured w.r.t. the equatorial plane of the Earth;
- the angle Ω w.r.t. a reference plane that is orthogonal to the equatorial one, but fixed in inertial space.

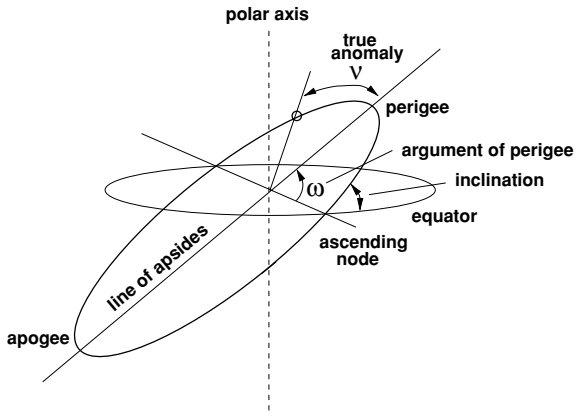

Figure 2.2. Definition of orbit parameters.

As the Earth rotates, one has to find a fixed point in space for the definition of this second reference plane. Convenient fix points for this purpose are the equinoctial points, defined by the intersection of the equatorial plane with the plane of the orbit of the Earth around the Sun (ecliptic).

The crossing points of a satellite's orbit plane with the equatorial plane are called the 'nodes'. The 'ascending' node refers to the point where the satellite is crossing in a northbound direction, and the 'descending node' refers to the southbound crossing point. This second angle, Ω, required for the definition of the orbit plane, is measured between the point of the vernal (spring) equinox and the ascending node (see figure 2.3). This angle is called the 'right ascension of ascending node' (RAAN).

An elliptic orbit is further defined by the size of its major (a) and minor (b) axes and by the location of its apogee and perigee w.r.t. the nodes (ω) or by corresponding expressions. The instantaneous position of a satellite on its orbit is defined by the 'true anomaly', which is the angle (ν) measured from the perigee of the orbit. These parameters are shown in figures 2.2 and 3.6.

2.1.3 Launch operations flexibility

In order to provide for sufficient flexibility of the launch operations, i.e. to provide as much margin as possible for possible interruptions of the countdown, one will attempt always to launch at the beginning of the launch window, whereas the nominal launch time will be in the middle of the launch window. The corresponding plane errors will

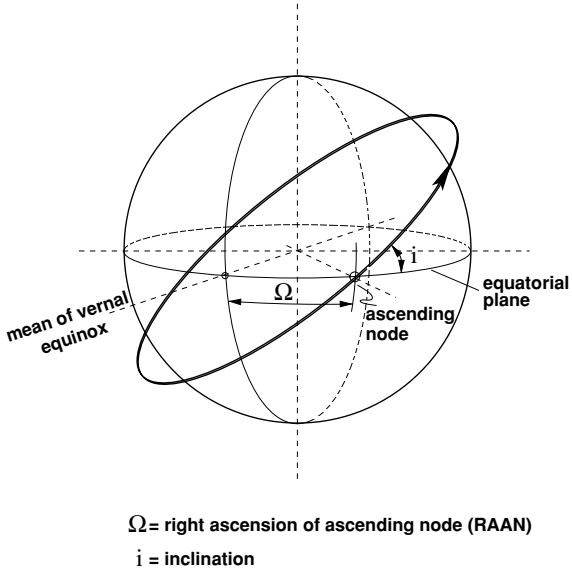

Figure 2.3. Definition of orbit plane.

be corrected, as discussed above, mainly during the early part of the launch phase. The subsequent phasing and rendezvous phases will also have to provide correction possibilities for residual launch dispersions, for achievement of the nominal arrival time and for other errors and perturbations.

2.1.4 Vehicle state at end of launch phase

At the end of the launch phase, the chaser vehicle has been brought by the launcher (and additionally, where necessary, by the spacecraft's own means of propulsion) into a stable orbit in the target orbital plane.[1] The chaser vehicle is then on a lower orbit and may be at an arbitrary phase angle behind the target (see figure 2.4) which depends on the orbit parameters of the target and on the actual launch date.

After separation from the launcher, the spacecraft has to deploy its solar arrays and antennas and must initialise all its subsystems. This phase may be particularly critical if the launcher injects the spacecraft into a non-viable orbit, i.e. into an orbit which would decay after a few revolutions. In this case it is of utmost importance that all necessary subsystems and equipment are in operation at the first apogee, so that a perigee raising manoeuvre can be performed.

[1] Actually, the chaser will be launched into a 'virtual' target plane, as the target orbit plane will drift with time; see section 5.2.1.

2.2 Phasing and transfer to near target orbit

2.2.1 Objective of phasing and state at end of phasing

The objective of this first orbital phase of a rendezvous mission is to reduce the phase angle between the chaser and target spacecraft (figure 2.4), by making use of the fact that a lower orbit has a shorter orbital period. During this phase, launch injection errors for inclination and RAAN will successively be corrected. As a rule, all phasing manoeuvres are controlled from ground. Phasing ends with the acquisition of either an 'initial aim point', or with the achievement of a set of margins for position and velocity values at a certain range, called the 'trajectory gate' or 'entry gate'. The margins of the 'aim point' or the 'gate' must be achieved to make the final part of the approach possible. The aim point or 'gate' will be on the target orbit, or very close to it, and from this position the far range relative rendezvous operations can commence.

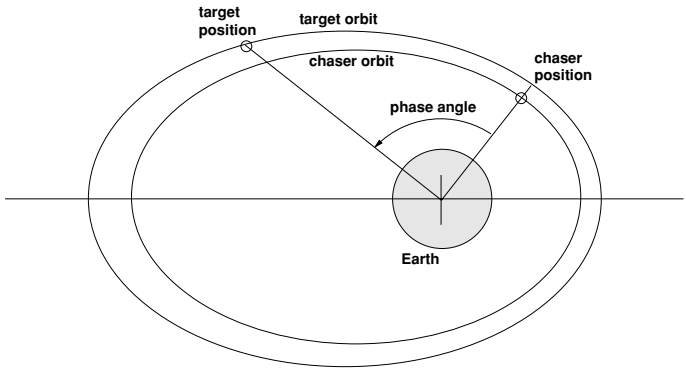

Figure 2.4. Definition of phase angle.

2.2.2 Correction of time deviations and orbit parameters

Depending on the phase angle to the target at the end of the launch phase, and given the time constraints for the total flight up to docking and the necessary correction of orbit parameters after launch, there is a multitude of possible phasing strategies, which will include the following choices of orbit and manoeuvre types:

- forward/backward phasing,
- circular/elliptic phasing orbits,
- change of orbit height in the case of circular orbits,
- change of apogee/perigee height in the case of elliptical orbits,
- lateral correction manoeuvres for inclination and RAAN corrections.

A more detailed discussion on the arrival time constraints of a rendezvous mission is given in chapter 5.

2.2.3 Coordinate frames during rendezvous

During launch and phasing, navigation is based on absolute measurements in an Earth-centred inertial frame. Trajectories of these phases will, therefore, usually also be represented in an Earth-centred frame, i.e. for the launch phase, when the desired orbital parameters have to be achieved, the 'Earth-centred equatorial frame' (see section 3.1.1), and for phasing, when the manoeuvres are mainly in the orbital plane, the 'orbital plane frame' (see section 3.1.2). During the far and close range rendezvous phases, when the trajectory evolution has to be shown in relation to the target position and over several orbital revolutions, it is more convenient to analyse the chaser motion in relation to the motion of the target and to represent it in a frame centred in the target and moving with it along the orbit. This is the 'target local orbital frame', defined in section 3.1.3. The curvilinear orbit direction is shown as a straight line and is named V-bar after the orbital velocity vector $\vec{V}$. The coordinate in the direction of the centre of the Earth is named R-bar after the radius vector $\vec{R}$, and the third coordinate completing the system is named H-bar after the orbital angular momentum vector $\vec{H}$. The centre of the system is the centre of mass of the target vehicle. As an example, figure 2.5 shows the trajectories of the target (target orbit) and of the chaser in both the orbital plane frame and the local orbital frame of the target. The chaser trajectory in this example is an eccentric orbit with an apogee on the target orbit and a perigee at a distance of Δh below it.

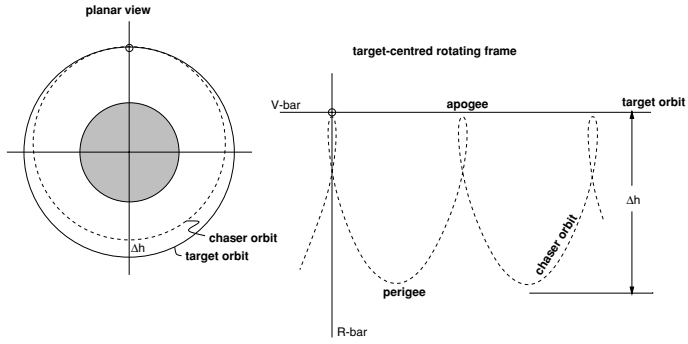

Figure 2.5. From planar view (inertial frame) to target-centred rotating frame.

2.2.4 Forward/backward phasing

When, at the time of the launch of the chaser, the phase angle to the target is too small (see figure 2.4), a direct transfer from the launch injection point to the target point may

become too costly, as a forward phasing would need more than 360 degrees. This may have to be excluded because of mission duration constraints, e.g. due to battery power limitations or due to limitations of life support expendables in manned space missions. The propellant consumption for attitude control during the long phasing duration may also be a factor. In such cases, backward phasing may have to be considered. The chaser vehicle is then transferred to an orbit that is higher than the target one, where it will drift backward toward the target (see figure 2.6). Generally, one will try to avoid backward phasing because of the higher cost in terms of the ΔV needed to achieve the higher orbit.

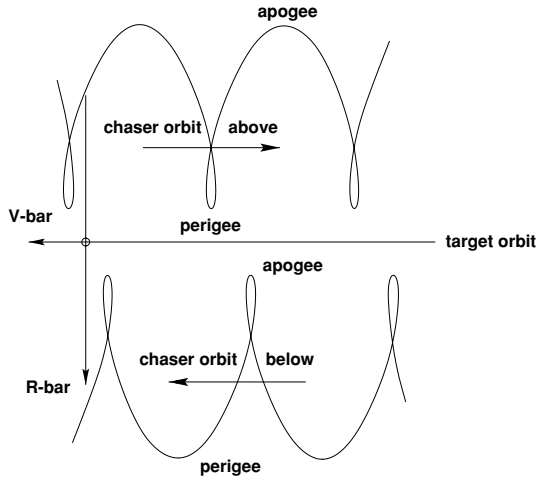

Figure 2.6. Forward and backward phasing below and above target orbit.

2.2.5 Different phasing strategy for each mission

Since for each launch day the phase angle conditions will be different, there can be no fixed phasing trajectories or strategies. Trajectories and manoeuvres will have to be calculated individually for each launch opportunity. For smaller phase angle uncertainties, arrival time adjustment can be achieved during flight by a strategy of drifting for different durations on orbits of different altitudes (see figure 5.22). With such a strategy, time deviations due to the constraints imposed by the launch window, or for example due to delays caused by operations of the target, can be compensated for. The problem of proper arrival time is addressed in more detail in chapter 5.

Figures 2.7 and 2.8 show two examples of possible phasing strategies. In the first strategy, both the apogee and perigee of the elliptic phasing orbits are raised at certain points in time, which slows down the phasing rate. The points at which the orbit is

changed will be chosen such that the vehicle will arrive at the initial aim point at the proper time. If a global positioning system (GPS) receiver is available aboard the spacecraft, the necessary navigation and thrust execution accuracy is permanently available. In the second strategy, one attempts to raise the apogee of the chaser vehicle as soon as possible to the height of the target orbit. This requires, on the one hand, a higher thrust capacity, but, on the other hand, offers somewhat lower propellant consumption as well as the possibility of adjusting iteratively, based on ground measurements, the apogee of the chaser orbit to the orbital altitude of the target. Such a strategy has particular merits when autonomous onboard navigation is not available. The two examples show that the thrust capabilities of the vehicle and the available navigation means play a role in the selection of the phasing strategy. The perigee and apogee raising manoeuvres, along with Hohmann transfer manoeuvres, are discussed in more detail in section 3.2.2.

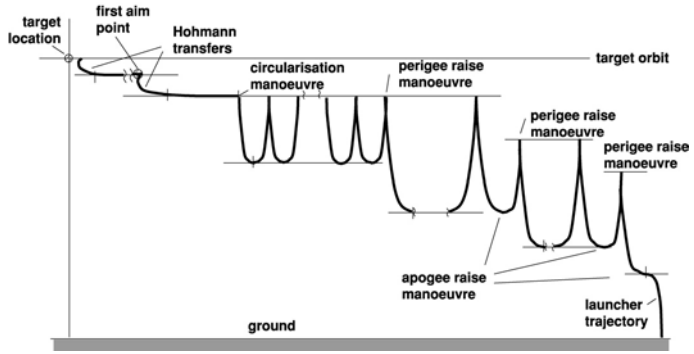

Figure 2.7. Phasing strategy.

2.2.6 Location of the initial aim point

The end point of phasing is often called the 'initial aim point' (see figure 2.7; see also point S0 in figure 2.9). This end point is, however, not a hold point. The location of this first aim point, i.e. whether it is on the + or − V-bar side, whether it is on or below/above the target orbit and whether it is at a larger or shorter distance from the target, will depend on a number of factors. The most important of them are the location of the docking port and the direction of the docking axis on the target and the operational range of the navigation sensor, which will be used for the subsequent first rendezvous phase (see section 5.3 for more details concerning the influence of port location and sensor characteristics on the approach strategy). Locating this point behind and slightly below the target is the most convenient solution, as the natural drift will move the chaser slowly toward the target without additional propulsion manoeuvres. During such drift, residual errors after the last manoeuvre in terms of Δ-height, Δ-eccentricity and

out-of-plane errors (Δ-inclination and Δ-RAAN; for definition of these terms see section 3.2.1) can be corrected.

2.2.7 Strategy with entry gate instead of aim point

As already mentioned, instead of a scheme with a fixed aim point, a strategy with an 'entry gate' can be used for the transition from phasing to the far range rendezvous (see figure 2.8). In this strategy, first the apogee is raised to the height of the target orbit, then the perigee is raised successively, reducing the phasing rate. The final goal of phasing is the passing through the entry gate, which fulfils the conditions for the start of far range rendezvous operations in terms of *x,y,z* positions and velocities. This strategy is convenient when a phasing strategy is used, in which the apogees of all orbital revolutions are on V-bar and when a continuous approach without interruptions is planned. In this case, the 'gate' conditions are applied for the last apogee prior to the final rendezvous operations.

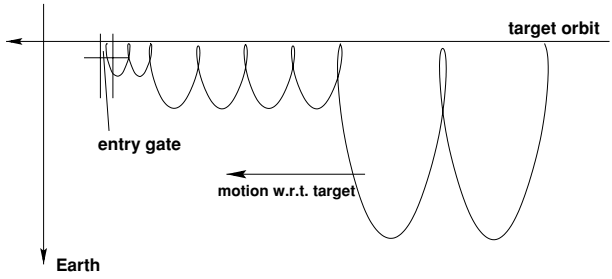

Figure 2.8. Alternative strategy: entry gate.

2.2.8 Final accuracy of open loop manoeuvres

Manoeuvres during phasing are usually performed in open loop, i.e. first the manoeuvre is calculated, then it is executed, and the achieved result is verified thereafter. As typical two-pulse manoeuvres have only limited accuracy, it may be necessary to perform several consecutive manoeuvres at the end of phasing to achieve the required accuracy for the initial aim point or entry gate for far range rendezvous. For reasons of safety (risk of collision with the target), most critical will be the achievement within close tolerances of the proper orbital height, in circular orbits, or of the apogee height, in elliptical orbits. The positioning accuracy, which eventually can be achieved on the basis of absolute navigation by open loop manoeuvres, e.g. by a Hohmann transfer, is typically of the order of a few hundreds of metres in height and a few kilometres in orbital direction. The errors arising from such open loop manoeuvres are discussed in section 4.3.

2.3 Far range rendezvous operations

2.3.1 Objectives and goals of far range rendezvous

In many publications this phase is called ‘homing’, by analogy to the navigation term used for aircraft when approaching an airport. The major objective of the far range rendezvous phase is the reduction of trajectory dispersions, i.e. the achievement of position, velocity and angular rate conditions which are necessary for the initiation of the close range rendezvous operations. Major tasks of this phase are the acquisition of the target orbit, the reduction of approach velocity and the synchronisation of the mission timeline. Far range rendezvous can start when relative navigation between chaser and target is available. The end point of this phase (see point S2 in figure 2.9) is usually a point from which standard rendezvous operations on standard trajectories at a fixed timeline can commence, a feature which is particularly desirable for an automatic rendezvous process.

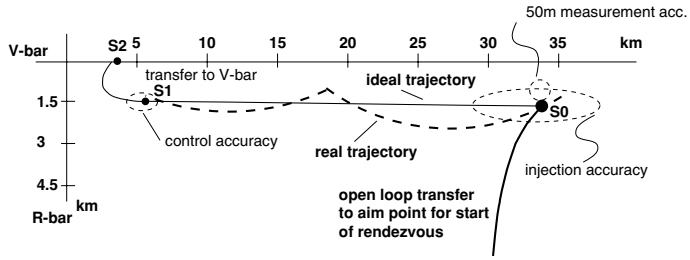

Figure 2.9. Transfer from phasing orbit to rendezvous drift orbit.

A constraint on the location of the end point of the far range rendezvous may result from operational requirements imposed by the target station. For example, for the ISS an ‘Approach Ellipsoid’ is defined with a major half-axis of 2 km along the target orbit direction and minor ones of 1 km (see section 5.6, figure 5.24). The requirement is that the approach initiation for final rendezvous manoeuvres should be located outside the Approach Ellipsoid. As a result, far range rendezvous typically starts in this scenario at a range of a few tens of kilometres and ends at a range of few kilometres from the target.

2.3.2 Relative navigation during rendezvous

Whereas during phasing all manoeuvres are based on absolute navigation measurements, provided either by sensors aboard the chaser (e.g. GPS) or on ground, navigation during rendezvous operations proper (i.e. far range and close range rendezvous) is based on relative measurements of range and direction (e.g. radar) or directly by the relative position (e.g. relative GPS or RGPS) between chaser and target vehicles. The final open loop manoeuvres at the end of phasing must lead to conditions which bring the chaser

into the acquisition range of the relative navigation sensor for far range rendezvous (for types and details of navigation sensors, see chapter 7). The required measurement accuracy of the relative navigation sensor at the beginning of the far range rendezvous phase is of the order of 100 m. In the same way, the accuracy of the last part of the far range rendezvous trajectory must be commensurate with the requirements for the start of the close range rendezvous operations. The required positioning accuracy is typically of the order of a few tens of metres and the measurement accuracy is of the order of 10 m.

2.3.3 Trajectory elements/time-flexible elements

Trajectory elements during far range rendezvous may include free drift trajectories on circular or elliptic orbits, tangential and radial transfers (see section 3.3.2) and hold points (see section 3.3.3). In order to be able to synchronise the mission timeline with external events, such as Sun illumination, communication windows and crew operations timeline, the far range rendezvous strategy may need to include 'time-flexible' elements. We have identified such a time-flexible element already during phasing, where faster and slower phasing rates could be achieved by varying the orbital height. Although this technique can be used here as well, other time-flexible elements become possible because the chaser is now close to target orbit. The most important one is, of course, a hold point on the target orbit, where the vehicle can stay indefinitely at nominally zero ΔV costs. If such a hold point on V-bar is used, it is usually implemented at the end of the far range rendezvous phase (figure 2.10). Other possibilities include forward and backward drifts below or above the target orbit, or an elliptical motion with the mean orbital height equal to the target orbit. For more details on time-flexible elements, see section 5.4.4.

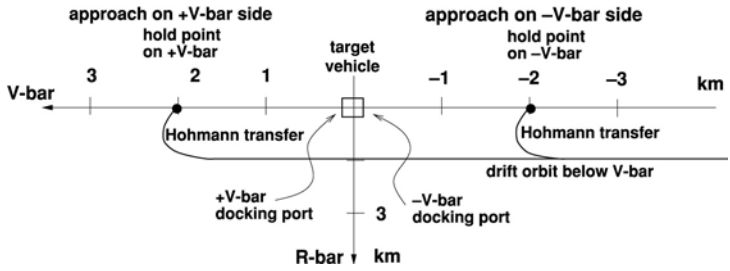

Figure 2.10. Time-flexible element: hold point on V-bar.

2.3.4 Communication with the target station

Generally prior to or shortly after the start of the far range rendezvous phase, communication between chaser and target vehicles will be established. Communication capability

between the two vehicles may be required for operational and safety reasons and possibly also for navigation sensor functions (e.g. for RGPS). In fact, apart from the possible communication requirements for the sensor function, the complete approach up to mating could be conducted without communications between the vehicles, i.e. all communications going via ground. However, as the communication links with ground are more prone to disturbances and black-outs, in rendezvous missions with manned target vehicles safety considerations require the establishment of such links prior to the start of close range rendezvous operations. The target crew must be able to monitor the trajectory and attitude of the incoming vehicle and must be able to command the chaser to stop or retreat in case of problems with either chaser or target vehicle. The crew must also be able to initiate a collision avoidance manoeuvre in case of dangerous trajectory situations. As a result, direct communication between the vehicles is not necessarily a requirement in cases where both vehicles are unmanned.

2.4 Close range rendezvous operations

The close range rendezvous phase is usually divided into two subphases: a preparatory phase leading to the final approach corridor, often called 'closing', and a final approach phase leading to the mating conditions. There are, of course, cases where no distinction can be made between a closing and a final approach subphase. This may be the case, e.g., for a V-bar approach, where the direction of motion remains the same and where no change of sensor type occurs.

The following features are important for the initiation of close range rendezvous operations: out-of-plane errors (inclination, RAAN) have been corrected to the same accuracy as the in-plane errors; the mission timeline up to capture has been synchronised with the external constraints; and all parties involved, i.e. space and ground segment of both vehicles, are ready for the final operation up to mating. The proximity to the target makes all operations safety-critical, requiring particular safety features for trajectory and onboard system design and continuous monitoring and interaction possibility by operators on ground and in the target station.

2.4.1 Closing

Objectives and end conditions of closing

The objectives of the closing phase are the reduction of the range to the target and the achievement of conditions allowing the acquisition of the final approach corridor. This means that at the end of this phase the chaser is, concerning position, velocities, attitude and angular rates, ready to start the final approach on the proper approach axis within the constraints of the safety corridor. If the approach axis for mating is not in the $+$ or $-$ V-bar direction, the closing phase may include a fly-around manoeuvre to acquire the approach axis. Because of the increased navigation accuracy requirements, in many

cases a different type of sensor than in the previous phase has to be used for the final approach. In this case, toward the end of the closing phase, the acquisition conditions for the new sensor type have to be met. The rule of thumb is that the measurement accuracy must be of the order of 1% of range or better.

Trajectory elements/time-flexible elements

Because of the safety criticality of the close range rendezvous operations, trajectory strategies have to be conceived such that the incapacity to execute a thrust manoeuvre, whether fully or partially, does not leave the vehicle on a trajectory which eventually leads to a collision. The following observations are relevant for the choice of trajectory in the closing phase.

- Because of their resulting trajectory characteristics, pure tangential thrust manoeuvres are rarely used (see figures 4.11 and 4.12).
- Radial manoeuvres result in eccentric orbit trajectories without changing the average orbital altitude, i.e. in stationary ellipses when initiated on V-bar (see figure 4.13). However, when they are, e.g., due to navigation errors initiated at a position which is higher or lower than the target orbit, they will result in 'walking ellipses', moving toward or away from the target. This problem and possible counter measures are discussed in more detail in section 4.4.2.
- If the closing phase extends over around 2000 m, straight line approaches are not used because of the comparatively high ΔV costs.

It must be ensured that if trajectory control ceases, there will be no risk of colliding with the target for at least a number of revolutions. The number of collision-free revolutions required will depend on the time the target vehicle needs to prepare and execute an escape manoeuvre.

Although the mission timeline is assumed to be already synchronised with external constraints prior to start of closing, time-flexible elements in the form of hold points may still be needed for fine-tuning and for operational reasons. Another consideration is that the rendezvous process may have to be interrupted for some larger time because of contingencies arising at either vehicle. In this case, the chaser vehicle may need to return to a hold point at a safe distance, where it can wait until the approach can be resumed. Trajectory design will, therefore, have to take into account the return to such a hold point. This can be, e.g., the point from which the closing trajectory is started or a safer point at larger distance from the target, if resolution of the contingency is expected to take more time.

Fly-around and direct R-bar acquisition

The different acquisition strategies for V-bar and R-bar approaches are shown in figure 2.11. Final approaches on V-bar (trajectories (a) and (b)), can commence directly from

a V-bar hold point on the + or − V-bar side (trajectories (a) and (b)). For the acquisition of an R-bar approach corridor, several possible strategies can be employed.

- The first is a fly-around starting from a position on V-bar (trajectory (c)). The advantage of starting from a V-bar position is the operational flexibility due to the possibility of an unlimited stay time at a V-bar hold point.
- The second is to acquire the starting point of the R-bar trajectory directly from an orbit lower than the target orbit (trajectory (e)), making use of the natural upward motion at the end of a radial impulse transfer trajectory. This strategy has the advantages of a short approach time and low propellant propulsion, as intermediate trajectories are omitted; however, there are disadvantages of no time flexibility and less favourable collision safety features.
- The third possibility is trajectory (d), which is a drift toward the R-bar approach corridor on a slightly lower orbit than the target orbit and has the advantages of a lower propellant consumption and inherent collision safety of the trajectory. By selection of the altitude difference to the target orbit, a certain amount of time flexibility can be achieved.

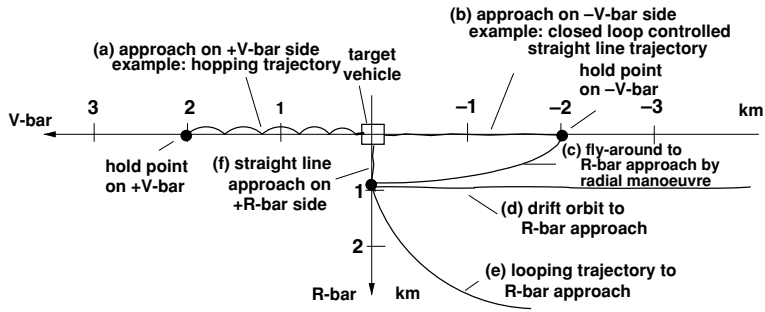

Figure 2.11. Acquisition of V-bar and R-bar final approach.

The eventual choice of acquisition strategy for an R-bar approach will depend on many safety constraints (see chapter 4) and operational constraints (see chapter 5).

2.4.2 Final approach to contact

Objectives and end conditions of final approach

The objective of the final approach phase is to achieve docking or berthing capture conditions in terms of positions and velocities and of relative attitude and angular rates. The attempted end condition is the delivery of chaser docking or capture interfaces into the reception range of the target docking mechanism or of the capture tool of the manipulator in the case of berthing. In the case of passive capture latches (impact docking),

there must be a certain axial contact velocity, as the energy is needed to operate the capture latches. In the case of active capture latches (soft docking), the capture latches are motorised and triggered by sensors. This type of docking mechanism will work also with very low contact velocities (see sections 8.3.4 and 8.3.5). For berthing, the capture interface for the manipulator, mounted on the chaser, must remain for a certain duration within a volume which can be reached by the manipulator within that time.

Trajectories during final approach

The trajectory types used for the final approach are closed loop controlled straight line trajectories or quasi-straight line trajectories realised by a multitude of small hops (see figure 2.11, trajectory (a)). The first type is the preferred choice for automatic onboard control systems, whereas the latter is more convenient for man-controlled approaches, as fixed thrust pulses can be commanded, e.g. when a reference line of the target image crosses the horizontal centre line of the field of view of a camera or sensor. Straight line or quasi-straight line trajectories are preferred during this phase, on one hand because of the limited field of view of the rendezvous sensors, and on the other hand because the docking interfaces have to enter each other along their symmetry axes.

Navigation and control requirements

The rule of thumb for the navigation measurement accuracy of approximately 1% of the range can, for a preliminary assessment, also be applied for the final approach. It is compatible with the final control accuracies for docking, which are, depending on the reception range of the docking mechanism, a few centimetres in lateral position, about 1 deg for attitude and of the order of 1 cm/s for axial and lateral rates and 0.1 deg/s for angular rates.

For berthing, the absolute position and attitude accuracies are less critical, i.e. values approximately a factor of 5 higher than those for docking may be still acceptable. In contrast, linear and angular rates must be a factor of approximately 5 lower than those acceptable for docking. For safety reasons, the target station may require that the reaction control system of the incoming vehicle is switched off prior to the start of the grappling operations by the manipulator. The manipulator operations from initiation until capture may take more than 60 s, within which time the grapple interfaces of the incoming vehicle must remain in the capture range. This is one of the reasons why berthing conditions may be more difficult to achieve by the GNC system than docking conditions (cf. section 5.3.1).

For docking, the GNC system has to fulfil an additional condition. The V-bar and R-bar approach axis, discussed so far, concern the nominal docking axis. The actual docking axis will deviate from the nominal direction due to (i) attitude bias, (ii) attitude control motions, and (iii) bending of the structure of the target vehicle. It is, therefore, important that the chaser vehicle acquires and follows the instantaneous docking axis (see figure 2.12). This is possible only when the chaser has the navigation means to

identify and track the centre of the docking port and the direction of the docking axis. For this purpose the rendezvous sensor for the final approach must be able to measure, in addition to axial and lateral positions (or range and direction), the relative attitude between the docking ports of chaser and target (see section 6.2.3, figure 6.12). This requirement does not exist for berthing.

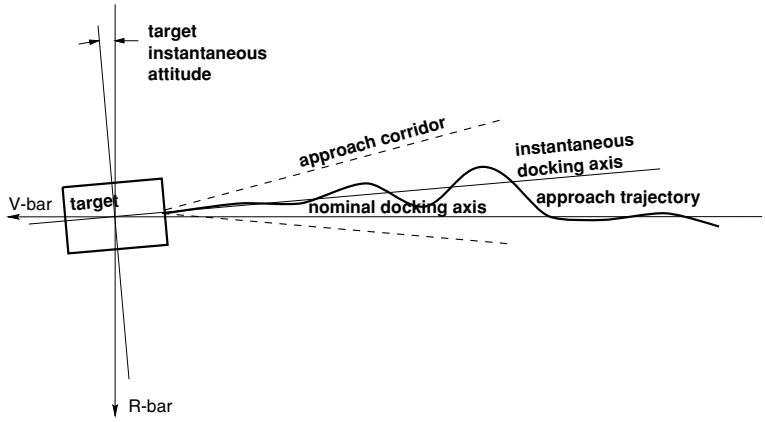

Figure 2.12. Acquisition of instantaneous docking axis.

Other constraints during final approach

For observability and safety reasons a cone-shaped approach corridor will usually be defined, within which the approach trajectory has to remain. The cone originates from the mating point at the target vehicle, i.e. from the docking port or from the berthing box, and has a half cone angle of 10–15 deg. Such a corridor allows ground operators and/or target crew to assess via video cameras or other sensor information the accuracy of the approach trajectory. If corridor boundaries are violated, stop, retreat, or collision avoidance manoeuvre commands can be issued (for further details concerning approach safety, see chapter 4).

Another issue which plays an important role when the approaching vehicle comes close, is the effect of the thruster plumes on the target vehicle. Three major effects can be distinguished:

- the forces exerted on the target vehicle by the plume pressure;
- the heat load on the structure of the target vehicle by the hot plume gases;
- the contamination of the surface of the target vehicle by the combustion products and unburned propellant components.

In order to reduce the approach velocity, the approaching vehicle has to apply forces in the opposite direction, i.e. it has to thrust directly toward the target. In addition, the attitude of the vehicle has to be controlled, resulting in thruster burns in all directions. The resulting effects on the target vehicle from the thrust plumes of the chaser can be:

- disturbance of the attitude and position, depending on the mass and inertia of the target in relation to the plume pressure;
- overheating of parts of the surface and underlying structure;
- contamination of sensitive elements on the target surface, in particular of optical elements, such as the target reflectors for the rendezvous sensor and the lenses on monitoring cameras, and of, e.g., the sealing elements of the docking mechanism.

In order to minimise these effects, for docking the final contact velocity will be achieved at some distance from the target and will thereafter be kept constant. The final braking burn toward the target then takes place at a distance which is far enough away such that the gas temperature has sufficiently cooled to avoid damage of the structure, and such that the density of contaminating particles is sufficiently reduced to avoid significant condensation when arriving at the target surface. For berthing, these effects are less pronounced, as the berthing box will always be located as far away from the target structure as the reach of the manipulator arm allows.

2.5 Mating: docking or berthing

2.5.1 Objectives and end conditions of the mating phase

The mating phase starts when the GNC system of the chaser has delivered the capture interfaces of the chaser into the reception range of those of the target vehicle. This must be achieved within the constraints of the interface conditions, concerning

- approach velocity, lateral alignment, angular alignment, lateral and angular rates for docking;
- position and attitude accuracy, residual linear and angular rates for berthing.

It is then the task and responsibility of the mating system to:

- achieve capture, i.e. the condition of no escape (task 1);
- attenuate the residual relative motion between the vehicles (task 2);
- bring the interfaces of the structural latches into their operational range (task 3);
- achieve rigid structural connection (task 4);

- achieve gas-tight sealing of the connection of a pressurised passage between the vehicles (task 5) – this is achieved usually in connection with the process of structural connection;

- establish the connection of data, power and possibly of fluid (propellant, water, air supply) interfaces (task 6).

Docking and berthing operations to achieve these tasks are described in sections 8.1.1 and 8.1.2. When these tasks are fulfilled, the mating phase is concluded. The subsequent phase of joint operations is outside the scope of this book.

2.5.2 Capture issues

In docking, all tasks are concentrated in one system, the docking mechanism. In berthing, tasks 1, 2 and 3 are performed by a manipulator arm, and the residual tasks are performed by a berthing mechanism. Another difference between docking and berthing is that the capture interface for berthing, the so-called grapple fixture, does not need to be located on the chaser vehicle in the vicinity of the other mating interface elements. In fact, for better acquisition and handling it is usually located in a different plane on a different part of the surface of the vehicle.

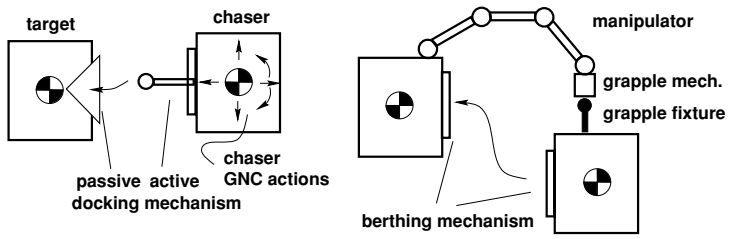

Figure 2.13. Docking and berthing.

For the purpose of this chapter, the most important mating function is capture, as it is the natural end of the rendezvous process. The subsequent structural and utility connection tasks are, for the success of the mission, of no less importance; however, they are independent from the dynamic processes of approach, contact and capture. The connection tasks will be addressed in section 8.4.1.

The basic difference concerning capture between docking and berthing is that in docking the body of the approaching vehicle is actively controlled to guide its capture interfaces into the corresponding interfaces on the target vehicle. In berthing, the manipulator arm plays the active role, guiding its grapple mechanism to capture the passive grapple fixture on the other vehicle. As a matter of fact, the manipulator arm can be located on either the target station or the approaching vehicle, and vice versa for the passive grapple fixture. The basic differences between the docking and berthing processes are illustrated

in figure 2.13. The physical effects at the contact and capture interfaces are, however, very similar.

Since at contact the two bodies will rebound and will separate again (see figure 2.14), capture must be accomplished in the short time before the interfaces have left the capture volume. For example, in the case of free motion of a rigid body with a relative velocity of 0.1 m/s into a concave cone of a fixed body with an opening diameter of $d = 0.1$ m, the body would leave the cone again after two (perfect) rebounds within 1 s (see figure 2.14). The methods of how to achieve capture under such conditions and how to increase the time for capture will be discussed in more detail in section 8.3.

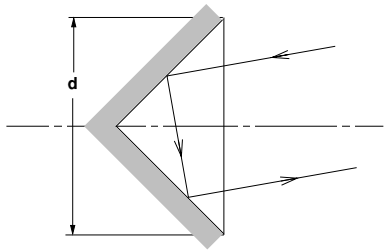

Figure 2.14. Rebound trajectory in a concave cone.

2.6 Departure

2.6.1 Objectives and end conditions of the departure phase

All rendezvous missions, except for assembly missions, will eventually include the separation and departure from the target spacecraft. This phase includes the re-initiation of the GNC system, the opening of the utility and structural connections and the departure from the target station. The end conditions of this phase are that the departing vehicle moves on a non-returning trajectory, and has arrived at a sufficiently safe distance w.r.t. the station, when the large thrust manoeuvre for de-orbitation will be performed.

2.6.2 Constraints and issues during departure

After the opening of the structural latches, an impulse has to be applied to the centre of mass (CoM) of the departing vehicle (assuming the target station remains passive) to achieve the necessary departure velocity. This is generally the task of the propulsion system of the departing vehicle. However, an impulse large enough to achieve the required safe departure trajectory implies a relatively large thrust in very close proximity to the target vehicle surface. The potential effects in terms of thermal loads and surface contamination have already been addressed in section 2.4.2. Solutions to this problem may include, as first manoeuvre steps, the application of spring forces at release of the structural latches, providing the impulse for the first few metres of motion, and there-

after the application of thrusts in a direction orthogonal to the docking port direction. Another constraint is the requirement for observability of the departure trajectory by a sensor or video camera, in the same way as for the final approach. This leads to the definition of a departure corridor analogous to the docking corridor.

A typical trajectory and corridor for departure from a −V-bar docking port is shown in figure 2.15 and for departure from an R-bar port in figure 2.16. The manoeuvre strategy in both examples fulfils the requirement of minimum plume impact on the target station and trajectory inside the departure corridor.

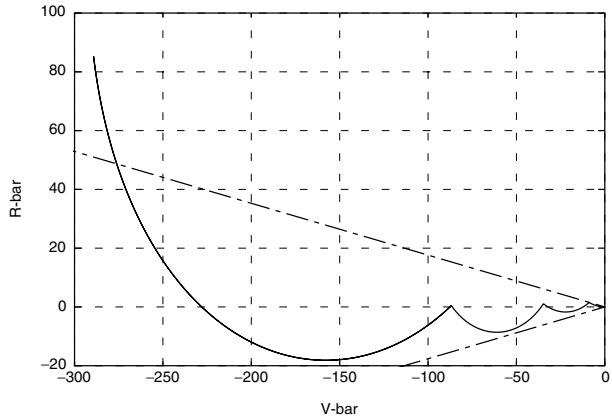

Figure 2.15. −V-bar departure.

The V-bar departure strategy shown in figure 2.15 assumes a first small ΔV of 0.06 m/s applied to the departing vehicle by the springs of the docking mechanism. The resulting trajectory would soon leave the departure cone, which has been assumed to have a half cone angle of 10 deg. The first impulse by the propulsion system after 150 s is a thrust of 0.05 m/s in the −R-direction to minimise the plume impact on the station. A further radial manoeuvre of −0.08 m/s follows after 420 s to keep the vehicle inside the departure corridor. After a further 720 s, at a distance of ≈80 m, a combined radial and axial boost of −0.2 m/s each can be applied without too much impact by the plume on the station. A departure corridor is usually defined for a distance of a few hundred metres, after which the departure trajectory is free to assume any shape, as long as it is moving away from the target.

The first elements of the trajectory in such a departure corridor are not inherently safe, since, in the case of loss of control capability, the resulting free drift trajectory would lead to collision with the target station. In this case, as a last resort, a collision avoidance manoeuvre (see section 4.5) must be initiated, for which, of course, potential plume effects must be acceptable for the target. The corresponding departure trajectory on the +V-bar side can be obtained by mirroring the −V-bar trajectory on the R-bar and V-bar axes.

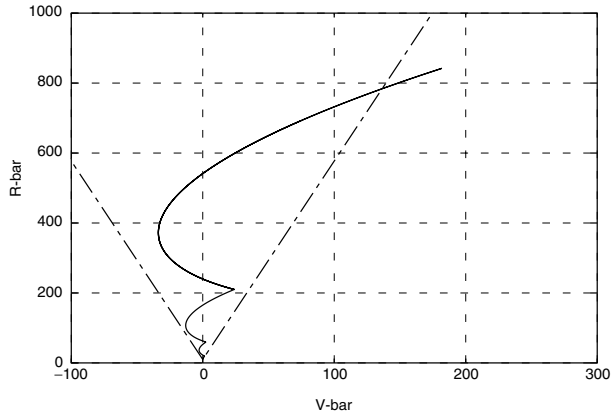

Figure 2.16. R-bar departure.

The departure from an R-bar docking port or from a berthing location is somewhat less critical concerning trajectory safety and contamination. Due to the fact that the CoM of the departing vehicle will be below V-bar, the natural motion after release of the structural latches will be downward and forward (figure 2.16). In order to remain in the departure corridor, the first thrusts, as well as the final departure burn, will be in the $-$V-bar direction, i.e. not toward the target surface, as in the case of the V-bar departure.

In the example it is assumed that the CoM of the departing vehicle is 10 m below the CoM of the station and receives a ΔV of 0.06 m/s from the springs of the docking mechanism. This results in a position change in the $+$ R-bar direction of $\approx$1.7 m after 300 s. At that point, a small thrust manoeuvre in the $-$V-bar direction of 0.06 m/s is applied. Thereafter, further $-$V-bar thrusts may have to be applied in order to keep the trajectory inside the departure corridor. Only at a distance of $>$200 m can the final departure manoeuvre be applied. This will be a large boost in the $-$V-bar direction.

In contrast to the approach, the required accuracy of the departure trajectory is decreasing, and there is in principle no need for a departure cone as narrow as that given in the two examples. The departure cone axis could even be at an angle w.r.t. V-bar, better following the natural motion. To monitor trajectory safety, the departure cone must be, however, in the field of view of the observation camera.

As shown in this section, departure strategies are formed by two or more impulsive manoeuvres and are therefore simple and straightforward. Since the complexity of the departure process in terms of trajectory implementation is comparatively low, and, accordingly, sensor and GNC requirements are fully covered by the relevant discussions for the approach phase, the rest of the book can concentrate on the rendezvous phases only.

3

Orbit dynamics and trajectory elements

In this chapter the basic equations for the calculation of orbits and trajectories are given, and the properties of the most important types of trajectories used in rendezvous missions are discussed. In sections 3.1 and 3.2 the reference frames are defined and the laws of motion in elliptic and circular orbits in the 'orbital plane' coordinate frame are addressed. Equations of motion, expressed in this frame, are conveniently used during launch and phasing operations. In sections 3.3 and 3.4, the trajectories between chaser and target vehicle which are used in the far and close range rendezvous approaches are discussed. They are treated as relative trajectories in the 'local orbital frame' of the target. Only the ideal undisturbed trajectories are looked at in this chapter, and the necessary velocity changes, or continuous forces to be applied and the resulting position changes, are derived for ideal cases. The major sources of trajectory disturbances are addressed in chapter 4.

3.1 Reference frames

The purpose of this section is to define the coordinate frames used in this book for the description of the orbital motion, for absolute and relative trajectory and attitude motions and for the relations of these motions to geometric features on the spacecraft. Each frame $\mathbf{F}_i$ is defined by its origin $\mathbf{O}_i$ and a set of three orthogonal vectors $\mathbf{a}_1, \mathbf{a}_2, \mathbf{a}_3$. Generally three types of coordinate frames are needed:

- *Orbit reference frames:* to describe the orientation of the orbit relative to inertial space and to the Earth and to describe the motion of a spacecraft within an orbit.
- *Spacecraft local orbital reference frames:* to describe the motion relative to a particular point in orbit or to another spacecraft.

- *Spacecraft attitude and body frames:* to describe dynamic and kinematic processes (attitude, attitude manoeuvres) of the spacecraft relative to its centre of mass and to describe features relative to the geometry and to a particular point of the spacecraft.

3.1.1 Earth-centred equatorial frame $F_{\mathbf{eq}}$

The F_{eq} coordinate frame will be used to describe the orbital motion around the centre of the Earth and w.r.t. inertially fixed directions. The Earth is assumed to be truly spherical, i.e. its geometric centre is its centre of mass and the focal point of orbital motions.

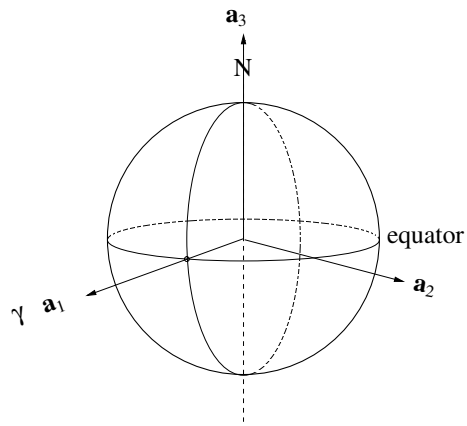

Figure 3.1. F_{eq} frame.

In figure 3.1 we have:

- origin $\mathbf{O}_{\mathrm{eq}}$: centre of the Earth;
- axis $\mathbf{a}_1$: in the equatorial plane, pointing toward the mean of the vernal equinox;
- axis $\mathbf{a}_2$: in the equatorial plane, such that $\mathbf{a}_3 = \mathbf{a}_1 \times \mathbf{a}_2$;
- axis $\mathbf{a}_3$: normal to the equatorial plane and pointing north.

$\boldsymbol{F}_{\mathbf{eq}}$ can be used as a quasi-inertial frame.

3.1.2 Orbital plane frame $\boldsymbol{F}_{\mathbf{op}}$

The F_{op} coordinate frame is used when only the motion within the orbital plane has to be described.

In figure 3.2 we have:

- origin $\boldsymbol{O}_{\mathbf{op}}$: centre of the Earth;

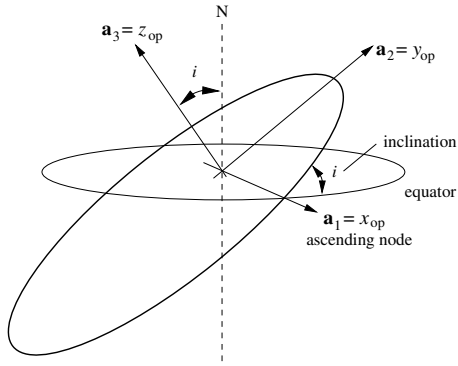

Figure 3.2. F_{op} frame.

- axis $\mathbf{a}_1$: in the orbital plane, pointing toward the ascending node;
- axis $\mathbf{a}_2$: in the orbital plane, such that $\mathbf{a}_3 = \mathbf{a}_1 \times \mathbf{a}_2$;
- axis $\mathbf{a}_3$: normal to orbital plane, inclined to the north direction by the angle i.

The coordinate transformation from the Earth-centred equatorial frame $\boldsymbol{F}_{\mathbf{eq}}$ to the orbital plane frame $\boldsymbol{F}_{\mathbf{op}}$ is obtained by a rotation about z_{eq} by the RAAN angle Ω (see figure 2.3) and by a further rotation about the axis through the nodes by the inclination angle i:

$$\begin{bmatrix} x_{\mathrm{op}} \\ y_{\mathrm{op}} \\ z_{\mathrm{op}} \end{bmatrix} = \begin{bmatrix} 1 & 0 & 0 \\ 0 & \cos i & \sin i \\ 0 & -\sin i & \cos i \end{bmatrix} \begin{bmatrix} \cos\Omega & \sin\Omega & 0 \\ -\sin\Omega & \cos\Omega & 0 \\ 0 & 0 & 1 \end{bmatrix} \begin{bmatrix} x_{\mathrm{eq}} \\ y_{\mathrm{eq}} \\ z_{\mathrm{eq}} \end{bmatrix}$$

$\boldsymbol{F}_{\mathbf{op}}$ can be used to describe orbital transfer manoeuvres.

3.1.3 Spacecraft local orbital frame $\boldsymbol{F}_{\mathbf{lo}}$

The F_{lo} coordinate frame is used to describe motions w.r.t. the moving position and direction towards the centre of the Earth of an orbiting body.

In figure 3.3 we have:

- origin $\boldsymbol{O}_{\mathbf{lo}}$: centre of mass of the spacecraft;
- axis $\mathbf{a}_1$: $\mathbf{a}_1 = \mathbf{a}_2 \times \mathbf{a}_3$ ($\mathbf{a}_1$ is in the direction of the orbital velocity vector but not necessarily aligned with it). In the rendezvous literature this coordinate is also called **V-bar**;
- axis $\mathbf{a}_2$: in the opposite direction of the angular momentum vector of the orbit. In the rendezvous literature this coordinate is also called **H-bar**;

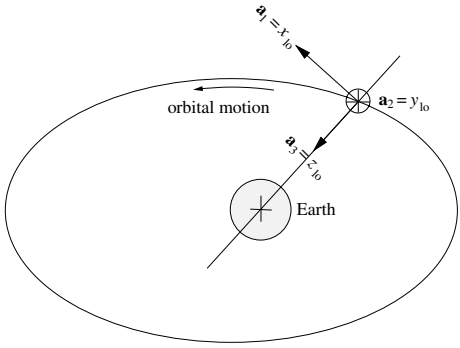

Figure 3.3. F_{lo} frame.

- axis $\mathbf{a}_3$: radial from the spacecraft CoM to the centre of the Earth.
  In the rendezvous literature this coordinate is also called **R-bar**.

In this way the local orbital frame for both the target and the chaser can be defined. The approach trajectories of the chaser are usually shown in the local orbital frame of the target. This frame is often referred to as the local-vertical/local-horizontal (LVLH) frame.

The coordinate transformation from the orbital plane frame $\boldsymbol{F}_{\mathbf{op}}$ to the spacecraft local orbital frame $\boldsymbol{F}_{\mathbf{lo}}$ is obtained by a rotation about z_{op} by the orbital phase angle ϕ, measured from the ascending node, and by two 90 deg rotations to put x_{lo} into the orbital velocity direction and z_{lo} toward the centre of the Earth. For a circular orbit $\phi = \omega\, t$. For near circular orbits, as used in most rendezvous missions, this is a good approximation:

$$\begin{bmatrix} x_{\mathrm{lo}} \\ y_{\mathrm{lo}} \\ z_{\mathrm{lo}} \end{bmatrix} = \begin{bmatrix} 1 & 0 & 0 \\ 0 & 0 & -1 \\ 0 & 1 & 0 \end{bmatrix} \begin{bmatrix} 0 & 1 & 0 \\ -1 & 0 & 0 \\ 0 & 0 & 1 \end{bmatrix} \begin{bmatrix} \cos\phi & \sin\phi & 0 \\ -\sin\phi & \cos\phi & 0 \\ 0 & 0 & 1 \end{bmatrix} \begin{bmatrix} x_{\mathrm{op}} \\ y_{\mathrm{op}} \\ z_{\mathrm{op}} \end{bmatrix}$$

3.1.4 Spacecraft attitude frame $F_{\mathbf{a}}$

The spacecraft attitude frame is used to describe all rotations of the body of a spacecraft. The attitude frame is often referred to as the 'body frame'. However, as the CoM may move during flight, e.g. due to depletion of propellant, this frame is not firmly fixed to the spacecraft geometry.

The nominal direction of the spacecraft attitude frame depends on the manoeuvre strategy of the mission. The axis $\mathbf{a}_1$ may point in the direction of the orbital velocity vector, toward the Earth, the Sun or in other directions. For example, in the final phase of a rendezvous and docking mission, the axis $\mathbf{a}_1$ is usually pointing in the direction of the docking axis. The lateral axis $\mathbf{a}_2$ is often aligned with the positive or negative direction of the angular momentum vector of the orbit. In figure 3.4 we have

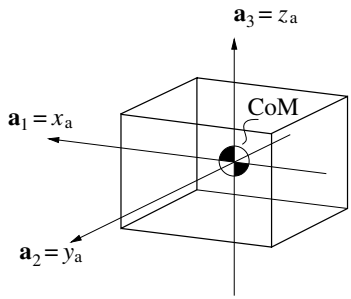

Figure 3.4.

- origin $\boldsymbol{O}_\mathbf{a}$: centre of mass of the spacecraft;
- direction of axes $\mathbf{a}_1, \mathbf{a}_2, \mathbf{a}_3$ depending on mission and mission phase, $\mathbf{a}_3 = \mathbf{a}_1 \times \mathbf{a}_2$ forming a right handed system.

The coordinate transformation from the LVLH frame $\boldsymbol{F}_\mathbf{lo}$ to the spacecraft nominal attitude frame $\boldsymbol{F}_\mathbf{a}$ is obtained by a rotation of the frame by the attitude angles α_z (azimuth), α_y (elevation) and α_x (roll):

$$\begin{bmatrix} x_\mathrm{a} \\ y_\mathrm{a} \\ z_\mathrm{a} \end{bmatrix} = \begin{bmatrix} 1 & 0 & 0 \\ 0 & c\alpha_x & s\alpha_x \\ 0 & -s\alpha_x & c\alpha_x \end{bmatrix} \begin{bmatrix} -s\alpha_y & 0 & c\alpha_y \\ 0 & 1 & 0 \\ c\alpha_y & 0 & s\alpha_y \end{bmatrix} \begin{bmatrix} c\alpha_z & s\alpha_z & 0 \\ -s\alpha_z & c\alpha_z & 0 \\ 0 & 0 & 1 \end{bmatrix} \begin{bmatrix} x_\mathrm{lo} \\ y_\mathrm{lo} \\ z_\mathrm{lo} \end{bmatrix}$$

$$s\alpha = \sin\alpha$$
$$c\alpha = \cos\alpha$$

3.1.5 Spacecraft geometric frames $\boldsymbol{F}_\mathbf{ge}$

These coordinate frames are used to describe translations and rotations of the spacecraft w.r.t. location and direction of equipment, such as sensors, thrusters or docking mechanism. In figure 3.5 we have

- origin $\boldsymbol{O}_\mathbf{ge}$: a particular point on the spacecraft, e.g.
  - the point defining the origin of the spacecraft coordinate system,
  - the centre of the docking port, defining the docking frame,
  - the centre of a sensor, defining the measurement frame;
- axes $\mathbf{a}_1, \mathbf{a}_2, \mathbf{a}_3$: coordinate-aligned with, or under a fixed angle to, the attitude frame.

The transformation from the spacecraft attitude frame to one of the geometric frames is a parallel shift in *x*, *y*, *z* from the centre of mass of the spacecraft and a fixed rotation ϕ_x, ϕ_y, ϕ_z around the origin of the frame. It requires, therefore, the knowledge of the instantaneous position of the CoM of the spacecraft.

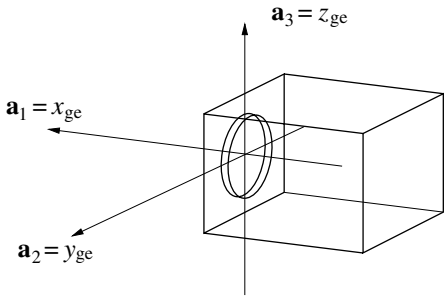

Figure 3.5. F_{ge} frame.

3.2 Orbit dynamics

3.2.1 Orbital motion around a central body

The equations of motion in an orbit around a central body can be derived from Kepler's and Newton's laws. The detailed derivation of these equations is provided in many textbooks, such as Kaplan (1976), Roy (1988), Renner, Nauck & Balteas (1988), Wertz & Larson (1991), Carrou (1995) and Sidi (1997).

To enable the understanding of rendezvous trajectories, only the most important relations will be repeated here; these are valid for the case of an undisturbed spherical gravitational field (relations are given in the orbital plane frame).

Combining Newton's laws of gravitation

$$F = -G\frac{m_c m_s}{r^2} \tag{3.1}$$

with his second law, relating force and acceleration,

$$F = m_s \ddot{r} \tag{3.2}$$

one obtains the equation for the orbital motion of a satellite:

$$\ddot{r} = -\frac{\mu}{r^2} \tag{3.3}$$

In these equations $G = 6.674 \times 10^{-11}\,\mathrm{N\,m^2/kg^2}$ is the universal gravitational constant, m_c is the mass of the central body, m_s is the mass of the satellite and r is the distance between their centres. The term $\mu = G \cdot m_c$ is the gravitational constant of the celestial body around which the satellite orbits. The gravitational constant of the Earth is $\mu_E = 398\,600\,\mathrm{km^3/s^2}$. A solution to Eq. (3.3) is:

$$r = \frac{p}{1 + e\cos\nu} \tag{3.4}$$

with p being a parameter defining the geometric extension of the curve, e the eccentricity and ν the polar angle measured from the pericentre (true anomaly). This is the general equation for conic sections. Derivations can be found in Roy (1988), Renner *et al.* (1988) and Sidi (1997). The value of *e* defines the shape of the curve:

for $e = 0$ the curve is a circle,
for $0 < e < 1$ the curve is an ellipse,
for $e = 1$ the curve is a parabola,
for $e > 1$ the curve is a hyperbola.

Of these four possible conic sections, circle, ellipse, parabola and hyperbola, only the first two are of interest for the discussion of rendezvous trajectories in this book.

Elliptic orbits

In an elliptic orbit, Eq. (3.4) becomes at the apocentre for $\nu = 180$ deg

$$r_{\mathrm{a}} = \frac{p}{1-e}$$

and at the pericentre for $\nu = 0$

$$r_{\mathrm{p}} = \frac{p}{1+e}$$

and with $r_{\mathrm{a}} + r_{\mathrm{p}} = 2a$, the parameter becomes $p = a(1-e^2)$. The polar equation of an elliptic orbit is then

$$r = \frac{a(1-e^2)}{1 + e\,\cos\,\nu} \tag{3.5}$$

The *true anomaly* ν, the *semi-major axis* a and the *eccentricity* e are defined in figure 3.6 and in figures 2.2–2.4 of chapter 2. The eccentricity e can be expressed as a function of the semi-major axis a and of the radii of apocentre and pericentre, r_{a} and r_{p}:

$$\begin{array}{rcl} r_{\mathrm{p}} & = & a(1-e) \\ r_{\mathrm{a}} & = & a(1+e) \end{array} \tag{3.6}$$

In an Earth orbit, apocentre and pericentre are called apogee and perigee.

The rate of the true anomaly can be derived from Kepler's second law, $h = \sqrt{\mu\, p} = \sqrt{\mu a(1-e^2)}$, and the specific angular momentum of the orbit, $h = \dot{\nu} r^2$. With these relations and r from Eq. (3.5), one obtains

$$\dot{\nu} = (1 + e\,\cos\,\nu)^2 \sqrt{\frac{\mu}{a^3(1-e^2)^3}} \tag{3.7}$$

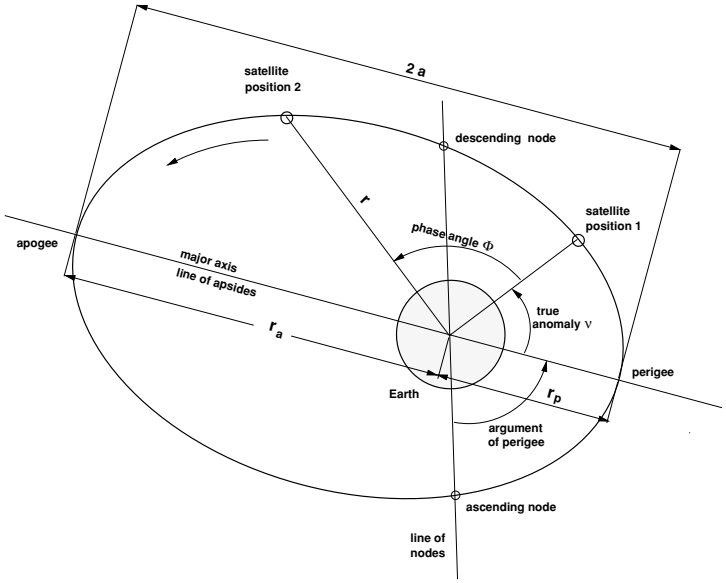

Figure 3.6. Definition of orbital elements in an Earth orbit.

The orbital period of an elliptic orbit can be derived from Eq. (3.7) by integration over one orbital revolution:

$$T = 2\pi\sqrt{\frac{a^3}{\mu}} \tag{3.8}$$

From Eq. (3.8) a mean motion n of an elliptical orbit can be defined as

$$n = \frac{2\pi}{T} = \sqrt{\frac{\mu}{a^3}} \tag{3.9}$$

From the energy conservation law, $E = \frac{V^2}{2} - \frac{\mu}{r} = -\frac{\mu}{2a}$, the velocity in the orbit direction can be derived:

$$V = \sqrt{\mu\left(\frac{2}{r} - \frac{1}{a}\right)} \tag{3.10}$$

The change of the mean phase difference between chaser and the target over time is $\Delta\Phi = (n_\mathrm{c} - n_\mathrm{t})\Delta t$. Per orbital revolution of the target, the phase advance of the chaser becomes, with Eq. (3.9),

$$\Delta\Phi = 2\pi\left(\frac{1}{T_\mathrm{c}} - \frac{1}{T_\mathrm{t}}\right)T_t = 2\pi\left(\frac{T_\mathrm{t}}{T_\mathrm{c}} - 1\right) \tag{3.11}$$

where T_t is the orbital period of the target and T_c is the period of the chaser.

Circular orbits

Most important for the application to rendezvous trajectories is the special case of the circular orbit, as practically all of the rendezvous missions are performed in near circular low Earth orbits (LEO). By setting $a = r$ and $e = 0$, the equations for the circular orbit can be obtained from the above equations for elliptic orbits as follows.

The rate of the true anomaly in a circular orbit is equal to the angular velocity of the orbit $\omega = \dot{\nu}$:

$$\omega_{\odot} = \sqrt{\frac{\mu}{r^3}} \tag{3.12}$$

The velocity in a circular orbit is

$$V_{\odot} = \sqrt{\frac{\mu}{r}} \tag{3.13}$$

and the orbital period is

$$T_{\odot} = 2\pi\sqrt{\frac{r^3}{\mu}} \tag{3.14}$$

3.2.2 Orbit corrections

The discussion of orbit corrections in this section assumes that all manoeuvres are impulsive, i.e. that they consist of an instantaneous change of velocity at the point where the manoeuvre is applied. This is a first approximation, which is convenient and sufficient to explain the effects in principle. Accurate manoeuvre calculation needs to take into account the maximum thrust level available and the necessary duration of the thrust to achieve the required ΔV.

Apogee and perigee raise manoeuvres

A tangential thrust at perigee in the direction of the orbital velocity vector will increase the semi-major axis of the orbit and thus raise the apogee. With Eq. (3.10) the ΔV required to achieve the new semi-major axis a_2 becomes

$$\Delta V_{\mathrm{p}} = V_{\mathrm{p}2} - V_{\mathrm{p}1} = \sqrt{\mu}\left(\sqrt{\frac{2}{r_{\mathrm{p}}} - \frac{1}{a_2}} - \sqrt{\frac{2}{r_{\mathrm{p}}} - \frac{1}{a_1}}\right) \tag{3.15}$$

$V_{\mathrm{p}1}$ and $V_{\mathrm{p}2}$ are the velocities at perigee before and after the manoeuvre. To raise the perigee, a corresponding tangential thrust in apogee in the direction of the orbital velocity vector must be provided:

$$\Delta V_{\mathrm{a}} = V_{\mathrm{a}2} - V_{\mathrm{a}1} = \sqrt{\mu}\left(\sqrt{\frac{2}{r_{\mathrm{a}}} - \frac{1}{a_2}} - \sqrt{\frac{2}{r_{\mathrm{a}}} - \frac{1}{a_1}}\right) \tag{3.16}$$

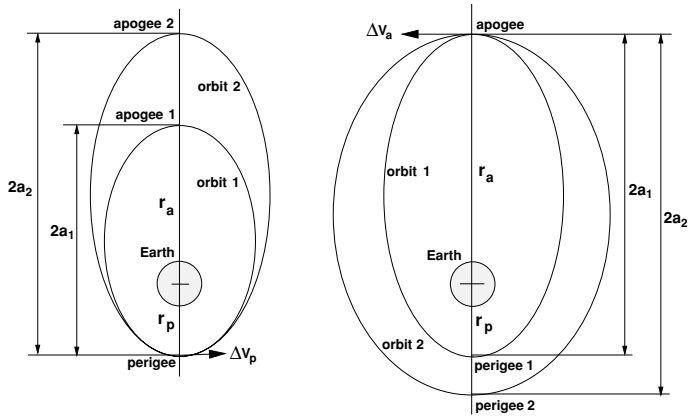

Figure 3.7. Apogee and perigee raise manoeuvres.

$V_{\mathrm{a}1}$ and $V_{\mathrm{a}2}$ are now the velocities at apogee before and after the manoeuvre. Remembering that $r_{\mathrm{p}} = a(1-e)$ and $r_{\mathrm{a}} = a(1+e)$, it can be seen that an increase of velocity at perigee will increase the eccentricity of the orbit, and an increase of velocity at apogee will decrease it.

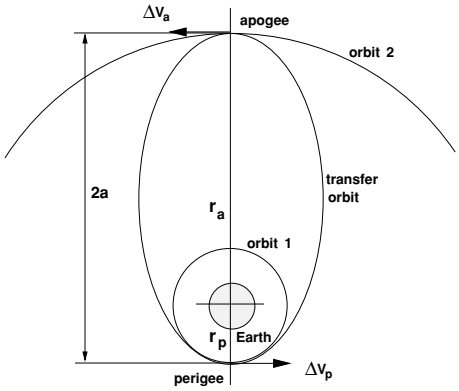

Figure 3.8. Orbit relations in a Hohmann transfer.

When starting and ending at circular orbits the combined perigee and apogee manoeuvres become the well known *Hohmann transfer* (Hohmann 1925) (figure 3.8). With Eqs. (3.10) and (3.13) one obtains

$$\Delta V_{\mathrm{p}} = \sqrt{\mu\left(\frac{2}{r_1} - \frac{1}{a}\right)} - \sqrt{\frac{\mu}{r_1}} \tag{3.17}$$

and

$$\Delta V_{\mathrm{a}} = \sqrt{\frac{\mu}{r_2}} - \sqrt{\mu\left(\frac{2}{r_2} - \frac{1}{a}\right)} \tag{3.18}$$

The semi-major axis of the transfer ellipse is

$$a = \frac{r_1 + r_2}{2} \tag{3.19}$$

Correction of inclination and RAAN errors

The plane of an orbit is given by the inclination i and the right ascension of ascending node (RAAN) Ω, as defined in figure 2.2. For a pure change of the orbital plane, the ΔV must be applied perpendicular to the plane. Any component in the orbit plane will lead to a change of eccentricity or orbit size or both. Further, since the new orbit will go through the point at which the manoeuvre has been applied, the correction ΔV must be applied at the intersection of the initial orbit with the intended one. So, for a change of inclination, the ΔV must be applied at the ascending or descending node, and for a change of RAAN it must be applied at half the arc between those nodes.

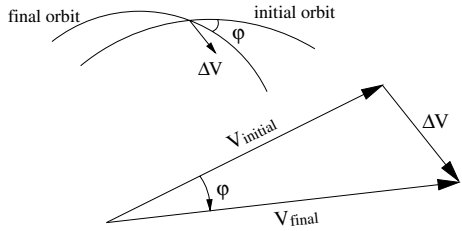

Figure 3.9. Corrections of orbital plane.

However, since pure plane change manoeuvres are relatively expensive, plane angle corrections are usually combined with in-plane transfer manoeuvres. With the cosine law one obtains

$$\Delta V = \sqrt{V_{\mathrm{i}}^2 + V_{\mathrm{f}}^2 - 2V_{\mathrm{i}}V_{\mathrm{f}}\cos\varphi} \tag{3.20}$$

where φ is the angle between the initial and the final orbit plane (see figure 3.9). The need for plane corrections arises mainly from the launch errors and from the drift of nodes due to the J_2-disturbance (see section 4.2.3).

A detailed discussion of the launch and phasing orbit manoeuvres has been provided by J. Legenne in Carrou (1995).

3.2.3 The equations of motion in the target reference frame

The equations of orbital motion discussed in section 3.2.1 are given in the orbital plane frame $\boldsymbol{F}_{\mathbf{op}}$. Equations of motion in this frame can conveniently be used for trajectory analysis until the chaser vehicle is in the close vicinity of the target. For relative navigation it becomes more convenient to keep one of the spacecraft as a fixed point. For the analysis of rendezvous trajectories, it is best to use a reference frame originating in the CoM of the target vehicle, i.e. to look at the chaser motion as an astronaut sitting in the target vehicle would. This frame is the spacecraft local orbital frame of the target, $\boldsymbol{F}_{\mathbf{lo}}$, defined in section 3.1.

For circular orbits the equations of relative motion are the Hill equations (see also appendix A):

$$\begin{aligned} \ddot{x} - 2\omega\dot{z} &= \frac{1}{m_\mathrm{c}} F_x \\ \ddot{y} + \omega^2 y &= \frac{1}{m_\mathrm{c}} F_y \\ \ddot{z} + 2\omega\dot{x} - 3\omega^2 z &= \frac{1}{m_\mathrm{c}} F_z \end{aligned} \tag{3.21}$$

In these equations $\omega = \frac{2\pi}{T}$ is the angular frequency of the circular target orbit and m_c is the mass of the chaser vehicle. The motion can be disturbed by imposed accelerations $\gamma_{x,y,z} = \frac{F_{x,y,z}}{m_\mathrm{c}}$. Eqs. (3.21) are a system of linear differential equations, which can be solved using the Laplace transformation method. For distances between chaser and target vehicles that are very small compared with the distance to the centre of the Earth, a linearised solution of the equations of relative motion has been derived from the Hill equations by W. H. Clohessy and R. S. Wiltshire (Clohessy & Wiltshire 1960).

A derivation of the Clohessy–Wiltshire equations from Eqs. (3.21) can be found in appendix A both for the homogeneous solution (no input forces) and for a particular solution, where the special case of input pulses with constant amplitudes is considered. This case is of particular interest for spacecraft applications, as practically all gas jet thrusters produce pulses of constant amplitude. Unfortunately this particular solution leads to relatively long mathematical expressions, which can be well processed by computers, but are less perceptual in the discussion of trajectory properties. For ease of discussion of the various trajectory types, it has been assumed that thrust manoeuvres are of an impulsive nature, i.e. step changes of velocity, and that longer term accelerations $\gamma_{x,y,z}$, whether resulting from thruster activities or from external disturbances, are constant over the time period considered. The constant force solution can be seen as a special case of Eqs. (A.43)–(A.47) and can be obtained by setting the start time of the pulse $t_1 = 0$ and the stop time $t_2 = t$. The resulting equations of motion for constant

input forces are

$$\begin{aligned} x(t) &= \left(\frac{4\dot{x}_0}{\omega} - 6z_0\right)\sin(\omega t) - \frac{2\dot{z}_0}{\omega}\cos(\omega t) + (6\omega z_0 - 3\dot{x}_0)t + \left(x_0 + \frac{2\dot{z}_0}{\omega}\right) + \cdots \\ &\quad + \frac{2}{\omega^2}\gamma_z(\omega t - \sin(\omega t)) + \gamma_x\left(\frac{4}{\omega^2}(1-\cos(\omega t)) - \frac{3}{2}t^2\right) \\ y(t) &= y_0\cos(\omega t) + \frac{\dot{y}_0}{\omega}\sin(\omega t) + \frac{\gamma_y}{\omega^2}(1-\cos(\omega t)) \qquad (3.22) \\ z(t) &= \left(\frac{2\dot{x}_0}{\omega} - 3z_0\right)\cos(\omega t) + \frac{\dot{z}_0}{\omega}\sin(\omega t) + \left(4z_0 - \frac{2\dot{x}_0}{\omega}\right) + \cdots \\ &\quad + \frac{2}{\omega^2}\gamma_x(\sin(\omega t) - \omega t) + \frac{\gamma_z}{\omega^2}(1-\cos(\omega t)) \end{aligned}$$

Because of the linearisation, the accuracy of the Clohessy–Wiltshire (CW) equations decreases with the distance from the origin of the coordinate-ordinate frame. In a LEO rendezvous mission, position errors will become significant at a distance of a few tens of kilometres from the origin. For example, the error in the z-direction due to the curvature of the orbit will be $\Delta z = r(1 - \cos\frac{x}{r})$, which for an orbit with $h = 400$ km, $r = 6766$ km at a distance of $x = 10$ km, becomes $\Delta z = 7.4$ m, and at a distance of $x = 30$ km becomes $\Delta z = 66.5$ m. If a curved definition of the x-coordinate were used, according to the actual circular orbit, the useful range of the CW equations can be significantly increased.

Many attempts have been made to solve the Hill equations (3.21) also for elliptical orbits (Wolfsberger 1983; Carter 1998). An elegant solution has been described in Yamanaka & Ankersen (2002), which includes the CW equations as a special case for zero eccentricity. The treatment of elliptical orbits is, however, outside the scope of this book, as practically all rendezvous missions are in circular orbit and as discussing the elliptical cases would not add anything to the basic understanding of trajectories of current rendezvous missions.

3.3 Discussion of trajectory types

The objective of this section is to describe the motion of the chaser spacecraft, and other properties of the chaser trajectory, in order to provide the basis for the discussion of trajectory safety and of approach/departure strategies in later chapters. For all trajectory discussions hereafter, the $\boldsymbol{F}_{\mathrm{lo}}$ frame of the target will be used. The trajectory elements can be grouped for the purpose of this discussion into three types:

- *Free drift trajectories*: these are trajectories evolving from a set of initial conditions for position and velocity, without application of thrust impulses or forces.
- *Impulsive manoeuvre trajectories*: these are trajectories evolving from a set of initial conditions plus an instant change of velocity, representing a boost manoeuvre.

- *Continuous thrust trajectories*: these are trajectories evolving from a set of initial conditions plus the continuous application of control forces (open loop) along the trajectory.

This grouping is somewhat arbitrary, as for the trajectory dynamics, e.g., it does not make any difference whether a certain velocity was present as an initial condition at the starting time t_0, or whether it has been applied as a step function at the time t_0. Also, boost manoeuvres are in reality not purely impulsive manoeuvres. In fact, with a limited thrust level available, thrust forces have to be applied over a certain time to achieve a certain ΔV. The grouping applied here is motivated rather by the typical questions in practical applications, where one would like to know: (a) the trajectory evolution when no impulses or forces are applied, (b) the trajectory evolution when a particular thrust manoeuvre is applied, or (c) the impulses or forces which need to be applied when certain trajectories shall be achieved.

The trajectory types discussed are intended to cover the most important types used in rendezvous approach and departure missions. However, whereas in a real mission a large part of the trajectories may be closed loop controlled and/or will be subject to external and internal disturbances, the trajectories in this section are treated as ideal open loop cases, without any disturbances. Trajectory deviations as a result of external and internal disturbances are discussed in sections 4.2 and 4.3.

For each trajectory type discussed in the following sections of this chapter,

- the assumed initial conditions,
- the equations of motion,
- the position after a fixed time (e.g. half or one orbital revolution),
- or, where applicable, the duration of a transfer to a certain position

will be derived. For free drift and impulsive manoeuvre cases, one example of a plot of each type of trajectory will be given and its characteristics discussed. Further, for impulsive and continuous force manoeuvres the required ΔV will be derived. Application examples will be given for all trajectories addressed.

Note: In general trajectory drawings the $+x$-direction (+V-bar) points to the left and the $+z$-direction (+R-bar) points downwards. This is in accordance with the convention used in the ISS scenario. For the example plots, which are produced using the $MATRIX_x$ tool, the x-direction (+V-bar) is pointing in the usual way to the right, but the z-direction (+R-bar) points upwards. The examples shown in the plots are calculated for 400 km altitude circular orbits.

3.3.1 Free drift motions

In this section, four cases will be discussed, selected because of their significance as elements of approach and departure strategies in rendezvous missions. These are

- the motion on a coplanar orbit at different altitude;
- the release from a station at a positive or negative distance in the z-direction (R-bar) from the CoM of the station;
- the release from a station at a positive or negative distance in the y-direction (H-bar) from the CoM of the station;
- the release (inhibit of control) from a forced motion along the target orbit or along the radius vector.

In all four cases no thrust manoeuvre is applied to the orbit at the initial point of the trajectory section under discussion. Except for the first one, in all cases there is, however, an instantaneous change of conditions assumed to take place at the initial trajectory point.

Relative motion on orbit with different altitude

This is the case of a chaser moving coplanar with the target in an orbit slightly lower or higher than the target orbit. The difference between the angular frequency of a chaser orbit w.r.t. the target orbit can be obtained for small differences by differentiation of Eq. (3.12):

$$\omega = \sqrt{\frac{\mu}{r^3}}$$

$$\mathrm{d}\omega = -\frac{3}{2r}\omega \mathrm{d}r \tag{3.23}$$

In the $\boldsymbol{F}_{\mathbf{lo}}$ frame of the target $\mathrm{d}z = -\mathrm{d}r$.

Further, by defining $\omega_\mathrm{t} = \omega$ of target and $\omega_\mathrm{c} = \omega$ of chaser, and replacing $\mathrm{d}\omega$ in Eq. (3.23) by $\Delta\omega = (\omega_\mathrm{t} - \omega_\mathrm{c})$, and setting $\Delta\omega r = \dot{x}$ and $\mathrm{d}z = z_\mathrm{c}$, the velocity of a chaser becomes

$$\dot{x}_\mathrm{c} = \frac{3}{2}\omega_\mathrm{t} z_\mathrm{c} \tag{3.24}$$

With this relation for a free orbit motion at a different altitude, the following initial conditions can be defined:

$$\begin{array}{rclrcl} x_0, y_0 & = & 0 & \dot{x}_0 & = & \frac{3}{2}\omega Z_0 \\ z_0 & = & Z_0 & \dot{y}_0, \dot{z}_0 & = & 0 \end{array}$$

Inserting the initial conditions into Eqs. (3.22), the equations of motion become for this case:

$$\begin{array}{rcl} x(t) & = & \frac{3}{2}\omega Z_0 t \\ y(t) & = & 0 \\ z(t) & = & Z_0 \end{array} \tag{3.25}$$

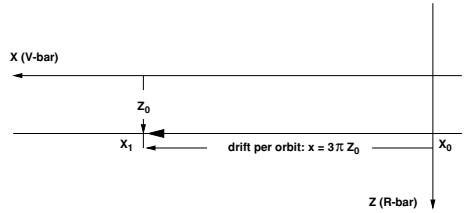

Figure 3.10. Coplanar motion at different orbital height.

After one orbital period of the target ($t = T$, $\omega t = 2\pi$) the advance of the chaser w.r.t. the target in the orbit direction is, as shown in figure 3.10:

$$X_T = 3\pi Z_0$$

This is a motion parallel to the target orbit with the relative velocity of $V_x = \frac{3}{2}\omega Z_0$. In rendezvous approach strategies, this type of trajectory can be used where a motion toward the target in the orbit direction together with a safe distance in the z-direction is required for safety reasons.

The motion due to different orbital height is de-coupled from the eccentricity and out-of-plane motions, i.e. the above result can be added to the equations of motion of all cases for $z_0 = 0$ to obtain the solution for initial conditions with a difference in altitude $z_0 = Z_0$.

Release at a distance from the station CoM in the z-direction

This is the case of a vehicle starting above or below the target orbit with the velocity of the target. Such a case can be imagined by considering a vehicle which was attached to the target structure at a distance Z_0 from the CoM and was subsequently released at time $t = t_0$. The initial conditions are then:

$$\begin{aligned} x_0, y_0 &= 0 \\ z_0 &= Z_0 \end{aligned} \qquad \dot{x}_0, \dot{y}_0, \dot{z}_0 = 0$$

Inserting the initial conditions into Eqs. (3.22), the equations of motion become for this case:

$$\begin{aligned} x(t) &= 6Z_0(\omega t - \sin(\omega t)) \\ y(t) &= 0 \\ z(t) &= Z_0(4 - 3\cos(\omega t)) \end{aligned} \tag{3.26}$$

After one orbital period of the target, the advance in orbit direction is

$$\begin{aligned} x_T &= 12\pi Z_0 \\ z_T &= Z_0 \end{aligned}$$

The cyclic motion with the orbital period T has an amplitude of $6Z_0$, i.e. starting at Z_0, arriving after $T/2$ at $7Z_0$ and returning after T to Z_0. The average z-distance of this orbit is

$$z_{\mathrm{m}} = 4z_0$$

which, inserted into Eqs. (3.25), yields the same result after one revolution, $x_T = 12\pi Z_0$, as above.

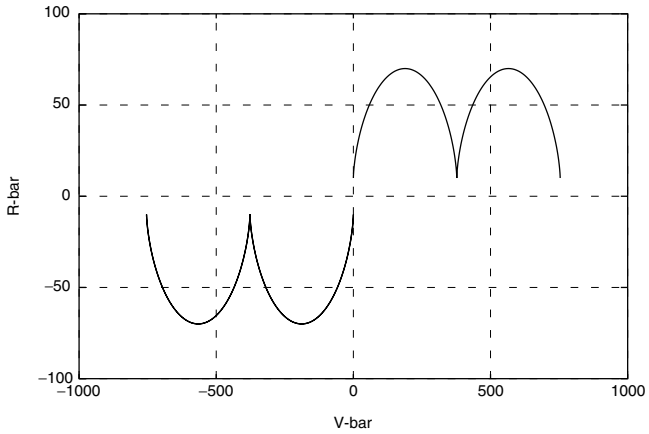

Figure 3.11. Example: trajectories after release at $Z_0 = +10$ m and $Z_0 = -10$ m.

The example shown in figure 3.11 indicates the significant effects caused by orbit dynamics for a release at small z-distances from the target orbit. Two examples are shown with a release distance of $Z_0 = +10$ m (below target CoM) and $Z_0 = -10$ m (above target CoM). After half an orbit the trajectory has reached a z-distance of 70 m, and after one orbit it has reached an x-distance of 377 m, where the trajectory starting above the target orbit $(-z)$ moves backward, and the one starting at a $+z$-position moves forward w.r.t. the target.

This result is very interesting for departure operations because of the significant advance in the x-direction. An application example for this trajectory case is the undocking of a vehicle from a port above or below the target orbit, or the release by a manipulator arm, at a distance in the $\pm z$-direction from the CoM of the station.

Release at a distance from the station CoM in the *y*-direction

This is the case of a vehicle moving at an out-of-plane distance to the target orbit with the velocity of the target. Again, such a case can be imagined by consideration of a vehicle which was attached to the target structure at a distance Y_0 from the CoM and

was released at time $t = t_0$. The initial conditions for the simplest case are:

$$\begin{aligned} x_0, z_0 &= 0 \\ y_0 &= Y_0 \end{aligned} \qquad \dot{x}_0, \dot{y_0}, \dot{z_0} = 0$$

Inserting the initial conditions into Eqs. (3.22), the equations of motion are

$$\begin{aligned} x(t) &= 0 \\ y(t) &= Y_0 \cos(\omega t) \\ z(t) &= 0 \end{aligned} \tag{3.27}$$

The result is the expected pure sinusoidal motion starting with Y_0. As this motion is de-coupled from the in-plane motions, this result can be superimposed to all in-plane cases.

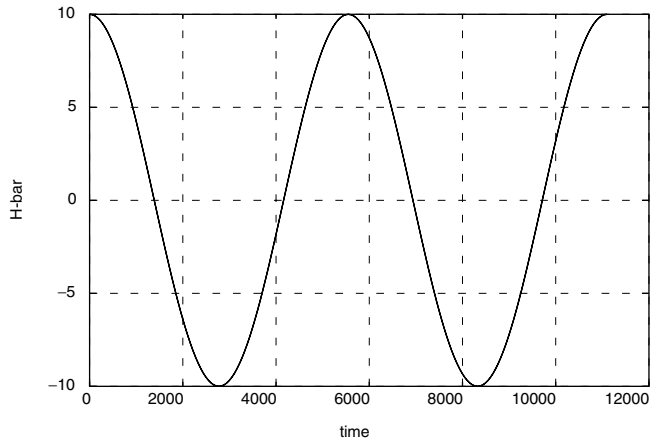

Figure 3.12. Example: motion over time after release at an out-of-plane distance of $Y_0 = 10$ m.

The example in figure 3.12 depicts the motion of a body after the release at a y-distance of $Y_0 = 10$ m from the target orbit (target CoM). If there are no obstacles, the body will pass the target orbit after a quarter orbit with a velocity of $\dot{y} = -Y_0 \cdot \omega = -0.0138$ m/s. After half an orbit it will reach the opposite extreme position of $y = -10$ m and after one orbit it will return to the initial position.

Again, this could be the case of a release by a manipulator arm of a departing vehicle at an out-of-plane distance Y_0 from the CoM of a space station. As a body to be released under these conditions tends to move along the y-axis toward the CoM of the vehicle, from where it is released, the above initial conditions would of course be meaningful only if the manipulator can easily establish the necessary distances X_0 or Z_0 to break free from the structure of the station.

Release from a forced motion along the target orbit (V-bar) or along the radius vector (R-bar)

These 'releases' are, e.g., the cases of thrust inhibit during forced motion straight line approaches on V-bar or R-bar (treated in section 3.3.3). When the continuous thrust necessary to implement the straight line trajectory is stopped at a certain point, the vehicle continues to move on V-bar, or on R-bar, respectively, with a velocity that is different from that belonging to a circular orbit of this altitude. As a result the Coriolis forces will move the vehicle away from the approach line, i.e. from the x-axis in the case of a V-bar approach, and from the z-axis in the case of an R-bar approach. Examples of such release trajectories are shown in figure 3.13 for V-bar and in figure 3.14 for R-bar.

Since there is no difference for the evolution of the trajectory whether a velocity is applied as a ΔV at the starting time t_0, or is present as an initial condition, the equations of motion are the same as those for impulsive manoeuvres, i.e. Eqs. (3.28) for the V-bar approach case and Eqs. (3.34) for the R-bar approach case given in section 3.3.2. In the case of a release at an initial z-position different from $Z_0 = 0$, the motion due to a different altitude, see Eqs. (3.25), has to be added.

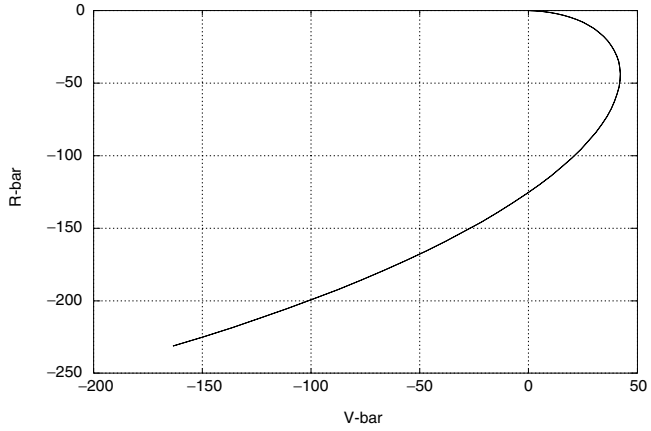

Figure 3.13. Example: release on V-bar with $V_x = +0.1$ m/s.

The example in figure 3.13 shows the free drift after thrust inhibit during a straight line approach along V-bar with a velocity of $\dot{x} = +0.1$ m/s. The resulting drift trajectory continues first to move forward, but at the same time it starts to move upward ($-z$-direction $= -$R-bar) and eventually backward ($-x$-direction $= -$V-bar). With the assumed initial velocity, it will touch again the target orbit after one orbital revolution at a distance of $x_T = -1656$ m. The maximum travel in the positive x-direction would be of the order of 45 m. The trajectory type is identical to the one shown in figures 3.15 and 3.17. The use of this type of trajectory to achieve passive trajectory safety w.r.t. collision is discussed in section 4.4.2 and is shown in figure 4.14.

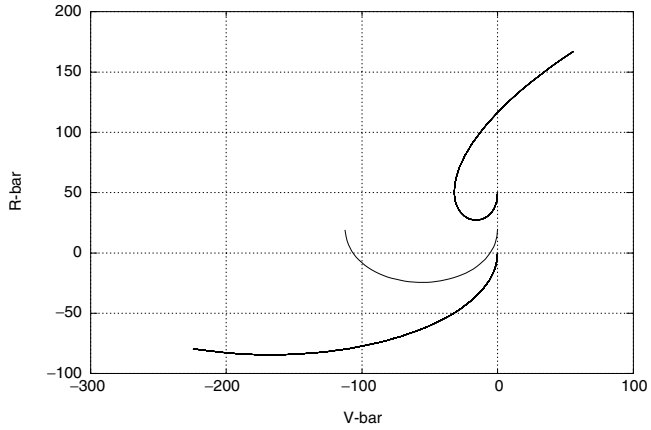

Figure 3.14. Example: release on R-bar with $V_z = -0.1$ m/s at $Z_0 = 0$, 20 m and 50 m.

Figure 3.14 shows three examples of drift trajectories after thrust inhibit during a straight line R-bar approach with a velocity of $\dot{z} = -0.1$ m/s. The difference between the three trajectories is the z-position at which thrust control is inhibited. For a release at $Z_0 = 0$ the trajectory is identical to the type described in figures 3.20 and 3.21. For the releases at $Z_0 = 20$ m and $Z_0 = 50$ m, the trajectory is a combination of the types shown in figure 3.11 (release at a z-distance) and figure 3.20 (impulse in z-direction), i.e. an addition of Eqs. (3.26) and (3.34). Whereas the trajectory in the case of a release at $Z_0 = 0$ will return after one orbital revolution to its starting point, in the other two cases with $Z_0 \neq 0$ a looping motion is initiated, which will result after one revolution in an x-distance from the release point. This behaviour can again be exploited for passive trajectory protection against collision (see section 4.4.2).

3.3.2 Impulsive manoeuvres

Thrust manoeuvres, to a first approximation, can be treated as impulses, i.e. as instantaneous changes of velocity at the time of manoeuvre. The acceleration terms of the CW equations can, therefore, be set to zero. In reality, due to limitations of thrust level available, such ideal impulsive manoeuvres do not exist and constant thrust forces have to be applied over a particular time to realise the manoeuvre (see section 3.3.3). The ideal case of a pure impulse allows us, however, to calculate manoeuvres easily, analyse manoeuvre strategies and assess the minimum ΔV required. As mentioned above, with the assumption of pure impulses, the equations of motion for impulsive manoeuvres are identical to the ones for the cases of 'release to free drift', where the initial velocity is different from that belonging to a circular orbit at the point of release.

Within this section the cases of impulsive manoeuvres with ΔV values in orbital and in radial directions will be discussed. Examples will be shown of how a combination of

such manoeuvres can be applied in advance in an orbital direction to change the orbital height and to fly around a particular point in orbit, e.g. a target station. For each of the applications, the required ΔV and duration will be indicated and the particular advantages or disadvantages discussed.

ΔV in an orbital direction

Thrust manoeuvres with a ΔV in a $\pm\, x$-direction (tangential manoeuvres) are used for transfers along the target orbit, for transfers to an orbit of a different height and for fly-arounds, e.g. from V-bar to a point where an R-bar approach can commence.

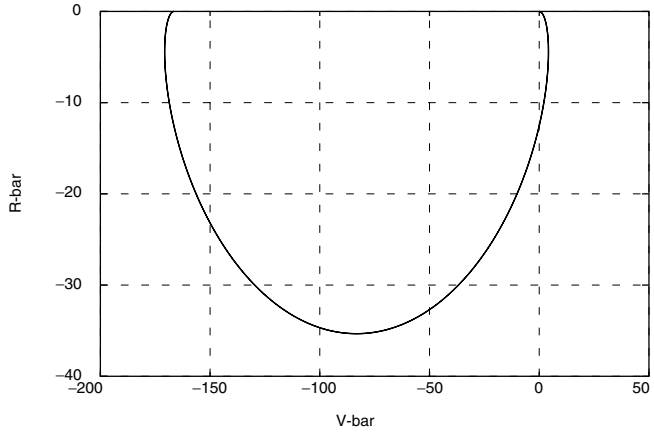

Figure 3.15. Example: impulse of $\Delta V_x = 0.01$ m/s, starting at $x = 0$, $z = 0$.

The simplest case is presented here, i.e. the manoeuvre takes place on the target orbit at the position of the target station $\boldsymbol{O_{lo}}$. The initial conditions are then:

$$x_0, y_0, z_0 = 0 \qquad \begin{aligned} \dot{x}_0 &= \Delta V_x \\ \dot{y}_0, \dot{z}_0 &= 0 \end{aligned}$$

Inserting the initial conditions into Eqs. (3.22), the equations of motion after a ΔV_x manoeuvre become:

$$\begin{aligned} x(t) &= \frac{1}{\omega}\Delta V_x(4\sin(\omega t) - 3\omega t) \\ y(t) &= 0 \\ z(t) &= \frac{2}{\omega}\Delta V_x(\cos(\omega t) - 1) \end{aligned} \tag{3.28}$$

Figure 3.15 shows an example of a trajectory after a tangential impulse in an orbit direction of $V_x = +0.01$ m/s, starting at $x = 0$, $z = 0$. The example indicates the

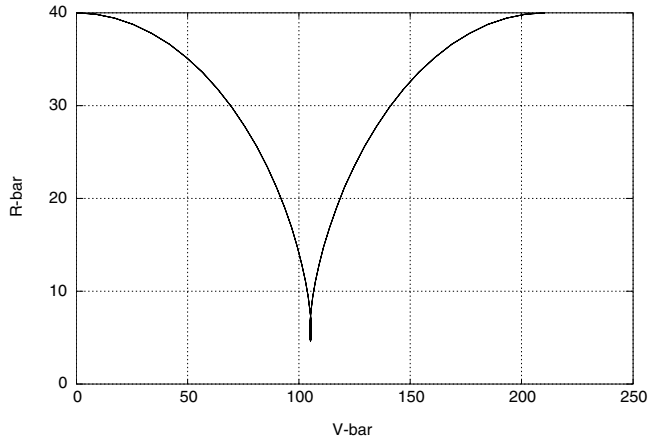

Figure 3.16. Example: impulse of $\Delta V_x = 0.01$ m/s, starting 40 m below target orbit.

sensitivity of the trajectory to velocity changes in orbit direction. A relatively small ΔV results in significant displacements, i.e. after half an orbital revolution more than 35 m in a $-z$-direction (above the initial orbit) and after one revolution more than 170 m in the $-x$-direction (behind the initial position).

ΔV_x on a higher or lower orbit than the target orbit The simple initial conditions which are used for Eqs. (3.28), i.e. all positions and all velocities (except for the applied ΔV) are zero, are of course not given in most cases of interest. For a position $x \neq 0$ the result is trivial, as in the CW equation for $x(t)$, Eqs. (3.22); the initial position x_0 is a constant, which will be added to each point of the motion, but has no further impact on the trajectory evolution. In contrast, for an initial position $z_0 \neq 0$, the additional relative velocity in the x-direction due to a different orbital altitude has to be taken into account. This motion is, however, independent from the other motions, as we have seen already in section 3.3.1. The initial conditions and equations of motion for the ΔV_x manoeuvre on a circular orbit of different altitude can therefore be obtained by adding to Eqs. (3.28) for the impulsive manoeuvre the equations for motion (3.25) at a different altitude. Figure 3.16 shows an example of how initial, non-zero, x- and z-positions influence the trajectory evolution.

The tangential impulse of $\Delta V_x = +1$ cm/s in the example of figure 3.16 is applied on an orbit that is $z = 40$ m below the target orbit. The result shows that the forward motion in the x-direction due to the z-distance of 40 m is predominant. In contrast to the example given in figure 3.15 for the same ΔV_x, the motion is now in the $+x$-direction, whereas the maximum displacement in the $-z$-direction is the same as in the previous case.

Applications of tangential thrust manoeuvres

Tangential impulse transfer along V-bar The principle of a transfer along V-bar by tangential thrusts is shown in figure 3.17. Starting at a point x_1 with a ΔV_{x1}, after one

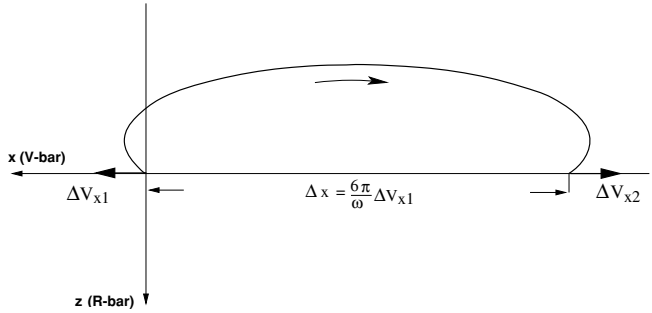

Figure 3.17. Transfer along V-bar by tangential impulses.

orbital period of the target, i.e. at $t = T$ and $\omega t = 2\pi$, the trajectory, Eqs. (3.28), has reached

$$\begin{aligned} x_T &= x_1 + \Delta x = x_1 - \frac{6\pi}{\omega}\Delta V_{x1} \\ z_T &= z_1 = 0 \end{aligned} \tag{3.29}$$

The required ΔV is accordingly

$$\Delta V_{x1} = -\frac{\omega}{6\pi}\Delta x \tag{3.30}$$

To come to a rest at the new position x_T on the target orbit, a stop impulse of the same size but in the opposite direction, $\Delta V_{x2} = -\Delta V_{x1}$, must be applied. The magnitude of the required ΔV in both cases is

$$|\Delta V_{x1}| = |\Delta V_{x2}| = \frac{\omega}{6\pi}\Delta x$$

The total ΔV expenditure for such a two-pulse manoeuvre is

$$\Delta V_{\text{total}} = \frac{\omega}{3\pi}\ \Delta x$$

Transfer to an orbit of different altitude To transfer a vehicle to an orbit of different altitude (see figure 3.18), the elliptical motion has to be stopped after half an orbital period, i.e. at $t = T/2$ and $\omega t = \pi$. Starting at x_1, z_1 with ΔV_{x1}, the trajectory,

Eqs. (3.28), has reached, after $t = T/2$, the maximum amplitude in z:

$$\begin{aligned} x_{T/2} &= x_1 + \Delta x = x_1 - \frac{3\pi}{\omega}\Delta V_{x1} \\ z_{T/2} &= z_1 + \Delta z = z_1 - \frac{4}{\omega}\Delta V_{x1} \end{aligned} \tag{3.31}$$

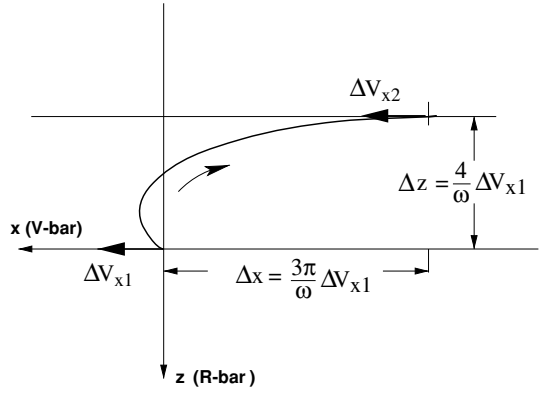

Figure 3.18. Transfer to orbit of different height (Hohmann transfer).

By the first impulse the new orbit becomes eccentric. To circularise it again at the altitude of $z_{T/2}$, an impulse of the same size and in the same direction must be applied (this is true only within the limitations of validity of the CW equations; for large differences in altitude, see Eqs. (3.17) and (3.18)). This manoeuvre is the well known *Hohmann transfer* already mentioned in section 3.2.2. Of interest for the design of trajectory strategies and operations is the fixed relation between the change of position in the z- and x-directions:

$$\Delta x = \frac{3\pi}{4}\Delta z$$

With $\Delta z = z_2 - z_1$, the magnitude of the required ΔV in both cases results from Eqs. (3.31):

$$\Delta V_{x1} = \Delta V_{x2} = \frac{\omega}{4}\Delta z \tag{3.32}$$

The total ΔV required for such a two-pulse manoeuvre is

$$\Delta V_{\text{total}} = \frac{\omega}{2}\,\Delta z$$

Tangential impulse fly-around manoeuvre For a fly-around to an R-bar approach (see figure 3.19), the same manoeuvres have to be applied as for the transfer to a different altitude. In order to arrive at the docking axis ($x = 0$) without a velocity in the z-

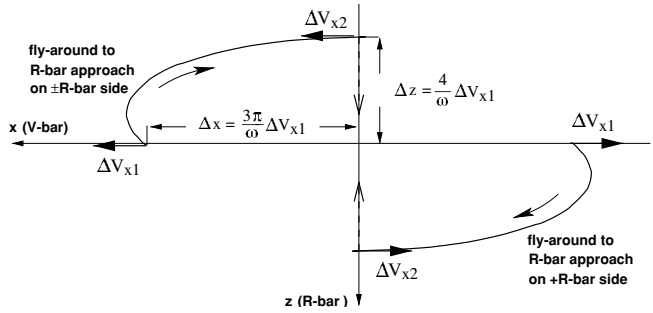

Figure 3.19. Fly-around by tangential impulse

direction ($V_z = 0$), the first pulse has to be given at a position $x_1 = \pm\frac{3\pi}{\omega}\Delta V_x$ on V-bar and the second one at $x_2 = 0$ (see figure 3.19). After a second impulse ΔV_{x2}, which would just achieve circularisation, as in a Hohmann transfer, the vehicle would move with a velocity V_x belonging to an orbit of that particular altitude. For a straight line R-bar approach the velocity V_x must, however, be the same as that of the target station all along the trajectory. The difference between the velocity at the end of the Hohmann transfer and the target orbit is, according to Eq. (3.24), $\dot{x} = \frac{3}{2}\omega\Delta Z$. This is the amount that has to be added to the second impulse. With Eq. (3.32) the ΔV for the second pulse of a fly-around manoeuvre becomes

$$\begin{aligned} \Delta V_{x2} &= \frac{\omega}{4}\Delta z + \frac{3\omega}{2}\Delta z \\ &= \frac{7\omega}{4}\Delta z \end{aligned} \tag{3.33}$$

Together with, or immediately after, the second fly-around impulse, the R-bar approach manoeuvre or a station keeping manoeuvre (see section 3.3.3) has to be initiated. Otherwise the vehicle will start the motion shown in figure 3.11.

ΔV in a radial direction

Thrust manoeuvres with a ΔV in $\pm z$-direction (radial manoeuvres) can be used, similar to the tangential manoeuvres, for transfer along the target orbit and for fly-around to an R-bar approach. A particular property of radial manoeuvres is that they affect only the eccentricity, not the orbital period, and thus cause no drift w.r.t. the target orbit. The differences in transfer distances and ΔV cost are given below in the discussion of equivalent cases.

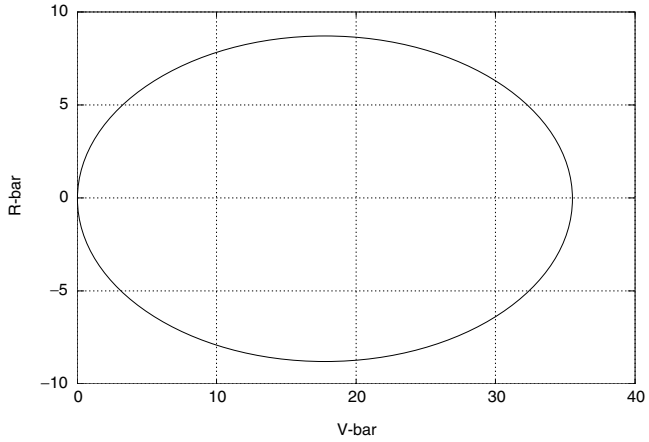

Figure 3.20. Example: impulse of $\Delta V_{z0} = 0.01$ m/s, starting on target orbit at $x = 0$.

For the simplest case of a manoeuvre starting in $\boldsymbol{O}_{\mathbf{lo}}$ the initial conditions are:

$$x_0, y_0, z_0 = 0 \qquad \begin{aligned} \dot{x}_0, \dot{y}_0 &= 0 \\ \dot{z}_0 &= \Delta V_z \end{aligned}$$

Inserting the initial conditions into Eqs. (3.22), the equations of motion become

$$\begin{aligned} x(t) &= \frac{2}{\omega}\Delta V_z(1 - \cos(\omega t)) \\ y(t) &= 0 \\ z(t) &= \frac{1}{\omega}\Delta V_z \sin(\omega t) \end{aligned} \tag{3.34}$$

In the $\boldsymbol{F}_{\mathbf{lo}}$ frame this trajectory is an ellipse, i.e. it returns to its starting point after each orbital revolution. After half an orbital period, i.e. at $t = T/2$ and $\omega t = \pi$, the trajectory, Eqs. (3.34), has reached its maximum amplitude in x:

$$\begin{aligned} x_{T/2} &= \frac{4}{\omega}\Delta V_z \\ z_{T/2} &= 0 \end{aligned} \tag{3.35}$$

The maximum amplitude in z has been reached after $t = T/4$:

$$z_{T/4} = \frac{1}{\omega}\Delta V_z \tag{3.36}$$

The example in figure 3.20 shows the behaviour described in Eqs. (3.34)–(3.36) for a small impulse in the z-direction of $\Delta V = +1$ cm/s, starting at an initial position of

$x = 0$, $z = 0$. In the first half of an orbital revolution, the trajectory moves in the $+z$-direction (below the initial orbit) and in the $+x$-direction; in the second half it moves in the opposite directions. The ratio of the maximum excursions in the x- and z-directions is $2 : 1$, as can be seen immediately from Eqs. (3.34). In comparison with figure 3.15 this example shows that the displacements due to a radial ΔV are much smaller than those due to a tangential ΔV of the same size, i.e. a factor of $\frac{2}{3\pi}$ (i.e. 35 m instead of 170 m) for the displacements in the x-direction and a factor of $\frac{1}{4}$ (i.e. 9 m instead of 35 m) for the ones in the z-direction.

Applications of radial thrust manoeuvres

Radial impulse transfer along V-bar Figure 3.21 shows the application of ΔVs in a radial direction as another possibility for a transfer to a different position on the target orbit. Starting at x_1, the transfer time to x_2 is half an orbital period $\left(\frac{T}{2}\right)$. To stop the motion at x_2, an impulse of the same size and direction, $\Delta V_{z1} = \Delta V_{z2}$, must be applied. With Eq. (3.35) and $\Delta x = x_2 - x_1$ the required ΔV in both cases becomes

$$\Delta V_{z1} = \Delta V_{z2} = \frac{\omega}{4}\Delta x \tag{3.37}$$

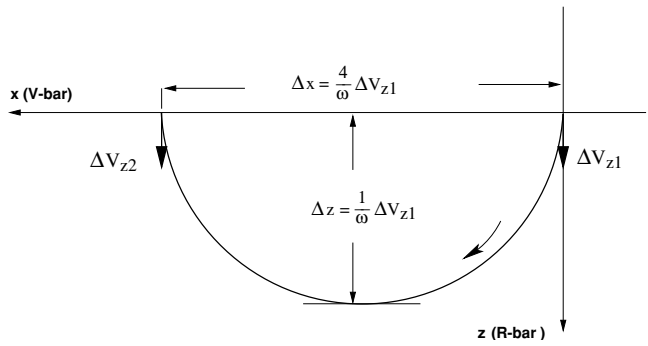

Figure 3.21. Transfer along V-bar by radial impulses.

The total ΔV required for such a two-pulse manoeuvre is

$$\Delta V_{\text{total}} = \frac{\omega}{2}\Delta x$$

In comparison with the transfer along V-bar by impulses in the orbit direction, the transfer by radial impulses is significantly more costly, i.e. by a factor of $\frac{3\pi}{2}$. Nevertheless, this transfer may be of interest because of safety and operational reasons (see chapters 4 and 5). One of the interesting features of this type of manoeuvre is the fact that, without the second impulse, the trajectory returns, if there are no disturbances, after one orbital revolution to its starting point. This allows, in the case of non-execution of the second boost, the repetition of the transfer trajectory without extra ΔV cost.

Radial impulse fly-around manoeuvre For a fly-around manoeuvre to an R-bar approach (see figure 3.22), the velocity component in the z-direction must be zero at arrival at the approach axis, i.e. the maximum amplitude $\Delta z = \frac{1}{\omega}\Delta V_{z1}$ of the trajectory (see Eq. (3.36)) must be reached at the beginning of an R-bar approach corridor at $x_2 = 0$. For a $\pm$ R-bar approach, the first pulse ΔV_{z1} must then be applied at a position $x_1 = \pm\frac{2}{\omega}\Delta V_z$ on V-bar and the motion, Eqs. (3.34), has to be stopped at $x_2 = 0, t = \frac{T}{4}, \omega t = \pi/2$. The impulse necessary to stop the motion in the $\pm x$-direction is

$$|\Delta V_x| = 2|\Delta V_{z1}| \tag{3.38}$$

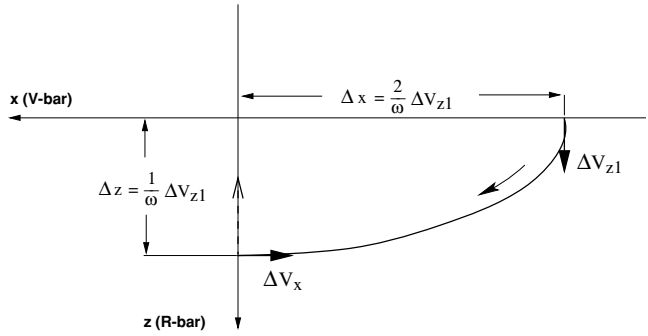

Figure 3.22. Fly-around by radial impulse.

The total ΔV required for such a fly-around manoeuvre is, with Eqs. (3.36) and (3.38),

$$\begin{aligned} \Delta V_{\text{total}} &= |\Delta V_{z1}| + |\Delta V_x| \\ \Delta V_{\text{total}} &= 3\Delta V_{z1} \end{aligned} \tag{3.39}$$

As in the case of the ΔV_x fly-around, together with, or immediately after, the second fly-around impulse of the ΔV_z fly-around, the R-bar approach manoeuvre or a station keeping manoeuvre (see section 3.3.3) has to be initiated. Otherwise the vehicle will start to describe the motion shown in figure 3.11.

ΔV in out-of-plane direction, orbit plane corrections

For the simplest case of a manoeuvre in O_{lo} the initial conditions are

$$x_0, y_0, z_0 = 0 \qquad \begin{aligned} \dot{x}_0, \dot{z}_0 &= 0 \\ \dot{y}_0 &= \Delta V_y \end{aligned}$$

Inserting these initial conditions into Eqs. (3.22), the equations of motion become

$$\begin{aligned} x(t) &= 0 \\ y(t) &= \frac{1}{\omega}\Delta V_y \sin(\omega t) \\ z(t) &= 0 \end{aligned} \tag{3.40}$$

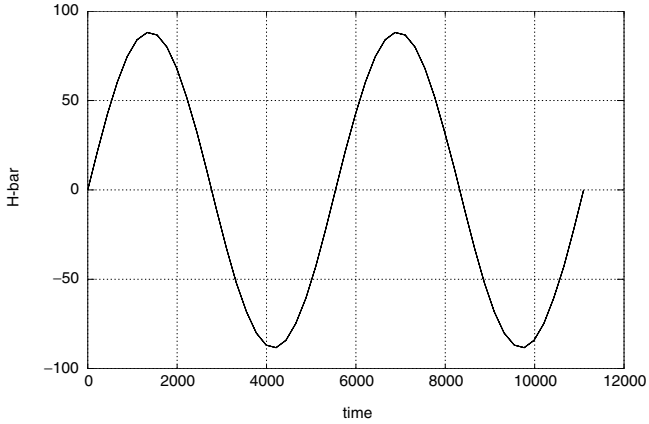

Figure 3.23. Impulse of $\Delta V_y = 0.1$ m/s, starting on target orbit.

The result is a pure sinusoidal motion starting with $y_0 = 0$. An example is shown in figure 3.23. The displacement in the y-direction is, for the same impulse, the same as the z-displacement for a radial impulse, shown in figure 3.20. The out-of-plane impulse does not cause displacements in other directions. As this motion is de-coupled from the in-plane motions, Eqs. (3.40) can be added to all in-plane cases.

Corrections of lateral motions can be performed, as has been shown in section 3.2.2, most efficiently at the intersection with the target orbit, i.e. when $y = 0$. In the rendezvous phase, when navigation is performed relative to the target in the $\boldsymbol{F}_{\mathbf{lo}}$ frame, there is no need to decompose the out-of-plane motion into inclination and RAAN components (which are used in the $\boldsymbol{F}_{\mathbf{eq}}$ frame to describe the orbit plane).

Impulsive transfer between arbitrary points (Lambert transfer)

In the previous sections, trajectory changes or transfers in one of the main directions of the local orbital frame have been discussed. Whereas out-of-plane manoeuvres are de-coupled from the two other axes, tangential and radial manoeuvres both produce trajectories with excursions in the x- and z-directions. The excursions have, however, different phasing over the orbital period, as we have seen in the previous sections. As a result, a combination of impulses in tangential and radial directions can be used if there

is a direct transfer between arbitrary points in the orbital plane. This type of transfer is known as a 'Lambert transfer'. The shape of the transfer trajectory depends not only on the x- and z-coordinates of the start and end points, but also on the time within which the transfer has to be performed. The required ΔVs in the x- and z-directions for the initial impulse to be applied at the position x_0, z_0 can be obtained by solving the CW equations (3.22) for $\dot{x}_0$ and $\dot{z}_0$:

$$\begin{aligned}\dot{x}_0 &= \frac{-\omega\sin(\omega t)(x-x_0)+\omega[6\omega t\sin(\omega t)-14(1-\cos(\omega t))]z_0+2\omega(1-\cos(\omega t))z}{3\omega t\sin(\omega t)-8(1-\cos(\omega t))}\\ \dot{z}_0 &= \frac{\omega[2(x_0-x)(1-\cos(\omega t))+(4sin(\omega t)-3\omega t\cos(\omega t))z_0+(3\omega t-4sin(\omega t))z]}{3\omega t\sin(\omega t)-8(1-\cos(\omega t))}\end{aligned} \tag{3.41}$$

by setting the chosen transfer time $t = t_1$, and by defining the initial velocities as

$$\begin{aligned}\dot{x}_0 &= V_{x0}+\Delta V_{x0}\\ \dot{z}_0 &= V_{z0}+\Delta V_{z0}\end{aligned}$$

V_{x0} and V_{z0} are the existing velocities prior to the application of the transfer impulses ΔV_{x0} and ΔV_{z0}.

The velocities at the final position x_1, z_1 can be obtained by differentiation of the CW equations (3.22), resulting in

$$\begin{aligned}\dot{x}(t_1) &= (4\dot{x}_0-6z_0\omega)\cos(\omega t_1)+2\dot{z}_0\sin(\omega t_1)+6z_0\omega-3\dot{x}_0\\ \dot{z}(t_1) &= (3z_0\omega-2\dot{x}_0)\sin(\omega t_1)+\dot{z}_0\cos(\omega t_1)\end{aligned} \tag{3.42}$$

and by inserting the chosen transfer time t_1 and the values found for $\dot{x}_0$ and $\dot{z}_0$ from Eqs. (3.41). The ΔVs for the second impulse at the position x_1, z_1 depend on the final velocity to be achieved. If the final condition is to be a point on a circular orbit, the final velocity in the local orbital frame of the target is given by Eq. (3.24). The ΔVs to be applied are

$$\begin{aligned}\Delta V_{x1} &= \frac{3}{2}\omega z_1-\dot{x}(t_1)\\ \Delta V_{z1} &= -\dot{z}(t_1)\end{aligned} \tag{3.43}$$

The evolution of the trajectory between the first and second ΔV can be calculated by inserting the assumed values for x_0, z_0 and the values calculated from Eqs. (3.41) for $\dot{x}_0$, $\dot{z}_0$ into the CW equations (3.22).

3.3.3 Continuous thrust manoeuvres

In this section a number of trajectories or manoeuvres will be addressed which, in contrast to all previous cases, need the application of continuous thrust forces in order to achieve a certain shape of trajectory or to keep a position. The following types of trajectories will be discussed:

- straight line trajectories on V-bar and R-bar;
- station keeping on different altitude and on out-of-plane distance w.r.t. the target;
- transfer by continuous thrust of limited level to a different altitude or to a different position along the target orbit;
- circular fly-around.

Whereas this is not an exhaustive list of trajectories with continuous thrust, the intention of this section is to address examples of the most important types of forced motion trajectories and to indicate how the equations for such cases can be derived.

Applications of straight line approach trajectories

Straight line trajectories are of interest for the final approach to the docking port or berthing position at the target station. With a straight line trajectory, lateral position errors in- and out-of-plane can easily be controlled w.r.t. the line of sight of a sensor. Also, monitoring of a straight line trajectory by human operators using direct eye sight or cameras will be easier than for a curved trajectory. Two general cases will be discussed for each approach direction: the special case of an approach with constant velocity and the general case of approaches with a pre-determined velocity profile. In real applications, straight line trajectories will always be closed loop controlled. The open loop solutions for simple trajectory and ΔV calculations are given below for the V-bar approach and in the subsequent section for the R-bar approach.

Straight line V-bar approach

Straight line V-bar approach with constant velocity This is the type of trajectory where a constant velocity of V_x w.r.t. the target is to be achieved between x_0 and x_1, with the velocities in the other directions kept zero. In the easiest case the motion is started with an impulse ΔV_{x1}, which produces the velocity in the x-direction V_x, and is stopped with an impulse of the same magnitude but in the opposite direction ΔV_{x2} (figure 3.24).

The initial conditions for the simplest case of a trajectory starting in x_0 are

$$\begin{array}{rrcll} x_0 = X_0 & \dot{x}_0 & = & \Delta V_{x1} & \\ y_0, z_0 = 0 & \dot{y}_0, \dot{z}_0 & = & 0 & \gamma_x, \gamma_y = 0 \end{array}$$

The equation of motion for $x(t) \in [x_0;\, x_1]$

$$x(t) = X_0 + V_x \cdot t \tag{3.44}$$

The force per mass unit γ_z that must be applied can be obtained from the Hill equations (3.21) by inserting the above assumed initial conditions:

$$\gamma_z = 2\omega V_x \tag{3.45}$$

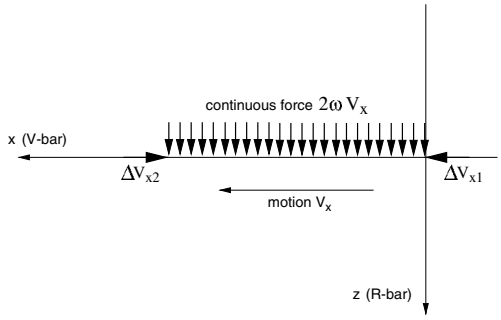

Figure 3.24. Straight line V-bar trajectory ($X_0 = 0$).

The total ΔV required for the transfer from x_0 to x_1 is

$$\Delta V_{\text{total}} = |\Delta V_x|_1 + |\gamma_z \Delta t| + |\Delta V_x|_2$$

The duration of the transfer is, with $\Delta x = x_1 - x_0$,

$$\Delta t = t_1 - t_0 = \frac{\Delta x}{V_x}$$

In reality, ΔV_{x1} and ΔV_{x2} will also be manoeuvres with a finite thrust and thrust duration, so that there will be a velocity profile (see the following section).

Straight line V-bar approach with velocity profile Assuming the initial conditions are the same as in the case above for constant velocity, the relations for a given velocity profile $V_x(t)$ are:

- The equation of motion for $x(t) \in [x_0;\, x_1]$

$$x(t) = x_0 + \int V_x(t) dt \tag{3.46}$$

- The force per unit of mass to be applied to keep the trajectory on the target orbit

$$\gamma_z(t) = 2\omega V_x(t) \tag{3.47}$$

- The total ΔV expenditure for the implementation of the velocity profile $V_x(t)$

$$\Delta V_{\text{total}} = \int_{t_0}^{t_1} \gamma_z(t) dt \tag{3.48}$$

Once the velocity profile $V(t)$ is defined, the equation of motion, the forces to be applied and the ΔV required can be calculated from the above equations.

Straight line R-bar approach

The special case of a constant velocity profile and the general case of a profile with changing velocity over time will be discussed.

Straight line R-bar approach with constant velocity At first, the velocity is assumed to be $V_z = \text{constant}$ between z_0 and z_1. Considering again the simplest case: the motion is started at z_0, t_0 with an impulse ΔV_{z1}, which produces the velocity in the z-direction V_{z1}, and is stopped at x_1, t_1 with an impulse ΔV_{z2} of the same magnitude but in the opposite direction (figure 3.25).

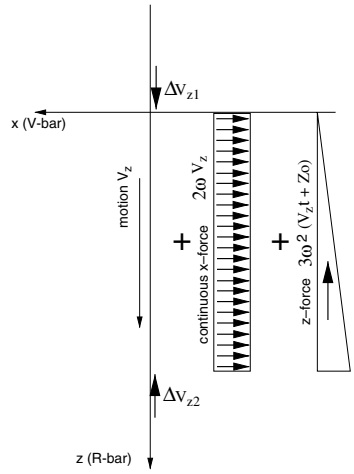

Figure 3.25. Straight line R-bar trajectory ($Z_0 = 0$).

The initial conditions for a trajectory starting in z_0 are

$$\begin{array}{rclrcl} x_0, y_0 & = & 0 & \dot{x_0}, \dot{y_0} & = & 0 \\ z_0 & = & Z_0 & \dot{z_0} & = & \Delta V_z \end{array} \qquad \gamma_y = 0$$

The equation of motion for $z(t) \in [z_0;\ z_1]$ is

$$z(t) = Z_0 + V_z \cdot t \tag{3.49}$$

The forces per unit of mass, γ_x and γ_z, which must be applied to counteract the orbital forces, can be obtained from the Hill equations (3.21) by inserting the above assumed initial conditions:

$$\begin{array}{rcl} \gamma_x & = & -2\omega V_z \\ \gamma_z & = & -3\omega^2 (V_z t + Z_0) \end{array} \tag{3.50}$$

The profiles for γ_x and γ_z are shown in figure 3.25. The total ΔV required for the transfer $z_0 - z_1$ is

$$\Delta V_{\text{total}} = |\Delta V_z|_1 + |\gamma_x \Delta t| + |\gamma_z \Delta t| + |\Delta V_z|_2$$

The duration of the transfer is, with $\Delta z = z_1 - z_0$,

$$\Delta t = t_1 - t_0 = \frac{\Delta z}{V_z}$$

Straight line R-bar approach with velocity profile Assuming the initial conditions are the same as in the case for constant velocity, the relations for a given velocity profile $V_z(t)$ are:

- the equation of motion for $z(t) \in [z_0; z_1]$

$$z(t) = z_0 + \int V_z(t) dt \tag{3.51}$$

- the forces per unit of mass to be applied to keep the trajectory on the target orbit

$$\begin{aligned} \gamma_x(t) &= -2\omega V_z(t) \\ \gamma_z(t) &= -3\omega^2 (V_z(t)t + Z_0) \end{aligned} \tag{3.52}$$

- the total ΔV expenditure for the implementation of the given velocity profile $V_z(t)$

$$\Delta V_{\text{total}} = |\int_{t_0}^{t_1} \gamma_x(t) dt| + |\int_{t_0}^{t_1} \gamma_z(t) dt| \tag{3.53}$$

As in the case for the straight line V-bar approach, once the velocity profile $V(t)$ is defined, the equation of motion, the forces to be applied and the ΔV required can be calculated from the above equations.

Station keeping on a position outside the target orbit

The attempted ideal conditions for station keeping are a fixed position w.r.t. the target and zero motion in any direction. For a position on the target orbit no control forces need to be applied. The cases to be discussed here are positions either at a different orbital height or at an out-of-plane distance. Station keeping elements of a trajectory sequence are usually closed loop controlled, as small errors in the assumed initial position and in the forces to be applied will lead to significant drift motions (see chapter 4). For this reason open loop station keeping manoeuvres can be applied only for short duration and at sufficient distance from the target station.

Station keeping below or above the target orbit The following initial conditions are assumed:

$$\begin{array}{rcl} x_0, y_0 & = & 0 \qquad \dot{x_0}, \dot{y_0}, \dot{z_0} = 0 \qquad \gamma_x, \gamma_y = 0 \\ z_0 & = & Z_0 \end{array}$$

The equations of motion are, by definition,

$$\begin{array}{r} x(t), y(t) = 0 \\ z(t) = Z_0 \end{array} \tag{3.54}$$

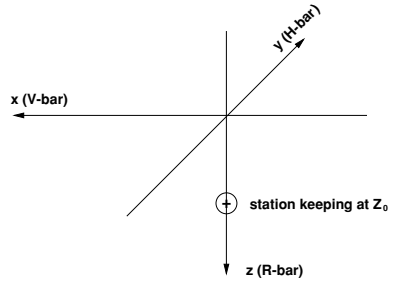

Figure 3.26. Station keeping below or above the target orbit.

The force per unit of mass γ_z, which must be applied to counteract the orbital forces, when a position below or above the target orbit is to be held, can be obtained from the Hill equations (3.21) by inserting the above initial conditions:

$$\gamma_z = -3\omega^2 Z_0 \tag{3.55}$$

The total ΔV required for station keeping at a position z_0 above or below the target orbit is

$$\Delta V_{\text{total}} = \gamma_z \Delta t = -3\omega^2 Z_0 \Delta t \tag{3.56}$$

The results are independent of the initial position x_0. The results for in-plane- and out-of-plane positions (see below) can be added for the case of a combined z_0, y_0 initial position.

Station keeping at out-of-plane position The following initial conditions are assumed:

$$\begin{array}{rcl} x_0, z_0 & = & 0 \qquad \dot{x_0}, \dot{y_0}, \dot{z_0} = 0 \qquad \gamma_x, \gamma_z = 0 \\ y_0 & = & Y_0 \end{array}$$

The equations of motion are accordingly

$$\begin{array}{rcl} x(t), z(t) & = & 0 \\ y(t) & = & Y_0 \end{array} \tag{3.57}$$

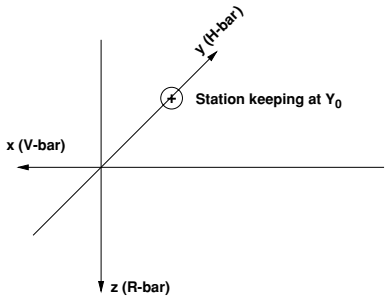

Figure 3.27. Station keeping at out-of-plane position.

The force per unit of mass γ_y, which must be applied to counteract the orbital forces, when an out-of-plane position is to be held, can be obtained for the above initial conditions from the Hill equations (3.21):

$$\gamma_y = \omega^2 Y_0 \tag{3.58}$$

The total ΔV required for station keeping at an out-of plane position Y_0 is

$$\Delta V_{\text{total}} = \gamma_y \Delta t = \omega^2 Y_0 \Delta t$$

Transfer by continuous *x*-thrust

In the impulsive manoeuvre cases discussed above (section 3.3.2), it has been assumed that the change of velocity is a step function. In reality all thrusters have a finite force level, so that a constant force has to be applied over a certain time in order to achieve a particular ΔV. A further case of interest concerning a constant force in the x-direction is the drag force of the residual atmosphere, which will be treated in more detail in section 4.2.1.

For the easiest case, with the trajectory starting in $\boldsymbol{O_{lo}}$, the initial conditions are

$$x_0, y_0, z_0 = 0 \qquad \dot{x_0}, \dot{y_0}, \dot{z_0} = 0 \qquad \gamma_y, \gamma_z \;=\; 0$$

Inserting these conditions into Eqs. (3.22) and defining γ_x as the constant thrust force per unit of mass to be applied over the time t, the equations of motion become

$$\begin{aligned} x(t) &= \frac{1}{\omega^2}\gamma_x \left(4(1-\cos(\omega t)) - \frac{3}{2}\omega^2 t^2\right) \\ z(t) &= \frac{2}{\omega^2}\gamma_x(\sin(\omega t) - \omega t) \end{aligned} \tag{3.59}$$

By differentiation one obtains the velocities

$$\begin{aligned} \dot{x}(t) &= \gamma_x \left(\frac{4}{\omega} \sin(\omega t) - 3t \right) \\ \dot{z}(t) &= \frac{2}{\omega} \gamma_x \left(\cos(\omega t) - 1 \right) \end{aligned} \tag{3.60}$$

Applications of tangential thrust manoeuvres with finite duration

Quasi-impulsive x-thrust manoeuvres The exact solution for the realistic case of thrust manoeuvres with limited thrust level and duration is given in appendix A, Eqs. (A.43)–(A.49). The position and velocities achieved after applying a constant thrust force per unit of mass γ_x, for time t, can easily be calculated, however, by using Eqs. (3.59) and (3.60). The total ΔV applied after time $t = \tau$ is, for a constant thrust level,

$$\Delta V = \gamma_x \tau$$

Further evolution of the trajectory can be obtained (using the simple tools provided in this chapter) by inserting the position and velocities achieved at the end of the thrust at time τ as initial conditions into Eqs. (3.22) and setting the forces $\gamma_x, \gamma_y, \gamma_z$ to zero, for the further free motion.

Example. Tangential transfer with finite boosts to a different orbit altitude (Hohmann transfer)

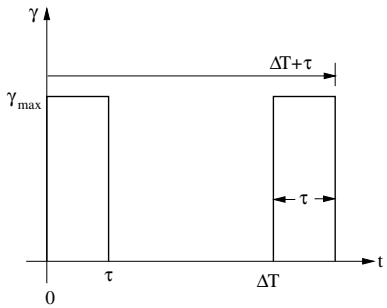

Figure 3.28. Two-boost transfer manoeuvres with finite pulse duration.

The manoeuvre starts at a distance $Z_0 = \Delta z$ from the target orbit. For an impulsive transfer, the necessary ΔV_x to achieve the desired change of altitude Δz is, according to Eq. (3.32),

$$\Delta V_x = \frac{\omega}{4} \Delta z$$

In order to achieve the same Δz in the case of a finite thrust transfer with a limited $\gamma_x = \gamma_{x-\max}$, the same $\Delta V_x = \gamma_x \tau$ must be applied (valid only for $\tau \ll \Delta T$). The necessary boost duration is then

$$\tau = \frac{\omega \Delta z}{4\gamma_x} \tag{3.61}$$

The interval from the start of the first to the start of the second tangential boost is still half an orbital revolution:

$$\Delta T = \frac{\pi}{\omega}$$

The equations of motion during the boost can be obtained from Eqs. (3.59) by inserting the chosen Z_0, τ and γ_x, γ_z. The equations of the free motion between the boosts are obtained by inserting the obtained results for $x(\tau)$, $\dot{x}(\tau)$ and $z(\tau)$, $\dot{z}(\tau)$ into the CW equations (3.22):

$$\begin{aligned} x(t) &= X_0 + \frac{3}{2}(\omega Z_0 - 2\gamma_x \tau)t + \frac{3}{2}\gamma_x \tau^2 + \frac{4}{\omega}\gamma_x \tau \sin\left(\omega\left(t - \frac{\tau}{2}\right)\right) \\ z(t) &= Z_0 - \frac{2}{\omega}\gamma_x \tau + \frac{2}{\omega}\gamma_x \tau \cos\left(\omega\left(t - \frac{\tau}{2}\right)\right) \end{aligned} \tag{3.62}$$

Continuous x-thrust transfer to a different altitude The following example is the extreme case of a continuous thrust over one entire orbital revolution. It shows that the most important difference between purely impulsive manoeuvres and constant thrust manoeuvres is the difference in duration. The change in orbital height, which can be achieved with a particular amount of ΔV, is the same.

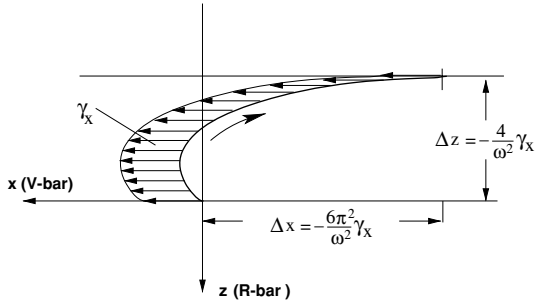

Figure 3.29. Continuous x-thrust transfer to different altitude.

The special case shown in figure 3.29, i.e. a transfer to a different orbital altitude by continuous thrust over one orbital revolution, can be of interest, either because of thrust level limitations or because of safety considerations (see section 4.1). For the transfer

time of one orbital period, $t = T$, $\omega t = 2\pi$, and for the general case of a trajectory starting at x_0, z_0, Eqs. (3.59) become

$$\begin{aligned} \Delta x = x_T - x_0 &= -\frac{6\pi^2}{\omega^2}\gamma_x \\ \Delta z = z_T - z_0 &= -\frac{4\pi}{\omega^2}\gamma_x \end{aligned} \tag{3.63}$$

and Eqs. (3.60) become

$$\begin{aligned} \dot{x_T} &= \frac{-6\pi}{\omega}\gamma_x \\ \dot{z_T} &= 0 \end{aligned} \tag{3.64}$$

The continuous thrust force per mass unit required over T to achieve the difference in altitude Δz is then

$$\gamma_x = \frac{-\omega^2}{4\pi}\Delta z \tag{3.65}$$

With Eq. (3.65) the total ΔV required is

$$|\Delta V_{\text{total}}| = |\gamma_x|\, T = \frac{\omega}{2}\Delta z$$

This is the same ΔV requirement as for the impulsive (Hohmann) transfer. The continuous thrust orbit raising manoeuvre is in its results indeed similar to the Hohmann transfer, except for a transfer duration of T instead of $T/2$ and for the progress in x-direction, which is double.

Transfer by continuous z-thrust

This case is similar to that for the x-thrust transfer, i.e. we are interested in limitation of thrust level and trajectory safety.

For the easiest case, with the trajectory starting in $\boldsymbol{O_{lo}}$, the initial conditions are

$$x_0, y_0, z_0 = 0 \qquad \dot{x_0}, \dot{y_0}, \dot{z_0} = 0 \qquad \gamma_x, \gamma_y = 0$$

Inserting the initial conditions into Eqs. (3.22) and defining γ_z as the constant thrust force to be applied, the equations of motion become

$$\begin{aligned} x(t) &= \frac{2}{\omega^2}\gamma_z(\omega t - \sin(\omega t)) \\ z(t) &= \frac{1}{\omega^2}\gamma_z(1 - \cos(\omega t)) \end{aligned} \tag{3.66}$$

By differentiation one obtains the velocities

$$\begin{aligned} \dot{x}(t) &= \frac{2}{\omega}\gamma_z\,(1-\cos(\omega t)) \\ \dot{z}(t) &= \frac{1}{\omega}\gamma_z\sin(\omega t) \end{aligned} \tag{3.67}$$

Applications of radial thrust manoeuvres with finite duration

Quasi-impulsive z-thrust manoeuvres In analogy to the case of continuous x-thrust transfer, Eqs. (3.66) and (3.67) can be used for the calculation of trajectory and velocity of a z-thrust manoeuvre with the boost duration $t = \tau$. The total ΔV is correspondingly

$$\Delta V = \gamma_z \tau$$

Example. Radial thrust transfer with finite boosts to a new x-position on V-bar

The radial boost starts at a position X_0 on the target orbit. For an impulsive transfer the necessary ΔV_z to achieve the desired change of x-position $\Delta x = X_\mathrm{F} - X_0$ is, according to Eq. (3.37),

$$\Delta V_z = \frac{\omega}{4}\Delta x$$

For a finite thrust transfer, the interval between the boosts is again half an orbital revolution. To achieve the same Δx with a limited $\gamma_z = \gamma_{z-\max}$ the necessary boost duration is (valid only for $\tau \ll \Delta T$, $\Delta T =$ time between the boosts)

$$\tau_z = \frac{\omega \Delta x}{4\gamma_z} \tag{3.68}$$

The equations of motion during the boost can be obtained from Eqs. (3.66) by inserting x_0, τ_z and γ_z. The equations of the free motion between the boosts are obtained by inserting the calculated results for $x(\tau_z)$, $\dot{x}(\tau_z)$ and $z(\tau_z)$, $\dot{z}(\tau_z)$ into the CW equations (3.22):

$$\begin{aligned} x(t) &= X_0 + \frac{2}{\omega}\gamma_z\ \tau_z \left[1 - \cos\left(\omega\left(t - \frac{\tau_z}{2}\right)\right)\right] \\ z(t) &= \frac{1}{\omega}\gamma_z\ \tau_z\ \sin\left(\omega\left(t - \frac{\tau_z}{2}\right)\right) \end{aligned} \tag{3.69}$$

If the transfer does not take place exactly on the target orbit, but at a distance Δz, the x-velocity according to Eq. (3.24), $\dot{x} = \frac{3}{2}\omega\,\Delta z$, has to be taken into account and must be compensated for by corresponding x-thrusts. The resulting equations of motion will then also include γ_x and τ_x terms. The duration of the additional boost in the x-direction is, according to Eq. (3.61), again

$$\tau_x = \frac{\omega \Delta z}{4\gamma_x}$$

The time interval between the boosts is (MATRA 1993)

$$\Delta T = \frac{\pi}{\omega} + \frac{2}{\omega}\arctan\left(\frac{4\Delta z}{\Delta x}\right) \tag{3.70}$$

The resulting free motion between the boosts is (MATRA 1993)

$$\begin{aligned} x(t) &= X_0 + 6\Delta z(\omega t - \sin(\omega t)) + \frac{\gamma_x}{\omega}\tau_x\left[4\sin\left(\omega\left(t-\frac{\tau_x}{2}\right)\right) - 3\omega\left(t-\frac{\tau_x}{2}\right)\right] + \cdots \\ &\quad + 2\frac{\gamma_z}{\omega}\tau_z\left[1-\cos\left(\omega\left(t-\frac{\tau_z}{2}\right)\right)\right] \\ z(t) &= \Delta z(4-3\cos\omega t) - 2\frac{\gamma_x}{\omega}\tau_x\left[1-\cos\left(\omega\left(t-\frac{\tau_x}{2}\right)\right)\right] + \frac{\gamma_z}{\omega}\tau_z\sin\left(\omega\left(t-\frac{\tau_z}{2}\right)\right) \end{aligned} \tag{3.71}$$

Continuous thrust transfer along V-bar The interest in the special case of a transfer along V-bar by continuous thrust (figure 3.30) is the same as in the previous case, i.e. thrust limitations and safety considerations. For the transfer time of one orbital period

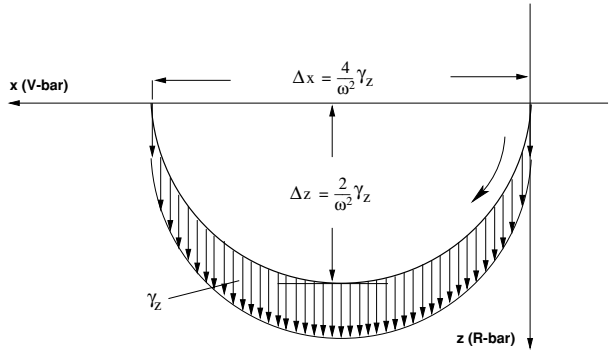

Figure 3.30. Transfer along V-bar by continuous z-thrust.

($t = T, \omega t = 2\pi$) and for the general case of a trajectory starting at x_0, z_0, Eqs. (3.66) become

$$\begin{aligned} \Delta x = x_T - x_0 &= \frac{4\pi}{\omega^2}\gamma_z \\ \Delta z = z_T - z_0 &= 0 \end{aligned} \tag{3.72}$$

The maximum extension of the trajectory in the z-direction is at $t = T/2$:

$$z_{T/2} = \frac{2}{\omega^2}\gamma_z \tag{3.73}$$

The continuous thrust required over T to achieve the intended Δx is, from Eqs. (3.72),

$$\gamma_z = \frac{\omega^2}{4\pi}\Delta x \tag{3.74}$$

This transfer along V-bar is similar to the radial impulse transfer, with a transfer time of T instead of $T/2$ and with continuous radial thrust along the arc. In contrast to the straight line V-bar transfer, there are no thrusts in the $+$ and $-x$-direction at the beginning and end of the transfer trajectory. The total ΔV is

$$\Delta V_{\text{total}} = \gamma_z T = \frac{\omega}{2}\Delta x$$

This is the same ΔV requirement as for the impulsive transfer along V-bar with radial impulses ΔV_z.

Continuous thrust in the *y*-direction

For reasons of completeness, the equations for a continuous constant thrust manoeuvre in the y-direction are given here. For a trajectory starting in $\boldsymbol{O_{lo}}$ the initial conditions are

$$x_0, y_0, z_0 = 0 \qquad \dot{x_0}, \dot{y_0}, \dot{z_0} = 0 \qquad \gamma_x, \gamma_z \;=\; 0$$

With these initial conditions and with γ_y defined as the continuous thrust force, Eqs. (3.22) become

$$\begin{aligned} x(t) &= 0 \\ y(t) &= \frac{1}{\omega^2}\gamma_y(1-\cos(\omega t)) \\ z(t) &= 0 \end{aligned} \tag{3.75}$$

By differentiation one obtains the velocity

$$\dot{y}(t) \;=\; \frac{1}{\omega}\gamma_y \sin(\omega t) \tag{3.76}$$

As in the case of continuous x- and z-thrust transfer, Eqs. (3.75) and (3.76) can be used for the calculation of trajectory and velocity of a y-thrust manoeuvre with the duration t_t. The ΔV cost is correspondingly

$$\Delta V = \gamma_y t_t$$

Forced motion circular fly-around

The forced motion circular fly-around can be of interest when a certain fly-around angle has to be reached and when the distance between chaser and target vehicles has to be kept constant because of safety or other reasons. Such a transfer trajectory can be used, e.g., when the docking axis has a small angle w.r.t. V-bar or when the fly-around has to be performed against the natural orbital motion, e.g. from $+$V-bar to $+$R-bar. For larger angles in the direction of orbital motion, e.g. for a 90 deg fly-around from $-$V-bar

to +R-bar, tangential or radial impulsive manoeuvres will be preferred because of the lower expenditure on ΔV. The following initial conditions are assumed:

$$\begin{array}{ll} x_0 = -R_{\rm fa} & \dot{x_0}, \dot{y_0} = 0 \\ y_0, z_0 = 0 & \dot{z_0} = \Delta V_{zi} \end{array} \qquad \gamma_y = 0$$

where $R_{\rm fa}$ is the fly-around radius. With $\dot{\alpha}$ being the angular rate of the fly-around, the equations of motion become, for the case shown in figure 3.31,

$$\begin{aligned} x(t) &= -R_{\rm fa}\cos(\dot{\alpha}t) \\ y(t) &= 0 \\ z(t) &= R_{\rm fa}\sin(\dot{\alpha}t) \end{aligned} \tag{3.77}$$

The initial ΔV that has to be applied is

$$\Delta V_{z\rm i} = R_{\rm fa}\dot{\alpha} \tag{3.78}$$

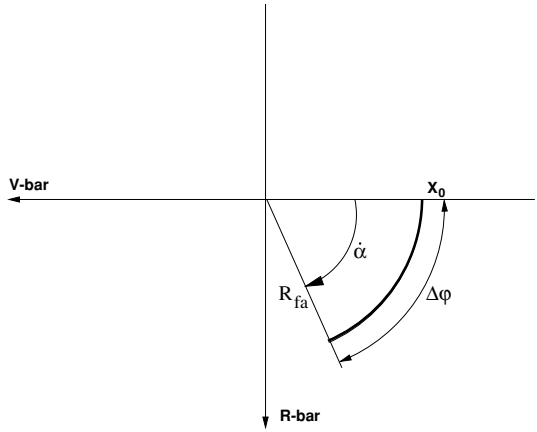

Figure 3.31. Forced motion circular fly-around.

The forces γ_x and γ_z that have to be applied over the arc can be obtained by inserting into Eqs. (3.21) the above initial conditions, the $x(t)$ and $z(t)$ positions from Eq. (3.77) and the velocities and accelerations obtained by differentiation of Eq. (3.77):

$$\begin{aligned} \gamma_x(t) &= -R_{\rm fa}\dot{\alpha}(2\omega - \dot{\alpha})\cos(\dot{\alpha}t) \\ \gamma_z(t) &= -R_{\rm fa}(\dot{\alpha}^2 - 2\omega\dot{\alpha} + 3\omega^2)\sin(\dot{\alpha}t) \end{aligned} \tag{3.79}$$

where ω is the angular rate of the orbit.

The final ΔVs that have to be applied in the x- and z-directions to stop the motion at the fly-around angle $\Delta\varphi = \dot{\alpha}t$ are

$$\begin{aligned} \Delta V_{x\rm f} &= R_{\rm fa}\dot{\alpha}\sin(\Delta\varphi) \\ \Delta V_{z\rm f} &= R_{\rm fa}\dot{\alpha}\cos(\Delta\varphi) \end{aligned} \tag{3.80}$$

The transfer time for a fly-around angle $\Delta\varphi$ is $\Delta t = t_1 - t_0 = \Delta\varphi/\dot{\alpha}$.

To the above final ΔVs must be added the velocities which the vehicle is intended to assume at the end of the fly-around, otherwise a motion as shown in figure 3.11 will commence. In the case of station keeping at this point, the continuous force per unit of mass of Eq. (3.55) for $z = R_{\mathrm{fa}} \sin(\Delta\varphi)$ has to be applied.

The ΔVs required during the transfer $\Delta\varphi$ are

$$\begin{aligned} \Delta V_{x\varphi} &= \int_{t_0}^{t_1} \gamma_x(t)\mathrm{d}t \\ \Delta V_{z\varphi} &= \int_{t_0}^{t_1} \gamma_z(t)\mathrm{d}t \end{aligned} \tag{3.81}$$

The total ΔV expenditure for a circular fly-around over an angle $\Delta\varphi$ is

$$\Delta V_{\mathrm{total}} = |\Delta V_{\mathrm{zi}}| + |\Delta V_{x\varphi}| + |\Delta V_{z\varphi}| + |\Delta V_{\mathrm{xf}}| + |\Delta V_{\mathrm{zf}}|$$

3.4 Final remark on the equations of motion

The intention of this chapter was to provide a sort of tool-kit for the calculation of properties of the most important types of trajectories and manoeuvres used in rendezvous approaches. Whereas all trajectories have been treated so far as undisturbed cases, in reality external disturbance forces and errors in the assumed initial conditions and applied ΔVs have to be taken into account. These are, in the first instance, not included in the equations derived here. However, in most cases:

- external disturbance forces can be treated as additional constant force components γ, at least over a particular time;
- thrust errors can be treated as additional x-, y-, z-components in the applied ΔV; and
- navigation errors can be treated as additional x-, y-, z-components in the initial conditions.

The disturbed trajectories can then be calculated, using the same set of equations as for the undisturbed ones, by simply adding the additional initial conditions and constant forces.

The most important equations of the undisturbed open loop trajectories are listed in Table 3.1, and examples for the combination of initial conditions and equations of motion are shown in the following sections. The sources and effects of trajectory deviations due to external disturbances and errors of the onboard system are addressed in sections 4.2 and 4.3 of the following chapter.

Table 3.1. Equations of motion.

Type of manoeuvre and equation numbers	Initial conditions	Equations of motion
Impuls. change V_x (3.28)	$\boldsymbol{O}_{\mathbf{lo}}$, ΔV_x, $t = 0$	$x(t) = \frac{1}{\omega}\Delta V_x(4\sin(\omega t) - 3\omega t)$ $z(t) = \frac{2}{\omega}\Delta V_x(\cos(\omega t) - 1)$
Impuls. change V_y (3.40)	$\boldsymbol{O}_{\mathbf{lo}}$, ΔV_y, $t = 0$	$y(t) = \frac{1}{\omega}\Delta V_y \sin(\omega t)$
Impuls. change V_z (3.34)	$\boldsymbol{O}_{\mathbf{lo}}$, ΔV_z, $t = 0$	$x(t) = \frac{2}{\omega}\Delta V_z(1 - \cos(\omega t))$ $z(t) = \frac{1}{\omega}\Delta V_z \sin(\omega t)$
Contin. force, x-dir. (3.59)	$\boldsymbol{O}_{\mathbf{lo}}$, γ_x, $t = 0$	$x(t) = \frac{1}{\omega^2}\gamma_x\,(4(1 - \cos(\omega t))$ $-\frac{3}{2}\omega^2 t^2\big)$ $z(t) = \frac{2}{\omega^2}\gamma_x(\sin(\omega t) - \omega t)$
Contin. force, y-dir. (3.75)	$\boldsymbol{O}_{\mathbf{lo}}$, γ_y, $t = 0$	$y(t) = \frac{1}{\omega^2}\gamma_y(1 - \cos(\omega t))$
Contin. force, z-dir. (3.66)	$\boldsymbol{O}_{\mathbf{lo}}$, γ_z, $t = 0$	$x(t) = \frac{2}{\omega^2}\gamma_z(\omega t - \sin(\omega t))$ $z(t) = \frac{1}{\omega^2}\gamma_z(1 - \cos(\omega t))$
Straight line V-bar (3.44), (3.45)	$\boldsymbol{O}_{\mathbf{lo}}$, ΔV_{x0}, $t = 0$	$x(t) = \Delta V_x t$, $\gamma_z = 2\omega\Delta V_x$
Straight line R-bar (3.49), (3.50)	$\boldsymbol{O}_{\mathbf{lo}}$, ΔV_{z0}, $t = 0$	$z(t) = \Delta V_z t$ $\gamma_x = -2\omega\Delta V_z$ $\gamma_z = -3\omega^2\Delta V_z t$
Circular fly-around (3.77), (3.79)	$x = -R_{fa}$, $t = 0$ $\dot{z_0} = \Delta V_{z0}$	$x(t) = -R_{fa}\cos(\dot{\alpha}t)$ $z(t) = R_{fa}\sin(\dot{\alpha}t)$ $\gamma_x(t) = -R_{fa}\dot{\alpha}(2\omega - \dot{\alpha})\cos(\dot{\alpha}t)$ $\gamma_z(t) = -R_{fa}(\dot{\alpha}^2 - 2\omega\dot{\alpha}$ $+3\omega^2)\sin(\dot{\alpha}t)$
Hold point at z_0 (3.55)	$x_0 = 0, \dot{x}_0 = 0, t = 0$ $z_0 = Z_0$	$x(t), y(t) = 0$ $z(t) = Z_0$, $\gamma_z = -3\omega^2 Z_0$
Hold point at y_0 (3.58)	$x_0 = 0, \dot{x}_0 = 0, t = 0$ $y_0 = Y_0$	$x(t), z(t) = 0$ $y(t) = Y_0$, $\gamma_y = \omega^2 Y_0$

Table 3.1. (*continued*). Equations of motion.

Type of manoeuvre and equation numbers	Initial conditions	Equations of motion
Free drift, start at z_0 on circular orbit (3.25)	$x_0 = 0, \dot{x}_0 = \frac{3}{2}\omega Z_0$ $z_0 = Z_0, t = 0$	$x(t) = \frac{3}{2}\omega Z_0 t$ $z(t) = Z_0$
Free drift, release at Z_0 with velocity of target (3.26)	$x_0 = 0, \dot{x}_0 = 0, t = 0$ $z_0 = Z_0, \dot{z}_0 = 0$	$x(t) = 6Z_0(\omega t - \sin(\omega t))$ $z(t) = Z_0(4 - 3\cos(\omega t))$
Free drift, start at y_0	$y_0 = Y_0, \dot{y}_0 = 0, t = 0$	$y(t) = Y_0 \cos(\omega t)$
Free drift, start at x_0 (3.27)	$x_0 = X_0, \dot{x}_0 = 0, t = 0$	$x(t) = X_0$

3.4.1 Examples for combined cases

Combined cases can be obtained by adding, where applicable, the equations of motion and the initial conditions belonging to each single manoeuvre.

Example 1

To obtain a trajectory with continuous force in the x-direction starting at $x_0 = X_0$ and $z_0 = Z_0$ on a lower orbit, we add initial conditions and equations of motion of the following cases (see Table 3.1):

(1) 'contin. force, x-dir.',

(2) 'free drift, start at x_0',

(3) 'free drift, start at z_0 on circular orbit'.

The results are as follows. For combined initial conditions $(1) + (2) + (3)$

$$\begin{array}{lllllllll} x_0 & = & 0 + X_0 + 0 & \quad \dot{x}_0 & = & 0 + 0 + \frac{3}{2}\omega Z_0 & \quad \gamma_x & = & \gamma_x + 0 + 0 \\ y_0 & = & 0 + 0 + 0 & \quad \dot{y}_0 & = & 0 & \quad \gamma_y & = & 0 \\ z_0 & = & 0 + 0 + Z_0 & \quad \dot{z}_0 & = & 0 & \quad \gamma_z & = & 0 \end{array}$$

For combined equations of motion $(1)+(2)+(3)$

$$\begin{aligned} x(t) &= \gamma_x \left(\frac{4}{\omega^2}(1-\cos(\omega t)) - \frac{3}{2}t^2 \right) + X_0 + \frac{3}{2}Z_0\omega t \\ z(t) &= \frac{2}{\omega^2}\gamma_x(\sin(\omega t) - \omega t) + 0 + Z_0 \end{aligned}$$

Example 2

To obtain a forced motion R-bar trajectory starting at $x_0 = X_0$ and $z_0 = Z_0$ with $\dot{x}_0 = 0$ we add initial conditions and equations of motion of the following cases:

(1) 'straight line R-bar',

(2) 'hold point at x_0' = 'free drift, start at x_0',

(3) 'hold point at z_0'.

The results are as follows. For combined initial conditions $(1)+(2)+(3)$

$$\begin{array}{lllllll} x_0 &=& 0+X_0+0 & \qquad \dot{x}_0 &=& 0+0+0 \\ y_0 &=& 0+0+0 & \qquad \dot{y}_0 &=& 0 \\ z_0 &=& 0+0+Z_0 & \qquad \dot{z}_0 &=& \Delta V_z + 0 \end{array}$$

For combined equations of motion $(1)+(2)+(3)$

$$\begin{array}{lllllll} x(t) &=& 0+x_0+0 & \qquad \gamma_x &=& -2\omega\Delta V_z \\ z(t) &=& \Delta V_z t + 0 + z_0 & \qquad \gamma_z &=& -3\omega^2\Delta V_z t - 3\omega^2 z_0 \end{array}$$

4

Approach safety and collision avoidance

The objective of this chapter is to explain the requirements for trajectory safety, to discuss the causes for trajectory deviations due to the orbital environment and to imperfections and errors of the onboard system, and to investigate the possibilities of employing protection against trajectory deviations. The discussions concerning trajectory deviations and trajectory safety concentrate on the rendezvous phases, since the mission phases of launch and phasing are generally controlled by operators or computer functions on ground. In the rendezvous phases the two spacecraft are relatively close together, their orbital planes are well aligned and the trajectory of the chaser, by definition, leads toward the target, so that any deviation from the planned trajectory can potentially lead to a collision, directly or after one or more orbital revolutions.

4.1 Trajectory safety – trajectory deviations

Rendezvous and docking is in fact a 'planned collision' of two spacecraft, which is controlled by considering the geometric location of the contact points on the two vehicles and the linear velocities and angular rates at contact. To achieve the contact conditions within the allowed margins, the trajectories have to be maintained within close tolerances prior to contact. Any deviation from such tolerances may lead either to a loss of the rendezvous and mating opportunity or even to the danger of collision of the two spacecraft at unsuitable points and dynamic conditions, with the risk of serious damage. For this reason, rendezvous operations, and all functions and systems involved in them, have to comply with failure tolerance and safety requirements.

The level of failure tolerance required for safety and mission success depends on the type of mission. The term *safety* is used in the context of space operations usually for the

safety of human life. It is, therefore, only applicable to missions involving at least one manned vehicle, which could be either the target or chaser vehicle. These missions require the highest level of failure tolerance. Failure tolerance requirements of unmanned missions are lower or, at most, equal to those of manned missions. Instead of *safety of human life*, the most important protection in unmanned missions must be given to the investment made in the missions of the two spacecraft involved. For this issue, instead of *safety* the term *spacecraft security* has been proposed by some authors. However, as there is no difference between manned and unmanned missions when considering the effects of trajectory deviations and the danger of collision, it would lead only to confusion if different terms were to be used in the two cases for the same problem. The terms *approach/departure safety* and *trajectory safety* will, therefore, be used in the following regardless of whether a manned or an unmanned mission is under discussion.

4.1.1 Failure tolerance and trajectory design requirements

Failure tolerance requirements are usually defined for general application, i.e. for all systems of the vehicle(s) and for all payloads in a given mission scenario. They need to be interpreted, however, on considering their consequences for each particular application. For example, in the International Space Station (ISS) Programme the following requirements have been defined (NASA 1998b).

(1) No single failure shall cause major consequences.

(2) No combination of two failures shall have catastrophic consequences.

A *single failure* is defined as 'the inability of either a system, subsystem or item (hardware and software) to perform its required function', or as any 'operator failure'; a *major consequence* is defined as 'the loss of the particular mission', e.g. of the rendezvous mission of another vehicle with the ISS; and a *catastrophic failure* is defined as either 'loss of life or disabling injury of crew', or 'loss of the space station or of one of its major elements'.

For spacecraft operations this can be translated into the familiar *fail operational–fail-safe* requirement. It can be expected that such a two-level requirement would also be applicable for, e.g., the case of a satellite servicing mission by an unmanned servicing vehicle, which is a typical rendezvous and capture mission scenario with two unmanned vehicles. For the rendezvous and capture operations proper, these failure tolerance requirements can be interpreted in the following way.

- *Approach up to contact*

  After one failure the trajectory must remain safe (collision-free), and it must be possible to continue or resume the rendezvous mission.

  After two failures the resulting trajectory must be collision-free, without requirement to continue the mission.

- *Capture*

  After one failure the approaching vehicle must be able to retreat and re-try.

  After two failures the chaser vehicle must be able to leave the target safely (collision-free), without requirement to resume the mission.

- *Departure*

  After one failure the chaser vehicle must be able to continue the nominal departure and de-orbitation operations.

  After two failures the chaser vehicle must be able to leave the target safely (collision-free), without further requirements.

A more detailed interpretation of failure tolerance requirements for other rendezvous related mission phases, such as structural connection/disconnection and operations preparing the attached phase, is not needed for the purpose of this book, as they are in no way different from other operations aboard a spacecraft.

4.1.2 Design rules for trajectory safety

For the approach phase it will be indicated in the following how such safety requirements can be translated into design requirements for the approach trajectory strategy and for the onboard system.

(1) The approach and departure strategies and their trajectory elements must be designed to be as safe as possible concerning the risk of collision. This means that, the natural development of each trajectory element shall be collision-free for as long as possible, taking into account all possible dispersions and including the possibility of a failure of the onboard system. This is of course not possible up to the end, as eventually the chaser vehicle will make physical contact with the target vehicle.

(2) In the vicinity of the target station, the onboard system of the chaser must be able to monitor the relative state vector w.r.t. the target at each point along the trajectory, and must be able to correct it automatically when deviations from the planned trajectory become too large.

(3) The onboard system must be able to detect failures of its subsystems, functions or equipment and must be able to engage redundant equipment, functions or subsystems within a time limit, which allows either the continuation of the present trajectory or the initiation of a back-up operation which permits a later resumption of the mission.

(4) In any case, at each point of the approach and departure trajectories, when all control fails and the actual state vector exceeds safety boundaries, the onboard

system must be able to execute an operation which ensures collision avoidance between chaser and target. Where natural collision-free trajectories are available (see (1)), such an operation could simply be the inhibition of all thruster action. In other cases the execution of a single boost may be sufficient to remove the chaser from the target vicinity (see section 4.5).

To be able to assess possibilities and constraints in the trajectory strategy design concerning the implementation of the first of the above design requirements, it will be necessary first to identify the causes of trajectory deviations and thereafter to find suitable safeguards against such deviations. The second and third design requirements regard the design of the automatic onboard control system, which will be discussed in detail in chapter 6. The last of these design requirements, the availability of a safe collision avoidance manoeuvre (CAM), has two implementation aspects:

- the design of the trajectories and manoeuvres for each case, which will be treated in section 4.5;
- the detection of deviations from the planned state vector at any point of the trajectory and the initiation of the appropriate actions, which is the task of the onboard control system, and will be treated in chapter 6.

4.1.3 Causes of deviations from the planned trajectory

Potential causes of deviations of the actual trajectory from the planned one are the following:

- orbital disturbances,
- navigation errors,
- control errors,
- thrust vector errors,
- thruster failures.

Orbital disturbances are forces acting on the spacecraft that change its trajectory, e.g. due to the deviations of the Earth's gravitational potential from a sphere (this plays a role during phasing and very far range rendezvous operations), due to atmospheric drag and solar pressure (this plays a role in all ranges, but not in all altitudes), thruster plume pressure (this plays a role only at very short distances), etc. These disturbances are the subject of the next section.

Navigation errors are the differences between the state as perceived by the onboard system and the real state (position, velocities, attitude, angular rates) of the vehicle. Initial navigation errors can be amplified over time by effects of orbital dynamics and by thrust manoeuvres (see section 4.3.1).

Control errors are the differences between the proper corrections of the values to be controlled and the ones actually produced by the controller. The effects of control errors are due in equal part to navigation errors and to thrust vector errors; therefore they should not be discussed separately.

Thrust vector errors are deviations in magnitude and direction from the assumed applied force and torque vectors (see section 4.3.2) .

Thruster failures could, strictly speaking, also be covered by the term 'thrust vector errors'. However, under this title only hard failures will be discussed, such as thruster valves stuck open and closed, the results of which are much more dramatic and require quite different measures from the small deviations to be treated under 'thrust vector errors'. It is, therefore, kept as a separate category of causes for trajectory deviations (see section 4.3.3).

The most important causes for trajectory deviations will be discussed in more detail in the following sections of this chapter.

4.2 Trajectory disturbances

The intention of this section is to provide an overview of only the most important trajectory disturbances, those which have a significant effect on the rendezvous trajectories, i.e. disturbances after which the spacecraft position is noticeably changed after one or a few orbits. The most significant disturbances depend on the class of orbit in which the rendezvous takes place. In LEO for instance, the most significant disturbance is the drag due to the residual atmosphere and, in the far range of the approach (in particular during phasing), the effect of the geopotential anomaly. In GEO, on the other hand, the most significant disturbance is the pressure of the solar radiation.[1] In both cases, the largest disturbance forces will occur, however, as a result of the pressure of thruster plumes of one vehicle on the surfaces of the other one when the two spacecraft are in close proximity. The disturbance due to the deviation of the gravitational potential of the Earth from a sphere results mainly in a drift of nodes (change of RAAN), which is of importance for the absolute trajectories, e.g. during phasing, but plays a minor role for the relative trajectories between chaser and target during close range operations. The effects of other disturbances on rendezvous trajectories, such as the luni–solar potential and the higher order harmonics of the Earth potential, are orders of magnitude lower.

Expected or known trajectory disturbances can be taken into account and compensated for. The largest uncertainties will occur in the knowledge of the actual values of absolute and differential drag and, for the last tens of metres of the approach, of the plume dynamic forces. Because of the large variation in density of the residual atmosphere over one orbit and over time in general, and because of the variation of the cross section of the spacecraft due to rotating solar arrays, significant uncertainties will always remain for the disturbance by air drag. Large uncertainties will also remain for the

[1] This book concentrates on rendezvous in LEO, where the majority of rendezvous missions are performed.

disturbance by plume forces due to the limited knowledge of the actual pressure distribution in the thruster plumes and due to the modelling errors of the spacecraft surfaces and of their interaction with the pressure fields.

4.2.1 Drag due to residual atmosphere

The drag force by the residual atmosphere acting on a spacecraft is

$$F_{\mathrm{D}} = -\frac{\rho}{2} V_x^2 C_{\mathrm{D}} A \tag{4.1}$$

where $V_x = \omega r$ is the orbital velocity; C_{D} is the drag coefficient; and A is the cross section of the body. As both vehicles are affected by drag, and as the difference of their absolute velocities is negligible, the differential drag force per unit of mass $\gamma_{\mathrm{D}} = \frac{F_{\mathrm{d}}}{m}$ acting on the chaser w.r.t. the target in a circular orbit is

$$\Delta\gamma_{\mathrm{D}} = \gamma_{\mathrm{Dc}} - \gamma_{\mathrm{Dt}} = -\frac{\rho}{2}\omega^2 r^2 \left(\frac{C_{\mathrm{Dc}} A_{\mathrm{c}}}{m_{\mathrm{c}}} - \frac{C_{\mathrm{Dt}} A_{\mathrm{t}}}{m_{\mathrm{t}}} \right) \tag{4.2}$$

where m is the mass of the vehicles and the indices c and t indicate chaser and target, respectively. The relation

$$C_{\mathrm{B}} = \frac{m}{C_{\mathrm{D}} A}$$

is called the ballistic coefficient of the vehicle. With this term, which is often used in rendezvous analysis, the equation becomes

$$\Delta\gamma_{\mathrm{D}} = -\frac{\rho}{2}\omega^2 r^2 \frac{1}{C_{\mathrm{Bc}}} \left(1 - \frac{C_{\mathrm{Bc}}}{C_{\mathrm{Bt}}} \right) \tag{4.3}$$

The effect of this disturbance on the trajectory can be calculated by introducing the value for $\Delta\gamma_{\mathrm{D}}$ as γ_x into Eqs. (3.59) and (3.66). For a more detailed model, not only the cross section of the vehicle, but the individual surfaces and their direction w.r.t. the orbital velocity vector, have to be taken into account.

The atmospheric density ρ is the value known with least accuracy in this equation. If the value for a certain orbital height is known, it can be modelled locally around this point by an exponential function:

$$\rho(z) = \rho(z_0) \mathrm{e}^{\frac{z - z_0}{H(z_0)}} \tag{4.4}$$

where $H(z_0)$ is a scale height coefficient (Carrou 1995). The atmospheric density at a particular height is dependent on the temperature of the atmosphere. For instance, on the side illuminated by the Sun, the atmosphere will expand and denser parts of the atmosphere will rise to higher altitudes. The density at a certain orbital height will, therefore, not be constant but will increase (solar bulge) on the illuminated side of the orbit, and

vice versa on the opposite side. The effect of the solar bulge on the relative motion between the chaser and target vehicles will, however, be much lower than the change of the absolute value of the density, as both vehicles are equally affected. Also, as this effect is periodic with the orbit, for manoeuvres with a transfer time of one revolution, the effect will be averaged out to a large extent. For preliminary trajectory assessments, an orbital average can therefore be assumed. For detailed analysis and simulations, however, the effect of the solar bulge needs to be taken into account.

A large influence on the density of the atmosphere at a certain orbital height is the solar flux, which heats up the outer atmosphere. Three periodic variations of the solar flux effects on the atmosphere can be distinguished:

- a period of about 27 days, which is due to the rotation of the Sun about its axis;
- a period of 1 year, which is due to the change of attitude of the Earth w.r.t. the Sun's axis during one orbit of the Earth around the Sun;
- a period of about 11 years, which is due to the solar activity cycle.

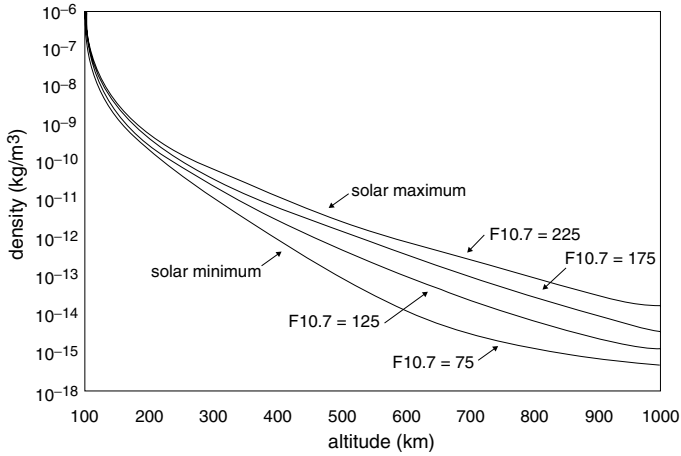

Figure 4.1. Density vs. altitude at various levels of solar flux. Taken from Larson & Wertz (1992), with the kind permission of Kluwer Academic Publishers.

The last effect has the most significant influence. For example, in a 400 km altitude orbit the density can vary between approximately $5 \times 10^{-10}\ \mathrm{kg/m^3}$ at high solar activity and $1 \times 10^{-12}\ \mathrm{kg/m^3}$ at low solar activity. A lot of research work has been performed to provide a model of the atmosphere. Well known are two empirical models: JACCHIA (Jacchia 1977) and MSIS (mass spectrometer incoherent scatter) (Hedin 1986). The variation of the density with the solar flux is shown in figure 4.1, which is taken from Larson & Wertz (1992).

In applications where a complex space station with large surfaces of solar generators and radiators is the target, and relatively compact vehicles comprise the chaser, the ratio of the ballistic coefficients $\frac{C_{\mathrm{Bc}}}{C_{\mathrm{Bt}}}$ can become quite large (4–8). Because of the fact that the solar arrays are pointing toward the Sun, the ballistic coefficient of spacecraft with articulated solar panels will change over one orbit. In cases where solar arrays can be articulated in two axes (to align the pointing axis also with the lateral Sun direction), the ballistic coefficient also varies over the year. If both target and chaser have articulated solar panels, the variation of the ratio of ballistic coefficient will, however, be lower than the variation of the absolute values. Whereas in first trajectory assessments this effect can be neglected, in simulations for performance verification (see sections 10.3.2 and 10.3.3) the variation of the ballistic coefficients must be properly taken into account. To simplify the discussion of the qualitative effects, drag forces are assumed to be constant in the following examples. To demonstrate the effect of the residual atmospheric drag, examples for free drift motions and for motion after impulsive manoeuvres are discussed below.

Free drift motion and impulsive manoeuvres with drag

The first type of trajectory discussed here is the release of a spacecraft on a circular orbit, e.g. from a controlled station keeping to a free motion. Prior to release, the drag force acting on it is counteracted by the control forces. The free drift motion of the spacecraft after release is given by the equations for a constant force transfer, into which the acceleration due to drag has to be inserted. For a trajectory starting in $\boldsymbol{O}_{\mathrm{lo}}$, the equation of motion is thus obtained by inserting Eq. (4.3) into Eqs. (3.59):

$$\begin{aligned} x(t) &= -\frac{\rho}{2}\omega^2 r^2 \frac{1}{C_{\mathrm{Bc}}}\left(1-\frac{C_{\mathrm{Bc}}}{C_{\mathrm{Bt}}}\right)\left(\frac{4}{\omega^2}(1-\cos(\omega t))-\frac{3}{2}t^2\right) \\ z(t) &= -\frac{2}{\omega^2}\frac{\rho}{2}\omega^2 r^2 \frac{1}{C_{\mathrm{Bc}}}\left(1-\frac{C_{\mathrm{Bc}}}{C_{\mathrm{Bt}}}\right)(\sin(\omega t)-\omega t) \end{aligned} \tag{4.5}$$

Since the relative motion between chaser and target is negligible compared with the absolute orbital velocity, the difference of velocity does not enter into the calculation of the drag forces. The results of Eqs. (4.5) can, therefore, be added to the results of the other trajectory cases; e.g., for a trajectory starting on a different altitude from the target orbit, Eqs. (3.25) have to be added to Eqs. (3.59).

The absolute motion of a spacecraft w.r.t. a local orbital frame of constant altitude is obtained by setting the ratio of ballistic coefficients $C_{\mathrm{Bc}}/C_{\mathrm{Bt}} = 0$, i.e. $C_{\mathrm{Bt}} = \infty$. The resulting trajectory is shown in figure 4.2 for a 400 km circular orbit, an assumed drag acceleration of $\gamma_{\mathrm{D}} = -1.38 \times 10^{-6}\ \mathrm{m/s^2}$, which corresponds to a density of about $10^{-11}\ \mathrm{kg/m^3}$ and a ballistic coefficient of $C_{\mathrm{Bc}} \approx 215$, which is valid for a relatively compact spacecraft.

Figure 4.2 shows the beginning of the natural decay (three revolutions) of a satellite orbit due to the drag of the residual atmosphere (note: the Earth is in the +R-bar di-

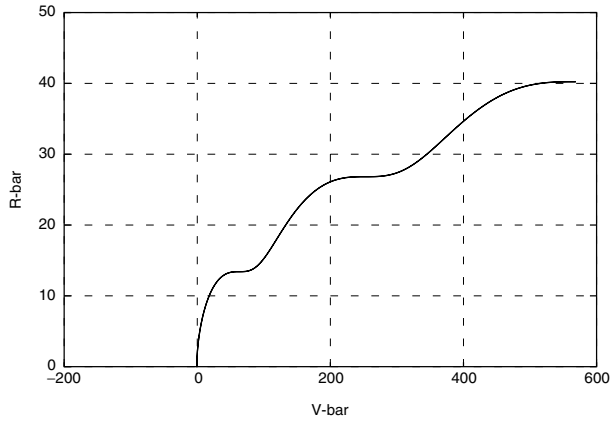

Figure 4.2. Free motion with drag $-1.38 \times 10^{-6}\ \mathrm{m/s^2}$ starting at $\boldsymbol{O}_{\mathbf{lo}}$ (400 km orbit, three revolutions).

rection). The sinusoidal component of the trajectories in figures 4.2 and 4.3 is due to the fact that the drag force is added at the starting point as a step function (release from station keeping).

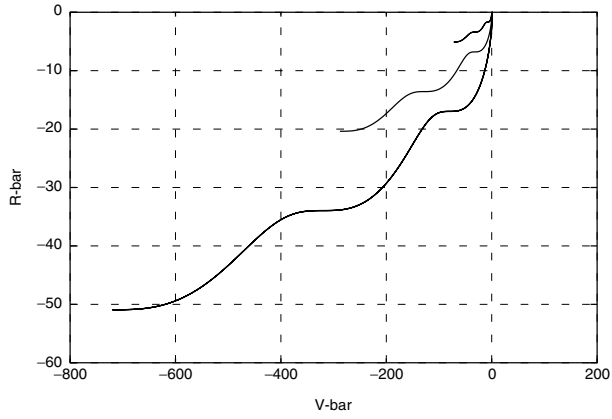

Figure 4.3. Example: motion with differential drag (start: $\mathbf{O}_{\mathrm{lo}}$, $C_{\mathrm{Bc}}/C_{\mathrm{Bt}} = 1.5, 3, 6$).

If chaser and target have the same ballistic coefficient, no effect will be seen in the target-centred orbital frame. However, if, e.g., the target has a lower ballistic coefficient, i.e. a higher resistance, it will decay faster than the chaser, causing the chaser to move over time to a higher position ($-$R-bar direction) behind the target. This is the case for the examples shown in figure 4.3, which are calculated for three orbital revolutions and for the same altitude and density as in figure 4.2. The ballistic coefficient of the chaser

of $C_{\mathrm{Bc}} = 470\ \mathrm{kg/m^2}$ is that of a very compact vehicle. The ratio of the ballistic coefficients $C_{\mathrm{Bc}}/C_{\mathrm{Bt}}$ has been varied between 1 and 6, with the higher values belonging to a target with larger (or chaser with smaller) surfaces. The results demonstrate the importance of the differential drag effect on the development of the free drift motion between chaser and target. Starting on the target orbit, a free drifting chaser with a ballistic coefficient only 1.5 times as large as that of the target vehicle would have reached, after three orbital revolutions, a position of about 5 m above and 70 m behind the target.

As a second case, the effect of differential drag on trajectories after impulsive manoeuvres will be analysed. The equations of motion for a tangential impulse manoeuvre with drag can be obtained by adding to Eqs. (3.28), for the impulsive manoeuvre, the above derived Eqs. (4.5), for free motion with constant drag force. Correspondingly, the equations for a radial impulse manoeuvre with drag are obtained by adding Eqs. (4.5) to Eqs. (3.34) for the impulsive radial manoeuvre.

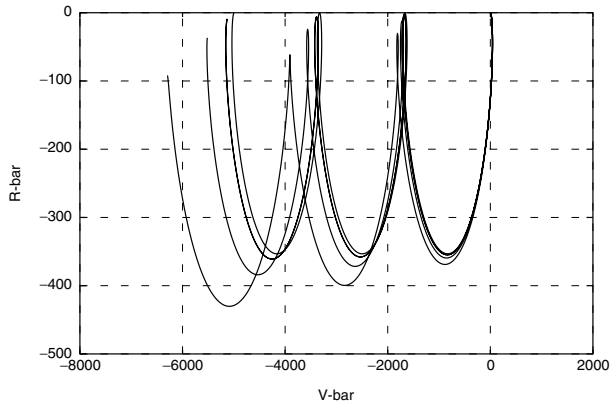

Figure 4.4. Tangential impulse 0.1 m/s with differential drag (400 km, $C_{\mathrm{Bc}}/C_{\mathrm{Bt}} = 1, 1.5, 3, 6$).

Results are shown for a manoeuvre with a tangential initial impulse in figure 4.4 and for a manoeuvre with a radial initial impulse in figure 4.5, assuming the same conditions as for figure 4.3 above. The absolute change of position is the same for all cases with the same density and ballistic coefficient and is equal to that of the drift case (figure 4.3). The relative effect is, however, larger on the radial impulse manoeuvre than on the tangential one, as a radial impulse of the same magnitude produces roughly a five times lower maximum change of position than a tangential manoeuvre.

4.2.2 Disturbances due to geopotential anomaly

Due to the fact that the shape of the Earth deviates from an ideal sphere, and that its mass is not distributed homogeneously inside its body, the gravitational forces are not entirely directed toward the orbit centre, but can have components in other directions in

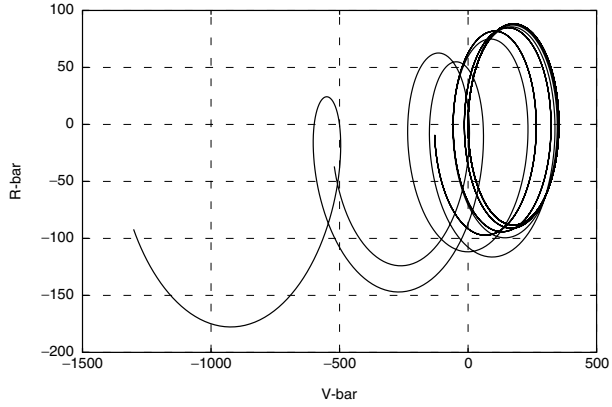

Figure 4.5. Radial impulse 0.1 m/s with differential drag (400 km, $C_{\mathrm{Bc}}/C_{\mathrm{Bt}} = 1, 1.5, 3, 6$).

and out of the orbit plane. These forces will vary over one orbital revolution and can cause changes in the orbital parameters. The gravitational potential of the Earth can be approximated by the function

$$\Phi = \frac{\mu}{r}\left(1 - \sum_{n=2}^{\infty} J_n \left(\frac{R_{\mathrm{E}}}{r}\right)^n P_n(\sin\varphi)\right) \tag{4.6}$$

where J_n are harmonic coefficients of the potential, R_{E} is the Earth radius at the equator, r is the distance of the satellite from the centre of the Earth, P_n are Legendre polynomials, φ is the latitude and μ is the gravitational constant of the Earth. This approximation uses only the zonal deviations from the sphere, i.e. the ones depending on the latitude. More elaborate models include also the sectoral (depending on longitude) and tesseral (combined zonal and sectoral) terms, which are, for most cases of trajectory analysis and particularly for the relatively short duration of a rendezvous mission, of low importance. A detailed discussion of the modelling of the gravitational potential of the Earth can be found in many textbooks, e.g. Carrou (1995).

The most significant effect on near Earth orbits is caused by the second harmonic of the Earth potential, which represents the Earth's oblateness. The coefficient J_2 is more than two orders of magnitude larger than all other ones, hence the name J_2-effect for the most significant gravitational disturbance. Seen in the $\boldsymbol{F}_{\mathbf{eq}}$ frame, the effect of the oblateness of the Earth on the orbits results in the following motions:

- a motion of the line of nodes, i.e. a change over time of the RAAN ($\dot{\Omega}$), called the 'drift of nodes' or 'regression of nodes',
- a rotation of the line of apsides ($\dot{\omega}$) for an elliptical orbit.

Although most rendezvous missions take place in near circular orbits, both effects are of importance for rendezvous operations during phasing and far range rendezvous manoeuvres, where elliptical orbits are often used. For circular orbits the absolute value of the regression of nodes remains significant and has to be taken into account for all issues depending on absolute orbit development, such as ground track, communication windows with relay satellites, GPS satellite visibility and illumination conditions. The difference between the regression of nodes of chaser and target orbit, however, will decrease and eventually disappear when the two vehicles come close to each other.

In the literature (e.g. Wertz & Larson 1994) the following formulas are given for the rate of change of the line of nodes and the line of apsides:

- regression of nodes:

$$\begin{aligned} \dot{\Omega}_{J2} &= -1.5nJ_2(R_{\mathrm{E}}/a)^2(\cos\, i)(1-e^2)^{-2} \\ \dot{\Omega}_{J2} &\approx -2.06474 \times 10^{14} a^{-7/2}(\cos\, i)(1-e^2)^{-2} \end{aligned} \tag{4.7}$$

- rotation of line of apsides:

$$\begin{aligned} \dot{\omega}_{J2} &= 0.75nJ_2(R_{\mathrm{E}}/a)^2(4-5\,\sin^2 i)(1-e^2)^{-2} \\ \dot{\omega}_{J2} &\approx 1.03237 \times 10^{14} a^{-7/2}(4-5\,\sin^2 i)(1-e^2)^{-2} \end{aligned} \tag{4.8}$$

where n is the mean orbital motion in deg/day, R_{E} is the Earth radius at the equator, a is the semi-major axis in kilometres, e is the eccentricity and i is the inclination. The results $\dot{\Omega}$ and $\dot{\omega}$ are in degrees per day. As already mentioned, the rotation of the line of apsides is, for a rendezvous mission, of lower importance, as long as the target is on a quasi-circular orbit.

Examples

For a circular orbit of, e.g., 400 km altitude and 52 deg inclination (International Space Station), the regression of nodes would be, according to Eq. (4.7) $\dot{\Omega}_{J_2} = -4.989$ deg/day. For an elliptic phasing orbit of, e.g., 350/200 km apogee/perigee height, the regression of nodes would be $\dot{\Omega}_{J_2} = -5.326$ deg/day.

For an inclination of 28.5 deg (Cape Canaveral launches), but otherwise the same orbit relations, the drift of nodes would be $\dot{\Omega}_{J_2} = -7.121$ deg/day for the 400 km altitude circular orbit and $\dot{\Omega}_{J_2} = -7.603$ deg/day for the 350/200 km elliptic phasing orbit.

4.2.3 Solar pressure

Solar radiation produces a force on a spacecraft in the Sun–satellite direction:

$$\vec{F}_{\mathrm{SP}} = -p \cdot A \cdot \vec{u}_{\mathrm{S}} \tag{4.9}$$

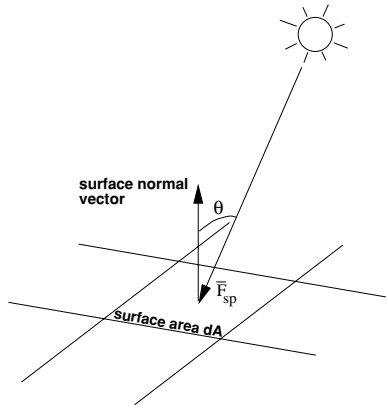

Figure 4.6. Solar pressure force on surface area.

Per unit of mass of the satellite this is

$$\vec{\gamma}_{\mathrm{SP}} = -p\frac{A}{m}\vec{u}_{\mathrm{S}} \tag{4.10}$$

where p is the radiation momentum flux, A is the cross section of the satellite, m is the mass of the satellite and $\vec{u}_{\mathrm{S}}$ is the Sun–satellite direction unity vector. The radiation momentum flux varies periodically with the orbit of the Earth around the Sun and is

$$p = 4.38 \times 10^{-6}\ \mathrm{N/m^2} \text{ at aphelion}$$
$$p = 4.68 \times 10^{-6}\ \mathrm{N/m^2} \text{ at perihelion}$$

As the forces due to solar pressure have in- and out-of-plane components, depending on the Sun direction w.r.t the orbital plane, the solar pressure will have some effect on all orbital parameters, with the most important ones being on eccentricity and on inclination. Depending on orbital height and Sun direction, the force will be intermittent, i.e. the force will be zero when the satellite is in the shadow of the Earth.

Solar pressure is the most prominent disturbance for rendezvous trajectories in geosynchronous orbits, where drag is practically zero but where solar pressure, in combination with a difference in the ballistic coefficients of chaser and target vehicles, can lead to different accelerations of the two. Because the Sun–satellite direction varies along the orbit and with the year, the actual effects of solar pressure need to be calculated separately for each case. In a more detailed analysis, and for verification purposes, the individual surfaces of the satellite body have to be taken into account concerning their direction w.r.t. the Sun–satellite vector and their reflection properties, i.e. whether absorptive, diffuse reflective or specular reflective.

In a 400 km altitude orbit, the acceleration due to solar pressure and the resulting

effect on the rendezvous trajectories is about two to three orders of magnitude lower than that of atmospheric drag.

4.2.4 Dynamic interaction of thruster plumes between chaser and target

Plume interaction becomes an important disturbance when spacecraft are operating in close proximity. Depending on the size of the thrusters and the geometric extension of the opposite spacecraft's surfaces, the effects are significant in a range below a few tens of metres through a few hundred metres. As thruster plumes are limited in their extension, and since the various spacecraft surfaces are at those distances equal to or larger than the plume diameter, there is no possibility of treating the disturbance more globally, as can be done for air drag or solar pressure. Rather, the forces must be integrated over the various surfaces, taking into account the thrust direction w.r.t. the particular surface and the pressure distribution of the plume as a function of range and angle from the centre line.

The force exerted by a thruster plume on a surface element $\mathrm{d}S$ can be described by the plume pressure $P(r, \theta)$ and the direction γ of the gas flux w.r.t the surface:

$$\mathrm{d}F = -P(r, \theta) \cos\gamma \, \mathrm{d}S \tag{4.11}$$

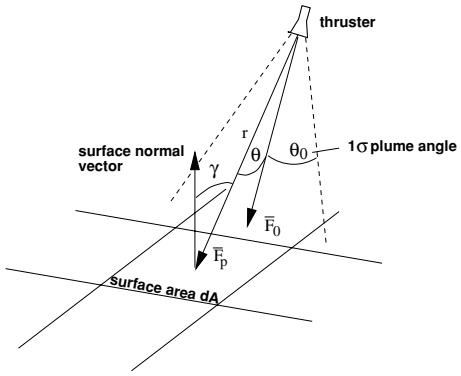

Figure 4.7. Thruster plume force on surface area.

A model of the pressure in a thruster plume as a function of the range r and the angle from the centre line θ has been given in Desplats (1988) by the following equation:

$$P(r, \theta) = \frac{\phi_0}{r^2} \, \mathrm{e}^{\frac{-\theta^2}{2\theta_0^2}} \tag{4.12}$$

where ϕ_0 is a flux constant characterising the thruster, θ_0 is the half cone angle, representing the 1σ value of the gas jet (assuming a Gaussian distribution), i.e. 3σ or 99.7 %

of the plume cross section is covered at $3\theta_0$. The value of ϕ_0 as a function of the standard deviation cone angle θ_0 can be computed from the following force conservation law:

- The force exerted by the plume on a unit sphere of 1 m range around the thruster must be equal to the thrust level F_0 of the thruster.

Integrating Eq. (4.11) over the surface of the unit sphere with the pressure profile of Eq. (4.12) yields, for the characteristic flux,

$$\phi_0 = \frac{F_0}{\pi} \frac{1}{\int_0^\pi (\mathrm{e}^{-\frac{\theta^2}{2\theta_0^2}} \sin(2\theta) \mathrm{d}\theta)} \tag{4.13}$$

The model has been validated for the Hermes–Columbus Free-Flyer scenario in Retali (1990) Typical values of the 1σ half cone angle θ_0 are of the order of 13 deg.

Accelerations due to plume interaction from one spacecraft on another one can (at short distance) be one to two orders of magnitude higher than that of air drag. Braking boosts close to the spacecraft, where the plume is directed toward the target vehicle, must therefore be avoided. Attitude control thrust could be in all directions, but the single thrusts are relatively short in time. Force and torques exerted on the target vehicle by such thrusts can properly be evaluated only by closed loop simulation of the chaser GNC operation, with detailed modelling of spacecraft geometry, thruster locations and thruster plumes.

4.3 Trajectory deviations generated by the spacecraft systems

The following discussion of trajectory deviations, caused by errors of systems or equipment, assumes that all manoeuvres are performed in open loop. The intention is, for each type of error to establish equations, which allow the assessment of type and magnitude of the trajectory deviation caused. Numerical examples are given to provide an understanding of the magnitude of the error effects.

4.3.1 Trajectory deviations due to navigation errors

As stated in section 4.1.3, navigation errors are the deviations of the measured or predicted state vector of the vehicle from the real one. Such deviations can result from alignment errors between the sensor and the spacecraft axes, from measurement performance limitations of the sensors used (see chapter 7), from aberrations caused by the measurement environment, and from performance limitations of the information processing in the navigation filter (see section 6.2.1). The parameters to be measured are position, linear velocities, attitude and angular rates. The following discussion will identify the trajectory uncertainties and errors, which may occur as a result of such measurement errors after a certain time of motion.

Position measurement errors

Position measurement errors in the *x*-direction have no further effects on the trajectory development than the position error itself. Position errors in the *y*-direction will result, according to Eqs. (3.27), in a sinusoidal development of the error over time. Position errors in the *z*-direction can have two effects depending on the *x*-velocity at measurement: either they will result, according to Eqs. (3.25), in an error of the velocity in the *x*-direction without further errors in *z*, or they will result, according to Eqs. (3.26), in a looping motion with significant *z* excursions.

- Measurement error $\Delta x_{\mathrm{m}} \Longrightarrow$ trajectory error of

$$\Delta x_{\mathrm{m}} \tag{4.14}$$

- Measurement error $\Delta y_{\mathrm{m}} \Longrightarrow$ trajectory error of

$$\Delta y(t) = \Delta y_{\mathrm{m}} \cos(\omega t) \tag{4.15}$$

- Measurement error $\Delta z_{\mathrm{m}} \Longrightarrow$ trajectory error of

$$\Delta x(t) = \frac{3}{2} \omega \Delta z_m t \tag{4.16}$$

  if the chaser is on a circular orbit below or above the target orbit, i.e. moving with the velocity belonging to this orbit.

- Measurement error $\Delta z_m \Longrightarrow$ trajectory errors of

$$\begin{aligned} \Delta x(t) &= 6\Delta z_m(\omega t - \sin(\omega t)) \\ \Delta z(t) &= \Delta z_m(4 - 3\cos(\omega t)) \end{aligned} \tag{4.17}$$

  if the chaser is moving with the same velocity as the target.

For error assessments, both possibilities of a measurement error in the *z*-position must be taken into account as extreme cases, if the velocity measurement accuracy does not permit a clear distinction.

Example: Initial position measurement error in the z-direction of 10 m

If the chaser is moving on a parallel orbit:

- the position uncertainty in the *x*-direction according to Eqs. (3.25) after one orbital revolution is 94.25 m;
- the uncertainty in the velocity V_x according to Eq. (3.24) will be 0.01 m/s after one orbital revolution;

If the chaser is moving with the same velocity as the target:

- the uncertainty in the z-direction will be a maximum of 70 m after half an orbital revolution;
- the uncertainty in the x-direction is 370 m after one revolution.

To assess the potential error ellipsoid along the trajectory, the worst values of both cases would have to be considered, if the actual velocity cannot be measured with sufficient accuracy.

Velocity measurement errors

The effects of velocity measurement errors are the same as those of an initial velocity in a certain direction. Trajectory deviations due to velocity errors in the x-direction follow from Eq. (3.28) due to velocity errors in the y-direction from Eq. (3.40) and due to velocity errors in the z-direction from Eq. (3.34). The position errors are a linear function of the velocity error.

- Measurement error $\Delta V_{xm} \Longrightarrow$ trajectory errors of

$$\begin{aligned} \Delta x(t) &= \Delta V_{x\mathrm{m}} \left(\frac{4}{\omega} \sin(\omega t) - 3t \right) \\ \Delta z(t) &= \frac{2}{\omega} \Delta V_{x\mathrm{m}} (\cos(\omega t) - 1) \end{aligned} \tag{4.18}$$

- Measurement error $\Delta V_{y\mathrm{m}} \Longrightarrow$ trajectory error of

$$\Delta y(t) = \frac{1}{\omega} \Delta V_{y\mathrm{m}} \sin(\omega t) \tag{4.19}$$

- Measurement error $\Delta V_{z\mathrm{m}} \Longrightarrow$ trajectory errors of

$$\begin{aligned} \Delta x(t) &= \frac{2}{\omega} \Delta V_{z\mathrm{m}} (1 - \cos(\omega t)) \\ \Delta z(t) &= \frac{1}{\omega} \Delta V_{z\mathrm{m}} \sin(\omega t) \end{aligned} \tag{4.20}$$

For the following examples a 400 km orbit is assumed.

Example: Velocity measurement error in the x-direction

The position error will evolve according to the trajectory type shown in figure 3.15 for a ΔV in the x-direction. A velocity measurement error of 0.01 m/s in the x-direction results in a position error in the x-direction of 166 m per orbit and in a maximum of the position error in the z-direction (double amplitude) of 35 m after half an orbit.

Example: Velocity measurement error in the z-direction

The position error will evolve according to the trajectory type shown in figure 3.20 for a ΔV in the z-direction. A velocity measurement error of 0.01 m/s in the z-direction results in a maximum of the position error in the x-direction of 35 m after half an orbit and in an amplitude of the position error in the z-direction of 8.8 m after one quarter orbit.

Example: Velocity measurement error in the y-direction

The position error will evolve according to the trajectory type shown in figure 3.23 for a ΔV in the y-direction. A velocity measurement error of 0.01 m/s in the y-direction results in an amplitude of the position error in the y-direction of 8.8 m after one quarter orbit.

Attitude and angular rate measurement errors

Attitude errors have no direct effect on the trajectory evolution. However, they do have an effect on the trajectory during boost manoeuvres, as they result in undesirable components of the thrust in directions other than the intended ones. This case is treated in section 4.3.2 under 'thrust direction errors'.

Angular rates have no direct effect on the trajectory evolution, except for the attitude achieved at the boost manoeuvre (see above).

4.3.2 Trajectory deviations due to thrust errors

Thrust errors can be caused by errors in the magnitude of the thrust force (ΔF), in the actual mass of the spacecraft (Δm), in the thrust duration (Δt) and in the thrust direction ($\Delta \alpha$) w.r.t. the values assumed in the calculation. These errors can be due to mounting errors, to misalignments of the exhaust flow velocity vector w.r.t. the mechanical axis of the nozzle, to impingement of the thrust plumes on the structure of the own spacecraft, to deviation of the actual specific impulse from the nominal one, to non-linearities of the delivered ΔV w.r.t the valve opening time, etc.

Thrust force and duration errors

The applied thrust force per unit mass is

$$\gamma_{\mathrm{t}} = \frac{F_{\mathrm{t}}}{m_{\mathrm{c}}}$$

where F_t is the nominal thrust force and m_c is the mass of the spacecraft. The actual thrust force per unit mass including errors can be defined as

$$\begin{aligned} \gamma &= \gamma_\mathrm{t} + \Delta\gamma \\ \gamma &= \gamma_\mathrm{t}\,\epsilon_\gamma \end{aligned}$$

where γ_t is the nominal thrust force/mass and ϵ_γ is the thrust error factor,

$$\epsilon_\gamma = 1 + \frac{\Delta\gamma}{\gamma_t}$$

If the thrust error is due to the assumed thrust force level, then

$$\epsilon_\gamma = 1 + \frac{\Delta F}{F_\mathrm{t}}$$

If the thrust error is due to an error of the assumed mass, then

$$\epsilon_\gamma = 1 + \frac{m_\mathrm{c}}{\Delta m}$$

The actual duration of the thrust, including errors, can be defined as

$$\begin{aligned} t &= t_\mathrm{t} + \Delta t \\ t &= t_\mathrm{t}\,\epsilon_\mathrm{t} \end{aligned}$$

where t_t is the nominal thrust duration and ϵ_t is the duration error factor,

$$\epsilon_t = 1 + \frac{\Delta t}{t_t}$$

Resulting position and velocity errors

The actual position x_act and the actual velocity $\dot{x}_\mathrm{act}$ may be similarly defined:

$$\begin{aligned} x_\mathrm{act}(t) &= x_\mathrm{th} + \Delta x \\ x_\mathrm{act}(t) &= x_\mathrm{th}\,\epsilon_x \end{aligned}$$

where x_th is the nominal x-component and $\epsilon_x =$ trajectory error factor,

$$\epsilon_x = 1 + \frac{\Delta x}{x_\mathrm{th}}$$

and

$$\begin{aligned} \dot{x}_\mathrm{act}(t) &= \dot{x}_\mathrm{th} + \Delta\dot{x} \\ \dot{x}_\mathrm{act}(t) &= \dot{x}_\mathrm{th}\,\epsilon_{Vx} \end{aligned}$$

where $\dot{x}_{\rm th}$ is the nominal x-component and ϵ_{Vx} is the velocity error factor,

$$\epsilon_{Vx} = 1 + \frac{\Delta\dot{x}}{\dot{x}_{\rm th}}$$

(correspondingly for y, z, $\dot{y}$, $\dot{z}$).

Using the above relations, the equations of motion for continuous thrust manoeuvres with deviations due to thrust errors become as follows.

Thrust in the x-direction The actual trajectory with thrust errors ($x_{\rm th}$, $z_{\rm th}$ from Eq. (3.59)) is

$$\begin{aligned} x_{\rm act}(t) = x_{\rm th}(t)\,\epsilon_x &= \gamma_x\epsilon_\gamma\left(\frac{4}{\omega^2}(1-\cos(\omega t_{\rm t}\epsilon_{\rm t})) - \frac{3}{2}t_{\rm t}^2\epsilon_{\rm t}^2\right) \\ z_{\rm act}(t) = z_{\rm th}(t)\,\epsilon_z &= \frac{2}{\omega^2}\gamma_x\epsilon_\gamma(\sin(\omega t\epsilon_{\rm t}) - \omega t\epsilon_{\rm t}) \end{aligned} \tag{4.21}$$

The actual velocities with thrust errors ($\dot{x}_{\rm th}$, $\dot{z}_{\rm th}$ from Eq. (3.60)) are

$$\begin{aligned} \dot{x}_{\rm act}(t) = \dot{x}_{\rm th}(t)\,\epsilon_{Vx} &= \gamma_x\epsilon_\gamma\left(\frac{4}{\omega}\sin(\omega t\epsilon_{\rm t}) - 3t\epsilon_{\rm t}\right) \\ \dot{z}_{\rm act}(t) = \dot{z}_{\rm th}(t)\,\epsilon_{Vz} &= \frac{2}{\omega}\gamma_x\epsilon_\gamma\left(\cos(\omega t\epsilon_{\rm t}) - 1\right) \end{aligned} \tag{4.22}$$

Thrust in the y-direction The actual trajectory with thrust errors ($y_{\rm th}$ from Eq. (3.75)) is

$$y_{\rm act}(t) = y_{\rm th}(t)\,\epsilon_y = \frac{1}{\omega^2}\gamma_y\epsilon_\gamma(1-\cos(\omega t\epsilon_{\rm t})) \tag{4.23}$$

The actual velocities with thrust errors ($\dot{y}_{\rm th}$ from Eq. (3.76)) are

$$\dot{y}_{\rm act}(t) = \dot{y}_{\rm th}(t)\,\epsilon_{Vy} = \frac{1}{\omega}\gamma_y\epsilon_\gamma\sin(\omega t\epsilon_{\rm t}) \tag{4.24}$$

Thrust in the z-direction The actual trajectory with thrust errors ($x_{\rm th}$, $z_{\rm th}$ from Eq. (3.66)) is

$$\begin{aligned} x_{\rm act}(t) = x_{\rm th}(t)\,\epsilon_x &= \frac{2}{\omega^2}\gamma_z\epsilon_\gamma(\omega t\epsilon_{\rm t} - \sin(\omega t\epsilon_{\rm t})) \\ z_{\rm act}(t) = z_{\rm th}(t)\,\epsilon_z &= \frac{1}{\omega^2}\gamma_z\epsilon_\gamma(1-\cos(\omega t\epsilon_{\rm t})) \end{aligned} \tag{4.25}$$

The actual velocities with thrust errors ($\dot{x}_{\rm th}$, $\dot{z}_{\rm th}$ from Eq. (3.67)) are

$$\begin{aligned} \dot{x}_{\rm act}(t) = \dot{x}_{\rm th}(t)\,\epsilon_{Vx} &= \frac{2}{\omega}\gamma_z\epsilon_\gamma\left(1-\cos(\omega t\epsilon_{\rm t})\right) \\ \dot{z}_{\rm act}(t) = \dot{z}_{\rm th}(t)\,\epsilon_{Vz} &= \frac{1}{\omega}\gamma_z\epsilon_\gamma\sin(\omega t\epsilon_{\rm t}) \end{aligned} \tag{4.26}$$

From the above equations it follows immediately that errors in the applied force per unit mass lead to directly proportional errors in trajectory and velocity. Errors in thrust duration, on the other hand, repercuss on the development of trajectory and velocities via the more complex time dependent terms in the above equations.

Thrust duration errors are for all nominal operations very small, as time can be measured very accurately and delays due to valve operations are low. Nevertheless, there is one case where thrust duration errors are important, i.e. in the case of 'thruster-open' failures. In such cases, the failure condition can be detected usually only by observation of secondary effects, such as temperature and pressure in the thruster, saturation of control commands, state vector deviations, etc. Detection of 'thruster-open' failure may, therefore, take some time, during which thrust continues to the full extent.

Examples

In the following examples only the position and velocity errors due to thrust duration errors are considered. The absolute values of γ and ω do not play a role as they are identical for the actual and theoretical values. The position and velocity errors are, according to Eqs. (4.21)–(4.26), a function of time. The examples have been calculated for a nominal thrust duration of 10% of the orbital revolution ($\approx$ 550 s in a 400 km orbit) and a thrust duration error of 5% . At the end of the thrust the trajectory and velocity errors are as follows:

X-thrust	$\epsilon_x = 1.086$ (8.6 % error)	$\epsilon_{Vx} = 1.014$ (1.4 % error)
	$\epsilon_z = 1.155$ (15.5 % error)	$\epsilon_{Vz} = 1.099$ (9.9 % error)
Y-thrust	$\epsilon_y = 1.099$ ((9.9 % error)	$\epsilon_{Vy} = 1.043$ (4.3 % error)
Z-thrust	$\epsilon_x = 1.155$ (15.5 % error)	$\epsilon_{Vx} = 1.099$ (9.9 % error)
	$\epsilon_z = 1.099$ (9.9 % error)	$\epsilon_{Vz} = 1.043$ (4.3 % error)

A thrust duration for a single manoeuvre of one tenth of an orbital revolution ($\approx$ 9 min) is very long and a duration error of 5% (27 s) is of course, even for detection of thruster failures, very high. These values have been chosen simply to demonstrate the effects. For thrust durations which are fractions of one orbital revolution, the errors will of course be different. The example shows, however, that the relative trajectory and velocity errors may, depending on the direction of thrust, be much higher than the relative duration error.

Thrust direction errors

Thrust direction errors can be caused by the attitude error of the vehicle w.r.t. the orbital frame, by geometric misalignment of the thruster hardware, or by a misalignment of the thrust vector w.r.t. the centre line of the thruster nozzle. This latter may be caused by flow-dynamic asymmetries. As in the case of attitude measurement errors, thrust direction errors lead to a component of thrust in a perpendicular direction.

Example

For a ΔV of 1 m/s, an attitude error of 1 deg results in an undesired component in a perpendicular direction of 0.0175 m/s, with the effects described above under 'Resulting position velocity errors'. For an impulsive manoeuvre in a 400 km orbit, e.g., the position error in the *x*-direction would be approximately 290 m per orbit, and the amplitude in the *z*-direction would be about 31 m.

For finite thrust manoeuvres, the direction of the applied force vector has to be taken into account:

$$\Delta\gamma_{\perp} = \gamma_{\mathrm{t}} \sin \Delta\alpha_{\mathrm{t}} \tag{4.27}$$

where $\Delta\alpha_{\mathrm{t}}$ is the direction error.

Depending on the original thrust direction and on the direction of the error angle, the corresponding trajectory and velocity errors in a perpendicular direction can be obtained by inserting the value found for $\Delta\gamma_{\mathrm{t}}$ into Eqs. (3.59)–(3.76), as in the previous cases.

4.3.3 Trajectory deviations due to thruster failures

Under the term 'thruster failure', as explained in section 4.1.3, two failure conditions are understood; these correspond to the inability to close the thruster valves at the end of operation (*thruster-open failure*) and to the inability to open the valves for operation (*thruster-closed failure*). Other failure conditions, where a thruster permanently produces a partial thrust level, are qualitatively equivalent to a thruster-open failure.

Thruster-open failure

A rendezvous vehicle must have the capability of producing control forces in all directions and will have an according combination of thrusters. Depending on the direction of the failed thruster, thruster-open failures, if not counteracted in time, can lead to any type of trajectory. The magnitude of the eventual trajectory and velocity errors depends on the duration of the failure condition. As a result, there is no other protection against thruster-open failures but to detect this failure condition as early as possible and to stop the thrust force (see section 4.4.1). The residual maximum possible trajectory and velocity errors can then be calculated from the worst case time difference between failure occurrence and closure of the faulty thruster (see the remark about thrust duration errors in section 4.3.2).

Thruster-closed failure

Thruster-closed failures, if no more redundancy is available and if not resolved in time, lead to loss of attitude control around one axis and loss of trajectory control in one direction. A resulting uncontrolled angular motion about this axis may, after time, cause a coupling of trajectory control forces from one axis in the others, resulting in trajectory deviations. The effects of an unresolved thruster-closed failure are, in the short term,

the inability to perform a planned trajectory manoeuvre and, in the longer term, the loss of attitude and the build-up of trajectory deviations. If the failed thruster can be identified, and as long as redundancy is available, the obvious solution is to inhibit the failed thruster and to switch over to a redundant one. Otherwise, a certain protection against the long term effects of thruster-closed failures concerning the collision with the target spacecraft would be the inhibition of all thrusters, provided the resulting trajectory would be collision-free (see section 4.4.2).

4.4 Protection against trajectory deviations

According to the failure tolerance requirements and design rules discussed in section 4.1.1, the trajectory strategy has to be designed such that if, due to errors and failures, the planned trajectory cannot be maintained, the resulting motion of the chaser vehicle will not lead to collision with the target. To ensure adherence to the planned trajectory, considering the various causes of trajectory deviations and the possibility of thruster failures as discussed above, the active detection and correction of trajectory deviations is the sole option (*active trajectory protection*). If it is no longer possible, for whatever reasons, to maintain this active protection, it must be attempted to keep the vehicle on a 'safe trajectory', i.e. a trajectory which remains collision-free when all thrust is inhibited (*passive trajectory protection*). This would also be the ultimate protection of the target vehicle against collision in the case of a complete loss of all control functions (examples would be the complete loss of power, an explosion or (e.g.) damage by meteorite or debris impact). However, not all parts of the approach trajectory sequence can be protected in this way. When the approaching vehicle is in very close proximity to the target, trajectories are designed 'to make contact', whether directly with a particular location on the target geometry (docking), or with a virtual 'reception box' in the very close vicinity (berthing). In such cases only an active *collision avoidance manoeuvre* (CAM) by the chaser can provide the required protection of the target vehicle. It should be pointed out that there are limitations concerning the range down to which a CAM can be defined. These may be given on one hand by the distance required for braking and on the other hand by thermal loads and contamination of the target surface due to the thruster plume of the CAM. As a result, a CAM cannot be used during the last metre prior to contact.

4.4.1 Active trajectory protection

Active trajectory protection requires the detection and correction in time of trajectory deviations. This principle of closed loop detection and correction is already applied in practically all spacecraft for attitude control. Another convenient solution to the problem of the control of trajectory deviations would be for the evolution of the trajectory to be closed loop controlled. Such active control is usually performed for forced trajectories, such as straight line V-bar and R-bar approaches and manoeuvres. This principle

can also be applied, however, to free drift and impulsive trajectories. In these cases the evolution of the nominal trajectory and velocities over time will be pre-calculated and closed loop controlled within narrow margins (controlled nominal trajectory scheme). As attitude and angular rate will also be closed loop controlled, the control of the spacecraft's state vector would comprise the control of a total of 12 values, i.e. three positions, three velocities, three angles and three angular rates. For two-pulse manoeuvres, the

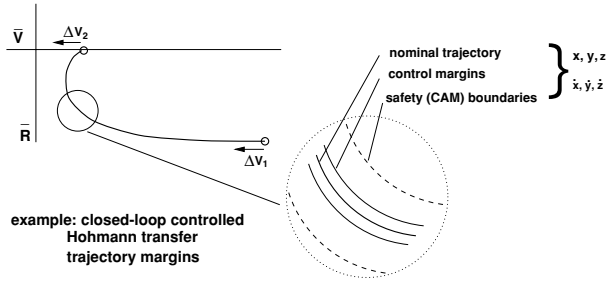

Figure 4.8. Example of the monitoring of safety of state vector: Hohmann transfer.

boost phases of the transfer can also be closed loop controlled. In this case the boosts are entered as feed-forward commands into the control loop by the guidance function (see chapter 7), while the controller minimises the control error w.r.t. the pre-calculated nominal trajectory. In order to keep the control effort small, known disturbances such as differential drag can be included in the calculation of the 'nominal' trajectory, where by nominal we mean 'to the extent known'.

Other methods of trajectory protection for free drift and impulsive manoeuvres include the application of one or more 'mid-course manoeuvres', where corrective ΔVs will be applied to achieve the intended final position. Compared with the continuous control of the nominal trajectory, a scheme with a few mid-course correction manoeuvres will of course result in a lower propellant consumption, which is why it is often preferred to the 'continuous nominal trajectory control scheme'.

A special case of this 'mid-course manoeuvre' strategy is the 'continuous targeting scheme', where the final position is continuously closed loop controlled, i.e. for each control cycle the ΔVs to reach this point are calculated from the instantaneous position, velocities and time.

During the rendezvous phase, i.e. in proximity of the target, the two latter schemes must be considered less safe than the 'controlled nominal trajectory scheme', as only the final position is actively controlled rather than the state vector at each point of the trajectory. In case of failure of the control system, all state vector values are, at the instance of failure, for the 'controlled nominal trajectory scheme' still nominal, whereas, for the 'continuous targeting scheme' the deviation of the actual from the nominal state vector values is uncontrolled. This can have repercussions on the validity of the passive trajectory protection concept (see the following section), the concept of which is based

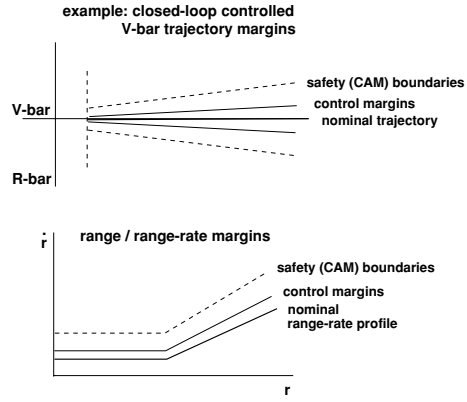

Figure 4.9. Example of monitoring of safety of state vector: V-bar approach.

on the nominal evolution of trajectories plus certain margins.

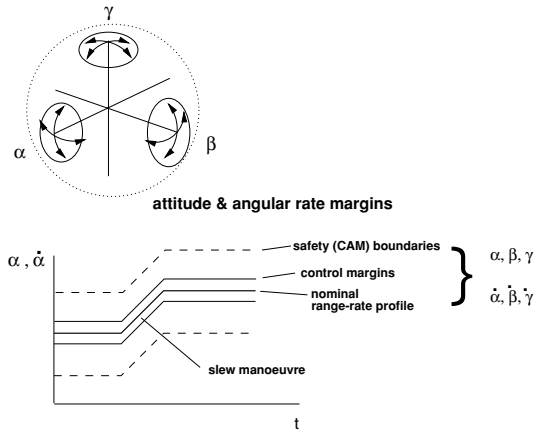

Figure 4.10. Monitoring of safety of state vector, attitude and attitude rate.

Closed loop control of a nominal trajectory also allows easy implementation of criteria for the initiation of a CAM. If the pre-calculated boundaries of safety margins around the nominal state vector values have been reached, the trajectory will be judged 'unsafe' (whether by the onboard system or by human observers) and a CAM will be commanded. For other schemes, safety criteria for position and velocities are more difficult to establish, and, in the case of the 'continuous targeting scheme', would have to be re-calculated continuously. Figures 4.8, 4.9 and 4.10 show schematically the con-

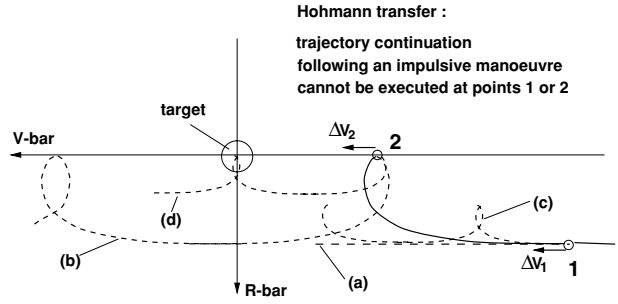

Figure 4.11. Passively safe trajectories: Hohmann transfer.

trol margins and safety boundaries for an impulsive transfer trajectory for a straight line V-bar approach with velocity profile and for attitude control.

Other important trajectory elements of the rendezvous phase, which require closed loop control and safety boundary monitoring, are hold points. If not actively controlled, a drift motion as shown in figure 4.3 will commence. Active trajectory protection requires sufficiently accurate navigation information on all state vector values throughout the entire duration of the trajectory element.

4.4.2 Passive trajectory protection

The basic idea of passive trajectory protection is, as stated above, to design all trajectory elements in an approach trajectory sequence such that if, at any point of the trajectory, thrust control ceases, the resulting 'free trajectory' will remain collision-free for TBD time. Such a property would not only be protection against the case of total disablement of the approaching vehicle, but would also allow the implementation of a straightforward and effective way of achieving collision safety by simply commanding the thrust to stop. Actually, a complete inhibition of thrust may often be the sole possible immediate action after thruster-open failures and malfunction of the control system, as long as the failure source has not been identified. This concept, of course, will not work in the very close vicinity of the target. Eventually the chaser vehicle will be so close that actual limits are determined by the geometric extensions of the two vehicles and by the absolute value and control margins of their motion. Unfortunately also prior to this closest range for passive trajectory safety, thrust failures can cause trajectory evolutions, which may lead to collision with the target. In the following, various types of trajectories will be analysed concerning their passive safety properties for thruster-closed failures (thruster-open failures must be dealt with by active means; see section 4.3.3). The examples shown in figures 4.11–4.14, are given for an approach on $-$V-bar. For an approach on +V-bar the trajectories have to be mirrored on both the V-bar and R-bar axes.

Hohmann transfer

The first type of trajectory to be analysed is the transfer to a different altitude by a two-pulse tangential thrust manoeuvre, i.e. a Hohmann transfer (figure 4.11). The first boost is to be applied at point 1 in the +V-bar direction, and the second, at point 2 after one half revolution, must be of the same magnitude and direction to stop the motion at the new z-position. To achieve the required ΔV, the available thrust force γ_x has to be applied during the nominal thrust time t (see the equations of motion (3.59)). The following failure cases have to be considered:

(1) When the first boost (ΔV_1 at point 1) cannot be executed, the trajectory continues as a free drift (trajectory (a)). This trajectory is safe w.r.t. collision.

(2) When the second boost (ΔV_2 at point 2) cannot be executed, the trajectory continues looping with an apogee at V-bar and a perigee at the z-distance of point 1 (trajectory (b)). The x-positions of point 1 and point 2 have to be chosen in such a way that the next following perigee will be near the x-location of the target and the next following apogee will be in front of the target. Under these conditions this trajectory is safe w.r.t. collision.

(3) When control ceases somewhere between the first and the second boost, the result is the same as for (2), i.e. trajectory (b).

(4) When the first boost is interrupted somewhere within its nominal duration, the motion in the x-direction up to the first apogee will be shorter, but also the z-position of the apogee will be lower (trajectory (c)). Only in cases involving a very large extension of the target geometry in the z-direction might there be a danger of collision. By adapting the position of point 1 accordingly, this can be avoided for each individual case. Under these conditions this trajectory is safe w.r.t. collision.

(5) When the second boost is interrupted somewhere within its nominal duration, the trajectory will not stop at point 2 but will continue with smaller loops with an apogee very near to V-bar and a perigee depending on the percentage of the planned second boost realised (trajectory d). In this case a very large region within the nominal duration of the second boost, where propulsion is stopped, could lead to collision with the target. This part of a Hohmann transfer cannot be rendered passively safe. The sole protection against a thruster-closed failure during the second boost is a CAM.

Tangential thrust transfer along V-bar

The second type of trajectory to be analysed here is a transfer along V-bar by two tangential boosts (figure 4.12). The first boost (thrust force γ_x over nominal thrust duration t, Eqs. (3.59)) to be applied in point 1 is in the $-$V-bar direction, and the second, at point

2 after one orbital revolution, is of the same magnitude but in the opposite direction to stop the motion at the new x-position.

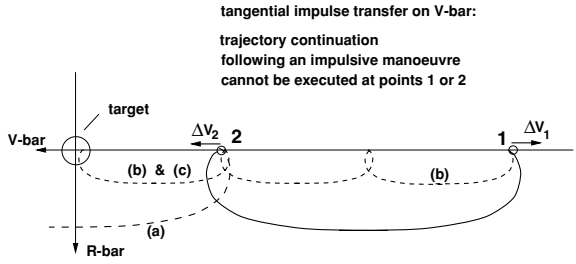

Figure 4.12. Passively safe trajectories: tangential boost transfer.

The following failure cases have to be considered:

(1) When the first boost at point 1 cannot be performed, the vehicle remains at that point. This condition is safe (for the influence of differential drag see below).

(2) When the second boost (ΔV_2 at point 2) cannot be executed, the trajectory continues looping with an apogee at V-bar and a perigee at the z-distance of point 1 (trajectory (a)). This situation is very similar to the case of the Hohmann transfer, discussed in the first example. The x-positions of point 1 and point 2 have to be chosen in such a way that the next following perigee will be near the x-location of the target and the next following apogee will be in front of the target. Under these conditions this trajectory is safe w.r.t. collision.

(3) When control ceases somewhere between the first and the second boost, the result is the same as for (2), i.e. trajectory (a).

(4) When the first boost is interrupted somewhere within its nominal duration, the trajectory will start with smaller loops, with an apogee at V-bar and a perigee depending on the percentage of the planned first boost that has been realised (trajectory (b)). For a propulsion failure which cannot be resolved within one orbital revolution, the trajectory continues looping, with a large chance that at one of the following apogees the target is hit, or that the perigee is of the same order of magnitude as the extension of the target geometry in the z-direction and the target will be hit in any case. This case is unsafe. The sole protection against a thruster-closed failure during the first boost of the tangential thrust V-bar transfer is a CAM.

(5) When the second boost is interrupted somewhere within its nominal duration, the situation is identical to the previous one: the trajectory continues looping, with a large chance that the target is hit at one of the following apogees, or that the

perigee distance is so small that the target will be hit anyway (trajectory (c)). Again, the sole protection is a CAM.

The analysis shows that the tangential thrust transfer on V-bar has relatively bad passive safety properties, as a thruster-closed failure at partial burns (of both burns) can lead to collision. The tangential thrust type of trajectory is, for this reason, less suitable as the trajectory element for close range approach. For other purposes, however, this trajectory may have advantages w.r.t. ground station visibility (communication window) and illumination conditions. Due to its transfer time of one orbit, such conditions may be equal or similar in the following revolution.

Radial thrust transfer along V-bar

The third type of trajectory to be analysed for passive safety is the transfer on V-bar by radial impulses, as shown in figure 4.13. The first boost (thrust force γ_z over nominal thrust time t, Eqs. (3.66)) is to be applied at point 1 in the +R-bar direction, and the second, at point 2 after one half orbital revolution, has to be of the same magnitude and direction.

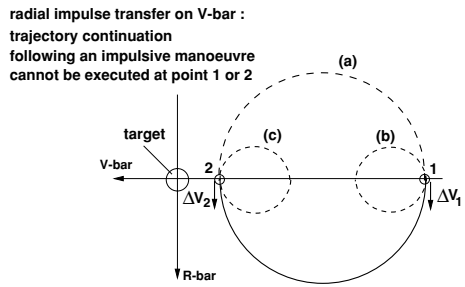

Figure 4.13. Passively safe trajectories: radial boost transfer.

The following failure cases have to be considered:

(1) When the first boost at point 1 cannot be performed, the vehicle remains at that point. This condition is safe (for the influence of differential drag see below).

(2) When the second boost at point 2 cannot be performed, the trajectory will return after each orbit, if no disturbance forces are acting, to the starting point 1 (trajectory (a)). This trajectory is safe w.r.t. collision in the short term. This also means that under the influence of differential drag the trajectory will not hit the target for at least one orbital revolution or more, the number of revolutions depending on the ratio of ballistic coefficients of the two vehicles and on the distance between point 2 and the target.
If the ratio of the ballistic coefficients of chaser and target is such that an average motion toward the target would result, an additional small tangential boost in

the $+x$-direction can be applied at point 1 to ensure that the trajectory will, on average, move away from the target, at least for a number of orbital revolutions.

(3) When control ceases somewhere between the first and the second boost, the result is the same as for (2), i.e. trajectory (a).

(4) When the first boost is interrupted somewhere within its nominal duration, the motion in the x-direction up to the first return to V-bar will, depending on the percentage of the planned first boost that has been realised, be shorter, and the trajectory will, if not stopped, loop between this point and point 1 (trajectory (b)). The trajectory is safe in the same way as in failure case (1), except that the shortest distance to the target is larger.

(5) When the second boost is interrupted somewhere within its nominal duration, the trajectory will loop back after half an orbit to a point on V-bar between point 1 and point 2, depending on the percentage of the planned second boost that has been realised. It would return without drag after each following revolution to point 2. The trajectory is safe in the same way as in failure case (1).

Straight line V-bar and R-bar approaches

The next class of trajectories to be analysed comprises the straight line forced motion trajectories used for V-bar and R-bar final approaches to the docking port or to a berthing position at the target. These types of trajectories (see section 3.3.3) require the continuous application of thrust to counteract the Coriolis forces. If these thrust forces are stopped, the resulting trajectories are as shown in figures 3.13 and 3.14.

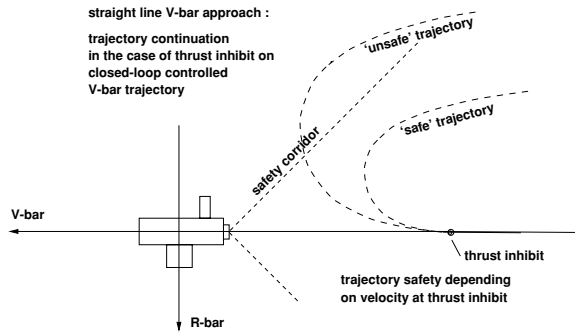

Figure 4.14. Passively safe trajectories: V-bar approach.

The passive safety of these trajectories depends on the approach velocity and on the distance from the docking port of the target. The trajectory can be kept safe by reducing the velocity according to the distance from the target. However, as (a) the target has a geometric extension in the $+$ and $-z$-directions, (b) trajectory and velocity control

margins have to be taken into account and (c) in the case of docking a final velocity has to be maintained, the last part of a straight line final approach trajectory cannot be made passively safe in this way. In addition, safety corridors may have to be observed (see also section 5.6). The situation w.r.t. safety corridors of free drift trajectories after inhibiting thrust forces is shown schematically in figure 4.14. For all these practical reasons, in the last 100 m of the approach passive trajectory safety cannot be relied on, and the sole protection, when active trajectory control has failed, is a CAM.

Long term trajectory safety

In the above discussion of the various trajectories concerning passive trajectory safety, no trajectory disturbance forces have been considered, and it was sufficient, for assessing trajectory safety, to look at the trajectory evolution for only one or very few orbital revolutions. However, as in reality drag forces are always present, the obtained results can be valid only for a short time. In the example shown in figure 4.15, where the trajectory starts with a tangential impulse of $\Delta V = 0.06$ m/s, it returns after about ten orbital revolutions to its origin. In this example an average density of 9.4×10^{-12} $\mathrm{km/m^3}$ has been assumed, which is similar to that assumed for the examples shown in figures 4.2–4.5. The ballistic coefficient of the chaser is again $C_{\mathrm{BC}} = 470$ kg/m^2 and the ratio of the ballistic coefficients of chaser and target is assumed to be $C_{\mathrm{Bc}}/C_{\mathrm{Bt}} = 5$. The direction and magnitude of the long term effect of the differential drag on the

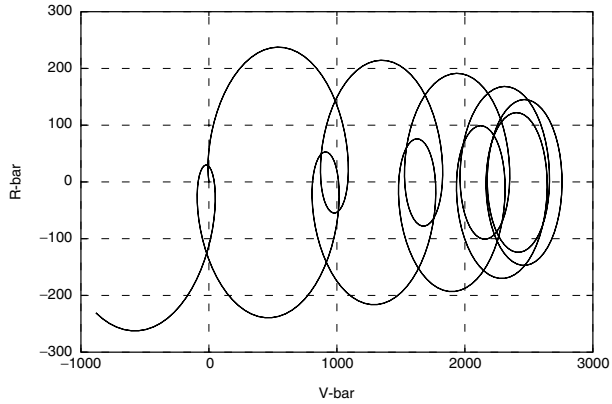

Figure 4.15. Tangential impulse -0.06 m/s with differential drag (400 km orbit).

trajectory development of the chaser depends, of course, on the value of $C_{\mathrm{Bc}}/C_{\mathrm{Bt}}$ (see Eq. (4.3)), as already shown in figures 4.3–4.5. Because of the differential drag effects, the approach from the $-$V-bar side is generally safer for a chaser with a higher C_{B} (and vice versa).

4.5 Collision avoidance manoeuvres

It has been identified above that the execution of a CAM will become necessary when active trajectory control has failed and when the present trajectory, or the present part of it, is not passively safe. Failure of active trajectory control can be caused by a number of reasons, e.g. by sensors, thrusters, GNC functional problems, software problems, etc. Such failures can be identified either on the level of the hardware and software functions involved in the process, or, e.g., by detection of violation of the safety margins of the various nominal state vector values, as discussed above (see also section 6.4).

Detection of contingencies due to violation of safety margins and corridors or due to loss of functions may be performed both by the onboard system and by remote human operators in the target spacecraft or on ground (see also section 9.1.2). After detection of a contingency case, a scheme for recovery could consist of the following steps:

(1) Switch to the redundant single equipment if the faulty equipment can be identified.

(2) Switch to the redundant string if the failure cannot be isolated. This includes switching to a redundant processor with identical rendezvous control software.

(3) If problems cannot be solved by redundancy switching, and the danger of collision still exists, either execute a CAM or inhibit trajectory control actuation, to leave the vehicle on a safe drift trajectory (if available).

In order to fulfil the failure tolerance requirements discussed in sections 4.1.1 and 4.1.2, the onboard system for rendezvous control and its constituents must of course provide sufficient redundancy. For essential equipment, such as data management equipment, reaction control system hardware, gyros, etc., double redundancy must be available.

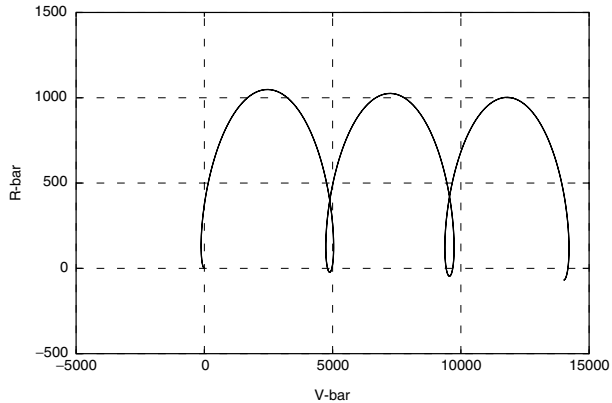

Figure 4.16. CAM on −V-bar: 0.3 m/s $-x$-boost, influence of differential drag.

As a collision avoidance manoeuvre must still function when the GNC system has failed or is malfunctioning, such a manoeuvre must be as simple as possible and be executable with a minimum of onboard resources. The simplest case is a single boost in the opposite approach direction. As such a manoeuvre is not very sensitive to the attitude (even at an attitude error of 15 deg, the cosine is still 0.966, i.e. the reduction in thrust is less than 4%), the thrust manoeuvre can be assigned to a fixed direction in the spacecraft geometric frame $\boldsymbol{F}_{\mathbf{ge}}$ instead of the local orbital frame $\boldsymbol{F}_{\mathbf{lo}}$. Then, no functioning onboard GNC system is required, since the operation consists only of addressing the specific thrusters and opening the thruster valves for a fixed time period.

An example of a CAM for a $-$V-bar approach is shown in figure 4.16. The CAM consists of an application of a ΔV in the $-x$-direction. The drag conditions are assumed to be the same as in figure 4.15, i.e. the average density is $9.4 \times 10^{-12}\ \mathrm{km/m^3}$ and the ratio of ballistic coefficients is $C_{\mathrm{Bc}}/C_{\mathrm{Bt}} = 5$. The boost is five times as strong as in figure 4.15, and the relative influence of differential drag is accordingly lower. For an approach on $+$V-bar, the same type of manoeuvre in the $+x$-direction would be applied, with the resulting trajectory mirrored on the *x*- and *z*-axes.

The amount of ΔV to be applied for a CAM depends on (a) the geometric extension of the target in the *z*-direction, (b) the relative velocity the chaser has at CAM initiation (or the maximum velocity of the trajectory element for which the CAM shall be valid) and (c) the time for which the CAM trajectory must be guaranteed collision-free. The primary requirement, i.e. to render the escape trajectory collision-free over the next few orbits, can be fulfilled with relatively small ΔVs. For very large chaser to target C_{B} ratios of 5–10, and for guaranteed collision protection over a long duration, such as 24 h, ΔVs of more than 1 m/s may be required for a V-bar CAM.

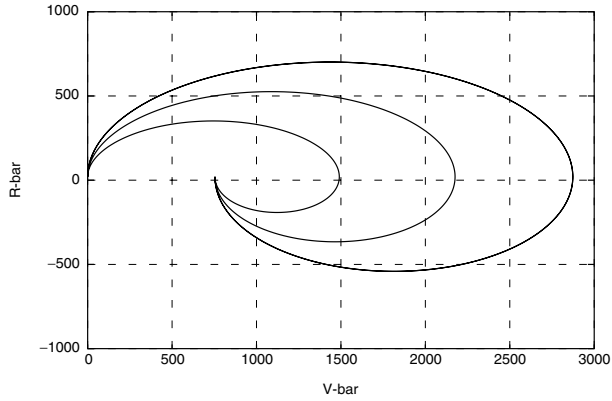

Figure 4.17. CAM on R-bar: $\Delta V_z = 0.3,\ 0.5,\ 0.7$ m/s, z = 20 m (one orbit).

For CAM on R-bar the situation is less simple. If the CAM were to consist of an application of a ΔV in the *z*-direction, the advance in the *x*-direction would depend

only on the z-position, where the CAM is applied. The resulting motion is obtained by addition of the equation for the release at a z-position moving with the velocity of the target (Eqs. (3.25)) and of the equation for a radial ΔV, Eqs. (3.34). As the latter equation does not include an average advance over one orbit, the average motion in the x-direction is only due to the z-distance of the CAM initiation point from the target orbit. This is shown clearly by the examples in figures 4.17 and 4.18. In figure 4.17, the CAM trajectory starts at 20 m, and three values for the radial ΔV have been assumed: 0.3 m/s, 0.5 m/s and 0.7 m/s. Figure 4.17 shows that the undisturbed trajectories all end, after one revolution, at the same point. In figure 4.18, the same ΔV is applied for all trajectories, but the initiation points are different, i.e. 20 m, 50 m and 100 m below the target orbit. This figure shows that the x-position after one revolution is strongly dependent on the z-position.

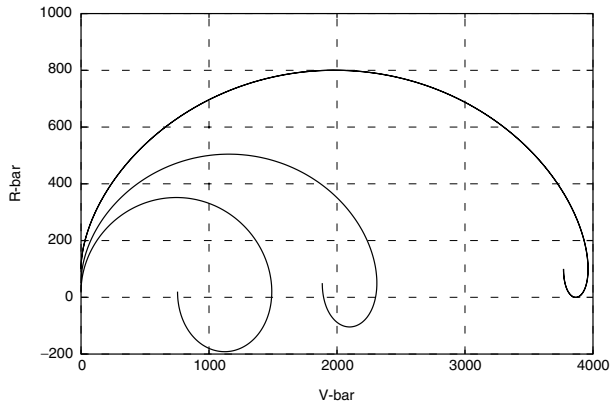

Figure 4.18. CAM on R-bar: $\Delta V_z = 0.3$ m/s, $z = 20$, 50, 100 m (one orbit).

A pure radial ΔV will, therefore, not be sufficient when the chaser vehicle is very close to the target. When the distance to the target orbit becomes only a few metres, the net advance after one revolution may be less than the diameter of a safety zone defined around the target (see section 5.6). An additional ΔV in the $-x$-direction could provide in this case the required advance in the orbital direction. The initial direction of the trajectory resulting from this combined x- and z-boost will, however, not necessarily be aligned with the approach axis. If there are elements of the target structure around the R-bar docking port or berthing box (see section 5.3), the ratio of $\Delta V_x/\Delta V_z$ must be chosen carefully to ensure that the escape trajectory will remain within the volume available for departure, including all dispersion and geometric extensions and margins of chaser and target.

An example of a CAM at the end of an R-bar approach at 15 m below the target orbit is shown in figures 4.19 and 4.20. The ratio of the ΔVs in the z- and x-directions

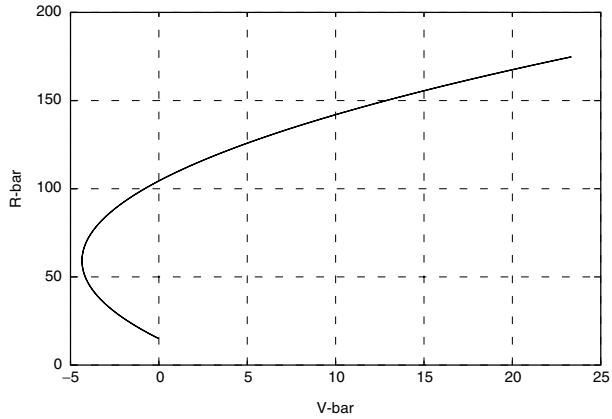

Figure 4.19. Example. CAM on R-bar: $\Delta V_z = 0.5$ m/s, $\Delta V_x = -0.1$ m/s (5 min).

is 5:1. Figure 4.19 shows that the trajectory in the first minutes will safely move below potential structural elements of the target. Figure 4.20 (same dynamic conditions) shows that after one orbital revolution the chaser will end up at a distance of more than 2000 m in front of the target.

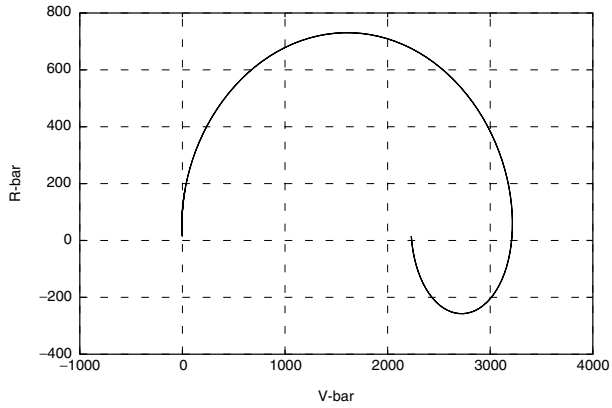

Figure 4.20. Example. CAM on R-bar: $\Delta V_z = 0.5m/s$, $\Delta V_x = -0.1$ m/s (one orbit).

Other important considerations which should be taken into account for the definition of the ΔV for a CAM are the time and propellant for recovery. The larger the CAM, the more time it will take for recovery, and consequently other resources of the vehicle have to be taken into account, in particular power. For the majority of the cases the time between the occurrence of a failure and the potential collision with the target is relatively long (from a couple of minutes up to one or more orbital revolutions), and therefore it

is very important that the human operators on ground or in the target station have other means at their disposal to stop or re-direct the motion of the spacecraft and to recover the mission (see chapter 9).

A CAM is the last resort in achieving safety against collision, which must still be available even after two failures, e.g. when the GNC system is no longer available. An open loop CAM requires that the attitude of the vehicle at initiation and during execution is approximately in the nominal direction. We have seen above that an attitude error of ± 15 deg is still not critical. However, as a failure situation which requires a CAM may also lead to uncontrolled angular rates, and as the achievement of a certain ΔV will take some time according to the mass of the vehicle and the size of the thrusters, there will be limitations to the application of open loop CAM manoeuvres.

In the case of a contingency situation, it must be possible for a CAM to be initiated both automatically by the onboard system according to certain failure criteria (see section 6.4), and directly by remote operators. However, as a CAM can endanger mission success and might not be absolutely necessary in all contingency cases, a human operator must be able to override the decision of the onboard system. The operator may decide, using all the information available, if the resources allow and if the situation is safe enough, just to interrupt the mission. Depending on the trajectory, this may be done by stopping the motion on the trajectory or by transferring the vehicle to a hold on V-bar and attempting to solve the problem there (for more details see chapter 9).

5

The drivers for the approach strategy

The major natural and technical features and constraints which (along with trajectory safety) are the driving forces behind the design of the approach strategy will be discussed in this chapter. The consequences on trajectory elements and approach strategy for the various natural and technical issues will be indicated. Trajectory safety remains the overriding requirement; this always has to be kept in mind when discussing all other potential design drivers. Three examples of approach strategies with different constraints are discussed at the end of the chapter, for which, within the context of a complete approach scenario, a detailed explanation of the rationale behind the choice of trajectory elements of the different rendezvous phases is provided.

5.1 Overview of constraints on the approach strategy

The most important disturbance which has to be taken into account in the *launch strategy* is the drift of nodes due to the J_2-effect, described in section 4.2.2. Because of the difference in orbital altitude, this drift will be different for chaser and target over the duration of the approach. The difference will therefore have to be compensated for by corrective measures during launch and phasing. The *phasing strategy* is mainly driven by the difference in position between the target station and the chaser vehicle after launch and by the required arrival time at the target. The *strategy of the rendezvous and final approach phases* will be determined additionally by many other physical, technical and operational constraints that will be present as a result of:

- geometrical conditions for mating at the target station, such as the location of capture interface on the target station, the availability and location of sensor interfaces on the target station, and the attitude of the target station;

- the capabilities of the sensors for trajectory and attitude control and of other equipment aboard the chaser and target vehicles, and on ground, which are used in the rendezvous process (this includes issues such as measurement range, measurement accuracy and field of view);
- needs and capabilities for monitoring on ground and by the target crew;
- availability of crew on the target vehicle for such operations;
- rules for the approach defined by the target;
- constraints by onboard resources.

All rendezvous strategies consist of a sequence of orbital manoeuvres and trajectories, which mostly have a fixed duration, i.e. typically one or one half orbital revolution. Visual monitoring of the last few metres of approach and capture by remote operators on the target station or on ground requires, however, particular illumination and communication conditions. Unfortunately, the occurrence of such conditions is not necessarily synchronised with the sequence of orbital motions required by the approach scheme. Such monitoring conditions and constraints are as follows.

- The illumination of the capture interfaces, i.e.
  - in the case of docking, the docking port of either chaser or target, depending on the location of video equipment or viewing capability,
  - in the case of berthing, the grapple fixture for capture by a manipulator.

  Either natural illumination by the Sun or artificial illumination can be used. For Sun illumination, availability and direction of sunlight is a major issue for visual monitoring during the last part of the final approach and during the mating process (see section 5.4.1). For artificial illumination, the last few metres of approach and capture can best be performed during orbital night, in order to avoid light disturbances by the Sun.
- The visibility windows, during which ground can communicate with the chaser and target spacecraft, either directly by ground stations or via relay satellites (see section 5.4.2).
- The data rate transmission and reception capabilities of space and ground equipment, in particular when video pictures are required for monitoring (see section 9.3).
- The communications delay due to space–ground signal travel time, e.g. via relay satellites, and due to ground link delays.
- The maximum range of direct communication between chaser and target station.

- The work, rest and sleep schedule of the crew in the case of a manned target (section 5.4.3). Monitoring by crew is a 'must' for manned vehicles, but availability of crew is usually limited.

Synchronisation of the timeline will obviously become more difficult as more and more of these requirements have to be met at the same time. In particular, the combination of Sun illumination requirements during the last part of the approach and capture with the requirement for communication windows can, in some cases, lead to an extreme reduction in mission opportunities.

Another issue that plays an important role in the concept of the approach strategy is the amount of participation of the target in the final approach operations. This cooperation can range from completely uncontrolled and passive (e.g. the case of an incapacitated target vehicle); via passively cooperative (e.g. a target vehicle with fixed attitude, communication and sensor interfaces); to actively cooperative (e.g. the target performs attitude manoeuvres to facilitate docking, or performs actively the berthing operations, etc.).

If the target crew has to fulfil an active role as back-up for the automatic GNC of the chaser vehicle (see section 6.5), the trajectory has to be designed such that an immediate take-over by manual control is possible. This is generally the case only for straight line trajectories.

A further issue, which has significant repercussions on the approach strategy, concerns the above-mentioned control rules defined by the target. These include, e.g., the traffic and safety control zones around the target, as defined by the International Space Station, and the rules which have to be observed therein. This subject will be addressed in more detail in section 5.6.

The constraints due to onboard resources in terms of propellant, power and heat dissipation capabilities will be addressed shortly. Such constraints can affect both nominal and back-up strategies. The latter determine the necessary time and propellant for retreat and return, and potentially include long waiting times, with repercussions on power resources. As the nominal approach strategy has to foresee, at all points of the approach, a back-up solution, the back-up needs will in turn influence the concept for the nominal approach strategy.

5.2 Launch and phasing constraints

5.2.1 The drift of nodes

With otherwise identical orbit parameters, the rate of drift of nodes depends on the altitude of the orbit (see Eq. (4.8)). The difference in the drift of nodes between chaser and target during phasing can be several tenths of a degree per day. In the example in

section 4.2.2, it was assumed that the target is in a 400 km altitude circular orbit and that the chaser is in a 350/200 km elliptical orbit, leading to a difference of 0.337 deg/day for a 52 deg inclination orbit plane and of 0.482 deg/day for a 28.5 deg inclination orbit plane.

As a result, when launched into the same orbital plane as the target, the chaser would end up, when arriving at rendezvous distance, in a plane with the same inclination but a different RAAN angle. For this reason it will have to be injected into a 'virtual target plane' with a different RAAN, such that the difference will have disappeared when the chaser arrives at the target, due to different drift of nodes along the way. This 'virtual target plane', into which the chaser has to be launched, can only be estimated, as it obviously depends on the further evolution of the actual trajectories until mating. Final adjustment of the RAAN angle has to be performed during phasing and must be concluded, except for minor calibrations, prior to the start of the close range rendezvous operations.

5.2.2 Adjustment of arrival time

Because of the problem of synchronisation of the approach timeline with the occurrence of suitable illumination conditions and communication windows, the phasing duration of the chaser after launch will not only be determined by the phase angle to the target. Since (a) launch has to take place at a certain point in time to meet the orbital plane conditions, and (b) final approach and mating have to take place at another independent fixed point in time to meet illumination and communication conditions, some flexibility in time will be needed on the way between those two points. The approach trajectories between launch and mating thus have to be designed such that the time conditions can be met in addition to compensation of the differential drift of nodes addressed above. For this purpose, time-flexible trajectory elements (see section 5.4.4) will be needed to ensure compliance with both requirements. For phasing this could be a drift for different durations at two fixed altitudes, as shown in figure 5.22.

For a given orbit plane and target position, the required conditions of launch window, Sun illumination and communication windows at mating will not be available at all times of the year. Once the point in time where all synchronisation requirements for the final approach and mating can be met has been determined, planning for the operations of all entities involved must commence. These are the control centres of the chaser and target, the target crew, and the communication infrastructure, such as relay satellites and ground links (see chapter 9). In particular, use of this infrastructure is costly, and its availability must precisely be planned for this time. After a missed final approach opportunity, the following one may be available only after some considerable waiting time, due to the necessary re-acquisition operations and the duration of all necessary preparations by the parties involved.

5.3 Geometrical and equipment constraints

5.3.1 Location and direction of target capture interfaces

The strategy for the last part of the final approach depends to a large extent on the location of the docking axis or the berthing box. This will determine whether a $+$V-bar, a $-$V-bar or an R-bar approach has to be performed, which in turn will determine the strategy of the previous phase. Depending on whether or not a potentially longer waiting time is needed, because of operational or other reasons (cf. section 9.1), a hold point on V-bar may be required. For an R-bar approach this will require first a V-bar acquisition and, after the hold point, a fly-around manoeuvre to acquire R-bar. If it can be foreseen that no such hold will be required, an R-bar approach can, of course, be initiated directly, e.g. from a lower (drift) orbit, without transferring the chaser to the target orbit first. However, as long as it is uncertain whether the possibility of a waiting time has to be envisaged, the application of an approach strategy with a hold point will be advisable.

Repercussions of port locations on the approach strategy

In cases where the target is a large orbital assembly consisting of several modules, final translation may not take place on V-bar or R-bar, but on lines parallel to it, according to the location of the docking port or the berthing box in relation to the CoM of the station. For docking this situation is shown schematically in figure 5.1, and for berthing it is shown in figure. 5.4.

Whereas the approach on a line parallel to R-bar (line through the CoM of the target vehicle) has no further consequences concerning the orbital dynamics, for an approach parallel to V-bar, orbit dynamics have to be taken into account (Eqs. (3.25), (3.44) and (3.26)). For example, the loss of control during a hold point on a docking axis above V-bar ($-\Delta z$) would result in a looping motion in the $-$V-bar direction and on an approach axis below V-bar ($+\Delta z$) in a looping motion in the $+$V-bar direction (see figure 3.11). For the approach in a closed loop controlled motion, the result would just be somewhat higher or lower propellant consumption, depending on the direction of approach, i.e. whether to a $+$V-bar or $-$V-bar port or a berthing box.

The distance in the z-direction of the approach axis from the actual target orbit line is very important for trajectory safety. In the case of loss of control, the resulting drift trajectory will become more or less safe, which means it will move either away from or toward the target. Direction and velocity of the relative motion will depend on side and direction of the approach, on the approach velocity and on the distance from V-bar. This influence, e.g., of the z-distance is shown in the two examples of figure 5.2 for the loss of control during a straight line approach. The chosen z-distances are 10 m above or below V-bar, and the assumed approach velocity is $+0.1$ m/s in the V-bar direction. Thrust is inhibited at a distance of $x = 60$ m from the CoM of the target. The trajectory starting below V-bar (positive R-bar side) is less safe, as it moves closer to the target.

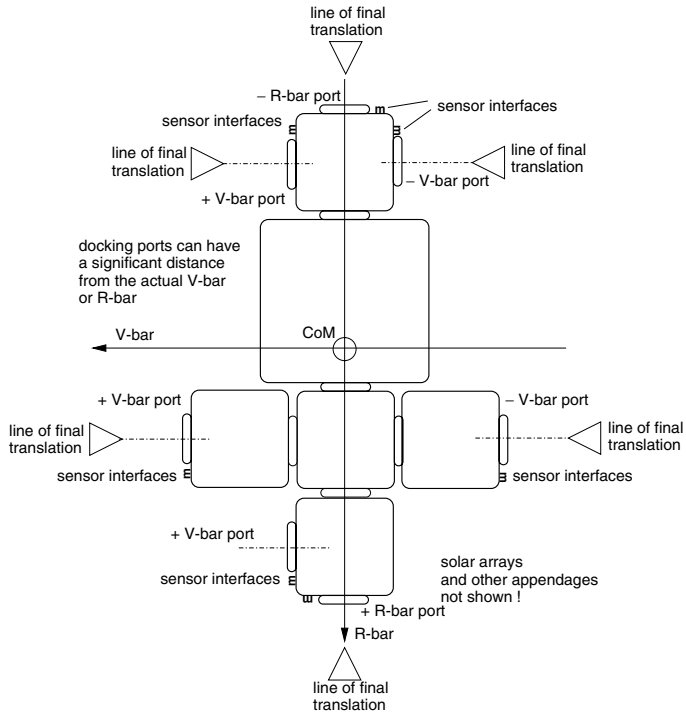

Figure 5.1. Location of docking ports w.r.t. the local orbital frame.

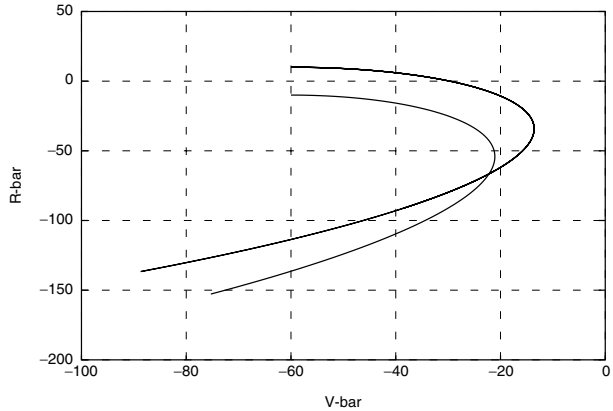

Figure 5.2. Thrust inhibit on 0.1 m/s V-bar approach at $z = \pm 10$ m.

Particularly sensitive in the cases of thrust inhibit or loss of control are hold points at a z-distance from V-bar. In these examples, shown in figure 5.3, it is assumed that the hold point is on the approach line to a docking port or berthing box at a z-distance of 10 m above or below V-bar and at a distance of $x = \pm 20$ m from the CoM of the target. For an approach on the $-$V-bar side, the critical condition concerning trajectory safety is a docking port below V-bar, i.e. with an approach trajectory at a $+$ z-distance from V-bar. For an approach on the $+$V-bar side, a docking port above V-bar, i.e. with an approach trajectory at a $-$z-distance, will be more critical.

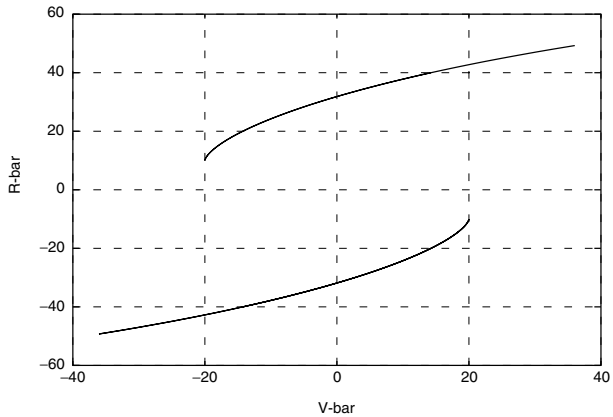

Figure 5.3. Example. Loss of control on hold points at z $= \pm 10$ m.

Any direct approach to a port located at $\pm$H-bar is inherently unsafe. In the cases of thrust inhibit or loss of control of the spacecraft due to other failures, the vehicle will continue to move toward the station, with the highest velocity achieved when crossing V-bar (see Eqs. (3.27)). For the connection to H-bar ports, berthing is preferred, whether by transfer directly from a berthing box or after initial docking from V-bar or R-bar docking ports.

Approach to a berthing box

The direction of approach to a berthing box is dictated neither by the location nor the direction of the berthing port axis. Depending on the reach and articulation capabilities of the manipulator arm used, convenient berthing box locations can be selected, from where the captured vehicle can be transferred to the structural interfaces of the berthing port, i.e. the berthing mechanism. The approach direction to a berthing box is then driven by the geometric shape of the vehicles, by the location and reach capability of the manipulator, by the location and nominal attitude of the corresponding capture interfaces (grapple fixture) and by trajectory safety considerations. The location of the berthing boxes, their relation to manipulator and berthing port positions on the target station,

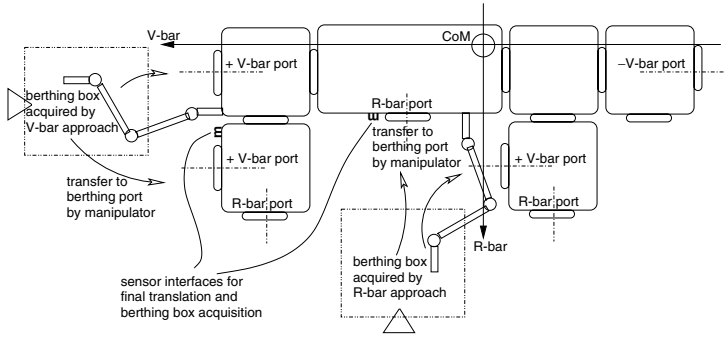

Figure 5.4. Location of berthing ports and berthing boxes w.r.t. the local orbital frame.

and their access by V-bar or R-bar approaches, are shown schematically in figure 5.4. In this example, the manipulator is located on the target, which is usually the case for large space stations (it can also be located, however, on the chaser, as in the Space Shuttle). In addition to geometric conditions and manipulator reach, availability and location of relevant rendezvous sensor interfaces will be major drivers for the location of, and approach direction to, the berthing box.

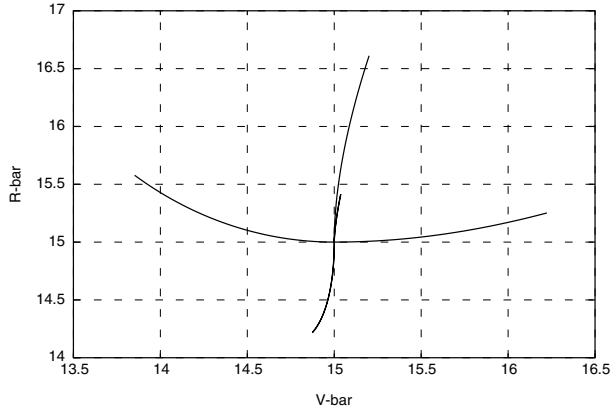

Figure 5.5. Example. Drift trajectories in berthing box, (v_x, $v_z = \pm 0.01$ m/s).

In the berthing box, control of the chaser will have to be switched off prior to capture to avoid competing control actions between chaser GNC and manipulator. In cases where the berthing box is located above or below V-bar, orbit dynamics will move the vehicle according to Eqs. (3.26) after control inhibition. For this reason, there will be only limited time for the manipulator to grapple the vehicle's capture interfaces. In the example shown in figure 5.5 the centre of the berthing box has been assumed to be 15 m below V-bar and the trajectory evolution has been calculated for 2 minutes. For the

nominal case, the natural motion during this time would be approximately 0.4 m in the R-bar direction. However, there will always be residual motion after shut down of the control system, which in addition will determine the trajectory evolution. In the example, residual velocities of 0.01 m/s in the $\pm x$- and $\pm z$-directions have been assumed. As a result, drifts of more than 1.5 m occur. The example indicates three important rules for design and operation:

(1) the berthing box should be as close as possible to V-bar,
(2) the residual velocities after control inhibition shall be as low as possible,
(3) the manipulator should be able to grapple the vehicle within a very short time.

Three different regions (volumes) can be identified for the berthing box, as defined in figure 5.6 (Lupo 1995; Bielski 1998):

- the station keeping volume (inner berthing box), which is required for the accuracy with which the chaser GNC can position the grapple interfaces w.r.t. the target coordinates and which includes the control motion;
- the capture volume, in which the capture of the vehicle has to be achieved; this adds to the station keeping volume the free drift which takes place after thrust inhibit up to the point in time when the manipulator end effector has captured the grapple interfaces;
- the total berthing box volume (outer berthing box), which adds to the capture volume the distance necessary to stop the manipulator motion.

In order to determine the allowable position of the box, the maximum outlines of the chaser vehicle (as measured from the grapple interface and including maximum possible attitude angle after capture) must be added to the outer berthing box volume, and a safety margin around the target vehicle structure must be considered. The manipulator must be able to reach the entire envelope of the outer berthing box, i.e. the capture box plus the braking envelope. For this reason, the resulting volume, taking all constraints into account, will not necessarily be of cubic form.

Since, after capture, the transfer to a berthing port does not depend on the approach direction but on the capabilities of the arm, the axis of the berthing port can have a completely different direction than the approach line. This is one of the major advantages of

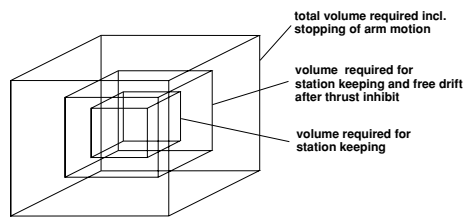

Figure 5.6. Definition of berthing boxes.

berthing. In this way connections of new elements can be made to the target station at places which are not accessible or difficult to access by direct docking. The major disadvantage of berthing is the much increased complexity of the mating process in terms of hardware, software and human operator functions involved, and of operations to be performed, with the corresponding consequences on duration and use of resources. This will also have repercussions on reliability and safety of the process, as there are now three additional active elements involved in the process, i.e. the target vehicle systems, the human operator and the manipulator arm, each adding potential failures and errors.

Approach to a docking port with an attitude angle

For a number of reasons, the target station may not be aligned with the local vertical/local horizontal (LVLH) directions. It could be pointing toward the Sun (e.g. for power reasons), be in a natural stable torque equilibrium attitude (equilibrium of major torques acting on the spacecraft, e.g. caused by gravity gradient and residual air drag effects), or pointing in a particular direction for communications reasons, etc. Although in the case of docking the chaser vehicle will eventually have to acquire the docking axis to be able to perform capture and docking, not all parts of the final approach need to be performed on the docking axis.

When the short range rendezvous sensor on the chaser acquires the sensor interfaces on the target (e.g. retro-reflectors for optical rendezvous sensors) at a distance of a few hundred metres, the parameters to be measured are the range and direction between the two vehicles. Measurement of relative attitude will typically commence (due to sensor limitations) only at a relatively short range, i.e. below 50 m. The range for which relative attitude information must be available results from the dynamics of the acquisition of the docking axis. This means that acquisition of the docking axis must take place at a distance that is large enough for the lateral trajectory oscillations to be damped out before arriving at the docking port (cf. figure 2.12).

The approach to a target with large attitude angle can be envisaged in the following way. Up to the point where relative attitude measurement is available, the attitude of the chaser will be controlled by the absolute attitude sensors, e.g. w.r.t. the LVLH frame. Assuming the use of optical sensors, the position of the chaser can be controlled such that the target reflectors will be in the centre of the field of view of the rendezvous sensor, whereby the absolute attitude of the chaser will be kept aligned to LVLH. The result will be that the approach trajectory of the chaser is a line parallel to V-bar or R-bar (depending on the direction of the docking axis), defined by the position of the sensor interfaces on the target.

This situation is shown for a V-bar approach in figure 5.7. On the right side of the figure the dispersion ellipsoid is shown, which results from the measurement accuracy of the sensor used in the previous phase. In the upper example an error radius of $r_{\max} = 10$ m is assumed; in the lower one there is an error radius of $r_{\max} = 20$ m. Further, it is assumed that the docking port is at a distance of 30 m from the CoM of the target station and that the station has an attitude angle of $+20$ deg (upper example) and -15 deg (lower

example), respectively. After sensor acquisition, the GNC system will guide the chaser automatically to the approach line determined by the sensor interfaces and by its own attitude control accuracy. Note: with these measurements the GNC system of the chaser cannot determine where V-bar is (V-bar is defined in the target local orbital frame). This fact has to be taken into account for trajectory safety considerations.

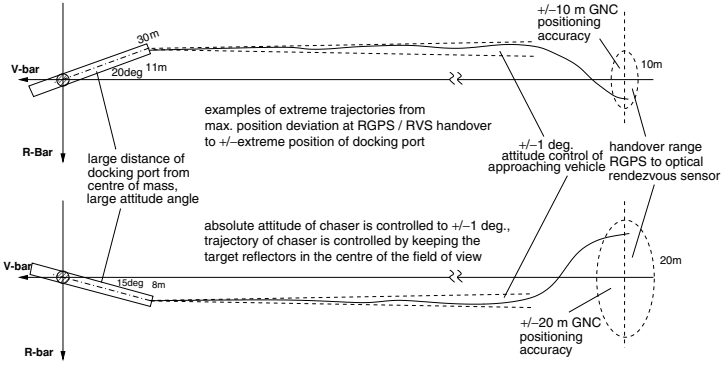

Figure 5.7. Final approach trajectory to target station with attitude angle.

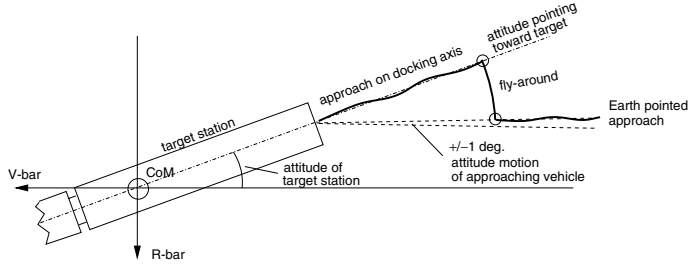

Figure 5.8. Acquisition of docking axis on target station with large attitude angle.

As the angular reception range of the docking mechanism is limited, the chaser will eventually have to acquire the instantaneous docking axis in order to perform the last part of the approach into the mechanical interfaces along this centre line. For this purpose, knowledge of the relative attitude between the two vehicles is necessary. The acquisition of the instantaneous docking axis in the case of small relative attitude deviations has been addressed already in section 2.4.2 and is illustrated in figure 2.12. For larger relative attitude angles, the visibility of the retro-reflectors may be lost, and it may no longer be possible to handle the acquisition of the docking axis by the same GNC mode as used for the approach. In this case, a fly-around manoeuvre has to be implemented. This situation is illustrated in figure 5.8. The fly-around could be implemented, e.g., as a circular fly-around manoeuvre, such as in figure 3.31, or as a two-impulse radial

manoeuvre, as illustrated in figures 3.19 and 3.22. As such manoeuvres have to be performed in the very close vicinity of the target vehicle, trajectory safety will be the over-riding consideration for its implementation.

Large attitude angles of the docking port w.r.t. V-bar or R-bar direction can occur when a module carrying the port is attached to the target station under a certain angle, when the station itself flies under a certain angle, e.g. a torque equilibrium attitude (TEA), or is inertially pointing, e.g., toward the Sun for power reasons.

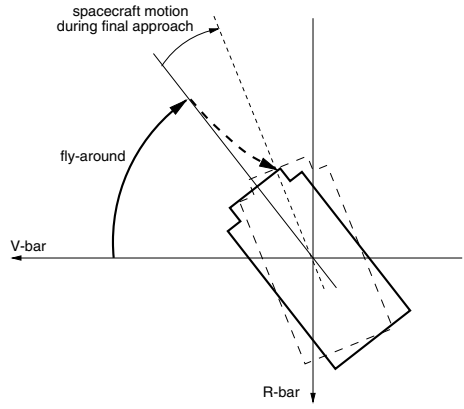

Figure 5.9. Fly-around and approach to inertially pointing target.

The case of an inertially pointing target (see figure 5.9) is very different from all the other cases, as the target is rotating, i.e. it is continuously changing its attitude w.r.t the local orbital frame $\boldsymbol{F}_{\mathbf{lo}}$. This requires the chaser, when on the docking axis, to follow the motion with the orbital rate ω of the target docking frame, which is 1.14×10^{-3} rad/s in a 400 km orbit. As a result, the chaser has to provide this rotation and the corresponding lateral velocity $r \cdot \omega$, which amounts to 0.114 m/s at $r = 100$ m and 0.0114 m/s at $r = 10$ m from the docking port. For an inertially pointing target, the acquisition of the docking axis can take place when the latter has turned, e.g., into either the $+$ or $-$V-bar direction, where the chaser is waiting. Docking axis acquisition may possibly be combined with a fly-around manoeuvre to obtain a suitable attitude of antennas w.r.t. ground or other satellites. The latter case is shown in figure 5.9. A radial impulse fly-around will have, in this context, the advantage of keeping a constant direction of chaser–target line w.r.t. the Sun. Approaches to an inertially pointing target have been used in the past in the Russian Mir Space Station scenario. However, as trajectory safety conditions are changing continuously for an approach to an inertially pointing target, a CAM would have to be calculated separately for each point of the trajectory. For this reason, V-bar and R-bar approaches are generally preferred. Approaches to an inertially pointing docking axis are nowadays mainly considered for rescue and repair missions to target spacecraft, which are in Sun-pointing mode for power reasons.

5.3.2 Range of operation of rendezvous sensors

The rendezvous approach process requires that the lateral displacements and velocities relative to the target will decrease commensurate with the decrease of distance on the approach line to the target. This results in a continuous increase of navigation accuracy requirements over the approach sequence, which cannot be fulfilled by one sensor over the entire approach range. Most sensors have a limited range of operation, which determines the extension of the particular approach phase in which it will be used. The required accuracy of the sensor measurements follows from the error ellipsoid for position and velocity, which has to be achieved in the following manoeuvre. This is explained in more detail in section 7.1.1.

The maximum operational range of a sensor is, in most cases, constrained by the power with which it can emit its signal. Exceptions are satellite navigation systems, such as GPS and GLONASS, and sensor principles, which make use of external power sources, such as Sun illumination.

- For radio-frequency based rendezvous sensors (e.g. radar) the maximum range is typically of the order of 100 km.

- For absolute GPS there is no limitation concerning the range of use in a RVD approach trajectory, as GPS satellites cover the entire surface of the Earth.

- For relative GPS, which uses the raw data of the GPS receivers on both chaser and target, the maximum range will be limited by the range of direct communication between the two vehicles.

- For optical sensors the maximum range is typically a few tens of metres to a few hundred metres, depending on the target area to be illuminated.

An overview of operational ranges and accuracies of sensors for rendezvous trajectory control is shown schematically in figure 5.10. The following remarks need to be made in support of this diagram.

The use of GPS and RGPS will be constrained at the lower end of the range of the operating range by shadowing and multi-path effects (see section 7.3.4). In particular, for large and complex structures such as a space station, with many large surfaces in various directions and even very large rotating elements, such as the solar arrays and radiators, shadowing is a significant problem.

After abandonment of the process of degradation of the GPS signal, known as 'selective availability' (SA), the accuracy of position determination by absolute GPS has improved by a factor of 10 (for further details, see section 7.3.2). The absolute GPS accuracy in figure 5.10 comes close to that of relative GPS. It has to be taken into account, however, that the calculation of the relative state of the chaser w.r.t. the target still requires measurements on the target side with the same accuracy and that the subtraction of very large numbers introduces the possibility of large errors.

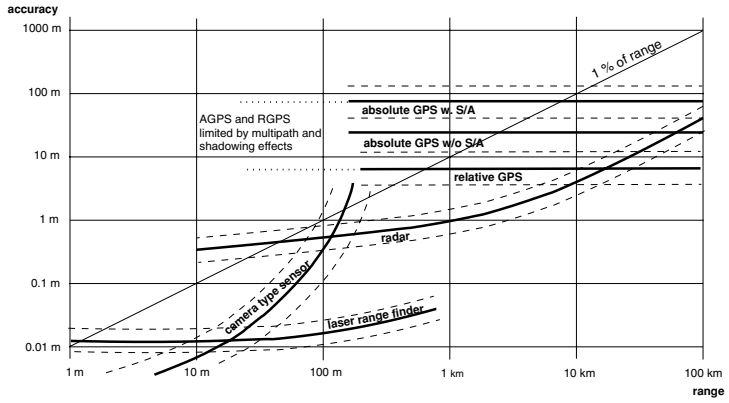

Figure 5.10. Typical operational ranges and measurement accuracies of rendezvous sensors.

Optical sensors, e.g. camera and laser range finder types (for more details see chapter 7), have an additional operational constraint for the approach trajectory design, i.e. a limited field of view (FOV). This puts limits on the lateral extension of the trajectory. An example is shown in figure 5.11: in the case of a transfer along V-bar by impulsive radial manoeuvres, the extension of the trajectory in the y-direction is one half of the advance in the x-direction, with the maximum half way. To cover such a trajectory very close to the target, an optical sensor would need to have a 60 deg FOV (30 deg half cone angle). Because of the power required to illuminate (camera sensor), or the duration required to scan such a large FOV (scanning laser), compromises have to be made, which result in relatively small FOV for most optical sensors.

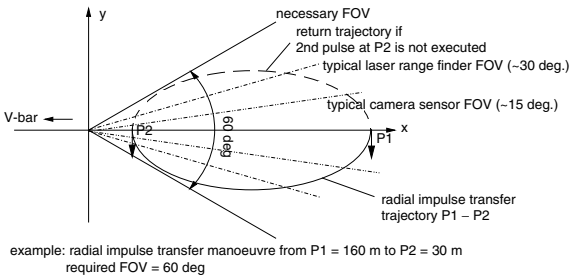

Figure 5.11. Required and available field of view (FOV) for a radial impulse transfer.

Optical sensors, with their limited FOV, are particularly suitable for the last part of the docking approach. During the final part of the approach to the docking port, the trajectory needs to be close to and the attitude aligned with the docking axis, in order to meet the reception range of the mechanical interfaces. During the last part of an

approach to a berthing box, sensors with a small FOV are also quite suitable, if the chaser can point towards the sensor interface on the target. For other parts of the approach strategy, which include impulsive manoeuvres, fly-arounds and attitudes, which are not necessarily pointing towards the target, sensors with larger FOV will be required.

As a result, for the various rendezvous phases, different sensor types will have to be chosen, and, in turn, according to the operating range and performance of sensors, the various rendezvous phases will have the appropriate ranges. The following list gives the approximate ranges of approach phases and the preferred types of sensors (see section 7.1.1).

- *Final approach*. Sensor: laser range finder or camera type of optical sensor, from 100–500 m to contact.
- *Close range rendezvous*. Sensor: relative GPS, radar or other type of RF sensor, from a few thousand metres to final approach range.
- *Far range rendezvous*. Sensor: absolute GPS, radar or other type of RF sensor, from 10–100 km to the start of close range rendezvous.
- *Phasing*. Sensor: absolute GPS or ground based navigation, from launch to start of far range rendezvous.

5.4 Synchronisation monitoring needs

Most of the synchronisation problems in rendezvous operations are related to the requirement that monitoring by human operators is necessary for the last part for final approach and for capture operations. Such synchronisation problems will be most severe when the human operators are located on ground. Many problems, however, will also occur when the operator is in the target station or even in the approaching vehicle itself. Those external events which must be synchronised with the final rendezvous events are as follows.

- *Proper Sun illumination conditions* during the last part of the final approach and during docking/berthing, since, in most cases, visual monitoring will rely for power reasons on Sun illumination.
- *Availability of a communication window* for transmission of video data (data rate) to ground, either directly to a ground station or via relay satellite. Video monitoring of the last part of the approach and capture operations is required by ground operators in any case if monitoring by target crew operators is not available. Even if visual or video monitoring by operators in the target is established, additional transmission of video data to ground will be advisable for safety reasons (see section 9.1.2).

- *Availability of crew member(s)* for monitoring within the crew activity timeline (only in the case of a manned target vehicle). It is assumed that, for safety reasons, target crew must always be able to supervise the last part of the approach and mating process. In some mission scenarios, target crew may be required, in contingency situations, to take over the control of the chaser vehicle manually, in order to ensure mission success (see section 6.5.3).

5.4.1 Sun illumination

Orbital day and night occur with an orbital period depending on the actual orbital radius (in a low Earth orbit (LEO) this is every 90–95 minutes). Due to the altitude above the Earth, orbital day is generally a bit longer than half the orbital period, except when the position of the Sun is nearly orthogonal w.r.t. the orbital plane. In this case, all of the orbit would be illuminated. However, not all of the illuminated part of an orbit will be suitable for visual monitoring of rendezvous and capture operations, as shadowing may make monitoring impossible. Due to the lack of refraction from the surrounding air, the contrast between light and shadowing is much more severe in space than on ground.

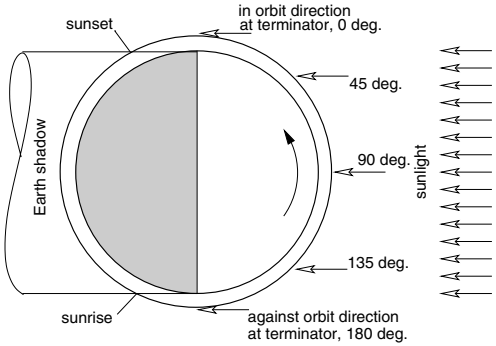

Figure 5.12. Variation of Sun elevation angle component over one orbit.

As an example, the elevation component of the Sun angle shall be considered for the easy case of an orbit with low lateral Sun angle, i.e. with the Sun being more or less in the orbital plane. This case is illustrated in figure 5.12. At orbital dawn the Sun shines in a direction opposite to the orbital velocity vector. At orbital sunset it shines in the same direction as the orbital velocity vector. At orbital noon sunlight and the orbital velocity vector are orthogonal. Assuming LVLH attitude of chaser and target, depending on the direction of the final approach, i.e. whether in $+$V-bar, $-$V-bar, the Sun will, at sunrise, illuminate fully the capture interface plane of the target station, and at sunset that of the chaser vehicle, or vice versa. For an R-bar approach, the chaser interfaces would be fully illuminated at orbital noon. If the docking port in question is fully illuminated, i.e. the Sun direction is orthogonal to the interface plane, it will be difficult to distinguish any

feature on the illuminated surface. For the human eye, or a video camera, looking along the approach line, the surfaces will, in this case, all be equally illuminated and there will not be much shadowing. Also, when at close distances, one vehicle will cast its shadow on the other. On the other hand, when the Sun is orthogonal to the approach axis, structural features with extensions along the approach line will cast long shadows, resulting in little or no illumination of surfaces in the capture interface plane. This is an equally unsuitable situation for visual monitoring. Best illumination conditions for monitoring are obtained at intermediate angles, where the interface plane for capture is illuminated, shadows of structural features are not too long and shadow casting from one vehicle on the other is limited to a minimum.

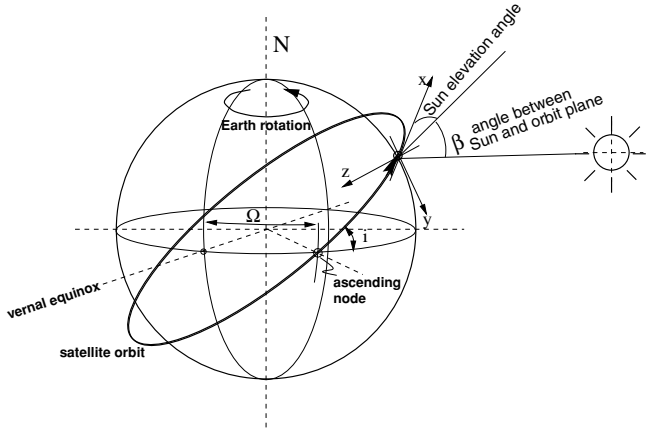

Figure 5.13. Sun angles seen from spacecraft.

In the general case, the orbit plane is not aligned with the ecliptic plane and the Sun direction will also have a lateral component β, as illustrated in figure 5.13. The maximum and minimum values that the β-angle can assume are given by the orbit inclination i plus the angle of the ecliptic w.r.t. the equator, $\varepsilon = 23.5$ deg., as shown in figure 5.14. Depending on the annual season and on the location Ω of the ascending node, the relevant component of the ecliptic angle ε has to be added to or subtracted from the orbit inclination angle i. Due to the drift of the nodes (see section 4.2.2), which can amount to several degrees per day, the β-angle can assume over time any value between the two extremes.

The direction of the Sun in the spacecraft local orbital frame F_{lo} (LVLH frame) can be calculated using the following coordinate transformations:

$$S_{\mathrm{lo}} = A_{\mathrm{lo/b}} \cdot A_{\mathrm{b/so}} \cdot A_{\mathrm{so/op}} \cdot A_{\mathrm{op/an}} \cdot A_{\mathrm{an/eq}} \cdot A_{\mathrm{eq/ec}} \cdot S_{\mathrm{ec}} \tag{5.1}$$

The position of the Sun w.r.t. the orbital plane frame is the first part of these

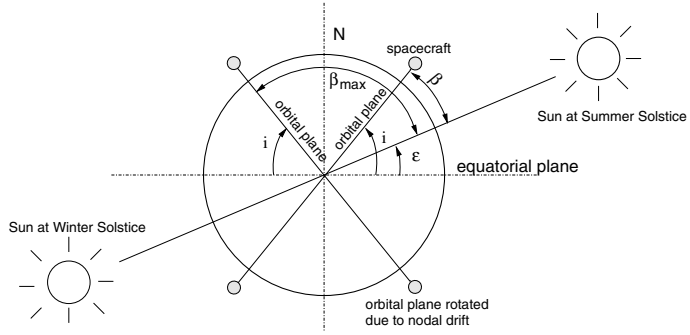

Figure 5.14. β-angle variation due to season and drift of nodes.

transformations:

$$S_{\mathrm{op}} = A_{\mathrm{op/an}} \cdot A_{\mathrm{an/eq}} \cdot A_{\mathrm{eq/ec}} \cdot S_{ec} \tag{5.2}$$

The β-angle is the arcsin of the y-component of the Sun unit vector S_{lo} in the spacecraft local orbital frame, which is the same as the $-z$-component of the Sun unit vector S_{op} in the orbital plane frame:

S_{ec} : unit vector of Sun in the ecliptic frame;

S_{op} : unit vector of Sun in the orbital plane frame;

S_{lo} : unit vector of Sun in the spacecraft local orbital frame (LVLH frame).

The transformation matrices are (see also section 3.1):

$A_{\mathrm{eq/ec}}$: from the ecliptic frame to the Earth-centred equatorial frame, rotation about x_{ec} by $-\varepsilon$;

$A_{\mathrm{an/eq}}$: from the Earth-centred equatorial frame to the ascending node frame, rotation about z_{eq} by the angle Ω (RAAN);

$A_{\mathrm{op/an}}$: from the ascending node frame to the orbital plane frame, rotation about x_{an} by the inclination i;

$A_{\mathrm{so/op}}$: from the orbital plane frame to the spacecraft orbital frame, rotation about z_{op} by the orbital phase angle ωt;

$A_{\mathrm{B/so}}$: from the spacecraft orbital frame to an auxiliary (B) frame, rotation about z_{so} by 90 deg;

$A_{\mathrm{lo/B}}$: from the auxiliary (B) frame to the spacecraft local orbital (LVLH) frame, rotation about x_{B} by -90 deg.

The relationships between the various frames used are shown in figure 5.15.

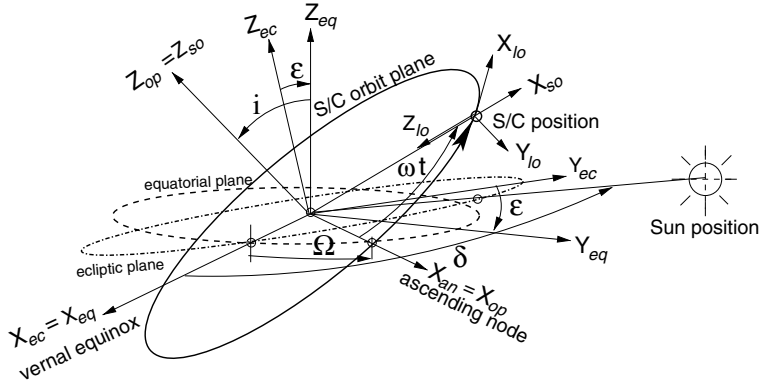

Figure 5.15. Relationships between Sun, Earth and orbit frames.

The unit vector of the Sun in the ecliptic frame is

$$S_{\mathrm{ec}} = \begin{bmatrix} \cos\,\delta \\ \sin\,\delta \\ 0 \end{bmatrix} \tag{5.3}$$

where δ is the day angle of the Sun measured from the vernal equinox.

The transformation matrices for the rotations to the various intermediate frames as defined above are

$$A_{\mathrm{eq/ec}} = A^{\mathrm{T}}_{\mathrm{ec/eq}} = \begin{bmatrix} 1 & 0 & 0 \\ 0 & \cos\,\varepsilon & -\sin\,\varepsilon \\ 0 & \sin\,\varepsilon & \cos\,\varepsilon \end{bmatrix} \tag{5.4}$$

$$A_{\mathrm{an/eq}} = \begin{bmatrix} \cos\,\Omega & \sin\,\Omega & 0 \\ -\sin\,\Omega & \cos\,\Omega & 0 \\ 0 & 0 & 1 \end{bmatrix} \tag{5.5}$$

$$A_{\mathrm{op/an}} = \begin{bmatrix} 1 & 0 & 0 \\ 0 & \cos\,i & \sin\,i \\ 0 & -\sin\,i & \cos\,i \end{bmatrix} \tag{5.6}$$

$$A_{\mathrm{so/op}} = \begin{bmatrix} \cos\,\omega t & \sin\,\omega t & 0 \\ -\sin\,\omega t & \cos\,\omega t & 0 \\ 0 & 0 & 1 \end{bmatrix} \tag{5.7}$$

$$A_{\mathrm{B/so}} = \begin{bmatrix} 0 & 1 & 0 \\ -1 & 0 & 0 \\ 0 & 0 & 1 \end{bmatrix} \tag{5.8}$$

$$A_{\mathrm{lo/B}} = \begin{bmatrix} 1 & 0 & 0 \\ 0 & 0 & -1 \\ 0 & 1 & 0 \end{bmatrix} \tag{5.9}$$

The calculation of the position of the Sun in the spacecraft local orbital frame for a given set of numerical values, for δ, ε, Ω, i and $\omega\, t$ with these transformation matrices, is easy and straightforward. The multiplication of all matrices in a general form leads, however, to very large expressions for the matrix elements, which are too complex to be used for a general assessment of the illumination situation under various conditions. It is much easier to produce the solutions in numerical or graphical form with the help of computer programs for matrix calculation.

The β-angle is variable and depends on the orbit inclination i, on the RAAN angle $\omega = f(t)$ and on the day angle δ, as shown in figures 5.13, 5.14 and 5.15. An example for the evolution of the β-angle over one year is shown in figure 5.16 for a 400 km altitude orbit with an inclination of 52 deg. It is assumed that the start time is the vernal equinox and that the ascending node of the orbit at start time is at $\Omega = 0$. The drift of nodes for this orbit is -4.989 deg/day (see section 4.2.2).

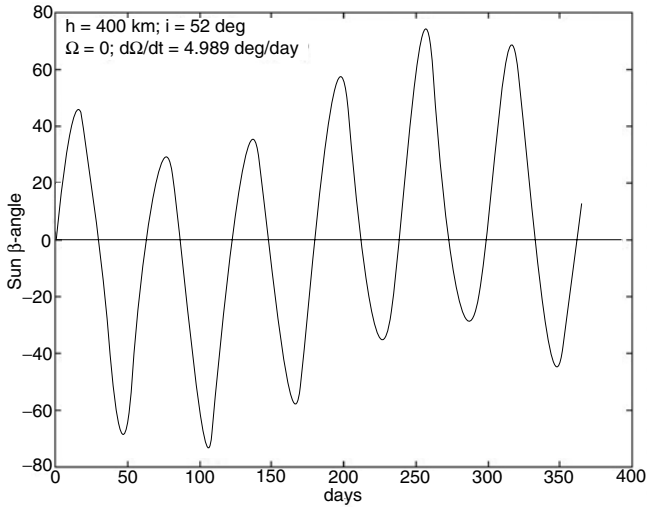

Figure 5.16. Evolution of the β-angle over time, $h = 400$ km, $i = 52$ deg.

For an approach to the target from the $-$V-bar side, at orbital sunrise the Sun will be in front of the chaser spacecraft, i.e. in the direction of the target, and will illuminate the chaser docking port side. At orbital sunset it will be the opposite way, i.e. the Sun will be behind the chaser and will illuminate the docking port side of the target (see figure 5.12). The best illumination conditions of the target docking port side will occur at intermediate angles between orbital noon and sunset, i.e. in a region around three-quarters through the orbital day corresponding to an in-plane component of the Sun angle of 135 deg. Depending on the geometric configuration of chaser and target, suitable illumination conditions may exist in a region of a maximum of $\pm$ 20–30 deg around this Sun angle point, i.e. between about 105 deg and 165 deg, corresponding to

a maximum duration of a quarter of an hour. This is the case when the β-angle is zero. The useful time will be reduced with increasing β-angle. Eventually, when the β-angle becomes 90 deg, there will be no suitable illumination conditions over the entire orbital day, as the Sun direction is always orthogonal to the docking axis. To achieve suitable illumination conditions, the β-angle must differ from 90 deg by at least 20 deg.

If at a $-$V-bar approach, for monitoring reasons, a maximum of the final approach is to be performed under Sun illumination conditions, it will be necessary to plan capture towards the end of the orbital day, i.e. when the target is illuminated. As a consequence, for approaches on the $-$V-bar side, the visual target pattern is best mounted on the target side and the video camera on the chaser side. The video signal needs then to be transmitted to the target crew and to ground to enable monitoring.

For an approach to the target from the $+$V-bar side, the illumination conditions occur in the opposite order: at orbital sunrise the Sun will be behind the chaser, illuminating the target, and at orbital sunset behind the target, illuminating the chaser. In order to achieve a maximum of the final approach under Sun illumination, it is in this case better to have the visual target pattern on the chaser and the video camera on the target. For the same reason, direct visual monitoring by a target crew member looking out of a window will experience better conditions when the approach comes from the $+$V-bar side. For this approach direction, the same time constraints will result as for the approach from the $-$V-bar side: i.e. for a zero β-angle a maximum duration of about 40 minutes prior to docking under Sun illumination, out of which the last 15 minutes will provide suitable illumination conditions for the visual target pattern.

For an R-bar approach the illumination conditions are somewhat different. Sunrise will occur on the side of the chaser in the V-bar direction, with the Sun moving from the $+$V-bar- to the $-$V-bar side in the hemisphere above the chaser. Since the Sun is always in the upper hemisphere, there will be no illumination of the target docking port during a $+$R-bar approach. As a consequence, for approaches from the $+$R-bar side, the visual target pattern is best mounted on the chaser and the video camera on the target. For the opposite arrangement of camera and target pattern, an approach from the $-$R-bar side (approach direction toward Earth) will be more suitable (see figure B.8). For a β-angle near zero, i.e. the Sun in the orbital plane, optimal illumination conditions of the chaser docking port will occur in two regions around 45 deg and 135 deg of the elevation (in-plane) Sun angle. The range of suitable illumination conditions around these points will be of the order of $\pm$20–30 deg. If β is between 20 and 70 deg, favourable illumination conditions would also exist at orbital noon, whereas suitable duration would be shortened at the beginning and end. If the β-angle becomes larger than 70 deg, no suitable illumination conditions will be available during the entire orbit.

The illumination conditions for $\pm$V-bar and $+$R-bar approaches are shown schematically in figure 5.17, which indicates the local orbital frame of the chaser, the relative trajectory of the Sun, position and local horizon of the chaser (the orbital altitude is not taken into account) and the relative position of the target for the various approach directions. The approach direction of the chaser is indicated by arrows, and the target docking port for the different approach directions has to be imagined at the point of these arrows.

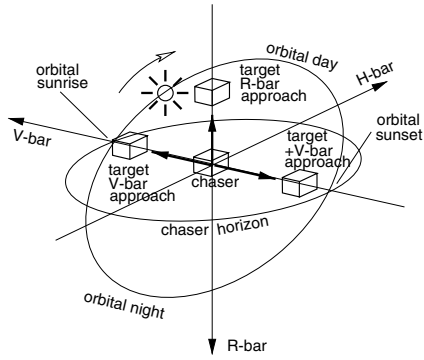

Figure 5.17. Illumination conditions during ±V-bar and R-bar approaches.

Taking all requirements together, it has to be taken into account that, for a given set of orbit parameters of the target in conjunction with the particular set of communication opportunities (ground stations, relay satellites) available for the rendezvous mission in question, proper illumination and communication conditions (see section 5.4.2) for monitoring of the last part of the approach and capture will not be achievable for all days of the year. This will be one of the most important criteria for planning the launch date of the chaser.

5.4.2 Communication windows

Communication from the chaser and target spacecraft to ground can be performed either directly between the antennas of spacecraft and ground or via a relay satellite in geostationary orbit. In the case of direct communication with a ground station, the duration of contact is limited by the altitude of the orbit, by the radiation/reception cone angle of the ground antenna (see figure 5.18) and by the part of the cone which will actually be crossed by the orbit. The resulting time for possible radio contact is called the communication window with the ground station. The useful cone of ground station antennas is

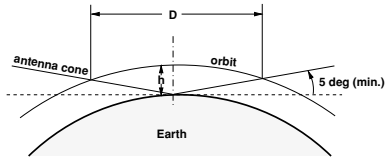

Figure 5.18. Visibility of ground stations, geometrical relation.

constrained by obstacles on ground and by reflections of ground atmosphere and other disturbances, occurring at very low elevation angles. The useful range starts at elevation angles of 5–7 deg, i.e. the maximum half cone angle of the antenna's radiation/reception

cone will be less than 85 deg. In a low Earth orbit, under the best conditions, i.e. when flying over the centre of the cone, the maximum communications duration would be for a 400 km orbital altitude of the order of 10 min and for a 300 km orbital altitude about 7.5 min. When the ground track of the orbit crosses the cone at a lateral distance to the centre, the communication window will be accordingly smaller. Also, because of obstacles and disturbances the shape of the communication range may not always be circular.

Owing to the rotation of the Earth, after one orbital revolution the ground track of the next orbit will have moved by approximately $\Delta\lambda$ degrees westward, which is for a 400 km LEO orbit approximately 23 deg:

$$\Delta\lambda = \frac{-T \cdot 360\,\mathrm{deg}}{24\,\mathrm{h}} \tag{5.10}$$

where $\Delta\lambda$ is the change of longitude and T is the orbital period (see figure 5.19).

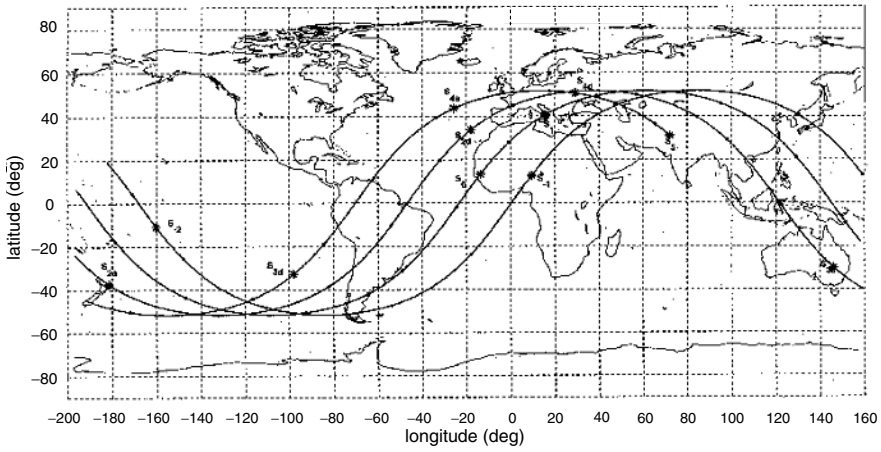

Figure 5.19. Ground track of a 400 km altitude, 51 deg inclination orbit. Dots represent 10 minute intervals.

For exact calculations, the orbital motion of the Earth around the Sun and the drift of the nodes $\dot{\Omega}$ (see section 5.2.1) will have to be taken into account, resulting in $\Delta\lambda = -T(15.041 + \dot{\Omega})$. Measured from the centre of the Earth, the half cone angle of a ground station visibility zone will be no more than 20 deg. Therefore, a communication window with a ground station, contacted in the previous orbit, may in the following one be reduced or non-existent.

In planning recovery operations after contingencies, it is desirable to achieve the same conditions as for the nominal approach. Neglecting the drift of nodes, a ground station passes the orbital plane after each 12 and 24 h, where after 12 h the direction of the orbital velocity vector will be opposite. However, due to the fact that orbital period (e.g.

92.3 min for a 400 km orbit and 90 min for a 300 km orbit) is not synchronised with the rotation of the Earth, the vehicle will not necessarily be directly over that ground station after 12 or 24 h. As a result, the nearest pass over the same ground station may happen somewhat before or after this ground station passes the orbital plane, resulting in a different contact duration.

It is obvious from the above considerations that a single ground station will not be sufficient in order to monitor the close range rendezvous phases. To achieve communication windows of 20 min or more, which would be desirable for monitoring the last part of the final approach including capture, a large number of adjacent ground stations would have to be established. This number would have to be even larger should a second approach and docking attempt be possible in the event of contingencies. Such an arrangement of adjacent ground stations has been established by the former Soviet Union for the rendezvous and docking of the space station programmes Salyut and Mir, and this is still operated by Russia. This unique system comprises seven ground stations, covering the major part of the Eurasian continent (see figure 5.20).

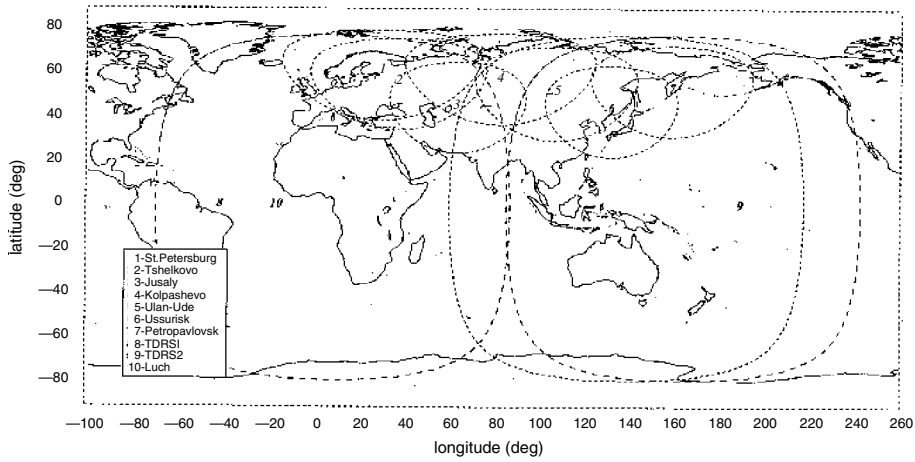

Figure 5.20. Coverage of relay satellites and Russian ground stations for RVD.

Longer communication windows can be achieved via relay satellites in geostationary orbit, which provide approximately half an orbit coverage each. The dashed lines in figure 5.20 show the boundaries of communication of the American TDRS1 and TDRS2, and of the Russian Luch relay satellites. In contrast to the ground stations, where communication is possible inside the closed dashed and dotted line, for relay satellites communication is possible outside the closed lines.

Because of the location of the presently available data relay satellites over the Earth, there will be an area where no communication is possible. In addition, the visibility constraints due to the antenna accommodation on the chaser vehicle must be taken into account. For the data exchange with a satellite in GEO, the antenna of the satellite

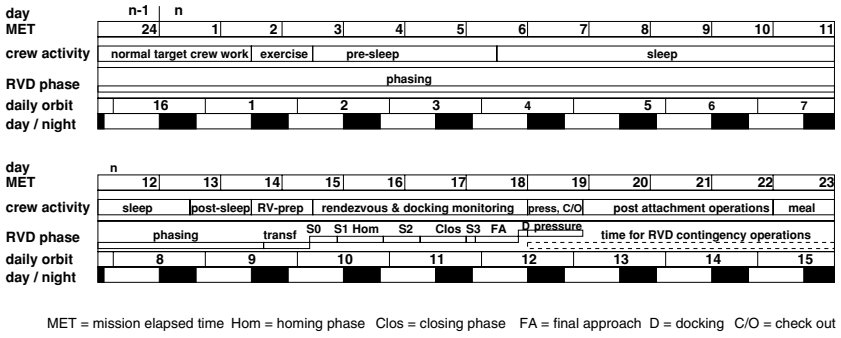

Figure 5.21. Typical 24 h crew activity timeline with RVD operations.

in LEO needs continuously to change its direction in order to point toward the GEO satellite. This requires an articulated antenna mount with two degrees of freedom. The available FOV will be limited by the articulation range of the antenna mount and by the geometry of the satellite. The available communication window via relay satellites will be reduced by these constraints.

The most important problem concerning transmission of monitoring data is, as we have seen, to arrange the approach timeline in such a way that the chaser enters the communication window when the last part of the final approach and capture commences. An additional constraint is that monitoring by video pictures requires a very large data transmission rate (high bandwidth), which may not necessarily be available on the frequencies and channels generally assigned to the mission (see section 9.3). Because of the relatively high cost, high data rate channels will usually be booked for the envisaged monitoring period only.

5.4.3 Crew activities

A large part of the available crew time will be taken up with the supervision of the approach and the preparation of docking/berthing and post-contact activities. As the total number of crew at the target station will be limited, it cannot generally be assumed that shift work around the clock is a realistic option. The time needed for approach/contact monitoring and mating operations, including the time for potential contingency handling, must therefore fit into the work, rest and sleeping schedule of the target crew. A maximum of 10 hours can be assumed for one working session, into which all nominal and contingency operations must fit, i.e. rendezvous and docking/berthing operations up to utility connection, plus potential contingency operations until acquisition of a hold point. Such a hold point must be at a sufficient distance from the target, to be at least one night safe, until crew can again take action.

The target crew will have to monitor all rendezvous phases, which include a potential collision danger. These are all phases, starting from the transfer to the target orbit and

including the possibility of reaching the target within very few orbital revolutions. In the examples of figures 5.25 and 5.28, the manoeuvres, beginning with the transfer to the target orbit, take a duration of typically three half orbits. Including hold points, the total time of the approach which has to be monitored by the crew may take in the order of 2.5–3 hours. Adding the preparation time for the rendezvous related activities aboard the target, e.g. for check-out activities and for the time needed for post contact activities, e.g. pressurisation, verification of connections, preparation for hatch opening, the nominal duration of crew involvement in the rendezvous and docking process will be 4–6 hours. Because of the additional tasks for the manipulator operations, the total nominal duration of crew involvement in a berthing mission will be longer. The planning must include sufficient margins for contingency operations.

Although there will be a certain flexibility in the work/rest schedule by perhaps an hour forward or backward, larger shifts to provide synchronisation with the approach timeline and illumination conditions will have to be planned well in advance. Recovery operations after a contingency or a CAM and retreat to a far hold point can be performed at the earliest opportunity during the following working day.

5.4.4 Time-flexible elements in phasing and approach

Synchronisation of the rendezvous timeline with external constraints is, as shown above, a major issue in the design of the approach strategy at mission planning. During the mission, corrective synchronisation starts right after launch, and continues up to the final approach, to compensate for launch margins and manoeuvre tolerances. The trajectory elements and operational methods used to achieve synchronisation have been termed ‘time-flexible elements’. They can be grouped into drifts at different orbital heights and hold points. To a limited extent, the velocity profile of the straight line final approach can be modified to fine tune the arrival time.

Drift at different orbital heights

Three drift cases can be distinguished:

- drift on elliptic orbits – the advance depends on the size of the major axis;
- drift on circular orbits – the advance depends on the orbit radius, i.e. on the orbital height above ground;
- drift on two fixed major axes or orbital heights – variation of time of transfer.

The last method, which allows for adjustments during the mission, is shown in figure 5.22. Since phasing lasts for a number of orbital revolutions, the basic idea is to prepare at all times for two standard orbits of different sizes, either of different radii, in the case of circular orbits, or of different major axes in the case of elliptical orbits. According to synchronisation needs, the total duration of phasing can be decreased by leaving the chaser for a longer time on the lower orbit and it can be increased by transferring the

chaser earlier to the higher orbit. The standard orbits can be used for all missions of a certain type of vehicle, so such a strategy would be well suited for an automatic system.

Because of the relatively long time available during phasing and the complexity of the rendezvous phases after approach initiation ('S1' in figures 5.25 and 5.28) in terms of manoeuvres and of parties involved, it is usual to perform the synchronisation tasks, as far as possible, during phasing. The chaser arrives then at the approach initiation point at the proper time, leading to the proper illumination and communication conditions at capture, when all subsequent manoeuvre elements are executed nominally. In this case, hold points will be kept as short as possible, and they will be used for functional check-out and last fine tuning of arrival time only.

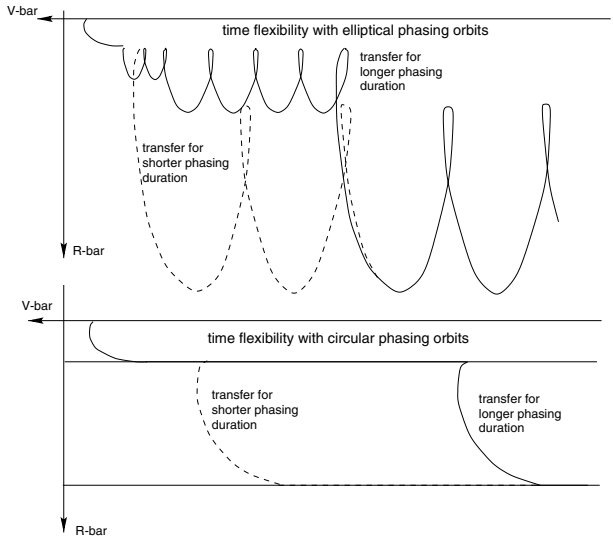

Figure 5.22. Time flexibility during phasing.

Hold points

Three trajectory elements with nominally zero average motion after one orbit exist:

- passive hold points only on V-bar,
- active hold points,
- safety ellipse.

Because of the increasing forces to be applied (see Eqs. (3.55) and (3.58)) with increasing distance from V-bar, this type of trajectory element is feasible only when the vehicle is on V-bar, or at least very near to it. Hold points on V-bar are in principle a very effective time-flexible element, as (theoretically) for their maintenance no forces are required. However, exact positioning on V-bar will not be possible, considering the

measurement and manoeuvre errors discussed in section 4.3. In reality, on passive hold points with no position control, the chaser will always drift either toward or away from the target. Drift direction and velocity will be as given in Eq. (3.24), according to its actual z-position below or above V-bar. A further cause of drift will be the effect of differential drag, discussed in section 4.2. Both sources can lead, even after very few orbits, to a significant change of position along V-bar. Because of this drift sensitivity, passive hold points can be used only for relatively short duration and at sufficiently long distances from the target.

The drift can of course be avoided by actively controlling the hold point position; this requires proper sensors and more propellant. The duration of a closed loop controlled hold point is constrained only by the consumption of propellant. However, in the case of a failure which results in a loss of control, it still must be ensured that no drift toward the target which may lead to collision will occur. A possible solution to the drift problem is the location of the hold point at a sufficiently large z-distance for an approach from the $-$V-bar side above the target orbit and for an approach from the $+$V-bar side below it. This z-distance must be chosen such that, for all conditions of differential drag and navigation errors, it is ensured that the chaser will never move toward the target. For a closed loop controlled hold point this will increase the propellant consumption significantly. In the open loop case, one could no longer call it a 'hold point'; a 'slow retro-drift' would be more correct.

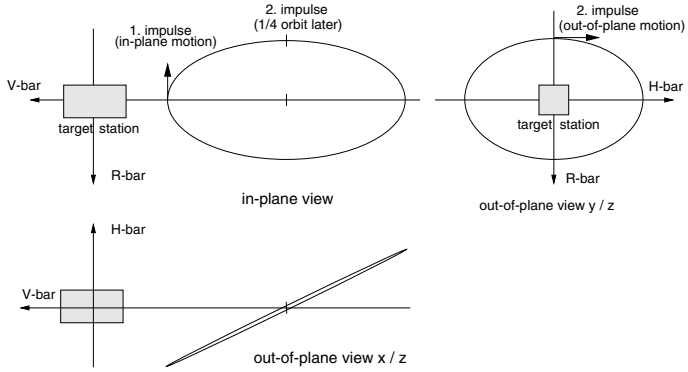

Figure 5.23. Safety ellipse.

Safety ellipse

The safety ellipse shown in figure 5.23 can be applied in cases where active hold point control or the above described 'slow retro-drift' is not possible (for whatever reason) and where a hold point type of time-flexible element is required for operational reasons. It consists of a combined in-plane and out-of-plane elliptic motion, which ensures that even in case of a drift toward the target, there will never be a collision, as the chaser will move around it on a distance given by the in-plane and out-of-plane excursions.

A safety ellipse can be implemented by applying a radial impulse (± R-bar direction) at the starting position on V-bar and an out-of-plane impulse (± H-bar direction) a quarter of an orbit later. It has to be pointed out also that the 'safety ellipse' will be only 'short term safe', as over a larger number of orbits the uncertainty of the differential drag has to be taken into account.

Velocity of straight line approach

The last chance of adjusting the arrival time is theoretically the variation of the approach velocity on the closed loop controlled straight line approach to a docking port or a berthing box. In practice this option will not be used, as the final approach will start only when it is proven that all conditions, including synchronisation, are nominal. Also, for reasons of approach safety, i.e. the assessment of the 'safe state' of the incoming vehicle by human operators in the target and on ground, it is preferred that the final part of the approach is performed with a standard velocity profile.

5.5 Onboard resources and operational reserves

Limitations concerning the availability of onboard resources can have significant repercussions on the approach concept. The most important resources in this respect are:

- electrical power,
- heat rejection capacity,
- propellant.

Limitations in available electrical power can be a reason to change the vehicle's attitude at regular intervals during the approach, e.g. from LVLH to Sun-pointing attitude, in order to obtain maximum output from the solar generators. This may lead to a strategy in which a Sun-pointing attitude will have to be assumed after any impulsive manoeuvre boosts and in the case of hold points. Hold points may be required to have a longer duration, or a larger number of hold points may be included in the approach to re-charge batteries than in cases without power constraints.

Limitations in the heat rejection capabilities may also result in a particular strategy, changing the attitude of a vehicle during approach whenever possible to a direction in which the heat radiating surfaces point toward deep space. Such requirements may have repercussions on the possibility of closed loop control of trajectories or hold points, as trajectory control sensors may not be available when the chaser is, e.g., in Sun-pointing attitude.

Propellant limitations may lead to the avoidance particularly of ΔV consuming trajectory types, such as straight line forced motion trajectories. Also, closed loop control of a trajectory after a boost, as described in section 4.4.1, may have to be excluded because of the significant additional propellant cost.

Mission planning for any rendezvous mission has to take into account the resources necessary for, e.g., a potential waiting time of a specified number of hours prior to start of the final rendezvous, or for the capability to repeat the approach a specified number of times. Such requirements are intended to cover the possibility of failures and delays caused by any party involved, i.e. chaser, target or all other elements of the space and ground segment. Considerations on how to minimise resources for recovery already have an influence on the design of the nominal approach strategy. For example, during close range rendezvous there will be a requirement to be able to retreat in the case of problems to a hold point from any point of the approach trajectory. This may be to the last hold point for those problems that are expected to be solved within same working session, or to a more distant hold point, where a longer period for resolution of the problems is expected. In order to minimise the cost for acquiring such hold points, the trajectory and manoeuvre of the nominal approach must be designed such that a retreat to the previous hold point is possible without excessive boost manoeuvres and within reasonable time. For example, such a requirement can lead, amongst other reasons, to the choice of a two-pulse *radial* boost transfer (see figures 3.20 and 3.21) for a certain part of the nominal approach strategy, as this type of trajectory will return to its starting point when the second boost is not executed. This means that whenever a retreat to the previous hold point is ordered, it can be achieved without extra cost within a time of between a half and one orbital revolution.

5.6 Approach rules defined by the target

Whereas during launch and phasing the approaching vehicle does not have many operational interfaces with the target vehicle and will be controlled by its control centre just as any single spacecraft, from some point during the far range rendezvous onwards, operations of chaser and target vehicles have to be planned and supervised in a coordinated way. As there will be different control teams responsible for the control of chaser and target vehicle, and as these teams may even belong to different organisations and space powers, a hierarchy of control authority and procedures of joint operation have to be established for the rendezvous operations in the proximity of the target (see chapter 9). In cases where one of the two vehicles, chaser or target, is manned and the other one is unmanned, the highest authority will have to be with the manned vehicle. This means that for an automated rendezvous of an unmanned chaser vehicle, the manned target space station, or its control centre on ground, will at a certain distance take over mission control authority for the rest of the rendezvous mission (for a definition of the various types of control authority see section 9.1.2).

In all cases a hand-over of control authority can best be achieved at defined points in the approach strategy, where the actual state of the vehicle w.r.t. the nominal one can be verified, or where there is subsequently sufficient time and opportunity for such verification. Hand-over of control authority does not necessarily include the hand-over of the actual command authority to control the vehicle, but concerns rather the highest level

decision making concerning trajectories and operations to be performed (see sections 9.1.1 and 9.1.2). Because of the need for defined interface and verification conditions at hand-over, this may have, amongst other conditions and rules, repercussions on the choice of the type of trajectory element during which hand-over has to take place.

Space stations, with their large and complex structures, can allow approach and departure of visiting vehicles only within certain spherical sectors, originating for docking at the docking ports or, in the case of berthing, at the nominal locations of grapple and release by the manipulator. In both cases, at implementation the origin and centre line of such cones will be determined by sensor and target pattern accommodation on chaser and target. Furthermore, safety of the station requires monitoring of the approaching or departing vehicles by the crew of the station and/or by the ground control centre of the station, in order to ensure that the trajectory and the other state vector parameters do not deviate from the planned ones. To establish references for control, volumes around the station can be defined in which visiting vehicles are subjected to certain rules (NASA 1994). Within such control zones, the hierarchy of control authority of the parties involved may be defined, maximum ΔVs allowed, operational procedures determined, approach and departure corridors defined, etc. Drivers and constraints for the definition of control zones can, for example, be

- the range where direct communication between the station and the visiting vehicle is available;
- the range from which the station could be reached within one orbital revolution, with a ΔV exceeding some defined small value;
- the range within which the visiting vehicle must fly inside approach and departure corridors in order to protect the structure of the station sufficiently against collision in the case of failures of the visiting vehicle;
- the range within which monitoring by video camera is possible, etc.

There are of course no exact physical laws to establish the size of such control zones, and their definition will, therefore, always be somewhat arbitrary. The purpose will rather be the definition of easily understandable and easily controllable boundaries at which the trajectory and state of the visiting vehicle can be checked against fixed criteria. The order of magnitude of potential effects will roughly determine the range of such boundaries. For instance, the boundary of the zone in which the visiting vehicle must move inside a defined corridor will be related to the size of the target vehicle. To be comfortable, the length of the corridor should be roughly one order of magnitude larger than the geometric extensions of the target station in that direction. If, e.g., the extension of the station in the x-direction is of the order of 20 m from the CoM, the length of the corridor can be envisaged to be 200 m. The definition of a control zone, in which execution of manoeuvres of a visiting vehicle will have to be agreed by the target, will depend on the typical size of such manoeuvres. If the ΔVs used in the rendezvous phase are, e.g., up to 0.1 m/s, a related control zone must be larger than 1800 m in $\pm$ V-bar direction (see Eqs. (3.28)). Drivers and constraints for the definition of the diameter of the approach and departure corridors include the following.

- *Observability*. In addition to the onboard data transmitted by the visiting vehicle, ground controllers and crew must be able to judge quickly upon the safety of the trajectory by means of direct vision or video. The nominal trajectory must be within a defined region of the field of view.
- *Thermal loads and contamination* by the thruster plumes of the approaching or departing vehicle on the surfaces of the target station must be limited.
- *Safety margins w.r.t. collision* around the geometry of the target station are necessary to prevent immediate impact in the case of failure of the visiting vehicle functions. This is a protection on the target side, which is independent of the failure tolerance requirements to be fulfilled on the side of the visiting vehicle (see section 4.1.1).

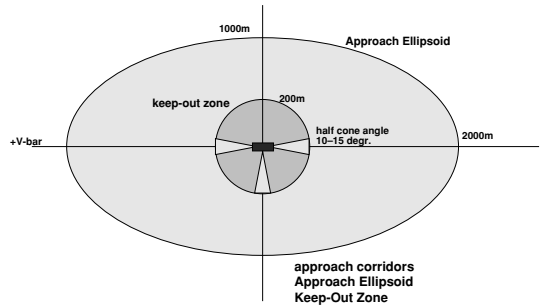

Figure 5.24. Control zones of the ISS.

Approach and departure corridors, however, must not be confused with the trajectory safety boundaries discussed in section tolerance requirements w.r.t. the target station, whereas the approach and departure corridors permit the target station to ensure observability and to limit thermal loads and contamination for the nominal approach and departure cases. Nominal approach and departure trajectories, including the safety boundaries, must be inside these corridors. Also, the corridors will also have to include some margin for the initiation of contingency operations by the visiting vehicle in the case of failure. In addition, margins must be taken into account for the attitude motion of the station itself. Depending on the range and the uncertainty of the attitude motion of the target, half cone angles of approach corridors (defined for the CoM of the approaching vehicle) may be between $\pm$ 5 deg and $\pm$ 15 deg.

For trajectories without thruster firings, e.g. after inhibition of thrust, after the nominal departure boost, after a boost for a contingency departure, or after a CAM, wider corridors may be defined. For this type of corridors, only protection against collision is the issue, rather than observability by cameras and protection against thruster plumes. It has to be noted that these wider approach and departure corridors will have to be defined not for the motion of the CoM but for that of the envelope of the vehicle, i.e. no part of the geometry of the visiting vehicle must exceed the corridor.

As an example, the control zones and approach/departure corridors of the ISS are shown in figure 5.24. The outer zone, called the 'Approach Ellipsoid' (AE), has an extension of $\pm$ 2000 m in the x-direction and $\pm$ 1000 m in the other directions. Prior to entering the AE, overall control authority will be taken over by the ISS Control Centre. The inner control zone, the so-called 'Keep-Out Zone', is a sphere of 200 m radius, which can be entered only through one of the approach and departure corridors, which are available for $\pm$ V-bar and $+$R-bar approaches. If they are defined w.r.t. the docking port axes or other body features of the station, the precise position and direction of these corridors will depend not only on the exact location of the docking ports and berthing boxes, but also on the main attitude of the station at the time of approach or departure.

5.7 Examples of approach strategies

In order to show the repercussions of various constraints on the choice of the trajectory elements used in the approach sequence, three examples of approach strategies will be discussed in this section. It is not the intention to analyse existing approach strategies of American and Russian vehicles, since these strategies have evolved over a very long time; some of the considerations leading to their design may have been driven by historical situations and are generally not known to the author. A brief description of the approach schemes of the US Space Shuttle and of the Russian vehicles Soyuz and Progress can be found in appendix B.

The three examples chosen are characterised by different directions of the final approach axis, by different sensor sets and by different mating methods, i.e. docking or berthing. These are as follows.

(1) Approach to a docking port on $-$V-bar; space station scenario with control zone setup; RGPS and optical laser scanner as rendezvous sensors.

(2) Approach to a berthing box on R-bar; space station scenario with control zone setup; RGPS and optical laser scanner as rendezvous sensors.

(3) Approach to a docking port on the $+$V-bar side with the docking axis skewed under an angle β w.r.t. the orbital velocity vector; radar and optical camera sensor as rendezvous sensors; no control zone constraints.

For all three examples a 400 km altitude quasi-circular orbit has been assumed. As launch and phasing will not be affected by the constraints for the relative navigation phases of a rendezvous mission, the discussion will start at the transition from phasing to the far range rendezvous.

5.7.1 Approach strategy, example 1

Strategy overview

This example of an approach to a $-$V-bar docking port in the ISS scenario is illustrated in figure 5.25. It is similar to the approach strategy of the European ATV (Cornier *et al.*

1999; Fabrega, Frezet & Gonnaud 1996) to the ISS. It is not the intention, however, to discuss here the actual approach strategy of the ATV project. The purpose of this example is rather to address the typical considerations for the design of a −V-bar approach concept to a docking port.

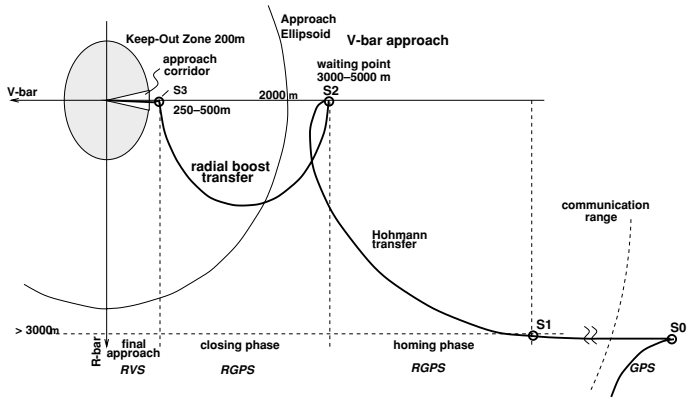

Figure 5.25. Approach strategy to −V-bar docking port (example 1).

The trajectory strategy consists of the following:

(1) *A free drift*. After the last phasing manoeuvre the chaser moves on a quasi-circular, 3000–5000 m lower orbit, parallel to V-bar. During the drift on this orbit, acquisition of the communication link to the target takes place and the navigation filter for RGPS converges.

(2) *A Hohmann transfer to the target orbit under RGPS navigation*. The transfer trajectory with all possible dispersions must not enter the approach ellipsoid of the ISS.

(3) *A hold point on the target orbit outside the Approach Ellipsoid*. At this point, last check-outs of the chaser system and last synchronisation corrections with external events, such as lighting conditions, crew schedule, etc., can take place. Further approach into the AE can commence only after permission from the ISS.

(4) *A radial boost transfer manoeuvre into the AE under RGPS navigation*. This transfer leads to a point where acquisition of the target reflectors by the optical rendezvous sensor can take place.

(5) *A forced motion straight line approach on, or parallel to, V-bar under optical RVS navigation*. This trajectory leads to the docking port. There may be optional stops on the straight line approach, e.g. to acquire a new navigation mode with relative attitude measurements.

The nominal attitude during the entire rendezvous approach is assumed for this example to be LVLH, i.e. aligned with the local orbital frame $\boldsymbol{F}_{\mathrm{lo}}$ of the chaser.

Acquisition of the target orbit

Location of the final aim point for phasing The rendezvous scenario starts at a point, identified in the figures as S0, which is the final point of the last phasing manoeuvre (initial aim point) and which is located below and behind the target. The location of this point will be defined by a number of desirable conditions on one side and constraints on the other side. The desirable conditions for initiation of far range rendezvous at S0 are as follows.

- Relative navigation should start at a distance behind the target, which is large enough to have sufficient time and range available for the manoeuvres necessary to reduce step-by-step position errors and velocities to those required for docking.
- The chaser orbit after the final phasing manoeuvre should be as close as possible to the altitude of the target orbit, to reduce the difference in orbital rate between the two vehicles and to create sufficient time for the above-mentioned manoeuvres.

The navigation sensor prior to S0 is, in this approach strategy example, assumed to be absolute GPS. RGPS will be acquired only during the drift between S0 and S1, after the chaser has entered the communication range with the target. The communication range is assumed to be 30 km for the purpose of this example. Navigation accuracy for absolute GPS is assumed to be of the order of 100 m and 0.1 m/s (i.e. the accuracy before abandonment of 'selective availability' for GPS; see section 7.3.2). Navigation errors can be cumulative, i.e. the existing position error at the start of the manoeuvre and the additional error after the second boost have to be taken into account. The initial velocity measurement error translates after the manoeuvre into a position error. Thrust errors of the last phasing manoeuvre depend on the type of thruster used and on the size of boost applied. The errors are assumed to be of the order of 0.2 m/s. The knowledge of the target position is assumed to be within 100 m and the evolution of the position error over one orbit is known to be not more than 50 m. The extension in the z-direction of the Approach Ellipsoid of the ISS is 1000 m (see figure 5.24). Summing up, the contributions to be taken into account for the definition of the altitude of S0 are:

- the required altitude difference due to rules for approach safety, set by the target, e.g. the Approach Ellipsoid in the case of the ISS (Δz_{AE} = 1000 m);
- the altitude uncertainties $\Delta z_{\epsilon\mathrm{targ}}$ due to the knowledge of the instantaneous position and due to the forecast accuracy for the evolution of the orbit of the target in the time between the manoeuvre boosts ($\Delta z_{\epsilon\mathrm{targ}} = 150$–$200$ m);
- the altitude errors $\Delta z_{\epsilon\mathrm{nav}}$ due to the navigation sensor accuracy, which is available to acquire S0 (due to position measurement error, $\Delta z_{\epsilon\mathrm{nav}} = 100$–$200$ m; due to velocity measurement error, $\Delta z_{\epsilon\mathrm{nav}} = 350$–$450$ m);
- the altitude errors $\Delta z_{\epsilon\mathrm{thr}}$ due to the thrust errors of the manoeuvres leading to S0 ($\Delta z_{\epsilon\mathrm{thr}} = 700$–$800$ m).

Additionally, a margin $\Delta z_{\mathrm{margin}}$ of 250–500 m has to be added for the definition of the nominal altitude of S0. This margin will have to cover such effects as the change of

relative orbital height between the vehicles due to differential drag during the drift phase after S0. The nominal relative altitude of the aim point w.r.t. the target orbit can then be calculated to be

$$\Delta z_{\mathrm{S0}} = \Delta z_{\mathrm{AE}} + \Delta z_{\epsilon\mathrm{targ}} + \Delta z_{\epsilon\mathrm{nav}} + \Delta z_{\epsilon\mathrm{thr}} + \Delta z_{\mathrm{margin}}$$

Adding up all errors and margins, the aim point for the final phasing manoeuvre will have to be of the order of 3000–5000 m below the nominal target orbit.

The contributions which have to be taken into account for definition of the location of S0 in orbit direction are as follows.

- The required distance Δx_{AE} due to the rules for approach safety set by the target, e.g. the Approach Ellipsoid in the case of the ISS ($\Delta x_{\mathrm{AE}} = 2000$ m).
- The position uncertainties $\Delta x_{\epsilon\mathrm{targ}}$ due to the knowledge of the instantaneous position and the forecast accuracy for the evolution of the orbit of the target between the manoeuvre boosts ($\Delta x_{\epsilon\mathrm{targ}} = 150$–$200$ m).
- Position errors $\Delta x_{\epsilon\mathrm{thr}}$ due to the thrust errors of the manoeuvres leading to S0 ($\Delta x_{\epsilon\mathrm{thr}} = 3400$–$3600$ m).
- Position errors $\Delta x_{\epsilon\mathrm{nav}}$ due to the navigation sensor accuracy available to acquire S0 (position measurement error, $\Delta x_{\epsilon\mathrm{nav}} = 100$–$200$ m, velocity measurement error, $\Delta x_{\epsilon\mathrm{nav}} \approx 3500$ m).
- The distance in orbit direction Δx_{Hoh} required for the Hohmann transfer from the S0 altitude to the target orbit, which is $\Delta x_{\mathrm{Hoh}} = \frac{3\pi}{4}\Delta z$ (see Eqs. (3.31)). With a Δz at S0 of 3000–5000 m, the x-distance for the Hohmann transfer becomes $\Delta x_{\mathrm{Hoh}} = 7000$–$12000$ m.
- A free drift distance $\Delta x_{\mathrm{drift}}$ between S0 and the starting point of the transfer manoeuvre, S1, equivalent to the time required for the preparation of the transfer manoeuvre. This may require manoeuvre confirmation by ground. Since the advance on a lower orbit per orbital revolution according to Eqs. (3.25) is $\Delta x = 3\pi\Delta z$, a total time for preparation of the manoeuvre and validation by ground of, e.g., 3 minutes, would result in an advance of the order of $\Delta x_{\mathrm{prep}} = 900$ m for a Δz of 3000 m and of $\Delta x_{\mathrm{prep}} = 1500$ m for a Δz of 5000 m.

  As the range of the communication link between chaser and target is assumed not large enough for RGPS navigation to be acquired prior to arrival at S0, a drift distance equivalent to the time required for convergence of the RGPS navigation filter (see chapters 6 and 7) needs to be added. With a time for filter convergence of 10 minutes, the advance in orbit direction would approach $\Delta x_{\mathrm{converg}} = 3000$ m for a Δz of 3000 m and of $\Delta x_{\mathrm{converg}} = 5000$ m for a Δz of 5000 m. The minimum required drift range is then $\Delta x_{\mathrm{drift}} = \Delta x_{\mathrm{prep}} + \Delta x_{\mathrm{converg}}$, which would amount to 3900 m for a 3000 m altitude difference and to 6500 m for a 5000 m altitude difference.

A margin must be added to these contributions, which takes into account further uncertainties and ensures that the hold point S2 on the target orbit will be outside the

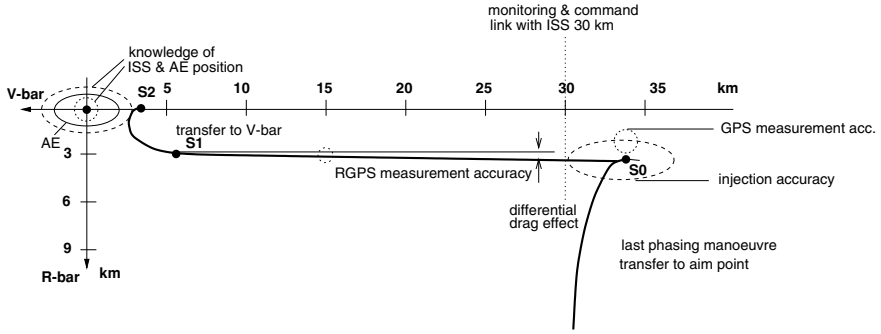

Figure 5.26. Acquisition of the target orbit (example 1).

Approach Ellipsoid. This margin should be at least of the order of 500–1000 m. The minimum relative distance in the orbit direction of the aim point w.r.t. the target position can then be calculated to be

$$\Delta x_{\mathrm{S0}} = \Delta x_{\mathrm{AE}} + \Delta x_{\epsilon\mathrm{targ}} + \Delta x_{\epsilon\mathrm{nav}} + \Delta x_{\epsilon\mathrm{thr}} + \Delta x_{\mathrm{Hoh}} + \Delta x_{\mathrm{drift}} + \Delta x_{\mathrm{margin}}$$

Adding up all worst case errors and margins, the minimum x-distance of the aim point for the final phasing manoeuvre would have to be of the order of 28 000 m behind the nominal target position. However, as S0 cannot be placed sufficiently inside the communication range of 30 000 m to prepare the second transfer manoeuvre under RGPS navigation, it will be better to place S0 such that its nominal position plus all possible dispersions are outside the communication range. This will make the approach more robust, as it ensures that sufficient time for filter convergence, manoeuvre preparation S1–S2, and validation by ground is available, and that short time communication interruptions can be covered.

Transfer to the target orbit From the above considerations it can be deduced that the hold point S2, i.e. the position after the Hohmann transfer to the target orbit, should, under no circumstances, be closer than 500 m to the boundary of the Approach Ellipsoid. For the definition of the nominal position and the dispersions of S2, the location of the starting point of the Hohmann transfer, S1, needs to be identified first. Three different strategies for the location of S1 can be considered.

(1) Start the Hohmann transfer at a fixed time after acquisition of the communication link between chaser and target, taking into account the time required for RGPS filter convergence plus a margin. This strategy results in a wide range of S2 locations, leading to a large variation of the ΔV required for the subsequent manoeuvre. The rationale for this strategy would be to obtain a more or less fixed duration of the drift phase between S0 and S1.

(2) Calculate the starting point S1 of the Hohmann transfer according to the altitude difference between drift orbit and target orbit such that the final point S2 will

always have the same nominal distance from the target. The rationale for this strategy would be to enable a standard manoeuvre strategy after arrival at S2.

(3) At a fixed time after acquisition of the communication link between chaser and target, start a two-pulse transfer with tangential and radial thrust components (Lambert targeting), aiming at a nominal position of S2. The rationale for this strategy would be to combine the rationales of (1) and (2).

Because of the necessary effort of verification and validation of manoeuvres and trajectories in a proximity operations scenario, and in particular within a multiple control authority environment, such as the ISS scenario, the second strategy is considered preferable, as for the transfer between S1 and S2 the verification and validation of tangential boost manoeuvres will be easier and more credible. Also, monitoring by operators on ground and in the target station will be easier with a nominal trajectory, which ends at a fixed nominal position and which does not cross V-bar. The variation in duration of the drift between S0 and S1 in the second strategy can easily be compensated for by a variable stay time at the hold point S2. For the approach after S2, in both cases (2) and (3) only one single manoeuvre plan has to be verified, which can be done prior to launch. The validation of the actual manoeuvres prior to execution will then be much easier, as it is then only necessary to check that the dispersions are within the tolerable margins. It must be kept in mind, however, that even with a standard manoeuvre plan the individual manoeuvres still have to be calculated and will vary due to the dispersions of the previous manoeuvre. These dispersions need to be corrected in the following manoeuvre, to remain as close as possible to the nominal trajectory plan.

Taking into account all the above considerations, the nominal position of the hold point S2 on the target orbit has been chosen, for the purpose of this example, to be 3000 m behind the target position. The start of the Hohmann transfer, i.e. the manoeuvre point S1, would then be for a 3000 m altitude difference of the drift orbit at $x_{\mathrm{S1}} = -10\,070$ m and for a 5000 m altitude difference at $x_{\mathrm{S1}} = -14\,780$ m.

Correction of out-of-plane errors Residual out-of-plane errors will be corrected successively during the last phasing manoeuvre and during the Hohmann transfer between S1 and S2. Such corrections can be executed either at a node crossing, or by manoeuvres separated by one quarter of an orbit, or by continuous corrections. The latter possibility would typically be used for closed loop controlled trajectory transfers.

Trajectory safety S0–S2 The final aim point for phasing, S0, has been placed, as discussed above, sufficiently below the approach ellipsoid such that the subsequent drift trajectory will never enter the AE, if no further manoeuvre is executed.

The passive trajectory safety features of a Hohmann transfer have been discussed already in section 4.4.2. If the second manoeuvre at S2 cannot be executed, the trajectory would loop below the AE and would, according to Eq. (3.29), return to the target orbit altitude in front of the target. This will be at a distance of about 4070 m, not taking

into account differential drag, for a transfer which had started from 3000 m below and about 8800 m behind the target. This distance of about 4000 m in front of the target for the return of the trajectory leaves sufficient margin for dispersions and drag effects. The figures indicate also that the nominal position of S2 should not be further than 5000 m behind the target position for this altitude difference. For partially executed manoeuvres, the possibility of collision cannot be excluded, and therefore a CAM must be available, the magnitude of which at least cancels the nominal boosts at S1 or S2. As a result, the ΔV of a CAM during a Hohmann transfer from, e.g., a 5000 m lower drift orbit must be at least 1.5 m/s.

Further, it has been assumed for this strategy example that the trajectory of the Hohmann transfer is closed loop controlled, as described in section 4.4.1, which adds active trajectory protection. The additional propellant expenditure for closed loop control is quite substantial when compared with the theoretical expenditure for a pure impulsive manoeuvre. As all ΔV cost for the rendezvous phase is, however, small compared with the ΔV required for phasing, the extra costs for closed loop control are considered worth the gain in trajectory safety and accuracy.

Approach recovery For all mission interruptions between the manoeuvre points S0 and S2, whether resulting from a cease of propulsion at S1 or S2, or from a CAM, the chaser will end up on a drift trajectory and will be a couple of kilometres in front of the target after one orbital revolution. As the communication link with the target may no longer exist, the first part of the recovery manoeuvres may have to be performed under absolute GPS navigation accuracy (for the purpose of this example, in the order of 100 m, the accuracy with SA). The recovery strategy would then be as follows:

(1) Acquire V-bar to reduce the relative motion between chaser and target as much as possible. Because of the assumed relatively low navigation accuracy of absolute GPS, V-bar acquisition will have to take place at a sufficiently large distance in front of the target ($\geq$10 km).
(2) Tangential boost transfer to a position at the $-$V-bar side at large distance ($>$50 km). To save propellant, this can be done in several loops, provided that the trajectory never enters the AE.
(3) From the position on $-$V-bar, further transfer to a 3000–5000 m lower drift orbit, such that on entering the communication range (30 km) the automatic approach can be re-acquired.

Acquisition of the final approach corridor (V-bar approach)

This phase is also called ‘closing’. Its task is to transfer the chaser vehicle from the hold point S2, outside the AE, to a point S3, which is inside the AE but outside the ‘Keep-Out Zone’ (KOZ). S3 is the point from which the final approach to docking can commence. The two major issues which determine the strategy for this phase are:

- the best location of the target point for closing, S3,
- the type of trajectory to be used for the transfer from S2 to S3.

The location of S3 will be determined essentially by four features:

(1) the radius of the KOZ;
(2) the maximum operational range of the rendezvous sensor, used for the final approach;
(3) the worst case position dispersion at S3 in case of loss of control after S2;
(4) the minimum useful range of RGPS, which is the trajectory sensor used during closing.

As already indicated in section 5.3.2, the lower boundary of the useful range of GPS and RGPS is given by multi-path and shadowing effects. The geometric extensions of the ISS are of the order of 100 m and include very large rotating solar arrays. Shadowing and multi-path effects on the GPS antenna of the chaser will become more pronounced when the distance is close to a few times the extension of the target. Since the visibility of GPS satellites by the ISS GPS antenna will also be constrained by the various structural elements of the station (see figures C.1 and C.2 for ISS configuration), the GPS receiver on the ISS will not be able to track all GPS satellites on the hemisphere. As a result, the number of common GPS satellites which can be tracked by both chaser and target receivers will become more and more reduced the closer the chaser gets. There will be a danger that the RGPS measurement function will be interrupted for longer than tolerable periods. In the ISS scenario it has, therefore, been concluded that GPS cannot safely be used below a range of 300 m. The maximum range of a laser range-finder, the sensor for the final approach, is a function of the emitting power of the laser beam (see section 7.4.1). Because of the limited power available on a spacecraft, sensors are designed to cover, along with the necessary margin, just the operational range needed. Laser range-finder sensors on the market or under development have, therefore, a maximum range of typically 500–1000 m. From these considerations, it can be concluded that, for the conditions of this strategy example, manoeuvre point S3 should be located between 300 m and 500 m from the target.

When selecting of the type of trajectory to be used for closing, the following features need to be considered:

- passive trajectory safety (no collision with ISS in the cases of missed or partial boosts);
- open loop dispersion of S3 (no penetration of KOZ in the case of loss of control after the first boost);
- ease of approach recovery (in the case of missed or partial boost or loss of control, trajectory should stay on $-$V-bar side);
- propellant expenditure (for comparison between trajectory types);
- transfer duration (short transfer times are preferable, because of the overall operational constraint addressed in section 5.4.3).

Concerning the type of trajectory, three options for closing are considered here:

(1) tangential boost transfer along V-bar,
(2) radial boost transfer along V-bar,
(3) straight line forced motion on V-bar.

These three types of trajectories are shown as solid lines in figure 5.27. Their follow-on drift trajectories after cease of thrust, indicating passive trajectory features, are shown as dotted lines.

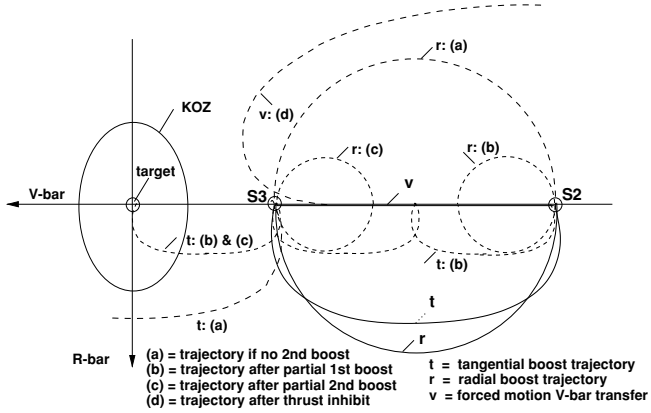

Figure 5.27. Passive safety of closing trajectories (example 1).

Tangential boost transfer The tangential boost transfer has the lowest propellant consumption of all trajectory types: the reference value for a theoretical impulsive transfer from 3000 m to 300 m is 0.33 m/s for the tangential transfer, whereas it is 4.7 times ($\frac{3\pi}{2}$) higher for the radial transfer. The transfer duration is one revolution, which may still be acceptable, but is twice as long as for the radial boost transfer. In the case of a missed burn in S3, the trajectory would loop forward under the target and reach the target orbit again at ≈2700 m in front of the target. However, passive trajectory safety requirements are not fulfilled in the case of partial burns, where collision with the target cannot be excluded (see section 4.4.2 and figure 5.27).

Sensitivity to thrust errors in terms of absolute values is higher than with the radial transfer, e.g. a thrust error of 0.01 m/s would result, for tangential transfer, in an x-position error of about 170 m, whereas for radial transfer there is an error of about 36 m. Approach recovery would have to start from the +V-bar side, in the same way as for the previous phase, whereas for radial transfer approach recovery it can commence in practically all cases (except for thruster open failures) from S2, i.e. from the conditions given in the mission interruption case (see below).

Straight line forced motion transfer The major disadvantage of the straight line forced motion approach for closing is the high propellant consumption. For transfer from 3000 m to 300 m the reference value for a theoretical transfer as defined in figure

3.24 would be, for a transfer duration of one orbital revolution, a factor of nearly 22 higher, and for one half revolution, 44 times higher than that for the tangential transfer. The straight line forced motion is passively safe. The type of trajectory, resulting after thrust inhibit, is shown in figures 3.13, 4.14 and 5.27. As the trajectory moves backward and returns to the target orbital altitude on the $-$V-bar side, approach recovery is easier than for tangential transfer, which, in the case of thrust inhibit, continues to move forward, always ending up at the $+$V-bar side. Trajectory recovery would not be as straightforward, however, as for radial transfer.

Choice of trajectory type Considering all criteria, conditions and features assumed for this strategy example, the radial boost transfer comes out as the best choice for the closing phase.

Trajectory safety of chosen strategy S2–S3 The basic features of passive trajectory safety of the radial boost transfer are discussed in section 4.4.2 and illustrated in figure 4.13. For completeness of the picture, these features are repeated here.

- If control ceases during the arc S2–S3, or second boost cannot be executed, return after one orbit to the starting point S2.
- If the first boost can be executed only partially, a loop of smaller size through S2 will commence.
- If the second boost can be executed only partially, a loop of smaller size through S3 will commence.

To compensate for the effects of differential drag in an open loop trajectory, a small tangential component could be added (its magnitude depending on the ratio of the ballistic coefficients), which ensures that the centre of the trajectory loop moves slowly away from the target. Since there will always be significant uncertainties concerning the actual value of differential drag, worst case assumptions have to be applied to achieve trajectory safety. As for the Hohmann transfer it has been assumed for the purpose of this strategy example that the trajectory will be closed loop controlled w.r.t. a nominal trajectory. This nominal trajectory will be calculated before the manoeuvre, taking the above-mentioned compensatory tangential component into account. If closed loop control ceases, the chaser remains on a short term safe trajectory.

Approach recovery Except for the case of a thruster-open failure and a subsequent CAM, approach recovery is, for this part of the approach, straightforward, as the free drift trajectories after thrust inhibit or partial boosts remain within the loop (plus some dispersions) described by the nominal S2–S3 arc and its corresponding return trajectory. Approach recovery can, therefore, be achieved in these cases by return to S2, and by application under ground control of a stop pulse to achieve a hold point. From S2 the automatic approach can be resumed. In the case of a CAM, the approach recovery procedure is as described for the Hohmann transfer.

Acquisition of the docking axis

The over-riding requirement for the last approach phase is that the trajectory, including all dispersions, has to be inside the approach corridor defined by the target station (discussed in section 5.6). The trajectory type of the last rendezvous phase is a straight line forced motion V-bar approach of the type described in section 3.3.2, which has been chosen for the following reasons.

- The setup of a narrow approach corridor of $\pm$ 10 deg (see figure 5.24) excludes any other trajectory choice for the last 200 m, if the approach time shall not become excessively long. Radial and tangential boost transfers would require a number of smaller loops of one or one half orbital revolution each to stay inside the corridor.
- The engagement of the docking interfaces of the two vehicles requires for the last few metres a straight approach line anyway. As the docking port may be located at a z-distance from V-bar (see figure 5.1), the approach line will not necessarily be exactly on the target orbit (V-bar) but at some distance from it (see figure 5.7).
- Monitoring of the final approach trajectory is much easier when this trajectory is a straight line.

The velocity profile along the approach line will consist of an acceleration phase at S3, a constant velocity phase and a deceleration phase when approaching the docking port. Velocity profiles are addressed in section 6.2.2. The deceleration phase ends when the final docking velocity is reached. It is followed by a constant velocity phase for the last few metres until contact with the target interfaces. The problem of acquisition and control of the instantaneous docking axis has been addressed already in section 2.4.2 and will be addressed again in section 6.2.3 (concerning the controller requirements) and in section 8.3.6 (concerning the required reception range of the capture mechanism).

If docking is to be performed under Sun illumination, the starting time w.r.t. orbital day and night at S3 and the approach velocity have to be chosen such that for the last few tens of metres optimal illumination conditions for optical monitoring (discussed in section 5.4.1) will be achieved. Another option would be to perform the final approach during orbital night and to illuminate the relevant docking and monitoring interfaces artificially. This would require, however, sufficient power resources and illumination equipment (floodlight, stroboscopic lamps, etc.) on at least one of the spacecraft.

Trajectory safety S3–contact Due to the trajectory rules of the Keep-Out Zone, which exclude any trajectory outside the approach corridor, in this phase passively safe trajectories as illustrated in figure 4.13 cannot be considered as a practical solution for approach safety. As a result of the geometric extension of the target in the z-direction, such safe trajectories would exist, in any case, only for large distances of 200 m or more.

The straight line approach on, or near, V-bar has, however, one very advantageous feature w.r.t. approach safety, i.e. that it can be stopped and held at any point, and that a hold is not very expensive in terms of propellant consumption. This can be seen as an additional safety feature for those types of failures which are not related to the control

and propulsion systems of the chaser, but would not allow continuation of the approach. If either a serious malfunction of a GNC function or of the propulsion system occurs during this phase, a CAM is again the sole safety means available.

Approach recovery The strategy for approach recovery after a CAM is identical to that of the previous phases. Approach recovery after a hold on V-bar is trivial, as only an acceleration to the nominal approach velocity at the particular distance is needed, from where switch-over to the nominal automatic approach is possible.

5.7.2 Approach strategy, example 2

Strategy overview

The second example is an R-bar approach to a berthing box in the ISS scenario. The example is, to a certain extent, similar to the approach strategy of the Japanese HTV (Kawasaki *et al*. 2000). Again, it is not intended to discuss here the approach strategy of an actual space project, but rather to address the typical constraints and considerations for the choice of trajectories. The trajectory sequence is shown in figure 5.28.The strategy for the acquisition of the target orbit is, in principle, the same as for example 1. It has been assumed, however, that in this case the last phasing manoeuvre to acquire manoeuvre point S0 can be performed inside the communication range with the target station. As a result, this last phasing manoeuvre can be performed with RGPS navigation accuracy, and the aim point S0 can be located more accurately at an altitude range of 2500–3000 m below the target orbit. The trajectory elements of the approach strategy after S0 in this second example consist of:

(1) a free drift from S0 until the first Hohmann boost at S1;
(2) a Hohmann transfer from S1 to a position S2 on the target orbit outside the AE;
(3) a hold point at S2 for approach synchronisation and check-out;
(4) a Hohmann transfer S2–S3 to a drift orbit 500 m below the target orbit;
(5) a drift trajectory toward the target at an altitude of 500 m below V-bar;
(6) a stop boost at S4 to cancel the drift velocity; S4 is located at, or close to, the x-position of the berthing box;
(7) a straight line closed loop controlled R-bar approach to the berthing box, which is assumed to be 15 m below V-bar;
(8) a closed loop controlled position keeping in the berthing box until the manipulator is ready for grappling.

Acquisition of the target orbit

As mentioned above, the scenario until S2 is very similar to the first example, except for the fact that the altitude difference between S0 and the target orbit is reduced due to the

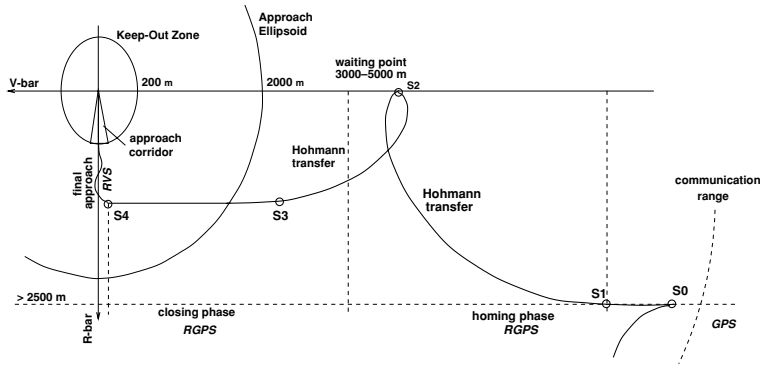

Figure 5.28. Approach strategy to berthing box on R-bar.

better navigation performance. The immediate consequence of this assumption is that the x-distance of S0 can be significantly reduced, because (a) there is no time needed for the RGPS filter convergence (this is assumed to have taken place prior to S0) and (b) the Δx required for the Hohmann transfer is smaller for the reduced altitude difference. The contributions which have to be taken into account for the definition of the altitude of S0 are, for this type of strategy:

- the extension in the x-direction of the AE (2000 m);
- the position errors due to the thrust errors of the manoeuvre leading to S0, when only the second boost can be performed under RGPS navigation (estimated 1500–3000 m);
- the distance on the drift orbit, due to the time required for the preparation of the manoeuvre S1–S2 (3 min drift at 3000 m altitude difference $\approx$900 m is assumed);
- the Δx required for the Hohmann transfer to S2 (7000 m for an altitude difference of 3000 m);
- the distance required between S2 and the AE boundary (this distance will depend on the safety features of the manoeuvres to be performed for the strategy of the subsequent approach phase – see below – and will be between 500 and 3000 m);
- a margin (500–1000 m) to cover boost errors, disturbances, etc.

For the initial aim point S0 of the last phasing manoeuvre, this adds up to a total Δx of 15 000–17 000 m behind the target position. This value also includes navigation errors, which are, however, comparatively small when using RGPS. Trajectory safety and approach recovery considerations for this approach phase from S0 until S2 are the same as in the first example.

Alternative strategies The question is, of course, why a transfer to the target orbit and a hold point on the target orbit at S2 would be necessary at all, since the approach

to the berthing box along a line parallel to R-bar needs to start for a lower orbit altitude anyway. Alternative strategies would be:

- a straight line forced motion R-bar approach from a 3000 m lower position to the berthing box;
- a tangential transfer from the 3000 m lower drift orbit to a point S2 on an orbit 300–500 m below the berthing box. This is followed by a drift to point S4 (in figure 5.28) from where the straight line R-bar approach to the berthing box can commence.

The first alternative has to be excluded because of excessive propellant cost. The second one would, on the contrary, have a lower propellant consumption and approach duration than the one proposed in the example and would also provide good trajectory safety properties. It would not provide, however, much time flexibility to achieve final approach conditions and to cover holds for operational reasons. If for any reason a stop of the approach for more than a few minutes became necessary, a transfer to a hold point on the target orbit would become indispensable. For this reason a hold point S2 on V-bar prior to the manoeuvres for acquisition of the final approach corridor has been considered advantageous and included in the chosen strategy. If, in a real mission, operational experience showed that so much time flexibility were not really required and the hold point on V-bar not necessary, the second alternative strategy would be the natural choice.

Acquisition of the final approach corridor (R-bar approach)

The retro-reflectors for final approach sensors are assumed to be mounted on the Earth-facing side of one of the modules of the station (see figure 5.30). Therefore, the approach taken to acquire the berthing box needs to start from a position S4 directly below these target reflectors. The location of manoeuvre point S4 has to be 300–500 m below the location of the target station to comply with both safety considerations (KOZ) and operational range of the RV-sensor. The selected strategy is

- a Hohmann transfer S2–S3 to a 500 m lower drift orbit and a subsequent drift to S4.

According to Eqs. (3.31), the x-distance for a transfer to a different altitude of $\Delta z = 500\,\mathrm{m}$ will be $\Delta x = \frac{3\pi}{4}\Delta z = 1178\,\mathrm{m}$ (without drag). If the second boost of the transfer must be applied for safety reasons outside the AE, the distance of S2 must be, including some margin, at least 1500 m from the AE or 3500 m from the target CoM. Actually, for the selected strategy of this example, a distance of 5000 m from the target CoM has been chosen. The rationale is that, if the second transfer boost cannot be executed, it will be better to have the subsequent apogee (trajectory returns to the target orbit) outside the AE.

Alternative strategies There are many other strategies with which it is possible to acquire an R-bar approach axis. A direct transfer from S2 to the final approach corridor by tangential or radial impulsive manoeuvres raises too many safety questions, as the trajectory may penetrate the KOZ if it cannot be stopped when arriving on the approach

axis. In order to show the considerations for strategy selection, therefore, the following three trajectory examples (see figure 5.29) will also be discussed, for comparison with the selected one:

(1) straight line forced motion transfer from S2 to a point S3f on V-bar, plus forced motion circular fly-around S3f–S4, as shown in figure 3.31;

(2) tangential two-boost transfer from S2 to a point S3t on V-bar, plus a tangential two-boost fly-around S3t–S4;

(3) radial two-boost transfer from S2 to a point S3r on V-bar, plus a radial two-boost fly-around S3r–S4.

For these alternative three cases, the distance of the hold point S2 from the AE can be much smaller, i.e. not more than 500–1000 m, as it has to include only a safety margin which is needed to cover the dispersions of the acquisition of S2. As it is necessary to reduce the relative x-velocity w.r.t. the target to zero, to start the R-bar approach, a stop pulse has to be applied at S4 in all four cases.

Both the tangential (trajectory type 2) and the radial (trajectory type 3) fly-around trajectories have a fixed ratio of $\Delta x : \Delta z$, which requires a start from the location of a particular point S3 on V-bar. For the radial boost fly-around with a Δz of 500 m, this is a distance of 1000 m, and for the tangential one it is about 1180 m. For the forced motion circular fly-around, the location of S3 would be, of course, 500 m from the target CoM.

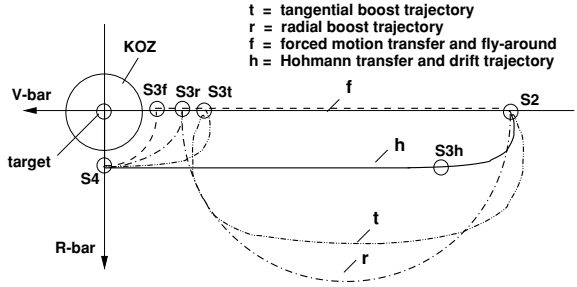

Figure 5.29. Alternative strategies for closing and fly-around (example 2).

Forced motion strategy The straight line transfer S2–S3f of alternative strategy (1) is extremely costly in terms of ΔV, as we have seen already in the first approach strategy example (section 5.7.1). This disadvantage outweighs by far the good monitoring and trajectory safety properties. The forced motion circular fly-around (strategy 1) is also much more propellant consuming than the other trajectory types, and does not provide any particular advantage over the other strategies in terms of trajectory safety or approach recovery. For this reason trajectory type (1) has to be discarded.

Radial boost strategy The advantage of the easy approach recovery with the radial transfer, which contributed to its selection in the case of the V-bar approach to docking

(approach strategy example 1), would be of course the same for the transfer from S2 to the starting point S3r of the fly-around. For the fly-around itself, this advantage is theoretically also present. However, the short distance to the KOZ and the lack of monitoring capabilities on the upper $(-z)$ side of the ISS would make a 360 deg fly-around unsafe. Also, the safety measure of a small additional ΔV in the tangential direction, as in the case of the closing transfer of strategy example (1), to ensure that the centre of the elliptic trajectory moves slowly away from the target, does not work for a fly-around.

The total duration of the closing and fly-around transfers with radial boosts would take three quarters of an orbital revolution, not including a potential hold after the closing transfer. Comparing the ΔV values for the theoretical impulsive transfers, the radial boost strategy (3) costs 4.2 times as much as the chosen strategy.

Tangential boost strategy The tangential transfer from S2 to the start of the fly-around is unsafe when considering the trajectory evolution after missed or partial thrusts. The same considerations as discussed in section 5.7.1 apply here (see figure 5.27). The tangential boost fly-around, which consists of the same size manoeuvre boosts as those of the last Hohmann transfer of the chosen strategy, is relatively safe. The next apogee would come back to V-bar in front of the target at a distance of about 1100 m, and the trajectory would loop out further in the forward direction. The total duration of the closing and fly-around transfers with tangential boosts would take one and a half orbital revolutions, not including a hold after the closing transfer. Comparing the ΔV values for the theoretical impulsive transfers, tangential boost strategy (2) costs 1.4 times as much as the chosen strategy.

Chosen strategy The easiest and least propellant consuming transfer method is, therefore, the Hohmann transfer to a 500 m lower orbit with subsequent drift (chosen strategy). The duration of the transfer S2–S4 is about 1.3 times an orbital revolution (T), i.e. $0.5T$ for the Hohmann transfer and $0.8T$ for the drift trajectory. Compared with the chosen strategy, the overall trajectory safety and approach recovery features of the radial boost strategy (2) would be no better, but those of tangential boost strategy (3) would be even worse.

Trajectory safety of the chosen strategy S2–S4 The sole critical part concerning trajectory safety is the Hohmann transfer to the 500 m lower drift orbit. Starting on the target orbit at S2, at $x = -5000$ m, the second manoeuvre boost has to be applied at S3h, at $x = 3822$ m. If the second boost cannot be applied, the undisturbed trajectory would return back to V-bar at an x-distance from the target of -2644 m (outside the AE) and, after a second revolution, at a distance of 288 m (outside the KOZ). The next return to V-bar would be at a safe distance in front of the target. However, considering differential drag and thrust errors, the free drift trajectory, following the missed second burn, could become safety-critical (depending on the ratio of the ballistic coefficients) at the second revolution. A shift in position of S2 further outwards would not change

the situation, as, in the case of a partial first burn, the target could be hit after a few revolutions anyway. It is, therefore, essential for this trajectory strategy to have a CAM available for the Hohmann transfer from S2 to S3h. The drift after S3h is safe: if the stop pulse in S4 cannot be applied, the chaser vehicle moves forward and eventually leaves the AE. In the case of a partial stop burn, the resulting velocity is slower than that of the corresponding circular orbit anyway, which results in a looping trajectory, starting in a downward ($+z$-direction) motion. The apogee of this trajectory is at the altitude of the drift orbit.

Approach recovery Approach recovery from positions on the drift orbit part of the trajectory S3–S4 would start with a continuation of the drift until the chaser vehicle is outside the KOZ or even outside the AE. This could become necessary, e.g., if the station denies further approach because of operational problems. As the relative drift velocity on a 500 m lower orbit is, at 0.85 m/s (about 4700 m per orbital revolution), still relatively slow, there will be sufficient time to plan and execute recovery manoeuvres. Whether the first recovery manoeuvre can still be executed inside the AE will depend on the ISS control authorities. The aim of the recovery strategy, which, due to the vicinity to the station, can probably be performed under RGPS navigation, will be to return to the hold point S2. From there, automatic approach can be re-initiated. In the case of a CAM, e.g. after failure during the S2–S3 transfer, approach recovery is identical to that from a CAM in the previous example.

Acquisition of the berthing box

The trajectory type for the approach to the berthing box is a straight line forced motion R-bar approach in the type described in section 3.3.3. As for the final approach in the previous example, the definition by the ISS of a narrow approach corridor of ± 10 deg excludes any other trajectory choice. Similar to the V-bar final approach, the velocity profile will contain an acceleration phase, a constant velocity phase and a deceleration phase, as illustrated in figure 6.6. The motion will be stopped at the nominal capture point, followed by a closed loop controlled position keeping mode. At that point, the manipulator end-effector will be moved into the close vicinity of the grapple fixture mounted on the target vehicle, and once it is ready for grappling the active control of the target will be switched off. The manipulator has then a limited time available to perform the grappling (section 5.3.1). It is important also that, during this time, the target station does not perform any manoeuvres which would make the grappling task more difficult. Station attitude motions should be as low as possible.

Trajectory safety S4–berthing box Passive trajectory safety properties, as illustrated in figure 4.14 for the forced motion V-bar approach, are in principle similarly available on a forced motion R-bar approach. Approaching on R-bar with velocity v_z, the trajectory which results after a thrust inhibit at a point z_0 is equivalent to a trajectory starting

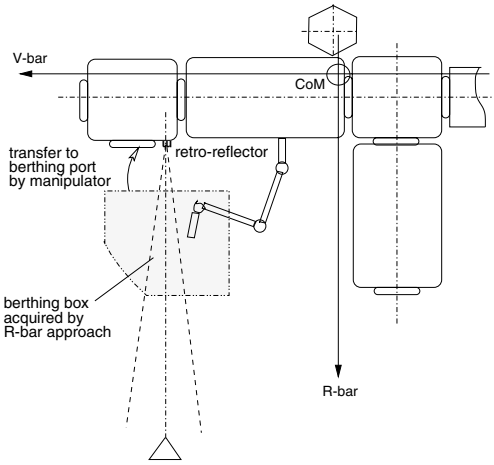

Figure 5.30. Approach to berthing box (ISS scenario).

at the same point z_0 with a radial ΔV_z of the same size. The trajectory evolution of this case can be obtained by addition of Eqs. (3.26) and (3.34). As the orbit dynamic forces, which move the trajectory away from the approach line, are, for a straight line R-bar approach, even stronger than in the V-bar case, it would be possible to design an approach velocity profile such that the trajectory remains passively safe until arrival in the berthing box. This requires, however, that the approach velocities are rather low (see

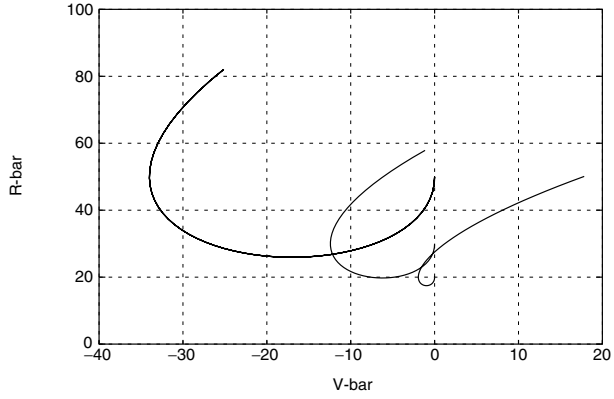

Figure 5.31. Example: trajectories after thrust inhibit during R-bar approach.

figure 5.31). Assuming an extension of the adjacent structure of the target vehicle in the z-direction, as shown in figure 5.30, of not more than 15 m, the approach velocity at

50 m should not exceed 0.1 m/s, at 30 m 0.05 m/s and at 20 m 0.02 m/s. This would result in a very long approach duration for the last few metres. Also, as in example 1, an approach/departure corridor is defined for free drift motions (no thruster activities). Taking into consideration the safety margins around the geometry of the ISS and the geometric extension of the chaser vehicle, the boundaries of this corridor would be exceeded by the free drift trajectories for practically all cases of position and velocity at thrust inhibit. For these reasons also in an R-bar scenario a CAM will be the sole safety measure for the final approach. A suitable CAM would, in contrast to the previous phases and to strategy example 1, consist of a ΔV in the $+z$-direction plus a ΔV in the $-x$-direction, as shown in figures 4.19 and 4.20.

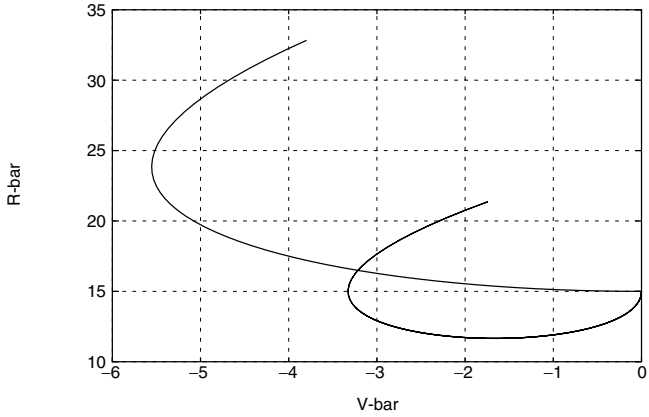

Figure 5.32. Example: trajectory safety at position keeping in berthing box.

The final trajectory element in this example of an R-bar approach to a berthing box is the active position keeping at a z-distance of 15 m from the target orbit. The safety of this part depends on the residual velocities at the time of loss of control.

Figure 5.32 shows the drift trajectories after inhibit of control for two cases: (a) a residual velocity of 0.02 m/s in the $-x$-direction and (b) a residual velocity of 0.02 m/s in the $-z$-direction. After sufficient time (shown are 10 min. for case (a) and 15 min. for case (b)), the free drift trajectories have turned away from the target. The two examples show, however, that within that time, with excursions of >3 m in the $-z$-direction and >5 m in the $-x$-direction, the trajectories would at least penetrate the safety margin around the station structure, if not lead to collision. It is obvious from this example that the residual velocities at thrust inhibit or loss of control in the berthing box would have to be much lower than 0.02 m/s, if one wanted to rely on passive trajectory safety. Otherwise, there would be the danger that the structure of the chaser, which may have geometrical extensions of a few metres, collides with that of the target within the first 5–10 min. As such a requirement would be unrealistic, for any malfunction of control and actuation in the berthing box a CAM will have to be applied.

The CAM for the berthing box will again be a combination of a ΔV in the $+z$- and in $-x$-directions, as in the final approach phase. As one will try for practical reasons to have only one fixed CAM manoeuvre stored per rendezvous phase, this CAM has to be defined according to the part of the trajectory with the maximum needs. For the R-bar trajectory, those maximum needs occur at the end of the approach, i.e. when arriving in the berthing box. In order to ensure that the trajectory after one orbital revolution will be, with sufficient margin, outside the AE, the CAM chosen for the final approach of this example is a boost of 0.5 m/s in the z-direction and 0.15 m/s in the $-x$-direction. The resulting trajectory is shown in figure 5.33. Starting at $z = 15$ m, the trajectory has moved at $z = 30$ m about 4 m into the $-x$-direction, reaching its maximum excursion in the $-x$-direction of less than 10 m at about $z = 80$ m. It can, therefore, be considered safe in the close vicinity of the berthing box. The trajectory does not return along the x-direction after one or more orbits closer than 2500 m to the target. The same CAM applied at the beginning of the trajectory, i.e. at $z = -500$ m, would be after one orbit at an x-distance of more than 21 km in front of the target, with an apogee at the same z-distance as the one at CAM initiation.

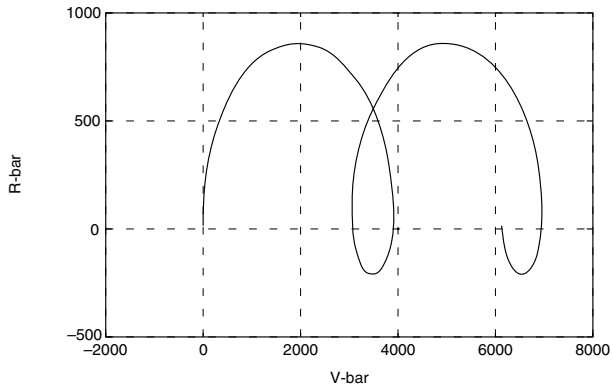

Figure 5.33. CAM trajectory $\Delta V_z = 0.5\,\mathrm{m/s}, \Delta V_x = -0.15$ m/s for R-bar approach.

Approach recovery The drift trajectory for the straight line R-bar approach following a CAM is, as we have seen, much more variable than for a straight line V-bar approach. The time and ΔV required for recovery will also depend much more on the conditions at CAM initiation, as for a V-bar CAM. The recovery strategy will therefore have to take time and propellant saving measures into account.

If the CAM had been initiated at the beginning of the straight line approach, i.e. at several hundred metres from the target orbit, the strategy will be to acquire V-bar as soon as possible, e.g. after the first revolution, to save time and propellant for recovery. Because of the large distance, navigation accuracy will be that of absolute GPS. The recovery strategy to return to S2 may include, e.g., a Hohmann transfer to a higher orbit,

after which the vehicle is drifting at a safe $-z$-distance above the target, and another one to acquire the manoeuvre point S2 on V-bar, from where the automatic approach can be initiated again.

If the CAM had been initiated at the end of the trajectory, i.e. near or in the berthing box, the x-distance after one orbit is still not very large and the apogee will even be above V-bar. The consequences are as follows: (a) there will be in this case more time available to implement corrective actions; (b) since the apogee of the trajectory is anyway above V-bar (see figure 5.33), it might be convenient to start a two-pulse or three-pulse transfer from there directly to S2.

5.7.3 Approach strategy, example 3

Strategy overview

The third example is a fictitious rescue mission to an incapacitated target vehicle, the docking port of which has a large attitude angle w.r.t. to the LVLH frame. It is assumed that the target has lost power and control, but that it had been designed to function as a target in a rendezvous mission. Because of the loss of control, the spacecraft has assumed a natural torque equilibrium attitude of the order of -30 deg w.r.t. V-bar, and because of the loss of power no communication of the target vehicle with the chaser or ground is possible. As a consequence, GPS on the target does not function, and therefore no RGPS navigation is available. The far and medium range rendezvous sensor used by the approaching vehicle is assumed to be radar. Furthermore, it is assumed that the incapacitated target vehicle possesses as interfaces for an optical rendezvous sensor the usual retro-reflectors near to the docking port and that the rescue vehicle has a camera type of rendezvous sensor.

The target vehicle is on a quasi-circular LEO orbit, the parameters of which are measured from ground by optical telescopes or radar with an accuracy of the order of 1 km. The chaser vehicle may have a GPS receiver, which can be used for absolute navigation, but would not be of much help for relative navigation with the target during rendezvous. In addition to the radar and the optical rendezvous sensor, it is assumed that the rescue vehicle has one or more navigation/observation cameras (e.g. star tracker type) available, which can be used for measurement of the direction of the target (azimuth and elevation angles) in the chaser attitude frame and for video monitoring of the target during approach.

For the far range, the approach strategy is to bring, relatively early, the apogee of the elliptic phasing orbit of the chaser to the altitude of the target orbit. This makes it possible, even at a large distance behind the target, to measure the elevation angle of the target using the navigation camera of the chaser. Using the camera measurements, the apogee of the chaser orbit can thereafter be adjusted more precisely to the target orbit, and also its perigee can be reduced successively. The aim of this series of manoeuvres is that the trajectory passes with its last apogee behind the target through a ‘gate’, as described in section 2.2.7. This ‘gate’ is a checkpoint which ensures that, at a defined

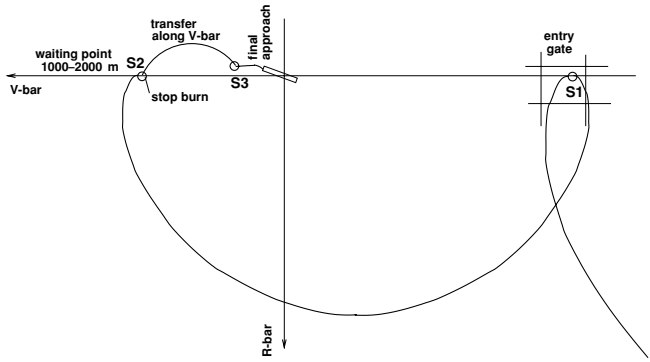

Figure 5.34. Approach strategy to docking port with large skew angle.

range, a defined set of orbit parameters w.r.t. the target is achieved; these parameters are necessary to initiate the close range rendezvous operations. The radar is assumed to have an operational range of the order of 50 km, from which point information on the range to the target is also available.

As the docking port is assumed to be on the +V-bar side, the further approach strategy from the entry gate onward is (see figure 5.34) as follows:

(1) Execution of a tangential boost manoeuvre in the +x-direction at the last apogee about 10 000 m behind the target (manoeuvre point S1), reducing the perigee such that the following apogee (manoeuvre point S2) will be at an x-position of 1000–2000 m in front of the target.

(2) Application of stop boost to acquire the closed loop controlled hold point S2 on the target orbit. The stay time in S2 is used for synchronisation with lighting conditions at docking,

(3) Radial boost transfer to a point S3 at 100–200 m from the docking port, where acquisition of the target retro-reflectors by the optical rendezvous sensor can take place.

(4) Short hold at S3 for inspection of the target docking interfaces by the navigation/observation camera prior to the final approach.

(5) Forced motion straight line approach parallel to V-bar down to a range between the sensor interfaces of 20–30 m.

(6) Circular fly-around of 30 deg to acquire the docking axis.

(7) Straight line approach up to contact on the docking axis, 30 deg canted w.r.t. V-bar.

Acquisition of the target orbit

As described above, the manoeuvres implemented to acquire the target orbit are assumed to be determined with the help of a camera. Assuming an angular resolution of the navigation camera measurements of the order of <0.05 deg, and a knowledge of the instantaneous attitude of the chaser in the LVLH frame of the same accuracy, the altitude uncertainty of the last apogee prior to S1 w.r.t. the target orbit can be reduced to a value of the order of 100 m. The above-mentioned 'entry gate' at S1 has to have an extension in the z-direction, which is equal to the navigation accuracy prior to radar acquisition, plus a margin. The extension of the 'gate' in the x-direction must be larger, according to Eq. (4.16), by a factor of at least 3π more. With the assumed operational range of the rendezvous radar of about 20–50 km, there may be, after radar acquisition, up to half an orbital revolution available to prepare the manoeuvre at S1 under radar navigation. This allows the subsequent transfer S1–S2 with a navigation accuracy of less than 10 m.

To see the target during radar navigation, the vehicle must point with the measurement axis of the radar toward the target, unless if the radar itself has articulation devices for pointing that are independent from the chaser vehicle. In the first case, because of the orbital arcs, the attitude of a vehicle pointing toward the target will change continuously, and with it the angles w.r.t. the Sun and the Earth. This fact will then have repercussions concerning (1) the resolution of ΔV commands into thrust commands for the individual thrusters, in the case of mid-course corrections, and (2) the power budget and the antenna coverage for communication with ground.

Because the mission assumed for this example 3 is not a routine mission, and that the position of S1 is not firmly fixed, the transfer S1–S2 will, in contrast to example 1, not be closed loop controlled. With mid-course corrections, the accuracy of the acquisition of S2 will be of the order of a few tens of metres. However, as the position of S2 will be closed loop controlled under radar navigation after the stop boost of the S1–S2 transfer, the dispersion of S2 can be reduced during station keeping to about 10–20 m. Since for this mission scenario no traffic control zones and rules are to be observed, as for the previous two examples, the hold point S2 could be moved closer to the target.

Trajectory safety S1–S2 For this phase, similar trajectory safety considerations exist as for the same phase of example 1. The big difference is, however, that if no, or only a partial, boost can be executed at S1 and S2, the trajectory is still safe. As the manoeuvre at S1 is a braking boost, a partial boost will lead to a larger loop than planned, putting the chaser further out in front of the target. A loss of boost or a partial boost at S2, which is, in contrast to example 1, now in front of the target, results in a forward motion, leading away from the target. Although the manoeuvres at, and the trajectory between, S1 and S2 are safe, it would still be advisable to have a CAM available to cover other malfunctions of the onboard system.

For the execution of a CAM during the phase S1–S2, the situation will be more complex if the radar antenna is not articulated and the vehicle has to point the docking axis and the axis of the radar antenna toward the target. At S1 and S2 the chaser is aligned

with the LVLH frame and its docking port points toward the target. In this attitude, a CAM in the opposite direction of the docking axis, as in example 1, can be executed. Between S1 and S2 there will be a point where the docking axis is pointing in such a direction that a simple CAM in the opposite direction of the docking axis will resolve to such ΔV_x and ΔV_z components that the resulting trajectory can hit the target. An example which would lead to a near collision with the target is given in figure 5.35, which is based on the following assumptions:

- The first part of the trajectory is the nominal transfer from S1 $= -10\,000$ m to S2 $= +1000$ m.
- After 0.76 orbital revolution, a severe malfunction of the attitude control system occurs and a CAM is initiated, i.e. a single boost of 1 m/s in the negative direction of the docking axis of the spacecraft.
  - The trajectory position at this instant is $x = 690$ m, $z = 1094$ m.
  - The pointing angle is $\phi = 57.8$ deg w.r.t. V-bar.
  - With this pointing angle, a CAM of 1 m/s has the components $\Delta V_x = 0.533\mathrm{m/s}$ and $\Delta V_z = 0.846$ m/s.

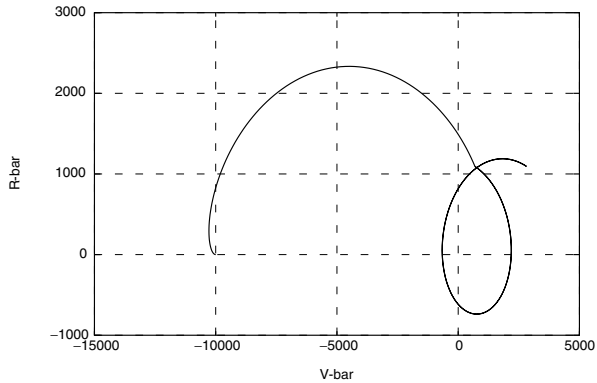

Figure 5.35. Example: CAM at transfer to S2 with target pointing chaser.

This example shows that, whenever the attitude changes significantly over the transfer trajectory, there is no immediate simple solution for a set of boosts which is valid for all points of the trajectory. In such cases, either a particular set of boosts has to be stored in the GNC system for each point, or the vehicle has first to be slewed to a LVLH attitude before the CAM is executed. Both possibilities require basic GNC functions to be available, which is not compatible with the concept of a CAM as a last resort.

Acquisition of the final approach corridor

For the transfer from S2 to S3, a radial boost manoeuvre has been chosen for the same reasons as in example 1. The transfer trajectory S2–S3 is assumed to be closed loop

controlled to achieve the necessary accuracy in manoeuvre point S3. The navigation accuracy of the radar improves with the approach, as indicated in figure 5.10. It is assumed that the radar can track particular known features on the target structure, so that the accuracy of the measurement is not corrupted by reflections from different unknown surfaces of the target. The requirements for the position accuracy in S3 come from two factors:

- *Safety*: the uncertainty of the position must not be more than 10% of the range to the target structure, leading to a position accuracy requirement in approach direction of about 10 m at S3.
- *RV-sensor*: the sensor has a field of view of $\pm$ 15 deg. This leads, for sensor acquisition, including margins for attitude control, to a position accuracy requirement in the lateral directions of $<$ 20 m. If the radar measurement has a different reference point on the target than the centre of the docking port, this difference, if not known, will reduce further the permitted lateral performance value.

The camera type of rendezvous sensor is assumed to have a position measurement performance at 200 m of better than 4 m and at 100 m of better than 1 m.

After optical RV-sensor acquisition, the hold point S3 will be position controlled w.r.t. the target reflector pattern on the target. With the assumed TEA angle of 30 deg and an assumed distance of the docking port from the target CoM of 20 m, S3 has a z-position of -11.5 m above V-bar.

Trajectory safety S2–S3 Because of the z-distance of more than 11 m above V-bar, the hold point S3 is not passively safe. In the case of loss of control, the chaser would advance during one orbital period according to Eqs. (3.25) by an amount $\Delta x = 3\pi\Delta z = 108\,\mathrm{m}$ toward the target. Passive trajectory safety and approach recovery considerations for the trajectory element S2–S3 are, for the rest of approach, the same as those of the same phase in example 1, as long as the chaser has an LVLH attitude.

If the radar antenna has no articulation and the chaser is pointing towards the target, as discussed already in the previous phase, the situation with a CAM would be more complicated. Due to the resulting changes of the vehicle attitude over the trajectory S2–S3, the CAM would have thrust components in the $+z$-direction, depending on the position of initiation along the trajectory. The effect of this z-component has to be considered in the evolution of the CAM trajectory. In the assumed scenario, the chaser attitude angle can have values up to $\phi = 35.2$ deg, resulting in a reduction in the x-component of the thrust by a factor of $\cos\phi = 0.817$, which still produces a large ΔV_x-component. In addition, for this trajectory the pointing angle always produces a ΔV_z-component in the $-z$-direction, which helps the escape.

An example for a CAM trajectory initiated at the position with the largest pointing angle ϕ is given in figure 5.36:

- the first part of the trajectory (small arc) is the nominal transfer from S2 $= +1000$ m to S3$= +100$ m;
- after 0.418 orbital revolution, a CAM is initiated;

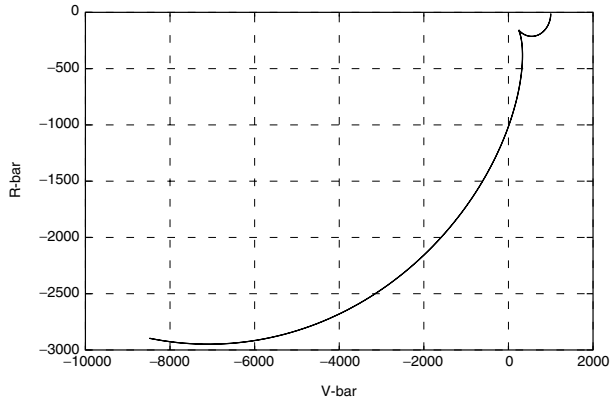

Figure 5.36. Example: CAM at transfer to S3 with target pointing chaser.

- the trajectory position is, at this point, $x = 240.9$ m and z $= -156.6$ m;
- the pointing angle at this point is $\phi = 33$ deg w.r.t V-bar;
- With a CAM of -1 m/s, the components are $\Delta V_x = 0.838$ m/s and $\Delta V_z = -0.545$ m/s.

For all other points, the pointing angle will be smaller and, because of the larger ΔV_x-component, the arc of the CAM trajectories will be larger. A single retro-boost in the opposite direction along the body axis of the chaser will, therefore, be sufficient as a CAM for this approach phase, even for a target pointing chaser.

Acquisition of the docking axis

The final approach up to S4 is in principle identical to that of example 1, described in section 5.7.1, with the exception that it will take place at a larger z-distance from V-bar. The repercussions of this fact on trajectory safety have been discussed already in section 5.3.1. There is in this third example no limitation by an approach corridor. However, the limited FOV of the camera type RV-sensor of ± 15 deg puts a comparable constraint on the trajectory design.

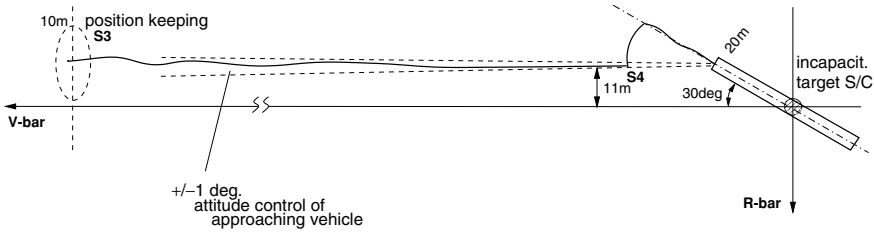

Figure 5.37. Final approach to docking port with large skew angle.

At a range of 20–30 m from the docking port, a closed loop controlled circular fly-around (see Eqs. (3.77) and (3.79)) will be performed. This can be implemented by keeping the range constant, controlling the centre of the target reflector pattern to remain in the centre of the FOV of the sensor, and commanding an attitude slew velocity, moving the chaser docking axis downward. The attitude slew, together with the control of a constant range and the target pattern in the centre, will result in an upward motion ($-z$-direction), which will be stopped when the relative attitude measured by the RVS becomes zero. From this position a straight line forced motion approach along the docking axis with a constant velocity of 0.05 m/s is performed until contact.

Trajectory safety S4–contact As in example 1, passive trajectory safety features cannot be exploited for the final approach. In this example, the passive trajectory features are even worse than in example 1 because of the z-distance of the approach line above V-bar . For this reason a CAM is the sole safety means available in all cases of loss of control. Similar to the first example, a hold and retreat on the trajectory is possible at reasonable propellant cost, as long as the GNC system is still functioning. The CAM for the final approach is again a boost in opposite approach direction. Even at an angle of 30 deg the component of the thrust in the x-direction is still 86% of the total thrust, which will result in an escape trajectory looping in a $-x$-direction. With a boost of, e.g., 0.5 m/s, this would cause the trajectory to return to the target orbit at about 7000 m behind the target.

6

The onboard rendezvous control system

The intention of this chapter is to provide the reader with a short overview of the typical tasks, functions and system hierarchy of an automatic onboard control system for a rendezvous and docking mission. It should provide a basic understanding of the concepts used for various functions, without entering into the details of actual designs. The functions required for automatic control of the vehicle's state vector, for automatic sequencing of manoeuvres and control modes and for automatic detection of failures and initiation of recovery actions are discussed. In section 6.5, the interaction of human operators with an automatic control system and the replacement of some of its functions by human operators is briefly addressed.

6.1 Tasks and functions

During the rendezvous and docking process, the automatic onboard system has to fulfil the following tasks:

(1) preparation and execution of manoeuvres and continuous control of trajectory and attitude (guidance, navigation and control = GNC);

(2) sequencing of phases, GNC modes or manoeuvres, and scheduling of equipment for such modes (mission and vehicle management = MVM);

(3) detection and recovery from system and equipment failures and from critical state vector deviations (failure detection, isolation and recovery = FDIR);

(4) data exchange concerning the rendezvous process and the onboard control system with the ground control centre and the target space station.

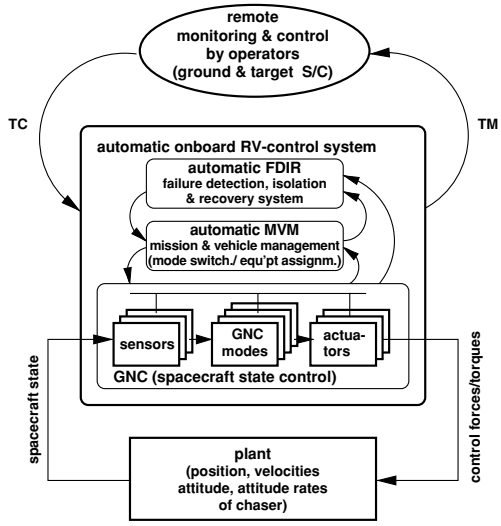

Figure 6.1. Hierarchy of control system for RVD.

There are obviously a number of other functions that the onboard system has to fulfil, such as power, thermal control and housekeeping functions. These functions, however, are not specific to rendezvous and capture, and therefore need not be addressed here. Repercussions on the trajectory strategy and GNC implementation of constraints concerning the resources for other such functions have been addressed in section 5.5.

To fulfil all the above listed tasks, the onboard control system for RVD will have to be designed according to a hierarchical structure, where the 'failure detection, isolation and recovery' (FDIR) function will have to exist at the highest level of authority. The typical hierarchy of the overall control setup for automatic rendezvous is shown in figure 6.1. This simplified figure shows only the levels of authority, not the actual functional relations within such a system. For instance, there will be the need to have failure detection functions at all levels, including on a lower level in the GNC software functions and in the sensor and actuator hardware, as will be explained in section 6.4.

As in an Earth orbit there is no need to perform the rendezvous process fully autonomously, there will be another hierarchical level above the FDIR function outside the chaser vehicle, i.e. the monitoring and control by human operators, aided by automatic tools, on ground and in the target space station. The onboard control system must be designed to allow monitoring and interaction by remote operators (see chapter 9). In the case of contingencies, operators, together with their support tools, may take over one or more of the above listed tasks. A particular case is the remote manual control of the GNC functions by human operators, which is addressed in more detail in section 6.5.

6.2 Guidance, navigation and control

The control loops for attitude and trajectory control include the sensors for position and attitude measurement, the GNC functions, which are implemented in software in the onboard computer, i.e. the navigation, guidance and control functions, and the thrusters and other actuators for attitude and position control. A block diagram of a typical control loop for one of the six degrees of freedom (DOF) is shown in figure 6.2. The disturbances acting on the spacecraft state, such as orbital disturbances and thrust errors, have been discussed already in chapter 4, whereas errors and disturbances of the sensors (block 'measurement environment and disturbances' in figure 6.2) will be covered in chapter 7.

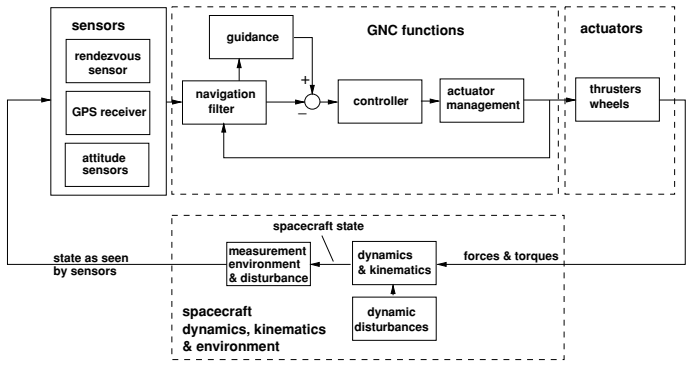

Figure 6.2. GNC functions.

Such a loop has to be implemented for each of the six degrees of freedom to be controlled, i.e. three for rotation and three for translation. During the approach, depending on the distance from the target vehicle, various translation and attitude manoeuvres have to be executed, and various types of trajectories must be controlled (see the previous chapter), for which different sensor types have to be used. This requires a reconfiguration of the control loops each time, in which algorithms and parameters of the navigation, guidance and control functions may have to be changed. The set of algorithms and parameters required for the execution of a particular manoeuvre or trajectory is termed 'GNC mode'. According to the main functions of a GNC system, the GNC modes consist of a set of different navigation, guidance and control modes. The management of these modes, i.e. the engagement of the proper algorithm and parameters, will be discussed in section 6.3.

As long as the distance between the two vehicles is large enough, each DOF rotation and translation may be controlled independently by a SISO (single-input–single-output) control system. For spacecraft with a symmetric shape, e.g. cylindrical ones, the individual body axes can be considered as decoupled. Therefore, SISO control design

techniques can be applied for attitude control as well. In docking, during the last part of the approach, when the docking mechanism of the chaser vehicle has to be aligned with the docking port of the target vehicle, all motions are coupled. In this case a MIMO (multiple-input–multiple-output) control system will have advantages. MIMO control may not be necessary, however, for the approach to a berthing box, as in this case angular alignment is less critical (see section 5.3).

For each navigation mode, the navigation function consists of a Kalman filter, which processes the various information of attitude (gyros, updated by Sun, Earth and/or star sensors) and trajectory sensors (RGPS, RVS) and propagates the vehicle state in position and attitude by using the knowledge of the dynamic behaviour and information on the actual thrust commands (see section 6.2.1). The guidance function defines the set values for the nominal evolution of the spacecraft state, i.e. the references for the control of position, velocities, attitude and angular rates at each point in time (see section 6.2.2). The control function produces the force and torque commands necessary to achieve the desired corrections in attitude and trajectory and to ensure stability of the vehicle. The thruster management function transforms the torque and force commands into 'on/off' commands for the individual thrusters. This function is of particular importance for vehicles which have their thrusters located in an unbalanced arrangement w.r.t. the centre of mass. In such cases each translation force and each rotation torque has to be produced by a combination of various thrusters with burns of different duration. Control function and thruster management function are addressed in section 6.2.3.

6.2.1 The navigation filter

The task of the navigation function is to provide the controller and the guidance function with the necessary information on the present state of the vehicle. As a rule, this function is implemented as a digital filter which processes the various information inputs related to the vehicle state obtained from different sensors, from the actuators or via communication links from external sources. The purpose of such a filter is to obtain out of several inputs related to the vehicle state an estimation of the state vector with reduced noise errors. A filter, which propagates the state, will also be helpful in cases where the sensor information is only intermittently available. If there were a single sensor continuously providing all necessary information on the state vector with sufficiently low noise, the navigation function could be reduced to converting the sensor information to formats as required by the guidance and control functions.

Principle of a Kalman filter

In a navigation system that is obtaining information from different sources, a best possible estimate for the actual state vector has to be calculated from the various inputs. In systems operating in computation cycles, the output of the navigation function has, in addition, to be a propagation of this estimate as an input to the following cycle of the control output calculation. The algorithms generally used for this estimation are those

relating to the Kalman filter (Kalman 1960), an optimal estimator in the 'least square' sense, which minimises the variance of the estimation error. The Kalman filter is well documented in the literature, and detailed descriptions and derivations of the filter equations can be found in many text books on digital control of dynamic processes, such as Issermann (1981) Brown & Hwang (1992) and Franklin, Powell & Workman (1998). For the description of the functional principles of a GNC system, it will not be necessary to repeat all the details relating to the Kalman filter; the intention of the following brief description is to familiarise the reader with the basic principles of the function of a Kalman filter, as far as is necessary for the understanding of the general operating principle of a navigation filter and in the possibilities of failure identification (see figure 6.18). The latter problems are discussed in more detail in section 6.4.

It shall be assumed here that the state of a discrete time invariant plant at the step '$k+1$' can be described by

$$\mathbf{x}_{k+1} = \mathbf{A}\mathbf{x}_k + \mathbf{B}\mathbf{u}_k + \mathbf{w} \tag{6.1}$$

(see also Eq. (A.16) in appendix A), and the measurements related to the state at the step 'k' can be described by

$$\mathbf{y}_k = \mathbf{G}\mathbf{x}_k + \mathbf{v} \tag{6.2}$$

where

$\mathbf{A}$ is the state transition matrix, which describes in the given dynamic process the changes of the state from step 'k' to '$k+1$';
$\mathbf{B}$ is the input matrix, which describes the relations between the inputs $\mathbf{u}$ and change of the state vector;
$\mathbf{u}$ are the external inputs to the system between steps 'k' and '$k+1$', e.g., in the case of a spacecraft, the control forces and torques;
$\mathbf{w}$ is the system noise;
$\mathbf{G}$ is the measurement model matrix (also called the output matrix), describing the theoretical relations between various measurements and the state vector;
$\mathbf{v}$ is the measurement noise.

The principle of filter operation is to provide, at each step, a prediction, i.e. a propagation in time, and a correction, i.e. an update based on measurements. The following calculations are performed. At each processing step the filter provides first a propagated value of the state vector for the new step

$$\mathbf{x}^*_{k+1} = \mathbf{A}\hat{\mathbf{x}}_k + \mathbf{B}\mathbf{u}_k \tag{6.3}$$

and a propagated (expected) value for the new measurement vector

$$\mathbf{y}^*_{k+1} = \mathbf{G}\mathbf{A}\hat{\mathbf{x}}_k \tag{6.4}$$

Both are calculated from the estimated state vector of the previous step and from the expected changes between 'k' and '$k+1$', given by the transition matrix.

The new estimate for the state vector at step '$k+1$' is calculated using the propagated value plus a correction, based on the difference between the new measurement vector $\mathbf{y}_{k+1}$ and the expected one:

$$\hat{\mathbf{x}}_{k+1} = \mathbf{x}^*_{k+1} + \mathbf{K}_{k+1}[\mathbf{y}_{k+1} - \mathbf{y}^*_{k+1}] \tag{6.5}$$

In words, we could state this as

$$\begin{matrix}\text{new}\\ \text{estimate}\end{matrix} = \begin{matrix}\text{predicted estimate,}\\ \text{based on old estimate}\end{matrix} + \begin{matrix}\text{correction}\\ \text{matrix}\end{matrix}\left(\begin{matrix}\text{new}\\ \text{measurement}\end{matrix} - \begin{matrix}\text{predicted measurement,}\\ \text{based on old estimate}\end{matrix}\right)$$

The difference between the new and the propagated observation, $\mathbf{y}_{k+1} - \mathbf{y}^*_{k+1}$, is in the literature often referred to as the 'innovation'.

We now need $\mathbf{K}$, the correction matrix (also called the 'gain matrix'), which provides a weighting factor for the contribution of the innovation information to the value of the new estimate:

$$\mathbf{K}_{k+1} = \mathbf{P}^*_{k+1}\mathbf{G}^{\mathrm{T}}[\mathbf{R} + \mathbf{G}\mathbf{P}^*_{k+1}\mathbf{G}^{\mathrm{T}}]^{-1} \tag{6.6}$$

where $\mathbf{P}^*_{k+1}$ is the estimation error covariance matrix propagated from the previous step, and $\mathbf{R}$ is the covariance matrix for the measurement noise $\mathbf{v}$.

The covariance matrix $\mathbf{P}_{k+1}$ of the state vector error for the new step '$k+1$' will be obtained using the propagated value $\mathbf{P}^*_{k+1}$ and the correction matrix K_{k+1}:

$$\mathbf{P}_{k+1} = \mathbf{P}^*_{k+1}[1 - \mathbf{K}_{k+1}\mathbf{G}] \tag{6.7}$$

The updated error covariance matrix $\mathbf{P}_{k+1}$ is not used in the gain matrix calculation of the present step, but will be used to calculate the propagated value for the subsequent step. In step '$k+1$' the propagated error covariance matrix $\mathbf{P}^*_{k+1}$ is calculated from the value obtained for the previous step 'k' as follows:

$$\mathbf{P}^*_{k+1} = \mathbf{A}\mathbf{P}_k\mathbf{A}^{\mathrm{T}} + \mathbf{Q} \tag{6.8}$$

where $\mathbf{Q}$ is a covariance matrix for the system noise $\mathbf{w}$, for which white noise is assumed. The values for $\mathbf{x}_{k+1}$ and $\mathbf{P}_{k+1}$ calculated from Eqs. (6.5) and (6.7) will become the $\mathbf{x}_k$ and $\mathbf{P}_k$ in Eqs. (6.3) and (6.8) of the calculations in the subsequent step.

The principle of operation of a Kalman filter is shown in figure 6.3, which indicates schematically the flow of data and the major calculations to be performed during one cycle. The interruption of the data flow return lines from the state estimation and error covariance matrix outputs to the propagation block indicate that these outputs will be used in the subsequent cycle. The block labelled 'preparation of measurement vector' indicates that the individual measurements obtained from various types of sensors may first have to be brought into a form suitable for further use in the subsequent calculations.

The Kalman solution has some practical implementation drawbacks. It is valid, in theory, only for cases where prediction and measurement errors are equal to Gaussian random processes with zero mean. The effects of errors with a different distribution law

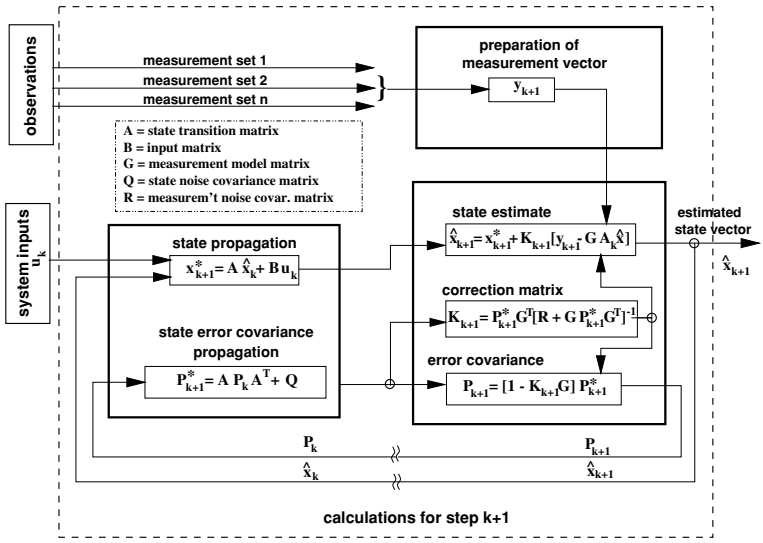

Figure 6.3. Block diagram of a Kalman filter.

(e.g. gravity errors in the prediction or measurement biases in the innovation), will have to be approximated by 'equivalent' zero-mean Gaussian random processes.

The Kalman gain computation, Eq. (6.6), and the associated covariance matrix propagation, Eqs. (6.3) and (6.8), can be extremely expensive in terms of computer load if the dimension of the state vector is not small. This can be problematic for the limited capabilities of the computer hardware available for operation in space at the time of writing, but may be less of a problem in the future, when more powerful space-qualified computers become available. The following solutions can be used to circumvent these limitations:

- the coefficients of the matrix $\mathbf{K}$ can be determined in simple SISO cases by pole placement, selecting a limited set of acceptable 'physical' coefficients, such as bandwidth and damping ratio, on the combined propagation, update equations;
- the Kalman equation can be solved to determine asymptotic gains, for k going to $+\infty$.

Performance evaluation analyses then permit convergence on an adequate set of gains. These are efficient methods for stationary systems, i.e. systems where measurements and transition matrices do not face significant variation w.r.t. time. One or the other of the above methods can be used on a sequential set of working set-points, in order to determine pre-programmed gains, which will be used in sequence as the mission advances. This feature is called 'gain scheduling'. An example is the use of a set of successive gain matrices for the rendezvous sensor based navigation estimation, in cases where the sensor accuracy improves commensurate with decreasing distance between sensor and target.

Rotational and translational motion components in the state vector

During the rendezvous phases, after relative navigation has started, the state vector $\mathbf{x}$ to be estimated consists of the instantaneous position $\mathbf{p}$ and the velocity vector $\mathbf{v}$, measured in the local orbital frame $\boldsymbol{F}_{\mathbf{lo}}$ of the target, and of the attitude angles $\boldsymbol{\alpha}$ and angular rates $\boldsymbol{\omega} = \dot{\boldsymbol{\alpha}}$, measured between the spacecraft attitude frame $\boldsymbol{F}_{\mathbf{a}}$ (body frame) and the reference frame (i.e. the local orbital frame $\boldsymbol{F}_{\mathbf{lo}}$ of the chaser), measured in the $\boldsymbol{F}_{\mathbf{a}}$ frame:[1]

$$\mathbf{x} = [\mathbf{p}, \mathbf{v}, \boldsymbol{\alpha}, \dot{\boldsymbol{\alpha}}]^{\mathrm{T}} \tag{6.9}$$

$$\mathbf{p} = \begin{bmatrix} x \\ y \\ x \end{bmatrix} \qquad \mathbf{v} = \begin{bmatrix} \dot{x} \\ \dot{y} \\ \dot{z} \end{bmatrix} \qquad \boldsymbol{\alpha} = \begin{bmatrix} \alpha_x \\ \alpha_y \\ \alpha_z \end{bmatrix} \qquad \boldsymbol{\omega} = \begin{bmatrix} \omega_x \\ \omega_y \\ \omega_z \end{bmatrix} \tag{6.10}$$

In docking, during the last part of the approach the navigation must be related to the docking frame of the chaser, which requires the availability of information on the relative attitude between the vehicles as an additional part of the state vector. The relative attitude vector $\boldsymbol{\delta} = \boldsymbol{\alpha}_{\mathrm{chaser}} - \boldsymbol{\alpha}_{\mathrm{target}}$ is measured in the $\boldsymbol{F}_{\mathbf{a}}$ of the chaser:

$$\boldsymbol{\delta} = \begin{bmatrix} \delta_x \\ \delta_y \\ \delta_z \end{bmatrix} \tag{6.11}$$

In the relative navigation phases the state transition matrix for the translational motion components $\mathbf{A}_{\mathrm{trans}}$ and the input matrix $\mathbf{B}_{\mathrm{trans}}$ in Eqs. (6.3), (6.4) and (6.8) can be derived from the Clohessy–Wiltshire equations (3.22). For the rotational motion components, the state transition matrix $\mathbf{A}_{\mathrm{rot}}$ can be derived from the angular momentum law. A derivation of the equations of motion is provided in appendix A.

Navigation filter issues relevant to rendezvous missions

After the initiation of the filter, time is needed to reach a steady state in the feedback system of predictions and corrections. Depending on the dynamics of the process, on the noise and on the tuning of the filter parameters, this may take, in the case of navigation filters for spacecraft, up to a few minutes. Filter convergence time has to be taken into account in the planning of manoeuvre schedules, since, when a new sensor is introduced, the full navigation performance required for calculation of the manoeuvre boost will be available only after convergence of the navigation filter.

Filter convergence requires that the error covariance matrix $\mathbf{P}_{\boldsymbol{k}}$ becomes stable, i.e. that the corrections to the state vector reach a consistent level. The filter can diverge, in which case the difference between the estimated state vector and the measurements increase with each cycle, when either:

[1] The angular velocity vector $\boldsymbol{\omega}$ should not be confused with the orbital rate ω_0.

- the measurement data are inconsistent, the measurement model matrix $\mathbf{G}$ and/or the input matrix $\mathbf{B}$ do not represent the relations to the real world correctly, or
- the state noise in relation to measurement noise has not been modelled correctly.

Whether the input matrix and the measurement model matrix are representative of the situation can be verified by analysis and test prior to the mission; inconsistencies in the measurement data, however, can be caused both by sensor failures and by disturbances in the measurement environment, which may be more difficult to determine beforehand. Also, extreme changes in the measurement noise may affect the balance between the covariance matrices for state noise and measurement noise.

Depending on the type of state vector information required for the different GNC modes in the various rendezvous approach phases, and on the type of sensors or other sources of information to be used, different navigation filters will have to be designed.

- A filter for absolute attitude estimation providing the attitude information for the other filters and for use as navigation filter in contingency situations where position information is no longer available.
- A filter for absolute position estimation using, e.g., absolute GPS information, required during phasing, in contingency phases and to provide observation input for the relative navigation filter.
- Filters for relative navigation between chaser and target for the rendezvous phases proper. Due to the different measurement principles, dynamics, noise and error characteristics, different filter designs will be needed per type of sensor used, e.g. for
  - relative GPS,
  - radio-frequency sensors, such as radar,
  - scanning laser range finders,
  - camera sensors.
- Different filter designs may be needed also in the case of the same type of sensor, where a different type of information is used, during the various approach/departure phases. This is the case, e.g., in the last part of the approach, when the rendezvous sensor also has to provide relative attitude.

The primary sensors providing the input for absolute attitude $\boldsymbol{\alpha}$ and angular rates $\dot{\boldsymbol{\alpha}}$ will be the gyroscopes. However, as gyro output drifts over time, updates will be necessary in regular intervals using measurements of extero-receptive sensors such as Earth, Sun or star sensors. Intervals of updating and the switching to the updating mode will have to be controlled by the mission management function (see section 6.3). Relative attitude information, required for the last part of the approach to docking, will usually be provided by an optical rendezvous sensor. The various types of rendezvous sensors, which provide measurements necessary for trajectory control in the different rendezvous phases (i.e. measurements of x-, y-, z-position, or of range r and direction angles ψ, θ, and of the relative attitude vector $\boldsymbol{\delta}$ for the last part of the final approach) will be discussed in more detail in chapter 7 (see figures 7.28, 7.29 and 7.31).

As navigation filters for different inputs and outputs can be active in parallel, the inputs to the measurement vector block are obtained either directly from trajectory sensors and attitude sensors or from another navigation filter, as described above. Information on the thrust commands, as produced by the thruster management function, will be used as the input for the state vector propagation. As the thrust command information is related to a geometric frame of the spacecraft ($\boldsymbol{F}_{\mathbf{ge}}$, see section 3.1.5), information on the absolute attitude must also be provided to the propagation block, in order to be able to propagate the translation motion in the local orbital frame $\boldsymbol{F}_{\mathbf{lo}}$.

6.2.2 The guidance function

The task of the guidance function is to provide at each point the set values for the state vector in time, which will then be compared with the estimated actual values, provided by the navigation function, enabling the control function to prepare the control commands. Depending on the manoeuvres and trajectories to be implemented, the guidance function has to:

- pre-calculate boost manoeuvres in terms of execution time and duration;
- generate position and velocity profiles, $\mathbf{p}(t)$ and $\mathbf{v}(t)$, in all axes for closed loop controlled trajectories and hold points;
- generate attitude profiles $\boldsymbol{\alpha}(t)$, e.g. for spacecraft pointing towards Earth, the Sun or a target vehicle, and angular rate profiles $\dot{\boldsymbol{\alpha}}(t)$ for closed loop controlled slew manoeuvres (large attitude angle rotation);
- propagate the instantaneous position of the centre of mass in the vehicle body frame according to the propellant consumption during the mission.

The last of the above tasks could have been grouped under a different function. As it is, however, neither a typical navigation task nor a typical control task, it has been listed here under the guidance tasks. The propagation of the instantaneous position of the spacecraft's CoM w.r.t. a body reference frame ($\boldsymbol{F}_{\mathbf{ge}}$) is a continuous update process throughout the mission, which does not depend on the type of manoeuvre executed or the state to be achieved, but rather on the amount of propellant consumed and on the location of the tank it is drawn from. The result of this update is used in the navigation function (e.g. in the input matrix of the navigation filter), in the control function (e.g. for the thruster management function) and in the guidance function (e.g. for the coordinate transformation from the sensor or docking frame to the nominal attitude frame).

The first three tasks are the classic guidance tasks, defining the state to be achieved over time. According to the strategy chosen for rendezvous and departure (see section 5.7), some of the following modes may have to be implemented. Typical nominal approach and departure modes are

- two-boost tangential and radial transfers,
- position keeping on V-bar and R-bar,
- fly-arounds to an R-bar approach line or to arbitrary x-, y-, z- positions,

- straight line approaches on V-bar and R-bar,
- straight line approach to a docking axis pointing in arbitrary directions,
- free drift (no position control) with and without attitude control,
- slew to an arbitrary attitude.

Typical contingency modes are

- braking and hold on V-bar,
- braking and straight line retreat on docking axis (V-bar and R-bar),
- two-boost radial transfer to, and acquisition of, a hold point,
- two-boost tangential transfer to, and acquisition of, a hold point,
- slew manoeuvre to Sun-pointing attitude.

The guidance laws for translation motion will be derived from the trajectory equations in chapter 3 for the various impulsive manoeuvres and continuous thrust trajectories. Disturbances, in particular differential drag between chaser and target, may have to be taken into account in the calculation of the nominal trajectory evolution. For open loop manoeuvres this will be a necessity in any case; for closed loop controlled trajectories, drag forces and other disturbances will continuously be counteracted by the control forces, as far as they have not been taken into account in the calculation of the nominal trajectory. For rotational motion, the guidance laws define the profile over time for the attitude angles relative to Earth, the Sun or the target vehicle, and for the angular rates in the case of slew manoeuvres.

Whereas the guidance laws can be validated prior to the mission and stored in the onboard data management system, the guidance parameters will in many cases have to be calculated from the actual state and the state to be achieved immediately prior to a manoeuvre. This is particularly so for the ΔVs to be applied and the time when they have to be executed. For instance two-boost transfers may be implemented as:

- open loop manoeuvres, in which case the guidance function has to calculate the start time and the duration of each boost;
- manoeuvres with mid-course corrections (figure 6.4), in which case the guidance function has to calculate, in addition, for pre-determined points in time, the correction boosts, derived from the nominal trajectory development vs. the actual one, as determined by the navigation function;
- closed loop controlled trajectories, in which case the guidance function provides the control function with the actual nominal value for the state vector at each process cycle between the boosts (see figures 4.8 and 4.9 in section 4.4.1).

The guidance laws have to take into account that the propulsion system can realise neither perfect impulses nor continuous accelerations. Thruster operation will always consist of a series of boosts of limited time. For two-pulse transfers the thrust duration t_2 of each pulse τ and the start time of the second pulse have to be calculated, as indicated for two examples in section 3.3.3. For constant thrust manoeuvres, such as straight line V-bar and R-bar approaches, the required thrust level has to be realised by pulse width modulation. Accordingly, the guidance laws have to take into account that there will be

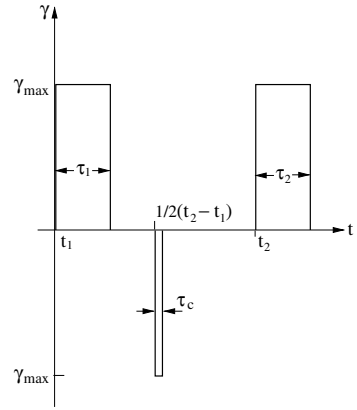

Figure 6.4. Two-boost transfer manoeuvres with mid-course correction.

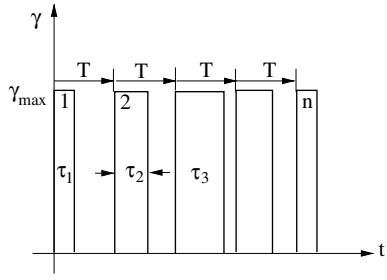

Figure 6.5. Pulse width modulation.

a minimum or threshold acceleration level, since the minimum pulse duration for τ in figures 6.4 and 6.5 will be determined by the characteristics of the thruster (minimum impulse bit, MIB) and by thrust efficiency considerations (see also figure 6.14). The minimum granularity will thus be given by the thrust duration $\tau_{\min}$ and the duration T of the computation cycle, i.e. the minimum average thrust level is

$$\gamma_{\min} = \frac{\tau_{\min}}{T}\gamma_{\max}$$

The maximum average thrust level is obviously achieved when the 'on' time τ is equal to the cycle duration T. In this case, the thruster will not be switched off at the end of the cycle. When large accelerations are required, this condition can last over many cycles. For modes where such large accelerations are not required, the condition of continuous 'thruster on' may be used as a failure criterion (see section 6.4). In any case, the guidance laws must be designed such that the acceleration request does not exceed the maximum possible thrust level.

For forced motion straight line approaches and similar trajectory elements, an acceleration profile has to be implemented at the start of the motion to achieve a desired approach velocity. Correspondingly, at the end a deceleration profile has to be implemented to arrive at the desired position with the desired velocity. At the start of motion a constant acceleration will bring the vehicle in the shortest possible time to the desired approach velocity, and thrust in this direction can be stopped when the velocity is achieved. For the deceleration phase constant thrust is less desirable, as not only a final velocity but also a final position has to be achieved, and thrust level errors would translate into position errors with the square of the time. For this reason, other guidance laws have been developed, such as exponential deceleration.

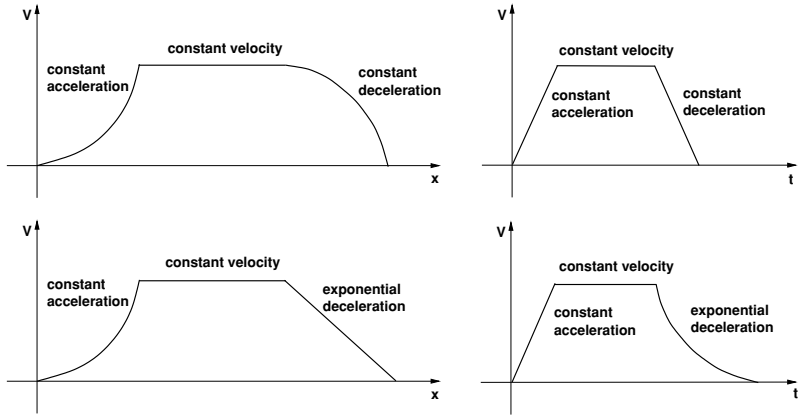

Figure 6.6. Examples of velocity profiles.

The exponential braking law, which has been formulated to fulfil passive safety criteria in case of loss of thrust (see figure 4.14), is characterised by an exponential change of position and velocity with time of the type

$$\begin{aligned} x(t) &= X_0 \cdot \mathrm{e}^{-\frac{t-t_0}{\lambda}} \\ \dot{x}(t) &= \dot{X}_0 \cdot \mathrm{e}^{-\frac{t-t_0}{\lambda}} \end{aligned}$$

which results in a linear profile in the approach phase plane of

$$\dot{x}(t) = \dot{X}_0 - \lambda(x(t) - X_0)$$

with λ being a proportionality factor, tuned to the safety area required by the target station.

Other schemes, such as proportional braking, are conceivable, which reduce the applied deceleration proportional to the elapsed time in order to allow a smooth acquisition

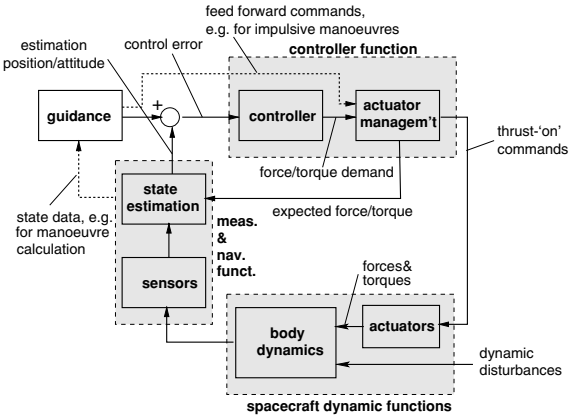

Figure 6.7. Functional block diagram of a closed loop controlled spacecraft.

of a pre-determined velocity at a particular position. Such a scheme would, however, result in even longer braking times.

Finally, another potential task of the guidance function should be mentioned, which has already been addressed in section 4.4.1, i.e., for closed loop controlled trajectories, the calculation of safety boundaries around each component of the state vector for each point in time, as discussed in section 4.4.1. This information will have to be provided to the FDI function (see section 6.4, figure 6.20) in case such state vector 'corridor' checks are included in the system design. The state vector safety boundaries have to be calculated together with the nominal trajectory.

6.2.3 The control function

The task of the control function is to provide the force and torque commands which will be executed by the reaction control system of the spacecraft to correct the deviations of the actual state vector from the nominal one. While the guidance function provides the nominal or reference state (previous section), and the navigation function estimates the actual state (addressed in section 6.2.1), from the differences of the two states the control function produces actuation commands to compensate for the effects of disturbances and errors. The performance of such a control loop is determined by the dynamic behaviour and errors of its elements and by the disturbances acting on them. The various disturbances and their points of interaction are shown in figure 6.8.

For the purpose of discussion of the control function, the functional blocks of figure 6.2 have been re-arranged into the reference functional block diagram, figure 6.7. Groups of functions which will be treated later in this section by a single mathematical model (transfer function) are marked by shaded boxes.

The *plant* in figure 6.7 is the block representing the six degree of freedom motion dynamics of the spacecraft, i.e. the dynamics of translational motion (position dynamics) and rotational motion (attitude dynamics). The coupling between translational and rotational motion is due to the orbital rotation (small) and the translational components $r \cdot \sin\alpha$ that result from a rotation angle α at a distance r from the centre of rotation. The latter effect plays a role when the vehicle is controlled w.r.t. a frame which does not originate in its CoM. This is the case when both lateral and rotational alignment with the target docking axis has to be achieved prior to contact. In all other cases, coupling of translational and rotational motions is rather small, and can usually be neglected. The position dynamics of motions of the CoM in orbit can be described, as already mentioned, by the Hill equations, Eq. (3.21), and the attitude dynamics by Euler's moment equations (see appendix A).

The *measurement and navigation function* includes the sensors and the state estimation, i.e. the navigation filter discussed in section 6.2.1. As already stated above, for measurement of the rotational motion the sensors used are inertial sensors, i.e. any type of gyroscopes. The measurement principles of sensors used for translational motion or position measurement are treated in chapter 7. Since all sensors are imperfect (bias, noise, disturbance by measurement environment, bandwidth), measurement performance enters the loop and impacts on the overall system behaviour.

The *controller function* includes, for the purpose of control loop analysis, the controller proper and the actuator management function, which translates the force/torque commands into 'on/off' commands for the individual thrusters. As the coupling between rotational and translational motion is rather small, for most of the approach, except for the last metres prior to docking, where the position and attitude loops can be separated. For the actuator management function this is true only provided the propulsion system allows independent control of position and attitude.

The *actuation system* is composed of thrusters, which in a spacecraft generally may be supported by rotating actuators (wheels) and magneto-torquers to reduce fuel consumption. In the case of a chaser vehicle for rendezvous, usually no rotating actuators are used, because (a) for such a short mission the added mass and complexity due to the additional hardware would outweigh the propellant mass saving by wheels, and (b) because the presence of an angular momentum would complicate the spacecraft dynamics in the last phase prior to contact. Concerning the forces and torques produced, the actuation system belongs in the control loop analysis to the block 'spacecraft dynamics'.

During the final phase of the rendezvous, the six degrees of freedom of motion of the vehicle must be controlled simultaneously. This could in principle be done by selecting a set of thrusters with components in three directions, and generating for each operating cycle the needed force/torque vector. Due to operational constraints of the thrusters, this may lead, however, to imperfect force and torque realisation, which creates input disturbances to both the position and attitude dynamics (see Eq. (6.30)).

Analytical relations in a control loop

For convenience of analysis, the closed loop system is usually described by a linear approximation about the operating point of the real function, which may be non-linear in its full range. This permits modelling of the system by a set of first order differential equations and the application of Laplace transforms, which transform the differential equations into easier to solve algebraic ones. From the controller design and analysis point of view, the block diagram, figure 6.7, may be redrawn into figure 6.8, which will be used as the reference diagram for the short explanation of control analysis in this section. The control loop is characterised by the transfer functions of its elements:

$$\begin{aligned} K(s) &= \text{transfer function of the controller} \\ G(s) &= \text{transfer function of the plant (spacecraft dynamics)} \\ M(s) &= \text{transfer function of the sensing function (measurement} \\ &\quad \text{and navigation function in figure 6.7)} \end{aligned}$$

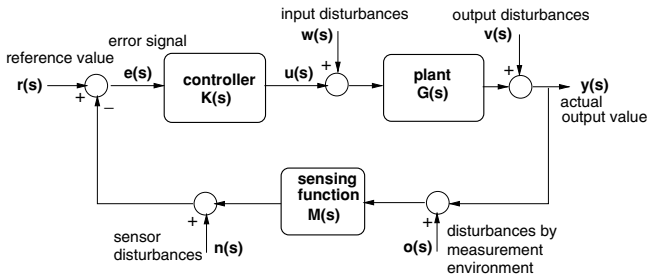

Figure 6.8. Reference control loop.

In our reference control loop diagram the guidance function becomes simply the reference input $r(s)$, the actuation system is merged with the plant in the transfer function $G(s)$, the navigation function and sensor dynamics are merged in the transfer function $M(s)$. In these functions s is the new variable in the Laplace domain of a function $f(t)$ in the time domain:

$$\mathcal{L}[f(t)] \equiv F(s)$$

which has the convenient property

$$\mathcal{L}[\dot{f}(t)] = sF(s) - f(0)$$

Without the disturbances, the ratio of reference and output values is the transfer function of the closed loop system:

$$\frac{y(s)}{r(s)} = T(s) = \frac{K(s)G(s)}{1 + K(s)G(s)M(s)} \tag{6.12}$$

The inputs, outputs and disturbances in figure 6.8 are as follows:

$r(s)$: reference signal (guidance value),

$e(s)$: error signal (difference between reference and measurement),

$u(s)$: control output,

$w(s)$: input disturbances (external disturbances on plant),

$v(s)$: output disturbances (internal disturbances of plant),

$o(s)$: disturbances from the measurement environment,

$n(s)$: sensor disturbances (bias, noise, etc.),

$y(s)$: plant output.

Depending on the characteristics of the errors and disturbances, some of them may be combined for convenience of analysis, e.g. the disturbance from the measurement environment $o(s)$ and from the sensor itself $n(s)$ are usually combined in $n(s)$.

The quality of the control action is determined by the *steady state error*, i.e. the difference between the reference and the output state achieved after settlement of transients, by the *transient response* characteristics and by the *noise rejection capability*. The transient response describes the time required to achieve steady state conditions and the output behaviour during this time. The latter includes the natural frequency of the system and the damping behaviour. These characteristics entirely depend on the transfer functions of the elements shown in figure 6.8.

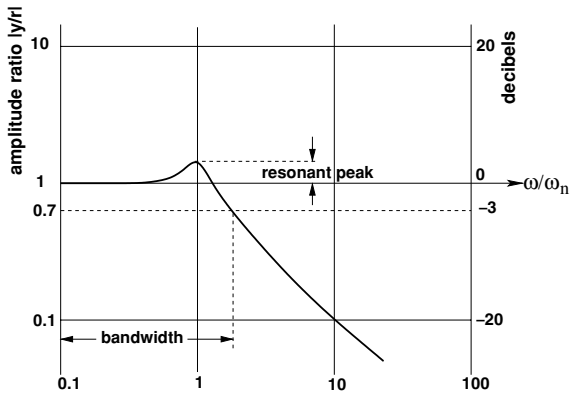

Figure 6.9. Bandwidth of a control loop.

The *transient response* will depend on the frequencies contained in the input signal. The response will be different if the input frequency is below or above the natural frequency of the loop. Far below the natural frequency, the relation of response to input amplitude will be equal to unity (or the value given by the loop gain); far above the natural frequency, it will approach zero. There is thus a limit in frequency up to which the output of a system will track a sinusoidal input. By convention, the frequency at

which the output amplitude has dropped by 3 dB, i.e. the output is 0.707 of the input magnitude, is called the *bandwidth*, ω_b.

In the following, a few basic properties and characteristics of a control loop will be briefly explained in the example of a simple second order system (mass/inertia-control stiffness-control damping), to provide a reference for the discussion of the performance of the control function in the rendezvous process. It goes without saying that in real applications systems may be more complex. The relations of resonant frequency, damping and steady state error can be explained in the example of a unity feedback system (figure 6.10), in which the full output is fed back. In most cases a given control loop can be reduced by manipulation of the transfer functions in a block diagram to a unity feedback system, so that the results of this discussion will be widely applicable.

Figure 6.10. Unity feedback system.

Combining the transfer functions of controller and plant into one transfer function, i.e. the open loop transfer function $G_\mathrm{u}(s)$, the closed loop transfer function, Eq. (6.12), of the unity feedback system becomes

$$T(s) = \frac{G_\mathrm{u}(s)}{1 + G_\mathrm{u}(s)} \tag{6.13}$$

The equation of motion of a second order system can generally be written in the form $A\ddot{x} + B\dot{x} + C = 0$, where x is the motion variable for translation or rotation, A is, for translational motion, the mass m and, for rotational motion, the inertia I, B is the factor of the rate depending term, and C is a constant gain representing the 'spring stiffness' of the system. The closed loop transfer function in a second order system can be expressed accordingly as

$$T(s) = \frac{C}{As^2 + Bs + C} \tag{6.14}$$

The *natural frequency* of the loop is given by

$$\omega_\mathrm{n} = \sqrt{\frac{C}{A}} \tag{6.15}$$

In our reference case of a simple second order feedback system, the value of ω_b is very close to the *natural frequency*, ω_n, of the system (see figure 6.9), so that in calculations the bandwidth is often taken for the resonant frequency.

The *damping ratio* is given by

$$d = \frac{B}{2\sqrt{CA}} \tag{6.16}$$

The amplitude ratio (magnitude) of the *resonance peak* in figure 6.9 is determined by the damping ratio d.

With Eqs. (6.15) and (6.16) the closed loop transfer function Eq. (6.14) can be written in a form which reveals the dynamic behaviour of the system,

$$T(s) = \frac{\omega_{\mathrm{n}}^2}{s^2 + 2d\omega_{\mathrm{n}}s + \omega_{\mathrm{n}}^2} \tag{6.17}$$

The transient response can be obtained from the roots of the denominator of Eq. (6.17) (characteristic equation). For $d = 1$ the system is critically damped; for $d = 0$ the system is undamped.

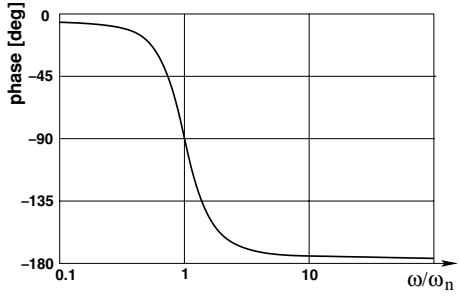

Figure 6.11. Phase shift over frequency.

As not only the amplitude response but also the phase response changes with the signal frequency, a feedback system can become unstable. The phase shift of the output signal due to the dynamic behaviour of the control loop is shown for a second order system in figure 6.11. Due to the fact that at frequency ratios $\gg 1$ the phase shift approaches -180 deg, an oscillation could in fact be amplified instead of damped if the amplitude of the feedback signal remained large enough. The assurance of stability is one of the major objectives of control analysis, and the according methods are well described in the literature, e.g. Anand (1984), Franklin *et al.* (1994) and D'Azzo (1995). For the purpose of this section, which will explain the effects and constraints of control loop features on the performance of trajectory and attitude control, these methods do not need to be discussed in detail. We can assume here that, for a control system implemented in a spacecraft, stability has been assured in the design and development process. With regard to the performance of a control loop, what has to be kept in mind is that stability requirements may put constraints on the achievable values for bandwidth, steady state error, etc.

The *steady state error* is defined as the difference between the reference signal and the output after settlement of transients:

$$e_{\mathrm{ss}}(t) = r(t) - y(t) \quad \text{for} \quad t \to \infty \quad \text{i.e.} \quad s \to 0$$

$$e_{\mathrm{ss}}(t) = \lim_{s\to 0} s\left[\frac{r(s)}{1+G_{\mathrm{u}}(s)}\right] \tag{6.18}$$

For a *position step* change at $t = 0$, e.g., the reference signal for all $t > 0$ is $r(t) = A$. The Laplace transform of the position step input is $r(s) = A/s$, with which the position steady state error of our unity feedback system becomes

$$e_{\mathrm{ss}}(t) = \lim_{s\to 0}\left[\frac{A}{1+G_{\mathrm{u}}(s)}\right] \tag{6.19}$$

$\lim_{s\to 0} G_{\mathrm{u}}(s)$ is the zero-frequency gain of the open loop transfer function.

A velocity step is a ramp input $r(t) = At$, which has the Laplace transform $r(s) = A/s^2$, and an acceleration step is a parabolic input $r(t) = At^2$, which has the Laplace transform $r(s) = A/s^3$, for which the steady state error can be derived accordingly.

The steady state error is thus proportional to a fraction with the zero-frequency open loop gain in the denominator, i.e. the larger the open loop gain, the smaller the steady state error e_{ss}. The steady state error can also be decreased by including an integrating behaviour in the feedback loop (integral feedback), at the expense, however, of increasing the transient response errors.

In the discussion of the control loop behaviour it is convenient to introduce an additional function, the so-called *sensitivity function* $S(s)$, which is the quotient of closed loop and open loop transfer function. For the unity feedback system of figure 6.10 this is

$$S(s) = \frac{1}{1+G_{\mathrm{u}}(s)} \tag{6.20}$$

The sum of the closed loop transfer function and the sensitivity function functions fulfils the relation

$$T(s) + S(s) = 1 \tag{6.21}$$

The sensitivity function indicates the advantage of close loop control: the error of a controlled parameter due to variations in the open loop gain $K(s)G(s)$ (e.g. by an input disturbance) is, in the case of closed loop control, by a factor of the 'sensitivity function' lower than in the case of open loop control.

General objectives of controller design

To simplify the discussion of the behaviour of our reference control loop, the reference block diagram figure 6.8 will now be transformed into a unity feedback system. This may be done as long as the bandwidth of the measurement system $M(s)$ is much higher than the closed loop control bandwidth, which is a desirable condition for the control loop design.[2] If this requirement is fulfilled, the transfer function $M(s)$ may be modelled

[2]This requires that the sensor has a sufficiently high bandwidth, which may not always be the case.

by a simple gain, which can be regarded to be resident within the controller $K(s)$ or within the plant $G(s)$. The closed loop transfer function Eq. (6.12) then becomes

$$T(s) = \frac{K(s)G(s)}{1 + K(s)G(s)} \tag{6.22}$$

and the sensitivity function becomes

$$S(s) = \frac{1}{1 + K(s)G(s)} \tag{6.23}$$

Making these assumptions, we can now assess the influence of the various inputs or disturbances shown in figure 6.8. The system output is driven by four input signals: the reference signal r, the input disturbances w, the output disturbances v and the sensor disturbances n (measurement environment $o(s)$ is included in sensor errors $n(s)$). It follows directly from figure 6.8 that the *system output* is

$$y(s) = T(s)r(s) + G(s)\frac{1}{1 + K(s)G(s)}w(s) + \frac{1}{1 + K(s)G(s)}v(s) - T(s)n(s)$$

which can be rewritten using the definition of $S(s)$, Eq. (6.23), as

$$y(s) = T(s)[r(s) - n(s)] + S(s)[G(s)w(s) + v(s)] \tag{6.24}$$

The *controller output* is

$$u(s) = \frac{K(s) \cdot [r(s) - n(s) - v(s) - G(s)w(s)]}{1 + K(s)G(s)}$$

which can be reduced to

$$u(s) = \frac{T(s)}{G(s)}[r(s) - n(s) - v(s) - G(s)w(s)] \tag{6.25}$$

From Eqs. (6.24) and (6.25), the following conclusions may be drawn for the control loop:

- Sensor disturbances are amplified by the closed loop gain $T(s)$ in the same way as the reference signal, i.e. there is no reduction of sensor errors/disturbances due to the feedback.
- Input and output disturbances are reduced due to the sensitivity function $S(s)$. As a result, tracking and disturbance rejection requires that the sensitivity function becomes small in the frequency domain of the disturbances, i.e. in the low and medium frequency range.
- To keep propellant consumption low, the energy of the control output $u(s)$ needs to be small, which requires the closed loop transfer function $T(s)$ to be small, at least where the transfer function of the plant, $G(s)$, is small.

- If the sensitivity function becomes small, $S(s) \ll 1$, the plant disturbances $w(s)$ and $v(s)$ are highly damped, i.e. the system has a large disturbance rejection capability. In this case, however, $T(s)$, according to Eq. (6.21), becomes very large and the control loop thus becomes very sensitive to the measurement noise $n(s)$ (cf. section 6.2.1, where one of the major objectives of the navigation filter was to reduce sensor noise).
- It should be noted that the system reference inputs, as well as the system disturbances, are generally in the low frequency range, whereas measurement noise lies in the high frequency range. The overall design guideline is, therefore, to achieve a small $T(s)$ for a high frequency range and a small $S(s)$ for the low frequency range. Consequently, the open loop transfer function $K(s)G(s)$ should be large for low frequencies and small for high frequencies.

As an '*a priori*' definition (setting) of the closed loop transfer function $T(s)$ may result in a non-realisable controller $K(s)$, the controller is therefore often designed via the open loop transfer function $K(s)G(s)$, for which specific characteristics may be required.

- The steady state error of, e.g., position, velocities and attitude angles may be required to not exceed certain limits. As a consequence, a requirement for a low steady state error for these parameters will result in a requirement for a high gain at low frequencies.
- Concerning the response time, the bandwidth must be selected such that the required frequency content of the guidance profiles and of the sensing function output can be tracked and that the disturbances are rejected with an acceptable damping ratio.
- Sufficient gain and phase margin is required for stability of the loop.

In conclusion, the controller will be designed such that it achieves sufficient performance in tracking the reference signal $r(s)$, without being too sensitive to measurement noise $n(s)$ and plant disturbances $v(s)$ and $w(s)$. Furthermore, the controller needs to be sufficiently robust w.r.t. plant parameter uncertainties, such as mass and inertia, and the control signal $u(s)$ should be kept small to minimise the propellant consumption.

Modelling of plant and disturbances

The description of the plant in the control loop design needs to include dynamic and kinematic models (see figure 10.10); the dynamic models are derived from the equations of motion and the kinematic models are derived from the spacecraft design. The modelling of input disturbances $w(s)$, such as air drag, gravity gradient, J_2 and sloshing effects, which are directly related to the dynamic and kinematic characteristics of the spacecraft, will need the spacecraft dynamic and kinematic models as input. These models will be needed in the design analysis of the control loop but are not necessarily part of the controller. To the extent that these disturbances are predictable, they can be compensated for in the guidance function. The modelling of dynamics and disturbance is addressed again in section 10.4.1 concerning the verification of the onboard system.

The major sources of disturbance for rendezvous trajectories have been addressed in section 4.2.

As already stated, the relative translational motion dynamics of one space vehicle w.r.t. another can be described by the Hill equations (3.21). For orbital motion, it was shown in section 3.3 that in-plane motion (x,z) and out-of-plane motion (y) are decoupled. The latter is an undamped oscillation with the orbital frequency. The in-plane coupling terms correspond to Coriolis and gravity forces in the Clohessy–Wiltshire solution, Eqs. (3.22) (see appendix A). For a closed loop controller design, these terms may be considered as low frequency disturbances and, for this reason, no longer need to appear in the design model. Consequently, a double integrator model, independent for each axis, can be applied for the position controller design. For the rotational motion of a three axis stabilised, Earth pointing satellite, Euler's moment equations can be linearised (Kaplan 1976) (see appendix A), so that for rotational motion basically a double integrator dynamic model can also be used for the controller design.

With this result, once damping d and closed loop bandwidth ω_b have been selected, a simple PD controller can directly be defined by

$$K(s) = K_\mathrm{P} + K_\mathrm{D} \cdot s$$

where for translational motion (position control) $K_\mathrm{P} = m \cdot \omega_\mathrm{b}^2$; for rotational motion (attitude control) $K_\mathrm{P} = I \cdot \omega_\mathrm{b}^2$; and the damping term $K_\mathrm{D} = 2d\sqrt{K_\mathrm{P}}$ (see also Eqs. (6.14)–(6.17)). For more detailed analysis, e.g. for stability analysis, the neglected coupling terms have to be taken into account.

In the phases prior to the final approach (see figure 2.1) position and attitude control is related to the CoM of the vehicle. This requires proper kinematic modelling of, e.g., the location w.r.t. the position of the CoM of the vehicle. The calculation of the actual position of the CoM has been assumed in section 6.2.2 to be the task of the guidance function. In the last part of an approach to docking, position and attitude of the chaser's docking port have to be aligned with that of the target (see figure 6.12). As a result, the vehicle has to be controlled w.r.t. its docking frame, which requires modelling of the geometric relations between the docking frame and the spacecraft attitude frame, which has its origin in the (moving) CoM. The corresponding kinematic model describing the motion coupling, resulting from location and direction of view of the sensors, is part of the navigation filter (see box labelled 'preparation of measurement vector' in figure 6.3).

Generally, the use of proper mathematical modelling of the disturbances and the system to be controlled will improve the performance of the control function. It is clear, however, that the real world cannot be described fully deterministically. The choice of the model fidelity therefore determines the quality of results, not only in the guidance but also in the control algorithms. This choice, i.e. whether the model is more or less accurate, most often also determines the complexity of the model and the computer effort for its processing. For this reason, there may be a limit in the degree of accuracy in the modelling of certain functions and effects.

Particular control issues in rendezvous missions

The performance requirements for the reduction of trajectory errors, i.e. the steady state errors for position and approach velocity, increase with decreasing range to the target. They will be particularly stringent in the last part of the approach, when entering the docking reception range. A short overview of the typical performances required is given in section 7.1, where sensor requirements are discussed.

For the coarse approach up to several hundred metres toward the target, orbital arc transfers are used (see sections 3.3.2, 3.3.3 and 5.7). If an impulsive transfer is used, boost and free flight phases have to be distinguished. For the rendezvous operations proper, which start in the vicinity of the target (typically 30 to 50 km), the necessary velocity increments ΔV per boost are rather small compared with the orbit transfer boosts needed during phasing to arrive at the target orbit. The small ΔV requirements either lead to large accelerations and short burn durations, when using large thrusters (e.g. the ones used during phasing), or to small accelerations and correspondingly long burn times, when using small thrusters (e.g. the ones for attitude control). In the first case, the ΔV errors may become larger and control performance may be lower; in the second case the burn time will, for the main boosts, cover a larger portion of the orbital arc. These considerations will be some of the driving factors in the selection of thrusters for a rendezvous spacecraft to be developed.

Open loop boost manoeuvres At larger distances from the target, trajectory manoeuvres can be performed with sufficient accuracy in open loop, i.e. the thrusters are fired for a duration calculated from the expected acceleration level and the required velocity increment. This will particularly be the case in the far range rendezvous phases, where accuracy requirements are still moderate. A major error contributor for the open loop trajectory implementation is the propulsion system itself (see also section 4.3.2).

In the free flight phase between the boosts, the errors made in the implementation of the first boost and the perturbations, which are not covered by the guidance function, can be observed and corrected open loop by mid-course manoeuvres.

Closed loop control of long boost manoeuvres Where longer boost duration is needed in the case of small thrusters, performance improvement can be achieved by closed loop control, using a high bandwidth velocity controller. For such a scheme, the navigation function (sensors and navigation filter) must be able to provide the state information with sufficiently high bandwidth.

It should be noted here that specific attention must be paid to the attitude control during the boost. Small centre of mass uncertainties and differences in the individual thrust levels can create significant disturbance torques, which have to be properly counteracted to maintain the correct orientation of the velocity increment (see also the 'Thrust direction errors' subsection in section 4.3.2). This requires a relatively high bandwidth

controller, which may challenge the assumption of a rigid body dynamics for cases where solar arrays or other flexible appendages are attached to the spacecraft.

Closed loop control between boost manoeuvres This case has been discussed in view of trajectory safety in section 4.4.1. During the free flight between manoeuvres, perturbations are caused by the air drag and other disturbances. As far as they can be predicted, they should be taken care of by the guidance function. The residual disturbances of the control loop are the unknown and neglected terms in the applied guidance model. Both are small and of low frequency, so that a low bandwidth controller will be sufficient, if closed loop control is applied at all during free flight phases. In fact, in this case the use of a controller is related to the correction of trajectory errors, caused by the preceding boost (navigation errors and thrust errors), or to the implementation of an active trajectory safety scheme, rather than to the compensation of the disturbance effects. Consequently the often applied alternative to closed loop control is the introduction of open loop correction boosts (mid-course manoeuvres), described above.

An alternative orbital arc transfer is based on low but continuous acceleration during the transfer (see section 3.3.3). Although this generally leads to a doubling of the transfer duration, it is well suited to a low bandwidth closed loop control concept, since the disturbances are small and constant.

Closed loop controlled straight line trajectories While approaching the target, the accuracy requirements in position and velocity control increase. Open loop techniques are no longer usable below a certain range. Constraints due to the angular operating range of optical sensors (visibility of target reflector pattern, see section 5.3.2) and due to approach corridors, defined by the target station (see section 5.6), require the spacecraft to stay on pre-defined trajectories.

For closed loop controlled trajectories, the required controller bandwidth will depend on the reference trajectory and velocities according to the guidance profile, on the performance requirements (response time, accuracy, consumption) and on the disturbances. The bandwidth of the necessary tracking system must be, on one hand, high enough to reach the required accuracy and, on the other hand, small enough not to waste fuel. The latter property can be improved when an appropriate dead-band is introduced in the closed loop.

Last metres approach to docking In the last part of the approach, an important driver for the controller design is the requirement that the chaser must be able to follow the motion of the docking port of the target. In the case of target thruster firings and of motions due to structural flexibility of the target during the final approach of the chaser, the frequency content of these motions may lead to higher bandwidth requirements than in the other approach phases. Although steady state errors of position and angular alignment may fit into the reception range of the docking mechanism, in case of (e.g.) rapid target motions, transient errors may be larger. The transient response of the controller must be such that, for the expected frequency content of such motions, the sum of the

instantaneous values of lateral position and angular misalignments between the docking interfaces of chaser and target will be smaller than the reception range (see figure 8.30).

As the motion between the coordinate frames of the docking interfaces of chaser and target has to be controlled in this phase, coupling of rotational and translational motion has to be considered, as indicated above. Any attitude motion of chaser or target will result both in a change of relative attitude and relative lateral positions of the docking frames of chaser and target.

At contact, the control system of the chaser must have achieved lateral position and angular alignment with the target docking mechanism, such that the residual errors fit into the reception range of the docking interfaces. To explain the control problem of the last phase prior to contact, three concepts of approach control shall be considered, where the chaser GNC system tracks different parameters of the target state:

(a) the position of the target CoM,
(b) the position of the target docking port,
(c) the position and the relative attitude of the target docking port.

Three different cases are shown in figure 6.12, in which the bold arrows represent the vehicle attitude frames, and the length of the x-component indicates the distance of the docking port from the CoM. The attitude control margins are shown on the target side, the position control margins on the chaser side. The maximum possible lateral and angular misalignments are indicated for each case above the figure.

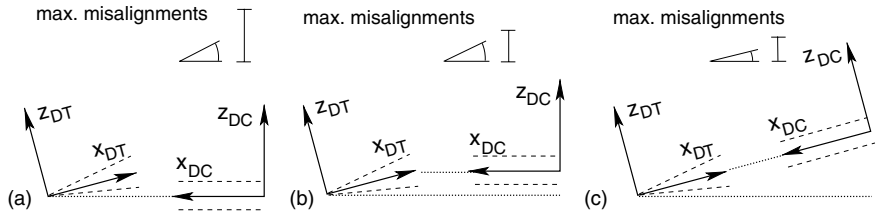

Figure 6.12. Control concepts for docking. (a) Tracking of target CoM, chaser attitude nominal. (b) Tracking of target docking port, chaser attitude nominal. (c) Tracking of target docking port and of chaser to target relative attitude.

Figure 6.12(a) represents the most simple control scheme, i.e. instead of controlling relative position and orientation of the docking ports, only the relative motion of the centres of mass and the absolute attitude of the vehicles are controlled, as in the previous approach phases. The aim point is the nominal, not the actual, location of the centre of the target docking port. The systematic alignment error at the docking interfaces is the sum of the angular error due to the target attitude deviation and the lateral error due to the distance of the docking port from the target CoM.

In figure 6.12(b), the lateral position of the chaser docking port is controlled w.r.t. the target one. A line of sight measurement to the target docking port is necessary. The attitude of each vehicle is controlled independently w.r.t. a nominal reference frame (e.g.

LVLH). The systematic alignment error at the docking interfaces is just the angular error due to attitude deviations between chaser and target.

In figure 6.12(c), both the relative lateral position and the relative attitude have to be controlled simultaneously to achieve full translational and rotational alignment of the docking interfaces. This needs, in addition to the lateral position, an onboard estimation of the relative orientation of the docking axes of chaser and target. A consequence of this scheme is that rotational and translational motions are now coupled, which has important repercussions on the controller, as it requires MIMO design.

The third case is the only one without systematic alignment errors. Alignment errors due to residual attitude and position control errors will be the smallest of the three cases. In RVD missions only cases shown in figure 6.12 (b) and (c) are actually used. In the following 'case (a)' will refer to figure 6.12(a), etc.

- *Case (a)* has never been applied, as generally it is not only too inaccurate as compared with realistic reception ranges of docking mechanism, but also it is not practical, as there is no sufficiently accurate sensing capability available to measure the relative position of the CoMs of chaser and target.
- *Case (b)* has been applied in some docking missions, whereby the position of the chaser has been controlled manually and the attitude of each vehicle automatically by its respective attitude control system. This option still requires a relatively large angular reception range of the docking interfaces, due to the steady state and transient errors of the individual attitude control systems (bang-bang control in most cases).
- *Case (c)* is applied in all automatic GNC systems for rendezvous and docking. In this case relative position and attitude measurements are processed in the navigation function to obtain an estimated six degrees of freedom relative state vector, the components of which have to be controlled simultaneously and will require the application of advanced controller design techniques. Case (c) is now also the standard concept for manually controlled approaches to docking (see section 6.5.3). Lateral position and relative attitude information can be obtained by the human operator, if a video camera and a suitable target pattern (see figure 6.25) is available. The nominal attitude will then be adjusted by commanding appropriate offsets.

During most of an RVD mission, the attitude control and the position control systems can be considered as de-coupled, except for the final approach to docking (case (c)). Furthermore, accuracies are, in these phases, less stringent than at close range. It shall nevertheless not be forgotten that for the position there are also the low frequency couplings for the in-plane motion of the Clohessy–Wiltshire equations, mentioned already under the 'Modelling of plant and of disturbances' section above (see also Eq. (3.22), for the 2ω terms).

These cross couplings can be taken into account during either the control design or as feed forward terms from the guidance part of the system in order to reduce transient errors, increase precision and reduce fuel consumption. For this part of the GNC design, classical PID type of designs will often suffice, but when low damped flexible modes are

present in the system, more advanced designs are needed. This can be a classical control design combined with separately tuned notch filters, but a more elegant and efficient design is to apply H_∞ design, which is well suited for such problems.

During the last metres of the final approach, the position and attitude angles and the translational velocities and angular rates are coupled, as a result of the control w.r.t. the target docking port (case (c)), and need to be controlled simultaneously. Such a control problem typically calls for a multi-variable design method. Owing to the nature of the system, the flexible modes to be controlled and the way in which the disturbances are described, a multi-variable robust design method is recommended for the synthesis, as well as for the analysis, part of the design.

As already discussed above, the actuators for this type of vehicle are usually thrusters, and their non-linear characteristics (see figure 6.15) require special attention during the stability analysis. For the part where SISO designs are applicable, the use of the negative inverse describing function is recommended, and for the MIMO methods an appropriate frequency domain weighting function should be chosen.

Discrete time control

Since onboard control systems are nowadays always implemented in software on digital computers, we are in fact dealing with discrete computer controlled systems rather than with analogue ones, assumed in Eqs. (6.12)–(6.25). Proper use of the discrete domain theories has, therefore, to be made in the entire design process. The type of systems we are dealing with here are sampled data systems with a fixed sampling time T for the feedback loop, in contrast to some interrupt driven free running discrete systems.

A sampled data system is described by difference equations, and a signal is described by a number sequence. These number sequences are obtained by sampling a continuous or analogue signal. An 'analogue to digital converter' (ADC) converts the analogue sensor signal to a digital signal, and a 'digital to analogue converter' (DAC) converts the digital controller output, which is fed to the actuators in the system. One can either view the real world as analogue, and the discrete the system as a special case, or, more conveniently, one can view the world as discrete and the continuous part as the special system; the latter is recommended. An analogue and an equivalent discrete control loop are illustrated in figure 6.13.

The sampling of the continuous signal must be performed at a sufficiently high frequency such that not too much phase margin is lost. The Nyquist frequency, which is twice the highest frequency in the signal, is the theoretical minimum. For practical purposes this is too slow, and one needs to sample at a frequency which is seven to ten times the fastest mode in the closed loop system. In this context, one also has to pay attention to aliasing of high frequency noise from sensors, which could show up as warped low frequency discrete signals. To avoid this, analogue anti-aliasing filters might need to be applied.

The output from the discrete system to the continuous one is typically through the DAC as well as a zero order hold (ZOH) network, which keeps the output signal constant over one sample.

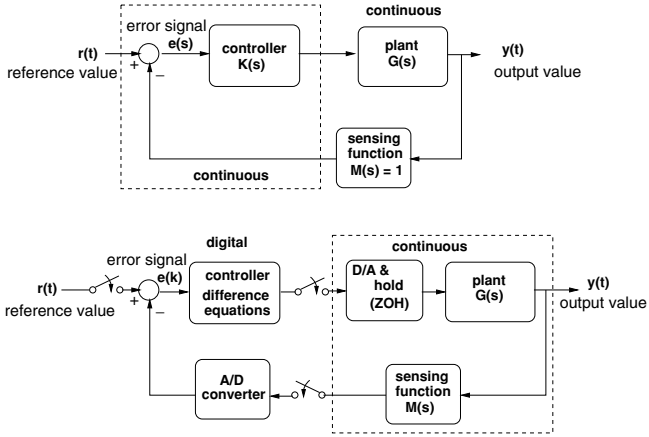

Figure 6.13. Continuous and digital control loop.

As a tool for the analysis of discrete systems (equivalent to the Laplace transform for the continuous domain), the $\mathcal{Z}$-transformation is available; it is defined as follows:

$$y(z) \triangleq \mathcal{Z}[y(k)] = \sum_{k=0}^{\infty} y(k) z^{-k} \tag{6.26}$$

The variable z can be viewed as a shift operator or as a complex variable in the z-plane, just as we view s as a differential operator or as a complex variable in the Laplace plane.

It should be noted that $y(z)$ often can be obtained from a known Laplace transform description, without going via the impulse response function $y(k)$ and the summation as given in the definition equation (6.26). This is typically performed by various approximations of the complex variable s for Euler forward, backward or bilinear transformations. These are approximations to the $\mathcal{Z}$-transformation, and will lead to a need for higher sampling frequencies followed by bigger computer load. A better method is to use the *pole-zero mapping*, where

$$z = \mathrm{e}^{sT} \tag{6.27}$$

and s is the Laplace variable and T is the sampling time. This leads to the smallest sampling frequencies and it is also mathematically exact. This means that at the sampling times the discrete signal is exactly equal to the continuous one and corresponds to the $\mathcal{Z}$-transformation.

The stability for discrete systems can be evaluated with respect to the unit circle, as we know from the conformal mapping that the left half-plane of the Laplace domain maps onto the inner part of a unit circle in the z-plane. Therefore systems having closed loop poles inside the circle are stable.

The best performance, lowest sampling rates and better stability margins will be achieved when designing discrete GNC systems directly in the discrete domain, i.e. transforming the plant into that domain. This will give better results than implementing first a continuous design and thereafter designing the controllers with some approximate transformations.

As a detailed discussion of digital control theory would be outside the objectives and scope of this chapter, the interested reader is referred to the literature, e.g. Franklin & Emami-Naeini (1990).

The thruster selection function

The task of the thruster management function is to translate the force and torque commands generated by the control function into 'on/off' commands for the individual thrusters according to their direction and to their location w.r.t. the momentary centre of mass of the vehicle. Depending upon the control error, a request for a force of varying level to be applied along the individual axes is made. The position controller generates force commands, and the attitude controller generates torque commands, of varying amplitude along and around the body axes. With the thruster hardware available for the realisation of such requests, two problems exist:

(1) The thruster either provides the nominal force or nothing, i.e. it is not possible to change the force level from zero to a maximum value.
(2) Due to thruster accommodation and redundancy constraints, dedicated thrusters for the individual controller outputs are most often not available, i.e. generally there is coupling between forces and torques, which has to be accounted for properly.

One solution to the first type of problem is the application of non-linear controllers with switching elements. For thruster control, pulse width pulse frequency (PWPF) modulation is usually applied (Noges & Frank 1975) (see figure 6.5).

During rendezvous, the sample interval for the discrete controller (typically 1 s) is large compared with the minimum pulse length of a thruster. Consequently, within the control cycle, the pulse length can be varied from zero to the control sample interval. The realised impulse is approximately a linear function of the pulse length. Therefore, as a first order approximation, the effect corresponds to an amplitude modulation of the force within the control cycle, where the average force is (see figure 6.14)

$$F_{\text{average}} = F_{\text{nom}} \frac{t_{\text{pulse}}}{t_{k+1} - t_k} \tag{6.28}$$

The output of the controller corresponds to F_{average}, and the command to the thruster control electronics is the pulse length t_{pulse}.

The pulses cannot of course be made arbitrarily small. The lower limit is the 'minimum impulse bit'. For a bi-liquid thruster of 200 N, for example, the MIB is in the order of 50 ms. Moreover, for small impulses, the steady state thrust level is not yet reached. Consequently, small force (or torque) requests are suppressed by a dead zone at the output of the controller.

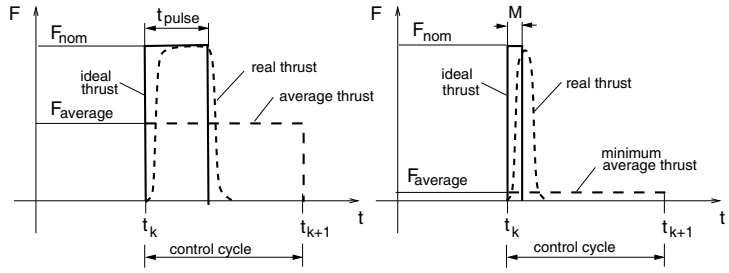

Figure 6.14. Thrust pulse characteristics.

When the thruster is operated close to the MIB, the simple equation (6.28) above may be modified by a calibration factor C_{F}, providing an appropriate correction as a function of the force request. We then have

$$t_{\mathrm{cmd}} = C_{\mathrm{F}} \frac{F_{\mathrm{ctrl}}}{F_{\mathrm{nom}}} (t_{k+1} - t_k) \tag{6.29}$$

Including the dead zone, the shape of the correction factor is shown in figure 6.15. The curve above the dashed level 1 may be approximated by an exponential function.

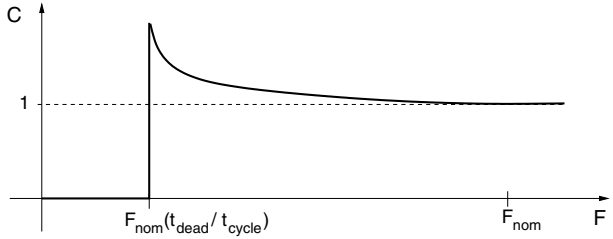

Figure 6.15. Control force correction factor as a function of nominal thrust.

The MIB of a thruster is generally a function of its maximum thrust. This may create a problem when the same set of thrusters has to be used both for larger thrusts, e.g. for transfer manoeuvres, and for fine control, e.g. for the last metres to docking or, e.g., for minimisation of the residual velocities in a berthing box. The minimum average force which can be applied during a control cycle will then be a constraint on the achievable GNC performance.

The coupling problem addressed under point (2) above may be treated by two different principles, depending on the complexity of coupling and on the envisaged thruster redundancy concept. If the accommodation can be kept close to the ideal configuration, where dedicated thrusters are used in the individual axes for force and torque requests, then so-called 'look-up tables' may be used. These tables allocate the thrusters to be

applied for specific force/torque requests. The actual commands are then composed of a scaled combination of the reference points.

The tables are only valid, however, for a specific thruster accommodation with a fixed CoM, and provide only sub-optimal solutions w.r.t. both fuel consumption and accuracy. However, this approach is rather fast and invokes only small CPU load. Since spacecraft systems have to be failure tolerant, a dedicated table is needed for any possible propulsion configuration, i.e. for any thruster (or thruster cluster) failure. Consequently, a large number of tables needs to be defined. If, furthermore, the CoM is subject to large variations, as is the case for a space station servicing vehicle during the various approach phases, even more tables are needed.

This problem can be reduced, when the optimal set of thrusters and the appropriate thruster-open duration are determined onboard. For this, the actual CoM position must be known precisely, which remains one of the major sources of errors. This task corresponds to a linear optimisation problem, which can be solved by a standard mathematical procedure such as the *Simplex* algorithm (see Press *et al*. (1992)). This algorithm works on a tableau representing the constraints on the optimisation variables, defined by linear equalities and the objective function. The latter contains the contribution of each free variable to the optimisation result.

The following problem has to be solved for the selection of thrusters:

$$\begin{bmatrix} f_{1x} & f_{2x} & \cdots & f_{nx} \\ f_{1y} & f_{2y} & \cdots & f_{ny} \\ f_{1z} & f_{2z} & \cdots & f_{nz} \\ t_{1x} & t_{2x} & \cdots & t_{nx} \\ t_{1y} & t_{2y} & \cdots & t_{ny} \\ t_{1z} & t_{2z} & \cdots & t_{nz} \end{bmatrix} \cdot \begin{bmatrix} u_1 \\ u_2 \\ \vdots \\ u_n \end{bmatrix} = \alpha \begin{bmatrix} F_x \\ F_y \\ F_z \\ T_x \\ T_y \\ T_z \end{bmatrix} \tag{6.30}$$

or

$$\mathbf{A} \cdot \mathbf{B} = \alpha \cdot \mathbf{C}$$

where

f is the x,y,z-force component of thruster 'n',
t is the x,y,z-torque component of thruster 'n',
n is the number of the available or usable thruster,
u is the normalized thruster open duration, $|u_i| \leq 1$.

The maximum value of u is limited to 1, i.e. the thruster is opened for the complete control cycle. A zero value for u_i means that the thruster is not used at all. The factor α allows us to account for thruster saturation. When the commanded force/torque control vector $\mathbf{C}$ cannot be realised with the available thruster, then at least the commanded direction will be kept, i.e. the $\mathbf{C}$-vector is appropriately scaled.

The optimisation criteria is the minimisation of the fuel consumption, while simultaneously maximising the scaling factor α. The cost function then can be given as

$$Z = -(c_1 u_1 + c_2 u_2 + \cdots + c_n u_n) + c_\alpha \alpha \implies \max. \tag{6.31}$$

where c_i is a coefficient for propellant consumption, and c_α is a weighting factor for the realisation.

Nominally, the simplex algorithm always finds a solution. Theoretically, however, the algorithm may enter the so-called 'circling' régime, i.e. the algorithm doesn't converge because a constantly repeated exchange series within the simplex tableau occurs. This rarely happens, but if it does it can be avoided, e.g. by enforcing the iteration loop to stop after a pre-defined number of iterations, or, in other words, accepting a potentially non-optimal solution.

Due to the optimisation scheme, the CPU load is significant, in particular when numerous thrusters ($>$20) are to be treated simultaneously. It provides, however, very high inherent flexibility with respect to thruster failures and CoM locations. The only things to be changed are the CoM location and a set of flags indicating whether or not a particular thruster can be used.

Since the processing power required for spacecraft computers is increasing over time (though much slower than in commercial products on Earth), the CPU load may become of lesser importance in the future. The inherent flexibility of this algorithm will then make its application interesting for a larger number of spacecraft, and it may be implemented in future, e.g. as a general service for thruster control.

6.3 Mode sequencing and equipment engagement

Because of the many different manoeuvres, trajectories and attitudes and the different sensors used in the various steps of the rendezvous approach, there will be, for each approach step, a different set of software functions (algorithm, parameter) and hardware functions (sensor), as explained above. For this reason, there must be a management function which activates for each new step the proper software modes for guidance, navigation and control (phase/mode management) and the sensor configuration (vehicle management) at the proper point in time, when a new manoeuvre or trajectory element has to commence. In addition, there will be the need for redundancy management of hardware functions, such as processors, data buses, sensors and reaction control equipment for contingency cases. All these functions can be grouped together under the term 'mission and vehicle management'.

In single satellite missions, only the redundancy management of critical hardware needs to be implemented as an onboard function; all other management functions can be performed by ground operators. In the case of a rendezvous mission of an unmanned vehicle many of these management functions are better performed on board. This is because of the possibility of interrupted communication with ground and the sensitivity of the trajectories to time delays of the manoeuvres. In particular it is the case

for the rendezvous phases proper, i.e. when the chaser is close enough to the target to perform relative navigation. The automatic mission and vehicle management functions are, therefore, key elements in the capability to perform automated rendezvous and capture.

The major task for the phase/mode management function is to determine the proper point in time when a new GNC mode has to be initiated. For this purpose both time and spacecraft state (position and attitude) criteria have to be checked to ensure that the intended state prior to initiation of the next trajectory element has been achieved. Except for the last phase of the approach, all trajectory elements last for a certain part of an orbital revolution (typically of the order of half or one orbital revolution), which can be pre-calculated according to the type of manoeuvre and the necessary thrust duration of the boosts to be applied. Considering the time as the only criterion will be, however, not sufficient, as e.g. thrust errors or failures may result in a position that is unsuitable to start the next approach step. In the same way, position or other spacecraft state parameters alone will not be sufficient, as e.g. the vehicle may (because of thrust errors) never reach the position that the criteria is requesting. Only if both time and the state parameter are within a certain margin can the next step can be initiated. Otherwise a contingency strategy has to be applied.

Figure 6.16 shows a flow diagram of nominal and contingency modes for the approach strategy given in the first example of section 5.7. From each nominal mode there are three possible transitions: (a) next mode, (b) mission interrupt, (c) mission abort. As explained in chapter 4, the mission abort (CAM) can be implemented as a simple retrograde boost, which may be, however, of different sizes in the different approach phases. The mission interrupt will consist of different guidance modes according to the approach phase. In the chosen example (see figure 5.25), mission interrupt modes in the rendezvous phases would be as follows.

- *Drift phase from S0–S1.* Continuation of drift after passing S1, if first pulse of homing manoeuvre cannot be executed because of onboard problems, or if it is not executed for reasons not related to the rendezvous onboard control system.
- *Homing S1–S2.* Either transition to next mode 'hold at S2', if mission has to be interrupted for reasons not related to the rendezvous onboard control system, or continuation of drift after passing S2, if second pulse of homing manoeuvre cannot be executed.
- *Hold point S2.* Tangential pulse to initiate a retrograde motion, looping away from the target. This pulse must be small enough to avoid the first part of the resulting trajectory entering the approach ellipsoid. By a further boost the motion could be stopped to acquire a new hold point.
- *Closing S2–S3.* Transition to next mode 'hold at S3' if mission has to be interrupted for reasons not related to the rendezvous onboard control system or, if the second pulse of the closing manoeuvre cannot be executed, continuation of drift after passing S3. In this case a second manoeuvre would have to be performed after half an orbit in order to stop the vehicle at S2, preventing it from moving again toward the target.

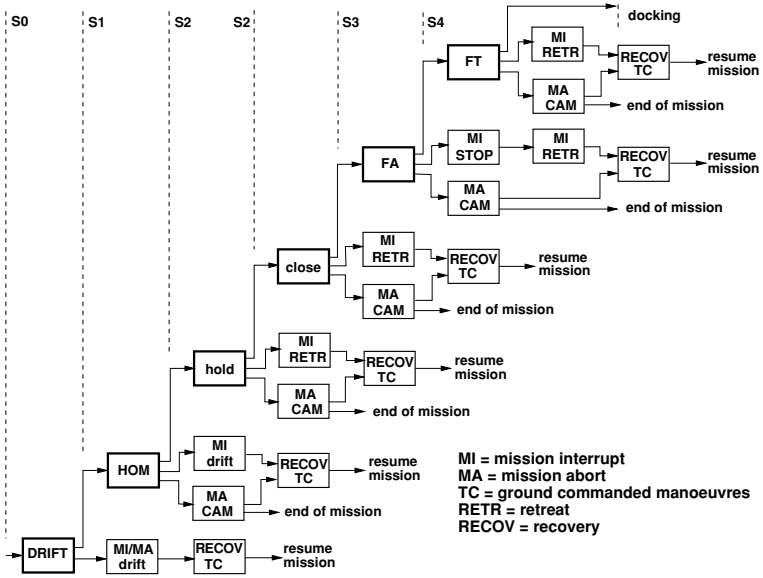

Figure 6.16. Sequencing of nominal and contingency modes.

- *Hold point S3*. Radial pulse manoeuvre to return to the previous hold point S2. Again, in this case a second manoeuvre would have to be performed after half an orbit in order to prevent the vehicle from moving again toward the target.
- *Final approach S3–S4*. Stop and hold on V-bar. In contrast to the previous modes, during the straight line approach the vehicle can be stopped at each point of the trajectory at the same cost. This braking manoeuvre may be followed by a retreat to the previous hold point S3.
- *Final translation to contact*. Retreat to S4. In this case stop and hold in very close vicinity of the target would be considered too hazardous.

Except for cases when the mission is stopped at a hold point or on V-bar, recovery from mission interrupts or mission aborts requires the calculation of a series of different recovery manoeuvres. A re-planning of the mission may have to be performed for all interrupts of more than a few minutes, as synchronisation with illumination conditions and communication windows may be lost. All mission re-planning will have to be done on ground, as it will be impossible to pre-plan all potential recovery manoeuvres. The recovery manoeuvres will have to be established based on the actual situation, and then would have to be transmitted to the vehicle by telecommand.

There are of course many ways in which such a phase/mode management function can be implemented. In order to provide an idea of how such a function would operate, a simplified concept is shown as an example in figure 6.17. This concept would work as follows.

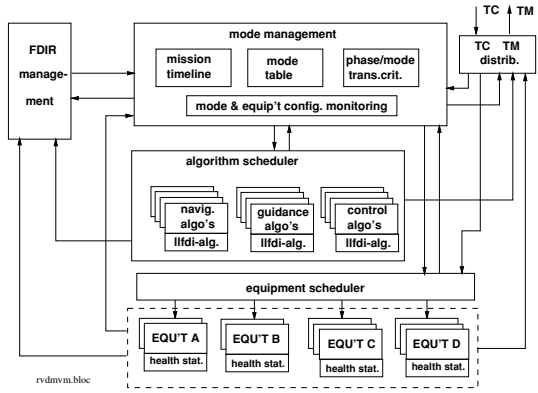

Figure 6.17. Mission and vehicle management functions.

(1) A 'mission timeline' function is implemented as a look-up table, which contains a schedule of the planned manoeuvres and trajectories.

(2) At a point in time when a pre-planned change of trajectory or attitude is due, the 'mission timeline' function requests a change of control mode (new manoeuvre, trajectory or attitude mode).

(3) Upon this request, the 'mode management' function fetches from the 'mode transition criteria' table the applicable criteria and checks whether the GNC data (navigation and guidance output) fulfil the criteria for a mode change.

(4) When the criteria are fulfilled, the new GNC mode will be loaded from the mode table and the corresponding commands will be transmitted to the 'algorithm scheduler' and the 'equipment scheduler'.

(5) If the switching criteria are not fulfilled, a contingency mode, pre-determined for each phase, will be loaded and the corresponding commands will be issued to the 'algorithm scheduler' and the 'equipment scheduler'.

(6) According to the commands from the 'mode management' function, the 'algorithm scheduler' fetches from the algorithm tables the different N, G and C algorithms belonging to the new mode, and the 'equipment scheduler' switches the relevant equipment combination.

The 'mode management' and 'equipment scheduler' functions in this concept would have to register the instantaneous configuration of software modes and of equipment, including their redundancy status, and would provide this information to the failure detection and isolation and recovery (FDIR) function. If the FDIR function detects a failure in equipment or the faulty behaviour of the complete string, it would request the 'equipment scheduler' function to execute the redundancy switching of sensor and actuator equipment. The mission timeline in the example concept would be a table containing

the latest planning of the time sequence of all mission events. It would be loaded prior to launch and would include the latest mission updates, based on the planned launch time and the evolution of the target orbit. For smaller changes of the actual timeline, this table and related parameters, e.g. time criteria for mode switching, could be adapted automatically by the onboard system. For larger deviations, the timeline table could be modified by telecommand from ground.

In any kind of design, the 'mission and vehicle management' functions will have to interact closely with the FDIR function, as the examples of mode switching failure and equipment redundancy management already indicate. Possible methods for failure detection and recovery will be discussed in more detail in the following section.

6.4 Fault identification and recovery concepts

The intention of this section is to describe some basic principles concerning how fault tolerance and recovery concepts can be implemented in the space and ground segments of rendezvous systems in general and in the design of onboard control systems in particular. As the first necessary step toward recovery from a failure is its detection and identification, the first question to be answered must be, therefore, 'What are the observables, and what are the criteria by which failures can be identified?'. On the highest level it may be possible to detect the deviation of the actual state of the vehicle from the planned one, e.g. in terms of position, velocity or attitude. On a subsystem level it may be possible to detect the deviation of a number of parameters and conditions from the nominal ones. On the lowest level it may be possible to detect the proper functioning of equipment by checking output data characteristics, power consumption and other physical parameters. Accordingly, the FDIR system of a chaser spacecraft will have to provide failure detection capabilities at three different levels.

- At the lowest level, all equipment will have to be checked either by internal or external agents (built-in test functions, criteria for voltage, temperature, pressure, etc.).
- At the GNC subsystem level, a number of criteria have to be checked, which will be related to the GNC modes engaged and to the manoeuvres and trajectories to be executed.
- At the highest level, concerning the spacecraft state, the transgression of safety margins around the nominal values of position, velocity, attitude and angular rates have to be checked.

The general concept for onboard FDIR implementation will always be to start the recovery at the lowest possible (equipment) level. If failure detection and recovery is not possible at equipment level, the onboard control system will have to try to recover the situation at the next highest level, i.e. the GNC subsystem level by, e.g., switching to a redundant string of the GNC subsystem. If recovery actions on the GNC subsystem level still do not bring the vehicle back into the allowable margins of state, actions at

mission level have to be taken. The options for the onboard FDIR at this level are, depending on the approach phase, e.g. a hold on V-bar, a free drift with contingency attitude mode and a mission abort (CAM).

In figures 6.1 and 6.17, the FDIR system has been presented as a single functional block. In a real design, the failure detection and identification (FDI) function will have to be, following the above three levels of failure detection, very closely related to the equipment (sensors, reaction control system, computers) and to the GNC functions, and will not form a separate subsystem. As we have seen for recovery, probably the same functions which are needed already for the management of the nominal mission will be used. In a real design implementation, the FDIR functions cannot, therefore, be separated from the MVM functions.

The following can be used for fault detection on the onboard GNC equipment.

- Information on equipment power status (i.e. switched-on or -off) or power consumption.
- Equipment can provide information on its health status (self-test data).
- Where equipment has different modes of operation, information on the mode status can be provided.
- For certain sensors, where the measurement principle includes different types of data, consistency checks of measurement data may be performed. This may be possible, e.g., for GPS and for a laser scanner type of rendezvous sensor, but not for sensor types where only one parameter is measured, as in the case of single gyros, Earth and Sun sensors, e.g. For single-parameter sensors, even where one hot redundant equipment is available, a failure condition cannot be allocated to one of the redundant sensors on the basis of the output signal alone.
- Failure of thrusters can, in principle, be detected on the equipment level by measurement of the pressure in the combustion chamber and of the equipment temperature. The first possibility is not always available with the hardware on the market, and the drawback of the second possibility is the duration after failure before the condition is observable. Hard failures of thrusters, i.e. stuck open and stuck closed, can probably be detected more quickly by observing the output of the control function (see below). The clear identification of a thruster failure will be, however, quite difficult, with complex thruster configurations, which are not fully symmetrical w.r.t. the CoM of the vehicle.

In accordance with the general description of a Kalman filter, figure 6.3, the navigation filter of an onboard system for automatic rendezvous can be represented by a general block diagram of the form shown in figure 6.18, in which the functional blocks correspond to the update and propagation blocks which process Eqs. (6.5)–(6.8). Comparison of the results produced by the measurement, propagation and update blocks can help to identify malfunctions in the navigation filter.

For the detection of failure conditions on the GNC subsystem level, including fault conditions on the sensor and thruster level and of the GNC functions proper, parameters and conditions such as the following can be checked.

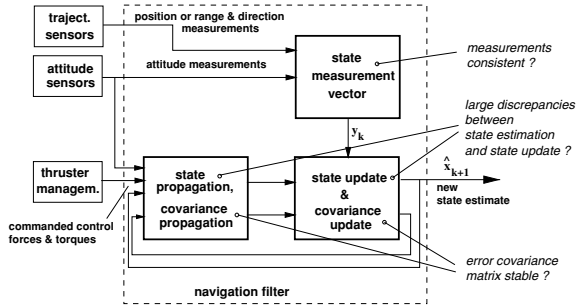

Figure 6.18. Navigation filter simplified: error detection possibilities.

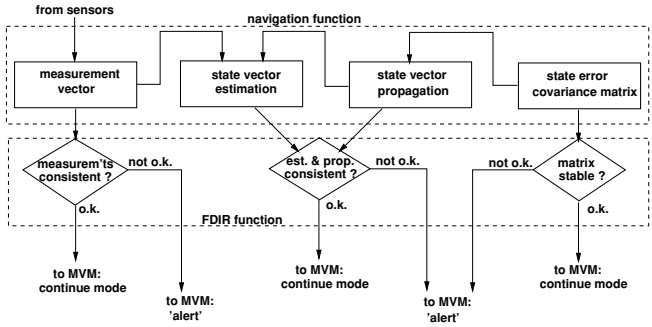

Figure 6.19. Failure detection related to the navigation function.

- Discrepancies between measured and propagated states (see figure 6.19). This condition points to a major problem in the navigation of the vehicle, which can be caused either by a faulty operation of one of the sensors or of the software of the navigation filter.

- Convergence of the navigation filter (see figure 6.19). Delay of convergence or even divergence of the filter can be caused by any of the data inputs, i.e. sensor data or thrust command feedback, or by errors in the filter software. Again, with this check only a failure condition can be identified without pointing to the failure source.

- Duration of manoeuvres (see figure 6.20) and check that the desired state has been achieved (this has been addressed in the previous section). The result of such checks relates to the achievement of a planned dynamic condition. The detection of a deviation will, however, not immediately point to the failure source.

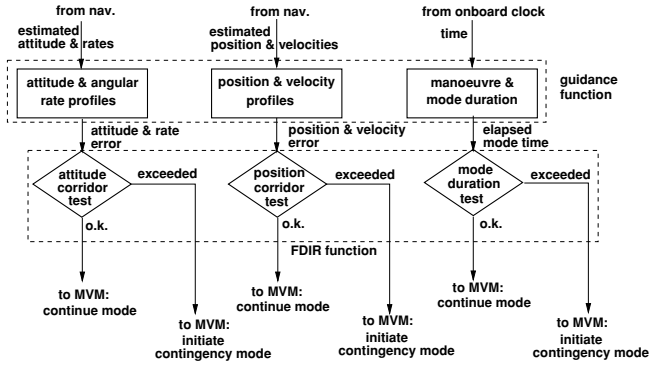

Figure 6.20. Failure detection related to the guidance function.

- Limits of forces and torques requested by the controller (see figure 6.21), e.g. saturation of command output to thrusters. Except in the case of boost manoeuvres, the continuous command of thrust in one direction can be caused either by a large deviation of the nominal state from the set value commanded by the guidance function or by a thruster-open failure.

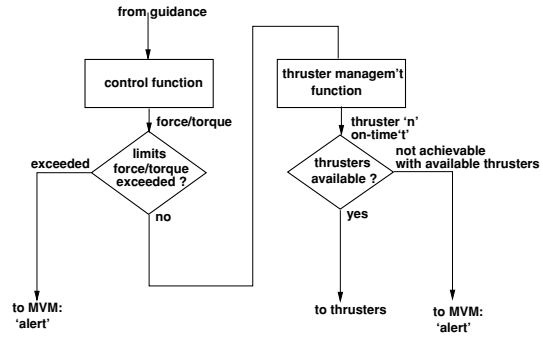

Figure 6.21. Failure detection related to the control function.

To detect a failure condition at the highest level, i.e. the transgression of safety margins around the nominal values of position, velocity, attitude and angular rates, in the first instance the nominal sensors and GNC functions can be used (see figure 6.20). This will cover failures of thrusters and 'hard' failures of sensors and of the GNC software. 'Soft' failures of sensors and GNC software can, however, not be detected in this way. The term 'soft failures' is used here as a general term for faulty outputs of the sensor and GNC functions, which are not immediately identifiable, but will cause over time critical deviations in the actual from the nominal spacecraft state. Serious malfunctions, such as

cease of operation, completely inconsistent output data or high noise, are what is meant by 'hard failures'.

To cover 'soft failures' (e.g. a slow build-up of bias on a sensor) by the onboard system, independent sensors and an independent guidance and navigation function would have to be installed on board, which in fact would have to be more reliable than the nominal GNC system. It is obvious that any design will eventually approach some technical and economical limits. This is one of the reasons that even a well-designed onboard FDIR system can assure protection against failures to a very large extent, but never 100% of the time. The availability of external agents, having independent means for remote monitoring, for assessment of contingency situations and for interaction with the automatic onboard system, will, therefore, always be highly desirable and will be necessary for safety reasons for the final part of the approach and capture. Such agents will be ground operators and the crew in the target station with their support tools, and the independent means of assessment may be direct vision, video or other measurement devices for range and direction (see chapter 9). Although fully automatic external supervision systems are conceivable, in the vicinity of a manned target station, monitoring by human operators will be indispensable.

Next in importance to failures in the onboard system is the interruption of the communication links; this can endanger the rendezvous approach, as these links may be essential both for the remote monitoring and control and for navigation, as in case of RGPS (see section 7.3.3). The following concepts concerning the fault detection of communication links can be envisaged:

- The link from the target station to the chaser vehicle can be checked by the chaser onboard system, e.g. reception of GPS data, where RGPS is used as rendezvous sensor. Otherwise, e.g., a continuous pulse or tone signal emitted by the target station could be monitored.
- In the close range rendezvous phases, the link from the chaser to the target station can continuously be checked by the target receivers, as the chaser will have to broadcast continuously its GNC and housekeeping data. For RGPS this will include implicitly also a check of the link from the target station to the chaser vehicle, as the data broadcast by the chaser will include the navigation data. Otherwise, if deemed necessary, a continuous signal transmitted by the target can be re-transmitted by the chaser, allowing (on the target side) monitoring of both directions of the link.
- The links between chaser and ground, whether via DRS or via ISS/TDRSS, including all ground links, can be checked by ground receiver equipment.

As we have seen, various criteria are available to enable the identification of a faulty situation, covering the large majority of potential failures. These criteria do not lead, however, in most cases to an immediate and unequivocal identification of the failure source. Only in the case of equipment failures, e.g., where health status information is available, will immediate decisions for redundancy switching on this level be possible. In most other cases, the sole recovery option will be to switch over to a redundant string on at least subsystem (e.g. GNC) level. To ensure the availability of the redundant chain,

the redundancy status of all necessary functions has to be monitored, and cross straps have to be managed, to engage equipment which has already lost its redundancy, as the choice of recovery operations or eventual safety measures (e.g. CAM) will depend on whether redundancy is available or the function has been lost.

It can be concluded from the above discussion that the recovery from the various types of contingencies will consist mainly of three types of actions:

(1) Switch-over to redundant single equipment, if faulty equipment can be identified.
(2) Switch-over to redundant string, if failure could not be isolated. This includes a switch to a redundant processor with identical RVC software.
(3) Interruption or abortion of mission, i.e.
   - interruption of mission (stop on V-bar, retreat to hold point),
   - execution of a CAM, where danger of collision exists,
   - inhibit of trajectory control actuation to leave the vehicle on a safe drift orbit (if available),

   in all cases where problems cannot be solved by redundancy switching.

In order to fulfil the failure tolerance requirements (described in section 4.1.1) for essential equipment such as data management equipment, reaction control system hardware, gyros, etc., double redundancy must be available. For other equipment, which is not essential for safety operations (CAM, survival mode), such as the rendezvous sensor, single redundancy will be sufficient. Functional redundancy will have to be included in the design, to the largest extent possible, in order to reduce the complexity of the system.

Detection of and recovery from contingencies due to violation of corridors or due to loss of functions can either be handled by the onboard system or by the target crew, or by ground operators assisted by support tools (see chapter 9). As mentioned above, re-planning and re-synchronisation of the mission after a contingency resulting in a change of the timeline can be achieved only by the ground system. Fast re-planning will require a faster than real time simulation capability, as the recovery strategy will have to be verified prior to up-linking to the chaser vehicle (see section 9.2.2).

6.5 Remote interaction with the automatic system

Although the onboard system of automated unmanned vehicles must be sufficiently failure tolerant to fulfil safety and mission success requirements (see section 4.1.1), it is obvious this can never cover all potential failure cases. Contingencies can be caused by external events (e.g. by problems in the target station), by design mistakes left undiscovered during the verification/validation process, or by manufacturing faults left undiscovered during the acceptance procedure. Remote control techniques could help to resolve those contingency situations during flight which are caused by such problems. This requires interaction with the various functions of the automatic onboard control system

depending on the contingency situation and type of failure. The following four levels of intervention into the automatic onboard system can be considered:

- High level intervention in the mode management concerning the mission sequence and in the equipment scheduler concerning the vehicle configuration. This type of intervention will be discussed in more detail in chapter 9.
- Intervention in the navigation, guidance or control functions while the automatic GNC system is still operating. In this case certain functions are modified or partially taken over by a remote operator.
- Manual navigation, guidance and control, i.e. the N, G and C functions of the automatic system are fully taken over by a remote operator. There is still a closed loop control, as the human operator continuously corrects the actual state w.r.t. the nominal one. Also, the actuator management function of the onboard system is still required.
- Open loop intervention, i.e. command by remote operators of discrete thrust manoeuvres to change trajectories or attitudes.

(The term 'remote operator' is applied here to human operators, computerised operator functions, or a combination of both, which are outside the chaser spacecraft.)

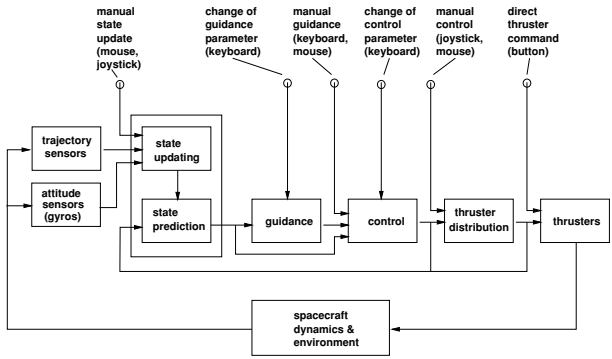

Figure 6.22. Potential points of intervention in the GNC loop.

6.5.1 Interaction with the GNC functions

Concerning the GNC functions, the possibilities available, in principle, of remote interaction with an automatic system are shown schematically in figure 6.22 and listed below:

- input of measurement data to the navigation function (manual state update);
- inputs to the guidance function:
  - fixed set values,
  - new guidance laws,

  - new guidance parameters;
- inputs to the control function:
  - new control laws,
  - new control parameters;
- input of force and torque commands to the actuator management function;
- input of valve open/close commands to individual thrusters.

Where guidance and control laws and parameters are concerned, interaction is by way of a software update, where the new software will be verified and validated on ground and up-linked to the onboard system off-line, e.g. during drift phases or hold points, when these guidance and control laws and parameters are not in use by the onboard system.

The direct command to thrusters from outside requires, in principle, a remote thruster management function, as the realisation of pure forces and torques will require generally the combined action of several thrusters. In the case of a CAM, however, where a fixed force in one body direction of the spacecraft has to be produced, a fixed set of thrusters with a fixed 'on'-time for each can be commanded.

Three of the points shown in figure 6.22 are of particular interest concerning a more continuous interaction by human operators in an automatic GNC system:

- manual state update, i.e. manual input of correction data to the propagated state, as produced by the navigation filter, to the actual state, as observed by the human operator;
- manual guidance, e.g. input of set points for velocities or angular rates by the human operator;
- manual control, i.e. input of force or torque commands into the thruster management function by the human operator.

6.5.2 Manual state update for the automatic GNC system

The manual state update can be useful as a backup mode, when the rendezvous sensor has failed but the automatic GNC system is still available and the human operator has continuous information from a video camera. If, e.g., an artificial contour of the target vehicle is produced and superimposed on the video picture, so simulating the same field of view as the video camera and driving the direction and size of the artificial view by the state update output of the navigation filter, the human operator can match the two images by varying the artificial view (i.e. by increasing/decreasing size, by changing position, and by rotation). This concept is illustrated by figure 6.23. Because the computer generated image has all the necessary data, such as range, line-of-sight angles etc., the modified values (after matching the images) can be entered into the update function of the navigation filter (MATRA 1993; Vankov *et al.* 1996).

In order to explain the principle, the real shape of the target spacecraft has, in figure 6.23, been replaced by that of a pyramid. The complete geometry of the target is, in principle, not needed for the artificial image. A minimum number of four points, of which

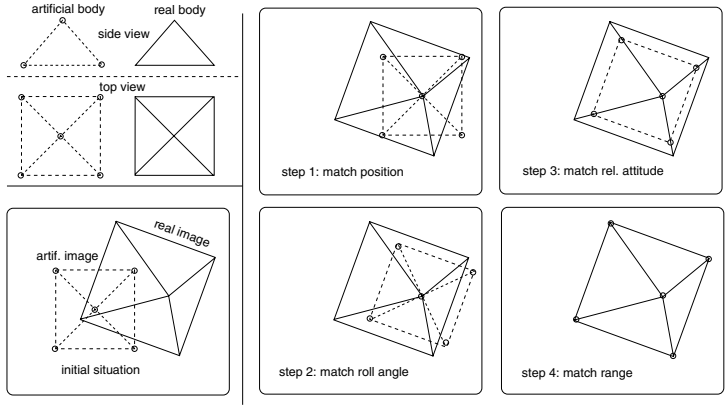

Figure 6.23. Manual state update by superposition of real and artificial images.

one must be outside the plane described by the other three, are required to define and manipulate a body. An artificial image more closely describing the spacecraft geometry will, however, be easier to match with the real target image because of the redundancy of information.

In the initial situation, the operator sees on the screen the unmatched video image of the target and the artificial image; this represents the state of the vehicle as propagated by the navigation filter. In the first step the operator will match the position (or azimuth/elevation angles, respectively) of the images by moving the artificial image, using, e.g., a computer mouse or a joystick. In the second and third steps the operator will rotate the artificial body about three axes to adjust the relative attitude, and in the final step he or she will match the size to adjust the range to the target. These steps may be performed iteratively. When the match is satisfactory, the result, which will be re-transformed by the computer into position and angles, will be supplied as a new measurement into the navigation filter. It has been found during simulations that an untrained operator can perform this task in real time with sufficient accuracy (Vankov *et al*. 1996).

6.5.3 Automatic GNC system with man-in-the-loop

Whereas in the rendezvous approach of the US Space Shuttle, the last part of the approach up to contact will always be controlled manually, the Russian vehicles, i.e. the manned Soyuz and the unmanned Progress, have manual control as a backup mode, which would be used only in case of failure of the automatic system. It should be noted that for any automatic vehicle such a manual backup control mode is a means by which to increase mission success rather than to increase safety. By itself, a manual control will be less safe, as there will be no automatic check of safety boundaries and the human controller will be the highest level of authority.

In the manual operating mode, as used, e.g., for the Russian Progress transporter, the unmanned vehicle will be manually remotely controlled by a crew member in the target station, or by a ground operator, using video images. Video pictures are sent by the approaching vehicle to the target station or ground. From the video pictures the remote human operator extracts the navigation information, and inputs commands to the system in the same way as if he were the pilot in the vehicle.

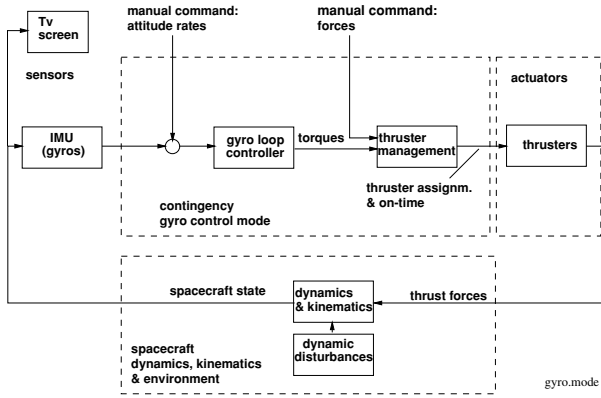

Figure 6.24. Manual operating mode with manual guidance and manual control inputs.

In the manual operating mode the human operator fulfils all GNC tasks except for stabilisation of attitude, which is performed by an automatic control loop based on gyro measurements (see figure 6.24). Changes of attitude will be entered by joystick command as change of attitude rate (guidance set value) into the gyro stabilisation loop. This is actually a replacement of the guidance function by the human operator, as he introduces the set values for the angular rates. Changes of translation velocities will be entered by joystick command directly into the thruster management function, which selects the thrusters and the length of thrust. In this case the human operator replaces the control function, as he directly commands the forces and torques to be executed.

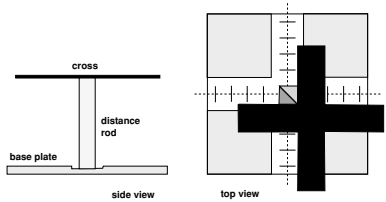

Figure 6.25. Visual target pattern for short range manual approach.

Navigation is performed by the human operator by assessing on the screen (with the help of reticles and fixed marks)

- the distance to the target (range) from the apparent size of the target image,
- the position or azimuth and elevation angles from the position of the target image relative to the centre of the screen,
- the relative attitude angles from the position of principal points of the target geometry w.r.t. the screen axes.

As long as the distance to the target is large enough that the full image of the target is on the screen, the operator will use the complete image for assessment. At shorter distances, only a part of the spacecraft will be on the screen. The operator will then use the largest available features for navigation assessment. Eventually, only a small section near to the docking port will be visible on the screen. It will then be necessary to have a particular visual target pattern, which must be sized such that its image does not exceed the screen up to contact. For monitoring the visual target pattern at medium and short range, cameras with two sets of lenses can be used. The concept of such a target pattern, as used in Russian and American space programmes, is shown in figure 6.25. The pattern consists of a base plate and a cross at a distance from the ground plane. Range, position and relative attitude can be assessed in the same way as described above from the relative position of the pattern w.r.t. the screen and from the size and position of the cross w.r.t. the base plate.

7

Sensors for rendezvous navigation

The subject of this chapter is the discussion of the measurement principles of sensors for relative navigation, required in the far and close range rendezvous phases to measure the relative state between the chaser and target vehicles. In the rendezvous phases proper (see figure 2.1), the accuracy of absolute navigation will no longer be sufficient. With one exception, sensor principles for absolute navigation will not be discussed here, since the measurement principles for absolute attitude and absolute position for spacecraft applications can be considered well-known. Measurement and control of absolute attitude is a feature of practically every spacecraft. Onboard measurement of absolute position is required, e.g., in Earth observation missions, where receivers for satellite navigation and for ground-based radio-positioning systems, e.g. DORIS (Carrou 1995), are accommodated on the spacecraft. In most other missions, absolute orbit and position determination is usually done by observations from ground, since, in the majority of cases, mission requirements do not justify the accommodation of an absolute position sensor aboard the spacecraft.

The above-mentioned exception, to be described in this chapter, comprises the basic functional principles of absolute position measurement by satellite navigation. At the time of writing, GPS and GLONASS are the satellite navigation services used, and, for the purpose of rendezvous navigation, the navigation results of, e.g., GPS receivers w.r.t. an Earth-fixed coordinate frame, are termed *absolute GPS*. The understanding of absolute GPS is a pre-requisite for the understanding of *relative GPS*, which is one of the major sensor principles used nowadays for far and medium range relative navigation in the rendezvous approach. If a GPS receiver is available on board, absolute GPS will of course also be the main source of absolute position information.

It is not intended to describe in this chapter the details of actual sensor design implementations. The detailed design depends to a large extent on the availability of particular

technologies at the time of development, which have been changing relatively quickly in the last decades. Also, for the comprehension of the typical function and performance of a particular sensor concept in the context of a rendezvous system, it is not absolutely necessary to have detailed knowledge of the actual design implementation. The purpose of this chapter is rather:

- to address briefly the requirements for the sensors in terms of parameters to be measured, the measurement performances in relation to trajectory errors and in relation to ranges of operation in the approach;
- to give a short overview of the physics which can be used for relative navigation measurements between two vehicles;
- to identify the basic functional principles of various categories of sensors actually used for rendezvous purposes;
- to discuss the potential disturbance effects which may result from the measurement environment for the various sensor principles;
- to identify typical features of the various sensor categories in terms of measurement performance, range, mass and power consumption and other constraints.

7.1 Basic measurement requirements and concepts

7.1.1 Measurement requirements

Measurements of the absolute state, such as the attitude of the vehicle w.r.t. the local orbital frame $\boldsymbol{F}_{\mathbf{lo}}$ and as position or orbital ephemerides of the vehicle in the Earth-centred equatorial frame $\boldsymbol{F}_{\mathbf{eq}}$, will be required during all phases of the rendezvous mission to determine spacecraft angles and position w.r.t. the Earth and the Sun for communication, power and illumination reasons. In addition, starting from the far range rendezvous, relative position and velocities need to be available in the target local orbital frame $\boldsymbol{F}_{\mathbf{lo}}$. Relative position and velocity information could of course be obtained by the differences of the absolute measurements made on chaser and target. However, as the subtraction of large values leads to large errors, this method can only be used at large distances. In the rendezvous phases proper, i.e. during far and close range rendezvous, an increasingly accurate knowledge of the relative position and velocities of the chaser w.r.t. the target is necessary. This requires direct measurements to be made between the two vehicles. Such measurements can in principle be performed on either vehicle. If performed on the target vehicle, the results would have to be transmitted to the chaser GNC system, which may cause additional noise and which includes the danger of link interruptions. If performed on the chaser, the vehicle's position or velocity cannot be measured directly in the target's $\boldsymbol{F}_{\mathbf{lo}}$ frame. In this case, the attitude of the sensor axes w.r.t. the $\boldsymbol{F}_{\mathbf{lo}}$ frame of the target must be known with sufficient accuracy in order to resolve the actual range

and direction measurements made in the chaser body frame into the needed values w.r.t. the target local orbital frame.

Measurement parameters

The following two alternatives can be used for the relative position measurements:

- Measurement of range and line-of-sight angles and of range-rate and angular velocities in the body frame $\boldsymbol{F}_{\mathbf{ge}}$ of chaser or target (for definition of frames see section 3.1). These measurements can be resolved into x-, y-, z-position and velocities in the $\boldsymbol{F}_{\mathbf{lo}}$ frame of the target, provided the attitude of the chaser in the target frame is known. The angular difference between the nominal attitude frames of chaser and target frame due to the curvature of the orbit can be calculated from the distance r between the vehicles. At very small ranges ($r \ll R$, where R = radius of orbit), the angular directions of chaser and target $\boldsymbol{F}_{\mathbf{lo}}$ frames are practically identical within the accuracy of attitude measurement and onboard calculation; e.g. below a range of 1 km the angular misalignment of the nominal frames of chaser and target is $<$0.009 deg.
- Measurement of range and/or range-rate on both chaser and target to a number of common external reference points, using the same type of tools and methods on both vehicles. The differential result will be calculated from the differences between the individual measurements on each vehicle, rather than taking the difference of the complete results. This is the type of measurement principle used, e.g., in RGPS, described in section 7.3.3. Because of the common reference points, tools and methods, and because the distance between chaser and target is small compared with the distance to the reference points, the major part of the errors will be the same on both chaser and target sides, and will therefore be cancelled during the subtraction of the measurements from both vehicles.

For the acquisition of the docking axis in the last part of the approach, control not only of the relative translational motion, but also of the angular motion between the docking frames of chaser and target is required. Therefore, additional information on relative attitude and relative attitude rate needs to be available. Again, the relative attitude between the two vehicles could in principle be obtained by calculating the difference between their absolute attitudes in the local orbital frame. However, because of the potential accumulation of errors, and because of the limitations of the reception range of the docking mechanism, it will, in most cases, be necessary to measure the relative attitude directly between the docking ports of the two vehicles. Deviations of the actual from the nominal relative attitude of the docking interfaces can be due to:

(1) potential unknown misalignments of the docking axes w.r.t. the nominal attitude frames on both vehicles, e.g. due to thermal expansion;

(2) motions of the docking axis, which are independent of motions of the vehicle's nominal attitude frame w.r.t. the $\boldsymbol{F}_{\mathbf{lo}}$ frame, e.g. due to structural flexibilities;

(3) instantaneous deviations from the nominal attitude due to the control motion (see figure 8.30),

The most important requirement for the rendezvous navigation is that the measurement errors for all parameters are decreasing commensurate with the decreasing range between the two vehicles. The second important requirement is that, in the vicinity of the docking port, the navigation errors become small enough to keep the control errors within the reception range of the docking mechanism (see section 8.3.6) or within the tolerances of the inner berthing box (see section 5.3.1). In order to arrive at the sensor requirements, the effects of measurement errors on the trajectory and the possibility of reducing the manoeuvre errors, or of achieving converging errors in the trajectory sequence by other means, will be discussed below.

Position measurement errors

Only position measurement errors in the z-direction (R-bar) have significant effects on the trajectory evolution. The lateral measurement error, Δz_{m}, can translate, as has been discussed in section 4.3.1, into an error in the x-direction in two ways. First, case (a), if the chaser is on a concentric orbit with a different radius from the target orbit, an unobserved altitude difference of Δz_{m} results, according to Eq. (4.16),

- after one orbital revolution (tangential boost transfer) in a position error along the orbit direction of $\Delta x = 3\pi\Delta z_{\mathrm{m}}$,
- after half an orbital revolution (radial boost transfer) accordingly in $\Delta x = 3/2\pi\Delta z_{\mathrm{m}}$.

Secondly, case (b), if the chaser is actually above or below the target orbit, but has the same velocity in the orbit direction as the target, an unobserved altitude difference of Δz_{m} results, according to Eq. (4.17),

- after one orbital revolution (T) in a position error along the orbit direction $\Delta x = 12\pi\Delta z_{\mathrm{m}}$,
- after half an orbital revolution ($T/2$) in an x-position error of $\Delta x = 6\pi\Delta z_{\mathrm{m}}$ and a z-position error of $\Delta z = 7\Delta z_{\mathrm{m}}$.

The numeric values given in section 4.3.1 are repeated here for reference. For a measurement error of $\Delta z = 10$ m, the results would be:

case (a) at $T/2$, $\Delta x = 47.12$ m; at T, $\Delta x = 94.25$ m

case (b) at $T/2$, $\Delta x = 188.5$ m, $\Delta z = 70$ m; at T, $\Delta x = 377$ m, $\Delta z = 0$

Whether measurement error case (a) or (b) is applicable could be decided only if very accurate velocity measurements were available. Since the accuracy of velocity measurement is, in most cases, worse than that of the position measurement, case (b) has to be taken into account as the worst case for the position error at arrival.

Velocity measurement errors

In addition to the position measurement errors, the dispersion of the final position is also sensitive to errors in the velocity measurement, as has been shown in section 4.3.1. According to Eq. (4.18), a velocity measurement error $\Delta V_{x\mathrm{m}}$ in the orbit direction will cause

- after half an orbital revolution (radial boost transfer) a position error of $\Delta x = -\frac{3}{2}\Delta V_{x\mathrm{m}} T$ and $\Delta z = -\frac{4}{\omega}\Delta V_{x\mathrm{m}}$,
- after one orbital revolution, a zero position error in the z-direction, and a position error in the x-direction of $\Delta x = -3\Delta V_{x\mathrm{m}} T$.

The numeric values given in section 4.3.1 are repeated here for reference. A velocity measurement error in the orbit direction of only 0.01 m/s would, after one orbital revolution, lead to an x-position error of about 170 m with no z-position error, and after half a revolution to an x-position error of about 85 m and a z-position error of about 36 m.

The effect of velocity measurement errors in the z-direction, $\Delta V_{z\mathrm{m}}$, is much smaller than that of $\Delta V_{x\mathrm{m}}$ errors, i.e. 0.21 times ($= \frac{2}{3\pi}$) on the x-position, and 0.25 times on the z-position (see Eq. (3.34)). Velocity measurement errors in the y-direction, $\Delta V_{y\mathrm{m}}$, result in position errors only in the y-direction. The effect of $\Delta V_{y\mathrm{m}}$ on the the y-position is the same as that of $\Delta V_{z\mathrm{m}}$ on the the z-position.

As for the position error, the velocity measurement error must decrease linearly with the range, in order to remain within a particular final position error in relation to the range. Otherwise, it must have the performance for the shortest distance over the entire range of use.

Angular measurement errors

For sensors which calculate position and velocities from line-of-sight (LOS) angles and range, the LOS measurement accuracy needs to be compatible with the range measurement accuracy. The lateral error is $\Delta z = r \cdot \sin \Delta\alpha$, where $\Delta\alpha$ is the LOS angle measurement error. The angular accuracy must be, therefore, at least 0.05 deg in order to correspond to the 0.1% of range requirement. Considering that errors in both range and LOS angle measurement will occur, the individual contributions must be accordingly lower.

Effects of measurement errors on absolute attitude are not considered here, as absolute attitude is not measured by rendezvous sensors. Relative attitude needs to be measured only in the last phase of approach on closed loop controlled straight line trajectories. Relative attitude errors will be addressed below in the context of capture conditions.

Effects on trajectory strategy and safety

From the above considerations, it is obvious that, with open loop transfers, a constant measurement accuracy for the lateral position will not be sufficient to achieve final contact

conditions. However, if the measurement accuracy is a certain percentage of the range, i.e. if the errors decrease steadily with the distance to the target, larger measurement errors can, to a certain extent, be compensated for in the approach strategy by more and shorter steps at the expense of a longer duration and higher propellant consumption.

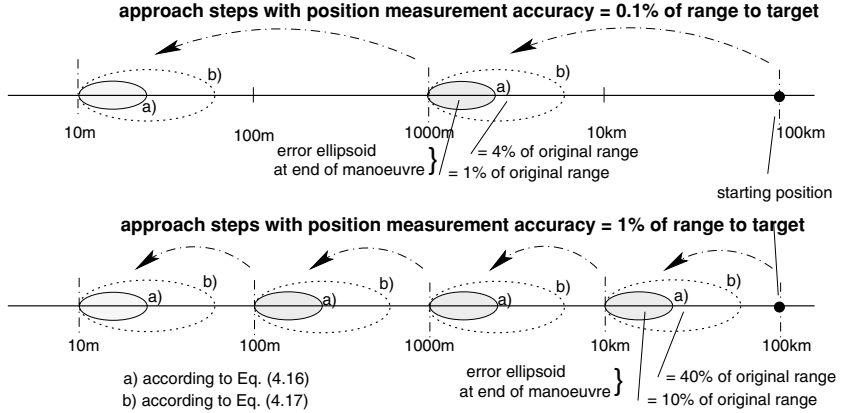

Figure 7.1. Approach steps with 0.1% and 1% of the range sensor accuracy.

Example 1

In figure 7.1, tangential boost transfers along the orbital axis are assumed, i.e. each transfer takes one orbital revolution. Two sensors are considered: the first has a measurement accuracy for lateral position of 0.1% of the range to the target, and the second has a position measurement accuracy of 1% of the range. Let us look at the transfer from a range of about 100 km to a range of 1000 m from a target station.

For a sensor with a lateral measurement error of 0.1% of the range, the range error would at arrival be approximately 1% of the original range, i.e. 1000 m for measurement error case (a) and about 4%, or 4000 m, for measurement error case (b).

In the second case, with a lateral measurement error of 1%, the range error at arrival would be 10% of the original range, i.e. 10 km for measurement error case (a) and about 40%, or 40 km, for measurement error case (b).

In the case of a 1% lateral measurement accuracy, the targeted position for a transfer in the x-direction must be no closer than 40 km for lateral measurement error case (b), in order to avoid the danger of collision with the target. As a result, the transfer from 100 km to 1 km must be performed with this sensor performance in at least two steps, whereas for a sensor of 0.1% accuracy, the same absolute final dispersion could be achieved in one step.

This example shows that, as a result of the measurement accuracy of the sensor, there is a limit to the size of the manoeuvres. By introducing a larger number of manoeuvre

steps of shorter transfer distance, using a lower performance sensor, the final accuracy can still be achieved. In any case, the error ellipsoid around the arrival position must be at sufficient distance from the target vehicle, so that there will be a limit to the acceptable sensor errors.

Whereas for tangential boost transfers, lateral measurement errors result, after one orbital revolution, in position errors only along the x-direction (V-bar), in the case of radial boost transfers, the position error after half an orbital revolution will also include, as we have seen, significant components in the z-direction. This will make the correction of position errors after each transfer step more complex, as corrective ΔVs in the tangential and radial directions will be required. Dispersions due to measurement errors in the z-position and the x-velocity are shown in figure 7.2. Combinations of position and velocity measurement errors can also lead to problems in the assessment of trajectory safety, which can be demonstrated by the following example.

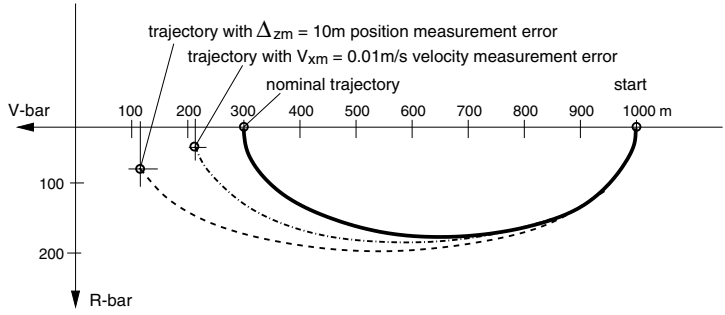

Figure 7.2. Dispersions due to measurement errors after radial boost transfer.

Example 2

Let us consider a radial boost manoeuvre along V-bar from a starting distance of 1000 m to an end distance of 300 m from the target: the z-position measurement error is -10 m and the x-velocity error is -0.006 m/s. Assuming that in reality the chaser is 10 m below V-bar and at zero relative velocity w.r.t. the target, the sensor would in this case indicate a position on the target orbit and a relative velocity of -0.006 m/s, i.e. a safe condition for a $-$V-bar approach. With the actual initial conditions, after half an orbital revolution the position error would be of the order of 190 m in the x-direction and 70 m in the z-direction.

The example shows that for an open loop radial boost transfer, starting at 1000 m and targeted at a few hundred metres, the assumed measurement accuracies of 1% of range and 0.006 m/s would lead to unacceptable end conditions for the transfer.

Velocity measurement by differentiation

In many cases the velocity cannot be measured directly or cannot be measured with the required accuracy. If a sensor can only measure the position, the average velocity can be obtained from the change of position over time. If, e.g., its position measurement accuracy were 10 m, an undisturbed measurement duration of 1667 s would be necessary to obtain a resolution of 0.006 m/s, i.e. the velocity measurement accuracy assumed in example 2 for a manoeuvre initiation at 1000 m. The measurement time will of course be shorter if velocities can be measured directly. With a direct velocity measurement capability of 0.1 m/s (the approach velocities are of the order of 10 m/s prior to the manoeuvre to acquire the target orbit, and 1–2 m/s during closing), it would take a measurement duration of only 16.7 s to reach the same resolution. However, the requirement to reduce position and velocity measurement errors commensurate with the decreasing distance to the target will, at close range for open loop transfers, eventually lead to unfeasible measurement requirements, both for accuracy and duration, and will rule out, for trajectory safety reasons, open loop transfers below a certain range to the target.

Mid-course corrections and closed loop control

The position accuracy of impulsive transfer manoeuvres can be improved by one or more intermediate corrections (mid-course corrections) or by closed loop control of the nominal trajectory, calculated for the nominal boosts (see section 4.4.1). In the case of a single mid-course correction manoeuvre, the final position errors can be reduced theoretically to one-half, by a further correction manoeuvre at three- quarters of the orbital revolution to one-quarter of the original value. As each manoeuvre will introduce new errors, this theoretical improvement may not be achievable in reality.

In the case of closed loop control over the entire transfer trajectory, the error at arrival will be the measurement error plus some additional control error. It is the major advantage of continuous closed loop control that the effects of initial measurement errors will be controlled out. This is due to the fact that, in closed loop trajectories, the position errors are a function of the range of the actual trajectory point, rather than of the range at manoeuvre initiation from the target, as in open loop transfers. As a result, for continuously controlled two-boost transfer trajectories, the requirements for position and velocity measurement in all directions will be less tight than in the case of the open loop transfers.

For closed loop trajectories the measurement accuracy should be, where possible, an order of magnitude (but as a minimum two to three times) better than that of the value to be controlled. For reasons already discussed above, the last part of the approach needs to be a straight line transfer. During the straight line final approach, not only the position, but also the velocity profile needs to be controlled accurately; this leads to additional velocity measurement requirements.

Measurement requirements at capture

The most critical measurement and control requirements must eventually be met at capture. The limiting features at capture are:

- in docking, the useful reception range of the docking mechanism in terms of lateral and angular misalignments and impact velocities (see section 8.3);
- in berthing the location and size of the inner berthing box (see section 5.3.1).

The following parameters are to be controlled, and performances are to be achieved, by the GNC system, for the interface with the capture operations.

- *For docking:* approach velocity, lateral alignment, lateral velocity, angular alignment and angular rate. Depending on the type of docking mechanism and vehicle characteristics, the typical values for docking are:

  approach velocity = 0.03–0.3 m/s

  lateral alignment = 0.05–0.2 m

  lateral velocity = 0.01–0.05 m/s

  angular misalignment = 1–5 deg

  angular rate = 0.05–0.25 deg/s

- *For berthing:* the nominal velocities at inhibit of actuation must be zero. The typical performance values to be achieved in the berthing box are:

  x-, y-, z-position = 0.1–0.5 m

  residual velocities = $<$ 0.01 m/s

  angular misalignment $\leq$ 10 deg

  angular rate: $\leq$ 0.1 deg/s

Because of the time required for the capture process to take place, the linear and angular rates are, in the case of berthing, more critical than the initial linear and angular misalignments.

It has been discussed in chapter 4 that navigation errors are not the only source of trajectory deviations and misalignments at capture. They will form, therefore, only a part of the overall error budget. In figure 7.3 an example of an allocation of error sources is shown for the closed loop controlled final translation to docking as a pie-chart. The main contributors to the final alignment accuracy at contact are:

- the sensor measurement error, including the sensor noise and any uncompensated bias resulting from the sensor itself and from misalignment between the sensor and the docking axis;

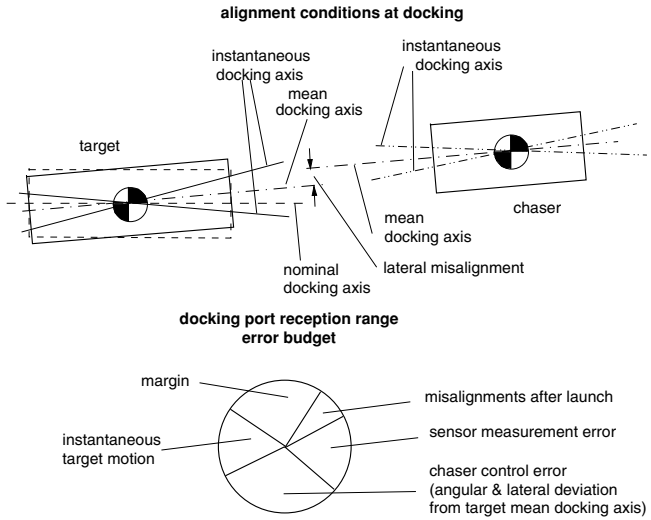

Figure 7.3. Error allocation for docking reception range.

- the control error, including all deviations of the actual vehicle state w.r.t the one according to the guidance set values and state as measured by the sensor;
- the uncompensated misalignments between the sensor axis and the chaser docking axis and between the target reflector axis and the target docking axis, e.g. due to residual calibration errors, launch impact and thermal deformations;
- the motion of the target which cannot be detected by the sensor, e.g. because of limited sensor bandwidth;
- a margin which covers all other unknown deviations and disturbances.

Conclusions on measurement performance

From the above discussion, the following conclusions on the effects of the performance of sensors for relative navigation can be drawn.

Impulsive transfers In open loop:

- The most significant trajectory deviations are caused by measurement errors of position in the z-direction (R-bar) and of velocity in the x-direction (V-bar).
- For open loop transfers, the end position of the transfer must be sufficiently far from the target such that the position dispersions at the end of the transfer do not lead to collision danger. The initial accuracy of position knowledge (all axes) should be

0.1% of range or better. An accuracy of only 1% may lead in two-pulse transfers to final position dispersions, which are unacceptable in the medium and short range rendezvous phases.

- Open loop transfer accuracy can be improved by mid-course corrections, taking advantage of the increased measurement accuracy at reduced distance to the target. In addition to a reduced transfer distance, one or more intermediate corrections will be necessary to make an approach with a 1% of range measurement accuracy viable down to ranges to the target of one or two kilometres. For an approach with mid-course corrections down to a few hundred metres, lateral position measurement accuracy would have to be at least 0.1% of range.

- If the lateral position is derived from range and LOS measurements, a range measurement accuracy of half the lateral measurement accuracy must be achieved as a minimum.

- LOS angles need to be measured with an accuracy of $\leq$0.25 deg, if, together with the range error of 0.5%, a lateral position measurement error of $<$1% of range shall be kept and accordingly a factor of 10 better, if a position measurement error of 0.1% has to be achieved.

- A 0.01 m/s velocity measurement error in the orbit direction will cause, in an impulsive, transfer a position error in the x-direction of about 85 m after half an orbital revolution and about 170 m after one revolution and a z-error of about 36 m after half a revolution. Errors of this size will not be acceptable at ranges to target below one or two kilometres. For an approach down to a few hundred metres to the target, the velocity measurement performance would have to be an order of magnitude better.

To achieve the required velocity measurement accuracy from position measurements, a long integration time may be necessary.

In closed loop:

- In impulsive transfers there is a possibility of reducing the dispersion at the arrival position by employing closed loop control w.r.t. a nominal trajectory. As measurement errors are a function of the range of the actual trajectory point, a 1% of range sensor accuracy, together with other error contributors, in a closed loop controlled transfer, may permit position accuracy of a few per cent of the actual range.

- For the closed loop controlled two-pulse transfers, the initial velocity measurement accuracy will be less critical, if along the trajectory the position measurement accuracy at each point is sufficiently accurate. A continuous position control with a measurement accuracy of 1% of range will provide sufficient integration over the transfer duration for effective correction of initial velocity errors.

Straight line transfers

- For closed controlled trajectories terminating with capture, it has to be kept in mind that the final position accuracy is determined also by other errors, as shown in figure 7.3. Measurement errors must be a factor of 2–5 lower than the desired final accuracy.
- For closed loop controlled trajectories with a velocity profile, the velocity measurement accuracy should be, if possible, one order of magnitude (but at least a factor of 2) better than the desired velocity accuracy. If, e.g., the nominal velocity of the last metre approach to contact were 0.1 m/s, and was to be controlled with 20% accuracy, the velocity measurement accuracy must be <1 cm/s.
- To achieve such velocity accuracy by position measurement, range and LOS angles must be measured with a bandwidth of the order of 1 Hz or better. Additional requirements for the bandwidth of the sensor can be imposed in the short range by the motion of the target, e.g. due to attitude control motions or structural oscillations. Lateral motion of the target which cannot be followed by the chaser is a major contributor to the error budget for docking.
- The measurement accuracy for relative attitude must be about 1 deg, if an angular alignment of the docking axes of <5 deg is to be achieved.

The above discussion was intended to show the driving factors for sensor requirements; it was not intended to yield a complete list of specifications for rendezvous sensors. Such specifications can be derived only after the definition of an approach strategy, including trajectory types and transfer distances, after decisions on mid-course correction schemes and closed loop control of trajectories, and after proper analysis of the other sources of trajectory deviations, such as external disturbances and thrust errors.

7.1.2 Measurement principles

The following basic physical phenomena and principles can be exploited for the measurement of the navigation parameters required during the rendezvous process.

Distance, range

- Triangulation. The range is calculated from measured angles and known target dimensions: measurement on the chaser of the direction angles toward a number of reference points on the target or vice versa (the relative position of those reference points w.r.t. each other must be known); measurement of the size of an image of a feature on the target in the focal plane of a camera on the chaser or vice versa (the dimensions of the feature must be known).
- Time of flight from a transmitter to a receiver of an electro-magnetic wave signal. This requires knowledge of the time t_0 when the signal is radiated (see figure 7.5).

- Phase shift of an electro-magnetic wave signal at a receiver w.r.t. the phase at the transmitter. This requires the knowledge of the phase when radiated (see figure 7.5).

- Integration over time of a velocity measurement. This will only provide the *changes* in range over the measurement period, not the absolute range.

Range-rate

- Doppler shift of transmitted frequency, when arriving at receiver (see figure 7.7). This requires the knowledge of the transmitter frequency.

- Differentiation w.r.t. time of range measurements. This requires a sufficiently low noise factor in the range measurements.

Line-of-sight direction

- Measurement of the position of a target point or of the centre of a target image in the focal plane of a camera (see figures 7.30 and 7.31).

- Difference of phase delay measurement by two antennas, mounted at a fixed distance on one of the vehicles, of an electro-magnetic wave transmitted or reflected by a target on the other vehicle (see figure 7.10).

- Difference of time delay measurement by two antennas, mounted at a fixed distance on one of the vehicles, of an electro-magnetic wave transmitted or reflected by a target on the other vehicle (see figure 7.10).

- Measurement of the signal transmitted or reflected by the other spacecraft concerning signal amplitude and instantaneous angle of the rotating receiver antenna at reception. The antenna must have a suitable pattern, with a pronounced maximum or minimum strength (see figures 7.11 and 7.12).

- Measurement of gimbal angle, or of electronic scan angle, at reception of a narrow beam signal, either transmitted or reflected by the other spacecraft (scanner type, see figure 7.9).

Relative attitude

- Triangulation. A three-axes frame on the target is established by: measurement of range and direction of at least three different known points, forming a plane (see figure 7.29); relative position of target image in the focal plane of a camera of at least four known target points forming a three-dimensional body (see figure 7.31).

- Single-axis measurement by superposition of two antenna patterns, i.e. by a fixed antenna with tone modulation and by a rotating antenna: an omni-directional antenna transmits a tone modulated signal, a second antenna with a particular antenna characteristic rotates with the modulation frequency, measurement of phase difference between the two-tone signals; this is similar to a VHF omni-directional range (VOR) in aircraft navigation (see figure 7.13).
- Single-axis measurement by two, and two-axis measurement by four, antenna beams with different modulation frequencies, measurement of amplitude difference (similar to instrument landing system (ILS) in aircraft navigation (see figure 7.14).

Angular rate

- Differentiation w.r.t. time of LOS and relative attitude measurements.
- Gyroscopes. Gyroscopic effects (mechanical: conservation of angular momentum; optical: Sagnac effect) are the only physical phenomena available for direct angular rate detection. Gyroscopes cover, however, only the angular motion of their own vehicle w.r.t. the inertial frame. They do not measure, e.g., the rate of LOS due to lateral motions of the target or the rate of relative attitude due to attitude changes of the target.

7.2 RF-sensors

7.2.1 Principles of range and range-rate measurement

General principle of range measurement

The range of the target can be measured either by measurement of the time of flight of the signal or by measurement of the phase shift of the incoming w.r.t. the outgoing signal. This requires recording in the first case the time and in the second case the phase both at transmission and reception. The relationship between the time-of-flight, $t_2 - t_1$, of an electro-magnetic wave and the travelled distance, r, is given by the speed of light c:

$$t_2 - t_1 = \frac{r}{c} \tag{7.1}$$

and the relationship between the shift of phase, $\phi_2 - \phi_1$, and the travelled distance, r, is

$$\phi_2 - \phi_1 = \frac{2\pi r}{\lambda} = \frac{2\pi r f}{c} \tag{7.2}$$

where λ is the wavelength and f is the frequency of the signal. In the general case these time or phase differences can be measured only when the transmitted signal is reflected by the target and the reflected signal is received again at the location of the

transmitter (for an exception see section 7.3.2). In all practical cases, a modulated RF signal is generated by a transmitter and is transmitted by an antenna toward a target. Part of the power of the signal is reflected by the target back in the direction of the transmitter, or the signal is re-transmitted by a transponder on the target, and is received by an antenna at the transmitter location. Transmitting and receiving antenna may be the same piece of hardware if there is a switching function between outgoing and incoming signal. Because of the modulation, the returning signal (echo) can be referenced to the outgoing signal.

Range measurement with pulse modulated signal

A high frequency carrier is modulated in pulse form. The time of the flank of the received pulse is related to that of the transmitted one. The total time will be double the amount given by Eq. (7.1), as the range R has to be travelled twice by the signal:

$$T = \frac{2R}{c}$$

Hence the range is

$$R = \frac{1}{2} T \cdot c \tag{7.3}$$

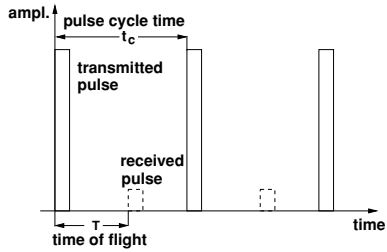

Figure 7.4. Functional principle of range measurement via time delay.

In order to avoid interference between the transmitted and received signals, in pulse radars, where the same pulse is repeatedly sent out, the subsequent pulse can only be sent after the echo of the previous one has been received. The receiver has to be blocked while a pulse is transmitted. This is true for the basic measurement principle of pulse type radars. In more modern developments the pulse is not created by switching the carrier frequency on and off, but by bi-phase modulation (see below). For a resolution of 1 m, the system must be able to measure a time difference of $\leq 6.6 \times 10^{-9}$ s.

Range measurement with continuous wave signal

Measurement of the phase difference between transmitted and received signals requires the knowledge of the phase at transmission. As in the time-of-flight measurement above, the initial conditions at transmission are available, in general, to a receiver, if it is collocated with the transmitter and if the signal is reflected by a target. This measurement principle is used by CW-type radars and also generally used by ground stations of satellites for so-called 'tone ranging' via two-way telemetry links. A continuous wave signal is transmitted toward the target. The phase difference between the transmitted and the echo signals is

$$\Phi = 2\frac{2\pi R}{\lambda} \tag{7.4}$$

where $\lambda = \frac{c}{f}$ is the wavelength. The range is then accordingly:

$$R = \frac{\Phi\lambda}{4\pi} \tag{7.5}$$

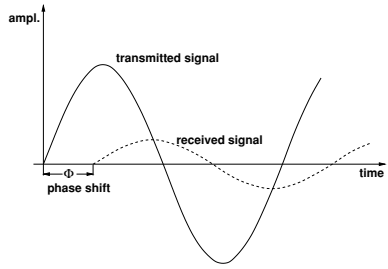

Figure 7.5. Functional principle of range measurement via phase shift.

As Φ can be measured unambiguously only between 0 and 2π, the measurements become ambiguous at ranges of $2R > \lambda$. On the other hand, the resolution of the range measurement increases when the wavelength decreases. If e.g. the frequency used for the measurement is 10 kHz, the maximum range which can be measured unambiguously

$$R = \frac{1}{2}\lambda = 15 \text{ km}$$

and if the phase angle can be measured with an accuracy of $\Delta\Phi = 0.01$ rad, the resolution will not be better than

$$\Delta R = \frac{1}{2}\frac{\lambda}{2\pi} = 24 \text{ m}$$

To improve the range, the wavelength would have to be increased, but to improve the resolution, it would have to be decreased. A solution to this dilemma is the use of two or more modulation frequencies, where the highest frequency determines the resolution and the lower ones determine the wave range (Hartl 1977). One possibility would be to modulate different subcarrier frequencies on the main carrier, which could again be modulated to transmit additional information.

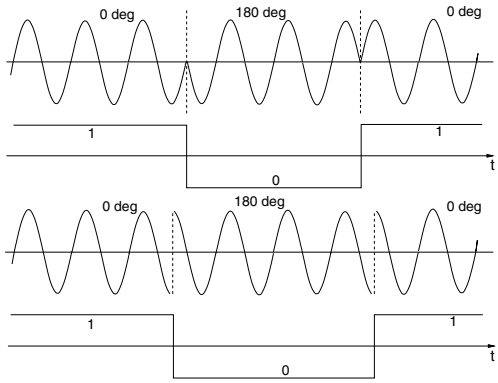

Figure 7.6. Bi-phase modulation of carrier frequency.

A method often used for such modulation is a phase modulation with the phase angles Φ equal to 0 and 180 deg, often called 'phase shift key' (PSK). This type of modulation, which can be used to transmit pulse type or digital information, is shown in figure 7.6. A logical '0' or a logical '1' corresponds in this case to one of the two phase angles. In radar applications, pulses of different length or a code of '0s' and '1s' can be used to indicate the start of the time measurement on the signal. Phase angle measurement according to Eq. (7.5) can be performed on the main and subcarriers, and time-of-flight measurement according to Eq. (7.3) on the digital code. Such a combination of pulse and phase radar principles is used in the Kurs system and in the satellite navigation systems described in sections 7.2.5 and 7.3.

Range-rate measurement

For the measurement of the range-rate, use can be made of the Doppler effect. The 'Doppler shift' of a frequency arriving at a receiver is directly proportional to the component of the relative velocity, $\dot{R}$, in the transmitter–receiver direction:

$$\Delta f = \frac{-\dot{R} f_{\mathrm{T}}}{c} \tag{7.6}$$

i.e. when the range-rate is positive, which means that the transmitter moves away from the receiver and the range increases with time, the frequency f_{R} arriving at the receiver

becomes lower; and vice versa, when the range decreases with time:

$$f_{\mathrm{R}} = f_{\mathrm{T}} + \Delta f = f_{\mathrm{T}} \left(1 - \frac{\dot{R}}{c} \right) \tag{7.7}$$

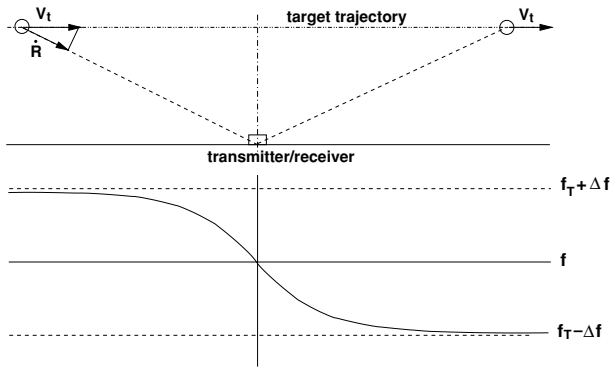

Figure 7.7. Doppler shift of received frequency due to target range-rate.

If the signal is reflected at a target, the Doppler shift will be applied twice. The frequency at the target is

$$f_{\mathrm{t}} = f_{\mathrm{T}} \left(1 - \frac{\dot{R}}{c} \right)$$

and the frequency at the receiver is

$$f_{\mathrm{R}} = f_{\mathrm{t}} \left(1 - \frac{\dot{R}}{c} \right)$$

resulting in

$$f_{\mathrm{R}} = f_{\mathrm{T}} \left(1 - \frac{\dot{R}}{c} \right)^2 \tag{7.8}$$

which, since the velocity of light, $c \gg \dot{R}$, is, to a good approximation,

$$f_{\mathrm{R}} = f_{\mathrm{T}} \left(1 - 2\frac{\dot{R}}{c} \right) \tag{7.9}$$

The range-rate is then

$$\dot{R} = \frac{1}{2}\frac{c}{f_{\mathrm{T}}}(f_{\mathrm{T}} - f_{\mathrm{R}}) \tag{7.10}$$

or

$$\dot{R} = \frac{1}{2}\lambda_{\mathrm{T}}(f_{\mathrm{T}} - f_{\mathrm{R}}) \tag{7.11}$$

where λ_{T} is the wavelength of the transmitted signal.

This measurement principle is used by Doppler radars. In order to obtain a velocity resolution of 0.01 m/s, such a sensor must be able to measure a ratio of $\frac{\Delta f}{f} = 6.7 \times 10^{-11}$, which requires transmission frequencies of the order of 100 GHz.

Power limitations of operating range

The maximum range of a radar is limited by the lowest power of the returning signal which can be detected on the receiver side. This means that the received signal must be at a sufficiently high level above the noise. Noise may be created both by external sources or by the receiver itself. Thermal noise will eventually form the limit for the receiver sensitivity. The power density of the signal when arriving at the target is equal to the transmitted power times the ratio of the transmitter antenna gain to the surface of a sphere with the radius of the range *R*:

$$S_{\mathrm{t}} = \frac{P_{\mathrm{T}} G_{\mathrm{T}}}{4\pi R^2} \tag{7.12}$$

where S_{t} is the power density of the signal at target, P_{T} is the power of the transmitted signal and G_{T} is the power gain of the transmitting antenna. The power reflected by the target is equal to the power density at the target times the effective reflecting area of the target. Assuming diffuse, i.e. omni-directional, reflection by the target, the power density of the echo signal when arriving at the receiver is

$$S_{\mathrm{echo}} = \frac{S_{\mathrm{t}} A_{\mathrm{te}}}{4\pi R^2} \tag{7.13}$$

where S_{echo} is the power density at the receiver antenna, A_{te} is the effective area of the target, resulting in the well-known 'radar equation' (Ehling 1967):

$$S_{\mathrm{echo}} = \frac{P_{\mathrm{T}} G_{\mathrm{T}} A_{\mathrm{te}}}{(4\pi R^2)^2} \tag{7.14}$$

Multiplying this result by the effective area A_{re} of the receiver antenna yields the received power:

$$P_{\mathrm{rec}} = S_{\mathrm{echo}} A_{\mathrm{re}} \tag{7.15}$$

These signal power considerations apply to all radar types with passive reflection.

Transponder on target

As the power of the echo is inversely proportional to the fourth power of the range, there will eventually be a limitation in the operational range, outside of which such a system cannot be used: for the long range by the signal-to-noise ratio and for the short range by saturation of the amplifiers. A passive measure taken to improve the power of the return signal is the placing of a corner-cube reflector on the target. A method used to increase significantly the power density of the return signal consists of placing a transponder on the target; this amplifies the received signal and re-transmits it toward the transmitter using a directional antenna and a different frequency. This has the additional advantages that a de-coupling of transmitted and received signals is achieved, and that no switching between transmit and receive mode is necessary. The time delay of the signal on its way through the transponder must of course be known and must be constant over time.

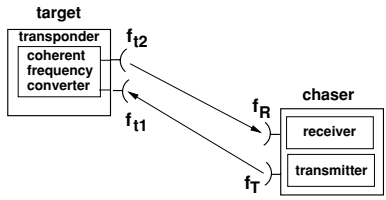

Figure 7.8. Frequency conversion and re-transmission by transponder.

For range measurement in Eq. (7.3), the transponder delay time t_t has to be added to the time-of-flight T, i.e. $T_\mathrm{tot} = T + t_\mathrm{t}$. In the same way, the phase delay of the transponder, $\phi_\mathrm{t} = 2\pi f \cdot t_\mathrm{t}$, has to be added to the phase shift Φ in Eq. (7.5), i.e. $\Phi_\mathrm{tot} = \Phi + \phi_\mathrm{t}$.

In a Doppler radar the frequency transmitted by the transponder must have a fixed relation to the received frequency, e.g. by a factor n, in order to take into account the Doppler shift correctly on both legs:

$$\frac{f_{\mathrm{t}1}}{f_{\mathrm{t}2}} = n$$

The frequency at the receiver is then

$$f_\mathrm{R} = n f_\mathrm{T} \left(1 - \frac{\dot{R}}{C}\right)^2 \tag{7.16}$$

which is, as seen before to a good approximation,

$$f_\mathrm{R} = n f_\mathrm{T} \left(1 - 2\frac{\dot{R}}{c}\right) \tag{7.17}$$

The range-rate is then

$$\dot{R} = \frac{1}{2}\lambda_{\mathrm{T}} \left(\frac{1}{n} f_{\mathrm{R}} - f_{\mathrm{T}} \right) \tag{7.18}$$

7.2.2 Principles of direction and relative attitude measurement

Many of the measurement principles for direction and relative attitude measurements used in RF-sensors and described hereafter can be found in the literature on aircraft navigation systems, such as Kendal (1987) and Jenkins (1991).

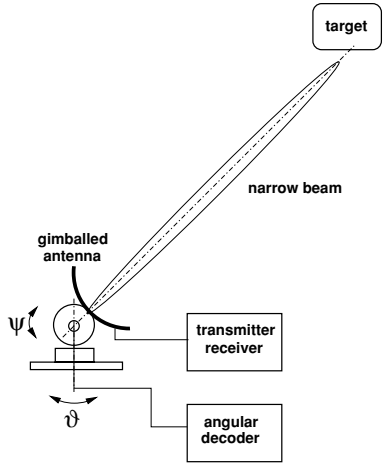

Figure 7.9. LOS measurement by pointing of narrow beam toward target.

Measurement of line-of-sight direction

Pointing of narrow beam antenna The most straightforward way of LOS direction measurement is the pointing of a narrow beam antenna toward the target. The transmitting/receiving antenna is mounted on a two-axis gimbal system, and the gimbal angles are measured for the maximum amplitude of the return signal. This maximum is usually found by scanning around the expected direction of the target. Since the time-of-flight of the reflected signal is very much smaller than a scan cycle, the gimbal angles at transmission and reception are identical within the accuracy of the angular read-out device. Electro-magnetic resolvers, optical encoders or similar devices can be used as read-out devices. This principle of LOS angle measurement by means of a scanning antenna is known from radar types of sensors, where range is measured according to Eqs. (7.3) or (7.5) and possibly range-rate according to Eqs. (7.10) or (7.11).

Instead of a gimbal system, which moves the entire antenna dish, scanning can be achieved also e.g. by angular motion of the antenna feeder or by electro-magnetic deflection of the antenna beam (electronic scanning). Where the achievable scan angle is sufficient, these methods will be preferred, because of reduced size and mass of the the assembly.

LOS measurement via time delay or phase shift In this type of sensor the time delay or phase shift is measured between a signal received by two antennas mounted on a baseline at a distance d. If the wave front is parallel to that baseline, both antennas receive the signal with the same phase. If the wave front is in line with the baseline, the phase shift and time delay will be according to their distance d. The signal arriving at antenna 1 (see figure 7.10) is

$$a_1(t) = a \cdot \sin(\omega t)$$

and at antenna 2 with the phase shift τ:

$$a_2(t) = a \cdot \sin(\omega t + \tau) \tag{7.19}$$

or with the time delay Δt:

$$a_2(t) = a \cdot \sin[\omega(t + \Delta t)] \tag{7.20}$$

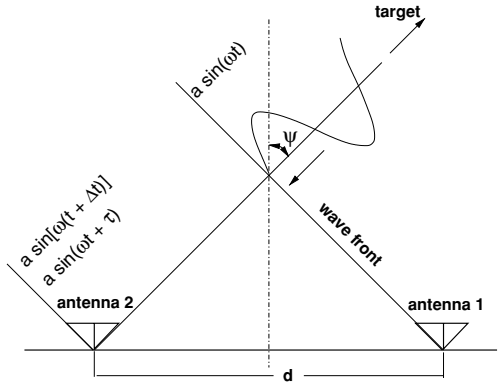

Figure 7.10. Functional principle of LOS measurement via two antennas.

The angle ϕ between the line toward the signal source and the line perpendicular to the baseline can be derived from the phase shift,

$$\tau = \frac{2\pi d}{\lambda} \sin \psi \tag{7.21}$$

or the time delay,

$$\Delta t = \frac{d}{c} \cos \psi \tag{7.22}$$

The resolution of the LOS angle ϕ will improve with increasing length of the baseline d and with increasing resolution of the measurements of the time delay Δt and the phase shift τ. In the latter case the resolution will actually improve with a decrease of the wavelength λ.

LOS measurement via amplitude and antenna rotation angle The antenna characteristic of a dipole has two pronounced directions with zero reception (see figure 7.11), which can be used for direction finding. This will provide ambiguous results when bearing angles up to 360 deg have to be measured. However, in many applications it is known in which part of the circle the target has to be searched, so that this ambiguity does not play a role. The induced voltage over the rotation angle in a dipole antenna is

$$V(\phi) = V_{\max} \sin \psi \tag{7.23}$$

If the direction angle needs to be measured in the full range of 360 deg, the dipole characteristic can be superimposed on to a circular antenna pattern with the same sensitivity. The resulting antenna pattern is that of a cardioid (figure 7.12), which has one zero point. The combined induced voltage over the rotation angle in this arrangement is

$$V(\phi) = V_{\max}(1 + \sin \psi) \tag{7.24}$$

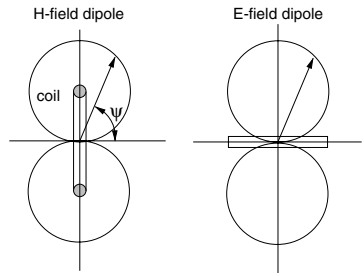

Figure 7.11. Antenna characteristic of dipoles.

Measurement of relative attitude

Relative attitude measurement through tone modulation and rotating pattern on target On the transmitter side, an antenna (1) with a defined single maximum or minimum over the circumference, e.g. a cardioid characteristic, is rotated with a frequency

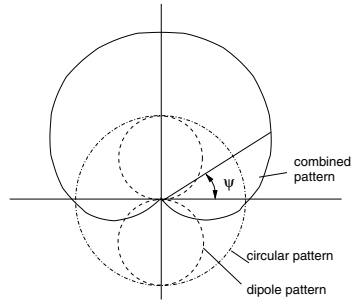

Figure 7.12. Cardioid antenna pattern.

of n hertz. The antenna transmits a carrier signal without modulation. The signal received at a receiver antenna will be amplitude modulated with the rotation frequency n of the transmitter antenna. A second antenna (2) on the transmitter side with a circular characteristic transmits a tone modulated signal with the frequency n. Rotation of antenna (1) and amplitude modulation of antenna (2) are adjusted in such a way that, in a particular direction, a receiver will receive both signals without phase difference. Other angular positions w.r.t. this particular direction can then directly be determined from the phase difference between the two received signals (see figure 7.13). This principle is used, e.g., in the VOR (VHF omni-range) in aircraft navigation.

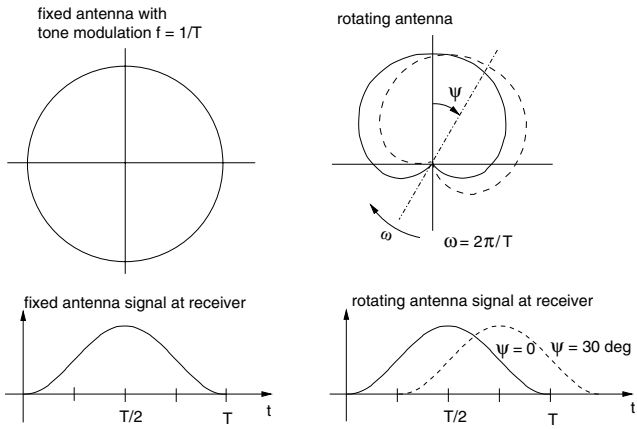

Figure 7.13. Relative attitude measurement through fixed and rotating antenna pattern on target.

Relative attitude measurement through antenna beams with different tone modulation Two antennas are radiating their patterns or beams under different angles and with the same carrier, but with different modulation frequencies f_1 and f_2. A receiver

with one channel for each carrier, located exactly in the middle between the centre lines of the two patterns, will receive both transmissions with the same amplitude. At the sides of the middle line between the two patterns, the amplitude of one of the modulation frequencies will become lower and the other one will become stronger. The angular position can thus be determined from the ratio of the amplitudes of the received modulation frequencies f_1 and f_2. Two cases are shown in figure 7.14: the first is the superposition of two dipole antennas, and the second shows the arrangement of two narrow beam antennas. The first can be used unambiguously in one quadrant. The second can be used only within a small angular range, but with higher accuracy. This type of angular position measurement is used, e.g., in the instrument landing system (ILS) for aircraft.

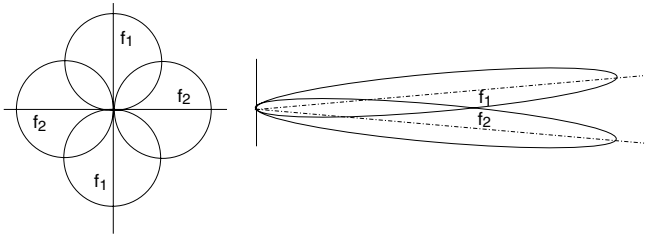

Figure 7.14. Relative attitude measurement through antenna beams on target with different modulation.

7.2.3 Measurement environment, disturbances

The performance of a sensor is usually described in terms of resolution, bias and noise. There are, however, other disturbances and effects which affect the performance but are neither caused inside the sensor itself nor are inherent to the measurement chain. They may be caused by effects of the environment of the measurement process and may be present in certain types of environment though not in others. For such external effects, the term 'measurement environment' is used here.

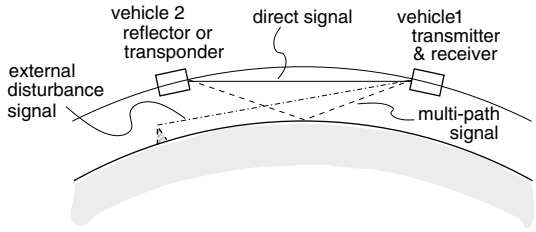

Figure 7.15. Multi-path signal reflected by Earth and external disturbances.

The major part of the disturbances due to the measurement environment are caused by one of the following effects:

- Multiple reflections of the transmitted signal by structural elements on transmitter spacecraft, resulting in the transmission of multiple or blurred target signals.
- Multi-path effects, i.e. signals arriving at the receiver via multiple paths due to reflection or refraction of the electro-magnetic waves by external bodies, e.g. reflections of transmitter or transponder signals by Earth and/or ionospheric layers; refraction and delays of signal by ionospheric and atmospheric layers; multi-path reflections of transmitter or transponder signal by different surfaces on the target spacecraft; multi-path reflections of the received signal by different surfaces on the receiver spacecraft.
- Shadowing by obstacles in the transmission direction due to structural elements on either transmitter or receiver spacecraft.
- Interference by signals transmitted from other sources using the same frequencies.

Some of the effects are more pronounced when the distance to the target is large and the returning signal is very weak. The last type of disturbance, i.e. signals from other sources, could play a role in such a case. Also, multi-path disturbances by the Earth will be more pronounced at long distances. On the contrary, multi-path and shadowing problems by the target structure are more pronounced in the close vicinity of the target.

Disturbances caused by reflections of the signal by the structure around the transmitting antenna can be avoided by proper design of the antenna and of the vehicle. Disturbances by external sources using the same frequency can of course be avoided by use of frequencies dedicated to a particular mission or application. An application of the above-mentioned passive corner-cube reflector would define a reference point on the target, which can be distinguished from all other spurious reflections by the power of the signal. As discussed above, a transponder on the target would improve the discrimination of the direct signal from spurious reflections and refractions by the target vehicle structure, but would require additional active equipment and power on the target side.

7.2.4 General assessment of RF-sensor application

Radio-frequency sensing devices have been used in all rendezvous missions so far for the measurement of range and direction or position. Examples are the rendezvous radars, used in the American rendezvous missions from Gemini up to the Space Shuttle, and the radio-frequency system ‘Kurs’ used by the Russian (Soviet) space programme. The Russian ‘Kurs’ system, which will be addressed as an example for an RF-sensor system in more detail in the following section, combines a number of principles for range and angular measurement that have been described above. Satellite navigation is a particular form of RF-sensing, applying time-of-flight and phase measurement principles to signals

transmitted by a set of navigation satellites. Because of its particular conditions, which are very different from the RF-sensor principles discussed so far, and because of its importance for future rendezvous missions, it will be treated separately in section 7.3.

The limitations of the operational ranges of sensors for rendezvous missions have been discussed in section 5.3.2 in the context of the approach strategy drivers, and an overview of range vs. accuracy has been given in figure 5.10. In addition to the emitted power, the maximum range of RF-sensors depends on the aperture of the antennas. The effective aperture or effective area of an antenna is

$$A_{\mathrm{e}} = \frac{D\lambda}{4\pi}$$

where D is the directivity of the antenna. This provides the relationship between the frequency and the size of an antenna. Assuming a receiving antenna at the range R and using the above relation for the effective area of the receiving antenna, Eq. (7.12) can be expanded to become (Kayton and Fried 1997)

$$\frac{\text{received power}}{\text{transmitted power}} = \frac{A_{\mathrm{re}} A_{\mathrm{te}}}{R^2 \lambda^2} \tag{7.25}$$

where A_{re} is the effective area of the receiving antenna A_{te} is the effective area of the transmitting antenna and R is the range between antennas and λ is the wavelength.

This shows that with fixed antenna areas the received power increases with the square of the frequency. The consequence is that very high frequencies (gigahertz range) have to be used to minimise mass and power. Equations (7.12) and (7.25) also show that eventually there will be, for RF-measurement systems (with the exception of satellite navigation systems, see the next section), a limitation of the maximum operational ranges due to the limitation of available power.

The typical operational range of RF-sensors is the long and medium range of the approach, whereas the very short range would require very high effort to mitigate disturbances and provide the required performance. As for medium and long ranges, the transmitted signal must still be sufficiently strong (with the above addressed consequences on power and antenna size), the RF-sensor techniques described above tend to have a comparatively high power consumption and mass.

It has been demonstrated above that for all navigation parameters required during a rendezvous mission, i.e. range, LOS, range-rate, and relative attitude, an RF-measurement principle is available. In the early development of automatic onboard rendezvous systems, when no alternatives were available, all sensor design was based on RF-techniques (see section 7.2.5). However, as a result of the development of new techniques and technologies, in many cases either measurement performance or mass and power consumption are nowadays more advantageous with other sensor principles. This is true in the long and medium range, mainly for satellite navigation, and in the short range for optical sensors, which are described in the subsequent sections 7.3 and 7.4.

7.2.5 Example: the Russian Kurs system

The Kurs system has been used for rendezvous navigation of the Russian Soyuz and Progress vehicles for a long time, first for approaches to the Russian space station Mir, and then to the ISS. Kurs is an example of the combination of various RF-sensor principles into one navigation system. The Kurs system is designed to provide all required navigation measurements during the entire approach from a few hundreds of kilometres down to contact. A short overview of its functions will be given here, since this system is, so far, the only sensor system used in automatic rendezvous and docking missions, and it is going to be used by Russia for many years to come. It can, therefore, be seen as a standard against which newer technologies can be evaluated. The following description is based on printed sources (Suslennikov 1993; *Data Book: Service Module 2000; Data Book: Soyus/Progress 2000*) and on updates (Semyachkin 2001) provided in a letter to the author, reflecting the state of design in 2001.

The Kurs system includes the following functions:

- Identification of the hemisphere of the target direction by two omni-directional antennas to permit the chaser docking port side to be directed into the hemisphere of the target position.
- Identification of the target direction within this hemisphere by a large angle scanning antenna.
- Range measurement based on the shift of a phase modulated signal during the travelling time from chaser to the target and back to the chaser, or vice versa.
- Range-rate measurement based on the Doppler shift of the carrier frequency.
- More precise LOS tracking in azimuth and elevation of the target by a scanning antenna in a ± 15 deg angular range. (In the original design of Kurs, an additional measurement of the LOS rate about the chaser y- and z-axes was made by gyros mounted on the gimballed antenna (Suslennikov 1993).
- Measurement in the proximity phase ($\leq$200 m) of relative attitude in pitch and yaw through evaluation of the scan beam pattern transmitted by the scanning antenna on the target and received by the fixed antenna on the chaser, and of LOS angles.
- In the original design, measurement in the proximity phase of the relative roll angle by tracking of antennas, at the circumference of the target, which are transmitting with different frequencies (Suslennikov 1993). This design has been changed: the roll angle is now calculated in the control system of the onboard computer complex from the other information available (Semyachkin 2001).

The Kurs system operates in the S-band using wavelengths of the order of 10 cm, with both continuous wave mode and bi-phase (0–180 deg) modulated signals. It comprises

active functions on both chaser and target vehicles, as shown in figures 7.17 and 7.18. The navigation parameters and their measurement range are as follows:

- coarse LOS angles: ψ_0, ϑ_0: $\pm$180 deg, during acquisition;
- range R: unambiguous in the range 0–100 km, beyond 100 km repeating, i.e. at 180 km the measurement is 80 km;
- range-rate $\dot{R}$: 400 m/s, all ranges after acquisition;
- LOS angles ψ_Γ, ϑ_Γ: $\pm$15 deg, all ranges after acquisition;
- LOS angles γ_ψ, γ_ϑ: $\pm$15 deg, in the proximity phase $\leq$200 m;
- relative attitude ψ_Π, ϑ_Π: $\pm$ 30 deg, in the proximity phase $\leq$ 200 m.

In the original design, the relative roll angle was also measured in the proximity phase ($\leq$200 m), and the LOS angular rates Ω_y, Ω_z were measured in all ranges after acquisition by gyros on the antenna platform (Suslennikov 1993). In the present design, the gyros have been omitted, and angular rate is no longer measured directly (Semyachkin 2001). The antennas used for these measurements are shown in figure 7.16. A short description of their functions is given in the following.

Antennas on the chaser vehicle

A1, A2 These are omni-directional antennas which transmit the frequency f_1 generated by the chaser and receive the frequency f_2 generated by the target. The antennas are used for acquisition to determine the hemisphere of the target position. After acquisition they transmit and receive the signal used in the range and range-rate determination process.

A3 This is a wide-angle mechanical scanning antenna with a special beam pattern and a scanning cone angle of 200 deg. It receives the frequency f_2 transmitted by the target and is used for coarse direction finding of the target position, i.e. providing the information for determination of the coarse LOS angles ψ_0, ϑ_0 w.r.t. the x-axis of the vehicle. Together with antennas A1 and A2, it is used in the acquisition process to point the chaser x-axis toward the target.

A4 This is a fixed antenna with an electronic scanning cone angle of 30 deg (Semyachkin 2001). (In the original design, it was mounted on a gimbal system with $\pm$15 deg freedom (Suslennikov 1993).) It transmits the interrogation frequency f_1 and receives, after acquisition, the frequency f_2 transmitted by antennas B1 and B2 on the target and, in addition, in the proximity phase ($\leq$200 m) the frequencies f_3 and f_4 transmitted by antennas B3, B4 and B5 on the target. The frequencies f_1 and f_2 are used for range (R), range-rate ($\dot{R}$) and LOS angles (ψ_Γ, ϑ_Γ) tracking. The frequencies f_3 and f_4

are used for roll determination by LOS angles γ_ψ and γ_ϑ (Semyachkin 2001).(In the original design these antennas were used for direct roll measurements, and, as already mentioned, two gyros mounted on the gimballed platform of the antenna delivered the LOS angular rates Ω_y and Ω_z (Suslennikov 1993).)

To establish a precise measurement axis, electronic beam switching is performed, which in turn establishes antenna sub-beams somewhat similar to the ones shown in figure 7.14, except that the different sub-beams are not separated by frequency but by time. If the antenna measurement axis is directly pointing toward the target, all sub-beams will receive the same signal amplitude.

A5 This is a fixed antenna with a narrow beam characteristic, receiving the frequency f_4 transmitted by antenna B5 on the target vehicle. A5 is used in the proximity phase ($\leq$200 m) for measurement of LOS angles ψ_Γ and ϑ_Γ. From the amplitude information of the received signal, the relative attitude angles (ψ_Π, ϑ_Π) are derived.

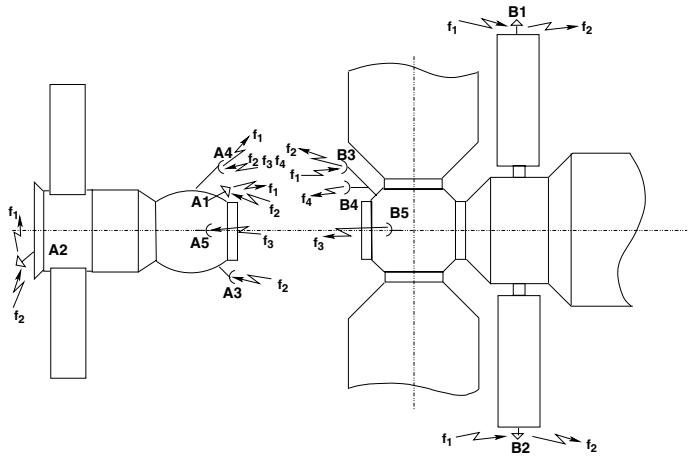

Figure 7.16. Location of Kurs antennas on Progress and Mir.

Antennas on the target vehicle

B1, B2 B1 and B2 are omni-directional antennas which transmit the frequency f_2 generated by the target and receive the frequency f_1 generated by the chaser. In function and performance they correspond to the antennas A1 and A2 on the chaser vehicle.

B3 B3 is a fixed antenna with a $\pm$30 deg antenna characteristic. In the proximity phase ($\leq$200 m) the transponder of the target switches to antenna B3 for transmitting frequency f_2. During this phase this antenna also receives frequency f_1 transmitted by the chaser and is used for determination of range and range-rate on the target side.

B4 The signal of antenna B4 is mainly used in the last 30 m for improved range measurement between chaser and target. B4 is a fixed antenna with a ± 20 deg beam characteristic transmitting a separate frequency f_4.

B5 B5 is a motor driven conical scanning antenna, rotating with 700 rpm (11.66 Hz) and describing a cone with a half-angle of 30 deg. The antenna transmits a frequency f_3 with an amplitude modulation at 11.66 Hz. The principle of measurement is somewhat similar to the one described in figure 7.13, except that the rotating pattern is not a cardioid: the 11.66 Hz amplitude modulated signal is compared with the amplitude variation of the carrier received by antenna A5 on the chaser. If the carrier signal is constant, the chaser is aligned with the target. If the carrier has an amplitude, the amplitude and phase difference with the modulation can be evaluated to determine the relative attitude.

Hardware of the Kurs system

The equipment on the chaser vehicle side (Soyuz or Progress), called the 'interrogator' since it contains most of the active measurement functions, is shown schematically in figure 7.17. The antennas are switches by the 'commutator' as selected by the 'logic unit' (not shown). The engagement of antennas also depends on mission progress and is controlled, as for all other Kurs equipment, by inputs from the onboard computer. The scan control functions are not shown in the figure.

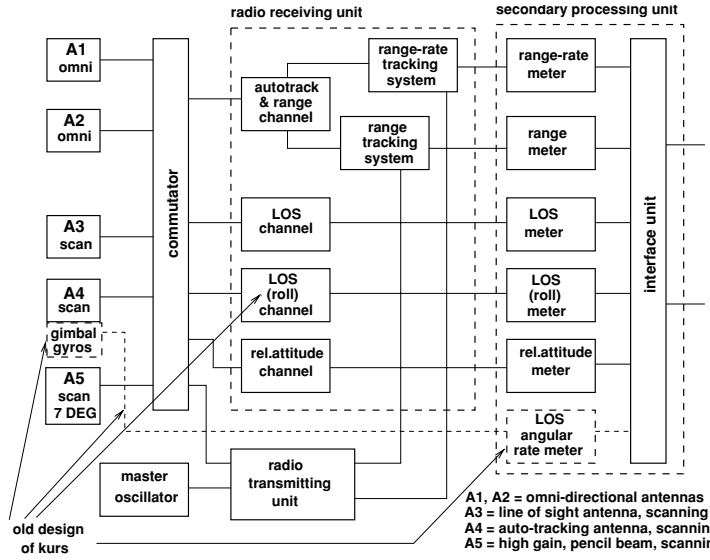

Figure 7.17. Functional block diagram of Kurs 'interrogator' equipment.

The information required for determination of range, range-rate, LOS angles and relative attitude are extracted in the 'radio receiving unit' from the signals received by the various antennas via the carrier frequencies f_2, f_3 and f_4. From these extracted signals the output navigation parameters range, range-rate, LOS angles and relative attitude are calculated in the 'processing unit' and are sent to the onboard computer of the vehicle for use in the GNC system and in the crew displays.

The 'radio transmitting unit' produces the carrier frequency f_1 and the bi-phase modulation for the interrogation signal to be transmitted to the target. The transmitted signals are also provided as a reference to the range and range-rate tracking loops in the 'radio receiving unit'.

The equipment on the target (Mir or ISS) is shown schematically figure 7.18. In addition to the transponder function proper, i.e. re-transmission of the interrogation signal on frequency f_2 back to the chaser, it has to provide the frequencies and modulations f_4 and f_3 to be transmitted by antennas B4 and B5. For antenna B5 the motorised drive for the conical scan also has to be provided. Further, the Kurs system on the target includes the range and range-rate measurement loops as the chaser system. The output is provided, via the 'processing unit', to the displays for the target crew.

The following values have been given for the mass and power consumption of the Kurs equipment on chaser and target (Suslennikov 1993; *Data Book: Soyus/Progress* 2000; *Data Book: Service Module* 2000; Semyachkin 2001):

total mass of redundant equipment on chaser side $\approx$ 85 kg

total power consumption on chaser side $\approx$ 270 W

total mass of redundant equipment on target side $\approx$ 80 kg

total power consumption on target side $\approx$ 250 W

Operation of antennas during rendezvous

At a range of about 200 km, the antennas B1 and B2 on the target will start to transmit the unmodulated frequency f_2, alternating between the two antennas at a rate of 1 kHz. The two antennas A1 and A2 on the front (docking port) and back-sides of the chaser vehicle are also switched at 1 kHz, receiving alternating the f_2 beacon signal of the target. The difference in strength of the signal received in A1 and A2 determines in which hemisphere the target is located. If necessary, an attitude manoeuvre is initiated to ensure that the chaser docking port is within the hemisphere of the target location. As the target is now located in the reception range of the scanning antenna A3 (200 deg cone), its pointing direction can be determined more precisely and the chaser can be moved to place the target into the reception range of the main tracking antenna A4.

The chaser Kurs system starts now to interrogate the target on carrier frequency f_1 with a bi-phase modulated signal at a modulation frequency of 800 Hz. The target

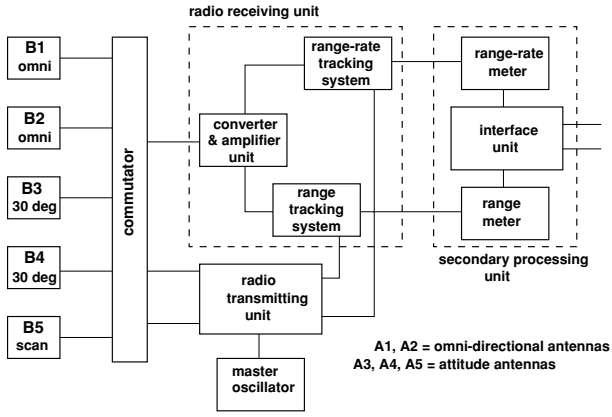

Figure 7.18. Functional block diagram of Kurs 'transponder' equipment.

system responds via antennas B1 and/or B2 by sending back the modulation signal on a different carrier f_2. The signal, which has been two times phase shifted over the range R, can be evaluated concerning the range, making use of the modulation signal (see Eq. (7.5)) and concerning the range-rate, making use of the carrier frequency (see Eq. (7.18)). The same process is also performed on the target, so that range and range-rate information is available on both vehicles.

During the fly-around or closing phase between 400 m and 200 m, the chaser will be aligned to the docking axis of the target. When all of the frequencies transmitted by the target alignment antennas, i.e. f_2 by antenna B3, f_4 by antenna B4 and f_3 by antenna B5, are received by their counterparts A4 and A5 on the chaser, station keeping will be performed at a range of $\approx$200 m.

During the subsequent final approach (from 200 m to 20 m) chaser antenna A4 will track target antenna B3 and chaser antenna A5 will track target antenna B5. B3 transmits in this range the Kurs transponder signals used to obtain range, range-rate and LOS angle information. B5 provides the reference for relative attitude detection in pitch and yaw. During the last 30 m of approach antenna A4 on the chaser receives in addition the signal from antenna B4 on the target, which is used together with the signal from B3 to determine the range by angle γ_ϑ.

7.3 Absolute and relative satellite navigation

7.3.1 Description of the navigation satellite system setup

As in the previous section, only the basic measurement principles required for a general understanding of absolute and relative navigation via navigation satellites will be described here. For more detailed information, readers are referred to the literature on

the subject, such as Ackroyd & Lorimer (1990), Scott *et al*. (1995), Kaplan (1996), Dye & Baylin (1997), Kayton & Fried (1997).

Satellite navigation systems are radio navigation systems based on signals transmitted by a set of satellites orbiting the Earth. They provide navigation information to the user through measurement of range and range-rate between a user receiver and a subset of these navigation satellites. Satellite navigation systems are generally composed of three segments:

(1) a space segment, including the navigation satellites as the active partners of the user in obtaining the navigation information;

(2) a ground segment, controlling the orbital parameters, the accuracy of onboard time and the accuracy of the navigation messages broadcast by the navigation satellites;

(3) a user segment, consisting of the navigation receivers, the locations of which are to be determined. More than one receiver may be used in cooperation to improve relative navigation accuracy between those receivers (see DGPS and RGPS).

At the time of writing, two major navigation satellite systems are deployed:

- the Global Positioning System (GPS), developed and operated by the United States of America;
- the Global Orbiting Navigation Satellite System (GLONASS), developed and operated by Russia.

Because of the importance satellite navigation has gained in all areas of terrestrial navigation for land vehicles, ships and aircraft, these systems will be further developed and enhanced. At the time of writing, within the frame of the international 'Global Positioning and Navigation Satellite System' (GNSS-1) programme, overlay systems by geostationary satellites are under development, i.e. the American 'Wide Area Augmentation System (WAAS), the 'European Geostationary Overlay Service' (EGNOS) and the Japanese 'MTSAT Satellite Based Augmentation System' (MSAS). These three systems will provide a seamless geostationary overlay service to the GPS and GLONASS systems and were planned, at the time of writing, to be available in the middle of the first decade of the twenty-first century. Further steps toward a GNSS-2 programme with new satellite configurations are being planned.

Setup of the space segment

GPS The American GPS space segment nominally consists of 24 operational satellites (the satellites are also called 'Navstar') in near circular orbits with an altitude of approximately 20 180 km (ARINC 1999). The satellites have an orbital period of 12 h, i.e. they make two revolutions per day, thus passing (due to the rotation of the Earth) over the same location once each day (i.e. every 23 h 56 min). There are four satellites

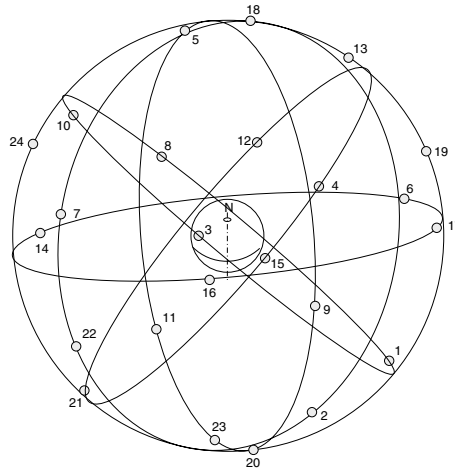

Figure 7.19. GPS satellites in orbit.

on each of the six orbital planes. All orbital planes have an inclination $i = 55$ deg, with their nodes separated by a RAAN angle of 60 deg. Due to disturbances, in particular by the oblateness of the Earth (J_2-effect), the nodes of these orbits will drift with time. The spacing of the four satellites in each of the orbital planes is not uniform. It is arranged such that a minimum of five satellites will be available to a user at any position on the Earth and at any time.

The Navstar satellites transmit on two L-band frequencies, i.e. on 1575.42 MHz and 1227.60 MHz, broadcasting a navigation message which includes pseudo-random number (PRN) codes and other information. The latter information includes the satellite identification and information on the orbital characteristics of each satellite and on its onboard clock.

GLONASS The Russian GLONASS space segment also nominally consists of 24 operational satellites, which are, however, arranged in three orbital planes separated by 120 deg. There are eight satellites per plane equidistantly arranged, i.e. with a separation of 30 deg. The orbital altitude is 19 130 km and the inclination of each plane is 64.8 deg. The ground track of a satellite repeats itself after 17 orbits, i.e. approximately after 8 days.

The GLONASS satellites transmit carrier frequencies, centred around two L-band frequencies, 1602 and 1246 MHz, with each satellite having its own frequency. GLONASS satellites also broadcast PRN codes, navigation messages etc., but in a slightly different way as compared with GPS.

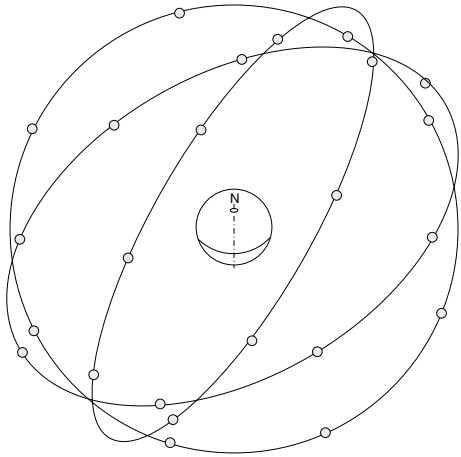

Figure 7.20. GLONASS satellites in orbit.

Galileo The next step in the development of a 'Global Positioning and Navigation Satellite System' (GNSS-2) will be the development of a global satellite navigation system by Europe, called 'Galileo'. This new constellation is planned to comprise 27 operational satellites and three spares in circular orbits of 24 000 km altitude, arranged in three orbital planes with 55–60 deg inclination. Full inter-operability with GPS and GLONASS is envisaged. An initial service is foreseen by 2008 with full operational capability by 2010. Positioning accuracies of down to 4 m are envisaged with the Galileo service.

Setup of the ground segment

To control a navigation satellite system, four ground antenna stations are needed at suitable locations on the Earth. When the positions of the stations are precisely known and the time at the stations is precisely synchronised, the navigation equations discussed below for the user segment can be used in an inverse way to determine exactly the location or the orbit ephemerides of the navigation satellites. Because of the orbital disturbances caused by the Earth, the Sun and the Moon, the orbital parameters of all satellites need to be measured, and forecasts of their development with time need to be calculated continuously. At regular intervals the navigation messages broadcast by each navigation satellite need to be updated accordingly. Furthermore, the clocks on the navigation satellites need to be monitored and corrected at regular intervals. The complete ground segment setup will therefore consist of:

- at least four monitoring stations with precisely located reception antennas and with high performance receivers;

- a master control station performing the calculations, generating the uplink data, controlling the time synchronisation and monitoring the links with monitoring and transmitting stations;
- a number of transmission stations to uplink commands and data to the navigation satellites.

7.3.2 Navigation processing at the user segment

Range measurement

To measure the range between navigation satellites and user by the 'time-of-flight' method (see section 7.2.1), the time at transmission of the signal by the navigation satellites must be known. Further, in order to re-constitute the position of the user in a particular coordinate system, the position of the navigation satellite in this system must be known. This requires that the navigation satellites broadcast continuously their position or their orbit ephemerides and time marks as reference, and that the clocks of the user receiver and the navigation satellites are synchronised. From time and orbit ephemerides, the actual position of the satellites at the time reference can then be calculated, and the range can be obtained from the travel time t_t and the speed of light c.

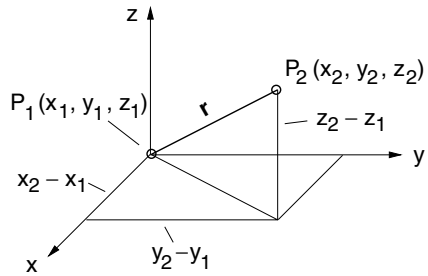

Figure 7.21. Relations for pseudo-range calculation.

As the user receiver's clock will not be fully synchronised with that of the transmitter, the measured range between user and navigation satellite is

$$p = c \cdot (t_1 + t_\mathrm{bias} - t_2) = r_{2,1} + c \cdot t_\mathrm{bias} \tag{7.26}$$

where c is the velocity of light and $t_\mathrm{t} = t_2 - t_1$ is the travel time between point P_2 (navigation satellite) and P_1 (user), and the term t_bias is the unknown bias of the user clock w.r.t. the navigation satellite clock. Because of this additional unknown, the range r measured by this method is not the real geometric distance $r_{2,1}$ between the user and the navigation satellite and is, therefore, called the 'pseudo-range'. If the position of

the transmitter is known, the coordinates of position of the user can be obtained from the following relation (see figure 7.21):

$$r_{2,1} = \sqrt{(x_2 - x_1)^2 + (y_2 - y_1)^2 + (z_2 - z_1)^2} \tag{7.27}$$

where x_1, y_1, z_1 and x_2, y_2, z_2 are the position coordinates of P_1 and P_2 in an inertial Earth-centred Cartesian coordinate system. Whereas a three-dimensional position can generally be determined by the range measurement to three known targets, the bias can be eliminated by the pseudo-range measurement w.r.t. a fourth navigation satellite, yielding four equations for the four unknowns:

$$\begin{aligned}
(x_{\mathrm{n}1} - x_{\mathrm{u}})^2 + (y_{\mathrm{n}1} - y_{\mathrm{u}})^2 + (z_{\mathrm{n}1} - z_{\mathrm{u}})^2 &= c^2 \cdot (t_{\mathrm{u}1} + t_{\mathrm{bias}} - t_{\mathrm{n}1})^2 \\
(x_{\mathrm{n}2} - x_{\mathrm{u}})^2 + (y_{\mathrm{n}2} - y_{\mathrm{u}})^2 + (z_{\mathrm{n}2} - z_{\mathrm{u}})^2 &= c^2 \cdot (t_{\mathrm{u}2} + t_{\mathrm{bias}} - t_{\mathrm{n}2})^2 \\
(x_{\mathrm{n}3} - x_{\mathrm{u}})^2 + (y_{\mathrm{n}3} - y_{\mathrm{u}})^2 + (z_{\mathrm{n}3} - z_{\mathrm{u}})^2 &= c^2 \cdot (t_{\mathrm{u}3} + t_{\mathrm{bias}} - t_{\mathrm{n}3})^2 \\
(x_{\mathrm{n}4} - x_{\mathrm{u}})^2 + (y_{\mathrm{n}4} - y_{\mathrm{u}})^2 + (z_{\mathrm{n}4} - z_{\mathrm{u}})^2 &= c^2 \cdot (t_{\mathrm{u}4} + t_{\mathrm{bias}} - t_{\mathrm{n}4})^2
\end{aligned} \tag{7.28}$$

In these equations the subscript ‘u’ denotes the user and the subscript ‘n’ denotes the navigation satellites. The positions $x_{\mathrm{n}}, y_{\mathrm{n}}, z_{\mathrm{n}}$ of satellites 1–4 can be calculated from the orbital data of the navigation message, which is broadcast by each of the satellites. The times $t_{\mathrm{u}i}$ are measured by the user receiver. The receiver bias is the same in all measurements. Eqs. (7.28) are non-linear and thus need to be linearised, e.g. by expansion into a Taylor series about an estimated position, and iteratively solved to arrive at sufficiently accurate solutions (an example for the derivation of such a solution is given in Kaplan (1996).

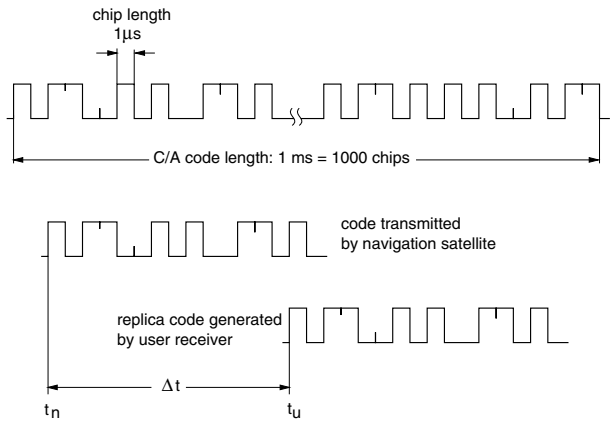

Figure 7.22. Pseudo-random number (PRN) sequence for coarse acquisition (C/A) code.

The next important question to be explained is, how can the user receiver continuously measure the time differences $t_{\mathrm{u}i} - t_{\mathrm{n}i}$? The navigation satellites continuously transmit

digital binary codes. These codes are called pseudo-random number (PRN) codes, because of their apparently random sequence of zeros and ones. They have, however, a certain length, after which they are repeated, and can therefore be compared to a melody which is continuously repeated. These PRN codes (or digital melodies) are generated and transmitted by the navigation satellite, with each navigation satellite broadcasting its own tune (GPS) or the same melody but on a slightly different carrier frequency (GLONASS). The user receiver can identify a navigation satellite either by its navigation message 'melody' (GPS) or by the carrier frequency (GLONASS). The receiver has a replica of the (civilian) PRN codes available and can correlate the emitted code once it has identified a navigation satellite.

In its navigation message, the navigation satellite also transmits information concerning the time of the transmission w.r.t. the reference time of the navigation satellite and concerning the start on the PRN code sequence. This is necessary because of the range ambiguity over a long distance of a signal, which repeats itself after 1 ms. In an overall travelling distance of about 20 000 km, it will repeat itself about 66 times. With the time of transmission and the code information available, the user receiver can compare the received PRN code with its replica code and can determine the shift in time (see figure 7.22) by auto-correlation techniques. With the found Δt, the pseudo-range can be calculated according to Eq. (7.26). With Δt measurements from four navigation satellites, the position can be determined by solving Eqs. (7.28).

Both GPS and GLONASS transmit two types of PRN codes, a 'coarse acquisition' (C/A) code and a 'precision' (P) code. To civil users only the C/A code is accessible. The C/A code is in both cases 1 ms long and constantly repeated. The chip length (length of a '0' or '1') of the C/A code is approximately 1 μs. The P code is extremely long, e. g. for the GPS it is 1 week, and is repeated after that period. Its chip length is 0.1 μs. Because of the exclusively military use of the P code, it is not necessary to discuss it here in more detail.

According to Eq. (7.4) the carrier phase can also be used for range measurement. Because of the large distance to the navigation satellites and the high frequency used, there will be a very large number of cycles over the range where the same phase angle occurs that is measured at the receiver. This will make it more difficult to establish the total range. The carrier phase measurement can be used, however, (via the Doppler effect) to improve the pseudo-range result (see the sub-section entitled 'Velocity and change-of-range measurement' below).

Measurement errors

In order to show the principle of the concept, it has been assumed so far that only errors in the clock time of the receiver exist. In reality there are a number of other errors which affect the accuracy of the pseudo-range measurement. Generally, the pseudo-range to a navigation satellite will include the following error components:

$$p = c\,\Delta t + E_{\mathrm{t-rec}} + E_{\mathrm{t-ion}} + E_{\mathrm{t-sat}} + E_{\mathrm{ephem}} + E_{\mathrm{n-rec}} + E_{\mathrm{t-trop}} \quad (7.29)$$

where

$E_{\mathrm{t-rec}}$ = error due to receiver clock bias ($\approx$ 1 m)
$E_{\mathrm{t-ion}}$ = error due to ionospheric delay (depending on user orbit $\approx$ 10 m)
$E_{\mathrm{t-sat}}$ = error due to remaining satellite clock error ($\approx$ 1 m)
E_{ephem} = error due to navigation satellite ephemeris error ($\approx$ 1 m)
$E_{\mathrm{n-rec}}$ = error due to receiver noise ($\approx$ 0.5 m)
$E_{\mathrm{t-trop}}$ = error due to tropospheric delay ($\approx$ 1 m)

Errors due to multi-path effects and shadowing are not inherent to the measurement process proper and will therefore be discussed later. Another artificial error, which has been introduced for GPS under the name of 'selective availability' will be addressed separately below. Combining all measurement errors, Eq. (7.29) can be written as

$$p = c\,\Delta t\,\sigma_{\mathrm{p}} \tag{7.30}$$

where σ_{p} is the pseudo-range error factor combining all errors listed in Eq. (7.29).

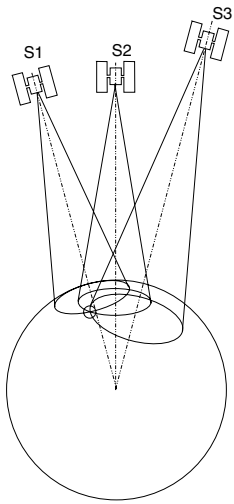

Figure 7.23. Locus of equal distance from navigation satellites.

Errors due to geometry of constellation

Independently of the above errors, not all visible combinations of four navigation satellites will, for the user, lead to the same position measurement accuracy. If the four satellites selected by the user receiver for position measurement are relatively close together, their loci of range (figure 7.23) will intersect at small angles, leading to poor results in the triangulation. The best result would be obtained in the hypothetical case that, seen from the user, one navigation satellite would be in zenith and the other three around the horizon, separated by 120 deg; this is, of course, not realistic. Generally, the

results will improve the farther apart the four satellites are. In order to obtain a quantisation of the effects of the geometric constellation of the selected satellites on the position accuracy result of the user, the concept of a 'geometric dilution of precision' (GDOP) has been introduced. The definition of GDOP can be explained as follows. The total of the standard deviations σ_{tot} relating to the user position and time in Eq. (7.27) (clock bias and geometric constellation effects included) can be expressed as

$$\sigma_{\mathrm{tot}} = \sqrt{\sigma_{x\mathrm{u}}^2 + \sigma_{y\mathrm{u}}^2 + \sigma_{z\mathrm{u}}^2 + \sigma_{\mathrm{ct}}^2} \tag{7.31}$$

where (x_{u}, y_{u}, z_{u}) is the position of the user, $\sigma_{x\mathrm{u},y\mathrm{u},z\mathrm{u}}$ is its deviation and σ_{ct} is the deviation due to clock errors. This total error can be defined as the pseudo-range error factor σ_{p} times the effect imposed by the GDOP due to the satellite constellation selected:

$$\mathrm{GDOP} \times \sigma_{\mathrm{p}} = \sigma_{\mathrm{tot}} \tag{7.32}$$

The GDOP factor is defined accordingly as

$$\mathrm{GDOP} = \frac{\sqrt{\sigma_{x\mathrm{u}}^2 + \sigma_{y\mathrm{u}}^2 + \sigma_{z\mathrm{u}}^2 + \sigma_{\mathrm{ct}}^2}}{\sigma_{\mathrm{p}}} \tag{7.33}$$

The calculation of the actual GDOP value from the constellation of the four satellites selected for measurement can be found in the literature; see, e.g., Kaplan (1996) and Kayton & Fried (1997). From the overall concept of a 'geometric dilution of precision' as an indicative factor of the quality of the solutions of Eqs. (7.28), other 'dilution of precision' factors can be established, e.g.

PDOP = position dilution of precision (three dimensions)
TDOP = time dilution of precision

According to the definition of GDOP, the position dilution of precision can be defined as

$$\mathrm{PDOP} = \frac{\sqrt{\sigma_{x\mathrm{u}}^2 + \sigma_{y\mathrm{u}}^2 + \sigma_{z\mathrm{u}}^2}}{\sigma_{\mathrm{p}}} \tag{7.34}$$

A value of PDOP = 6 is considered the limit for useful position results, a value of PDOP = 3 is considered to be good.

Velocity and change-of-range measurement

Measuring the Doppler shift of the carrier frequency provides information on the velocity and on the change of position (for the basic measurement principle see Eq. (7.6) and figure 7.7). The received frequency is, according to Eq. (7.7),

$$f_{\mathrm{R}} = f_{\mathrm{T}} \left(1 - \frac{\dot{r}}{c}\right)$$

where f_{T} is the frequency transmitted by the navigation satellite, c is the speed of light and r is the distance to the user. The range-rate is accordingly

$$\dot{r} = \frac{c}{f_{\mathrm{T}}}(f_{\mathrm{R}} - f_{\mathrm{T}}) \tag{7.35}$$

or in terms of the wavelength λ_{T} of the transmitted frequency

$$\dot{r} = \lambda_{\mathrm{T}}(f_{\mathrm{R}} - f_{\mathrm{T}}) \tag{7.36}$$

The measured range-rate, $\dot{r}_{\mathrm{n,u}}$, is the difference between the velocity component in the range direction of the navigation satellite v_{rn} and the velocity component in the range direction of the user receiver v_{ru}. As the velocity components of the navigation satellite can be estimated from the orbit ephemeris, the velocity of the user receiver in the range direction can be calculated from

$$v_{\mathrm{ru}} = v_{\mathrm{rn}} - \dot{r}_{\mathrm{n,u}} \tag{7.37}$$

The position of the navigation satellite can also be derived from the orbit ephemeris (navigation message), and the position of the user receiver is known from the pseudo-range calculations. From these values, the direction of the range-rate vector can be derived and the x-, y- and z-components of the velocity can be calculated.

The change in range can be obtained by integration of Eq. (7.35) or (7.36):

$$\Delta r = \int \dot{r}_{\mathrm{n,u}} \mathrm{d}t$$

$$\Delta r = \lambda_{\mathrm{T}} \int (f_{\mathrm{R}} - f_{\mathrm{T}})\, \mathrm{d}t \tag{7.38}$$

which can be obtained by counting the difference of the number of cycles between the received frequency and the known carrier frequency over a fixed period of time; this has lead to the term 'Integrated Doppler count',

$$N_{\mathrm{Da}} - N_{\mathrm{Di}} = \int_{\mathrm{ti}}^{ta} (f_{\mathrm{T}} - f_{\mathrm{R}})\, \mathrm{d}t \tag{7.39}$$

where $N_{\mathrm{D}a}$ is the count at the time t_a and N_{Di} is the initial count at the time t_{i}. The change in pseudo-range is then

$$\Delta r = (N_{\mathrm{D}} - N_{\mathrm{Di}})\lambda_{\mathrm{T}} - E_N \lambda_{\mathrm{T}} \tag{7.40}$$

where E_N is the sum of all errors in this measurement, comprising those presented in Eq. (7.29) and other errors due to the measurement environment (see section 7.3.4). Because one cycle of the carrier frequency ($\leq$1 ns) is much shorter than one chip of the PRN code (1 ms), the resolution of the change of range is more than two orders of magnitude better than that of the absolute range. According to the wavelength of the carrier, one cycle corresponds to a change of range $\Delta r = \lambda_{\mathrm{T}}$ of

$\lambda_T = 0.1903$ m for GPS L1-frequency
$\lambda_T = 0.2442$ m for GPS L2-frequency
$\lambda_T = 0.1873$ m for GLONASS L1-frequency
$\lambda_T = 0.2408$ m for GLONASS L2-frequency

A large part of the errors of both the pseudo-range and the Doppler measurements consist of noise. Because of the iterative techniques used to solve the navigation equations and used in order to minimise the noise of the navigation solutions, all GPS and GLONASS receivers make use of recursive Kalman filter techniques (see section 6.2.1), for the processing of the navigation results. With the computational resources typically available on spacecraft at the time of writing, the time required for convergence of the filter is usually a couple of minutes. This time has to be taken into account when considering the availability of navigation results after initiation of the receiver.

Selective availability

After deployment of the initial GPS satellites, it turned out that the navigation results obtained from the C/A code were much better than had been predicted by the designers. In order to protect their military interests, the United States decided for this reason to decrease artificially the C/A navigation accuracy by imposing a feature called 'selective availability' (SA). SA adds a random change to the GPS satellites clocks, which corrupts the reference time for the time-of-flight measurements, and also induces errors into the navigation messages. With SA applied, the following position accuracies can be achieved (Kaplan 1996):

horizontal 100 m (95% probability)
vertical 156 m (95%)

With SA removed, the position accuracies would be improved to (Kaplan 1996):

horizontal 25 m (95%)
vertical 43 m (95%)

For reasons not made public, the US Government decided to discontinue the application of SA with effect from 1 May 2000. The position accuracies which can be achieved with GLONASS are similar to that of GPS without SA.

7.3.3 Functional principle of differential GPS and relative GPS

In this section the terms 'differential GPS' (DGPS) and 'relative GPS' (RGPS) are introduced; this is because these relative navigation principles have become widely known under these names. These principles are, however, not specific to GPS, they can be

applied in the same way to GLONASS and also to potential future satellite navigation systems, such as Galileo.

In many applications, but in particular in rendezvous type navigation, it is not the absolute navigation w.r.t. some fixed frame which requires the highest precision of the state vector determination, but the relative navigation between a vehicle and a fixed point or between two vehicles operating in relatively close proximity. Using satellite navigation, the relative state vector can be determined by:

(1) relating the absolute measurements of a moving receiver to those of a fixed reference receiver, the position of which is known precisely (DGPS);

(2) the subtraction of the raw measurements of two receivers located at different positions for a number of common navigation satellites (at least four) and using these differential raw data as the measurement input to a navigation filter (RGPS).

In both cases, most errors will be eliminated only if the two receivers are in the vicinity of each other (not more than a few tens of kilometres).

Differential GPS

Differential GPS is the method most often used in terrestrial applications. There are several possible methods of implementation (figure 7.24):

(a) The *relative coordinates* of a moving receiver B w.r.t. a fixed reference receiver A are simply the difference of the results from Eqs. (7.28), measured at the same time in both receivers. This is the simplest method, which eliminates ionospheric and tropospheric errors in Eq. (7.29), but it leads to elimination of the satellite errors only if the same navigation satellites are used by both receivers.

(b) Reference receiver A calculates the difference between its known position and the instantaneous solution from the GPS measurements. These position corrections are transmitted to receiver B to correct its *absolute position* solution. The error elimination conditions are as in (a).

(c) Reference receiver A calculates, based on the knowledge of its own position, the corrections for the pseudo-ranges to *all* available navigation satellites. The corrections per satellite are transmitted (actually they may be broadcast for general use) to receiver B, which selects the corrections for the navigation satellites it will use to determine its *absolute position*. The advantage of this method is that the moving receiver is free in its selection of navigation satellites.

In methods (a) and (b), if the measurements by the two receivers are made asynchronously, a correction term

$$\Delta\mathbf{r}(\Delta t) = \Delta t(\dot{\mathbf{p}} + \dot{\mathbf{r}}_{\mathrm{c,t}}) \tag{7.41}$$

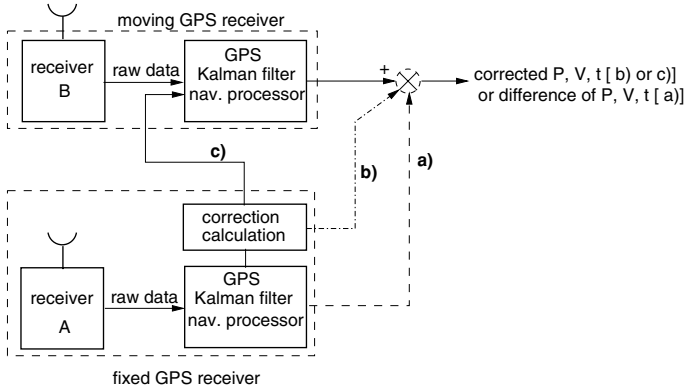

Figure 7.24. Functional principle of differential GPS.

has to be added to Eqs. (7.28) and (7.29), where Δt is the time difference between the measurements of chaser and target receivers, $\dot{\mathbf{p}}$ is the vector of the rate of change of the pseudo-range, and $\dot{\mathbf{r}}_{\mathrm{c,t}}$ is the vector of rate of change of the range between chaser and target during the time Δt. In method (c) the corrections to the pseudo-ranges will change relatively slowly with time, so that asynchronous measurement will not lead immediately to errors.

If the measurements of target and chaser receivers are based on the same navigation satellites, most of the errors in Eq. (7.29), except for the receiver noise, will be cancelled. However, as chaser and target receiver noises are treated independently in the Kalman filters of the chaser and target receivers, they cannot be treated optimally, and also the dynamics of the manoeuvring chaser vehicle cannot be taken into account in an optimal manner.

Since there is no fixed reference receiver available, the DGPS methods for improving absolute navigation are, of course, not possible in space applications. An exception may be the re-constitution of trajectories after flight, where the measurements of a fixed ground receiver may be taken into account for calibration (see section 10.7.2).

Relative GPS

In relative GPS, the raw data of both receivers, i.e. pseudo-range, Doppler data on the carrier frequency, and reference time, will be processed in the navigation filter of the chaser (see figure 7.25). If both chaser and target GPS receivers make their measurements at the same time, raw data from both receivers can be processed jointly and the linearised equations (7.28) and (7.40) can be solved in the RGPS navigation filter of the chaser for Δ-position and Δ-change of range between chaser and target (see figure 7.26). If the measurements are not performed at the same time, a correction according to Eq. (7.41) has to be applied. Usually, the GPS raw data of chaser and target are delivered

with a time tag, so that

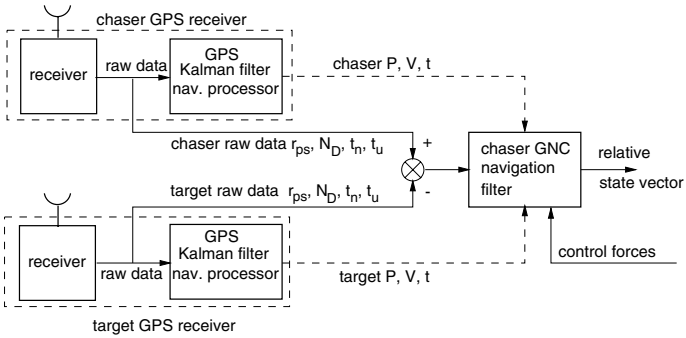

Figure 7.25. Functional principle of relative GPS.

they can be propagated to a common time reference. The single difference between the measurements of receivers A and B to the same navigation satellite i will eliminate satellite and ionospheric error terms in Eq. (7.29), which form the major part of the error budget:

$$\Delta p^{\mathrm{i}}_{\mathrm{A,B}} = p^{\mathrm{i}}_{\mathrm{A}} - p^{\mathrm{i}}_{\mathrm{B}} \tag{7.42}$$

where $\Delta p^{\mathrm{i}}_{\mathrm{A,B}}$ is the new observable, used as the input to the navigation filter of the chaser (see figure 7.26).

To eliminate the clock bias of the receiver in Eq. (7.29), double differences can be processed, i.e. differences between the pseudo-ranges to two different navigation satellites measured by the same receiver and differences between the pseudo-range measurements of the two receivers. Considering receivers A and B and navigation satellites i and j the 'double difference' input to the RGPS navigation filter will be

$$\nabla\Delta p^{\mathrm{i,j}}_{\mathrm{A,B}} = p^{\mathrm{i}}_{\mathrm{A}} - p^{\mathrm{j}}_{\mathrm{A}} - p^{\mathrm{i}}_{\mathrm{B}} - p^{\mathrm{j}}_{\mathrm{B}} \tag{7.43}$$

Because of 'double differencing' all errors except for receiver noise will be eliminated, so the equation can be written as

$$\nabla\Delta p^{\mathrm{i,j}}_{\mathrm{A,B}} = r^{\mathrm{i}}_{\mathrm{A}} - r^{\mathrm{j}}_{\mathrm{A}} - r^{\mathrm{i}}_{\mathrm{B}} - r^{\mathrm{j}}_{\mathrm{B}} + E_{\mathrm{n-A}} + E_{\mathrm{n-B}} \tag{7.44}$$

where $r^{\mathrm{i,j}}_{\mathrm{A,B}}$ are the real ranges of receivers A and B to navigation satellites i and j and $E_{\mathrm{n-A,B}}$ are the receiver noises. A set of four common navigation satellites yields the necessary number of 'double difference' observables $\nabla\Delta p^{\mathrm{i,j}}_{\mathrm{A,B}}$, to solve for the real ranges $r^{\mathrm{i,j}}_{\mathrm{A,B}}$ and to produce the relative position result. The same procedure can be

applied to carrier phase measurements, which can be used to smooth the more noisy pseudo-range measurements.

In the general case, each of the two receivers will see a number of navigation satellites, of which only a part will be common to both of them. In the navigation process, the first task is, therefore, to identify the common navigation satellites and select at least four suitable ones for relative navigation processing according to criteria such as GDOP. The raw data for the selected navigation satellites of the two receivers are then corrected for synchronisation of measurement time and subtracted. The accurate calculation of the measurement matrix of the Kalman filter requires knowledge of the absolute position and attitude. However, it may be less accurate than the relative navigation data. The measurements are then fed into the process of state update, gains and covariance computation and state and covariance propagation, as described in section 6.2.1. A simplified block diagram of a navigation filter for RGPS is shown in figure 7.26.

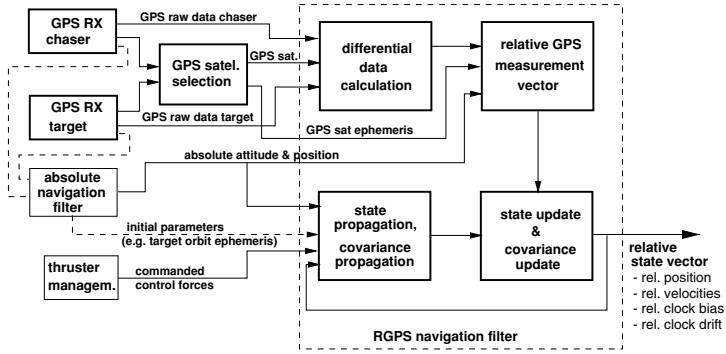

Figure 7.26. Block diagram of a relative GPS navigation filter.

Using this method and with the technology available at the time of writing, the accuracy achievable with RGPS is of the order of 10 m for position and 0.05 m/s for velocity, as compared with about 100 m (30 m without SA) position and 0.5 m/s velocity for absolute GPS. The range of operation of RGPS is limited by two constraints: one being the effectiveness of error cancellation, which decreases with increasing distance between the receivers, and the other being the range of the radio link between chaser and target that is necessary to transfer raw data from vehicle to the other. The maximum useful range may also be limited by the availability of a communication link. Link range may be limited on the far end by the transmitting power available and at short distances by shadowing from the structure of one of the two vehicles.

7.3.4 Measurement environment, disturbances

The most important disturbances and limitations of absolute and relative satellite navigation are due to shadowing and multi-path effects. The eventual outcome due to

multi-path effects is a distortion of both the code and the carrier of the direct signal of a navigation satellite. The term 'shadowing' is used here for the obstruction of view from a GPS receiver antenna to a navigation satellite by the structure of the other spacecraft. It plays a significant role when the chaser is in the close vicinity of the target, i.e. when the range to the target is of the same order or less than the geometric extensions of the target. For target stations with large rotating solar arrays, such as Mir and the ISS, the overall shadowing characteristics will also depend on the angles of the various solar generator surfaces w.r.t. the local orbital frame. As these surfaces are pointing toward the Sun, shadowing is dependent on the instant location of the navigation satellites to be used, on the position of the vehicles along the orbit (day/night phase), and on the time of year. The actual shadowing conditions can be obtained for a particular mission only by a proper simulation of the chaser and target orbital motion and of the orbital motions of the navigation satellites. At close range, for the most important approach directions, i.e. + or −V-bar direction, or below the target on the + R-bar side, the target will mask a part of the hemisphere, large enough that an uninterrupted view of four common satellites is not guaranteed. This is one of the effects which determine the lower limit of operational use of satellite navigation in rendezvous missions.

Multi-path effects due to reflection and refraction of navigation satellite signals by the Earth can affect the function of navigation satellites near to or under the horizon (tangential plane to the actual orbital position) of the receiver (GMV 1997). This effect does not influence the measurements if the antennas of the two vehicles are pointing mainly toward the zenith and are masked for low elevations.

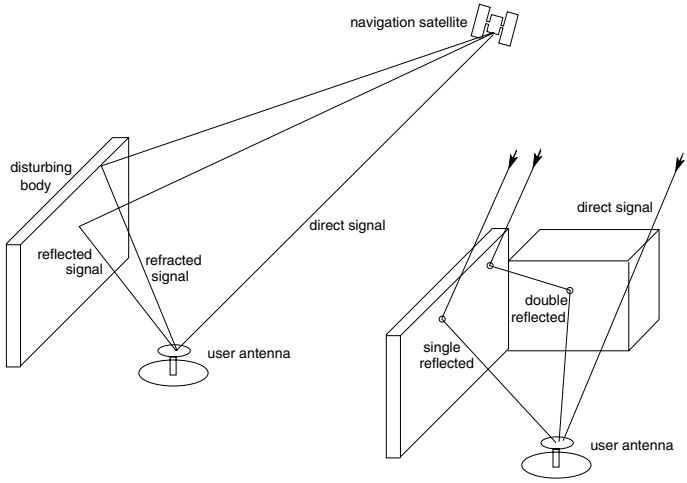

Figure 7.27. Multi-path effects due to external structures.

Multi-path effects by external structures can be caused by the following mechanisms (GMV 1997):

- specular reflections by surfaces,
- diffractions, e.g. by edges.

The amplitude of the diffracted signal is much lower than that of specular reflections. However, GPS antennas are designed for reception of the direct GPS signal, which is right hand polarised. Single reflections from planar metallic surfaces will change to a large extent the signal polarisation from right to left hand. Signals different from right hand polarisation should be strongly attenuated by the GPS antenna. The disturbance effect of single-reflected multi-path signals would, therefore, be low. Typical values for errors by single-reflected or diffracted signals are 5–10 m for pseudo-range and 5 cm for carrier phase. However, if such a signal is reflected a second time, polarisation will change again, from left to right hand. Double-reflected multi-path signals will therefore cause the strongest disturbance effects, which can be 40–100 m in pseudo-range and 2–3 cm in carrier phase (GMV 1997). ESA has observed in a flight experiment peaks of up to 300 m of error in pseudo-range (Ortega *et al*. 1998).

Another error is the so-called 'cycle slip', which occurs when a receiver loses the lock on a navigation satellite, e.g. due to shadowing. From the start of a measurement onward, the cycle count is precisely recorded and related to the start of a PRN code sequence (locking on a satellite). If reception of the satellite transmission is interrupted for a certain time, a 'loss of lock' will occur. On resumption, locking has to be established again. As a result there will be a 'jump' in the measurement data.

7.3.5 General assessment of satellite navigation for RVD

Satellite navigation provides a unique capability to determine the absolute position and velocity of a spacecraft in an Earth-centred coordinate frame during all mission phases. Without satellite navigation the absolute state of a space vehicle could be determined only by multiple measurements from ground or on board by complex RF- or astro-navigation. In addition, satellite navigation enables relative measurements of position and velocities between chaser and target, if both vehicles are equipped with appropriate navigation receivers and if the raw data of one of the receivers can be transmitted to the other vehicle. Relative navigation can be performed over relatively large distances between the vehicles (50 km or more) with an accuracy of the order of 10 m for position and 0.05 m/s for velocity, provided a communication link for that range is available. As relative navigation requires a cooperating target with navigation receiver and communication link to the chaser, this type of sensor will not be suitable for, e.g., rescue approaches to incapacitated spacecraft, where one or more of the necessary functions on the target side may have failed.

The range and range-rate measurement accuracy achieved by satellite navigation techniques is independent of the actual range between chaser and target. This is true to

a large extent also for relative satellite navigation. The advantage for the rendezvous approach lies in the relatively high manoeuvre precision that can be achieved at large ranges and which reduces the number of manoeuvre iterations necessary (see section 7.1.1). The lower limit of the operational range of satellite navigation for rendezvous missions, given by the relative navigation performance and by the disturbances discussed above, will be a few hundred metres from the target.

In contrast to other RF-sensor techniques, mass and power consumption of satellite navigation receivers are not dependent on the distance between chaser and target. Only for relative navigation is such a dependency given by the power required for the communication link between the two vehicles. A communication link such as this may, however, in practically all cases (except for the approach to an incapacitated spacecraft) also be required for operational reasons. The overall expenditure on power and mass is, for navigation systems based on satellite navigation receivers, considerably lower than for other RF-sensor systems for the same operational range.

7.4 Optical rendezvous sensors

In this section two types of optical sensors are considered: scanning laser range finders and camera sensors. Both require optical corner-cube reflectors as interfaces on the target. These two types of sensor principles were developed in the final two decades of the 20th century, precisely for the application in automated rendezvous and docking missions. With the advance of image recognition techniques and other new technologies, it can be expected that in future a larger variety of sensor principles will be both available and suitable for automated rendezvous.

7.4.1 Scanning laser range finder

Scanning laser range finder types of sensors (in some publications called 'telegoniometers') function according to the same basic physical principles (see section 7.1.2) as radar types of sensors, described in section 7.2. The difference in technology is due to the wavelength of the electro-magnetic signal. The wavelengths used for these types of optical sensors are in present applications in the near infrared range of the order of 1000 nm, depending on the available laser diode technology. The range can be determined either by measuring the time-of-flight (cf. Eq. (7.3) for pulse laser range finder) or by the shift of phase of the returning signal (cf. Eq. (7.5) for continuous wave laser range finder). The direction can be determined by scanning the laser beam and measuring the angle at which a return signal is received, either by guiding the transmitted and received laser signals via two mirrors or by placing the optical head of the laser range finder into a gimbal system, which is oscillating about orthogonal axes (see figure 7.28). The angles of the mirror axes can be read by optical encoders or resolvers to obtain the LOS angles to the target, ψ and ϑ. On the target side, the transmitted laser beam will be reflected back into the direction of the transmitter by optical corner-cube reflectors.

The design and development of laser range finder types of rendezvous sensors has been reported in several publications (NASA 1992; Moebius, Kolk & Manhart 1997; Kolk & Moebius 2000; Luther & Meissner 2000).

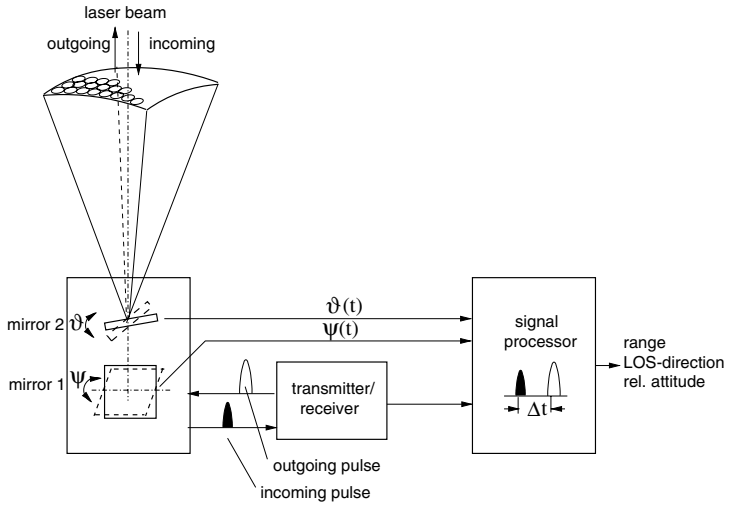

Figure 7.28. Functional principle of a scanning laser range finder.

As in the case of the RF radar, the received power is equal to the transmitted power times the ratio of effective reflector area to the cross section of the transmitted beam times the ratio of the effective receiver antenna area to the cross section of the reflected beam. With the cross section of the transmitted beam given by $\frac{\pi}{4}(R \cdot \varphi_\mathrm{t})^2$ and the cross section of the beam reflected by the corner-cubes $\frac{\pi}{4}(R \cdot \varphi_\mathrm{cc})^2$, the power of the received signal is (MBB 1988):

$$P_\mathrm{r} = P_\mathrm{t} \cdot \tau \cdot \frac{A_\mathrm{r} A_\mathrm{cc}}{\Omega_\mathrm{t} \Omega_\mathrm{cc}} \cdot \frac{1}{R^4} \tag{7.45}$$

where

P_t = transmitter power;

τ = transmittance of receiver optics;

A_r = receiver optics aperture = $\frac{\pi}{4} d_\mathrm{r}^2$;

A_cc = corner-cube reflector area = $\frac{\pi}{4} d_\mathrm{cc}^2$;

R = range to the target reflector;

$\Omega_\mathrm{t} = \frac{\pi}{4} \varphi_\mathrm{t}^2$;

φ_t = transmitted laser beam divergence;

$\Omega_{\mathrm{cc}} = \frac{\pi}{4}\varphi_{\mathrm{cc}}^2$;

$\varphi_{\mathrm{cc}}^2 = \varphi_a^2 + \varphi_b^2 + \varphi_c^2$;

$\varphi_a =$ corner-cube dihedral angle error;

$\varphi_b =$ corner-cube diffraction;

$\varphi_c = \frac{1}{R}(d_{\mathrm{t}} + 2d_{\mathrm{cc}}) =$ divergence of the return beam.

Figure 7.28 shows as an example the functional principle of a pulse radar type of laser range finder sensor. A continuous series of pulses with a high pulse repetition rate (order of kilohertz) is produced and bundled to a very narrow laser beam. The transmitted beam is deflected in the x- and y-directions by two mirrors with orthogonal axes, which can be controlled to perform various scan patterns. The rate of scan is small compared with the pulse repetition rate and the velocity of light. For a search scan covering the total rectangular FOV, the first mirror oscillates with a frequency of a few hertz, while the second one progresses slowly to start a new line when the motion of the first one returns. When the transmitted laser beam hits a corner-cube reflector on the target, it will be mirrored back toward the sensor and deflected by the mirrors into the receiver optics and compared with the outgoing signal. The range to the reflector is calculated using the time difference between the transmitted and received pulse.

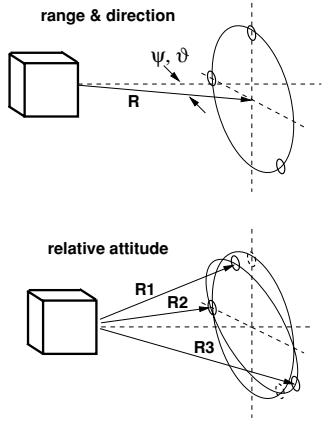

Figure 7.29. Target pattern for a laser range finder.

For the measurement of range and direction (LOS) only a single retro-reflector is necessary. Once the sensor has found the reflector, it will no longer be necessary to perform the scan over the total FOV; it will then track the reflector by scanning a narrow field around it. To increase the returning signal power, it may be useful, for very long distances, to increase the number of reflectors on the target. In this case the sensor will have to select at very short distances one of those reflectors for tracking, i.e. the most

central one. Range-rate is established by differentiation (after filtering) of the range measurements.

At least three retro-reflectors will be necessary for the measurement of relative attitude (see figure 7.29). After having identified them, either by a search scan in the total FOV or by previous tracking of the complete pattern at longer ranges, the sensor will track them individually. By knowing the coordinates of the reflectors on the target and measuring the distance to each of them, the sensor can establish the angles of the coordinate frame established by them on the target. The accuracy of the relative attitude measurement is given by the distance between the reflectors and the centre of the pattern and by the range resolution of the laser range finder sensor. As the three reflectors can only be scanned sequentially, the relative motion between chaser and target would lead to relative attitude errors if their distance measurements were not propagated to the same point in time.

Constraints due to RA measurement

The additional measurement of relative attitude will lead, however, to a number of consequences that do not exist when only range and LOS are measured.

Limitation of useful range The target pattern with three reflectors on a circle of a certain radius can be seen by a sensor with a certain maximum FOV only down to a certain range. For example, a sensor with a FOV of 30 deg, i.e. a half cone angle of $\psi_{\max} = 15$ deg, can see a target pattern with a radius of $r = 1$ m only down to a range of

$$R = \frac{r}{\tan\theta} = 3.75 \text{ m}$$

This phenomenon, which is inherent in the tracking of geometrical features, is also known by the term 'explosion of target in the FOV' during the approach. Unfortunately this effect cannot be compensated for by switching to a smaller target pattern, as the resolution of relative attitude will decrease with smaller target pattern if the resolution of the range measurement cannot be increased at the same time.

Limitation of bandwidth Since the time necessary to scan sequentially three retro-reflectors cannot be decreased below a minimum dictated by the scan mirror/motor dynamics, there will be a limitation in bandwidth of the measurements. This will also be the case not only for the relative attitude measurements but also for the range and LOS measurements, which are calculated from the same input data. The limitation of measurement bandwidth can be a problem for the overall control performance, if the GNC loop cannot observe and process the changes in the relative state between chaser and target. Such changes of the relative state can be due to the approach motion of the chaser or due to independent motion of the target.

Range of operation and performance

Range measurement The typical operating range of laser range finder sensors extends from less than 1 m up to a few kilometres, depending on the measurement principle, i.e. continuous wave or pulse radar type, and on the transmitter power. The continuous wave type of laser range finders can achieve high resolution in the very short range easier than pulse type sensors, as long as an accordingly high modulation frequency has been chosen. Pulse laser types, in turn, have advantages over the continuous wave type of sensors at longer ranges. The interdependency of maximum range, resolution and wavelength for continuous wave type radars has been discussed in section 7.2.1.

Line-of-sight measurement – field of view The size of the FOV will be a compromise between the requirements for acquisition, trajectory control and keeping at close distance the pattern in the FOV on one side, and the necessary size, mass and power consumption for gimbals or mirrors on the other. Typical FOV values for laser range finders developed for the final approach of a rendezvous mission are of the order of $\pm$ 10–20 deg.

Relative attitude measurement As discussed above, the lower limit of the range in which RA can be measured is given by the FOV, i.e. up to which point all target reflectors still can be seen by the optics. It must also be taken into account that lateral and angular relative motion between chaser and target have to be covered by the sensor, so that the reflectors for RA measurement may already move out of the FOV at larger distances than indicated in the above example. The upper limit is given by the range up to which the three reflectors can be tracked separately. If one assumes that the angular distance between the reflectors needs to be of the order of 1 deg for separate tracking, RA measurement would be possible for a target pattern of the above example up to ranges of the order of 100 m. This is quite sufficient, as RA measurement is needed only in the last 20–40 m to acquire the docking axis.

Measurement performance Range measurement performance is determined by the limitations in time or phase resolution. For pulse type laser range finders resolutions of 5–50 mm in commercial applications and 10–30 mm in developments for space applications, are preferred. For continuous wave type laser range finders, resolutions below 1 mm can be achieved, provided the modulation frequency is high enough and, correspondingly, the wavelength is short enough. For example, with a wavelength of 10 m (3 MHz) it will not be too difficult to obtain a resolution of 1 mm; however this will be at the expense that beyond 10 m the information will be ambiguous. From the measurement principle pulse type of laser range finders the resolution of range is *a priori* not dependent on the absolute value of the range, i.e. at a range of 100 m the resolution should not be much worse than at 10 m. In reality, this is true only for the shorter ranges, as beam divergence and correspondingly decreasing signal to noise ratio will

impair performance at large distances (see Eq. (7.45)). The angular resolution depends on the angular decoders of the mirror or gimbal axes. Using present technology, resolutions of 0.01 deg or better can be achieved for the above range of FOV.

7.4.2 Camera type of rendezvous sensor

The measurement principle of a camera type of rendezvous sensor (in some publications also called 'videometer') is based on the laws of imaging on the focal plane of a lens. With the advent of solid state charge transfer devices (CCDs and CIDs), extremely compact cameras with high resolution could be built, which opened the way for the principle of an optical camera as a solution for many sensor tasks. The basic functions of a camera sensor are shown in figure 7.30. An illuminator attached close to the optics illuminates the entire field of view of the camera. An optical pattern consisting of an arrangement of corner-cube reflectors is mounted on the target vehicle, each reflecting the received light back in the direction of the source. The image of the target pattern is read out by the CCD electronics, in which the coordinates of the reflector images are detected. Using the pattern evaluation algorithms, the information on range, LOS direction and relative attitude is computed in a data processor. The design and development of camera type RV-sensors is described in many publications, such as Bomer & Tulet (1990); MATRA (1994); Howard *et al.* (1997, 1999); Strietzel (1999).

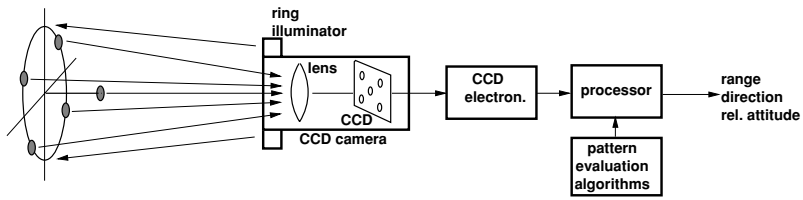

Figure 7.30. Functional principle of a camera rendezvous sensor.

The basic principle of measurement of the range R from the known distance D between two reflectors on the target, and from the distance d of the images of those reflectors in the focal plane of the camera, is represented by the relation

$$\frac{\text{range}}{\text{distance reflectors}} = \frac{\text{focal length}}{\text{distance image points}}$$

The range is then

$$R = D \cdot \frac{f}{d} \tag{7.46}$$

where f is the focal length.

The LOS angles ϕ and θ of a single reflector on the target vehicle can be determined from the position x_{fp}, y_{fp} of the image of this reflector on the focal plane of the camera.

The relationship between LOS angles and imaging parameters is

$$\frac{\text{LOS angle}}{\text{FOV angle}} = \frac{\text{distance of image point from centre}}{\text{max. extension of focal plane from centre}}$$

The maximum FOV angles are $\pm\psi_{\max}$, $\pm\vartheta_{\max}$, the total field of view is

$$\text{FOV} = 2|\psi_{\max}| \times 2|\vartheta_{\max}|$$

and the total area of the focal plane is

$$A_{\text{FP}} = 2|x_{\max}| \times 2|y_{\max}|$$

The LOS angles of a reflector on the target vehicle are accordingly

$$\begin{aligned} \psi &= \psi_{\max}\frac{x_{\text{fp}}}{x_{\max}} \\ \vartheta &= \vartheta_{\max}\frac{y_{\text{fp}}}{y_{\max}} \end{aligned} \tag{7.47}$$

Since the target may have a relative attitude angle w.r.t. the camera axis on the chaser, and the projection of the pattern plane on the plane normal to the camera axis may be shortened, the measurement of the coordinates of two reflectors is not sufficient. A minimum of three reflectors is necessary to define a plane on the target. However, in many applications a configuration of four reflectors in a plane is chosen to simplify computation algorithms. The change in positions of the reflector images on the focal plane due to a relative attitude angle is a function of the cosine of this angle, which does not provide the sign of this angle. For unambiguous detection of RA an additional reflector, arranged at an out-of-plane position w.r.t. the others, is necessary. Figure 7.31 shows a typical camera target with four reflectors in-plane and one out-of-plane. The parameters, which can be obtained by evaluation of the pattern, are indicated in the figure. The evaluation steps to produce the image of the target reflectors in the camera processor are as follows.

(1) Calculation of the centre of the ellipse defined by the images of the four reflectors on the focal plane.

(2) Determination of the major and minor axes of the ellipse and the calculation of the range from the major axis, which corresponds to the diameter D of the circle of the retro-reflectors.

(3) Calculation of the LOS angles from the x- and y-distances of the centre of the ellipse from the centre of the focal plane.

(4) Calculation of the pitch and yaw angles of relative attitude from the position of the image of the out-of-plane reflector on the focal plane.

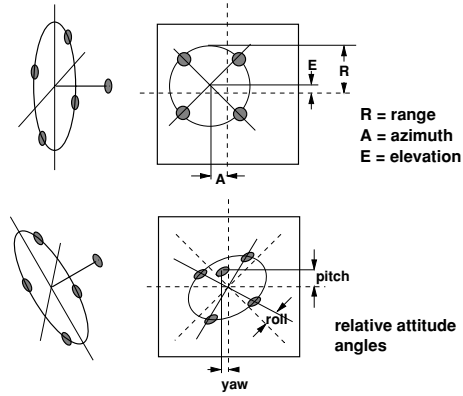

Figure 7.31. Target pattern for a camera rendezvous sensor

(5) Calculation of the roll angle from the angles of the axes of the pattern image w.r.t. the xy-axes of the focal plane.

The resolution of a camera is determined by the size of the FOV and by the number of pixels on the focal plane. There have been techniques developed to obtain subpixel resolution by defocusing (blurring) the image and calculating the centre of the spot from the signal strength of each pixel involved, so that the basic resolution of one pixel can be improved by a factor η. The effective resolution is then $\varepsilon_{\text{eff}} = \varepsilon \cdot \eta$. With such improvement techniques, up to an order of magnitude in resolution can be gained, i.e. the improvement factor may be $0.1 \leq \eta < 1$. The basic resolution ε is

$$\text{basic resolution} = \frac{\text{size of focal plane}}{\text{number of pixels}}$$

which is, for one row or one column,

$$\varepsilon = \frac{2|x_{\max}|}{N}; \quad \varepsilon = \frac{2|x_{\max}|}{M} \tag{7.48}$$

where N and M are the number of pixels in a row and column, respectively. With a being the diameter of 1 pixel, the size of the image of the target pattern d on the focal plane expressed in numbers of pixels is given by

$$d = n \cdot a \tag{7.49}$$

Inserting these definitions into Eq. (7.46) yields the number of pixels as a function of the range:

$$n = \frac{D}{R \cdot \varepsilon} \tag{7.50}$$

which gives an indication of the development of the error with the range R. Considering only the basic resolution ε, the uncertainty of the measurement would be 1 pixel, the reciprocal value of the integer of n would then be a direct measure of the range resolution. With the total FOV corresponding to a CCD of $N \times M$ pixels, the relationship between the FOV angles, $\psi_{\max}$ and $\vartheta_{\max}$, the focal length f and the number of pixels in one row or one column is given by

$$x_{\max} = \tan \psi_{\max} = \frac{1}{2} \frac{N \cdot a}{f} \tag{7.51}$$

$$y_{\max} = \tan \vartheta_{\max} = \frac{1}{2} \frac{M \cdot a}{f} \tag{7.52}$$

Equation (7.50) can then be written for a row as

$$n = \frac{D}{2R} \frac{N}{\tan \psi_{\max}} \tag{7.53}$$

and for a column with $\vartheta_{\max}$ and M replacing $\psi_{\max}$ and N accordingly.

A particular issue for the camera type of sensor is the illumination of the target pattern. Due to the fact that the total FOV has to be illuminated for each measurement, the power density of the reflected signal is much smaller than in the case of the sharp beam of the laser range finder. For a quadratic FOV, i.e. the FOV angles are $\psi_{\max} = \vartheta_{\max}$, the half cone angle of the illuminator must be $\phi_{\text{ill}} = \psi_{\max}\sqrt{2}$. The power received at the camera is, according to the radar equation,

$$P_{\text{r}} = P_{\text{t}} \frac{A_{\text{cc}}}{A_{\text{beam-ta}}} \cdot \frac{A_{\text{r}}}{A_{\text{beam-r}}} \tag{7.54}$$

where P_{t} = transmitted power; A_{cc} = area of corner-cube reflector; A_{r} = aperture of receiving optics; $A_{\text{beam-ta}}$ = cross section of illumination cone at target; $A_{\text{beam-r}}$ = cross section of reflected cone at receiver.

The cross section of the illumination cone at the target is

$$A_{\text{beam-ta}} = \frac{\pi}{4} (R \cdot \phi_{\text{ill}})^2$$

and the cross section of the reflected beam at the receiver optics is, to a good approximation, $A_{\text{beam-r}} = A_{\text{beam-ta}}$, which yields for the received power

$$P_{\text{r}} = P_{\text{t}} \frac{16 A_{\text{cc}} A_{\text{r}}}{\pi^2 R^4 \cdot \phi_{\text{ill}}^4} \tag{7.55}$$

This result shows that the received power decreases with the fourth power of the range and of the illumination cone angle.

Target pattern issues

As we have seen in Eq. (7.50), the resolution is a function of the ratio of target size to range. To keep the resolution at an acceptable level, the size of the pattern has to be increased with the range to be measured:

$$D = \frac{2n}{N} R \tan \psi_{\max}$$

where, e.g., the number of pixels n must be 100, if a 1% resolution is to be achieved. For the above example of a FOV of ± 10 deg and a CCD with 1000×1000 pixels, the size of the target pattern must be 3.5 m for an operational range of 100 m in order to keep the basic resolution at 1% of range. If a resolution enhancement factor η can be applied, the size would be correspondingly smaller. In any case, the necessary distance D between the reflectors increases linearly with the operational range. On the other hand, a larger target size will, in the approach, exceed already at a larger distance the available FOV of the camera. For our example of a pattern size of 3.5 m and a FOV of ± 10 deg, this would happen at a range of about 10 m. Before that point, the sensor would have to switch over to a smaller pattern, to be able to continue measurements during a rendezvous approach. In order to measure down to a range of 1 m between sensor optics and target pattern, the pattern would have to be, for our example, $\leq$0.35 m. This value has to be further reduced when lateral motions of the target have to be taken into account. As a pattern of 0.35 m diameter would, however, in our example yield a basic resolution of 1% only up to a range of 10 m, a third intermediate pattern would be required to cover the range of 100 m to 1 m with a resolution of 1%.

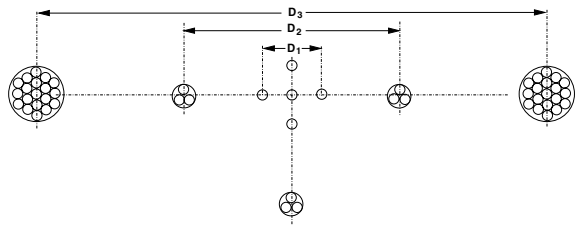

Figure 7.32. Typical target pattern set for long and short range.

The target pattern of camera type sensors will, therefore, consist of a set of concentric patterns of different sizes for the different subranges of operation. As relative attitude is required only in a range of 20–30 m, only the inner ones will have to have the out-of-plane reflector shown in figure 7.31. If the relative attitude is small, or will occur only in one known direction, it may be sufficient for longer ranges to have only two reflectors at a large distance on the target vehicle. This may be helpful for accommodation problems of the target pattern on the target vehicle. A typical set of reflector patterns is shown in figure 7.32, where the reflectors at distance D_3 are for the longest and the ones at distance D_1 for the shortest range (D_1, D_2, D_3 not to scale).

The second problem which affects the design of the target pattern for longer ranges is the low power density of the return signal, as has been shown above in Eq. (7.55). The operational range of a camera sensor will be limited by the signal-to-noise ratio of the reflected signal. In order to increase the power density at the camera optics, the area of the reflectors has to be increased. This leads for long range targets to the design of multi-reflector spots, as indicated in figure 7.32; these require less mass and volume than a single reflector with larger diameter.

Range of operation and performance

As we have seen above, the range of operation of a camera sensor is limited by the size of the target pattern and by the power density of the reflected light. The typical values for operational range and performance assume an improvement factor over the basic resolution of one pixel of η somewhere between 1 and 10. Typical limits for a sensor with a FOV and number of pixels corresponding to the example given above would be:

range: up to 200 m with a large target pattern (cf. figure 7.32)
LOS angles: up to $\pm$10 deg
relative attitude (pitch and yaw): up to $\pm$5 deg
relative attitude (roll): up to $\pm$180 deg, depending on target pattern
bandwidth: $>$1 Hz

Typical performance figures for the above example, assuming a target pattern size of 0.2 m for ranges $<$30 m and 1.5 m for ranges $>$30 m would be as follows. For range and lateral offset:

$<$10 m: $<$0.01 m
$<$30 m: $<$0.1 m
$<$100 m: $<$1 m

For LOS angles:

$<$0.1 deg

For relative attitude:

$<$10 m: $<$0.5 deg
$<$30 m: $<$2 deg

These figures are purely indicative; results of actual sensors may be better or worse, depending on design parameters and evaluation techniques applied.

7.4.3 Measurement environment, disturbances

Disturbance sources

All light sources in the FOV, in addition to the target retro-reflectors, are potential external disturbances for optical sensors. The following sources have to be considered according to the importance of their effects:

(1) the Sun;

(2) reflections of sunlight on target surfaces;

(3) reflections of sensor illuminator light on target surfaces;

(4) direct light or reflections of other light sources.

Potentially the most powerful disturbance source in the FOV of a sensor is obviously the Sun. The Sun radiates in practically all wavelengths of light so that sharp filtering of the illuminator wavelengths will not provide sufficient protection. The same is true for specular reflections of the Sun by features on the target vehicle. Specular reflection of the illuminator light is the third disturbance source which cannot be eliminated by filtering. Direct light or reflections from other sources have generally either a much lower intensity and/or have different wavelengths than the sensor illuminator. Accordingly they can be discriminated against the target reflectors by an intensity threshold or wavelength filter. In the following discussion, therefore, only the first three sources of disturbance light will be considered.

Sensitivity of different sensors to disturbances

Laser range finder type Due to the narrow beam and the very small instantaneous FOV, laser range finder types of sensors are, in their normal mode of operation, generally less sensitive to disturbances than camera type sensors. A large FOV is needed only for acquisition and in the case of a multi-target pattern, when the sensor is very close to the target vehicle. In the first case, the large FOV is needed only for a very short time; thereafter only very small areas around the reflectors are scanned. In the second case, the instantaneous FOV around a target reflector is still very small, and the three or four reflectors are distributed over a large part of the total FOV. Concerning possible disturbance by the Sun, a large part of the sensor FOV is covered in the second case by the structure of the target vehicle. Depending on the approach direction, i.e. $\pm$V-bar or $\pm$R-bar, a potential disturbance by the Sun is limited to a very short part of the approach trajectory and can, if necessary, also be excluded by operational means (e.g. change of start time of a trajectory or change of attitude for short time).

Camera type Camera types of sensors, because of the snapshot of the complete FOV taken at each measurement, are *a priori* more susceptible to disturbance light sources. To suppress the 'false' images a number of techniques can be applied, two of which are described below. Another problem for a camera type sensor is the 'blooming' of the CCD when an intense light source is in the FOV. In such a case, complete rows and columns of the pixels affected, and also neighbouring pixels, can become saturated, resulting in crossbars of rows and columns over the FOV, where no measurement is possible. There is not much possibility of protection against this effect in the case where one or more of the target reflectors are within these saturated crossbars. For reflectors outside the

saturated rows and columns, tracking of a very narrow instantaneous FOV, similar to the technique described above for the laser range finder sensor, can be performed also on a camera image. The other pixels will, in this case, be ignored in the evaluation.

Possible protection measures against 'false' images are:

- wavelength filters on camera optics;
- subtraction of measurement with and without sensor illumination (Howard *et al.* 1999);
- flash during transfer (Bomer & Tulet 1990).

The first measure will be effective in particular against artificial light sources or reflections of such sources onto the target. As already mentioned, it will not provide protection against direct sunlight and Sun reflections. The second technique consists of a comparison of two images, one taken with and one without sensor illumination. Because the retro-reflectors of the target pattern always reflect the light back along the direction of the source, the target reflectors will be visible only on the image with sensor illumination. The third technique consists of illuminating the scene with a short flash at exactly the time when the CCD charges are transferred from the photosensitive area to the memory area. For this purpose the CCD is operated in a non-standard mode, in which the charges continuously move along the columns, i.e. a chaining of transfer phase and a clean-up phase without interruption. Permanent light sources will, therefore, affect all pixels of a column, whereas reflections from the illumination flash will create a sharp image. This special mode is called 'flash during transfer' (FDT) and is the subject of a patent by MATRA (Bomer & Tulet 1900).

None of these measures provide any protection against spurious reflections of the sensor illuminator light. This is applicable also to the laser range finder type of sensor, though in this case the illuminated instantaneous FOV is very small. Protection against spurious reflections of the illuminator light can only be obtained by proper design of the interfacing target surface and by testing of the sensor within a representative target environment (see chapter 10).

7.4.4 General assessment of optical sensors for rendezvous

In the very short range from a few hundred metres to capture, optical sensors provide a solution to the rendezvous navigation requirements, a solution which cannot be matched for the combination of performance, mass, power consumption and complexity by sensor systems using other measurement principles. RF-sensor techniques will require complex and bulky antennas and electronic equipment on both chaser and target vehicles to provide all the parameters. Satellite navigation, even in relative mode, will not provide performances better than $\approx$5 m for position measurement and suffers, in addition, in the very short range from shadowing of the navigation satellites by the target structure.

Concerning the operational range, camera type sensors will be limited to the 100–200 m range, whereas laser range finder types could be used up to the kilometre range, as discussed above. The choice of measurement principle is, however, more complicated and will depend also on the type of mission to be flown, i.e. whether docking or berthing, whether or not fly-arounds will be included in the last few hundred metres, whether fast target motion has to be considered in the last metres prior to capture, etc. To assess the suitability for various mission requirements, the typical advantages and disadvantages of the two sensor types will be recalled here.

Laser range finder sensor

Advantages of a laser range finder sensor:

- Only one reflector is required on the target, if only range and LOS need to be measured.
- It has a large operational range from about 1 m to a few kilometres, depending on emitting power.
- Because of the operational principle, with its very small instantaneous FOV, the laser range finder sensor has an inherently low sensitivity w.r.t. Sun interference and other spurious light sources.

Disadvantages of a laser range finder sensor:

- This measurement principle requires moving mirrors or gimbals, resulting (a) in additional power consumption for scanning motion and (b) in reliability issues due to the sensitivity of bearings to launch and space conditions.
- Complex scan patterns for acquisition and tracking have to be performed, resulting in a limitation of bandwidth when more than a single reflector has to be scanned.
- Limitation of the minimum range, down to which relative attitude can be measured. This is due to the fact that the pattern moves out of the FOV in the last metres of approach. A reduction of the target pattern size, as in case of the camera sensor, does not help, as this would cause a corresponding increase of the measurement error.

Camera sensor

Advantages of a camera sensor:

- There is an increase of measurement accuracy with decreasing range.
- The measurement of all navigation parameters can be obtained in one shot at the same time.

- There is a high bandwidth of measurement output, as measurement shots can be repeated at a relatively high rate.
- The relative attitude measurement can be performed down to the minimum range by using sets of smaller target patterns.
- The sensor has no moving parts and is, therefore, less sensitive to launch and orbital environment.
- Any low range can be covered in principle by adding a sufficiently small sized target pattern, which fits into the FOV at the shortest range.

Disadvantages of a camera sensor:

- For larger ranges, target reflector spots must have be at a large distance D from each other and each spot may have to consist of a number of reflectors to return sufficient light (see figure 7.32). In addition, for the measurement of relative attitude in the short range, one reflector sticking out of the plane of the others is required. As a result, the accommodation of such a complex set of target patterns for short and long ranges on target spacecraft may be more difficult than that of a single pattern for the laser range finder type of sensor.
- The operating range will be limited due to the decrease of performance with the range by $1/R$ and due to the decrease of signal-to-noise ratio with the fourth power of the range and of the illumination angle.
- The FOV of this type of sensor has to be kept as small as possible due to illumination angle problems.

Choice of sensors for RV missions

As a medium range sensor, satellite navigation in relative mode can be used in a range no closer than a few hundred metres before problems with shadowing and multi-path effects limits its usefulness. This is also the limit of the range where its performance is still sufficient for a further approach. Below this range, optical sensors are the best choice considering all relevant features and properties. Although optical sensors inherently have a limited FOV, fly-around manoeuvres can be performed with them, provided the chaser is pointing, during the fly-around manoeuvre, toward the target, and on the target side a set of multiple reflectors is mounted under different angles covering all parts of the fly-around trajectory arc.

The choice of the type of optical sensor for RV missions ending with berthing is relatively easy. As measurement of relative attitude is not necessary, the laser range finder type of sensor is the best choice. For range and LOS angle measurement, only one reflector is required, and the sensor can cover the entire short range from the order of a kilometre down to the berthing box.

For RV missions ending with docking, the choice is more difficult. Concerning the characteristics and performance required in the different ranges from a few hundred metres down to contact, a combination of laser range finder types and camera types of sensors would provide optimal performance. The laser range finder type would provide range and LOS information in the entire range, whereas the camera sensor would provide all navigation parameters, including relative attitude, with increasing accuracy in the last part of the approach, e.g. at least from approximately 30 m to docking. The penalty to be paid is a duplication of sensor heads and sensor electronics on the chaser side and the accommodation of at least two different target patterns on the target side. The accommodation problems will be increased by the fact that, due to the particular safety criticality of the last part of the approach, all sensor functions on the chaser side may have to be duplicated and operated in hot redundancy. Because of the complexity and cost of accommodation and operation of two types of sensors, spacecraft designers will of course attempt in the first instance to solve the navigation problem of the final approach with only one type of sensor. The following criteria may play a role in the choice of sensor type.

- If a medium range sensor, i.e. satellite navigation or any other type, can be used down to less than 200 m, the use of a camera sensor only may become possible for the short range and may satisfy all requirements. In this case a very large target pattern for the 100–200 m range would have to be accommodated on the target.

- If the medium range sensor ceases to be useful at ranges larger than 200 m, the laser range finder type is the better choice. This type of sensor may cause difficulties, however, in the very short range concerning the measurement of relative attitude, when the target pattern is moving out of the FOV. It may also cause problems due to the limited bandwidth with which the navigation information is provided, when three reflectors have to be scanned for relative attitude measurements. The possibility of using a laser range finder sensor only, including the short range of approach, will depend, therefore, on the motion characteristics of the target.

- A combination of both types of sensors may have to be used if (a) the target attitude motion has amplitudes which would use up a significant part of the reception range of the docking port, if (b) the cycle time of the attitude motion is shorter than the residual approach duration after loss of relative attitude (see above) and if (c) the medium range sensor cannot be used at ranges closer than a few hundred metres.

These considerations can of course only indicate the issues directly connected to the measurement principles. In a spacecraft project, other design and operational constraints may also eventually determine the choice.

8

Mating systems

The objective of this chapter is to provide a basic understanding of the dynamic and kinematic processes which are taking place during docking or berthing of two vehicles, and to give an overview of the design principles used for docking and berthing mechanisms. Design driving requirements for these mechanisms are briefly discussed, and an overview of existing mechanism developments is given. The dynamic processes of contact and capture at docking are discussed using a simple model of an equivalent mass, which represents the masses of both spacecraft plus a central attenuation system. Basic functional concepts of the design elements used for shock attenuation, capture, structural connection and sealing are discussed at the end of the chapter.

8.1 Basic concepts of docking and berthing

The main tasks and issues arising during docking and berthing have already been addressed in section 2.5. Definitions of the terms 'docking' and 'berthing' have been given in chapter 1. For completeness of this chapter, these key definitions shall be recalled here.

- As a general term for the process of achieving contact, capture and connection, the term *mating* is used. This includes the two cases 'docking' and 'berthing'.
- The term *docking* is used for the case where the GNC system of the chaser controls the required vehicle state parameters necessary to ensure that its capture interfaces enter into those of the target vehicle, and where the capture location is also the location for structural connection.
- The term *berthing* is used for the case, where
  - the GNC system of the chaser delivers the vehicle to a meeting point with zero nominal relative velocities and angular rates;

– a manipulator, located on either target or chaser vehicle, grapples the corresponding capture interface on the other vehicle;
– the manipulator transfers the captured vehicle with its attachment interface to the final position at the relevant target berthing port and inserts it into the corresponding attachment interfaces of the target vehicle.

As already shown in figure 2.13, for docking, the capture and attachment interfaces are integrated into a single system, the main axis of which is the approach axis. In berthing, the approach axis and the axis of attachment, and hence the interfaces for capture and attachment, are fully de-coupled. The transfer from the capture position to the attachment position by a manipulator makes it possible to access different berthing ports, as shown in figure 5.4.

In order to give an overview of the functions and operations involved in the processes of mating of two spacecraft, and to recall the major constraints and interface requirements (some of them have been addressed already in previous chapters), the sequence of operations of a typical docking process and of a typical berthing process are described in the following sections.

8.1.1 Docking operations

Depending on the type of mission, unpressurised (usually for completely unmanned mission scenarios) or pressurised (for missions including astronauts in one or both vehicles) docking mechanisms will be used (see section 8.2). The following description of a typical docking process is based on a manned scenario, which involves the more complex functions, as an air-tight transfer passage has to be established.

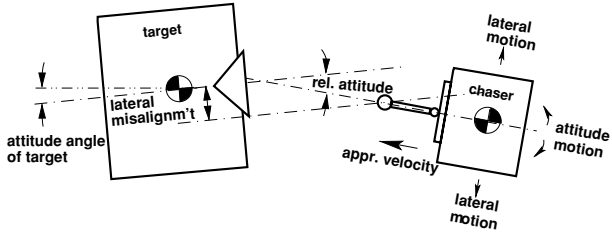

Figure 8.1. Alignment and motion parameters at docking contact.

(1) *Reduction of approach velocity and misalignments.* During and/or after acquisition of the docking axis, the chaser reduces its approach velocity to the final value. The last part of the approach down to contact will be flown with constant velocity, avoiding braking thrusts in the last few metres and plume impingement on the target at close distance. During the last few metres of approach the chaser GNC must achieve the lateral and angular alignment which is necessary to place docking interfaces of chaser and target into each other's reception range.

(2) *Reception*. In this phase, the docking interfaces of the two vehicles enter into each other's reception range. This is the range within which physical contact between the two vehicles occurs and capture of the according interfaces is possible. The reception range must be large enough to cover all residual dispersions of the chaser w.r.t. the target vehicle. The reception range must also cover all rebound motion, which may take place after first contact prior to completion of capture.

(3) *Impact attenuation*. If the interface structures impact on each other without shock absorbers, they would rebound, with the deceleration and re-acceleration dependent on the elastic and plastic deformations of the contacting structures and of their sub-structure. As the change of velocity would happen over a short distance, the accelerations would be high and the rebound would take place within a short time. For this reason, spring-damper devices have to be applied; these reduce the relative velocity (the velocity change occurs over a longer distance) to

- reduce the shock of impact on the structures of the two vehicles;
- make the alignment of the capture interfaces possible;
- decrease the rebound velocity; and
- increase the time available for the capture process.

(4) *Capture*. After entering into their reception ranges, the capture interface structures of both sides can guide each other (because of the compliance of the attenuation system) into the conditions of alignment, at which capture can be completed. The term 'capture' simply means that the vehicles can no longer escape from each other. It does not imply, however, that a rigid connection has been established. Operation of the capture latches can be achieved, e.g., by springs and by the kinetic energy available from the residual velocity between chaser and target; this is comparable to a spring-loaded door-latch falling into its catch. Otherwise, operation of capture latches can be initiated by sensors and actuated by electric motors. Such sensors could be contact or force sensors, or sensors observing the entry of interfaces into the capture range.

(5) *Retraction and structural alignment*. After capture, the two spacecraft are still only relatively loosely connected to each other, and the residual distance and the lateral and angular misalignments in general will not allow immediate engagement of the structural latches. On the contrary, in most designs, the springs of the shock attenuator system will push the two bodies away from each other up to the limits given by the capture latches. For this reason, in most designs a retraction mechanism will be necessary to pull the docking interface planes of the two craft together. This generally includes additional mechanical guiding features (e.g. pin–cone, ball–groove), ensuring improved alignment during the retraction motion, as is necessary for structural connection.

(6) *Structural connection*. Once they are properly aligned, the structural latches can be engaged. They will press the two interface planes together under a pre-load, which ensures a stiff structural connection under all load conditions which potentially could occur during operation as a combined spacecraft. In the case of pressurised docking ports, the structural latches also have to apply the compression forces for the sealing rings, which are required to achieve a gas-tight connection. In some docking mechanism designs, one or more of the functions of capture latch, attenuation system, retraction mechanism and structural latch can be combined.

(7) *Utilities connection*. After proper structural latching, utility connections can be engaged. This will be possible at this point in time only if connections are performed automatically. Otherwise, utility connections may be performed by the crew after pressurisation and hatch opening. In many cases, only electrical connections for power and data will be required. In some mission scenarios there are, however, also fluid and gas connections, e.g. for re-supply of propellant, water and/or air to the target spacecraft. After connection of the data lines, the systems of the chaser spacecraft can be directly monitored and, where necessary, commanded by the target.

(8) *Pressurisation*. In the case of pressurised docking ports, after successful structural latching, the pressurisation of the volume between the hatches can commence. Information provided by pressure sensors in the tunnel and between two concentric sealing rings will be monitored during pressurisation to verify gas tightness.

(9) *Opening of hatches*. When pressurisation has been established and gas tightness has been verified, the hatches can be opened and the post-docking operations according to the mission objectives can begin.

8.1.2 Berthing operations

In principle, the manipulator arm can be mounted either on the target or on the chaser vehicle, and correspondingly the grapple fixture should be mounted on the opposite vehicle (see figure 2.13).

In the following description, which is based on the ISS scenario, it is assumed that the manipulator is located on the target vehicle.

(1) *Acquisition of berthing box by chaser*. At the end of the approach, the chaser vehicle will perform station keeping in a berthing box, as described in sections 5.3.1 and 5.7.2. The berthing box is a volume located very close to the target station into which the chaser has to be placed, to make capture of the grapple interfaces by the manipulator arm possible.

(2) *Acquisition of readiness position by manipulator*. Once the chaser is in the berthing box, the manipulator front end with its end-effector will be moved to a position

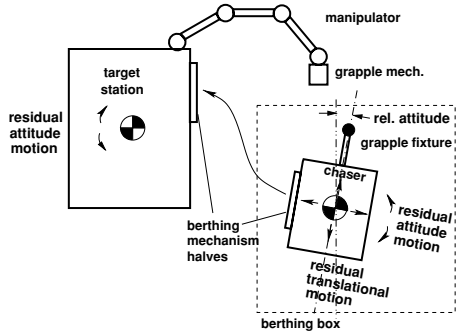

Figure 8.2. Berthing scenario: conditions at capture.

from where capture operations can start. As a rule, for safety reasons, the manipulator will not be in this position during acquisition of the berthing box by the chaser.

(3) *Switch-off of chaser thrusters and initiation of capture*. When the front end of the manipulator has acquired the readiness position and when it has been verified that the grapple fixture is within the 'inner berthing box' (see figure 5.6), the propulsion system of the chaser will be inhibited and the manipulator will be steered to pursue with its end-effector the grapple fixture on the chaser. After thrust inhibition, the chaser will start to move away due to the effects of orbital dynamics (see figure 5.5). As a result of this motion, capture has to be performed within a limited time, typically 1 or 2 minutes, depending on the position of the berthing box w.r.t. the target orbit (V-bar).

(4) *Grappling of capture interfaces by manipulator.* When the correct position of the capture tool (end-effector) is achieved, the grappling operation is initiated. Similar to the docking operation, grappling has to ensure that the interfaces can no longer escape each other, and subsequently that the connection between the manipulator and the captured vehicle is sufficiently rigid to comply with the needs for transfer and insertion.

Correct position of the capture tool w.r.t. the capture interface on the other vehicle (grapple fixture) requires a sensing function; this has to provide the same type of information as required for docking, i.e. range, LOS angles and relative attitude angles. At the time of writing, this sensor function has been fulfilled in all berthing missions by a human operator with the aid of a camera, mounted on the end-effector, and a target pattern near to the grapple fixture, similar to the one shown in figure 6.25. In future manipulator operations for berthing, this function may also be performed automatically.

(5) *Transfer to the berthing port.* The front end of the manipulator will be steered so as to perform all necessary translations and rotations to move the berthing mechanism interfaces of the captured vehicle to those of the target berthing port on the station. As the captured vehicle will in most cases obscure the vision of the manipulator camera used for capture (wrist camera of manipulator), different sensing functions are necessary for transfer. As the accuracy requirements for steering of the manipulator arm during transfer are moderate, the internal angular sensors of the manipulator joints may be generally sufficient. A path plan will be used which ensures that, during transfer, no collision between the body to be berthed and the structure of the station will occur.

(6) *Insertion into reception interfaces*. As for docking mechanisms, berthing mechanisms also have a reception range which must be measured according to the positioning accuracy of the manipulator. A sensing function is required to verify proper positioning of the berthing interfaces w.r.t. each other. If the joint angle sensors of the manipulator cannot provide sufficient accuracy, additional sensing devices (e.g. camera and visual target pattern) may have to be provided.

After proper positioning has been established, the manipulator will push the berthing interfaces of the captured vehicle gently into those on the berthing port of the station. Alignment will be achieved by the manipulator forces and guiding features (i.e. first by alignment petals and eventually by pin–cone or ball–groove combinations). The manipulator can provide these pushing forces until structural connection commences. In contrast to docking, insertion into the berthing interfaces can be a very slow process, as this is fully controlled by the manipulator.

(7) *Structural connection, utilities connection, pressurisation and hatch opening*. These operational steps and functions are in principle no different than the ones for docking, and therefore need not be repeated here.

Berthing techniques can be used also for other applications, e.g. the transfer of modules or other structural components from one location to another. Examples are the transfer of Mir modules from docking location to the final location, or the unloading and attachment to the ISS by manipulator arms of cargo items from the cargo bay of the Space Shuttle Orbiter. The transfer of the modules of the Mir Space Station from one fixed position to another one has been performed automatically without active control by a human operator.

8.1.3 Commonalities and major differences between docking and berthing

The above descriptions of operational sequences show that for both docking and berthing the same basic types of operations are required:

- acquisition of capture reception range;

- closure of capture devices;
- transfer to and alignment with operating range of structural latches;
- closure of structural latches;
- pressurisation of tunnel (mission dependent);
- hatch opening (mission dependent).

For *docking*, the functions for capture and attachment are concentrated at one location on each vehicle and integrated into one system, the active half of which, in the majority of cases, is on the chaser side. The acquisition of the capture range is performed by the GNC system of the chaser. Capture is initiated automatically either by passive spring-loaded latches falling into their corresponding catches on the other vehicle, or by active latches initiated by sensor signals. Due to the integration of capture and transfer functions, the transfer from the capture position to the attachment position is very short. It is typically performed by a simple retraction of the front end of the mechanism to the base structure.

For *berthing*, the functions for capture and attachment are at different locations on both vehicles. Capture is performed actively by a tool which is able to pursue and capture the according interface on the other vehicle in a much wider range of positions and attitudes than for docking. From the capture position, the captured body can be transferred to a wide range of potential attachment locations. As a result, in contrast to docking, this transfer has to be performed via a long and complex path. The price to be paid for the additional flexibility concerning capture location and attachment location is the much increased complexity in terms of tools and operations required for capture and transfer. The tools required are a large manipulator arm and an end-effector. The increased operational complexity is due to:

(a) the dynamic interactions between three systems, i.e. the approaching vehicle controlled by its GNC system, the body dynamics of the target station, with or without active GNC, and the manipulator system;

(b) the inherently more complex capture and transfer operations by a manipulator, which is actively controlled by the human operator in the loop.

For docking, the GNC performance parameters (i.e. velocity in approach direction, lateral and angular alignment and rates) will determine the size of the reception range and the size of the spring-damper equipment. Different design principles can be used for these functions, depending on whether the docking contact will be at high or very low speed. Generally, the better the GNC performance, the lower the approach velocity at contact can be.

In the case of capture for berthing, the absolute alignment of the chaser vehicle plays, compared with the residual rates, a secondary role, as already discussed in sections

5.3.1 and 7.1.1. In order to stay in a berthing box of, e.g., 1 m^3 for 1 minute, residual velocities in all directions must not be higher than 0.01 m/s. Residual angular rates must be compatible with the tracking capabilities of the manipulator and the human operator. Considering an initial misalignment of, e.g., 10 deg and a residual rate of 0.1 deg/s, the final misalignment after 1 minute would be 16 deg. This type of rate and misalignment could still be handled by a manipulator.

For completeness, the general advantages and disadvantages of docking and berthing shall be recalled here.

Docking operations are generally less complex, more reliable and less time consuming than berthing operations. Docking mechanisms generally require, however, larger reception and damping devices than berthing mechanisms. Capture has to be achieved in a few seconds after contact, otherwise the vehicles will move away from each other. Because of the angular motion (potentially induced by the contact of the vehicles), a failed capture is more safety-critical in docking than in berthing.

Berthing allows attachment to locations on the target vehicle which would be inaccessible for docking. As capture takes place at nominally zero relative velocity between the two vehicles, impact shocks and forces will be small. This requires, however, that the GNC of the chaser is capable of leaving the vehicle in the volume of the berthing box at very low residual velocities and angular rates after thrust inhibit. The time available for capture depends on the residual velocities, on the capture location w.r.t. V-bar, on the constraints imposed by the target vehicle geometry and on the capabilities of the manipulator. The capture window available after control inhibit of the chaser is typically of the order of 1 to 2 minutes. Failure of capture within this time leaves the chaser vehicle in a safe state w.r.t. collision with the target structure, if the rules of the berthing box definition (see section 5.3.1) have been followed. The necessity of a large manipulator is a penalty, in principle, in terms of mass to be launched and investment cost. These considerations may, however, play a secondary role for the mission design of the chaser, e.g. if such a manipulator is available on the target station anyway. The time required for capture, transfer and attachment to the berthing port is, in any case, a penalty concerning mission resources, in particular concerning crew time.

8.2 Types of docking and berthing mechanisms

In this section the characteristics of the different types of mechanisms for attachment will be discussed in general terms. The discussion looks, in particular, at the mutual dependence of the design driving functions. These are the capture function and the functions involved in the establishment of a passage for transfer of goods between the vehicles. The latter functions include the structural connection and, in the manned scenario, the seals and hatches required to establish a pressurised tunnel between the spacecraft. Examples are given of previously developed different types of mechanisms, and actual implementations of these features are shown. A very detailed description of central and peripheral docking mechanisms for manned spacecraft, together with a

comprehensive discussion of the major design elements of the Russian systems, can be found in (Syromiatnikov 1990). An overview of docking and berthing interfaces and of docking/berthing requirements and parameters, together with an extensive list of reference documents, is given in (AIAA 1993).

8.2.1 Design driving requirements

The design and size of mating mechanisms are determined by a number of factors, which depend on the mission objectives and the dynamic conditions at contact of the chaser and target halves of the mechanism.

Transfer of crew and goods

Unmanned missions In unmanned missions, i.e. where neither spacecraft is designed to be habitable, there is generally no need for a pressurised transfer tunnel. For this reason, the design of unpressurised docking and berthing mechanisms will typically be determined by requirements for load carrying capability, stiffness and, in some cases, alignment accuracy. Unpressurised mating mechanisms are much simpler in design, as no air-tight connection has to be established.

Manned missions In manned missions, at least one of the two spacecraft is permanently or intermittently manned; usually this is the orbiting target station. This requires transfer of goods to the pressurised areas of the station, and for this reason also a supply vehicle usually has a pressurised area so items may be used inside the station. For the transfer, a tunnel has to be formed after mating, which provides a pressurised passage. The diameter of the docking or berthing mechanism is mainly dependent on the size of the tunnel required for transfer of crew and goods. As a rule, the minimum cross section of hatch and tunnel should allow the passage of an astronaut in his space suit.

Contact parameters

The necessary reception range is mainly determined by the lateral and angular misalignments between the two halves of the attachment mechanism at insertion. The design and size of the attenuation devices are determined by the relative translational velocities and angular rates at contact. In the case of docking mechanisms, these are the approach velocity, lateral velocities and angular rates, determined by the GNC performance of the chaser. In berthing mechanisms, these values are determined by the performance of the manipulator and the sensors used to guide it. There are two occasions of capture which have to be considered in the case of berthing: capture of the grapple fixture, and capture after insertion of the berthing interfaces of the captured vehicle into those of the target station. As insertion velocities by a manipulator can be very low, for berthing there will be no need for large shock attenuation systems, and there will also be no driving constraints for the closure time of latches.

Requirements for utility transfer

Utility lines for, e.g., power, data, fluids, gas, require a certain area on the docking or berthing interface plane for connectors or line feed-throughs. Utility connections can be performed either automatically or, in the case of pressurised attachment interfaces, by hand. If performed automatically, additional areas for the connection mechanism must be provided. In pressurised mating mechanisms, such areas must be outside the minimum diameter required for the transfer of crew and goods. If performed by hand, the connections need to be inside the tunnel, whereas automatic connectors can be located either inside or outside. The latter location may be chosen, e.g., for safety reasons in case of fluid connectors for toxic propellants.

The sizing requirements for a pressurised mating mechanism are shown in figure 8.3. The design driving feature, shown here for the inner cross section, is a space-suited astronaut. There can, however, be other requirements, e.g. the transfer of standard racks, which are bigger than a space suit. This was the design driving feature, e.g., in the berthing mechanism for the ISS. A discussion of sizing requirements for docking/berthing systems can be found in Tobias,Venditti & Cable (1989).

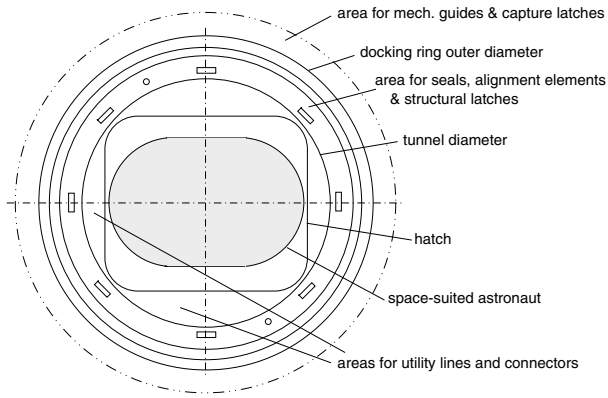

Figure 8.3. Sizing features for pressurised mating mechanisms.

The diameter of the pressurised tunnel eventually becomes a design driver for the choice of structural connection latches, as the latch forces will increase with the square of the tunnel diameter. The repercussions of this effect on the design of docking ring structure, seals and latches are discussed in more detail in section 8.3.6.

Mating devices which perfectly fit the needs of a particular mission can, in general, be designed only if both the chaser and the target are developed at the same time. In servicing missions, the target spacecraft will usually have been in orbit for a long time, and therefore the mating devices of the chaser will have to fit the interfaces available on the target. This is true in particular for a supply vehicle visiting a space station.

These interfaces are usually conceived and designed early in the development phase, or their design may even be taken from those used in former missions, and the operational phase in orbit may last one or two decades. In principle, for the operational lifetime of the station, visiting vehicles will have to comply with these interfaces. As a result, newly designed supply vehicles may have to use mating devices, the design of which may be very old and not fully optimised for the mission. Only in cases where later structural items are added to the station will there be a chance to add a new design for the mating devices.

8.2.2 Central vs. peripheral docking mechanisms

For docking mechanisms, the requirement for effective alignment for capture at the first contact can most easily be implemented by a central capture mechanism. This will consist (on the side of the active vehicle) of a rod (also called a probe) with one end flexibly connected to the spacecraft structure, and (on the side of the passive vehicle) of a hollow cone (also called a drogue) receiving the tip of the rod and guiding it to the cone centre, where it can be captured. This process is described in more detail in section 8.3. All early docking mechanism designs used in the American and Russian space programmes were based on this principle (Bloom and Campbell 1970; Syromiatnikov 1971; Syromiatnikov 1990). The disadvantage of a central docking mechanism is that, after successful attachment and hatch opening, the capture mechanism components, i.e. the rod mechanism on the active side and the capture cone on the passive side, are in the way of the transfer tunnel (see figure 8.4). They have to be removed and stored elsewhere before transfer of crew and goods can take place.

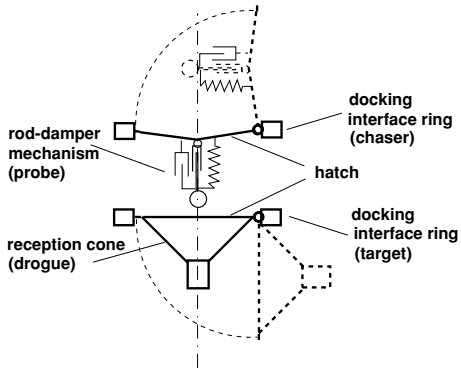

Figure 8.4. Central docking mechanism: obstacles after hatch opening.

To avoid this disadvantage, designers have looked into the possibilities of arranging the functional elements necessary for reception, mechanical guidance and capture at the periphery of the interface rings establishing the transfer tunnel (Syromiatnikov 1971, 1990). Most of the area inside the interface ring is then free for the passage, as only

a flat hatch has to be opened, as shown in figure 8.5. Reception and capture principles, such as the V-latch for unpressurised attachment (see figure 8.6), could be arranged in principle around the interface ring. Peripheral attachment systems also provide the possibility for an androgynous design. Whereas a central system will always have a male and a female side, a peripheral system can be arranged such that reception, guidance and capture functions are available on both sides. Such systems are called 'androgynous' (see also the next section) and have reception and guidance elements formed like the petals of a flower arranged around the docking ring. They were used for the first time in the Apollo–Soyuz docking project in 1975 (Swan 1976; Syromiatnikov 1990); figure 8.9. This basic design has been followed by practically all peripheral mating mechanism developments thereafter, and is presently used in the design of the APDS (Androgynous Peripheral Docking System, figure 8.10; Syromitnikov 1990), originally designed for the Russian space programme and now used for the docking of the US Space Shuttle with the ISS, and by the CBS (Common Berthing Mechanism, figure 8.13; Illi 1992), the attachment mechanism for the pressurised modules on the 'US' side of the ISS.

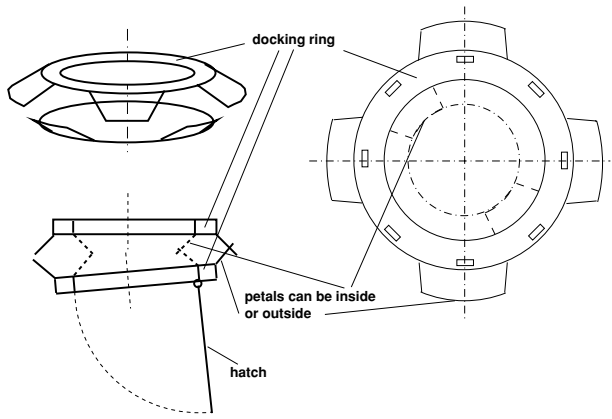

Figure 8.5. Peripheral docking/berthing mechanism: outside/inside petals, hatch opening.

Contact dynamics and shock attenuation systems are more complicated for peripheral docking systems than for central docking systems, due to the facts that the first contact will take place with peripheral systems on a point located on a circle around the docking axis with a diameter of the order of 1 m or more, and that, with the relatively large number of subsequent contacts at different places, a three-dimensional load pattern will be created. With central devices the first contact will occur at a distance from the docking axis of the order of 0.1 m, with not more than one or two subsequent contacts, which allows in many cases a representation of the contact dynamics by a two-dimensional model. Shock attenuation systems will be treated in more detail in section 8.3. As mentioned above, shock attenuation function will not be required in the case of berthing, as in this case the insertion velocities are generally very low.

8.2.3 Androgynous design of docking mechanisms

After the experience of the first manned space-flight programmes at the end of the 1960s, the idea of an androgynous docking mechanism emerged. Androgynous docking mechanisms have the same basic functions and interfaces on both sides, and both sides can play either the active or the passive role in the docking process. Androgynous design of the docking interfaces was seen as one of the prerequisites for the rescue of incapacitated spacecraft, and, further, as being able to provide increased operational flexibility, e.g. in the build-up and reconfiguration of more complex assemblies in space. A secondary effect of androgynous design is the increased reliability due to the redundancy of functions on both sides.

The price to be paid for these advantages is the increased mass, volume and complexity of the design and the according penalties on the vehicles concerning payload-carrying capability, concerning design for long term operation in space, etc. Then the question must be addressed of whether strict androgynous design is the optimal solution for all mission scenarios, or, in other words, whether there are design requirements which overrule the desire for identical functionality on both sides.

In a space station servicing scenario, the docking interfaces on the station's side may have to stay in orbit for a period of 10–20 years. Maintenance of all items of the docking mechanism facing outer space would have to be performed by extra-vehicular activity (EVA), which is not only technically difficult, but also a penalty concerning the operational resources (crew) available. It is, in this case, much better to arrange all design elements which may be sensitive to long term operation under space conditions on the side of the vehicle which is launched from ground to visit the space station. Such elements would be seals, damper elements and generally all active devices (electro-mechanical devices, lubricated bearings, etc.).

Considering the re-configuration of assemblies in space, it has to be taken into account (a) that for long term connections the priority of requirements may be different from those for a short term docking connection, and (b) that, for re-configuration, other assembly methods, i.e. berthing, may be available. In berthing, the issue of impact attenuation is of lesser importance, as we have already seen above, and bulky damper assemblies will not be necessary. If in a re-configuration two outside interfaces have to be mated, seals become a problem. However, since the connection to be made will, in such a re-configuration, be of long term nature, the potentially necessary extra effort of seal replacement by EVA would be justifiable. These few considerations show already that androgyny of the interfaces is a real advantage, although not all features of a docking mechanism need to be available in the assembly and re-configuration scenario of pressurised modules. In the design of the CBS of the ISS (see figure 8.13 below), these considerations have been taken into account.

For the rescue of incapacitated spacecraft, other overruling constraints play a role. An urgent need to bring back a spacecraft to ground exists only when it is manned. In the manned LEO scenarios, the spacecraft involved are either short term visiting vehicles or long term orbiting space stations. An orbital station needs to have a safe return vehicle

attached to it, as long as it has crew aboard. The type of mating mechanism by which this return vehicle is attached is of no importance, as long as it can quickly and safely depart in emergency situations. Manned visiting vehicles have their own re-entry and landing capabilities. If such spacecraft get into serious trouble before or after visiting the station, the chance of rescue by another vehicle would be very small, even if a fully androgynous docking system were available. The reasons for this are (a) the necessity to have a second vehicle and launch facilities to be in operational readiness during the flight and (b) the unpredictable orbital and operational conditions of the spacecraft to be rescued, for which no preparation is possible. Spacecraft designers will, therefore, rather invest their development efforts in making the vehicles more reliable concerning safe return to ground than in establishing a rescue capability.

In conclusion, neither the servicing scenario nor the rescue scenario can be considered as a driver for a fully androgynous design of docking mechanism. The greatest benefits from androgynous design of a mating mechanism can be obtained in a space station assembly scenario, where re-assembly of modules during build-up or later may become necessary. Such attachment mechanisms may, however, not need to include all functions of a docking mechanism. Further, not all features of an attachment mechanism for space station modules will need to have fully androgynous design. For instance, the CBS for the ISS, described below (figure 8.13), has an active half and a passive half.

8.2.4 Unpressurised docking/berthing mechanisms

If both of the vehicles to be mated are unmanned, a pressurised transfer tunnel and hermetic seals on the interface ring are generally not needed. This will significantly reduce the complexity of the mating mechanism. In the case of berthing, the mechanism can be reduced to the function of a structural connection latch. In docking the shock attenuation and capture functions are still necessary. The latter can be combined, however, with the structural connection function.

A typical example of the basic design principles of unpressurised docking or berthing mechanisms is the V-latch arrangement shown in figure 8.6. Such an arrangement typically consists of three or four latches arranged on the mating ring of the active vehicle, with handlebars as interfaces for the latches on the side of the passive vehicle. The latch consists of a V-shaped guiding structure and two arms, which after closure will prevent escape of the handlebar and will pull it down into its seat. In docking, if contact velocities are relatively small, the damping elements can be arranged between the fixed V-shaped structure and a V-shaped guiding structure, as indicated in the figure. For larger impact velocities, spring-damper elements may have to be arranged between the latches and the base structure, e.g. in an arrangement such as in the peripheral docking systems shown below.

This type of mechanism has been used in berthing operations by the US Space Shuttle, e.g. in the servicing and repair missions for the Hubble Space Telescope, and will be used in the ISS scenario for attachment of unpressurised payloads on to the truss. For docking,

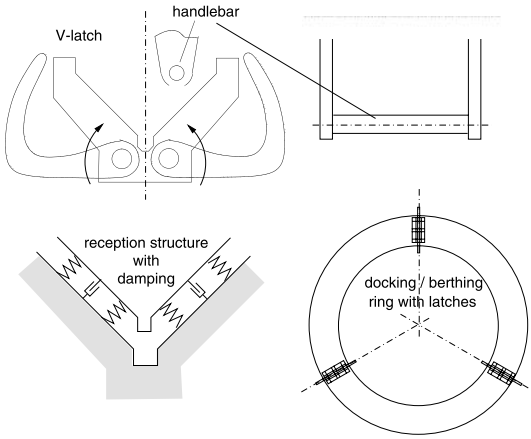

Figure 8.6. Unpressurised docking/berthing mechanism: V-latch.

this type of mechanism has been used in the rendezvous and docking demonstration of the Japanese ETS-VII mission in 1999 (Taniguchi *et al*. 1991; Ichikawa *et al*. 1993) described in section 10.7.3.

8.2.5 Examples of docking and berthing mechanisms

A few examples of previously developed docking mechanisms are described below. It is not the intention to provide here an exhaustive design description of these mechanisms, but rather to give them as examples for the requirements and features stated in the previous section. The functions of the typical elements of docking and berthing mechanisms are described in more detail in the following chapters. The first four of the examples given here are described in more detail in Syromiatnikov (1990).

The Apollo probe–drogue docking system

This is one of the first mature docking mechanism designs, and has been used in all Apollo missions in the Moon-landing and Skylab programmes.

The overall design is shown in figure 8.7. It is a central docking system of the type shown in figure 8.4, with a reception cone with a capture hole in the centre on the target side and a spherically suspended rod with shock attenuation on the chaser side. After first contact with the reception cone, the conical tip of the rod will be pushed into the capture hole. The tip is connected via a spherical bearing to the rod, allowing alignment with the surface of the reception cone. Upon entering into the capture hole, the spring-loaded capture latches on the tip of the rod will engage on the flange inside the entrance of the hole. Alignment between the two vehicles is achieved during retraction of the rod through a number of arms which form a cone and are connected to the base of the rod.

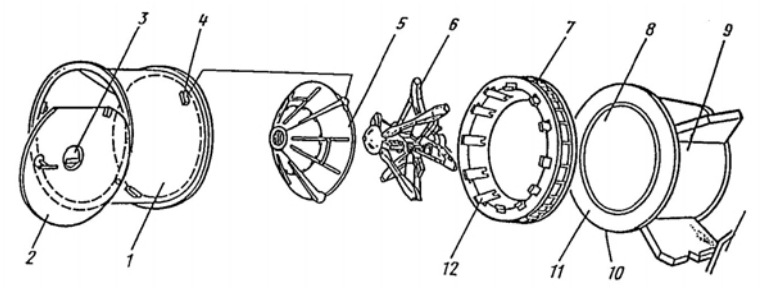

Figure 8.7. Example: Apollo docking mechanism (courtesy NASA).

Structural connection is achieved through 12 single-hook structural connection latches, which engage on the flange of the docking ring. The mechanism assembly for capture, damping and alignment has to be removed after opening of hatches to clear the transfer tunnel. The parts of figure 8.7 are as follows:

(1) docking ring of passive vehicle (on tunnel of Lunar Module),
(2) hatch of Lunar Module,
(3) valve for pressure equalisation,
(4) supports for receiving cone,
(5) receiving cone of passive vehicle,
(6) capture and alignment mechanism on active vehicle (Command Module),
(7) docking ring of active vehicle,
(8) (9), (10), (11) tunnel, hatch and sub-structure of active vehicle,
(12) structural latches of active vehicle.

The Russian probe–drogue docking system

This type of docking mechanism has been used in the Salyut and Mir Space Station scenarios for docking of the manned Soyuz and unmanned Progress spacecraft with the orbital station. It is also used in the ISS scenario for docking of the Soyuz, Progress and ATV vehicles at the Service Module side.

The first design without seals and latches for pressurised connection was developed at the same time as the Apollo system, and has been re-designed and refined thereafter during many years of application. The basic design of the system is shown in figure 8.8. It is similar to that of the Apollo probe–drogue docking system, i.e. a central docking system of the type shown in figure 8.5, with a reception cone and capture socket on the target side and a spherically suspended rod with shock attenuation on the chaser side. After first contact with the reception cone, the spherical tip of the rod will be pushed into the capture socket. Upon entering into it, the spring-loaded capture latches on the tip of the rod will engage their corresponding catches in the socket. Alignment between

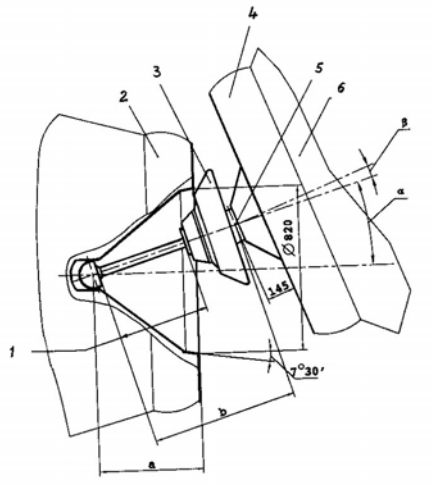

Figure 8.8. Example: Russian probe–drogue docking mechanism (courtesy RSC Energia).

the two vehicles is achieved during retraction of the rod through a convex cone (or a number of arms forming such a cone) at the base of the rod. For structural connection, double-hook type connection latches are used (see section 8.4.1). The hooks engage each other and can be operated from both the chaser and target side. As in the Apollo case, the mechanism complex for capture, damping and alignment has to be removed after opening of hatches to clear the transfer tunnel. Utility connections for power, data and fluid transfer are performed automatically. The parts of figure 8.8 are as follows:

(1) capture rod (probe) with extension stroke (in extended position),
(2) docking ring with receiving cone structure (drogue) of passive vehicle,
(3) angular limiting device,
(4) docking ring of active vehicle,
(5) spherical bearing of capture rod,
(6) substructure of active vehicle.

The Apollo–Soyuz androgynous peripheral docking system

This is the ancestor of all peripheral docking/berthing mechanisms. The two sides of the system were developed, according to a joint interface specification, independently by the USA and the Soviet Union for the Apollo–Soyuz demonstration mission in 1975. This was the first attempt to design an androgynous mechanism, i.e. each side can be active or passive, and each half mechanism could be mated with a copy of it. For the

demonstration mission both sides developed its own mechanism, in which the geometry of reception petals and contact ring, capture latch and structural latch interfaces was prescribed, but most of the detailed design was at the discretion of each of the parties. In the demonstration mission, each side assumed once the active and once the passive role. In figure 8.9, the Apollo side is shown in the passive configuration with the contact ring retracted to the docking ring, and the Soyuz side is shown in the active extended configuration.

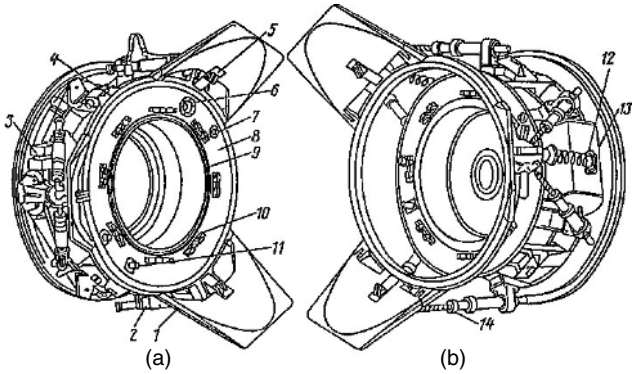

Figure 8.9. Example: Apollo–Soyuz docking mechanism assembly (courtesy NASA, RSC Energia). (a) Apollo side; (b) Soyuz side.

First contact occurs between the flanks of the three guiding petals mounted on the outside of each of the contact rings. The contact rings are separated from the structural connection ring (docking ring) by six dampers arranged in a 'Stewart platform' setup. On the active side, the dampers are extended; on the passive side they are retracted. Each petal carries a spring-loaded capture latch, which acts on a latch-catch on the opposite ring. After contact, the active contact ring will be pushed toward the passive one and will be aligned with it so that the capture latches will engage their corresponding catches. After successful capture, retraction of the contact ring is performed by motor drives via the damper screws on the Soyuz side and via three cables on the Apollo side. For structural connection, eight double-hook type latches of the Soyuz mechanism design described above were used. The parts of figure 8.9 are as follows:

(1) contact ring with petals,
(2) hydraulic shock attenuators,
(3) docking mechanism drive (retraction),
(4) capture latch-catch,
(5) capture latch,
(6) alignment guide socket,
(7) push rod (for separation),
(8) docking ring,
(9) seal rings,

(10) structural latches (hooks),
(11) alignment guide pin,
(12) flexible cable,
(13) differentials unit with docking mechanism drive,
(14) screw with bearing-screw converter.

The APDS Androgynous Peripheral Docking System

The APDS is an improved development of the Apollo–Soyuz docking system. It was intended originally for the Russian 'Buran' spaceplane, and an according interface was mounted on the Cristal module of the Mir Space Station. After termination of the Buran project, it was used with some modifications by the US Space Shuttle visits to Mir, and is now used for the docking of the Space Shuttle to the ISS.

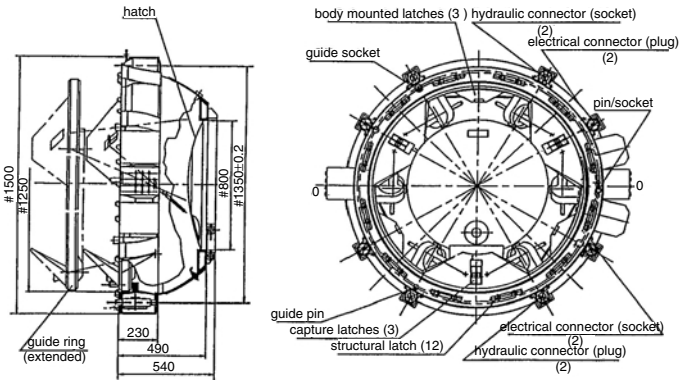

Figure 8.10. Example: APDS docking mechanism assembly (courtesy RSC Energia).

The basic functions of the APDS (see figure 8.10) are identical to those of the Apollo–Soyuz peripheral docking mechanism. First contact between the mechanism halves mounted on chaser and target will occur between the three petals mounted on the contact rings of each side. In contrast to the Apollo–Soyuz mechanism, the petals point to the inside of the docking tunnel. The contact ring (guide ring) is, as in the previous example, separated from the structural connection ring (docking ring) by a spring-damper system arranged in a 'Stewart platform' setup. In the middle of each petal is mounted a capture latch, which engages on a latch-catch, mounted on the docking ring flange of the opposite mechanism. After capture, the contact ring will be retracted using the screws of the damper elements. Because of the larger seal diameter (compared with that of the previous example), 12 double-hook type structural latches are arranged on the docking ring. Utility connections for power, data and fluid transfer are performed automatically.

The Hermes–Columbus docking system

This is an example of a peripheral docking mechanism design for very low approach velocities (0.01–0.03 m/s). Because of the discontinuation of the Hermes and Columbus

Free-Flyer Programmes, this mechanism has never been flown. However, a prototype has been built and dynamically tested (Gonzales-Vallejo *et al*. 1992). The design is discussed here because of the different design principles used for the capture and damping functions.

In this design (see figures 8.11 and 8.12), the functions of capture latch and retraction mechanism are combined. Only the active half of the docking system has capture latches and damping functions. Closure of a capture latch is initiated upon the entrance of the interface of the passive side into the reception range, which is detected by light sensors. First contact again occurs between the flanks of the guiding petals mounted either on the outside or the inside of each of the contact rings.

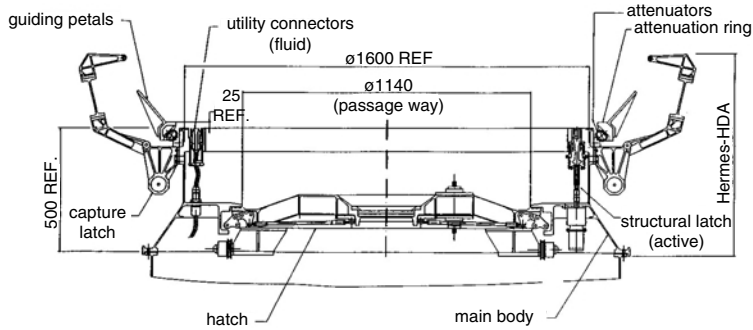

Figure 8.11. Example: Hermes–Columbus docking mechanism (courtesy ESA).

The contact ring and the structural connection ring of the active half of the system are separated by a friction damper ring. Because of the capture strategy (see section 8.3.5) and the very low approach velocity, damping by friction devices was found to be sufficient. These small devices are in the form of spring-friction coils (see figure 8.24), designed only for attenuation of the contact shock at very low velocities, but not for achieving alignment and capture. Four active capture latches are mounted either inside or outside the docking ring of the active side. Twelve structural latches of the bolt and nut type are arranged on the inside of the tunnel, i.e. inside the seals, allowing removal/replacement by intra-vehicular activity (IVA). Utility connections should be made manually after hatch opening. The type and number of latches have been chosen because of the large diameter of the sealing ring ($>$1.6 m).

The NASA ISS Common Berthing Mechanism

This mating system (see figure 8.13) has been designed for connection of large space station modules (Illi 1992). The major design requirement is a large hatch diameter, allowing the transfer of standard ISS double racks (1055×900 mm cross section). As a

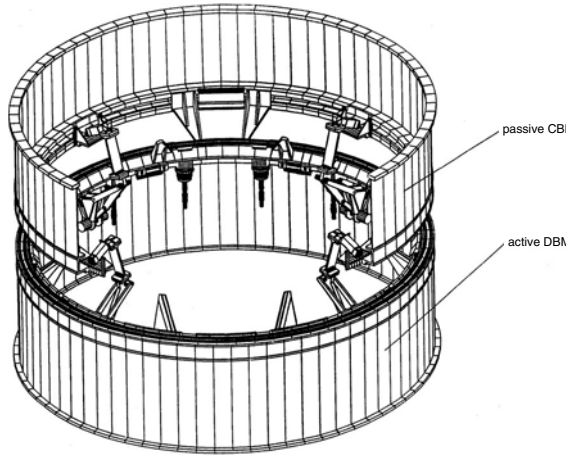

Figure 8.12. Example: Hermes–Columbus docking mechanism with inside petals (courtesy ESA).

result, the berthing ring has an inner diameter of about 1.8 m. Guiding petals are on the inside of the connection ring and can be removed after pressurisation and hatch opening. The mechanism does not need a damping function, as the insertion velocity during the manipulation is very low and as there is no limitation concerning the capture time.

Four capture latches are mounted on the inside of the connection ring, which are used for grappling the counterpart after insertion by the manipulator and fulfil the function of retraction and alignment of the two mechanism halves in preparation for structural connection. Similarly for the guiding petals, the capture latches are inside mounted, and will be removed, once long term connection has been established. Sixteen structural latches of the bolt and nut type are arranged inside the seals, allowing removal/replacement by IVA. Also, all utility connections are inside the seals, and connection will be established manually.

The NASA Low Impact Docking Mechanism

A prototype of this peripheral docking mechanism design has been developed by a team of NASA and Lockheed Martin engineers at the Johnson Space Center (JSC) for docking and berthing of the X-38 and crew return vehicles to the ISS (Lewis & Carroll 1999). An early version of this mechanism is shown in figure 8.14. The three petals for reception and mechanical guidance are directed to the inside. Along with the Stewart platform arrangement of the attenuation system they are analogue to other peripheral systems. This mating system has two interesting and novel design features: a force sensor driven, closed loop controlled electro-mechanical alignment and attenuation system with linear actuators and an electro-magnetic capture latch system.

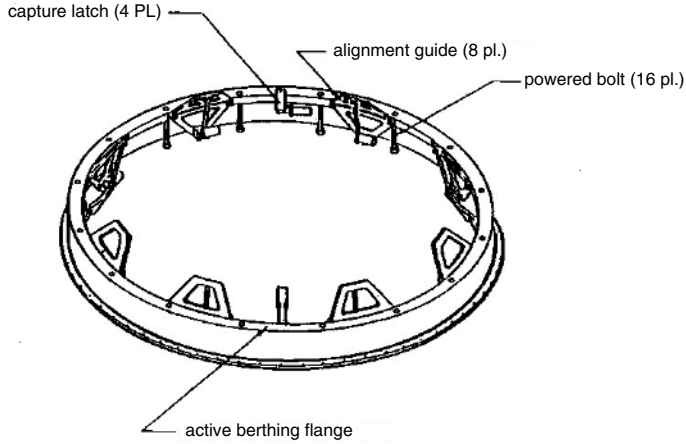

Figure 8.13. Example: ISS Common Berthing Mechanism (courtesy NASA).

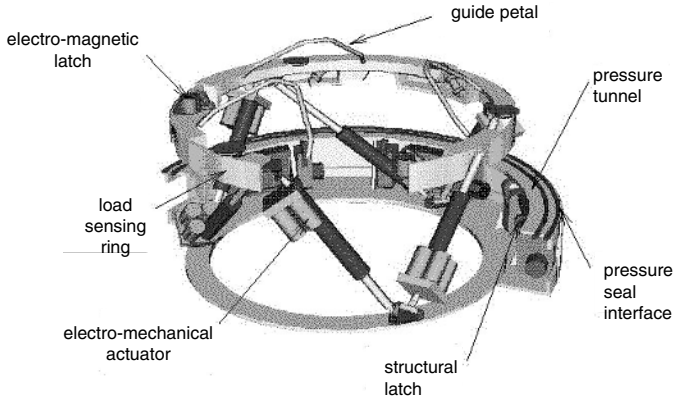

Figure 8.14. Example: cut away view of Low Impact Docking Mechanism (courtesy NASA).

At contact, the six force sensors, which are arranged at 45 deg w.r.t. the contact ring in a similar way to the linear actuators, determine magnitude and direction of the force vector and the point of force application. The control loops are closed via the six linear actuators to align the contact ring with the contact ring on the target, i.e. the forces sensed by the force sensors are balanced. At this stage, the three electromagnets are engaged to latch the contact ring of the target onto that of the chaser. The attenuation of the approach velocity is then achieved by the closed loop control system, where the required damping characteristics can be programmed into the control software. The retraction of the contact ring to join the structural connection ring with the seals is performed by further reduction of the extension of the six linear actuators.

8.3 Contact dynamics/capture

8.3.1 Momentum exchange at contact

The movement of and between two bodies after contact can be derived from the momentum law. For translational motion over the time period $\Delta t = t_1 - t_0$, the relation between the change of velocity vector $\Delta\mathbf{V}$ and the force $\mathbf{F}$ on a body with the mass m is

$$\int_{t_0}^{t_1} \mathbf{F}\mathrm{d}t = m \cdot \Delta\mathbf{V} \tag{8.1}$$

If the point of impact is not located on a line connecting the CoMs of the two bodies, the change of angular momentum must also be taken into account:

$$\mathbf{I} \cdot \Delta\boldsymbol{\omega} = \int_{t_0}^{t_1} (\mathbf{r} \times \mathbf{F})\, \mathrm{d}t \tag{8.2}$$

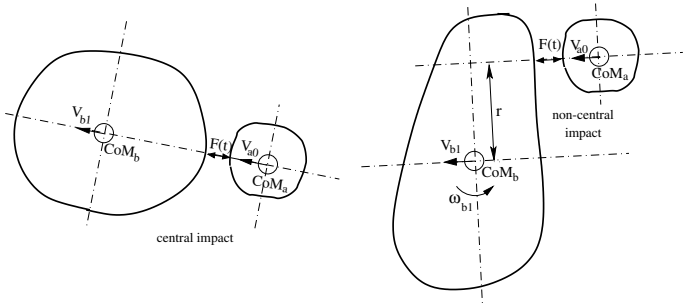

Figure 8.15. Basic relations at contact.

where $\Delta\boldsymbol{\omega}$ is the change in the angular velocity vector of the body during the time period $\Delta t = t_1 - t_0$, $\mathbf{I}$ is the inertia tensor of the body and $\mathbf{r}$ is the distance vector between the

contact point and the CoM of body b. The two types of impact are shown in figure 8.15. The first one, where the line of impact forces goes through the CoMs of both bodies, is called 'central' impact; the second one with a lever arm r w.r.t. the CoM of one or both of the bodies is called 'non-central' or 'eccentric' impact.

The effects of momentum exchange at contact between two bodies can be explained most simply by examining the simplified case of an impact along one of the main axes, e.g. the x-axis. For a central impact, Eq. (8.1) becomes

$$\int_{t_0}^{t_1} F_x(t)\mathrm{d}t = m\Delta V_x \tag{8.3}$$

Considering two impacting bodies a and b with masses m_a and m_b and velocities in the x-direction $V_\mathrm{a}(t)$ and $V_\mathrm{b}(t)$, respectively, the changes of velocity due to the impact are

$$m_\mathrm{a}(V_\mathrm{a1} - V_\mathrm{a0}) = -\int_{t_0}^{t_1} F_x\mathrm{d}t \tag{8.4}$$

$$m_\mathrm{b}(V_\mathrm{b1} - V_\mathrm{b0}) = \int_{t_0}^{t_1} F_x\mathrm{d}t \tag{8.5}$$

where V_a0 is the velocity of body a at contact, t_0 is the time at contact and t_1 can be any time during the impact, i.e. before the two bodies have separated again.

The impact can be divided into two parts: a compression phase and an expansion or restitution phase. At the end of the compression phase, i.e. when the two bodies have assumed the closest distance, they have the same joint velocity $V_\mathrm{c} = V_\mathrm{a1} = V_\mathrm{b1}$. This is also the case if we assume that capture takes place, i.e. the combined body will continue to move with the common velocity V_c. As the forces acting on the two bodies are equal in magnitude, but opposite in direction, we can write for the case of a central impact

$$m_\mathrm{b}(V_\mathrm{c} - V_\mathrm{b0}) = -m_\mathrm{a}(V_\mathrm{c} - V_\mathrm{a0}) \tag{8.6}$$

$$V_\mathrm{c} = \frac{m_\mathrm{a}V_\mathrm{a0} + m_\mathrm{b}V_\mathrm{b0}}{m_\mathrm{a} + m_\mathrm{b}} \tag{8.7}$$

If capture is not successful, the forces of the springs of the spring-damper system of the docking mechanism will cause the two vehicles to separate again after the impact.

For a non-central impact, let us consider again the simple case of an impact of body a on body b with a velocity V_a in the x-direction, where on body a the force line passes through the CoM, but where on body b a distance r exists in the y- or z-directions between the impact line and the CoM. Assuming further that the value of r will not change during the time $t_1 - t_0$, the angular momentum Eq. (8.2) for body b becomes

$$I_\mathrm{b} \cdot (\omega_\mathrm{b1} - \omega_\mathrm{b0}) = r \cdot \int_{t_0}^{t_1} F_x(t)\mathrm{d}t \tag{8.8}$$

For simplicity, we also assume that

$$V_{\mathrm{b}0} = 0 \tag{8.9}$$

$$\omega_{\mathrm{b}0} = 0 \tag{8.10}$$

At the end of the compression phase, or at the instant of capture, both bodies have, at the contact point, the same velocities, where on body b the velocity is the sum of a translation of the CoM and of an additional translation of the impact point due to the induced angular velocity about the CoM:

$$V_{\mathrm{c}} = V_{\mathrm{a}1} = V_{\mathrm{b}1} + r \cdot \omega_{\mathrm{b}1} \tag{8.11}$$

Whereas the momentum equation for body a is still Eq. (8.4), for body b the two equations (8.5) and (8.8) have to be considered for the momentum exchange. They become, with the initial conditions (8.10):

$$m_{\mathrm{b}} V_{\mathrm{b}1} = \int_{t_0}^{t_1} F_x \mathrm{d}t \tag{8.12}$$

$$\frac{I_{\mathrm{b}}}{r}\omega_{\mathrm{b}1} = \int_{t_0}^{t_1} F_x \mathrm{d}t \tag{8.13}$$

From these equations, and with Eqs. (8.4) and (8.11), one obtains for the translational motion of body b

$$V_{\mathrm{b}1} = V_{\mathrm{a}0} \frac{I_{\mathrm{b}} \cdot m_{\mathrm{a}}}{I_{\mathrm{b}}(m_{\mathrm{b}} + m_{\mathrm{a}}) - r^2 m_{\mathrm{a}} m_{\mathrm{b}}} \tag{8.14}$$

and, for the angular motion,

$$\omega_{\mathrm{b}1} = V_{\mathrm{a}0} \frac{r \cdot m_{\mathrm{a}} \cdot m_{\mathrm{b}}}{I_{\mathrm{b}}(m_{\mathrm{b}} + m_{\mathrm{a}}) - r^2 m_{\mathrm{a}} m_{\mathrm{b}}} \tag{8.15}$$

In a real case, the impact will not be along one of the main axes, nor will the docking axis necessarily go through the CoM. To calculate the impact forces and the dynamic reactions of the two vehicles during and after contact, the exact point of contact and the angles of the impact line w.r.t. the body coordinates of the two spacecraft will have to be determined as a first step. The details of these calculations depend on the geometry of the vehicles and their docking interfaces, and on the state vectors of both spacecraft. Because of the complex geometrical relations at contact, they will become quite elaborate. However, for a basic understanding of the contact and capture processes, they are not needed here.

8.3.2 Shock attenuation dynamics

If two compact bodies impact with each other, the elastic and/or plastic deformations will be relatively small, depending on the material properties. As a result, the impact

time will be relatively short, and accordingly the forces will be relatively high. For docking of two spacecraft, this would have as a consequence high structural loads and a very short time for capture. In order to reduce contact forces and to increase the time available for capture, shock absorber devices are applied in the docking mechanism which are designed to increase the amount of travel after contact due to elastic and plastic deformation and to absorb a part of the kinetic energy by viscous damping and/or friction. In both cases, velocity proportional damping or constant friction, a part of the kinetic energy of the relative motion is converted into heat.

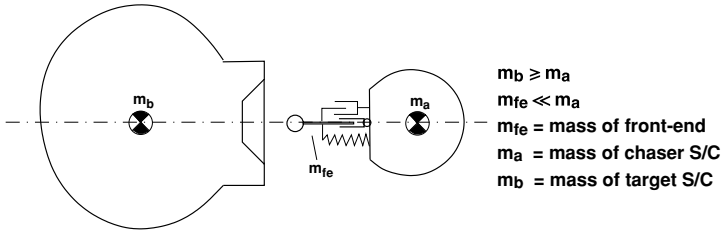

Figure 8.16. Simplified model: central impact with spring-damper system.

The function of shock attenuation systems for spacecraft mating can be best explained using the above simple example of a central impact along the x-axis of two impacting bodies and putting a shock attenuator in between (see figure 8.16). As a rule, shock attenuation systems consist of elastic elements, i.e. springs, and elements converting the motion energy into heat. The mass of the shock absorber system is assumed to be very small compared with the masses of each of the vehicles. The energy conversion functions are known as dampers, which can be implemented either as velocity dependent friction devices, as constant friction devices or as a combination of both. Velocity dependent friction devices can be, e.g., viscous dampers, where a fluid is pressed through a narrow gap or orifice and the resistance force is dependent on the speed through the gap, or, e.g., eddy current dampers, where the resistance torque is dependent on the angular velocity of a metal disc rotating in a magnetic field.

The equation of motion of a mass connected via a spring and a velocity proportional damper to a fixed point in an inertial frame is

$$F_x(t) = m\,\ddot{x} = -D\dot{x} - Cx \pm F_\mathrm{f} \tag{8.16}$$

where D is the damping constant, C is the spring constant and F_f is the constant friction force. The sign of the friction force is always opposite to the direction of motion.

For the case that two masses m_a and m_b are connected by a spring and viscous damper system (figure 8.16), the equations of motion are, for body a,

$$m_\mathrm{a}\,\ddot{x}_\mathrm{a} = -D\Delta\dot{x} - C\,\Delta x \tag{8.17}$$

and, for body b,

$$m_\mathrm{b}\,\ddot{x}_\mathrm{b} = +D\Delta\dot{x} + C\,\Delta x \tag{8.18}$$

where $\Delta x = x_1 - x_0$ is the distance and $\Delta \dot{x} = \dot{x}_1 - \dot{x}_0$ is the relative velocity between the two bodies. Subtraction of these equation yields

$$\Delta \ddot{x} = \ddot{x}_1 - \ddot{x}_0 = -(D\Delta \dot{x} + C\,\Delta x)\left(\frac{1}{m_\mathrm{a}} + \frac{1}{m_\mathrm{b}}\right)$$

which can be written as

$$\Delta \ddot{x} = -(D\Delta \dot{x} + C\,\Delta x)\frac{1}{m_\mathrm{e}} \tag{8.19}$$

where m_e is the equivalent mass of the system:

$$m_\mathrm{e} = \frac{m_\mathrm{a} \cdot m_\mathrm{b}}{m_\mathrm{a} + m_\mathrm{b}} \tag{8.20}$$

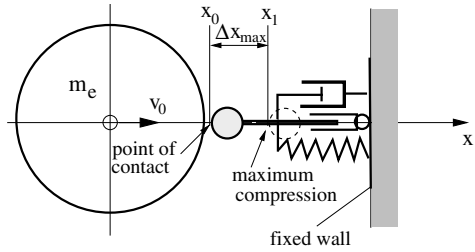

Figure 8.17. Simplified equivalent mass model for central impact.

The simplified spring-damper model with an equivalent mass is shown in figure 8.17. This definition has the advantage that only the relative motions between the two masses need to be considered, not the motions of the individual masses w.r.t. any other frame, e.g. related to pre-contact conditions. The definition of an equivalent mass is also valid for a constant friction damper system, as can be easily derived. Eq. (8.16) shows that there are several possible ways of reducing the kinetic energy $(1/2 \cdot m\dot{x}^2)$:

- by a spring,
- by solid friction braking,
- by velocity proportional braking,
- by a combination of two or all of these functions.

Shock attenuation by spring only

For this case the equation of motion becomes

$$m_\mathrm{e}\ddot{x} = -Cx \tag{8.21}$$

The well-known solution of this differential equation is

$$x(t) = c_1 \cos \omega_1 t + c_2 \sin \omega_1 t \tag{8.22}$$

where the resonant frequency $\omega_1 = \sqrt{C/m_\mathrm{e}}$. The constants can be obtained from the boundary conditions for t_0:

$$c_1 = x_0; \quad c_2 = \frac{v_0}{\omega_1} \tag{8.23}$$

Damping by solid friction braking only

For this case the equation of motion becomes

$$m_\mathrm{e} \ddot{x} = \pm F_\mathrm{f} \tag{8.24}$$

The direction of the friction force is always opposite to the direction of the velocity. The solution for the travel over time can be found easily by double integration:

$$x(t) - x_0 = \Delta x(t) = \left(v_0 \pm \frac{F_\mathrm{f}}{2m_\mathrm{e}} t \right) t \tag{8.25}$$

The equation is valid up to the time where $\mathrm{d}x/\mathrm{d}t$ becomes zero.

Damping by velocity proportional braking only

For this case, the equation of motion becomes

$$m_\mathrm{e} \ddot{x} = -D\dot{x} \tag{8.26}$$

This equation can easily be integrated once. Thereafter, the solution for the travel over time can be obtained, using the homogeneous solution ($y = c\cdot$) of a first order linear differential equation $\exp\left(\int_p dt\right)$ ($\dot{y}+py = 0$). With the substitutions $D/m_\mathrm{e}x(t) - c_1 = y$ and $D/m_\mathrm{e} = p$, the equation can be brought into the above form, yielding the following result:

$$x(t) - x_0 = \Delta x(t) = -\frac{m_\mathrm{e}}{D} v_0 (\mathrm{e}^{-\frac{D}{m_\mathrm{e}} t} - 1) \tag{8.27}$$

Combination of a velocity proportional braking device and spring

For this case the equation of motion becomes

$$F_x(t) = m\,\ddot{x} = -D\dot{x} - Cx \tag{8.28}$$

Solutions are available for this type of differential equation, if it is written in the following form:

$$\ddot{x} + 2\delta\dot{x} + \omega_1^2 x = 0$$

where the coefficients are $\omega_1^2 = C/m$ and $2\delta = D/m$. The constant ω_1 is again the resonant frequency of the spring–mass system. The solutions are

$$x(t) = \mathrm{e}^{-\delta t}(k_1 \cos \lambda t + k_2 \sin \lambda t) \text{ for } \lambda^2 = \omega_1^2 - \delta^2 > 0 \tag{8.29}$$

$$x(t) = \mathrm{e}^{-\delta t}(k_1 \cosh \lambda t + k_2 \sinh \lambda t) \text{ for } \lambda^2 = \omega_1^2 - \delta^2 < 0 \tag{8.30}$$

$$x(t) = \mathrm{e}^{-\delta t}(k_1 + k_2 t) \text{ for } \lambda^2 = \omega_1^2 - \delta^2 = 0 \tag{8.31}$$

The first case represents an oscillation with low damping, the second one with high damping and the last one is the boundary case of aperiodic damping. This third case, where $\omega_1^2 = \delta^2$, is the optimal case for avoidance of oscillations. This condition will in real cases never be met exactly, but it is very useful as a reference case for the assessment of spring-damper systems, as it leads to simple mathematical expressions which can be quickly evaluated. The constants k_1 and k_2 can easily be determined from the boundary conditions:

$$\begin{aligned} k_1 &= x_0 \\ k_2 &= v_0 + \delta x_0 \end{aligned} \tag{8.32}$$

where Δx_0 and v_0 are the conditions at the start of the motion. With these constants, and using the definitions of Eqs. (8.19) and (8.20), the equations for the relative position Δx (from Eq. (8.31)), the relative velocity $v = \Delta \dot{x}$, and the relative acceleration $\Delta \ddot{x}$ between the two bodies after contact become

$$\Delta x(t) = \mathrm{e}^{-\delta t}[\Delta x_0 + (v_0 + \delta \Delta x_0)t] \tag{8.33}$$

$$\Delta \dot{x}(t) = \mathrm{e}^{-\delta t}[v_0 - (v_0 + \delta \Delta x_0)\delta t] \tag{8.34}$$

$$\Delta \ddot{x}(t) = \delta \mathrm{e}^{-\delta t}[(v_0 + \delta \Delta x_0)\delta t - 2v_0 - \delta \Delta x_0] \tag{8.35}$$

For our application, Δx_0 is always zero, as the spring-damper system is in a neutral position at the instant of contact. The maximum possible compression, $\Delta x_{\max}$, shown in figure 8.17, is a constraint imposed by the design of the system; it is not the maximum excursion due to the dynamics of the impact. In fact, the spring-damper parameters, including the maximum possible excursion, have to be chosen such that they are valid for all dynamic conditions potentially occurring in a particular mission scenario.

The definition of the factor δ for the aperiodic case according to Eq. (8.31) is

$$\delta = \omega_1 = \sqrt{\frac{C}{m_\mathrm{e}}} \tag{8.36}$$

From Eqs. (8.33), (8.34) and (8.35) the relative motion and force over time between the two bodies can easily be calculated. For the central impact case, the force acting between the two sides is according to Eq. (8.28) and the definition of the equivalent mass in Eq. (8.20):

$$F_x(t) = m_\mathrm{e} \Delta \ddot{x}$$

8.3.3 Example case for momentum exchange and shock attenuation

Let us consider two spacecraft, which are docking with the following impact conditions:

- the chaser has mass $m_{\mathrm{a}} = 10 \times 10^3$ kg;
- the target has mass $m_{\mathrm{b}} = 100 \times 10^3$ kg;
- the target has an inertia about the y-axis of $I_{yy} = 10 \times 10^6\,\mathrm{kg\,m^2}$;
- the approach velocity is $V_{\mathrm{a1}} = v_0 = 0.1$ m/s;
- the target has no velocities w.r.t. the reference frame, i.e. $v_{\mathrm{b1}} = 0$ and $\omega_{\mathrm{b1}} = 0$.

Momentum exchange

For a central impact, the joint velocity after capture is, according to Eq. (8.7),

$$V_{\mathrm{c}} = \frac{m_{\mathrm{a}} V_{\mathrm{a0}} + m_{\mathrm{b}} V_{\mathrm{b0}}}{m_{\mathrm{a}} + m_{\mathrm{b}}} = 0.0091\,\mathrm{m/s}$$

The change in velocity of the combined target and chaser vehicle after docking is, in this example case, not very large. However, a velocity change of the order of 0.01 m/s results in an orbital motion of the combined spacecraft w.r.t. the original target position, as shown in figure 3.10, i.e. an advance of the order of 170 m per orbital revolution. In a non-central impact case, if we assume the impact line has a distance of $r = 10$ m to the CoM, the angular velocity induced on body b is, according to Eq. (8.15),

$$\omega_{\mathrm{b1}} = V_{\mathrm{a0}} \frac{r \cdot m_{\mathrm{a}} \cdot m_{\mathrm{b}}}{I_{\mathrm{b}}(m_{\mathrm{b}} + m_{\mathrm{a}}) - r^2 m_{\mathrm{a}} m_{\mathrm{b}}} = 10^{-3}\,\mathrm{rad/s} = 0.057\,\mathrm{deg/s}$$

The resulting angular velocity of the target vehicle is, in this example, very small and could easily be handled by the attitude control system.

Shock attenuation

The equivalent mass of the system is, according to Eq. (8.20),

$$m_{\mathrm{e}} = \frac{m_{\mathrm{a}} \cdot m_{\mathrm{b}}}{m_{\mathrm{a}} + m_{\mathrm{b}}} = 9091\ \mathrm{kg}$$

In the following, shock attenuation characteristics with different types of attenuators are discussed.

Spring only attenuator Selecting a spring constant of $C = 90.91$ N/m, the resonant frequency becomes

$$\omega_1 = \sqrt{\frac{C}{m_\mathrm{e}}} = 0.1\,/\mathrm{s}$$

With the selected value for ω_1 and with the constants $c_1 = x_0 = 0$ and $c_2 = v_0/\omega_1 = 1.00$ m, Eq. (8.22) becomes

$$x(t) = 1 \sin{(0.1t)}\ \mathrm{m}$$

The result is shown in the left hand curve of figure 8.18. The maximum excursion of 1 m is reached after approximately 16 s, and the reception range is left again after approximately 31 s.

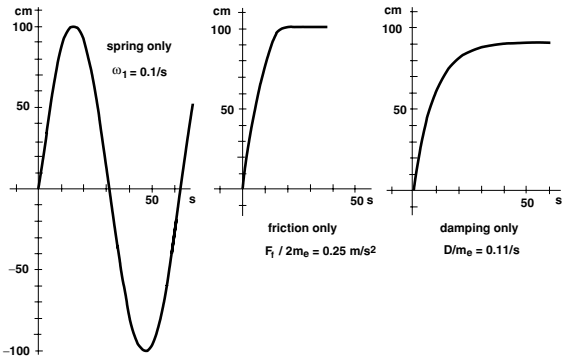

Figure 8.18. Travel after impact for spring only, friction only and damper only cases.

Friction only attenuator To achieve an attenuation curve which is comparable to the others, a factor of $F_\mathrm{f}/2m_\mathrm{e} = 0.0025\mathrm{m/s}^2$ has been chosen, which, for the equivalent mass of 9091 kg, corresponds to a friction force of $F_\mathrm{f} = 45.5$ N. With the boundary conditions $v_0 = 0.1$ m/s and $x_0 = 0$, Eq. (8.25) becomes

$$x(t) = 0.1t - 0.0025t^2\ \mathrm{m}$$

(valid for $\mathrm{d}x/\mathrm{d}t > 0$). The result is shown in the centre curve of figure 8.18. The curve is parabolic up to its maximum, where $\mathrm{d}x/\mathrm{d}t = 0$, and continues with $x(t) = \text{const}$. With the chosen friction force the maximum excursion is, as in the previous case, 1 m, which is reached after 20 s. The curve shows also that, due to the quadratic term in Eq. (8.25), the maximum braking effect occurs only toward the end. This makes the pure friction damper quite sensitive to parameter uncertainties. Such uncertainties may be due to friction at the start of motion and to variations of friction coefficient as a function of the surface properties.

Viscous damping only attenuator The damping factor has been chosen to be $D/m_e = 0.11$ 1/s, which for the chosen mass m_e corresponds to a damping constant of $D = 1000$ kg/s. This is half of the amount used in the next case of an aperiodic spring-damper system, but leads, concerning the maximum excursion, to more comparable results with the two previous cases. Equation (8.27) becomes, with $v_0 = 0.1$ m/s and $x_0 = 0$,

$$x(t) = -9.1 \times 0.1(\mathrm{e}^{-0.11t} - 1) \ \mathrm{m}$$

The right hand curve in figure 8.18 shows the advantage of velocity proportional damping over friction damping. The maximum excursion is reached after approximately 40 s and the velocity is reduced steadily. This behaviour is much less sensitive to parameter uncertainties than that owing to the pure friction case.

Aperiodic spring – viscous damper The coefficient δ is, for the aperiodic case, equal to the resonant frequency, i.e. $\delta = \omega_1 = 0.1$/s, which corresponds to a damping factor of $D = 2000$ kg/s. With v_0 = 0.1 m/s and $x_0 = 0$, we obtain from Eqs. (8.33)–(8.35) the behaviour over time for the relative distance, the relative velocity and the relative deceleration between the vehicles. The results are shown in figure 8.19.

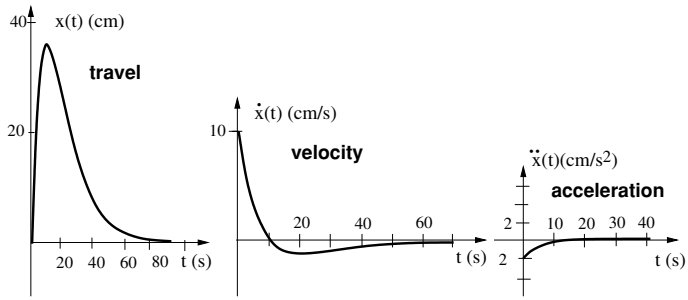

Figure 8.19. Travel, velocity and acceleration after impact for spring-damper case.

With the chosen parameters, the maximum travel of the spring-damper system is about 0.37 m after 10 s. The maximum deceleration at the beginning of the impact is 0.02 m/s^2, which is reduced to $<$0.004 m/s^2 after 20 s. The maximum force at the beginning of the impact is, in this example,

$$\Delta\ddot{x} \cdot m_e = 0.02 \ \mathrm{m/s^2} \times 9091 \ \mathrm{kg} = 181.82 \ \mathrm{kg \ m/s^2}$$

The force of 182 N is equivalent to that of a thruster, which is very small for a docking impact. The maximum time available for capture can be assumed to be the time at which the contact surface of body a (in figure 8.16 the body with the mass m_e) has moved back beyond the position x_0. In figure 8.19, this time is determined by the crossing with the x-axis of the tangent through the inflection point of the $x(t)$-curve, as the bodies would

separate with the maximum negative velocity gained during expansion. In our example, this time would be about 40 s.

The example shows that, with the chosen parameters, the available capture time is very long and the maximum forces are very low. This is at the expense of a large excursion of the spring-damper system, which would require a mechanism of large dimensions, resulting in an unnecessary mass and volume penalty to the spacecraft. Increasing the spring constant by a factor of 25, the parameter δ would be increased to $\delta = 0.5$, which would result in a maximum excursion of the spring-damper system of 0.075 m, in a maximum time available for capture of approximately 8 s and a maximum deceleration at start of impact of 0.1 m/s^2. Both capture time and maximum acceleration are still comfortable, but the necessary size of the mechanism can be decreased by a factor of 5.

Comparison of attenuator types

On comparing the different types of attenuators, the following conclusions can be drawn:

- A spring alone is an effective attenuator in its first quarter of oscillation. It will, however, change direction of motion after its maximum excursion and would eventually push the interfaces out of the reception range. If the time available for capture is long and the contact forces low, the resonant frequency needs to be low and the maximum excursion will be accordingly large.

- Solid friction can be easily made use of in attenuation devices; in fact, the friction present in practically all mechanisms can be included in the attenuation process. As a 'stand-alone' attenuator, however, it will be less suitable, because of its sensitivity to parameter variations.

- The velocity proportional damper is a very effective 'stand-alone' attenuator with smooth braking characteristics over time (with low decelerations). In contrast to all attenuators including a spring, it does not change its direction of motion. This makes it particularly suitable for motion braking prior to capture.

- The aperiodic spring-damper combination cancels all oscillations within the first cycle. For systems where capture is initiated immediately after entering the reception range, this attenuator type offers the combination of optimal oscillation damping with shorter excursion than the other types. For systems where capture is initiated toward the end of the excursion, the characteristics of this attenuator type are suitable for damping of the residual motion after capture.

As all of the attenuator types are obviously sensitive to the value of the initial contact velocity, the actual excursion after contact remains uncertain. This could cause a 'hard' impact if the excursion stroke available from the mechanism is smaller than the maximum excursion of the natural motion according to the contact velocity. For this reason,

a type of progressive spring function in the form of a stack of springs with increasing spring constant is implemented in many designs.

It must be kept in mind that the simplified one-dimensional model with a single 'equivalent' mass, used here for the discussion of attenuation behaviour, can provide no more than an idea of the real dynamic processes and only a rough order of magnitude of the expected forces, excursions and duration. Results of this simplified model can be used to assess the preliminary design of an attenuation system concerning the necessary stroke, spring and damping constants, etc. The reality, involving six DOF motion, multiple masses, inertias and flexibilities, leads to very complex models, which can only be evaluated numerically (e.g. using the Runge–Kutta integration method) by means of computer simulation programs.

8.3.4 Devices for shock attenuation and alignment for capture

Shock attenuation systems for central docking systems

As the active part of a central docking system is a rod which is elastically connected to the main body of the chaser, two main forces will occur at contact: a longitudinal force along the rod axis; and a lateral force which causes a torque about the connection point at its base. Accordingly, a longitudinal motion, i.e. a compression (and later, if there is a spring, an expansion) along the rod axis and an angular motion of the rod about the spherical bearing at its base have to be attenuated. The damping of the longitudinal motion can be performed with one of the damper types discussed above. For the damping of the angular motion of the rod in two directions, a system with possibly three or four linear damper elements in a plane normal to the rod axis can be used (see figure 8.20).

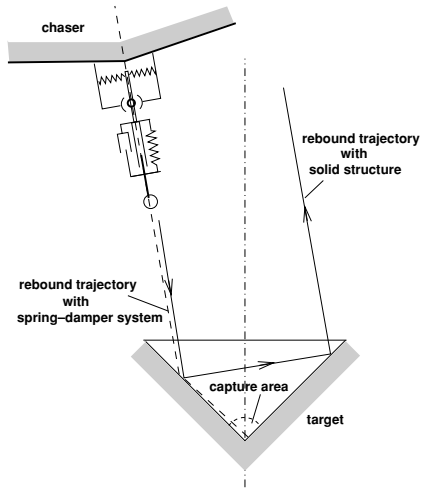

Figure 8.20. Central docking system: rebound with and without spring-damper.

Without any flexibility in the rod, in particular in its lateral direction, the tip of the rod would not move to the centre of the cone, which is the place where it can be captured. If the rod were rigid and firmly connected to the chaser body, its tip would behave as the contact point in a non-central impact according to Eqs. (8.14) and (8.15). In a cone, two rebounds with opposite translational and rotational motions would take place, as shown in figure 8.20. With axial and lateral flexibility and damping, the tip of the rod will move into the capture area in the centre of the cone.

As we have seen in Eqs. (8.25) and (8.27), motion attenuation in a longitudinal direction does not necessarily require the inclusion of springs. In fact, for capture it may be better, at least during the initial part of motion, to have only velocity proportional braking. A spring system could push the capture interfaces back after maximum excursion, if the system was not properly tuned for aperiodic damping. For the final part, in particular for damping of the residual motion after capture, spring-damper combinations, possibly together with solid friction devices, can be used.

Shock attenuation systems for peripheral docking systems

Shock attenuation and alignment for capture is, in peripheral docking systems, much more complex than that for central ones. Without damping, the motion reaction of two rings impacting on each other would be similar to the conical motion of a coin being dropped on a surface. Since the contact conditions also include lateral velocities, linear and angular misalignments and angular velocities, in addition to the velocity along the nominal approach axis, the docking system requires damper arrangements for motion in six DOF.

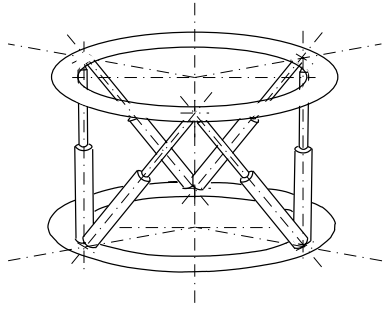

Figure 8.21. Stewart platform damper arrangement for peripheral docking mechanism.

The most commonly used arrangement used for this purpose is that of a ‘Stewart platform’, i.e. an arrangement of six linear motion elements, connected to three points each on the upper and lower rings (figure 8.21). The position of the connecting points between the two rings are shifted by 60 deg. This arrangement allows the use of six identical linear damper elements, and it fulfils the requirements of six DOF motion. It

also provides the necessary freedom of the tunnel area for transfer of astronauts and goods.

Docking dynamics with a peripheral system are also more complex because of the following effect. If passive capture latches are used on a peripheral system, capture will take place only once the two contact rings are aligned within very small margins, i.e. the above-mentioned conical motion must be fully damped out. In contrast, in a central docking system, the tip of a flexible rod will be pushed into the centre of the reception cone, where it can be captured by passive spring-loaded latches without prior alignment of the contact rings.

In order to achieve proper alignment of the two contact rings in a very short time, either the damper elements must initially be very 'soft', or the alignment must be achieved by active means. To achieve a very soft spring behaviour for alignment and a sufficiently strong spring behaviour for shock attenuation after capture, springs can be staged in several steps with increasing spring constant. To support actively the alignment of the contact rings, the APDS docking mechanism (figure 8.10) uses a complex system of differential gears, which ensures that when the contact ring is pushed down at a certain point, its opposite side will be moved up. The concept of an actively closed loop controlled alignment system has been used in the Low Impact Docking System shown in figure 8.14. The problem of accurate alignment of the contact rings to achieve capture can be avoided when active capture latches are used, as these ensure the condition of 'no escape' prior to full alignment (see section 8.3.5).

Shock attenuation elements

A few examples of typical concepts of damping elements are given below to illustrate how such functions can be implemented. Formulas describing their operation are not provided here, as this would go beyond the objectives of this chapter. They can be found in relevant textbooks on physics.

Velocity proportional viscous damper A combination of spring and hydraulic damper is the most common damping device in many applications. It is a well known system, used e.g., as shock absorbers for cars. In ground applications, a viscous damper is designed in most cases as a piston in a cylinder, where the gap between the piston and the wall is the flow restrictor. In space applications, this type of design is less suitable because of the sealing problems. A hermetically sealed viscous damper design can be achieved, e.g., by an arrangement of two bellows, connected by an orifice, as shown in figure 8.22. The orifice between the bellows is acting in this case as the flow restrictor, providing the velocity proportional damping. The bellows themselves provide a spring force, which acts in parallel to the spring arranged on the outside.

One problem with the bellow arrangement is that the ratio of extended to compressed length is relatively small. For applications where dampers with long excursions are needed, either the piston–cylinder principle would have to be used, with the sealing

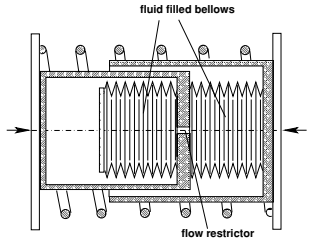

Figure 8.22. Principle of a spring viscous damper with bellows.

problem to be solved in some way, or a 'dry' solution may be applied, as described below.

Velocity proportional eddy current damper One way of realising a velocity proportional damper without using a liquid or gas is to use an eddy current using a damper. This principle uses the physical effect that eddy currents are induced in a piece of metal when the metal is moved in a magnetic field, and that these eddy currents interact with the magnetic field. As a result, energy is dissipated, and a magnetic drag force proportional to the velocity is produced; this tends to slow down the motion of the piece of metal.

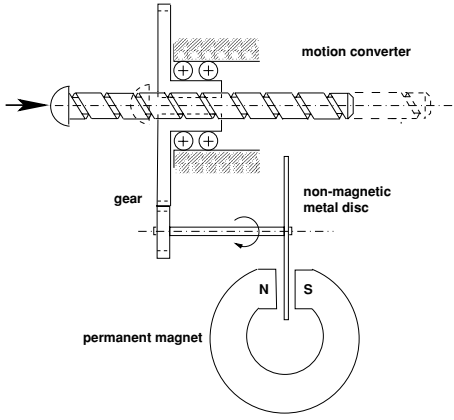

Figure 8.23. Translational/rotational motion converter and eddy current brakes.

This principle may be used to damp translational motions and may be envisaged in the way shown in figure 8.23. To produce a high damping effect, the relatively slow translational motion is converted into a rotation by a screw type of motion converter, which drives a metal disc, moving through the gap of a permanent magnet. Instead of an arrangement with a flat disc, moving in the planar gap between the poles of a magnet,

an arrangement with a thin-walled metal cylinder rotating in the cylindrical gap formed by the magnet poles could be used. The latter variant is used in the Soyuz/Progress probe–drogue docking mechanism (see figure 8.8).

Friction damper Solid friction is present in practically all mechanisms; in most cases it is caused by sliding or rolling friction in the bearings. As the friction force is proportional to a compression force normal to the sliding plane, friction dampers can be implemented, e.g., by moving a disc between two others which are compressed by spring pre-load. As in the eddy current damper, the relatively slow translational motion can be converted into a rotation. The amount of friction in a friction brake can be adjusted by spring pre-load. A typical design comprises a number of rotating discs running between fixed ones, i.e. an assembly similar to a clutch.

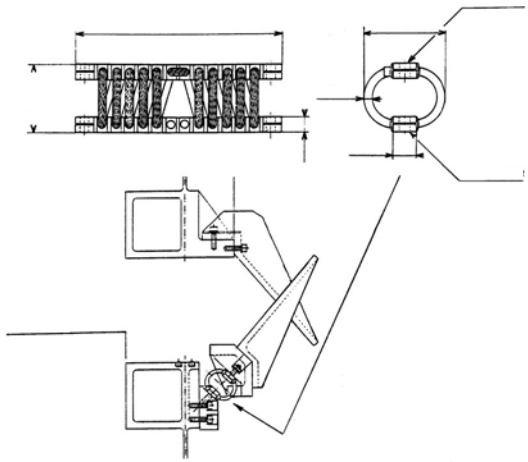

Figure 8.24. Example: friction coil element (of figure 8.11).

A different implementation of a friction damper is shown in figure 8.24 (Gonzales-Vallejo *et al*. 1993). It consists of coils of multiply twisted steel wires that rub against each other when the coils are deformed. This type of damper is used in machines for vibration attenuation. In docking mechanisms it has been implemented and successfully tested in the Hermes–Columbus docking system shown in figure 8.11. Since it allows for only relatively small deformations, this type of damper can be used only in systems with very low impact velocities.

Actively controlled motion damping The concept of a fully active alignment of the contact rings and damping of the motion by a closed loop control system has been used in the NASA development of the Low Impact Docking System (Lewis & Carrol 1999),

which has been described in section 8.2.5 and is shown in figure 8.14. In this system, the force vector and its application point is actively sensed by six load cells at the circumference of the contact ring, and damping and alignment is provided by motion control of the six linear actuators arranged in a Stewart platform configuration. The advantages of an active control of alignment and attenuation may have to be paid for by increased complexity and development effort.

The advantage of a system where attenuation is realised by a closed loop controlled electro-mechanical system, including force sensors, controller and linear actuators, is in the wide range of damping characteristics which can be achieved by a change of algorithm and parameters in the control software for this system. For instance, with a closed loop controlled system, a progressive spring-damper behaviour can be achieved, which otherwise would require a series arrangement of several sizes of spring-damper elements or combinations with friction dampers.

8.3.5 Capture devices

Capture strategies

In the above discussion on impact attenuation, it has been assumed that capture will take place somewhere in the period between the first contact and the instant where, in the expansion phase, the docking interfaces of the two vehicles have again left the contact position x_0. In the following, capture issues will be elaborated upon in more detail. The actual point in time where capture should take place during the docking or berthing process depends on the capture strategy chosen. The following capture strategies can be applied.

Capture after first contact In this case, capture operations are initiated at or after the first contact between the according docking interfaces of chaser and target. Three subcases can be distinguished:

- The capture latch is effected by the kinetic energy of the docking vehicles. The capture process is similar to a door latch falling into its catch. This type of latch requires a minimum contact velocity for successful capture to overcome friction and spring forces of the mechanical guides and latches. Capture has to take place before the attenuation system has reached its maximum compression state.
- The capture latch is motor driven, and the motor operation is initiated by an impact sensor. Capture has to take place in the time period between contact and separation, i.e. the speed of latch closure must be fast enough to ensure capture before the docking interfaces have separated again.
- The contact rings will be actively aligned after the first contact and capture takes place, when the alignment conditions are achieved. Capture has to take place before the attenuation system has reached its maximum compression state.

Capture before first contact This strategy requires, in any situation, a sensor function which identifies the entrance of the interfaces into the capture range. Such sensors can be light-barrier detectors, electro-magnetic or capacitive proximity sensors, etc. The optical rendezvous sensor could be used, if it is sufficiently accurate. In the case of berthing, human operators, with the aid of manipulator cameras, may fulfil the sensor function. Two cases can be distinguished for the strategy of 'capture before contact', i.e. the typical capture operations for berthing and the capture operations of an 'intelligent docking mechanism':

- Capture for berthing: the end-effector of the manipulator actively pursues and grapples the capture interface of the other vehicle. As we have seen in section 8.1.3, these operations must be completed within 1 or 2 minutes before the vehicle to be captured has left the berthing box.
- Capture for docking by motor driven latch: this is initiated upon sensing of the docking interfaces entering into reception range. As in the case of capture after contact (above), the speed of latch closure must be fast enough to ensure capture before the docking interfaces have separated again. The advantages of this case would be, however, that about double the time is available for the capture operations, and no precise alignment of the contact rings is necessary prior to engagement of the capture latches.

The choice of capture strategy is one of the most important design drivers for the design of a mating system. It will depend on issues such as the GNC performance and vehicle velocity at contact, availability and reliability of sensor information on the capture interface position, availability of a manipulator on either chaser or target, etc.

Types of capture systems

Capture mechanism for central docking systems Because of their basic design principle, central docking systems generally follow the strategy of 'capture after first contact'. As we have seen in figure 8.20, contact will occur somewhere on the surface of the reception cone, whereafter the tip of the rod will move toward the centre of the cone, where it will be captured. Capture is achieved by spring-loaded latches arranged on the tip of the rod, which fall into their corresponding catches in the socket at the centre of the cone, as shown in figure 8.25. In order to overcome the friction and spring forces of the capture latches, this system requires a minimum kinetic energy for successful capture. For this reason, this type of docking is known as 'impact docking'. Usually, an additional thruster boost will be applied to drive the capture latches into their catches. There may be three or four latches on the tip of the rod. The catches on the opposite side will provide sufficient oversize to account for all possible misalignments. They will provide coarse limitations for translational motion and will prevent large roll motion after capture. For release and separation of the probe from the drogue, the spring-loaded capture latches can be withdrawn by a release mechanism.

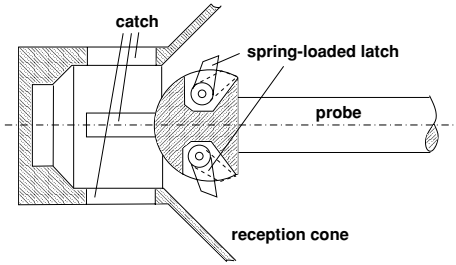

Figure 8.25. Central docking system: principle of capture latch.

Passive capture latch for peripheral systems Whereas the central docking system does not lend itself to a 'capture before first contact' strategy, the peripheral docking system can be designed in both ways. For passive capture latches, spring-loaded latches are typically arranged in the middle of each petal; these engage with corresponding catches between the petals on the opposite docking ring. Such latch–catch interfaces can be arranged on both chaser and target sides of the docking system (androgynous design), providing additional redundancy to the function (see figure 8.26). A special mechanism will be used for withdrawal of the capture latches if the two halves have to be separated for any reason during the docking process. The final alignment requirements, which have to be achieved for successful capture, are more critical for a peripheral system than for a central one. This is due to the design relations of a system, where all alignment and capture elements are arranged near the outer diameter. In particular, angular misalignments must be small to engage all capture latches. To achieve the alignment requirements, the shock attenuation system has to be sufficiently compliant. Friction forces due to the petals during mechanical guidance, and spring and friction forces of the capture latches, will be more critical for capture than in the other designs, because of the complex motion, after contact, of the multiple contact points and of the long lever arms at which these forces act w.r.t. the centre line. As a result, a relatively high contact velocity is required for successful capture. Also, in this type of docking system, additional boost along the chaser's longitudinal axis is usually applied to support capture.

Active capture latch for peripheral systems In contrast to the passive spring-loaded latch, latch engagement will in this case be operated by an electro-motor. The capture strategy to be applied will be 'capture before contact', in order to provide the maximum possible time available for the closure of the latches. It is obvious that this strategy leads to successful capture only if the approach velocity is small compared with the latch closure velocity. Closure of the capture latches has to be initiated immediately once all capture interfaces are within their according reception ranges. Proper capture conditions will either be detected by dedicated sensors, e.g. light-barrier sensors near the latches or petals, or will be reconstituted from the position and relative attitude measurements of the rendezvous sensor, if accurate enough. Requirements for final alignment at the

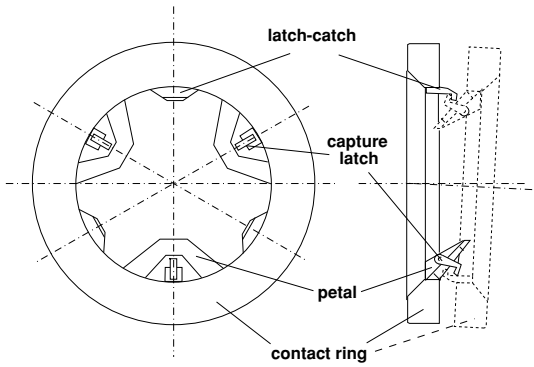

Figure 8.26. Peripheral docking system with passive capture latch.

instant of capture will be less demanding than for passive capture latches. This will make capture more reliable. However, larger misalignments at the entrance into the reception range, due to GNC performance, would have to be compensated for by relatively large dimensions of the capture latches.

An example of an active capture latch system is shown in figure 8.27. The design is an over-centre latch, which is self-locking in the closed position. The linkage is designed such that the trajectory of the latch tip after initiation travels, in a very short time (1–2 s), from the ready position to the capture position, at which the interfaces can no longer escape. The system includes a minimum of three capture latches, which are actuated individually. The second part of the latch trajectory serves the functions of retraction and alignment for structural connection. To keep the dimensions of the capture latch low, the combination of angular and lateral misalignments at a given docking ring diameter must not exceed a certain value. For a latch with the total dimension of $\approx$0.5 m, the typical longitudinal and lateral capture range is between 0.2 and 0.25 m. Assuming that lateral and angular misalignment share equally the reception range, the lateral misalignment must not exceed $\pm$0.1 m and the angular misalignment in pitch and yaw must not exceed $\pm$3 deg with a docking ring diameter of the order of 1.5 m. The acceptable angular misalignment on entering the reception range is further reduced by the approach velocity and rebound motion. The system was designed for a nominal approach velocity of 0.02 m/s and the acceptable angular misalignment was $\pm$1.5 deg.

Magnetic capture devices The capture device consists of a number of electro-magnets arranged on the circumference of the contact ring. The interface on the target vehicle consists of soft iron counterparts at places corresponding to those of the electro-magnets on the chaser side. When these interfaces are brought into close vicinity, they will attract each other, ensuring contact and attachment in an aligned state. The advantages of using electro-magnets as capture devices are that no mechanical capture latches are needed and that alignment occurs automatically. A problem with the application of magnetic

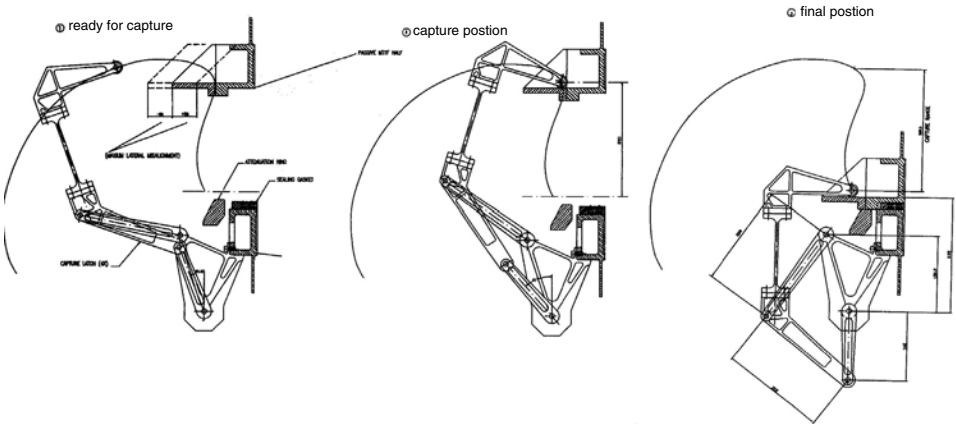

Figure 8.27. Peripheral docking system with active capture latch (courtesy ESA).

devices for docking is the force characteristic of magnets, which decreases by $1/r^2$ with the distance r. This means (a) that at larger distances the forces of the magnets may not be sufficient for capture, and (b) that at shorter distances, when the magnetic forces are large enough to initiate capture, the vehicles will accelerate toward each other, rather than decelerate, which is essential for smooth contact. This characteristic of magnets may be overcome either by actively controlling the magnet forces as a function of their distance, or by actively aligning the contact rings w.r.t. each other, and by engaging the electro-magnets only when the distance to their counterparts has become practically zero for all of them.

Capture mechanism for berthing (grappling/grasping) As already discussed above, there are two capture tasks in a berthing scenario: (a) to perform a first connection between the vehicles by a manipulator arm, and (b) once insertion into the berthing mechanism is achieved, to prepare for structural connection.

In order to be able to exploit the potential advantages of berthing, i.e. large envelope of position and relative attitude at capture, the capture system for the first connection must be able to cope with significant misalignments between the vehicles. The major part of these misalignments will be compensated for by appropriate articulation of the manipulator joints. As the arm is manually controlled, there will be residual misalignments, however. For this reason, the end-effector must have a sufficiently large reception range.

There are many types of end-effector designs developed for industrial and scientific applications. The design used for most berthing operations in space is the end-effector developed by the Canadian Space Agency (CSA) together with the manipulator arm for the US Space Shuttle (Ussher and Doetsch 1983). This design is now used also for the ISS. The principle of operation is shown in figure 8.28. The interface on the

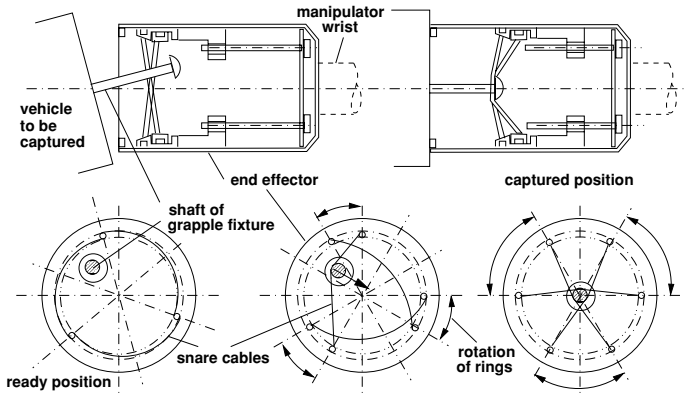

Figure 8.28. Manipulator end-effector and grapple fixture (developed by CSA).

vehicle to be captured consists of a rod (grapple fixture), which has a base structure for alignment and firm connection. The end-effector consists of a cylinder, which contains a mechanism with three snares. For a man-in-the-loop controlled capture, the operator of the manipulator steers the end-effector to follow the residual motion of the grapple fixture and to align the two interfaces with the aid of a visual target pattern, similar to the one shown in figure 6.23. When sufficiently aligned, the end-effector will be placed over the grapple rod and the snare mechanism activated. The snares will then close around the rod and prohibit escape, as shown in figure 8.28. During subsequent operation, the snares are further tightened and pulled in the direction of the wrist of the arm. This presses the end-effector cylinder against the base of the grapple fixture, providing a firm connection between the two.

The capture mechanism for insertion into a berthing mechanism, shown in figure 8.29, is the design for the Common Berthing Mechanism (CBS) developed by NASA for the Space Station. The design is an over-centre latch similar to the one shown in figure 8.27 for docking. The design criteria, however, are different. Whereas in docking the motion from the 'ready' position to the 'capture' position must be as fast as possible to prevent escape, such a requirement does not exist in this case, since the manipulator can hold the interfaces in position as long as necessary. Also, the misalignments at capture in a berthing mechanism will be comparatively small, as the manipulator arm can push the petal interfaces into each other, improving the preliminary alignment. The capture latch design will, therefore, be optimised for minimum size and mass, for small initial misalignments and for no time constraints. A spring is mounted between the first member of the linkage (the one with the hook) and the second member; this spring bends the upper member (hook) forward and provides the necessary flexibility in case of misalignment between the berthing interfaces. When all hooks are in contact with their corresponding catches on the opposite side, they will pull the two berthing rings together.

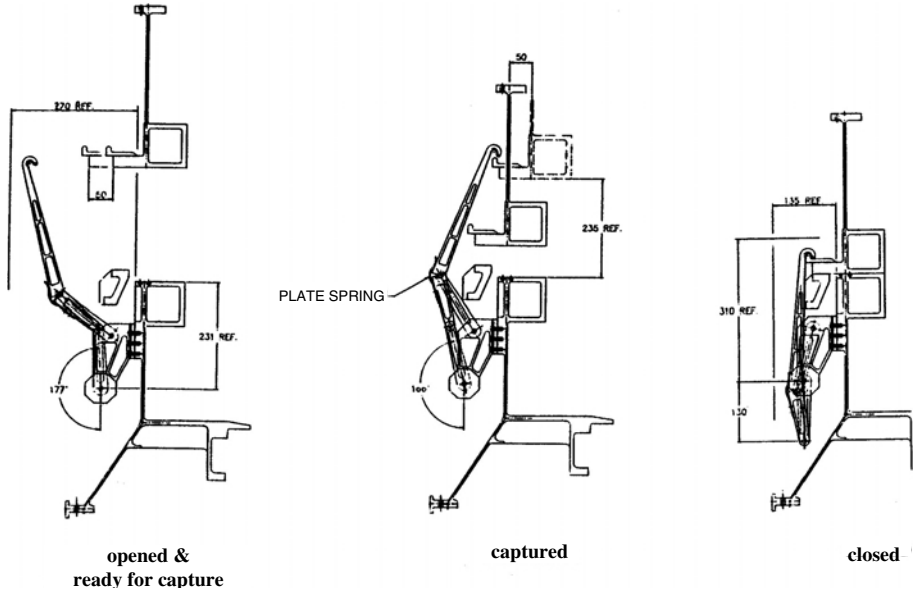

Figure 8.29. Capture latch of berthing mechanism (courtesy NASA).

8.3.6 The interface between the GNC and the mating system

As contact and capture dynamics are very closely related to the GNC performance, their interfaces will be addressed here before discussing structural connection and sealing issues and elements. In the previous sections of this chapter, we have already seen that the choice of functional principles and the detailed design of the elements for capture and shock attenuation depend on the lateral and angular displacements and on the translational and rotational velocities between the capture interfaces of chaser and target at the instant of contact or just prior to it ('capture before contact' strategy).

Generally, in the case of docking, to keep the impact, and therefore the size of the attenuation system, low, contact and lateral velocities and angular rates should be as low as possible. We have seen, however, that for the 'capture after contact' strategy, generally a minimum velocity is necessary to achieve mechanical guidance by the probe–cone or petal–petal interfaces and for actuation of the spring-loaded latches.

The requirements for berthing have been addressed already in section 5.3.1. The ideal conditions for capture by the manipulator would be zero relative translational and rotational rates; this situation is not possible, however, because of orbital dynamics and residual rates after switch-off of the reaction control system.

Performance requirements for the GNC system have already been addressed to a certain extent in chapters 6 and 7. In chapter 6, possible control strategies for docking (see figure 6.9) have been indicated, showing that it is necessary to control relative attitude

in addition to lateral trajectory deviations, in order to achieve sufficiently small misalignments at docking. Further, the causes of control deviations have been addressed in section 6.2.3. In chapter 7, the requirements for sensor performance at docking have been derived from an assumed reception range of a docking mechanism, giving an allocation to control performance and to uncompensated target motion (see figure 7.3).

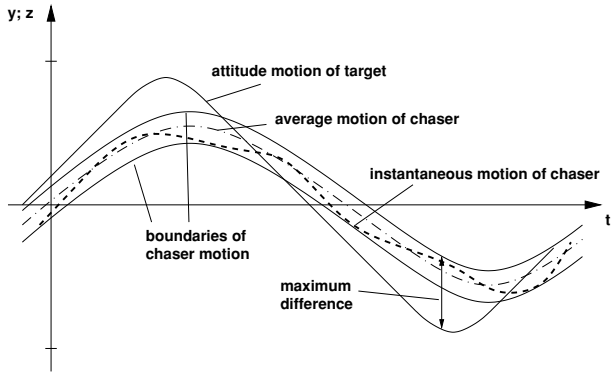

Figure 8.30. Motion of target and chaser at docking.

The effects on the reception requirements of the chaser GNC performance in pursuing the target motion will be investigated more closely in this section. The docking port of a vehicle is necessarily at a certain distance from the CoM. As a result, angular motions about the CoM of the vehicle translate into lateral motions of the docking port. The solid line in figure 8.30 is the lateral motion of the target docking port resulting from a typical two-sided limit cycle (saw-tooth) attitude motion. The rounded-off corners are due to the available thrust level and the inertia of the target spacecraft. Due to the filtering and control processes (see chapter 6), the chaser will follow the target motion with a certain delay. Further, its trajectory and relative attitude will deviate somewhat from the target motion due to sensor performance and the thruster selection process. The chaser motion may also exhibit lower amplitude, due to (e.g.) bandwidth limitations of the chaser GNC chain. As a result, the lateral motion of a chaser following the target motion may resemble the thick dashed curve in figure 8.30, labelled 'instantaneous motion of chaser'. The deviations are of a random nature and can be described by an average motion, with margins on both sides, indicated as 'boundaries of the chaser motion' in the figure. The reception range of the docking mechanism must be larger than the maximum possible difference between the lateral motion of the target docking interface and that of the chaser. The simplified diagram in figure 8.30 shows of course only one of the six degrees of freedom to be controlled.

In order to avoid unwanted reactions by the GNC system on the contact dynamics, the reaction control system (thrusters) of the chaser will have to be inhibited prior to, or at, contact. This can be initiated either upon detection of the docking interfaces entering

into their mutual reception range, at a certain distance measured by the rendezvous sensor, or upon detection of first contact. The navigation, guidance and control functions will have to continue operating, in order to facilitate immediate retreat if necessary, e.g. if the capture fails. For the auxiliary thrust that is necessary to support capture, which has been mentioned above, thrusters providing force components in the direction of the docking axis will be initiated upon detection of contact by an independent command string outside the GNC.

The conclusion of all the discussions so far is that the requirements concerning reception, shock attenuation and capture are interdependent with the GNC performance requirements. This means that a balance has to be found between the capabilities of the GNC and docking systems.

- High approach velocities, lateral and angular rates and misalignments at contact require large reception ranges and attenuation systems with large excursions. Capture can be performed only after contact, and the capture function can best be implemented by passive spring-loaded latches. From the dynamics point of view, the best docking system for high velocities, angular rates and misalignments is central docking, which offers large lateral and angular reception ranges and relative simple design implementation possibilities for the shock attenuation system, capable of coping with large impact shocks. Peripheral systems offer a better clearance of the transfer tunnel at the expense of significantly increased design complexity and potentially reduced reception capability.

- High GNC performance, with low approach velocities and misalignments, allows the application of a 'capture before contact' strategy. This involves the application of active capture latches, which do not require a certain residual relative velocity between the vehicles for successful capture. The reduced shock attenuation requirements allow for the application of small and simple damper devices.

- Capture by a manipulator for berthing does not require high positioning and angular alignment performance by the chaser GNC, but rather nominally zero velocities and angular rates. This requires also a relatively high GNC performance (see also sections 5.3.1 and 7.1.1).

8.4 Elements for final connection

The residual functions of docking and berthing mechanisms are the structural latches, seals, utility connections, and the sensor and detector functions. Only the structural latches and seals will be discussed in this section for completeness of understanding of the docking/berthing mechanism functions. These functions are fully independent of the flight (GNC) and contact dynamics (reception, shock attenuation, capture) complex, and can also be considered in the verification process (see chapter 10) completely independently. The subject of utility connections is outside the scope of this book, as additional

technical fields unconnected with the understanding of rendezvous and docking in space would have to be covered. The design principles used for these functions are basically no different from those used for automatic connection/disconnection mechanisms on ground.

8.4.1 Structural latches

The tasks of the structural latches are as follows:

(1) To provide the necessary strength and stiffness of the connection, necessary to transmit internal and external loads caused by, e.g., crew and payload motion, thruster firings, EVA, manipulator activities, further docking and berthing operations, and as required for attitude control of the joint vehicle.

(2) To provide the necessary compression force at all points of the circumference of the docking or berthing ring for optimum functioning of the seals.

The second task, which is required only in manned missions, puts the highest demand on the structural latches. If the inner pressure is equivalent to that of the normal Earth atmosphere at sea level, i.e. $p = 9.81$ N/cm^2, the total force to be carried by the structural latches is $f_\mathrm{p} = pd^2 \cdot \pi/4$. For example,

- at a diameter of the sealing ring of 1 m, $f_\mathrm{p} = 77\,048$ N;
- at a diameter of the sealing ring of 1.5 m, $f_\mathrm{p} = 172\,764$ N.

The actual pressure in a space station may be reduced to 50–60% of the sea level value, which has advantages w.r.t the structural loads, the consumable budget and the EVA activities. In addition to the pressure force, the latches have to provide the compression force for the seals, ensuring their gas tightness, plus a safety margin. The resulting force level is orders of magnitude higher than all the other loads, listed under point (1) above, which makes it the major design driver for the structural latches.

The quadratic increase of the pressure force with the diameter of the pressurised area eventually puts constraints on the design of structural latch assembly. To carry the pressure load at a given seal diameter, a certain number of latches may be required. Increasing the seal diameter by a factor of n would mean that the number of latches of the same design would have to be increased by a factor of n^2 to carry the increased pressure load. As the circumference of the ring has increased only linearly, this may eventually cause accommodation problems for the latches and may, as a result, require the use of latches with higher load carrying capability.

Another parameter which changes with the increase of the sealing ring diameter, and which affects the effectiveness of the sealing, is the stiffness of the structure. If all dimensions are increased linearly, the stiffness also increases linearly, whereas the pressure forces increase quadratically. As a result, the bending of the structure will increase,

which in turn requires a larger number of connection points to keep a sufficient and equally high pre-load on the seals along the circumference.

In summary, a significant increase in the tunnel diameter will lead to a requirement for both increased load carrying capability and a higher number of latches.
Examples

- *Soyuz/Progress central probe–drogue docking system.* The tunnel diameter is 0.8 m and the diameter of the sealing rings is approximately 0.95 m. The mechanism has eight structural latches of the hook type (plus eight redundant ones from the other half of the system).

- *APDS (androgynous peripheral docking system).* The sealing ring diameter is approximately 1.2 m. The mechanism has 12 structural latches of the hook type (plus 12 redundant ones from the other half of the system).

- *Hermes–Columbus docking system.* The diameter of the sealing rings is 1.6 m. The mechanism has 12 latches of the screw type (on the active side only).

- *ISS common berthing system.* The diameter of the sealing rings is about 2 m. The mechanism has 16 latches of the screw type (on the active side only).

There are two basic design principles used for the structural latches, i.e. the 'hook' type (figure 8.31) and the 'screw' type (figure 8.32). The hook type latch has been developed for the Soyuz/Progress and APDS docking systems. The trajectory of the hook latch is generated by a simple eccentric cam. The design includes at each latch location an active and a fixed passive hook. In the Soyuz/Progress system, all active hooks of one side are driven together by one actuator via a steel cable system. In the APDS system, because of the increased pressure forces and number of latches, there are two actuators which operate, via steel cables, six active latches each. The force transmitted in each string of steel cable must have a very high margin to ensure reliable operation under all conditions. An advantage of the hook system is that the 'fixed' hook can be designed such that it can be released if necessary (e.g. by pyrotechnics and springs). If a double hook arrangement is used, as in the Soyuz/Progress central docking system and in the APDS (principle shown in figure 8.31), a firm structural connection can be achieved also by actuating the latch system of the other side, which provides full redundancy to the system.

With increasing diameter of the sealed area, the forces become so high that eventually a reliable operation of the hook latch design becomes problematic. For this reason, for mating systems with a very large diameter of the sealed area, such as the common berthing system of the ISS or the Hermes–Columbus docking system, the screw type of structural latch with individual actuators has been chosen. With screw type latches, higher pre-loads can be achieved at a given torque delivered by the actuator.

A further advantage of the screw latch with individual actuator is the possibility of controlling the pre-load individually at each latch, which is not so in the case of a hook

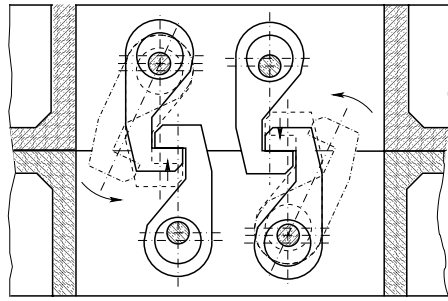

Figure 8.31. Structural latches, hook type.

latch arrangement. This advantage has to be paid for, however, by the increased expenditure in electrical circuitry and motors and by the increased amount of single-point failures. To provide redundancy and to mitigate single-point failure possibilities, screw latches must be capable of being operated from two sides, i.e. the bolt and nut must be capable of being operated independently.

For all structural connections which are not intended to be permanent, it is extremely important that they can be opened again. For separation and departure, if there are no capture latches, holding the two docking rings in position, the structural latches must open at the same time. In contrast to the hook latch arrangement, which is operated jointly by a steel cable, this condition will be more difficult to achieve with a large number of individually operated latches. For this reason, with the screw type of latch, it will be safer to re-engage first the capture latches, then to de-pressurise and open the structural latches, and eventually open the capture latches for separation. For individually operated capture latches, the problem of a single latch failure still exists. The immediate repercussions can be limited if, prior to capture latch opening, the attenuation system is expanded and does not exert spring forces on the latches. Opening of a failed latch can then be forced by a pyrotechnic release mechanism.

As the above-described redundancy by separate bolt and nut operation cannot cover all possible failures, e.g. cold-welding between the flanks in the thread, additional possibilities for opening of the latch have to be implemented. This can be done, e.g., by bolt-cutting pyrotechnic devices. However, as the expense in terms of design complexity may be relatively large, and the amount and size of the pyrotechnics may be unwanted because of safety-criticality, the screw latches are usually placed inside the sealing rings, so that they can be accessed by IVA operation. The solution would then be to remove and replace the complete latch manually, providing temporarily the pre-load by auxiliary clamps attached to the flanges of the docking/berthing rings. In docking mechanisms with smaller tunnel diameter, such as the Soyuz/Progress and APDS, structural latches and other devices which cannot be removed after connection are preferably arranged outside the sealing ring, to maximise the available cross-section for transfer. Since EVA will be required, this of course increases the complexity of such manual operations.

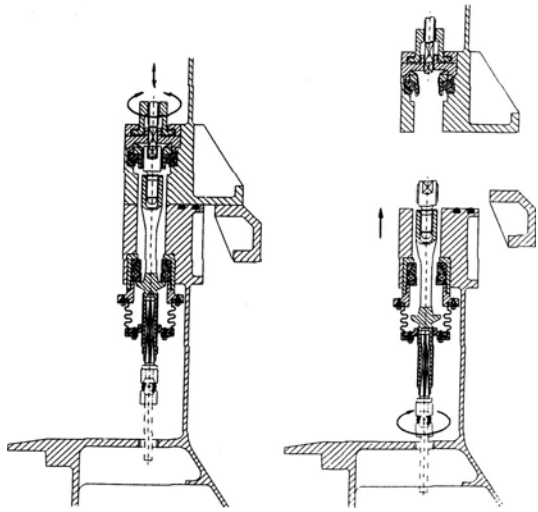

Figure 8.32. Structural latches, screw type (courtesy ESA).

A typical design of a screw type structural latch, which was developed for the Hermes–Columbus docking system, is shown in figure 8.32. In this case, the latches are mounted inside the seals. Both bolts and nuts are mounted in spherical bearings to compensate for misalignments. For contingency separation, the bolt can be operated from the nut side by rotation of a shaft in the centre of the nut assembly; this has a square cross section at the tip and can be moved downwards to fit into a square hole at the tip of the bolt.

8.4.2 Seals

To keep the forces which have to be applied by the latches to compress the seals low, the seals should be arranged at the smallest diameter possible. As we have seen, however, there may be overruling considerations, i.e. access to essential devices from the inside, which move the seals to the outer diameter of the interface ring (see figure 8.32). For redundancy reasons, generally two concentric seal rings are applied. Pressure measurements can be performed in the volume between these two rings, and these provide an indication of the leak-tightness of the seals (see figure 8.33). If the pressure of the volume is equal to the inner pressure, the inner ring is leaking. If the pressure is equal to the outer pressure, there are theoretically two possibilities: (a) the outer ring is leaking or (b) both rings are absolutely airtight. In case (b), after structural connection and subsequent pressurisation, the volume would still have the outside pressure. It would be possible to implement small diameter ducts, with valves to both inside and outside, which apply either the inside pressure or a vacuum and to determine the nature of a leakage from the pressure development.

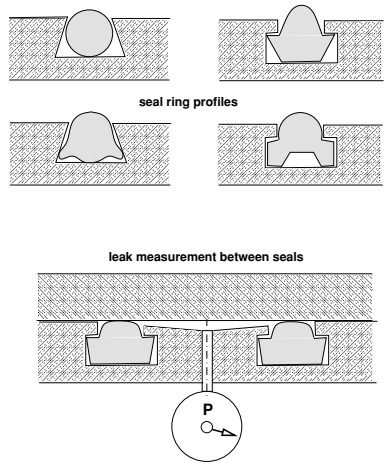

Figure 8.33. Seal ring profiles and leak measurement.

Seals must be sufficiently flexible so as to comply with the form of their interfaces, even on the scale of surface roughness; i.e. on one side with the groove in which they are held and with the interface surface on the opposite side. On ground, metals and elastomers are used as sealing materials, together with low-outgassing greases. In space, in docking/berthing applications, however, grease and metallic seals may not be used for a number of reasons, the most important of which are:

- grease: high adhesion force, causing a problem at separation; lack of chemical stability under conditions of radiation and atomic oxygen;
- metal seal: very high compression forces necessary to achieve air tightness; plastic deformation of metal allows for only one operation.

This leaves synthetic elastomer materials as the only possibility of providing the mechanical properties for docking/berthing seals. Unfortunately, these materials lose their properties during long term exposure to space conditions and, for this reason, missions have to be arranged such that seals are not exposed to orbital environments for more than a couple of days. This has the following consequences:

- docking/berthing interfaces on the outside of a space station must not carry seals;
- seals for docking/berthing connections must be located on the servicing vehicle side, which will be in orbit for only a few days up to a few weeks until it is connected to the target;
- at disassembly and re-assembly of modules for reconfiguration of an orbital complex, all seals must be covered again, either by the mating interface of its opposite module or by a hatch.

It is hoped that, in the future, materials and seal designs will be developed which are capable of long term exposure to space conditions. Until such seals become available, it is obvious that the idea of androgyny of docking/berthing interfaces cannot be fully implemented and the benefits of these designs cannot be exploited.

There are many types of seal cross sections used in applications on ground. A few examples are shown in figure 8.33. To be used in mating interfaces of space vehicles, the profiles of the seals and of their corresponding grooves must fulfil two requirements:

- The seal ring in its groove must be firmly attached such that it is capable of withstanding launch vibrations and accelerations, as well as possible lateral motions during closure and alignment for structural connection. Adhesion forces during separation must not lead to extraction of the seal from the groove.

- A maximum of the seal surface must press against the opposite mating ring and the groove walls at maximum compression, i.e. when metal to metal contact is reached between the interface rings.

Because of the second requirement, the seal profile must not only protrude from its interface ring, but the difference between seal and groove cross sections must be such that the groove is almost completely filled when maximum compression is reached. As the seal material is flexible but incompressible, seal and groove profiles have to be carefully matched, i.e. there must remain a very small amount of freedom when metal to metal contact is reached.

After compression of the seals, and in particular if the seals are attached for a certain time, there will be adhesion between the seal and the opposite wall, requiring a certain force to achieve separation. Even larger forces may be required to separate power and fluid connectors, if they do not have their own separation devices. For this reason some docking mechanism designs include a number of ‘pushers’ around the docking ring, which apply the necessary forces. These are passive spring-loaded rods, which have been compressed during structural latching and are released at separation. In other designs, the contact ring, which is connected to the shock attenuator devices, provides the separation force. In berthing, the vehicle or module to be removed is separated by means of the manipulator arm. The ‘pushers’ may be used additionally to provide the initial ΔV to the departing vehicle, so that the thrusters need to be operated only when a distance of a couple of metres has been reached.

9

Space and ground system setup

This chapter addresses the tasks and responsibilities of all parties outside the automatic onboard system involved in the control of a rendezvous mission. It looks at the hierarchy of authority, the support functions required and the constraints imposed by the communication links. Tasks and design principles of support tools for human operators are indicated.

As discussed already in chapter 6, in an Earth orbit there is no need to conduct the rendezvous and docking process fully autonomously. The interaction by external operators is, on the contrary, always desirable, when this will reduce the complexity of the system and increase safety and success probability. On the other hand, because of the limitations of the communication links, the complete control of the rendezvous and docking process cannot be performed entirely from ground. For this reason, the onboard control system of unmanned spacecraft must be able to perform automatically in the vicinity of the target vehicle the control tasks discussed in chapter 6:

- the control of the spacecraft state (attitude angles, position, velocities and angular rates);
- the sequencing of manoeuvres and modes at the right time and points of a trajectory;
- the detection of, and recovery from, anomalies and failures;
- in the case of docking, sequencing and control of mating operations.

A number of high level control tasks can be performed better by remote human operators, who can contribute the human capabilities of recognition and assessment of unpredicted situations, together with the much larger resources for information gathering and data processing than are available to the onboard system. Remote operators will, therefore, monitor the trajectory and attitude of the vehicles, the status of the automatic onboard systems and of the communication links; command, e.g., equipment reconfigurations or manoeuvres in case of contingencies not resolved by the onboard system; and

will re-plan the mission in case of deviations from the planned timeline due to delays or contingencies. Remote operators with their support tools will be in a better position than the onboard system to identify failures and to find the best solutions for long term recovery measures.

9.1 Functions and tasks of space and ground segments

The remote interaction by operators on ground and in the target station will include in the nominal case (a) monitoring and high level control of spacecraft functions and of the spacecraft state vector and (b) the initiation of manoeuvres or the next step in the automatic approach. The ground segment will, in addition, provide operational data to the spacecraft, such as the actual orbit ephemeris of both vehicles. After launch and during phasing, only attitude control and housekeeping functions are controlled automatically by the onboard system; all manoeuvres are planned, calculated and initiated from ground. In contrast, during the rendezvous phases, ground involvement is in the nominal mission mode generally reduced to monitoring and to high level decision making, e.g. approach initiation or command of holds, etc. The ground segment will have to assume a more active role if there are deviations from the nominal mission plan. If there are mission interruptions or delays, the most important task of the ground operators will be the re-planning of the mission sequence. In the case of onboard failures, the major task will also be the identification of the failure source and, if a failure situation cannot be resolved by the onboard system, immediate moderation of the situation and the initiation of recovery actions.

9.1.1 General system setup for a rendezvous mission

The general system setup of the space and ground segments of chaser and target is shown in figure 9.1. It is assumed here that each vehicle has its own control centre (CC). However, in cases where the chaser and the target are operated by the same authorities, a part or all of the ground segment functions of both vehicles may be performed by the same centre. In this case, each of the vehicles will probably have its own control team.

Chaser and target vehicles can be controlled independently during the mission phases of launch and phasing (figure 9.2). Except for mutual exchange of information concerning mission progress, only one type of data is required by the chaser CC from the target CC, i.e. the precise orbital parameters of the target station. As these parameters will change over time, regular updating will be required. All this information exchange can be performed off-line, e.g. by voice or electronic mail communication, as there is no need, at this stage, to involve the partner in the space–ground data stream of the other vehicle.

From the end of phasing onwards, when the chaser is transferred to an orbit close to that of the target (e.g. to an ‘initial aim point’), continuous information exchange

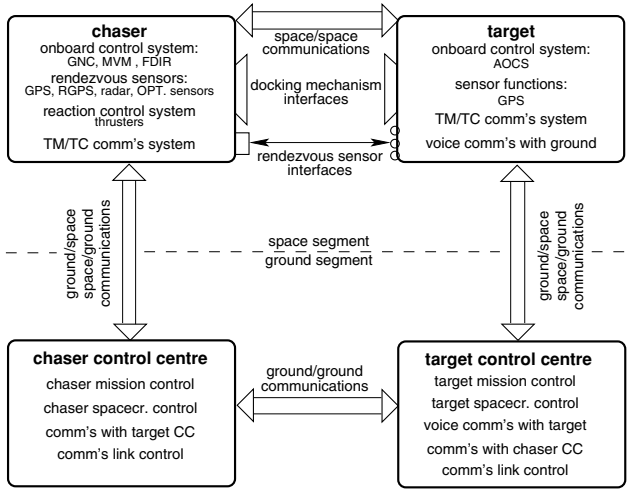

Figure 9.1. System functions and interfaces in a rendezvous mission.

between the two control teams is required. At this stage of the mission, space–space communication links between chaser and target have to be established and verified, operational schedules of both vehicles have to be synchronised, manoeuvres and trajectories of the chaser have to be assessed concerning collision safety, and decisions concerning continuation of the nominal approach at hold points or 'gates' have to be made jointly by the chaser and target control centres. During proximity operations, i.e. starting from a distance where the target or a safety zone around it (see figure 5.24) could be reached within the next following manoeuvre, a control hierarchy must be put in place which coordinates the operations of chaser and target space and ground segments (figure 9.3). One of the control centres must then have the lead concerning decisions on the further approach. In the case where an unmanned vehicle is the chaser and a manned space station is the target, the highest authority must be with the control centre of the manned vehicle, i.e. the target. In contrast, if the chaser is a manned vehicle, the highest authority will probably be with the chaser CC, as the chaser has the better manoeuvring capability.

During all phases of a rendezvous mission, each control centre will be responsible for monitoring and control of the subsystems and of all hardware and software of its own vehicle. After mating, the control centre of the target vehicle will, in a space station scenario, have the authority over the joint complex. In other cases, where the target is smaller, has less control intelligence on board, or is unmanned and the chaser is manned, the situation may be reversed. The various types of responsibilities and authorities during the rendezvous process are discussed in more detail below, after identifying the tasks which have to be performed by the ground segment during the mission.

Concerning the control of the approach and capture process, the major tasks of the chaser CC in the different phases of a rendezvous mission are as follows.

- After launch and during phasing:
  - preparation, initiation and verification of all manoeuvres.
- During the nominal rendezvous phases:
  - monitoring of manoeuvres/trajectories controlled by the onboard system;
  - issuing of 'go-ahead' commands for approach continuation at hold points.
- During capture:
  - monitoring of the capture process in the case of automatic docking.
- In case of contingencies:
  - issuing of commands for approach interruption in non-safety-critical contingencies;
  - issuing of commands for a CAM, in the case of major malfunctions of the onboard system, or of major trajectory deviations, which may lead to collision danger (if a CAM has not been executed by the onboard system);
  - preparation and implementation of recovery actions after CAM or mission interruptions.

It should be pointed out that various approach scenarios including all conceivable contingency cases will have to be worked out in detail, during mission planning prior to launch. The contingency actions to be taken by ground controllers and station crew must be well documented and agreed on by all parties, such that each individual knows immediately how to respond. However, not all types of contingencies can be foreseen, and not all recovery actions can be pre-planned. For the follow-on steps, *ad hoc* decisions may have to be taken.

In addition to the trajectory control tasks, the chaser CC has to perform a number of other tasks related to the control of the spacecraft and the space and ground infrastructure. The most important of these tasks are:

(1) monitoring and control of chaser spacecraft onboard systems and equipment;

(2) communication with the ground segment of the target;

(3) control of the communication links.

The first of these tasks is, in principle, no different from the ground control tasks for single spacecraft, except for the monitoring of the rendezvous specific onboard systems. Similarly, the third task is, in principle, no different from that for other space missions,

except for control of the communication links to the target CC. The communication and close cooperation with the control centre of another vehicle is, however, a new rendezvous specific task, which also includes the new problem of arrangement of the hierarchy of control authority.

Assuming a rendezvous mission between an unmanned chaser vehicle and a manned space station, the major tasks of target ground segment (target CC) during the rendezvous mission would be as follows.

- After launch and during phasing:
  - monitoring of the chaser's mission progress, using data provided by the chaser CC.
- During the nominal rendezvous phases:
  - preparation of target spacecraft for final rendezvous and mating phases;
  - involvement in 'go-ahead' decisions after hold points;
  - monitoring of final approach trajectory, capture and structural connection.
- Control of the joint complex after attachment of the chaser.

The tasks to be performed by the target CC during the rendezvous phases require detailed information on the chaser state vector and, for docking, on the functional status of the docking mechanism of the chaser.

In the last part of the approach in a space station scenario, the target crew also must possess all the available information on the trajectory and attitude of the chaser vehicle. Therefore, in the rendezvous phases these data will be transmitted on the local link from the chaser to the target station and then, together with the target data stream, to the target CC.

9.1.2 Control responsibilities and control hierarchy

From the above listed tasks, which have to be performed during the rendezvous phases by the remote operators in the chaser and target CC and in the target station, different types of responsibilities can be identified and a control hierarchy may be derived. The responsibilities of the various parties can be generally grouped into four categories:

(1) responsibility for proper operation and health of onboard functions of a vehicle;

(2) responsibility for initiation and execution of manoeuvres, for change of trajectory and attitude of a vehicle;

(3) responsibility for safety monitoring regarding collision danger and for initiation of collision avoidance actions if necessary;

(4) responsibility for mission plan execution and for mission re-planning.

Control responsibility for the onboard system

All remote operations related to the proper functioning of the onboard systems will remain, during the entire mission, the responsibility of the specific control centre of each vehicle. Such operations will include, e.g., the checking of hardware and software functions, failure identification following warnings or automatic redundancy switching by the onboard system and overriding of the decisions of the onboard system, if necessary.

Control responsibility for manoeuvres

The second type of responsibility, with one exception, will also remain during the entire rendezvous mission the responsibility of the control centre of each vehicle. This is the safest way of operation. A direct interaction with a spacecraft by a foreign team that does not possess all the detailed knowledge of design and behaviour of the vehicle would always compromise the functional security of the spacecraft. The one exception is the initiation of a stop, retreat or CAM command in the case of immediate danger of collision. Such interactions will therefore be restricted to very simple operations and single commands. If more complex interacting operations are foreseen, as (e.g.) with the remote manual control of the chaser vehicle to ensure mission success (see section 6.5), long and detailed training of the operator will be necessary.

Collision safety responsibility

This will, by nature, involve all participating parties of the mission. Although the onboard system has its own failure detection and CAM initiation function, there may be contingency cases where remote operators in the control centres of the chaser or in the target station can identify a collision danger situation which has not, or not yet, been detected by the onboard system.

The depth of involvement of target ground operators or crew will depend, however, on the phase of the mission, or rather on the time remaining up to a potential collision. As long as this time is relatively large, e.g. at the beginning of a typical half orbit duration manoeuvre, there will be still be time for the chaser ground operators to initiate a stop, retreat or CAM, when a dangerous situation has been detected by the target side. However, when the two spacecraft are at such a distance that collision could be imminent within a few minutes, it will no longer be safe to rely on an initiation of the manoeuvre by the chaser CC after a verbal CAM request by the target CC or crew. Because of the possibilities of communication link failures or operator mistakes it is necessary that, in addition to the chaser onboard system and chaser ground operators, the target ground operators and crew must also have in the last approach phase a direct command capability to stop the approaching chaser vehicle or to remove it from the close vicinity of the space station.

Mission responsibility

All decisions related to the mission have, in principle, to be taken jointly by both control centres. As there will be time restrictions, operation schemes must be set up according to the mission phase, to ensure that decisions can be made between the two control centres within the necessary time. For the nominal case, mission planning has been performed and agreed between the parties long before launch. The most important joint decisions to be made during the mission are the ones for 'go-ahead' at hold points or entry gates. For non-nominal situations, e.g. in case of interruption or delay of the nominal mission, contingency operations and mission re-planning have to be performed. Contingency operations fall under the control responsibilities for manoeuvres and collision safety, discussed above. The formation of a new mission plan may be performed by either of the control centres or jointly; the implementation will inevitably require joint decision making.

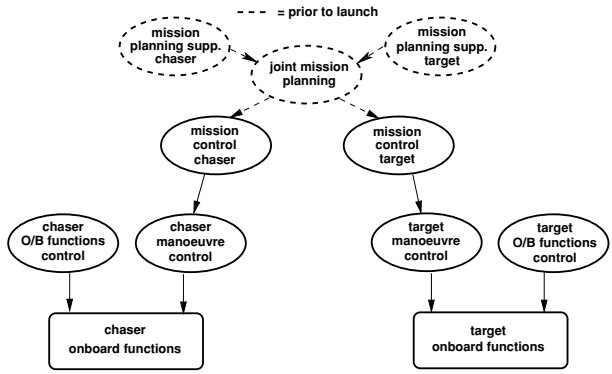

Figure 9.2. Responsibilities of ground control teams prior to the rendezvous phases.

Figures 9.2 and figure 9.3 show how the responsibilities are distributed for mission phases prior to rendezvous and for the final rendezvous phase, respectively. Before entering into the rendezvous phases proper (for a definition of rendezvous phases see figure 2.1), the two control centres can independently control the execution of the mission plan for their own vehicle. In the case of delays or more important contingencies, there is, at this stage of the mission, probably sufficient time available to prepare off-line a new mission plan and agree on it afterwards, while a (possibly pre-planned) contingency manoeuvre plan is executed by the chaser CC. This could be, e.g., a transfer to a higher orbit, gaining time by the slower phasing velocity, or a continuation of the nominal mission up to the first hold point and waiting there.

The situation is different during the rendezvous phases (figure 9.3). Any contingency leading to a delay, mission interruption or a mission abort must be handled in a coordinated manner. These types of contingencies will eventually lead to a loss of synchronisation with communication windows and illumination conditions and will instigate

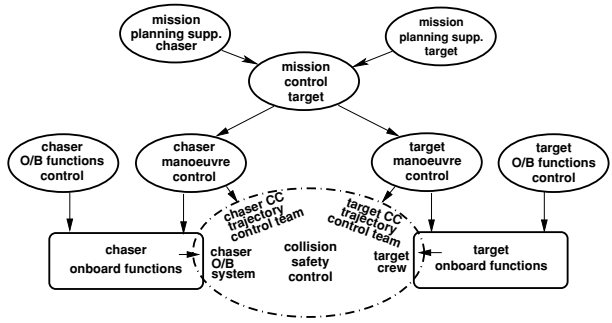

Figure 9.3. Responsibilities of ground control teams during final rendezvous.

re-planning of the approach. In contrast to the pre-rendezvous phases, there is, in the vicinity of the target, not much time available for re-synchronisation. As a result, at this stage any changes in the approach sequence immediately affect the operations planning of both vehicles. For this reason, a hierarchy of authority and rules must be established, which have to be followed in case of contingencies. This will ensure sufficiently fast and coordinated reactions, on either side, to ensure collision safety and to elaborate and implement recovery and mission re-planning. The rules to be followed will depend on the type of trajectory flown and on the distance to the target, i.e. the time left to a potential impact. For example, in the ISS scenario it is a requirement that prior to initiating a chaser trajectory which will enter the 'Approach Ellipsoid' (see section 5.6), mission authority will be transferred to the ISS CC, which at that point becomes the highest control authority for both vehicles.

The hand-over of the mission authority to the target CC at the start of the close range rendezvous operations requires that the target CC receives sufficiently detailed information on the chaser that enables it to make judgements on proper mission progress and on possible collision danger. The necessary information includes the chaser state vector (position, attitude and rates) and general information on health and redundancy status of chaser subsystems involved in the rendezvous process. If, in the case of a contingency, the mission authority decides on a mission hold (stop on straight line trajectory or retreat to a hold point), the mission timeline will have to be re-planned in order to synchronise the approach sequence with communication windows and Sun illumination, and possibly also with the work/sleep schedule of the crew in the target station. As the resources and corresponding infrastructures (e.g. relay satellites, ground links) of two vehicles are involved, re-planning will have to be carried out in cooperation with the mission planning support teams of both control centres. In the case of a CAM, both sides will have to analyse whether and how the remaining resources will allow a recovery strategy and/or a resumption of the mission.

As already mentioned, the chaser and the target may be controlled by two teams in the same control centre, as has been the case in the past in both Russian (Soviet) and

US rendezvous missions. In such cases, the separation of control authorities may be less pronounced. In future scenarios, such as that begun with the ISS, chaser and target vehicles will more often be owned by different powers. This requires a clear definition and separation of control authorities.

9.2 Ground segment monitoring and control functions for RVD

9.2.1 The concept of supervisory control

During the rendezvous phases of a nominal mission, the automatic control system of an unmanned chaser vehicle performs practically all the tasks necessary for the approach up to capture, so the human operator at the ground control centre mainly has to monitor the evolution of the trajectory and attitude of the vehicle and the status of its onboard systems. The term 'human operator' is used here for any member of the control team involved in monitoring and command, in contrast to the automatic operations by the onboard system or to automatic operational functions of the ground segment. In the nominal mission, in addition to the few tasks identified in section 9.1.1, the human operator may have to send to the onboard system an update of the mission timeline, e.g. if there are unexpected minor delays. Such delays may be caused by any reason, not necessarily only by the chaser.

Despite all analysis, design and verification efforts, it will never be possible to create an automatic system which can cover all contingency cases and take into account all possible causes and combinations of external and internal malfunctions and disturbances. Therefore, human operators need, in addition to the tasks identified for the nominal mission, to be able to interact with the onboard system, to command thrust manoeuvres, to change the onboard system configuration and potentially to up-link modified control software. This concept of monitoring and high level interaction in cases where extra intervention is required has been termed 'supervisory control'.

For unmanned vehicles, remote human operators on ground or in the target vehicle can, in the case of contingencies, to a certain extent take over the role of a pilot. In particular, for mission success probability, for which the automatic system usually provides only single failure tolerance, the direct control of the spacecraft motion by human operators may be helpful in rescuing the mission. In contrast to 'supervisory control', this concept is called 'manual control', and has been described already in section 6.5.3.

Whereas in contingency situations the pilots aboard manned vehicles can provide human intelligence to analyse the problems and find solutions, an automatic system can handle only those cases which had been considered already at its design. For automatic vehicles, it is, therefore, essential that the information necessary to analyse potential problems is provided to the human operator on ground. In contingency cases for normal

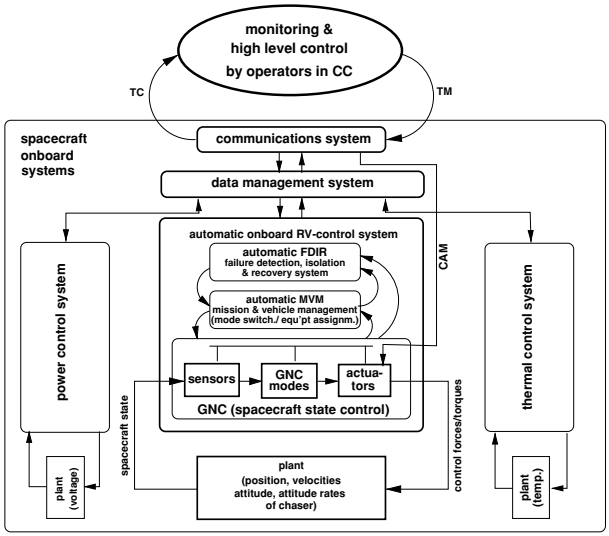

Figure 9.4. Supervisory control of automatic onboard system by ground operators.

satellites with more or less fixed orbits, comparatively large periods of time are available for the ground operator to fix a problem. On the contrary, in a rendezvous mission, the required reaction times are much shorter, ranging from a few seconds up to one half orbit maximum (3/4 h), depending on the trajectory and distance to the target. To perform the tasks of 'supervisory control', operators in the control centres need computerised support tools which facilitate fast recognition of the situation and immediate preparation of the necessary commands for trajectory safety and recovery.

To be aware of the situation, and to be able to analyse and predict the future state, the human operator needs to know the actual status of the vehicle functions and, as much as possible, the individual outputs of equipment and functions. These data must be compared with the planned data for the actual point in the mission timeline. To protect the target vehicle from collision danger, the operator must be able to identify very quickly the danger and provide commands to the chaser vehicle, e.g. for a stop on a straight line trajectory, for a retreat to a safe hold point, or for a CAM. To ensure mission success, the operator must be able, following any delay or change in trajectory sequence, to re-plan the mission and to provide the corresponding commands for manoeuvres, change of timeline and trajectory parameters to the onboard system.

To enable the operator to identify failure causes, the support systems should provide (in addition to the currently transmitted onboard data) detailed information on the nominal (expected) status of equipment and software and on the expected processing results of all subsystems at the time in question. The support systems should also be able to provide information on the effects of typical equipment and software failures.

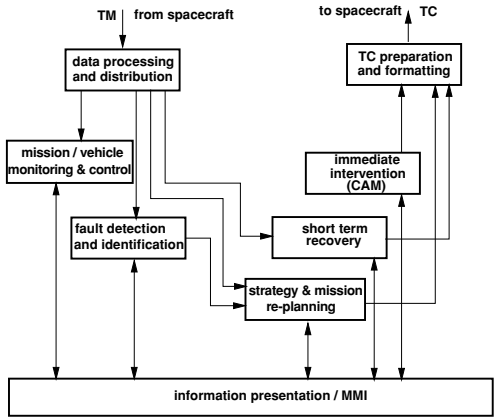

Figure 9.5. Ground operator support functions.

9.2.2 The functions of a support tool for ground operators

The typical functions of a support tool for operators in a control centre are shown in figure 9.5. The telemetry (TM) data received from the spacecraft are processed and distributed to the monitoring functions, to the failure detection and analysis functions and to the re-planning functions. The output of these functions to the operator and the operator's input to these functions are performed via the man–machine interface (MMI), which, in the simplest case could be a normal computer screen and a keyboard. Commands and data sent to the spacecraft need to be formatted, packaged and inserted into the telecommand (TC) data stream.

Monitoring

Monitoring information must contain the state of the vehicle concerning attitude, position and rates (together with the planned values) relating to the actual point in the mission timeline, the present GNC mode, the actual configuration of equipment and functions and the status of the communication links. For this purpose the telemetry data stream from the vehicle must provide update information on the state vector and onboard system conditions at sufficient frequency. The data must be processed and displayed in such a way that the operator can quickly grasp the situation and make appropriate decisions.

To provide the reader with an idea of the ways in which spacecraft data could be displayed, concepts of a trajectory monitoring display and of a system monitoring display are shown in figures 9.6 and 9.7. Similar concepts have been described in Fehse & Ortega (1998); Ortega & Alvarez (1998); Sarlo, Barrera & Ortega (1998); Ortega (1999); and Sarlo, Barrera, Ortega & Franco (1999). As not all information can be displayed on one screen, the basic concept includes a stack of displays, which can be called up by clicking via mouse and cursor on a button or a particular field in the display. This starts

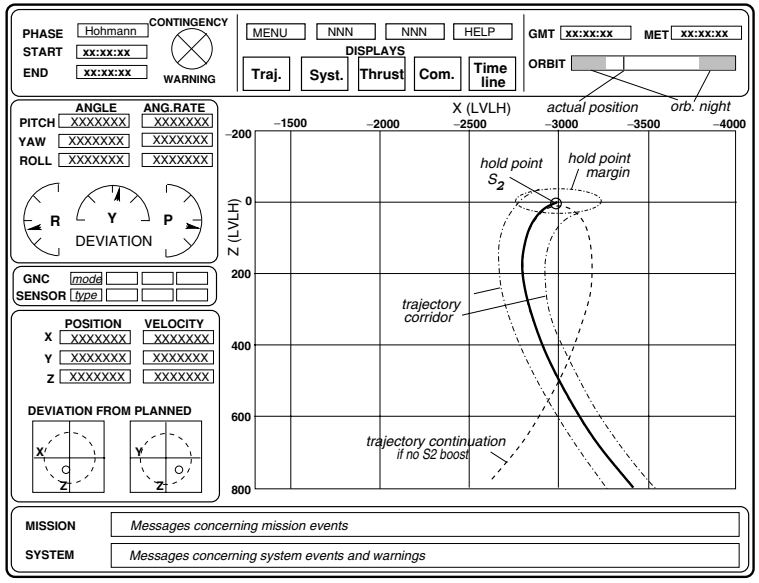

Figure 9.6. Concept of a trajectory monitoring display for ground operator.

the new display indicated by the button or field. For example, in the system display shown in figure 9.7, one could click on one of the fields, such as 'propulsion system' or 'data management system' to bring up on the screen a more detailed display of that particular function. Fields and buttons for particular functions should be colour coded to indicate the status of that function. Such colour codes could be, e.g.,

green = engaged – healthy
blue = not engaged – healthy
red = engaged – failed
violet = not engaged – failed

There may be top and bottom bars or windows arranged at the sides of the screen, which would be the same for all displays. These common fields for all displays could contain general information on the mission, e.g. on time, mission phase, orbit position, and further messages and warning lights for major contingencies and buttons to switch between major displays. The buttons in the fixed part of the display should be the ones needed by the operator to switch between those displays which are providing a complete high level overview on the status of the mission and of the spacecraft systems. The buttons for switching to the major displays could also be colour coded, indicating the display where the nature of the contingency can be found. In addition, there should be a flashlight in the fixed part of the display, to warn the operator in the event of critical

contingencies, whatever display is switched on. Such critical contingencies could be the interruption of communications between chaser and target for longer than a specified duration, the transgression of safe limits for state vector components (position, attitude, rates), unrecoverable thruster failures, loss of last redundancy level for critical equipment, etc.

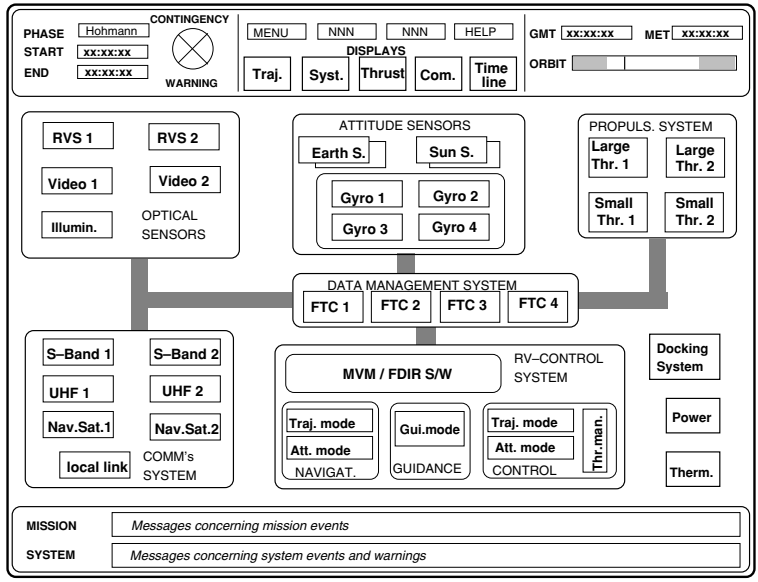

Figure 9.7. Concept of a system monitoring display for ground operator.

For the last few tens of metres of the approach up to contact, a display of a video picture of the opposite vehicle together with the relevant system information, as shown in the crew operator display, figure 9.8, would also be useful for the ground operator. This requires, however, the availability during this period of a downlink with the capability of transmitting video data (cf. table 9.1). This is not available with the normal links used for TM/TC transmission. In the Russian space programme, a chain of ground stations has been set up for this purpose, as shown in figure 5.20, from where the video information is transmitted to the control centre. In this case both the following synchronisation requirements have to be fulfilled: the last metres of approach and docking must take place at proper illumination conditions and when the vehicles pass over the dedicated ground stations.

Immediate intervention

In this function, pre-programmed commands or command sequences are stored, which can immediately be called up by the operator and sent via the TC formatting function to

the spacecraft. Pre-programmed commands will be used in the nominal case for, e.g., the 'go-ahead' commands after hold points. In contingency situations they are used for commands to stop motion on V-bar or to initiate a CAM. As the CAM may be different for each approach phase in terms of ΔV and thrust direction, the pre-programmed CAM command must be linked to the current approach phase. Also, a command for a stop on V-bar must be inhibited for all approach trajectories which do not follow a straight line V-bar approach. For safety-critical operations, such as the command of a CAM or of an immediate stop on V-bar, the input may be given via a separate protected button, hard-wired to the 'TC send' function.

Short term recovery

Procedures for manoeuvre sequences are stored in this function. These procedures are not fixed single commands or fixed command sequences, but require, for each point on a trajectory where a contingency happens, a new calculation of the starting time for the next thrust manoeuvre, or of the ΔV to be applied, or both. Also, different GNC modes and altered sequences of trajectories and attitudes can be stored in this function, e.g. to retreat from points on the nominal approach trajectory to the previous hold point.

These are all short term manoeuvres to be followed in cases of limited mission interruptions or delays, i.e. where the subsequently resumed approach follows the nominal sequence. In this case, the control software does not need to be changed and, for the resumed approach, only the timeline has to be updated such that it is re-synchronised with external events such as Sun illumination, communication windows, etc. Recovery of the nominal approach sequence may take place, e.g., after hold on V-bar, after return to a previous hold point or after retreat to a safe waiting point on V-bar. Opportunities for re-synchronisation may occur immediately in the next few orbits or otherwise after about 24 hours.

Mission re-planning

This function is required to ensure mission success after large deviations from the nominal trajectory or timeline. For instance, after a CAM, the position and velocities of the chaser vehicle would be so far away from the nominal state that a complex sequence of manoeuvres needs to be performed to return to a position from where the nominal automatic approach sequence can be re-initiated. As the amount of time and propellant required for recovery would rapidly increase with the duration of the contingency, a recovery strategy would need to be worked out, and the manoeuvres would have to be defined quickly. The function will, therefore, have to include a fast computer for strategy re-planning and a high fidelity orbit dynamics and environment simulator to verify the recovery mission plan.

Failure detection and identification

This function must permit the operator to arrive quickly at an assessment of the nature and severity of the failure. If possible, the operator should also identify the cause of the failure, in order to be able to judge the potential long term repercussions. Failure identification will begin with a general indication that a function or equipment has malfunctioned or that a parameter is outside the nominal margins. Failure identification can be supported by computer programs, which, e.g., can compare the actual values received from the onboard system with the nominal ones, obtained by support equipment in real time or by analysis prior to the mission. For fast identification of detailed causes of hardware and software malfunctions, so-called 'expert systems', i.e. knowledge based search programs, may be developed. For the constraints in transmitting onboard data to ground, see section 9.3.2.

It is obvious that the above description of functions can indicate only basic requirements and concepts. There are many ways of implementating the functions, and, as in the case of many other functions, the accumulated experience with available equipment and procedures may be the decisive factor for the actual implementation. Where the same parameters have to be monitored in the same mission by two different control centres for the close range rendezvous phases, a certain standardisation would be advantageous. A standardisation of essential display features would facilitate the communication between the control centres concerning the assessment of the particular situation when decisions become time-critical.

9.2.3 Monitoring and control functions for the target crew

As discussed above, in the close vicinity of the target, the crew aboard the target station must also be able to monitor the chaser's deviations from the planned state vector evolution, the status of the chaser's equipment essential for the control of the approach and the status of the communication links. The crew operator must further be able to command a stop, a retreat or a CAM, if the situation makes immediate action necessary and if there is no time available for the involvement of the ground operators. This requirement means that the crew should have available support tools similar to those in the charge of the ground operators. It will not be necessary, however, for the crew support tools to contain the more complex analysis and re-planning functions that are required for the support of the ground operators. Monitor display designs for crew operators in a space station need to be compatible with the computer screens available aboard the vehicle. In the past, television type cathode ray tubes (CRT) have been used in the Russian (Soviet) and American space programmes. The amount of graphic detail and text which could be displayed on such screens, however, was limited. On the laptop computer screens available to the crew in the ISS, probably less detail can be displayed than on a large computer screen on ground. In addition, on ground there will be a team of several people available for monitoring and control of the various parameters and features, whereas in orbit there is probably only one crew member available for this task.

The most important monitoring tool for the crew operator will be a monitoring display showing the relative state of the chaser vehicle w.r.t. the target. When the chaser is at a distance where only sensor information is available, this display can be designed to be similar to the trajectory display for the ground operators (see figure 9.6). In the close vicinity of the target, when the approach is additionally monitored by a video camera, a different type of display may be used, which would then include the video information. As it is advisable that the operator in the target station can concentrate during the most critical part of the approach on one single screen, it is preferable that trajectory and RV-control system information is superimposed on the video picture.

Such a system was developed in Russia to monitor the Soyuz and Progress rendezvous operations with the Mir Space Station. The system used analogue (television) techniques for video display, which included alphanumeric information on the relative state vector. At the time of writing, this system was still in use on the Russian part of the ISS.

A modern concept for such a display, integrating a digital video picture with control system information on a LCD computer screen, is shown in figure 9.8. A similar display has been shown in Sarlo *et al*. (1999). It is assumed here that the video camera is located on the chaser vehicle. In a $-$V-bar approach, this arrangement has (a) the advantage of better Sun illumination conditions at the end of the approach, and (b) provides the same view as a pilot in the chaser vehicle would have. On the target vehicle a visual target pattern of the type shown in figure 6.23 is assumed to be mounted in a position opposite to the camera when docked. If the chaser is on the nominal approach line with the correct relative attitude to the target, this target pattern would be in the centre of the image. Fixed grids would enable the operator to make judgements about linear and angular misalignments of the chaser vehicle during approach. In addition, position, velocities, attitude and angular rates could be displayed in alphanumeric form. Translational accelerations and angular rates could be displayed as arrows, which would enable the operator to assess the trend of trajectory and attitude development.

Flashing lights could warn the operator, e.g., about contingency situations in the automatic system and about critical link interruptions. For the chaser–target–chaser link the target operator has the main monitoring responsibility. Function buttons on the main monitoring screen would enable the operator to switch over to other displays, such as the trajectory display, the system display or (after contact) to the docking system display. In addition to the information on the chaser, some essential information on the status of the target system could be provided on a dedicated status display. Colour coding of the switch buttons could, as in the case of the ground operator tools, provide additional information on the type of contingency and could indicate where to look for more detailed information.

The onboard operator will also need a minimum of command capability for collision safety control, as discussed in section 9.1.2. Such commands may be:

- thrust inhibit,
- stop on V-bar,
- CAM.

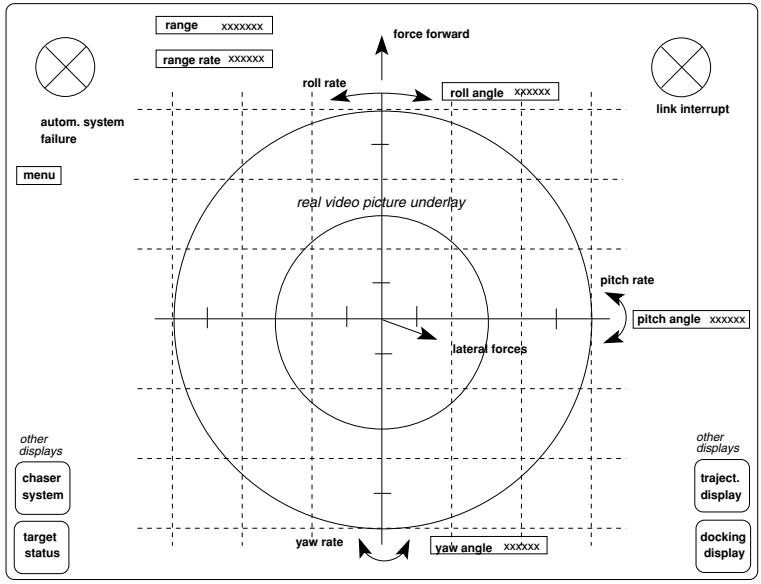

Figure 9.8. Concept of a final approach monitoring display for the target crew.

The available commands will depend on the stage of the approach, as the first two commands make sense only for particular trajectories and distances from the target. For instance, ‘thrust inhibit’ may not be of much use on two-pulse transfers, where the trajectory just naturally continues. Depending on the approach velocity, thrust inhibits may even be dangerous in the last part of a V-bar approach. A ‘thrust inhibit’ command would be a useful remedy in the first part of V-bar and R-bar straight line trajectory, when the resulting trajectory is collision safe (see section 4.4.2). The ‘stop on V-bar’ command must be inhibited for all guidance modes except ‘straight line V-bar trajectory’. The ‘stop on V-bar’ command requires that the chaser RV-control system is fully functional, as after reception of the command the onboard system has to engage automatically a deceleration mode and subsequently a position keeping mode.

The command interfaces for an operator in the target station will probably be just one or two physical buttons, hardwired to the communication function. These buttons, particularly the one for the CAM, will have to be specially protected to avoid inadvertent activation. In the nominal approach case there will be no interaction between the target crew and the chaser vehicle.

Manual control of the chaser by a target operator as a backup for mission recovery has been addressed already in section 6.5.3. The command interfaces for this case could consist, e.g., of two joysticks, where one is for the control of the three translational DOF and the other one for the three rotational DOF. This is the concept for manual control of the unmanned Progress vehicles implemented in the Mir and ISS scenarios.

9.3 Communication constraints

The purpose of this section is to give a short overview of the repercussion of communication constraints on the automatic rendezvous operations and on the monitoring and control by remote human operators. It is not the intention of this chapter to cover space communication systems and structures. Detailed information on these subjects can be found in, e.g., Morga & Gordon (1989) & Wertz & Larson (1991).

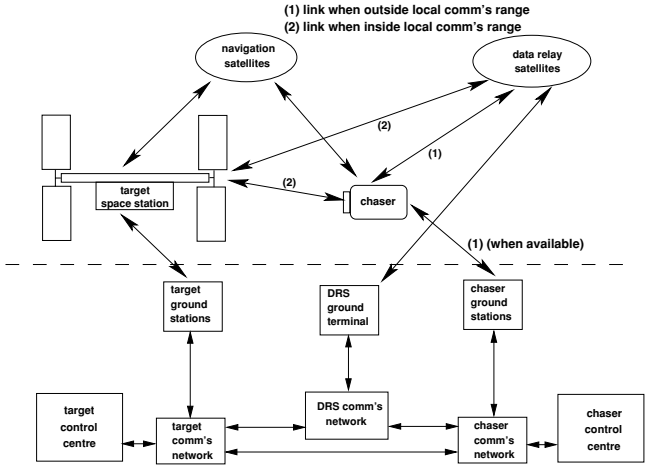

Figure 9.9. Overall communication scenario for a rendezvous mission.

A typical communications scenario for a rendezvous mission is shown in figure 9.9. Both vehicles communicate with their respective control centre via data relay satellites and, when available and if planned, via dedicated ground stations. In the rendezvous phases, when local communications and relative navigation have started, the information on the state vectors of both chaser and target must be available in both control centres and, during the very last part of the approach, also to the station crew. For this reason, communications may be routed via one of the two spacecraft, usually the target station, and the combined data stream will be distributed to the control centres. In the case of relative navigation using navigation satellites, a communication link between chaser and target needs to be available anyway (see section 7.3.3). The ground communication networks of chaser, target and relay satellites will use both dedicated lines and commercial ones, rented during the mission from local telecom organisations. The latter possibility has to be considered in particular for links with ground stations that are located in remote parts of the world, but is potentially used also for some of the other ground links. Whichever link is used, the space ground data stream will pass on its way from the spacecraft to the ground control centre, or vice versa, through many receivers, amplifiers and computers, potentially adding noise and delays. The major issues and

constraints associated with the communications links in a rendezvous mission are as follows.

- Communication windows: the point in time and duration for which data exchange between space and ground is possible.
- Availability and reliability of the links: the probability of deteriorations, interruptions or losses of the link and the corresponding loss of data.
- Constraints of the communication link due to bandwidth or data rate limitations: the capability of transmitting a certain amount of data per unit of time.

The first issue has been discussed already in section 5.4.2; the most important aspects of the two other issues are discussed below.

9.3.1 Data transfer reliability

Considering that the link budget is designed, under normal conditions, to provide sufficient margin for the sender–receiver distance, link deteriorations or interruptions can be causes by:

(1) equipment failure of communications equipment in the spacecraft, on the ground station and in the intermediate link constituents such as relay satellites, telephone lines, etc.;

(2) too low signal-to-noise ratio of the received signal due to (i) attenuation by atmosphere, e.g. at low elevation angles of the antenna LOS and by rain, due to (ii) attitude changes of the spacecraft, reducing the antenna gain, and to (iii) shadowing by structural elements of the spacecraft or by the other vehicle etc.;

(3) disturbances of the received signal by other radio sources sending on the same frequency and by multi-path effects.

Communication equipment (receivers, amplifiers, etc.) both on spacecraft and in the ground station can be made redundant. This is, however, generally not possible for the complete link. The radio link between the antennas of the spacecraft and the ground station, the links to and from the relay satellites, and the telephone lines on ground are generally not redundant. Except for the very limited possibility of parallel communication, e.g. (a) directly with a ground station and (b) via a relay satellite, there is no complete redundancy in ground–space communications. When considering the collision safety control aspects during the last part of the approach, the fact that that communication links are prone to failures is of particular importance.

There are systematic and random link interruptions. The systematic ones, e.g. those due to coverage by ground station and relay satellite, can be well predicted and taken into account during the mission planning. Random interruptions, e.g. those due to atmospheric disturbances and other causes (see points (1)–(3) above) can be predicted

only with a certain statistical probability. The duration of such interruptions will always remain uncertain. Typical data on length and frequency of occurrence of such interruptions can, however, be determined empirically in a scenario with frequent rendezvous missions, such as the Mir or ISS scenarios.

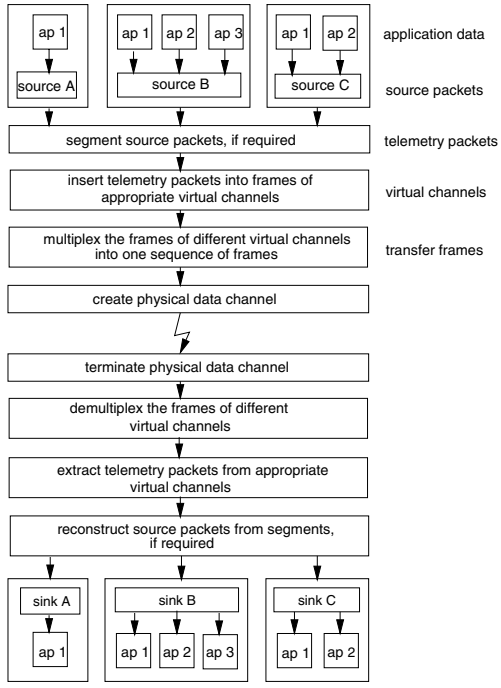

Figure 9.10. Packet telemetry data flow (after CCSDS 1987 a,b).

Because of the potential disturbances and interruptions, all communication between the spacecraft and ground, i.e. both the telemetry (TM) and the telecommand (TC) streams, need to be protected by encoding, to facilitate the checking of the integrity of received data. For this purpose, standards for packet telemetry and packet command streams have been developed, which are today used by most spacecraft (CCSDS, 1987 a,b). Figure 9.10 shows the various steps of encoding and decoding of a packetised TM-stream with application data from various sources of the spacecraft, i.e. spacecraft subsystems and payload.

The packet TM transmission protocol ensures that corrupted packets will not be used in the decoded application data and that an error message is issued when a package has not been received. A segmentation process permits the breaking up of very long source packages into shorter pieces to fit them into the data flow. By assigning each

group of sources to a dedicated sequence of transfer frames, virtual channels are created in accordance with the frequency requirements of the source data. The frames of the different channels will be inserted into a sequence of frames, which is the data stream transmitted to ground.

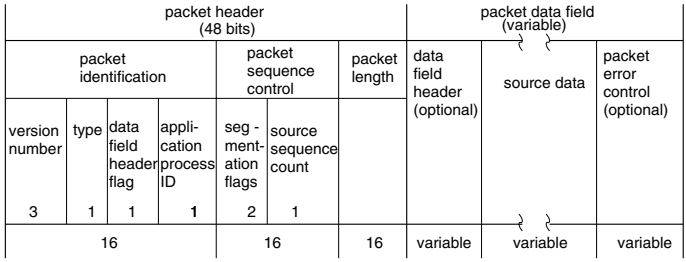

Figure 9.11. Format of a source packet (after CCSDS 1987 a,b).

The format of a source packet, figure 9.11, is the one described in CCSDS (1987b) as 'version 1' format. It is the firstlevel of encoding identified in figure 9.10. The source packet has a header, which includes identification, sequence control and length, and a data field, which can be arranged according to the needs of the source applications. Similar codes in headers and trailers will be added at each further step of encoding shown in figure 9.10. As most space communication systems are capacity-limited, the penalty to be paid for this reliability improvement mechanism is a reduction of transmittable data rate for the applications. To send the data flow from the transmitter to the receiver antenna, so-called 'channel coding' is applied, which has the effect that distinct messages are clearly distinguishable from others (CCSDS 1997). In combination with data compression techniques, 'channel coding' achieves transmission of higher bit rates at lower bit error rates.

Packet TC transmission is implemented in a similar way. In addition to the first measure, which concerns the completeness of the shell of the information package, the proper receipt of the information contents can be ensured by additional measures, e.g. the acknowledgment of TC by the onboard system.

9.3.2 Data transmission constraints

In addition to interruptions and distortions, the constraints for the data transmission between the ground and space segment during a mission are:

- the planned availability of the links,
- the delays with which the data arrive at their destination,
- the data rate or frequency bandwidth which can be transmitted.

Planned availability of links

Many of the ground links and the links via relay and communication satellites will be rented from other authorities (including commercial ones) for the time of the mission. Contingency situations causing approach delays will have to be taken into account in the planning of the availability time. For cost reasons it may, however, not be possible to cover all possible contingencies by a fixed duration of the planned link availability. This is true particularly for TV channels, if docking under video monitoring by ground is planned. As the recovery from a CAM (e.g.) may take one or more days, possibilities must be planned to re-open such an expensive link when required.

Communication delays: space–ground, ground–ground

Due to the altitude of the relay satellites (36 000 km), the two-way communication delay is 0.24 s. To this amount must be added the receiver–transmitter delays of the spacecraft (in the case of transmission from the chaser via the target, of both spacecrafts) and of the relay satellite as well as the delays due to the ground links. Because of the multitude of amplifiers and computers in the ground links and of the possibility of additional ground–space hops via communications satellites between the ground station (antenna) and the ground control centre, the total round-trip time may take a couple of seconds. This has to be taken into account in the timing of manoeuvre commands and in the evaluation of TM data. Solutions to this problem include the application of time tagging for manoeuvre execution and of time markers for TM, e.g. to identify the correct time relation of GNC data.

Communication data rates: space–space, space–ground

There are usually limitations of data flow between space and ground due to the data rate capacity of the link. As we have seen in the previous section, not all the total data rate of a link is available for transmission of user data, but in the case of encoding in packages a part of it will be needed for securing the integrity of the data transmitted. Because of the multiple encoding process shown in figure 9.10, a significant amount of overhead will be added to the source data in packet TM, which can be more than 10% of the total data rate, depending on the type of application and mission.

The data rate is defined as the number of samples per second times the number of bits per sample. For analogue signals the Nyquist theorem requires that the sampling frequency must be at least twice the highest frequency of the signal spectrum to be transmitted:

$$f_{\mathrm{sample}} > 2 f_{\mathrm{signal}}$$

In practice, because of filter limitations, a factor of 2.2 rather than 2 will be applied (Wertz & Larson 1991) for data transmission. For digital data transmission, the quantisation error must also be considered. The maximum quantisation error decreases from

Table 9.1. Bit rate required to transmit analogue information (after Wertz & Wiley 1991).

Analogue type of data	Max. input frequency f_m (Hz)	Sampling frequency (samples/s)	Number of bits per sample	Data rate R (bits/s)
Voice (PCM)	3600	8000	7	64×10^3
Voice (delta PCM)	3600	8000	6	56×10^3
Colour television (commercial quality)	4.0×10^6	8.8×10^6	5	44×10^6
Colour television	4.2×10^6	9.25×10^6	10	92.5×10^6

6.25% at 3 bits/sample to 1.56% at 5 bits/sample and to 0.05% at 10 bits/sample. The required bandwidth of the link will depend also on the required quality of the signal to be received. Table 9.1 gives examples of bit rates required for certain types of analogue input data. Data rates concerning television refer to US standards.

Typical TM/TC data rates required for the operation of satellites are in the range of a few tens of kilobits per second, comparable to voice channels, whereas the TM requirements of the payload will vary depending on the mission and can assume values of a few hundreds of megabits per second. A significantly higher TM data rate than for conventional satellite missions will be required for rendezvous missions, since guidance, navigation and control data for six DOF motions and information on the operations of the automatic system have to be transmitted comparatively frequently. In the example shown in figure 9.12, the total amount of information pertaining to the onboard RVC system which could be transmitted to ground is 9184 bytes or 73 472 bits. If this amount of data had to be transmitted once per second, it would exceed the capacity of a voice link. Of course, not all variables and parameters are changing or required with that frequency on ground. It could be that only a part of the information is needed at lower frequencies, at certain intervals, or only in particular situations, so that the actual data rate of this source can be significantly reduced to fit into the capacity (some tens of kilobits per second) of links for spacecraft operation. If video transmission is required during the last few metres of approach and contact, the downlink requirements increase significantly (see table 9.1). With modern compression techniques, however, the bit rate requirements can be reduced by large factors, and, due to the low velocity of approach, the number of frames per second can be reduced to values of 10 or less without significant loss of information.

Communication frequencies

Frequencies available for space operations are a scarce commodity which has to be shared by many users. With the development of radio-transmission applications, more

Table 9.2. Frequency bands used in non-commercial space applications.

Band	Frequency range	Frequency type	Use for space
	30–225 MHz	VHF	∼137 MHz (up), ∼149 MHz (down) ∼270 MHz (down)
	225–1000 MHz	UHF	400.15–401 MHz (proximity links) ∼450 MHz (up)
L-band	1.0–2.0 GHz	UHF	∼ 1.5–∼ 1.7 GHz
S-band	2.0–4.0 GHz	UHF	∼2.1GHz (up), ∼2.3 GHz (down)
C-band	4.0–8.0 GHz	SHF	∼7.2 GHz (up)
X-band	8.0–12.4 GHz	SHF	∼8.5 GHz (down)
Ku-band	12.4–18.0 GHz	SHF	13.23–15.35 GHz, (13.4–14.0 TDRSS)
K-band	18.0–26.5 GHz	EHF	16.6–17.1 GHz (down) 22.55–23.55, 25.25–27.5 GHz (DRS) ∼26 GHz (proximity, & multipoint)
Ka-band	26.5–40.0 GHz	EHF	∼32 GHz (down), ∼34 GHz (up) 37–38 GHz (lunar, planetary-down)
Q-band	40.0–60.0 GHZ	EHF	40–40.5 GHz (lunar, planetary-up)
V-band	60.0–75.0 GHz	EHF	∼65 GHz (no direction specified)
W-band	75.0–110.0 GHz	EHF	

and more frequency bands will be firmly occupied for fixed services on ground and in space. Frequency bands for any type of applications are assigned by the International Telecommunication Union (ITU), an intergovernmental body comprising representatives from the majority of countries in the world. Recommendations concerning frequencies and data formats for space applications are provided to the ITU by organisations such as the Space Frequency Coordination Group (SFCG) and the Consultative Committee for Space Data Systems (CCSDS). The frequency bands for space operations shown in table 9.2 allocated by the World Administrative Radio Conference, Geneva, are extracted from documents produced by these organisations (CCSDS, 1997). As the utilisation of radio-frequencies will evolve further in the future, re-allocation of frequencies may become necessary, and the bands available for space operations may change.

The available bands in the 2, 7 and 8 GHz regions are subdivided into channels of 100 kHz. If commercial telephone lines are used for transmission from ground stations to the control centre, the data rate limitations of these lines have to be taken into account too, e.g. 56 kbits/s for ISDN lines. Bandwidth requirements of 10 MHz and more are already now increasingly difficult to satisfy in the frequency bands for space application below 10 GHz. Frequencies above 15 GHz are, at the time of writing, less crowded. For video data transmission between the spacecraft, the 26 GHz band is suitable. Video

transmission to ground can be done, e.g., via TDRSS in the 14 MHz band, in which case a wide-band channel has to be rented for the planned transmission time. Otherwise, for direct transmission to ground stations (for communication window constraints see section 5.4.2), channels in other high frequency bands may have to be requested.

Since the capacity of the link available for user data transmission will have to be shared by the TM data from all the spacecraft subsystems and payloads, there will, for each of the subsystems, be only a very limited data rate available. In a rendezvous mission, payload data do not need to be transmitted, and the most important spacecraft subsystems are of course the GNC and propulsion systems. Nevertheless, in most cases the data rate available does not allow the transmission of all onboard data which would be of interest to the ground operator.

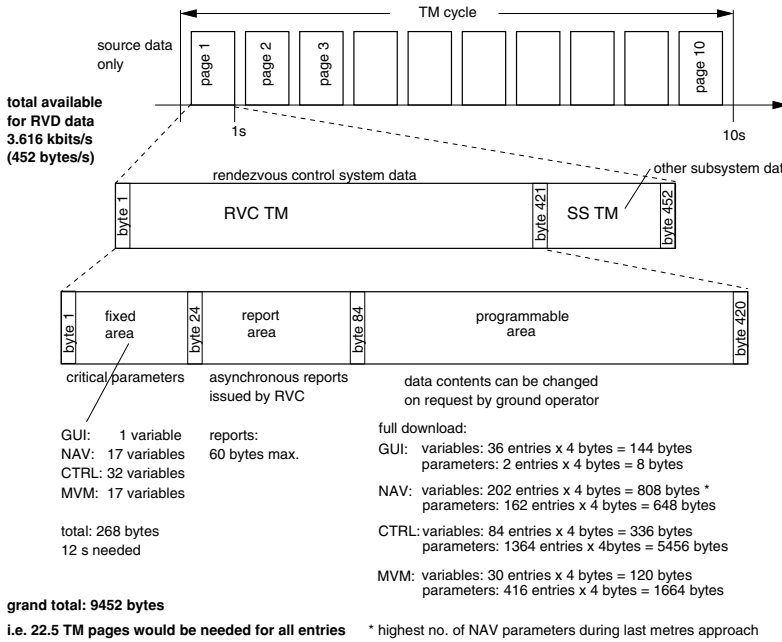

Figure 9.12. Typical GNC telemetry (TM) data transmission for a rendezvous mission.

Telemetry message format

An example of severe link limitations in the transmission of chaser onboard data is shown in figure 9.12. The availability of only 3.6 kbits/s = 452 bytes/s is assumed for the entire amount of RV-control data plus the necessary amounts of bytes for the packet header and error control. As the total amount of GNC and MVM data in this example is 9183 bytes (more than the entire capacity of a voice link), this will allow the transmission of a system overview, but no details. A possible solution to this problem could be the

creation of fixed and programmable areas in the TM-message format, where the contents of programmable area can be changed by request of the ground operator. If the data in the fixed area of the message indicate a problem in one of the functions guidance (GUI), navigation (NAV), control (CTRL) or mission and vehicle management (MVM), the ground operator can send a TC to the vehicle to change the content of the programmable area such that it obtains more detailed information on the particular function in trouble.

The problem with this arrangement is the amount of time necessary to obtain more detailed information. Another problem in this example is that the fixed data for GUI, NAV, CTRL and MVM alone have a total volume of 268 bytes = 2.14 kilobits/s, which is about 60% of the total data rate available for GNC and MVM. To have a reasonable capacity available for the programmable area, the fixed area has been limited to 23 bytes. The refreshment of all data in the fixed area would, therefore, take about 12 s.

With the target S/C (space station) acting as communications relay, additional constraints may have to be observed during proximity operations. The advantage of this arrangement is that all information which the chaser transmits to ground is automatically available also on the target spacecraft. The disadvantage is that the chaser data flow must share the total available bandwidth with the target data flow. As a result, data rate limitations as assumed in the above example can occur.

For the space–space communication link, the range which can be achieved depends on the transmitter power, the antenna areas and the frequency used, as shown in Eqs. (7.12) and (7.25). With the 400 MHz band allocated for proximity links, at reasonable transmission power only limited ranges can be achieved. The 26 GHz band offers capabilities for larger ranges.

10

Verification and validation

The final chapter of this book is dedicated to one of the most difficult issues in the development of an automated rendezvous system, i.e. the problem of gaining sufficient confidence prior to flight that the system will perform in orbit as required by the mission objectives and as intended in the design. Since orbit dynamics and the condition of 'zero-g' cannot be reproduced on ground, the function and performance of many features cannot physically be tested prior to flight. This is a general problem for all space missions. In addition to physical testing, the process of gaining this confidence will, therefore, have to include mathematical modelling of the orbital effects and spacecraft systems, and the evaluation of the behaviour of the spacecraft in the orbital environment by analysis and simulations will be based on those mathematical models. The entire process of obtaining confidence by physical testing, analysis and simulation is referred to as *verification* and *validation*, where these terms are used in the sense that:

- *verification* is the proof that
  - an item, function or process performs according to the specification, under which it has been developed;
- *validation* is the proof that
  - an item, function or process will behave as expected under real world conditions, or
  - the description by mathematical modelling represents, to a sufficient level of accuracy, the behaviour which an item, function or process would have under real world conditions.

In contrast to other space missions, in the final stages of a rendezvous and docking mission, flight operations have to be performed between two spacecraft in close proximity, and eventually physical contact has to be achieved. As these operations are safety-critical, it is particularly important to minimise prior to flight any risk concerning these

operations. This requires in the development phase a particularly rigorous verification of all functions, processes and interfaces involved in the proximity operations and a proper validation of all mathematical models and tools involved in the verification process.

10.1 Limitations of verification and validation

The highest possible confidence in the proper functioning of a function or item in the real mission will be obtained when it is subjected, during testing prior to flight, to the same environment and conditions as it will experience during the mission. Worst-case conditions of this environment need to be taken into account. Wherever possible, such functions and items should therefore be tested in a realistic physical environment, including sufficient margins to cover such worst-case conditions. For functions and performances which cannot be verified by direct physical tests on ground, two other ways of verification are available in principle: mathematical modelling and simulation or testing in orbit under the conditions of the real flight.

Verification by testing in orbit is very limited, however, not only for reasons of launch cost and opportunity. Full verification by testing in orbit is even more limited because generally the 'real world' conditions of a mission cannot be reproduced unless the complete mission is practically duplicated. Because of the cost involved, testing or demonstration in orbit is, in most cases, a matter of flight opportunity, where the test conditions have to be taken as available. In the best case, testing in orbit can be performed under similar conditions which must be proven to be sufficiently representative of the real mission. This general problem of in-orbit verification and validation will be addressed in more detail in section 10.7.

For the majority of all features in rendezvous and docking systems and operations which include orbit dynamics, contact dynamics and 'zero-g' effects, verification has to rely on tools and facilities containing mathematical modelling. For this reason, detailed mathematical models have to be established of the spacecraft, its dynamics and kinematics, of the actuators, of the sensors, of the capture equipment, of the onboard data management system and of the communications links and equipment. This modelling must include all effects that the orbital environment has on these features. To make them suitable for use in verification tools, these mathematical models need to be validated w.r.t. the according properties and effects of the real world, which are set by the spacecraft design and by the orbital environment. Development of a rendezvous and docking system therefore always includes both

- the development and verification of the onboard and remote control systems and of their constituents, and
- the development and validation of the verification tools and facilities.

The validation of these verification tools is, to a large extent, the validation of the mathematical models of the features and effects, as explained above. The goal of the

validation will be to provide evidence that the representation of the reality by the model is correct and sufficiently complete for the purpose of verification. The last requirement will be the most difficult one to fulfil, since it requires complete knowledge of the 'real world' with all its facets, knowledge that even with long experience will never be 100% complete.

Notwithstanding the above postulation of rigorous verification and validation of all functions, processes and interfaces involved in safety-critical operations, it has to be kept in mind that verification and validation are, in reality, tasks which by nature cannot result in absolute certainty, since they will always be limited in their extent. Furthermore, even if it were technically feasible to test the system, item or operation involving all environmental conditions relating to the mission, it would for reasons of time and cost be impossible to test all the potential variations and combinations of parameters and all possible contingency situations. The method generally applied is to test maximum and minimum values along with a certain representative number of combinations of such values. This is, however, not the same as testing the entire field of possible variations and combinations, as it leaves the possibility of unidentified harmful combinations. An additional problem is that tests can be performed only in anticipation of known effects, leaving the possibility of undetected side-effects.

The goal for all verification and validation efforts can, for the reasons given above, never be the achievement of absolute proof, but rather the acquisition of the highest possible level of confidence that an item, system or operation will perform as required in the real mission under the real conditions. In other words, even after the most rigorous verification and validation process, uncertainty and risk will always remain.

10.2 RVD verification/validation during development

In order to arrive at an acceptable level of confidence that the final product will fulfil its tasks, a number of questions must be answered positively during its development. The basic questions to be answered concerning the issues of verification/validation in any development project are as follows.

(1) Which functions/features are involved in the process; which of them have to be considered as particularly critical for the proper fulfilment of the task in question; and for which of them is experience gained from former developments and applications available?

(2) What risks have to be considered for these features; i.e. what can go wrong during development and, eventually, the operational phase?

(3) How can these risks be reduced; i.e. what needs to be done to obtain evidence for proper function and performance of these features?

These basic questions lead immediately to the next level of questions concerning the distribution of verification/validation efforts over the development life-cycle of a project

(see figure 10.1):

- What features and issues have to be verified/validated and when; i.e. what risk needs to be considered for which feature at which point in the development life-cycle?

- How can such features/issues be verified/validated; i.e. which methods or means of verification/validation will have to be applied at each point in the development life-cycle?

- How much effort needs to be invested for each verification/validation task; i.e. in how much depth do features have to be verified/validated to achieve sufficient confidence at each point of the development life-cycle? Considering the fact that proof of proper functioning according to a specification or according to real world conditions is an asymptotic process, which will never reach 100%, a conscious decision has to be made regarding how much effort needs to be invested and how much residual risk can be tolerated.

The sum of the answers to all these questions will eventually lead to the definition of an overall verification/validation approach for the development project in question.

10.2.1 Features particular to rendezvous and docking

As this book is exclusively concerned with rendezvous and docking/berthing, only those features which are particular to the mission task of rendezvous and docking, and which are not used in other types of mission, shall be treated here. For RVD/B, proper function and performance of the following features must be verified:

- the algorithms of onboard systems controlling the rendezvous, i.e. the GNC, MVM and FDIR algorithms;

- the control software in which the algorithms are implemented;

- the sensors required for the rendezvous trajectory and attitude control;

- the reaction control system for full six DOF motion capability;

- the compound of algorithms, software, data management system, sensors and reaction control system forming together the onboard RV-control system;

- the capture dynamics of the docking or berthing system and the physical connection;

- the remote interaction functions (ground, space station crew) with the automatic onboard system.

There are of course many other spacecraft hardware and software items which are also involved in the rendezvous system, e.g. normal attitude sensors, such as gyros, Sun and Earth sensors, the data management and communication subsystems, thrusters and valves, etc. These items, although essential elements in any rendezvous control system, will not be discussed here, as they are not rendezvous specific. Generally, the methods of their verification are well-known from other space or even ground applications. Also, other verification issues, e.g. those w.r.t. physical space environment, such as launch loads, thermal vacuum, radiation, electrical and electro-magnetic environment or the verification w.r.t. manufacture requirements of the spacecraft, or end-to-end verification of a functional chains, etc., are not considered here, as they are covered by the normal verification tasks within any spacecraft project.

An exception to this is the reaction control system. Thruster management function and thrusters are, of course, used in practically all other spacecraft. However, in RVD/B, thrusters are used in a different mode with a much higher number of duty cycles, and the thruster management function has to select actuators for six DOF control, which is different from that of spacecraft with attitude control only. Also, trajectory errors caused by thrust imperfections and the consequences of thruster failures concerning trajectory safety, are issues specific to a rendezvous approach. For this reason the reaction control system is counted here as a rendezvous specific function.

In conclusion, three distinct lines of verification have to be followed which are, to a certain extent, independent of each other:

- the functions in charge of trajectory implementation;
- the functions responsible for the physical mating process;
- the functions and operations involved in the supervisory control of the automatic onboard system.

The first line of verification concerns the GNC and MVM functions, including algorithms, sensors and reaction control functions. The second line includes the contact and capture dynamics until insertion into the structural latching interfaces. The verification of the structural latching itself will not be discussed here, as it is in no way different from similar functions in ground applications. The third line includes the operations by the ground controllers in the chaser and target control centres, the target station crew and the functions of the dedicated support equipment for these operators. Functions for communication, such as packeting, encryption, transmitters, receivers, ground links, etc., will not be addressed, since they are not specific to RVD/B.

10.2.2 Verification stages in the development life-cycle

Verification and validation are not constrained to a particular phase at the end of a project (e.g., the *qualification phase*, during which it will be proven that everything is functioning and performing according to the requirements under all conditions of the real

mission). On the contrary, verification and validation tasks start at the very beginning of a project and continue during each of the project phases. The methods of verification and validation in each phase have to be chosen such that confidence is achieved in those particular aspects which are at stake at the particular stage of development in question. In the development life-cycle of a space project the following major questions have to be answered at the various development stages.

- In the mission definition phase:
  - are mission concepts and requirements realistic and feasible?
  - do the requirements and specifications represent the real mission needs?
- In the design phase:
  - will a design be feasible which fulfils the specifications?
  - will the design be able to realise the mission concept and provide the required performance under real world conditions?
- In the development phase (concluding with qualification):
  - does the actual design function and perform according to the specification?
  - will the design implementation in hardware and software fulfil the function and performance requirements for the mission under real world conditions?
- In the flight item manufacturing phase:
  - do the flight items 'as built' in all aspects, i.e. physical, function and performance, fully correspond to the ones which passed through the qualification phase?
  - are all subsystems and items properly integrated?

It is the primary objective of the verification/validation process to ensure that the above goals of each particular phase are fulfilled. In the first instance, the verification task is to ensure that the specifications are followed. However, verification goals must of course always be related to the proper functioning and performance in the 'real world', i.e. under the conditions of the real mission. The second question at each step of the development life-cycle must therefore be

- Are there any effects in the real world, that would potentially cause a risk in the operational phase, which are not known and not sufficiently covered by the specification and verification process?

It is obvious that the detail and aspects of the 'real world' to be considered in the validation process will depend on the project phase in question. Unfortunately, the 'real world' will never fully be replicated before the mission is flown. As a result of analyses,

tests and (possibly) orbital experiments, knowledge of the 'real world' will steadily be increased during the development stages. However, even at the time of qualification of the system, a residual uncertainty will remain. The aim must be, rather than 100% proof, that, at the end of the development life-cycle, i.e. at completion of qualification, the risks for the operational phase will be reduced to an acceptable level.

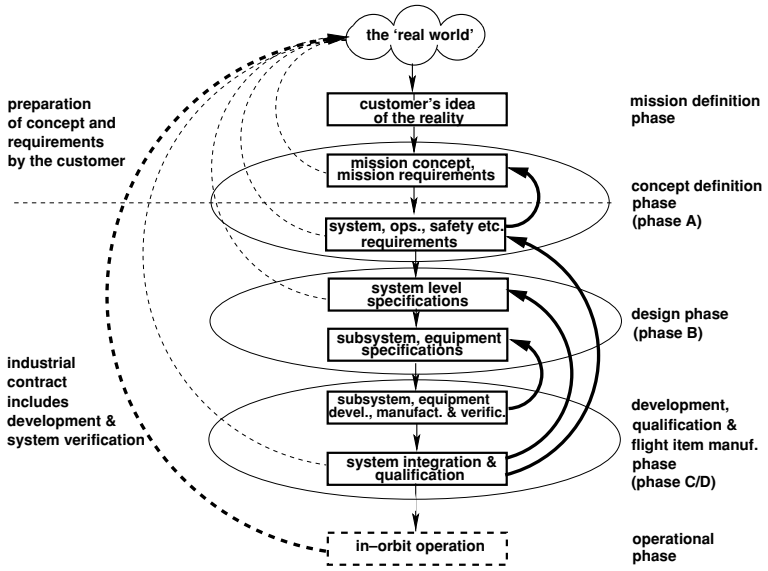

Figure 10.1. Verification and validation in the development life-cycle of a space project.

In figure 10.1, the arrows with solid lines on the right hand side represent the verification tasks, and the dotted lines on the left hand side represent the questions concerning validation. According to the above definition, verification tasks can begin only once the first products have been established according to a set of written requirements or specifications. The first task is usually the verification of the system specification w.r.t. the overall mission requirements.

A major validation task already exists, however, right at the beginning of a project. The customer, usually a national or international space agency, will have an idea of the mission to be performed. This includes also the first idea of the 'real world' which will exist during execution of the mission. Starting from this idea, the customer must establish a mission concept and define the mission requirements. These concepts and requirements need to be validated against the 'real world', which at that stage is known only to a limited extent. The investigation and description of the 'real world' in which the spacecraft and its subsystems and items will have to operate during the mission, is, next to the development of the spacecraft systems, subsystems and items, the other major development task during the entire development life-cycle of the project.

After the first definition of mission and system requirements, all subsequent lower level specifications and implementations have to be verified against the next higher level specifications and requirements. However, as all these sets of requirements and specifications refer to the 'real world' describing the future mission, there will also at each step be the need to validate the detailed description of the 'real world' required for the verification task of that particular step. The verification/validation effort culminates in the development phase, where it should be proven that a system or item will achieve its specified performance under all conditions of the real mission. The sum of all these activities is referred to as *qualification*. However, keeping in mind the limitations of all verification and validation efforts, it will eventually be only in the operational phase of the real mission that the spacecraft system will meet the 'real world' proper. Only then can final proof be achieved that the system indeed functions and performs properly, that all requirements were indeed defined correctly, comprehensively and in sufficient detail, and that the tools for verification have indeed been correctly validated to represent the 'real world' to the necessary extent.

10.3 Verification methods and tools

The objective of this section is to provide an understanding of the issues to be verified, the methods and types of tools employed, and the depth of modelling needed for verification in each of the various development phases. Verification concerning the effects of orbital environment, such as thermal vacuum, radiation and launch loads, will be addressed only if that environment is expected to cause a change in the parameters involved in the dynamic processes of rendezvous, contact and capture. As already stated above, the verification w.r.t. resistance to launch loads will therefore not be discussed here.

This section will also briefly address the possible and necessary depth of the validation of mathematical models or physical stimuli of test items used in the simulations of a particular development phase. Possible methods and constraints of validation for the various types of models will be treated in more detail in section 10.5.

As the intention is to show in principle the methods used for the verification and validation tasks at each development stage, the description can be limited in the case of the RV-control system to verification and validation of the guidance, navigation and control (GNC) functions, and in the case of the mating system to the verification and validation of the front end functions, i.e. the ones involved in contact dynamics and capture. In the case of a docking mechanism, the front end functions include the elements for reception, the attenuation devices and the capture latches.

For the RV-control system it will be indicated where MVM and FDIR functions will be integrated with the GNC functions. The verification of these functions will not, however, be discussed in any detail. Their final verification is, in any case, included in the overall verification of the rendezvous control software in the development phase. The description of contact dynamics and capture verification will be restricted to docking.

For berthing, the verification of capture of the interfaces of the other vehicle by the end-effector of a manipulator and the transfer to and insertion into the attachment interfaces, all of which are controlled by a human operator, are outside the scope of automated rendezvous and docking and will, therefore, not be discussed in any detail.

10.3.1 Mission definition and feasibility phase

In the first phase, the mission concept and mission requirements have to be validated, which means that the feasibility of trajectories, attitudes, thruster configuration and thrust level etc. have to be confirmed by analysis or simulations. These early simulations do not need, however, to include the modelling of a closed loop for the GNC functions, or the algorithms for mode sequencing, equipment engagement (MVM) and FDIR functions, or other detailed features of the onboard system. Analysis of the trajectories, of the ΔVs to be applied and of the duration of manoeuvres will yield the basic data required to assess the required thrust level and propellant budget, the type of sensors required, the feasibility of capture, etc.

Verification/validation of trajectory control issues

Verification objectives

- Feasibility of trajectory and attitude strategy and overall ΔV requirement for the trajectory sequence.
- Feasibility of thruster configuration, thrust level, and preliminary propellant budget.
- Identification of required navigation and control performance in the various stages of approach and preliminary selection of sensor types.

The particular requirements for the individual features of the rendezvous system (subsystems, equipment, functions, operations) are derived from the initial mission and system design analyses. Verification of these individual requirements is the first important part of the overall verification task.

Verification tools The most important tool required in this phase is a non-real time trajectory simulation based on the Clohessy–Wiltshire equations. Thrust level requirements and propellant budget or trajectory and attitude control are derived from the ΔV results by applying empirical factors. Navigation performance is estimated from available sensor data and from past experience. Concerning disturbances, the trajectory simulation needs to include only the modelling of differential drag, which is essential for the analysis of manoeuvre performance and long term safety of trajectories. This requires a first estimate of the geometry of chaser and target vehicles and of the atmospheric density in the rendezvous orbit. Other orbital disturbances are of lower importance and need not to be considered at this stage.

Verification/validation of contact dynamics and capture

Verification objectives

- Feasibility of capture with the velocities, lateral and angular misalignments at contact, resulting from the expected GNC performance of the chaser and attitude dynamics of the target.
- Vice versa, the identification of requirements for contact conditions to be fulfilled by the GNC system of the chaser.

Verification tools At this early stage, verification will consist of an assessment of the feasibility of capture by a comparison between the GNC performance expected at contact and the capture capabilities of existing mating systems. In the case of berthing, this can be an assessment of whether or not the GNC system will be able to fulfil the conditions of the berthing box.

If a docking mechanism design is already available, it may be of interest at this stage to check the probability of capture by means of a non-real time contact dynamics simulation, which would include a simplified modelling of the contact surfaces and capture mechanism. If a new docking mechanism has to be developed, there will not yet be a basis for any kind of simulation at this stage. Feasibility can in this case only be assessed by comparison with known parameters resulting from the successful use of existing designs.

10.3.2 Design phase

Verification/validation of trajectory control issues

The first important task in the design phase is the development of the guidance, navigation and control algorithms. They will initially be verified by running in closed loop with an environment simulation which is developed together with the GNC algorithms. As long as no detailed models are available, spacecraft and orbital environments will initially be modelled in this simulation with consideration only to their dominant effects. For example, the spacecraft will be modelled as rigid bodies; the sensors will be modelled according to their basic function, plus some bias and noise; and only drag or differential drag according to the spacecraft cross sections will be taken into account when considering orbital disturbances. The expected/required GNC performance obtained from such early simulations will be the driving factor for the specification of the trajectory sensors and front end functions of the mating system, i.e. for reception range and capture. The MVM and FDIR algorithms are, to a large degree, independent of the GNC algorithms and will have to be developed in parallel. They can be tested by applying the appropriate stimuli to trigger the state changes. At a later stage they will have to be merged with the GNC algorithms to form the complete onboard rendezvous control software.

In the final stage of the design phase the RV-control software will eventually have to be verified in a closed loop 'all software' simulation of all environment functions and effects. This must then include, in addition to the RV-control software, detailed models of the spacecraft body, including the flexibility, rotating appendages, fuel sloshing, etc., of the onboard data management and communication architecture, of all equipment and of orbital disturbances. The RV-control software consists of the GNC, MVM and FDIR algorithms. As no hardware is involved yet, such a simulation setup can still run in non-real time, i.e. faster than the real processes, to reduce simulation and evaluation time. Running the RV-control software in a simulation environment with such detailed and complete models will provide sufficient confidence that the rendezvous control software will work properly and provide the required performance in the real mission environment.

Verification objectives

- Feasibility of the design concepts for GNC, MVM and FDIR.
- Achievability of performance requirements for GNC.
- Feasibility of design implementation with the envisaged sensor and data management hardware.
- Correctness of environment modelling (validation task).

Verification tools In the first step, separate tools will be required for GNC, MVM and FDIR algorithm development. For instance, GNC algorithms may initially be developed in non-real time development environments for control systems, such as Matlab or MatrixX, and tested in closed loop non-real time 'all software' simulations in that development environment, with basic modelling of spacecraft dynamics in orbit and including orbital disturbances. At this stage of development, the modelling of spacecraft design, subsystems and equipment may still be of limited detail. Spacecraft and equipment developments are performed in parallel, and their design is usually not yet finalised in this early phase. Under these conditions, vehicle dynamics and disturbances will have to be modelled using the available preliminary spacecraft design, and sensors, actuators, etc. will have to be modelled according to their expected GNC behaviour, rather than to their detailed design. For instance, as long as the detailed design is unavailable, sensors will usually be modelled as a basic function, plus bias, plus noise. Modelling of the measurement environment will be simplified. For GPS, e.g., only the position and visibility of GPS satellites w.r.t. the antennas on the chaser and target vehicles may be simulated, and for optical sensors the disturbance effects of a measurement environment (e.g. specular reflections) can be neglected. A block diagram of an initial GNC simulation is shown in figure 10.2.

The preliminary models of the early design phase will have to be exchanged in later stages for more refined ones. For instance, the bias and noise type sensor models, which

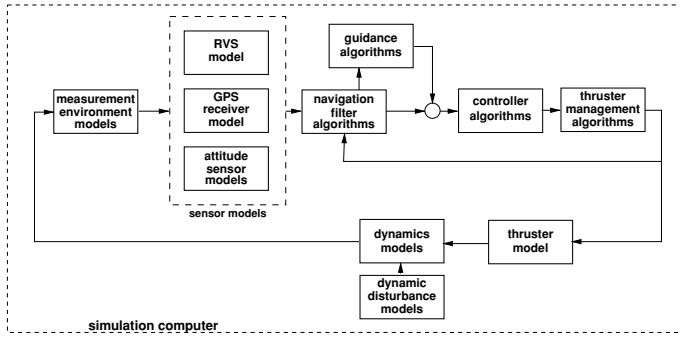

Figure 10.2. Closed loop GNC simulation on one platform.

try to approximate the behaviour of the sensor, will have to be replaced by more detailed models representing the actual design of the sensor in terms of field of view, maximum range, resolution, bandwidth, etc., and a more refined model will also have to include its operating modes. The measurement environment models will have to include the specific details of the sensor environment in question. This will include, in GPS and RGPS, e.g., the modelling of GPS satellite configurations and of multi-path and shadowing effects. In addition to run-time simulations, other tools, such as error co-variance analysis, will be used to assess the expected margins of GNC performance.

All analysis and verification tools used in the design phase will typically run in non-real time, as there is no hardware test item requiring a real time environment. Validation of the models of spacecraft and equipment will, at this stage, be limited to a comparison with the evolving design of these items. Validation of models for dynamic disturbances in the orbit and measurement environments will in most cases be limited to comparison with data known from previous missions.

Verification/validation of contact dynamics and capture

Verification of the contact and capture process will obviously depend on the type of mating used in the mission in question. For berthing this will require a simulation of a manipulator arm, with a human operator in the loop. As the manipulator and the human operator are usually located on the target station, verification of capture is the responsibility of the target project, and the chaser project will have only to provide evidence that its vehicle will be delivered into a berthing box as defined in figure 5.6, which is a GNC task.

If a docking mechanism has to be newly developed, the initial verification task is to prove that the design parameters for the reception, attenuation and capture functions have been chosen correctly. If an existing docking mechanism design has to be used, the verification objective will be to show that capture will be possible with the expected GNC performance. Otherwise, it must be determined how the GNC performance must

be improved, or what parameters of the docking mechanism need to be changed, to ensure capture.

Verification objectives

- Forces and torques acting between chaser and target vehicles at contact must be below acceptable limits.
- The choice of shock attenuator parameters in the design must be correct concerning capture capability and force limits.
- Capture must be achieved with the given GNC performance of the chaser and attitude dynamics of the target.

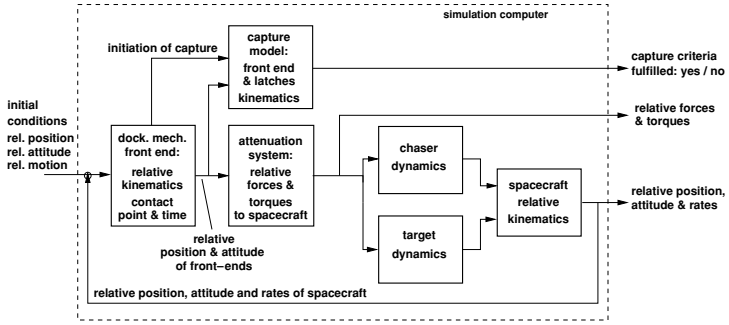

Figure 10.3. Docking system capture simulation.

Verification tools To analyse the probability of capture, a tool needs to be available which includes modelling of the following functions: the kinematics at contact of the docking front end interfaces on chaser and target; the forces and torques applied to both spacecraft via the attenuation system; the relative motion of the spacecraft as a result of these forces and torques; and the operation of the capture latches. A simplified block diagram of such a simulation is shown in figure 10.3. The first task of this simulation is the identification of the contact point and the direction of the contact forces. This requires modelling of the reception interfaces on both sides and the determination at each point of the distances of the surfaces between one side and the other as a result of relative position and attitude of the two vehicles. Contact point, force direction and the relative position and attitude of the capture interfaces determine the deformations of the attenuation system, which in turn determine the forces and torques acting on the vehicles. The closing motion of the capture latches, which will in reality be triggered by either contact force detection or an optical sensor, can be initiated in the early stage of the simulator development by a distance criterion. By changing the design parameters of

the reception structure and the attenuation system, the reception range, the time available for capture and the forces acting on the spacecraft can be varied to improve capture probability. As for GNC simulations, in the design phase there will be no need for a real time simulation, as no hardware or human operator is involved.

Validation of the geometric and dynamic models used in the simulation determining contact point, force direction and dynamic reactions of the attenuation system can, at that stage of development, only be achieved by comparison with the design of the available docking mechanism, and with the results of calculations, e.g. those concerning the forces at particular deformations of the attenuation system.

10.3.3 Development phase

Verification/validation of trajectory control items

In the development and qualification phase, the onboard control system for rendezvous has to be verified for function and performance in an environment and under conditions as close as possible to the real application. This requires that the hardware and software of the system will have to be tested in closed loop in a real time operation environment with as many as possible real items in the test chain. For the rendezvous control system this means that the RV-control software will have to run in its proper computer hardware and that eventually real sensor hardware will have to be connected to it. It is generally not possible to include the actuator hardware in closed loop performance tests, as this would require the proper orbital environment for thrusters and spacecraft dynamics to close the loop. To test the rendezvous system with sensor and controller hardware in the loop, all items involved in the dynamic process, e.g. spacecraft body and actuators, must still be represented by mathematical models.

Verification/validation objectives

- Proper function and performance of the complete rendezvous control system implemented in hardware and software.
- Function and performance of the navigation hardware and software in a realistic measurement environment.
- Proper function of the onboard system together with the remote control functions (ground, target station).

GNC verification tools During the development phase, the complete rendezvous control software (GNC, MVM and FDIR functions) will become available and its performance will have to be verified. The most important tool required for verification of the onboard rendezvous control system in the development and qualification phase will, therefore, be a real time simulation, which will be able to test the RV-control software together with the data management hardware and software, i.e. the onboard computer

and data bus in the loop. The rendezvous control software will be resident in the onboard computer, and the interfaces to sensors and propulsion control electronics, or to the mathematical models of these items, will be via the onboard data bus. In this way any modification of the behaviour of the control algorithms due to their implementation in the software and due to their operation in the data management environment will be included in the test results.

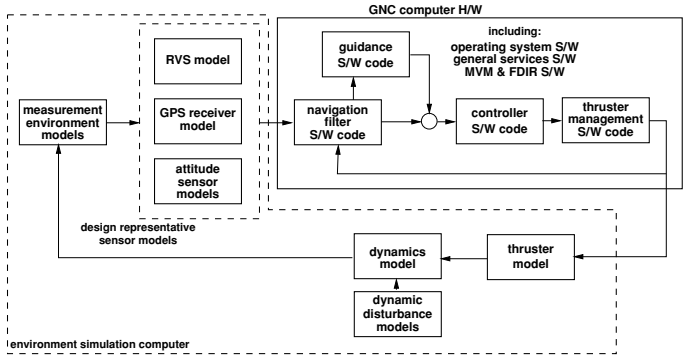

Figure 10.4. Closed loop GNC simulation with RV-control computer as test item.

The mathematical models for orbital perturbations, for the actuators and their drive electronics, for spacecraft dynamics and kinematics, and for sensors and their measurement environment, need to be available in sufficient detail and reliability to produce the same closed loop test result as in the real mission. All models need to be validated to fulfil these requirements, which means that, by test or comparison, sufficient confidence must be established that they represent the 'real world' to the extent necessary. The resulting simulation setup will be the main tool for verification of the function and performance of the rendezvous onboard control system (see section 10.4). It will be used for verification of the nominal mission and for all foreseeable non-nominal/contingency situations. A typical simulation setup for the GNC functions in the development phase is shown in figure 10.4. The MVM, FDIR and data management functions are not shown in this figure. They will, however, be included in the simulation runs and form part of the verification effort for nominal and contingency cases.

Sensor verification tools To verify the sensor hardware and software, test setups with physical stimulation of the sensors will be required. In the first instance, these will be open loop tests, where the physical stimulation is intended to provide an as realistic as possible measurement environment for the sensors in accordance with the trajectory and attitude motion of the chaser and target spacecraft and the motion of other reference points. These are, e.g., the navigation satellites for the case of GPS, RGPS or other satellite navigation systems, and, for optical sensors, the Sun at the time of the approach (figure 10.5). For attitude, Sun position and navigation satellite constellations, fixed

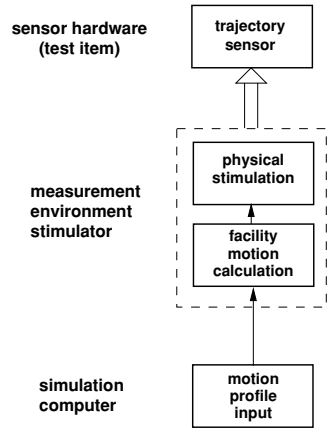

Figure 10.5. Open loop GNC stimulation of sensor hardware.

profiles can be used which have been calculated for the part of the approach to be tested. These open loop test setups with physical stimulation will be used as the primary means of validation of the mathematical models of the sensors, which will be used in the 'all software' simulations.

The non-systematic disturbance part of the measurement environment models used in the software simulations and for the stimulators can be validated only by practical experience in space, either by comparison with data from former missions or by dedicated in-orbit experiments (see section 10.7.2). Once the worst-case situations are known from experience, they can be used in the tests with physical stimulations to validate sensors and navigation function w.r.t. real world conditions.

GNC verification with sensor stimulation Eventually, stimulation facilities may also be included in the closed loop test of the GNC system (figure 10.6). These closed loop tests will be used mainly for the validation on the system level of the 'all software' simulation, in particular of the navigation function. As test preparations on such setups and test runs are complex, long and expensive, tests will have to be limited to a few particular test cases. Also, such test setups with physical sensor stimulation may not permit the reproduction of contingency situations, either because of physical limitations of the facility or because of operational safety of the test.

For RGPS, the physical stimulation will have to produce the RF data input to the GPS receivers on the chaser and target sides, as they would be received by their respective antennas according to the instantaneous GPS satellite constellation and to the actual position and attitude of chaser and target vehicles. To produce the RF data input, two GPS satellite constellation simulators will be required to simulate the position of the GPS satellites as seen by each of the two vehicles. For their input they will have to obtain

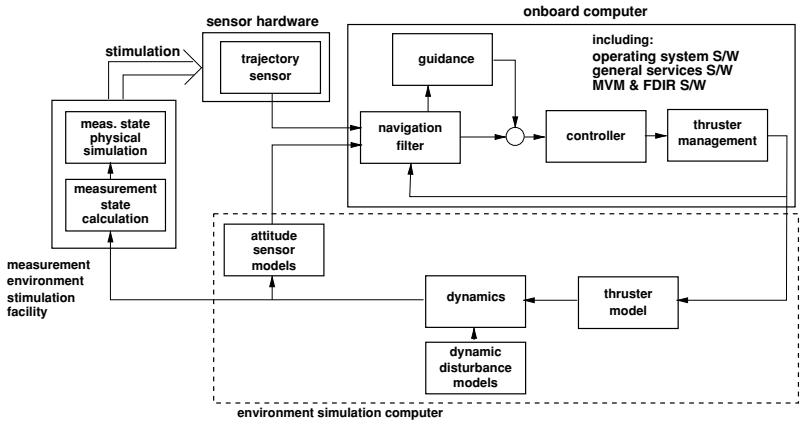

Figure 10.6. Closed loop simulation with GNC computer and navigation sensor hardware in the loop.

the actual position and attitude of chaser and target. The output of the receivers on chaser and target will be fed into the RGPS navigation filter of the GNC system, where the relative navigation data is actually produced (see figures 7.25 and 7.26). The modelling in the GPS satellite constellation simulation needs to include multi-path effects and shadowing according to the geometric conditions around the antennas on the chaser and target vehicles.

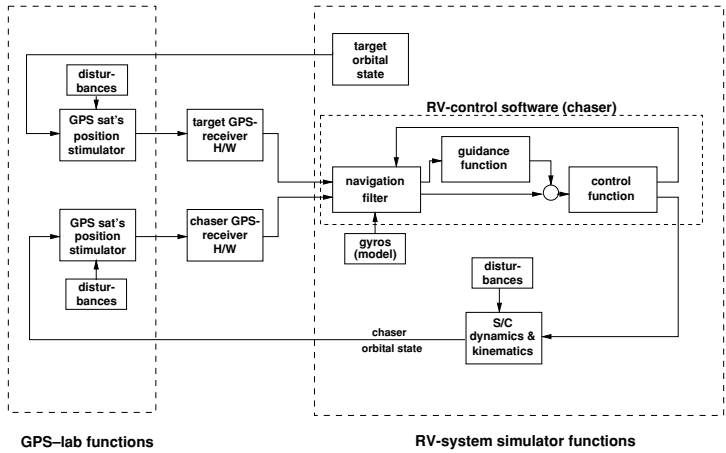

Figure 10.7. Measurement environment simulation for relative GPS navigation.

For optical rendezvous sensors, the physical stimulation needs to reproduce the conditions of the light signal to be measured by the sensor, whether emitted by the sensor

illuminator and reflected by a reflector pattern on the target or emitted by target lights. This will require a motion system which changes the direction and distance of the light sources to be sensed in accordance with the relative motion between chaser and target during the trajectory part to be tested. Also, the stimulation will have to provide a realistic representation of the disturbances (measurement environment) that the sensor might be subjected to in the real mission. Such disturbances will, in particular, be specular reflections by the target surface of sunlight and light emitted by the illuminator of the sensor, and direct sunlight in the FOV of the sensor. As chaser and target will have independent attitude motions w.r.t. the Sun, the angular motion of this disturbance stimulation will need to be implemented independently of the relative motion between chaser and target, resulting in a total of at least eight DOF for the facility.

Following the above described steps of verification of the RV-control software in its data management environment and of sensor and navigation functions in their respective measurement environment, only a few tests with different sets of initial conditions and variation disturbance parameters will be possible because of time and cost reasons. In a real time simulation, the test of each part of the trajectory will take between one half and one full orbit, i.e. about 45–90 minutes. The time necessary for test preparation has to be added to this. An evaluation of the limits of the system behaviour, taking into account the full specification ranges for system and equipment and the uncertainty of knowledge of the environment, and considering all possible combinations and variations of these parameters, would require an excessive amount of time in a real time simulation setup. For the full performance verification of the system, an updated 'all software simulation' will be required, with which 'Monte Carlo' runs can be performed in faster than real time. Such simulations will be in principle similar to the one shown in figure 10.2; however they will also include the final design of the GNC algorithms, the detailed modelling of sensor and actuator functions and disturbances, and a complete representation of the MVM and FDIR functions and of the data management system.

Verification/validation of contact dynamics and capture

As for the trajectory control related systems and items, the front end functions of a docking system have to be verified under conditions as close as possible to the real application. This requires (a) the front end hardware to be tested under the same dynamic conditions as that which occur during the real docking in space, and (b) the dynamic reactions of both spacecraft to be physically available in the test setup.

Verification/validation objectives for contact dynamics and capture

- Proper reception with final kinematic and dynamic conditions of the two spacecraft, according to GNC performance at zero distance.
- Successful capture by the latches under the given dynamic and kinematic conditions at contact.

- Maximum forces and torques acting on the spacecraft during the contact and capture process.

Capture dynamics verification tools During the development of a new docking mechanism, an analysis tool (described in the previous section and indicated in figure 10.3) will be used to verify the limits of the capture capability of the design concerning approach and lateral velocities and lateral and angular misalignments. The validation of the mechanism design, and of the modelling in the simulation tool, requires a test setup in which the docking mechanism hardware will be subjected to the kinematic and dynamic conditions of contact, i.e. linear and angular velocities and misalignments. Such a test setup needs to simulate the physical motion of the front ends of the chaser and target vehicles and will have to model masses, inertias and flexibilities of the two vehicles and to calculate their kinematic reactions.

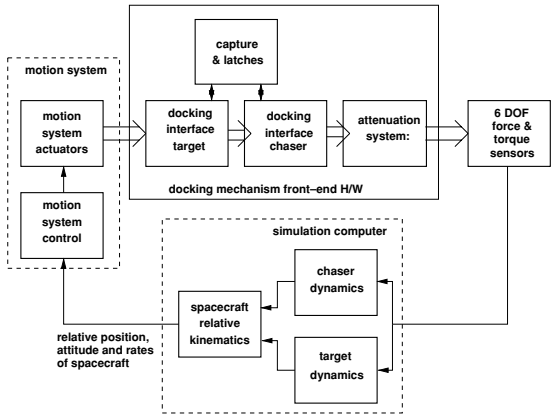

Figure 10.8. Docking system front end dynamic testing.

A block diagram of the typical functions required for such a facility is shown in figure 10.8. The six DOF physical motion will have to be provided by a motion system, which carries the front ends of the docking system on the chaser and target sides, which include the reception, capture and attenuation functions. Similarly to the physical stimulation facilities for the rendezvous sensor functions, the test of extreme or contingency situations on a contact dynamics facility will be limited because of the danger of damage to both the test item and the facility. As the time required for each test run will, however, be comparatively short, such a facility could be used also for the evaluation of optimum design parameters for capture.

The principles of verification of the other functions of a docking mechanism, i.e. retraction, structural latching and hermetic sealing, are no different from the verification of similar functions for ground applications. For this reason, there is no need to discuss them here.

Performance verification under thermal vacuum conditions

GNC functions Items which may be affected are the sensors and the actuators. Their behaviour can be tested on equipment level concerning the change in any performance parameter due to variations in environmental conditions. There will, however, be no need to test the complete system under thermal vacuum conditions.

Capture dynamic functions Considering the sensitivity of mechanisms to temperature and vacuum, all functions of the docking system need to be tested in a thermal vacuum. In particular the front end functions of attenuation and capture will have to be tested for change of performance with changing environmental conditions. For these tests, particular tools have to be developed in accordance with the actual design of those mechanisms. The performance of closed loop dynamic tests under such environmental conditions will, however, not be necessary, as the mathematical modelling can be validated at normal temperature in air, and the performance of the complete mechanism under thermal vacuum conditions can be obtained from the 'all software' capture simulation by introducing the changed parameters of the individual components, measured under those conditions. All other functions of the docking mechanism, such as retraction, structural latching and sealing must also be tested for proper functioning under thermal vacuum conditions, as postulated above. There is no need, however, to discuss such tests here in further detail.

10.3.4 Verification methods for operations and tools for remote operators

The verification of the space–ground system setup and of the requirements and concepts for support tools for remote operators will have to follow a different schedule from the verification of the automatic onboard rendezvous system, described in the previous sections. The tasks of ground operators in the chaser and target control centres and of crew members in the target station were identified and the requirements and concepts for support tools were discussed in the previous chapter. The development and verification of operational procedures governing the interactions between the players according to these tasks, and the verification of the support tools, can only start when the development of the onboard system design and its verification tools has progressed to a certain point and when real time software of both the onboard system and the environment simulation is already available. To avoid confusion with the development phases of the onboard system, the discussion and description of development and verification objectives and processes will be done here globally, without making reference to feasibility, design and development phases.

Overall verification/validation objectives for ground system tools and operations

- Proper function and performance of the support tools for ground and space operators.
- Proper interaction of chaser CC with chaser S/C during RV phases.
- Proper interaction of chaser CC with target CC during RV phases.
- Proper interaction of target crew members with the chaser vehicle in case of contingency operations.

Verification of support tool functions for ground operators and target crew

Items and issues to be verified

- Concerning the monitoring function of support tools for the ground operator and target crew member, it needs to be verified that the representation of trajectory, attitude and onboard functions status, warnings and messages is easily understandable by the human operator and will prompt him for the proper reactions.
- Concerning the immediate intervention and short term recovery functions, it needs to be verified that commands will be executed by the onboard system, that the intended trajectory/attitude changes will be achieved and that the operation of this function by the human operator will be easy and fast.
- Concerning the failure analysis function, it needs to be verified that onboard failures or contingency situations will be detected sufficiently quickly such that the human operator will be aware of them and can initiate pacifying or recovery actions in due time. Further, it will have to be verified that the identification of the location of the failure down to a certain level is possible, and that the specified tool will be able to support the operator during and following identification of the failure.
- Concerning the strategy and mission re-planning function, it needs to be verified that the tool is capable of quickly providing all data required for the implementation of a sequence of new trajectories, including the corresponding parameters of the applicable manoeuvres or GNC modes. It will further have to be verified that the results of this tool will be sufficiently accurate, such that they can safely be used for mission re-planning and trajectory implementation.

Verification methods

- *For the monitoring function*. Proper performance of the support tool can be verified by running it together with a real time simulator (representing the onboard system),

which provides the relevant onboard data. The major criterion in the verification will be the subjective experience of one or more human operators concerning the ease of understanding of the displayed information and its usefulness in the operation.

- *For the immediate intervention and short term recovery functions*. As above, performance of the support tool can be verified by running it together with a real time simulator representing the onboard system, in which the onboard RV-control system accepts and executes the commands issued by the remote operator via this function.

- *For the failure analysis function*. A full verification of such a function will be difficult, as this would in principle require the availability of the complete onboard system with all hardware and software in the test setup and the capability of producing any possible failure conditions. In a setup with the real hardware and software it would be difficult, however, to reproduce all possible failures or any particular one at any particular time. The only way to test the failure analysis function would be to run it together with a simulation of the onboard system, which includes a sufficiently detailed design modelling of sensors and the data management and propulsion systems, where failure conditions can be introduced on command.

- *For the strategy and mission re-planning function*. This function will have to consist of a fast simulation with detailed GNC, propulsion and environment modelling. It can be operated and verified off-line, assuming several particular contingency situation, e.g. after a CAM, retreat, long duration waiting, etc. The verification will consist of a comparison with a simulation of the same trajectory sequence, manoeuvre and GNC mode parameters using the most accurate simulation tool available.

Verification tools

- *For the monitoring function*. This requires a setup consisting of the operator support tool running together with the real time RV-system simulator, i.e. the RV-control software in the onboard computer hardware and the real time environment simulation. In addition, a communications simulator will be needed which models effects such as the space–ground time delay, communications windows, shadowing, signal-to-noise ratio, etc.

- *For the immediate intervention and short term recovery functions*. The same setup is required, i.e. the operator support tool running together with the real time RV-system simulator.

- *For the failure analysis function*. This requires a setup consisting of the failure analysis tool together with an all-software RV-system simulator with detailed modelling of the design of all subsystems and equipment.

- *For the strategy and mission re-planning function.* A fast non-real time RV-system simulator is necessary which could be, e.g., the non-real time RV-system simulator used for Monte Carlo simulations.

Verification of interactions between control centres and vehicles

Items and issues to be verified

- The operating procedures for nominal and contingency situations, and, together with these procedures, the interaction of chaser CC with chaser vehicle during RV phases.
- The operating procedures for interactions between chaser CC and target CC in the last phases of the rendezvous mission, e.g. hand-over of mission authority, decision making for approach continuation at hold points, contingency handling, etc.
- The operating procedures for interactions of the target CC with the chaser vehicle in the case of contingencies in the last part of the final approach.
- The operating procedures for the interaction of the target crew member with the chaser vehicle in the case of contingency operations.

Verification methods The real time simulation output of the state vector, of the navigation data and of the subsystem and equipment status of the chaser vehicle, must be available for that part of the mission which is to be monitored at one or both control centres and for the last part of the approach in the monitoring equipment for the operator in the space station.

Delays, noise and other constraints or disturbances of the communication flow between space and ground must be simulated. If the control centres for the chaser and target are at different locations, the real communication lines (or technically equivalent ones) should be used in the final verification test setup for communication between ground centres.

Verification tools The basic simulation setup will consist of the real time RV-system simulator, i.e. the RV-control software in the onboard computer hardware and the real time environment simulator, plus the communication simulator, which represents the constraints and disturbances of the space–ground communication links.

If the chaser and target control centres are at different locations, the final verification tests can make use of 'distributed interactive simulation' techniques (Miro *et al.* 1998; Vankov & Arguello 1998; Arguello & Miro 2000), for which a detailed simulation of each spacecraft will run in a different place, i.e. the chaser vehicle dynamic simulation

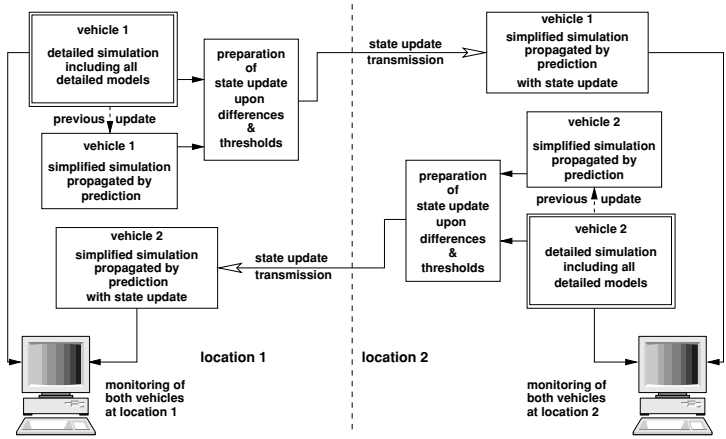

Figure 10.9. Principle of distributed interactive simulation.

in the chaser CC and the target vehicle dynamic simulation in the target CC, and a simplified dynamic simulation of each vehicle in the opposite CC. Each simplified dynamic simulation will be updated continuously via the ground communication links by state vector information from the detailed one. Communication delays between the CCs will be compensated for by a lead/lag algorithm. The principle of a distributed interactive simulation is shown in figure 10.9. The advantage of such an arrangement would be that each operator could remain in his normal environment, that the actual constraints and disturbances of the ground links will be included in the test, and that the space segment simulation of each side can be synchronised with the other to form an overall space–ground system simulation.

10.3.5 Flight item manufacture phase

Following production of the flight items, the risk introduced by manufacturing errors has to be eliminated. It has to be verified that the flight items ‘as built’ are in all aspects ‘as qualified’, i.e. that the qualification in terms of physical properties, functioning and performance performed on the final development items are fully applicable to the flight items.

To make this verification, not all of the tests performed for qualification need to be repeated. The verification of conformance of an item ‘as built’ with the design ‘as qualified’ usually will require less effort, as confidence in proper manufacture can be established by a few physical tests and simulation runs. This will have to include the verification of functioning and performance under nominal (and possibly a few contingency)

conditions, the verification of all interfaces and the verification of physical identity with the qualification items. It is important that flight item verification is performed up to the highest level, i.e. system integration and integration into the spacecraft, in order to verify proper integration and connection of all interfaces.

GNC verification tools

The rendezvous control software must, in addition to being subjected to comprehensive testing on software level, be acceptance tested in the real time RV-simulation setup with the data management hardware and software in the loop. This will be the easiest way of ensuring that the flight item hardware and software will work together without problems. The acceptance tests can be limited to the nominal mission sequence and a few contingency cases, in order to establish that there is no deviation in behaviour between qualification and flight software.

Except for the testing of the RV-control software in the data management hardware environment, there will be, in the flight item manufacture phase, no need for a GNC performance test with hardware in the loop. Hardware items will be tested individually in their own acceptance test programme using their own equipment level test tools and facilities. GNC level tests with sensor hardware in realistic measurement environments will not be necessary for acceptance, as this behaviour can be considered to be design dependent, rather than manufacture dependent. An end-to-end test with all hardware and software in a chain will have to be performed on a spacecraft level, using electric stimuli for the sensors and other hardware functions. The objective of such tests will be the verification of proper functioning, rather than performance, of the individual items and of the complete chain.

A similar final electrical test of the GNC system will have to be performed prior to flight, which will form part of the checkout of all functions of the spacecraft. As the spacecraft is completely assembled, this test can be, however, less comprehensive than the previous one.

Capture dynamics verification tools

The acceptance testing of the front end of the docking mechanism flight item will consist of both the individual tests of the attenuation and capture mechanisms under laboratory and thermal vacuum conditions and the test of the complete system under laboratory conditions on a six DOF motion facility. The verification tools will be the same ones as used in the development phase.

In contrast to the real time testing of the RV-control software, which will, as explained above, always take considerable time and will, therefore, be limited to a few test cases, the test of a single case of contact and capture will not take more than a few minutes.

For this reason, it will be worthwhile testing the flight item of the docking system within the full range of dynamic conditions specified for the GNC performance at contact.

10.4 Modelling of spacecraft items and orbital environment

In a test performed to evaluate the behaviour of an item or function under 'real world' conditions, every other item or feature involved in the system or process of the 'real world' must either be present in reality or be represented by an equivalent mathematical model. In a verification test setup, we call the function or item to be tested the *test item* and all other functions and features representing the 'real world' the *environment*.[1] For instance, when testing a sensor in its system environment, i.e. with the GNC system in closed loop, the sensor is the test item and the GNC algorithms and data management system belong to the environment. On the contrary, when testing the GNC algorithms in their system environment, i.e. with the sensor hardware in a closed loop, the algorithms are the test item and the sensors belong to the environment. Mathematical modelling is always related to items or features of the *environment*.

As explained in the previous section, modelling will start in the early stages of a project with simple behaviour models. For spacecraft equipment, such as sensors and actuators, the initial models will include the basic output function plus some errors or disturbances, modelled as bias and noise. For the measurement environment, this will be the basic effects; e.g., for GPS the basic effects are the positions of the individual navigation satellites. Orbital disturbances, such as drag or differential drag, will initially be modelled as constant forces. In the very early trajectory feasibility analysis, i.e. in the beginning of the mission definition and feasibility phase, ideal sensors and actuators with no errors are assumed, and ΔVs are applied as an impulse, rather than a force with a certain duration (see chapter 3). During the course of development, these models will have to be improved and refined, such that they will eventually represent realistically the spacecraft items, measurement environment and orbital disturbances required for the qualification of system and items for flight.

This section will identify the type and the contents of the models needed to satisfy the verification requirements for the final stage of the development process. Model requirements for the RV-control system and for the capture system of the docking mechanism will be addressed. Since these models depend on the actual design of spacecraft and equipment, it would not make much sense, however, to discuss their design details here. In many cases, the basic functions of the models have been addressed in the previous chapters of this book, which is indicated in the following by reference to the appropriate sections, figures or equations.

[1] Note, the term 'orbital environment' includes only that part of the simulation or test environment that relates to the effects in orbit experienced by the spacecraft.

10.4.1 Modelling of environment simulation for RV-control system test

In the example shown in figure 10.10, it is assumed that the test item is the complete RV-control system, i.e. the GNC, MVM and FDIR algorithms processed in the onboard computer. This is the type of test shown in figure 10.4. Figure 10.10 shows the various models of the environment simulation required for a closed loop rendezvous simulation with the described test item. It also shows the input and output data interfaces between the environment simulation and the test item. The inputs to the environment simulation are the GNC commands to the propulsion system for the execution of the actuation forces and torques and the information on orbit parameters and spacecraft attitude for the determination of the orbital disturbances. The outputs of the environment simulation to the RV-control system are the raw data of the GPS receivers of chaser and target (see figure 7.25), the absolute attitude of the chaser and (in the last part of the approach) range, line-of-sight and relative attitude angles provided by the optical rendezvous sensor.

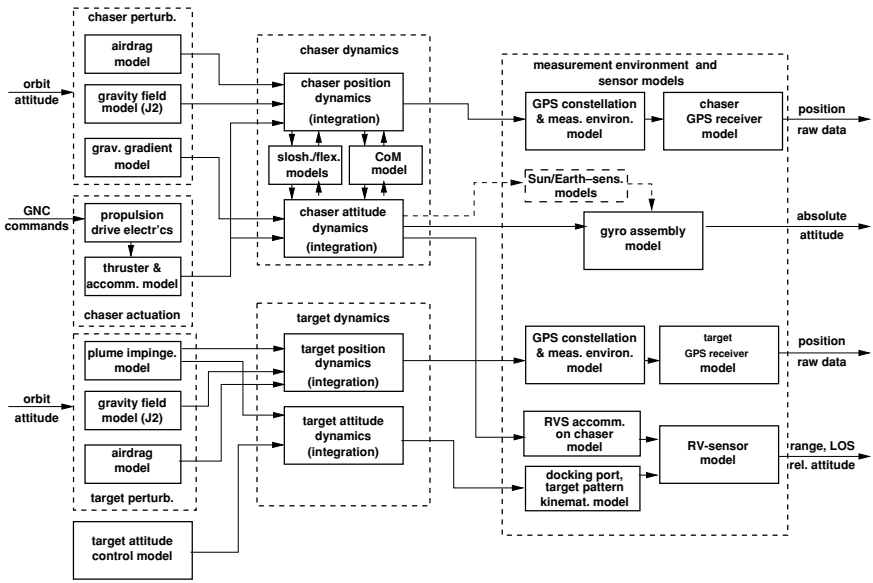

Figure 10.10. Simulation models for spacecraft items, dynamics, kinematics and orbital environment.

The models used in the environment simulation can be broken down into the following major groups:

- chaser actuation models,
- chaser perturbation models,

- chaser dynamics models,
- target perturbation models,
- target dynamics models,
- sensor and measurement environment models.

The major inputs/outputs to/from each model are also indicated in figure 10.10. However, in order not to comlicate the diagram, not all connections are shown (e.g. the inputs to the perturbation models, taken from the position and attitude dynamics output of chaser and target are not shown). In addition to the above model groups, the figure shows a 'target attitude control model', which models, in a simplified way, the control torque inputs to the target attitude dynamics. Where a more detailed description of the target GNC is not available, or such a detailed modelling is not necessary for the purpose of performance testing of the chaser GNC, the attitude motion of the target can be modelled by inputting a fixed command profile, e.g. a saw-tooth profile, into the target attitude dynamics model.

The major features, which have to be represented in these models are listed in the following.

Chaser actuation models

- *Propulsion drive electronics model:*
  - the time delay between the actuation of thruster valves and commands from the thruster management function, which is part of the GNC algorithms;
  - a representation of 'built-in test equipment' producing data on failed thrusters as input to MVM and FDIR;
  - data on redundant string main valve status as input information to MVM and FDIR.
- *Thruster accommodation model:*
  - location and angles of thruster accommodation on spacecraft;
  - errors of location and angles of thruster accommodation (see section 4.3.2);
  - thrust direction and magnitude errors due to plume impingement of spacecraft structure (see section 4.2.4) – this has to be modelled individually for those thrusters affected, depending on accommodation location and angle and on the design of the spacecraft structure.
- *Thruster equipment:*
  - minimum impulse bit (MIB), thrust magnitude and thrust pulse characteristics as a function of 'thruster-on time' (see figures 6.14 and 6.15);

- thrust direction and magnitude uncertainties (see section 4.3.2);
- 'thruster open' and 'thruster closed' failure modes.

Chaser perturbation models

- *Absolute and differential air drag (see section 4.2.1):*
  - evolution of air density along the orbit due to the temperature difference between the illuminated side and the shadow side of the orbit;
  - change of the cross section of the chaser along orbit due to the solar arrays rotating with the Sun direction;
  - determination of the absolute drag force acting on the chaser, calculated from the evolution along the orbit of the chaser cross section and the air density;
  - determination of torques due to drag. These occur when the centre of pressure and the centre of mass do not coincide in the cross section of the vehicle normal to the velocity vector. The CoM position will be obtained from the mass, inertia and CoM model below;
  - determination of the differential drag by subtraction of the absolute drag values of chaser and target;
  - correction of the differential drag value at close distance by determination of the areas on the chaser which are shadowed by the target structure.
- *Gravity field, J_2-effect (see section 4.2.2):* forces, due to the deviation of the gravity field of the Earth from an ideal sphere, which change the orbit of the vehicle (see Eqs. (4.8) and (4.9)).
- *Gravity gradient:* torques acting on the spacecraft body due to the gradient in the gravity field of the Earth in the radius direction (this attitude disturbance has not been discussed further in this book, since the effect is well analysed and described in all textbooks on attitude control).
- *Thruster plume interaction (see section* 4.2.4*):*
  - forces and torques due to the impact on the surfaces of the chaser vehicle of the thrust plumes emitted by the target vehicle;
  - kinematic model of location of thruster on target vehicle and of relative position and attitude between the two vehicles.

Note: the modelling of the target thruster plume interaction may not be necessary if target thrusters are inhibited during docking.

Chaser dynamics models

- *Chaser position dynamics:*
  - numerical integration of the Hill Eqs. (3.21) (note: the Clohessy–Wiltshire linearised solutions Eqs. (3.22) would be not accurate enough). Parameters are the vehicle properties, i.e. the mass and the CoM position of the spacecraft body, determined by the 'mass, inertia and CoM' model described below. Input values are the forces acting on the spacecraft, i.e. the thrust forces, the air drag forces and the J_2-effect;
  - internal features, modifying the solid body dynamic behaviour in terms of resonant frequencies, bandwidth, damping behaviour, etc., are flexible appendages, e.g. solar arrays and antennas, and the sloshing of liquid propellant in the tanks (see below);
  - correction of thrust force vectors by results from CoM position model. These will be necessary because there is in the general case not a single tank located in the geometric centre (see below).
- *Chaser attitude dynamics:*
  - numerical integration of Eq. (A.83), for which the input values are the inertia tensor of the vehicle determined by the mass, inertia and CoM model described below and the torque inputs, i.e. the control torques by the thrusters and the disturbance torques by drag and gravity gradient effects;
  - as for the position dynamics, internal features, modifying the solid body dynamic behaviour in terms of resonant frequencies, bandwidth, damping behaviour, etc., are flexible appendages, e.g. solar arrays and antennas, and the sloshing of liquid propellant in the tanks (see below);
  - correction of thrust force vectors by results from CoM position model, as described for the position dynamics model.
- *Flexible appendages:* part of the dynamics model block, modelling the dynamic interaction between items flexibly attached to the main body of the spacecraft and the rigid body dynamics. These are items such as solar arrays or antennas, which are usually modelled as separate masses attached to the main body by spring-damper links.
- *Fuel sloshing:* this model is part of the dynamics model block, modelling the motion of the propellant liquid in the tanks as a result of linear and angular accelerations. Several models are available, the most simple one being a pendulum model. The pendulum model, in which a single mass representing the propellant mass is hinged with three DOF motion capability at a point representing the centre of the tank, is typically used in simulations of the concept feasibility stage. In the final design stage more detailed models have to be used, taking into consideration the

shape and type of tank (e.g. surface tension tank, diaphragm or bladder tank) and the motion of liquid in those tanks under zero-g conditions.

- *Mass, inertia and CoM position:*
  - the changes of mass, inertia and CoM of the spacecraft during the mission, due to the consumption of propellant. The input to the model is the actual propellant consumption, determined from the thrust commands and from the scheme governing the depletion of tanks;
  - the inertia changes during one orbital revolution due to the rotation of the solar arrays.

Target attitude control modelling

- *Simplified modelling*. As already noted above, the modelling of the target can be kept relatively simple, as long as only the orbital motion of its CoM is of interest for the relative position determination of the chaser, and as long as only its typical attitude motion needs to be simulated to obtain realistic results for the docking port motion as inputs for the optical rendezvous sensor in the last part of the approach. If there is no need to represent the target attitude control by a closed control loop, attitude disturbances resulting from gravity gradient and air drag effects do not need to be modelled for the target. The target attitude evolution over time can then be modelled by a bias attitude, representing the torque equivalent attitude, where all external torques are in balance, and by a simplified attitude command model, representing, e.g., the torque commands in a limit cycle type of attitude control.

- *Closed loop modelling*. If a closed loop attitude control system is to be modelled for the target, disturbances and dynamic modelling will be the same as for the chaser. As actuators, the target may have, in addition to thrusters, reaction wheels or control-moment gyros. In the following, the simple type of modelling is assumed.

Target perturbation models

- *Absolute air drag model:*
  - evolution of air density along the orbit due to the temperature difference between the illuminated side and the shadow side of the orbit (input from chaser modelling);
  - change of the cross section of the target along orbit due to the solar arrays rotating with Sun direction;
  - determination of the absolute drag of the target, calculated from the evolution along the orbit of the target cross section and the air density.

- *Gravity field, J_2-effect (see section 4.2.2):* the forces due to the deviation of the gravity field of the Earth from an ideal sphere, which changes the orbit of the vehicle (see Eqs. (4.8) and (4.9)) (as in the chaser model, the numeric values will be different from the chaser values only as long as the target is at a different altitude from the chaser).

- *Thruster plume interaction model (see section 4.2.4):*

  – forces and torques due to the impact on the target surfaces of thrust plumes emitted by the chaser;

  – kinematic model of location of thruster on chaser vehicle and of relative position and attitude between the two vehicles.

Target dynamics models

- *Target position dynamics*. Numerical integration of the Hill equations Eqs. (3.21) with the absolute drag as the input. In the simplified modelling of the target motion it can be assumed that no position control of the target during the rendezvous approach of the chaser takes place. If the target performs position control during the approach of the chaser or other control forces are applied, an open loop control force profile can be used as the input to the position dynamics model in the same way as for the attitude control torques. In addition to the position control, residual forces may result from thruster operations during de-saturation of reaction wheels or control moment gyros.

- *Target attitude dynamics*. If the target attitude is not just defined by a simple kinematic model, numerical integration of the Eq. (A.83), with fixed inertia characteristics and control torque inputs from the target attitude control model.

Sensor and measurement environment models

Satellite navigation models *(see section 7.3)*

- *Navigation satellite position constellation for chaser:* determination of the navigation satellite positions w.r.t. the instantaneous position of the chaser.

- *Satellite navigation disturbance models (shadowing, multi-path) for chaser:*

  – fixed visibility constraints of chaser antennas for satellite navigation due to antenna characteristics, chaser structure and chaser attitude;

  – shadowing of navigation satellites by moving structural items on chaser, e.g. solar arrays. This model provides additional temporary masking features to the previous one;

  - shadowing of navigation satellites by target structure;
  - multi-path effects.

- *Satellite navigation receiver model for chaser.* Model of chaser satellite navigation receiver representing the basic functions (see section 7.3.2) and the particular features of the individual design. This model needs to include all the features that have any kind of interaction with the GNC, MVM and FDIR functions of the RV-control software. As a minimum the following values must be available from the model:

  - raw measurements with accuracy representative for receiver design,
  - output rate of data, accuracy of time measurement representative for receiver design,
  - time required for filter convergence,
  - criteria for switching between antennas,
  - criteria and functions for redundancy switching to redundant channels,
  - built-in test functions.

- The satellite navigation receiver model must represent the internal functions of the receiver equipment in such detail that the listed features and performances result from the modelling.

- *Navigation satellite position constellation for target:* determination of the navigation satellite positions w.r.t. the instantaneous position of the target.

- *Satellite navigation disturbance models (shadowing, multi-path) for target:*

  - fixed visibility constraints of chaser antennas for satellite navigation due to antenna characteristics, target structure and target attitude;
  - shadowing of navigation satellites by moving structural items on target, e.g. solar arrays. This model provides additional temporary masking features to the above one.

- *Satellite navigation receiver model for target:* same modelling as for chaser.

Optical rendezvous sensor models (*see section 7.4*)

- *Optical rendezvous sensor accommodation and kinematics model*:

  - relationship between the linear and angular motion at the position of the sensor and the angular motion of the CoM of the chaser;

  - relative position and relative attitude between sensor location and optical axis on chaser, and reflector pattern on target from relative position and attitude at spacecraft CoMs, target docking port kinematics model and chaser sensor location model.

- *Target docking port and reflector pattern kinematics model:*
  - relationship between the angular motion of the CoM of the target and the linear and angular motion at the docking port;
  - position of the sensor reflector pattern in the docking port plane.

- *Measurement environment model for rendezvous sensor:*
  - received light power as a function of range (Eq. (7.45) for laser range finder and Eq. (7.54) for camera type of sensor), signal-to-noise ratio criteria;
  - Sun in FOV of sensor determination;
  - specular reflection representation (if needed – sensor may not be sensitive).

- *Optical rendezvous sensor equipment model*. Rendezvous sensor model, representing the basic measurement function (see sections 7.4.1 and 7.4.2) and the particular features of the actual design of the equipment. The model must include all features and parameters that have any interaction with the GNC, MVM and FDIR functions of the RV-control software. As a minimum the following values must be available from the model:
  - sensor FOV,
  - performances,
  - operational limits for measured parameters,
  - bandwidth, output rate, delay of information,
  - built-in test functions.

  As for the satellite navigation receiver model, the rendezvous sensor model has to represent the internal functions of the equipment in such detail that the above features and performances are a product of the modelling.

Other sensors

- *Gyro assembly model*. Due to the host of applications on ground and in space, detailed models of gyro assemblies exist which can be adapted to the particular mission application. The model will have to include particular redundancy features, such as skewed gyros as backup for more than one measurement axis, with the corresponding reduction in accuracy. Also, as for rendezvous sensors and GPS receivers, all features and parameters that have any interaction with the GNC, MVM and FDIR functions of the RV-control software have to be modelled.

- *Sun and Earth sensors*. These models are well established, since they are used in the attitude control systems of a very large number of satellites. Modelling of the basic measurement function plus noise and bias will be sufficient in most cases. Existing models can easily be adapted to the particular items used in the mission.

10.4.2 Modelling for contact dynamics simulation

The basic groups of models used in a contact and capture simulation are shown in figure 10.3. The spacecraft features that play a role in the modelling of the dynamics of contact and capture are shown in figure 10.11. The detailed modelling will very much depend on the type of mechanism design (see section 8.2.5).

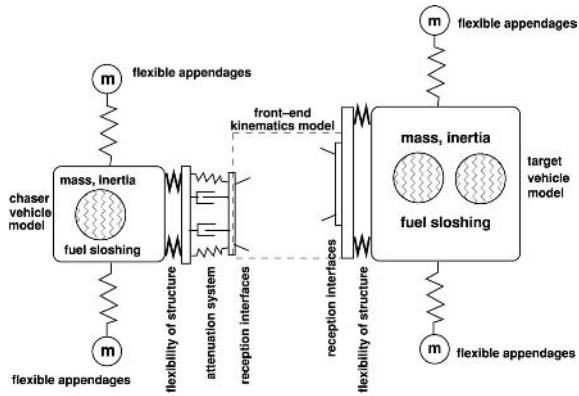

Figure 10.11. Principle of spacecraft modelling for contact dynamics analysis.

The following features have to be included in the modelling:

- *Relative kinematics between chaser and target:* determination of the relative position and relative attitude angles between the spacecraft at their CoMs. The initial conditions, which will be given as the input to the simulation, are the approach velocity and GNC performance values at the test start distance. In the subsequent computation steps, relative position and attitude are determined from the difference of the position and attitude output provided by the dynamics models of chaser and target.
- *Front-end kinematics model:*
  - geometric representation of reception configuration, i.e. rod–cone or contact rings with petals;
  - determination of relative position and angles of front end geometric features on chaser and target from the relative kinematics of the spacecraft and from the distance of these features from the spacecraft CoM;

  - determination of shortest distance between front end geometric features of chaser and target, and determination of contact point when distance becomes zero;
  - determination of contact force direction from the geometric features of chaser and target front ends at the contact point.

- *Capture latch kinematic model*. The latch model needs to include, as a minimum:
  - position of capture latches as a function of time after initiation;
  - comparison of latch positions with the position of their interfaces on the target side;
  - determination of latched condition.

  This model is closely related to the attenuation dynamics and front end kinematics models. Its design will depend on whether the capture latch is connected to the attenuation system (as, e.g., in the central docking system, see figures 8.8 and 8.25), to the contact ring (as in the peripheral docking system with passive capture latches, shown in figure 8.26), or to the docking ring (as in the peripheral docking system with active capture latches, shown in figure 8.27).

  In the case of a passive, spring-loaded capture latch, the model will have to determine whether the position and angles for engagement of the latches are fulfilled. It will also have to model the spring and friction forces acting between the spacecraft due to the capture latches.

  For active latches, the model will have to include the criteria for initiation of the latch operation, the kinematics of the latch motion, the determination of latch contact with the target interfaces and the forces and their direction applied by the latches to chaser and target.

- *Attenuation dynamics model*. Determination of the evolution over time of the deformation of the shock attenuation devices and of the forces acting between the spacecraft after contact, as described in section 8.3. Inputs are the contact point and force direction, determined by the front-end kinematics model and the instantaneous velocity vector.

- *Chaser body dynamics model*. Determination of the linear and angular accelerations of the chaser spacecraft body as a result of the forces transmitted by the attenuation system. For large spacecraft, the flexibility of the substructure of the docking port, flexible appendages and fuel sloshing may have to be taken into account for the calculation of the dynamic reactions, as shown in figure 10.11.

- *Target body dynamics model*. This model is, in structure and content, similar to the chaser body dynamics model, representing the structural design of the target, relevant to forces applied at the location of the docking port.

10.5 Validation of models, tools and facilities

All the models discussed above, and eventually also the tools and facilities in which they are used, need to be validated prior to use in verification tools for the onboard system. According to the definitions given at the beginning of this chapter, this means that sufficient confidence must be obtained that the models (individually for a particular effect) and the tools/facilities (globally for the complete environment of the test item) represent reality to the extent necessary for the verification to be performed. A validation can be achieved in principle by:

(1) comparison of model/simulation output with data obtained from physical testing of the item or the effect in question under the same conditions;

(2) comparison of model/simulation output with data derived from real space missions, where model or simulation parameters are tuned to that particular mission – if results conform to the conditions of an existing mission, confidence in the applicability of the model for other mission conditions will be increased;

(3) comparison of a mathematical model with a model of the same kind which has been obtained from other sources and which has been already validated;

(4) comparison of results of the complete simulation with results of other simulations of the same kind which have been obtained from other sources and are already validated.

10.5.1 Validation of GNC environment simulation models

Orbital perturbation models

For orbital features which are independent of the design of the spacecraft, its subsystems or equipment, validated models are, as a rule, already available from the flight experience and development work of former missions. This is the case for the orbital environment, e.g. for models of the residual atmosphere and for the anomaly (J_2-effect) and the gradient of the Earth gravity field. Although such environment models may be well established and validated, there may still be a residual uncertainty concerning the actual values to be expected when the mission is performed. This is true in particular for the residual air density, which varies with solar flux (see section 4.2.1).

In cases where the perturbation model depends on the actual design of the spacecraft in addition to the orbital environment, such as in the case of absolute and differential air drag forces and gravity gradient torques, the relevant geometric models of the spacecraft which are representative for the particular case must first be established and validated:

- For air drag, the model must represent all surfaces of the vehicle which are perpendicular to the direction of flight. To determine the disturbance torques due to drag, the centres of pressure of these surfaces and their distance from the CoM of the vehicle must be calculated.

- For the gravity gradient effect, a model has to be established which represents the distribution of masses on the spacecraft.

These models will have to be refined commensurate with the design evolution of the spacecraft, starting from rough preliminary values in the concept definition and feasibility phase up to the final versions, where the detailed design of the spacecraft, its moving parts, such as solar arrays and articulated antennas, the spacecraft attitude and the change of mass, CoM and inertias during flight have to be taken into account. Although the measured data for the mass and geometry of parts, and of the complete vehicle, will eventually become available once the spacecraft has been manufactured, validation of these geometric models can be obtained only by analysis and comparison of the model with the hardware design of the vehicle.

Since this type of disturbance model is obtained by a combination of orbital environment models and spacecraft geometric models, the combined model cannot easily be validated experimentally. The method of modelling can be validated, however, by applying it retroactively to spacecraft designs which have already been flown and for which flight data are available. For instance, the drag forces can be calculated from the decay of a spacecraft orbit. As the cross section of the vehicle is known, the drag coefficient C_{D} (see Eq. (4.1)) can be calculated if the residual air density is known; or, vice versa, if the drag coefficient is known with sufficient confidence, the density can be determined.

Plume interaction models

As in the case of drag, this is a combined model, depending on the plume properties of a thruster, on the geometric accommodation of the thruster, on the properties of the surface geometry of the opposite spacecraft and on the relative position and attitude between the two vehicles. Concerning the thruster plume properties, the model for the pressure field of the plume (see Eq. (4.11)) has to be validated. This has been done in many cases by measuring in a vacuum chamber the pressure distribution over the cross section and/or the forces acting on a plate at various distances from the thruster. Plume forces of a thruster exist and have measurable effects also at distances larger than those available in a vacuum chamber. As the plume expansion in a vacuum is well known, the pressure magnitude and distribution as a function of range can be calculated from the measured pressure field at shorter distances.

Spacecraft dynamic models

The equations of motion, i.e. Eqs. (3.21) for translational motion and Eq. (A.83) for rotational motion, are the basic laws of mechanics, which can be assumed to be proven. The accuracy of the numerical integration method used can be proven by mathematical means. The remaining models for the spacecraft dynamics which depend on the spacecraft design and which, for this reason, need to be validated are:

- the evolution during flight of spacecraft mass, CoM position and inertia,

- dynamic interaction caused by flexible appendages,
- dynamic interaction caused by fuel sloshing.

For the final spacecraft design, none of these models can be validated directly by experiment, as this would require the mass changes during flight and the dynamic reactions under zero-g conditions to be observed on the real spacecraft. In these cases, the method of validation will be to use a proven method of modelling and cross-checking by independent analysis to verify that the model provides correct, or at least credible, results for particular sets of parameters.

Evolution of mass, CoM position and inertia The evolution of mass, CoM position and inertia, which is a function of the propellant consumption and tank usage, can be validated only by analysis, e.g. by calculating precisely, for particular points in the mission time-line, the propellant consumption and the change of propellant mass in the tanks. Considering the uncertainties in propellant consumption and the liquid motion in the tanks, the values for mass, CoM position and inertia will also have a margin of uncertainty which cannot be improved by better modelling.

Flexible appendages Dynamic interaction of flexible appendages affects the dynamic response of a body to input forces and torques and has repercussions on the control performance, most significantly on attitude control. The methods used to model flexible appendages and the design of controllers to overcome the effects are well understood and have been experimentally verified and validated for particular configurations. Validation of the model for the actual spacecraft design in question can be performed with a sufficiently high level of confidence by analysis.

Fuel sloshing Models for the motion of liquids in a vessel under zero-g conditions are difficult to be validated experimentally on ground.

Fuel sloshing provides dynamic uncertainties in the attitude control, a phenomenon which is present in practically every satellite. For this reason, a lot of theoretical and experimental work has already been carried out. Theoretical work includes finite element fluid dynamics analysis. Experimental work has been done, using, e.g., drop towers and parabolic flights, which provide a short-time zero-g environment. A number of attempts have been made with orbital experiments, the most recent and most comprehensive one being the Sloshsat 'Flevo' project, was planned, at the time of writing, to be launched by the US Space Shuttle in 2003 (Vreeburg 1999 a,b).

Validation of a sloshing model for a particular spacecraft design can be performed only by analysis. The confidence level in such a model, depending on its level of detail, will be moderate. Comparing the magnitude of effects with other disturbances, however, simulation errors will not be very high for the purpose of a rendezvous mission.

Sensors

For satellite navigation receivers, optical sensors, gyro packages, etc., the models will be derived from the actual design and will be validated by comparison with the results of equipment tests on stimulation facilities as indicated in section 10.3.3, figure 10.5 and as described in section 10.6 below. Such tests need to include the evaluation of the types of values and parameters which have been listed for satellite navigation receivers and optical rendezvous sensors in section 10.4. The objective of orbital demonstrations of the sensor equipment will rather be to increase the confidence in proper performance of the equipment than to validate the model.

Measurement environment

Correct representation of sensor performance in a simulation depends both on the modelling of the sensor functions and on the modelling of the measurement environment.

The systematic part of the measurement environment, which is part of the sensing process, consists of defined geometric and time relations. For satellite navigation receivers, this is the position constellation of the navigation satellites w.r.t. the receiver position and satellite and receiver clock times. For optical sensors, this is the target reflector position, which is obtained from the accommodation and kinematics models for sensor and reflector hardware. This part of the model can be validated at high confidence level by analysis.

For the disturbance part of the measurement environment, i.e. shadowing and multipath effects in the case of satellite navigation receivers and, for optical sensors, spurious reflections of sensor illuminator or sunlight or direct sunlight in the FOV, validation of the models will be a very difficult task. Many experimental investigations, using measurement data from test setups and from real space missions, will be necessary to achieve sufficient confidence in such models. The requirement of validation of these disturbance effects in scope, magnitude and frequency of occurrence is one of the driving forces for building stimulation facilities (see section 10.6) and for performing experiments and demonstrations in orbit (see section 10.7).

Thrusters

Validation can be performed to a large extent by analysis. Due to the long experience with thrusters of all sizes and of many different design types, detailed modelling is available, and good confidence exists in modelling of thruster behaviour and performance. Nevertheless, for each individual design, the thrust level, minimum impulse bit, on/off profile and similar parameters should preferably be validated experimentally at least once for each design. Such experimental validation can be performed by comparison of the model output with results of thruster testing in a vacuum chamber.

10.5.2 Validation of contact dynamics simulation models

Chaser dynamic model

The model can be based on the one established for the GNC simulation, but needs to be modified to include the stiffness of the chaser body at the docking port. Validation by analysis will provide a sufficiently high level of confidence.

Target dynamic model

As for the chaser, the model established for GNC simulation can be used as a basis for and modified to include the stiffness of the target body at the docking port. Validation by analysis will provide a sufficiently high level of confidence.

Spacecraft relative kinematic model

This is a purely geometric model of relative position of the CoMs and relative attitude of vehicles. The current values in the simulation will be obtained by propagation of the initial conditions by integration of the dynamics output. Validation can easily be performed by analysis.

Front end kinematics and contact detection model

Validation is required of the determination of the points of shortest distances at each point in time and the determination of the force direction at contact. Validation will be performed in the development life-cycle, first by analysis for a particular set of parameters comprising initial position and velocities and relative attitude and angular rates. Final validation will be achieved by comparison with results from tests of real mechanisms on a docking dynamics test facility.

Attenuation dynamic model

For the validation of the spring and damper models, the elements can be physically tested and the results compared with the model output. For complex spring-damper arrangements further validation will be performed by analysis.

The model of the complete attenuation system could be validated by physical testing of the integrated attenuation system hardware, i.e. by measuring forces and displacements following well-defined impacts. Final validation can eventually be achieved when the complete docking mechanism is tested on a docking dynamics test facility.

Capture latch kinematic model

The modelling of the relative motion of all capture latches w.r.t. their counterparts (catches, interface ring) has to be validated. This includes the planar motion of a single

capture latch and the six DOF relative motion of the structures that they are mounted on. Capture success depends on both the kinematic condition of the latch and the front ends on both sides. The model is purely kinematic and can easily be validated by analysis. Again, final validation will be achieved by comparison of model and test results, once the complete docking mechanism is tested on a docking dynamics test facility.

10.5.3 Validation of simulator programs and stimulation facilities

Even when all models in a simulation program are properly validated, residual risks remain: the various parts of the program may not interact correctly, i.e. they may interfere with each other because of dynamic incompatibilities; there may be undetected hardware and/or software problems. Validation of proper functioning and performance can be achieved:

- by comparison with results from other simulations, on running the same test case on both simulations,
- by comparison of test results with flight data from a previous mission using the same parameters for initial conditions, disturbances, etc. in the simulation.

The validation of stimulation facilities depends not only on the type of sensor, but, as for the measurement environment models, also on the objective of the stimulation to be produced, i.e. whether the objective is:

- to test if correct measurement data are produced from the input data obtained by the sensor from the measurement environment,
- to test, if the sensor output is sensitive to disturbances by the measurement environment.

In the first case, the validation of the facility essentially consists of providing evidence that the geometric constellation, the velocities and time values produced by the facility are correct. This is the case, e.g., of a stimulator for a satellite navigation receiver, where the accuracy of the input signals for the test item, i.e. the receiver, have to be validated w.r.t. the real navigation satellite constellation. It is also the case for a stimulation facility for optical sensors, where it has to be proven that the geometric positions, angles and rates of the sensor and target pattern indicated by the facility represent, with the accuracy necessary for the verification test, the values produced by the facility.

In the second case, the validation consists of proof that the modelled disturbances are realistic. To verify the sensors it is important that measurement data are not affected under worst case disturbance conditions. Validation is, therefore, the proof that the facility provides such worst case conditions. For example, this is the case of a stimulator of light disturbance of optical sensors. It must be proven that the illumination source is equivalent to sunlight, both for the illumination of the target and for the simulation of the Sun in the FOV of the sensor. Worst case situations of reflection disturbances

will be specular reflections of sunlight and of the sensor's own illuminator. It must be proven that the stimulation facility creates such conditions. In the case of a stimulator for satellite navigation, it must be proven that disturbances due to multi-path effects and shadowing are worst case but realistic. The problem of validation has been addressed already above at the discussion of the measurement environment model validation.

To validate the physical motion stimulation output of docking facilities, in the first instance simple contact geometries (e.g. ball against plate) and simple models for the spacecraft bodies (e.g. spheres and cubes) can be used for which the resulting motion after contact can easily be verified by analysis. Such initial validation exercises will verify the proper functioning of the complete setup from force vector reconstitution and transformations via the spacecraft dynamics into actuator motion. The validation of the models has been addressed already in the previous section. The validation of the complete facility, including all models, can best be performed by comparison with results of an already validated simulation. The compatibility of results of two independently developed simulations, e.g. in this case the test result of the docking hardware on the facility and the results of a simulation based entirely on mathematical modelling, will also increase the confidence in both tools, even if neither of them has been validated before.

10.6 Major simulators and facilities for RVD

10.6.1 Verification facilities based on mathematical modelling

The term *verification facility* is used here for a simulator which provides the environment for verification of hardware and software items in closed loop with a simulated environment. In section 10.3.3 we have seen that such facilities are required for the verification of the RV-control software resident in the onboard computer (figure 10.4) and for the verification of trajectory sensor equipment together with the navigation function of the GNC system (figures 10.6 and 10.7). In these figures, only a high level representation of the GNC functions, sensors and models of the other features that play a role in the performance of the test item under 'real world' conditions are shown. In addition, a verification facility will have to provide a number of functions for the interface with the test item, for running the simulation environment and integration of the dynamics equations, for proper engagement of models, for data inputs and outputs, for pre-, post-processing and storage of data, as required for the tests. The major functions of such a test facility are summarised in figure 10.12.

In order to be able to communicate with the test item, the facility will have to provide all those data interfaces which the test item has in its nominal environment, e.g. data bus and hardwired signal line interfaces. In addition it may have to establish for the test item particular test data interfaces, e.g. if there is a need for measurement of values which are not included in the data stream through the data bus and direct lines, or for input of particular data, e.g. for the creation of a failure condition in a particular function of the test item.

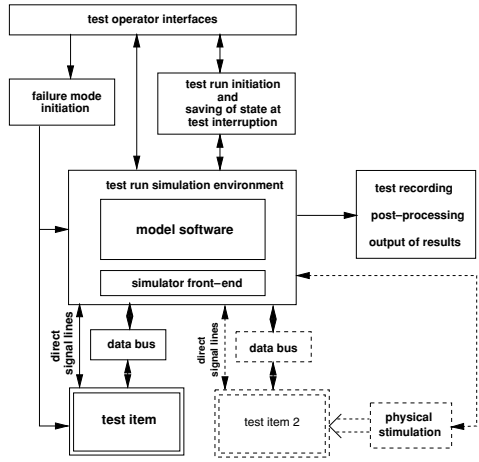

Figure 10.12. Functions of a simulation facility.

The primary function of the facility is to provide the simulation run environment, i.e. the real time execution of the integration of the differential equations describing the dynamic processes to be simulated, the engagement and calculation of the models and the transmission of the input and output data to and from the test item. Input and output data flow must be synchronised with the actual processing sequence and rate of the test item. Other features required for a verification facility are the introduction of failure conditions in the test run and the capability to stop and re-start the simulation run. Finally, a test facility must be capable of recording, post-processing and providing output of the test history and test results.

The introduction of failure conditions in the test item or in one of the functions modelled in the environment simulation can either be at pre-planned points during the simulation run or at the discretion of the test operator. In testing the FDIR functions, such failure simulation may concern both the consequences of failure conditions in the test item, and of equipment modelled in the environment simulation.

At any time during the simulation run, the test operator must be able to stop the simulation, e.g. for off-line analysis, and to resume it at the same state, i.e. with the same conditions and values of the models. The facility must provide all the necessary functions for the initiation of the test at a certain point of the mission, i.e. with the state of the models of the environment simulation according to that mission point. At interruption of the test, it must be possible to save this state and use the data as the initial values for the subsequent test run.

A second or third test item may be connected to the facility, e.g. a sensor or the GPS receivers of chaser and target, which may be physically stimulated by external stimulators, as already indicated in figures 10.4 and 10.7. In that case, the stimulator will be synchronised with the simulation environment and will be driven concerning the

motion of chaser and target by models contained in the model software. The physical stimulation can be in the form of electric signals, e.g. the antenna signal fed to a satellite navigation receiver, or in the form of light and motion, as for optical sensors. For the latter case, an example of a stimulator is described in more detail in the following section.

10.6.2 Example of a stimulation facility for optical sensors

A stimulation facility for optical rendezvous sensors must provide variable relative positions, relative attitudes, relative velocities and angular rates in all directions between the sensor head and the target pattern. It must further provide an emulation of the Sun in the FOV of the sensor and of sunlight illuminating reflective surfaces around the target pattern. The first features are required to test sensor performance within the limits of their operating ranges, the latter ones are required to test their sensitivity against disturbances of the measurement environment.

Although it would be desirable to have a test setup which covers the complete operational range of an optical sensor (typically a few 100 m in the LOS direction), the combination of all test functions with such an extreme range would be extremely difficult to implement and not worth the effort. Also, with increasing distance between the sensor head and the reflector pattern, slight differences of density due to temperature differences cause the air to move and will introduce increasing disturbances. The most critical range for optical rendezvous sensors is that of the last few tens of metres prior to docking. In this range, not only the highest performance requirements exist for the range and LOS angle measurements, but also the three relative attitude angles have to be measured. A stimulation facility for optical rendezvous sensors should, therefore, cover a significant part of this range. If the effects of spurious specular reflections of sensor illuminator or sunlight are to be tested, the target reflector pattern needs to have the capability of three DOF angular motion independently of the sensor head.

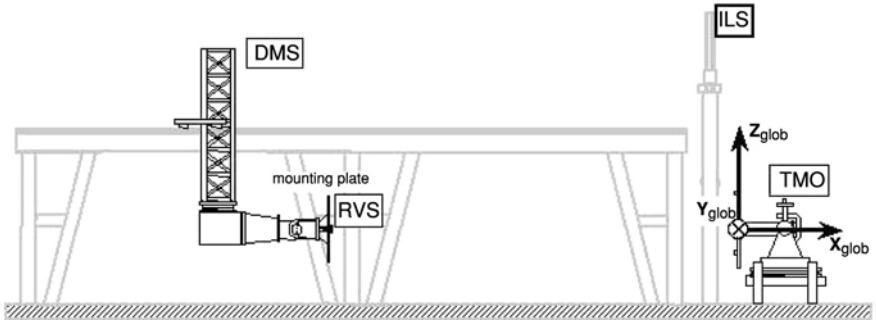

Figure 10.13. Measurement environment facility for optical sensors, EPOS (courtesy DLR).

For the operation as a GNC test facility in a closed loop with the rendezvous control software, as shown in figure 10.6, the motion system needs to be able to follow smoothly, in a slave mode, the state vector values produced by integration of the spacecraft dynamics equations in the environment simulation facility (see also figure 10.12). This requires that the bandwidth of the facility is at least as large as that of the closed loop system of the GNC and the spacecraft, and that the motion system of the facility does not produce additional oscillations to those contained in the spacecraft motions. The bandwidth requirement is another constraint for the size of the facility: the larger its dimensions, the lower the eigenfrequency.

An example of such a stimulation facility is the European Proximity Operations Simulator (EPOS) (Heimbold, Prins & Fehse 1987; Heimbold & Zunker 1996), which has been jointly developed by the European Space Agency and by DLR, the German Aerospace Centre. The facility is located at the DLR Flight Operations Centre in Oberpfaffenhofen, Germany. EPOS (figures 10.13 and 10.14) consists of a motion system (indicated as DMS) providing six DOF of motion capability, a target mount (indicated as TMO) with additional three DOF of angular motion and an illumination system (indicated as ILS) having a two DOF capability in translation and two DOF in rotation. The test item (indicated as RVS) is mounted on the front end of the DMS.

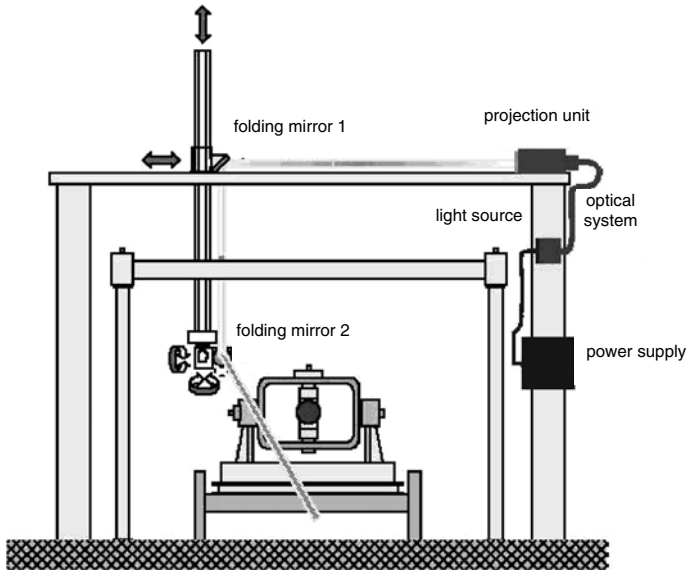

Figure 10.14. Illumination system of EPOS (courtesy DLR).

The *motion system* is a gantry robot, which has a working space of 12 m $\times$ 3 m $\times$ 2 m and provides maximum translation velocities of 0.5 m/s in all directions. The first carriage (gantry) moves in the $\pm x$-direction on two rails mounted at a distance

of >3 m on a base structure firmly connected to the foundation. The second carriage moves on the gantry in the $\pm y$-direction, and the third carriage, a vertical beam structure connected to the second one, moves in the $\pm z$-direction. Connected to the lower end of the vertically moving structure is the front end, which carries the test item. The front end has rotational freedom (without test item) of $360 \times 180 \times 360$ deg (yaw, pitch, roll) and provides maximum rotation rates of 6 deg/s. The bandwidth of the motion system is of the order of 2 Hz.

The *target mount* provides an operating range of $360 \times 180 \times 360$ deg (yaw, pitch, roll), which will be reduced, however, by the accommodation of the test item, i.e. the target pattern and possibly a model of the surrounding surface of the target spacecraft. The target mount can be re-located to increase the distance between the reflector pattern and the sensor head up to 25 m.

The *illumination system* (figure 10.14) is on another gantry type robot, which provides lateral translation capability in the y- and z-directions, and a pitch and yaw rotation capability by its gimballed front end. The Sun simulator consists of a projector which produces parallel light with the intensity of 1 solar constant and two folding mirrors, the first mounted on the moving part of the gantry and the second on the outer (pitch) gimbal of the front end. The illumination system produces a light beam of 12 cm diameter, which can point either to the sensor optics or to the target mount.

To test the sensors, the three systems can be operated by pre-defined profiles for position, angles, velocities and angular rates. All three robot systems can be steered in position and direction by the output of a real time GNC simulation facility connected to the EPOS facility, where the measurements of the sensor mounted on the DMS provide the input to the simulation.

10.6.3 Dynamic stimulation facilities for docking

Many attempts have been made to build a test facility for docking dynamics entirely by mechanical means. Each of the following requirements alone is already difficult to implement:

(1) six DOF motion capability;

(2) two spacecraft models with the correct mass, inertia and CoM position;

(3) compensation for the effects of gravity;

(4) the correct contact velocities;

(5) realistic translational and rotational misalignments;

The combination of all these requirements is practically impossible to achieve without reduction of the degrees of freedom and without arriving at extremely constraining compromises concerning the choice of test conditions. These constraints will apply to the range of contact conditions, spacecraft masses and inertias which can be tested and to

the freedom of motion of the emulated spacecraft bodies motion after contact. The design of a fully mechanical facility with five DOF has been described in Syromiatnikov (1990). This test setup has been used for the verification of the Apollo–Soyuz docking mechanism and for other Russian (Soviet) docking mechanisms. In figure 10.15 it can be seen how the mass and inertia of the two spacecraft are emulated (item 2 for target, item 4 for chaser), how the gravity effect is compensated for by hanging the two masses on cables, suspended in their CoM, how the pendulum effects are compensated for by spring compensators (items 1 and 6), how the chaser body is replaced w.r.t. the target body (item 7), etc.

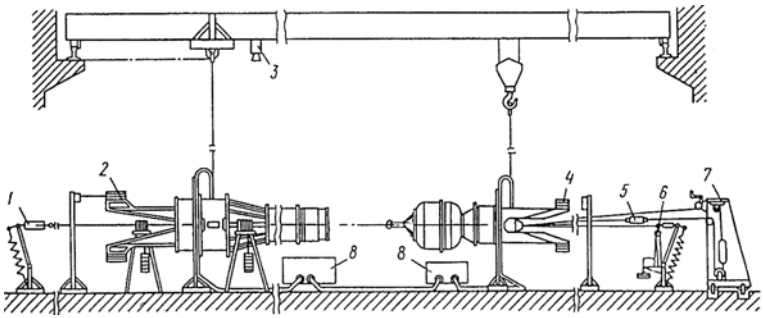

Figure 10.15. Mechanical docking test facility (Syromiatnikov 1990).

It is obvious that with increasing mass and inertia of the vehicles involved in the docking process, such an entirely mechanical facility will be even more difficult to realise. The main disadvantage of such a facility is that, due to the reduction of degrees of freedom, the actual dynamic reactions of the two model bodies will not properly represent the real dynamic reactions of the chaser and target spacecraft. Such setups may provide some indication of the contact point and magnitude of forces in the attenuator system. They may also be useful for testing the proper functioning of the attenuation system or of the latches, but they cannot prove that capture will be successful.

In order to be able to test docking systems in a full six DOF environment, computer controlled electro-mechanical facilities have been developed according to the concepts described in section 10.3.3 and shown in figure 10.8. In practically all the developments of such facilities performed so far, the principle of a Stewart platform has been used. (A Stewart platform is the configuration which provides a six DOF motion capability at maximum stiffness and a minimum number of actuators and moving parts.) The basic design principle of a dynamic docking test facility is shown in figure 10.16. Such facilities have been built for the American (Tobbe & Naumann 1992) and Russian (Syromiatnikov 1990) space programmes, and later also in Europe (Brondino *et al.* 1990) and Japan (Inoue 1991).

From the front end kinematics model, the required position of the platform will be calculated and transformed into the necessary extension of the linear actuators. The requirements for the mathematical models which have to be engaged for the computation

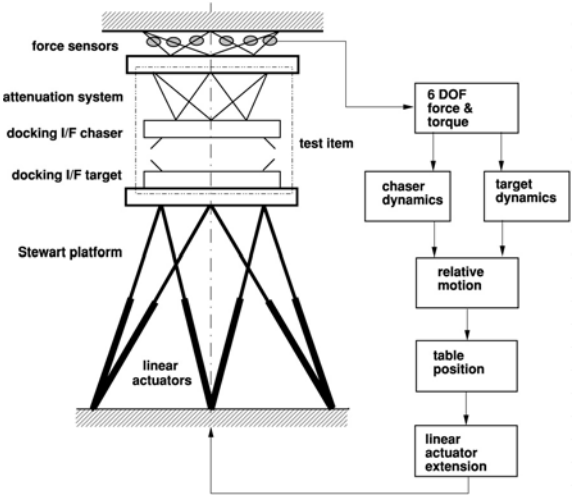

Figure 10.16. Principle of a docking dynamics test facility.

of the motion of the platform have been discussed already in section 10.4.2. Because of the large mass of manned docking mechanisms and the high loads in the case of impact docking, in most cases hydraulic actuators are used. Linear actuators driven by electric motors have been used in smaller test facilities originally designed for unpressurised docking test facilities (Brondino *et al*. 1990; Inoue 1991). Attempts to verify contact dynamics of docking mechanisms for manned scenarios on such small facilities have led to the development of scaled models and to the derivation of scaling laws (MATRA 1993). It has to be kept in mind, however, that although such tests on scaled down hardware is a useful approach for the investigation and verification of the capabilities of the design, and also for validation of models, they will not be sufficient for the final qualification of the flight item.

For better load carrying capability and compensation of the undesirable 1 g loads, the main motion axis (approach axis) of the facility should be vertical. In some implementations (Grimbert & Marshal, 1987; Brondino *et al*. 1990; Inoue 1991; RDOTS 1997) this has been compromised in favour of an additional capability for testing rendezvous sensors. Such a combination of objectives is, however, not advisable:

- A docking test facility requires a high stiffness to achieve a high bandwidth. This is necessary to be able to perform also the motions resulting from structural oscillations of the docking mechanism and the spacecraft substructure at impact. The range required in the approach direction is not much more than what is necessary to accelerate the platform plus the test item to the contact velocity.
- A sensor test facility must have relative large ranges in all directions, but only moderate stiffness requirements (see the previous section).

Large range and high stiffness are incompatible technical requirements. Whereas with very small and lightweight docking mechanisms, such as the ones for unpressurised mating, a combination of the types of facilities might just be possible, for large manned docking systems, such a combination of facility objectives would not lead to useful results for either type of test.

10.7 Demonstration of RVD/B technology in orbit

10.7.1 Purpose and limitations of in-orbit demonstrations

The term *demonstration* is used here for the operation of an item in front of witnesses, with the aim of providing evidence of proper function and performance. A demonstration is neither verification, as there will be no proof that a test item fulfils *all* specifications, nor is it a complete validation, as there will be no proof that a test item functions and performs as required under *all* real world conditions. Generally, a demonstration can show in the best case that for the single set of demonstration conditions the requirements are fulfilled. A successful demonstration in orbit, however, can significantly add to the level of confidence in the proper performance of an item.

Demonstration in orbit will provide in the first instance experience concerning the behaviour of an item under orbit dynamic and zero-g conditions. Further, depending on the demonstration item and the objectives, it may also provide experience concerning other environmental conditions, e.g. survival under launch load conditions, performance under real measurement environment conditions, etc. However, if the demonstration cannot be performed exactly under the same conditions as the real mission, its 'real world conditions' may be similar, but not equal, which reduces the value as a means of verification.

A particular problem of using the results of a demonstration in orbit with two spacecraft for verification/validation purposes, is the fact that this would require an independent measurement capability which is better than or at least equal to the performance of the item or process that is to be verified. For instance, the performance of a GNC system is mainly determined by the accuracy of its sensors. The GNC sensors have been selected, however, because they are the best available for this purpose. For this reason, it will generally not be possible to verify the performance of a GNC system and of its sensors in orbit by comparing it with independent measurements of higher accuracy. At best, a sensor of different or independent design with equal accuracy can be used.

The objective of a demonstration in orbit will, therefore, in most cases not be a verification or validation by direct measurement. The success of a demonstration will usually have to be judged either by the final state achieved in an operation, e.g. the end point of a manoeuvre, the capture of the docking interfaces, etc., or by indirect criteria which can more easily be performed either in orbit or from the ground. Orbital parameters and a position in an orbit at a particular time can, e.g., be reconstituted with relatively good accuracy after flight.

Flight demonstrations are extremely costly when this requires a dedicated mission including spacecraft, launch and mission operations. For this reason, in most cases, flight opportunities will be sought where the flight experiment is an add-on to an existing mission. Such opportunities are rare, however, in particular if a demonstration opportunity in the same type of orbit as the target mission is sought. For this reason, considering both the limited flight opportunities and the general limitations of achieving a demonstration in orbit, in most cases any flight opportunity will be accepted for a demonstration provided the orbit conditions are roughly similar (e.g. LEO for a LEO target mission).

10.7.2 Demonstration of critical features and equipment

In-orbit testing will be sought in particular for items or features where doubts exist that all potential effects or disturbances could be identified and covered to a sufficient extent by analysis, simulation or physical testing on ground. Such doubts typically exist for

- new technologies, for which no space experience yet exists;
- complex measurement environments, where disturbances may be caused by the complex structure of one or both spacecraft, by the atmosphere or by interference from ground, which cannot easily be modelled;
- complex dynamic disturbances and interactions.

A typical case in which it would be desirable to test a new technology in orbit is the demonstration of a rendezvous sensor. Since the performance of the sensors is crucial for the success of a rendezvous mission, it must be ensured that there will be, once in orbit, no effects which may compromise function and performance of the sensor during the mission. The objectives of a flight demonstration will be, therefore, to

- uncover potential side effects, due to orbital conditions, which may have slipped through analysis and testing;
- achieve a better understanding of the operational environment in which the equipment will have to function;
- obtain better information on the disturbance part of the measurement environment.

The possibile validation by an in-orbit demonstration of particular features has already been addressed, e.g. for drag and propellant sloshing, in section 10.5.1. The objective will be, in this case, confirmation or improvement of an existing model. The concept for the demonstration/test setup could be, e.g.,

- the measurement of dynamic reactions of the host spacecraft itself (for example, excitation of slosh by applying linear and angular accelerations, measurement of excitation and of reactions by accelerometers and by gyros (Vreeburg 1999), or

- the measurement of differences in trajectory and attitude between the host spacecraft and a sub-satellite (for example, measurement by optical rendezvous sensors or relative GPS of the trajectory of a sub-satellite with different ballistic coefficients to determine differential drag).

Relative GPS (see section 7.3.3) is an example of a complex sensor function which involves a measurement environment formed by a set of navigation satellites, sensor equipment, i.e. satellite navigation receivers on chaser and target spacecraft, a communication link between the vehicles and a navigation filter, receiving inputs from other functions on the chaser vehicle. Because of the complexity of this measurement principle and its dependency on many conditions and features, which are present only under the condition of two vehicles being in relative close vicinity in orbit, a demonstration prior to operational use is extremely desirable. Unfortunately, a flight opportunity providing all of the features of

- two spacecraft in close vicinity,
- GPS receivers on both chaser and target spacecraft,
- communication between spacecraft,
- an RGPS navigation filter with the real time inputs of actuation commands and attitude measurements of one of the vehicles,

will be rare, unless a dedicated demonstration mission can be implemented (see the ETS-VII demonstration mission in section 10.7.3). Obviously, any rendezvous mission to a space station and any deployment and recovery of spacecraft by the US Space Shuttle will provide some of these features. However, since in the Mir and ISS scenarios no spacecraft has used, up to the time of writing, RGPS for rendezvous and docking navigation, and since most deployment and retrieval missions did not include GPS receivers, all demonstrations of RGPS have so far required a particular experiment setup. A number of orbital experiments have already been performed at the time of writing, and the according experiment plans and results have been reported in, e.g., Hinkel, Park & Fehse (1995), Park *et al*. (1996), Ortega *et al.* (1998), Cislaghi *et al*. (1999) and Mokuno, Kawano & Kasai (1999). However, to achieve sufficient confidence for operational use, additional experience with RGPS will have to be gained in the proper environment of the envisaged spacecraft systems and mission operations.

RGPS flight demonstration example

As an example of the complexity of measurements and data reconstitution, an in-orbit demonstration of RGPS will be described which was performed by the European Space Agency in 1997 on the STS-84 and STS-86 rendezvous missions of the US Space Shuttle to the Russian Mir Space Station (Ortega *et al.* 1998; Cislaghi *et al.* 1999). The

demonstration campaign included also the demonstration of the optical rendezvous sensor RVS. However, for the purpose of this example, the description will concentrate on the RGPS part of the demonstration only. The objectives of the demonstration were threefold:

(1) a validation of the receiver equipment under actual space environment conditions;

(2) a validation of the RGPS navigation filter with real flight data inputs;

(3) a validation of the mathematical model of the GPS receiver.

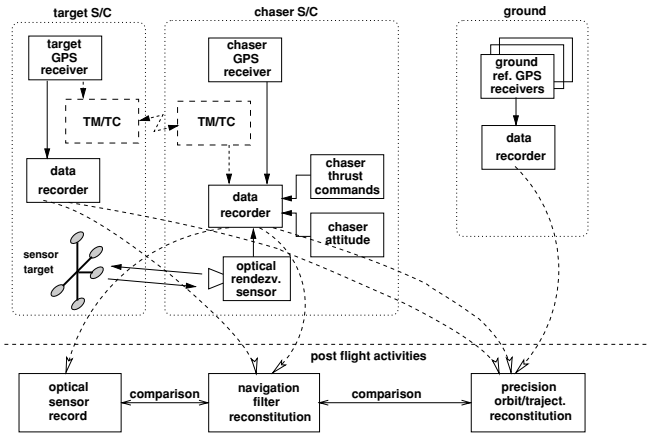

Figure 10.17. Experimental setup for flight demonstration of RGPS.

The RGPS demonstration setup consisted of the following elements:

- GPS receivers on both chaser and target vehicles. These receivers were of different design:
  - the target had a Motorola Viceroy receiver, which was part of the German navigation package MOMSNAV, mounted on the Priroda Module of the Mir Space Station;
  - the chaser had a Laben GPS receiver (based on the Loral TENSOR design), which was mounted as an ESA experiment near to the docking port on the orbiter. The antennas of both vehicles were nominally zenith pointing during the last part of the R-bar final approach of the Orbiter.
- An optical rendezvous sensor on the chaser to provide reference data for the short range. There were two sensors involved, the ESA rendezvous sensor (RVS) and the NASA trajectory control sensor (TCS). Both sensors were of the laser range finder type and mounted near to the docking port of the Orbiter. Corresponding target

reflectors were mounted on the docking module for the Orbiter, which was attached to the Kristal Module of the Mir station.

- A data recorder on the chaser vehicle (Orbiter):
  - to record the raw data of the chaser GPS receiver;
  - to record the accelerations and attitude values of the chaser;
  - to record the optical rendezvous sensor output.
- A data recording device in a laptop computer on the target vehicle (Mir), to record the raw data of the target GPS receiver. Other data pertaining to Mir could not be recorded. The actual time of the attitude changes of the station had to be obtained from the flight plan post-flight.
- A radio link for the transmission of the GPS raw data from the target (Mir) to the chaser (Orbiter) was originally planned, but could not be implemented.

To obtain the maximum opportunities for measurements, the GPS experiments were planned to take place during both approach to and departure from Mir by the Orbiter. The first part of the departure trajectory was similar to the approach trajectory (shown in figure 10.18), only in the opposite direction, with Mir in a LVLH attitude. The second part of the departure trajectory was a fly-around, while the Mir Station was in a Sun-pointing inertial attitude, with the Orbiter remaining opposite to the docking module on Mir at a constant distance.

During the mission no navigation filter processing was to be performed. Instead, the experiment plan was to reconstitute the data processing and output of the navigation filter from the recorded GPS raw data of the chaser and target and from the recorded attitude and thrust acceleration data of the inertial measurement unit of the Orbiter. GPS time was to be used for synchronisation of data. The absolute trajectories of chaser and target were planned to be reconstituted by differential GPS techniques (DGPS, see section 7.3.3) using the IGS (International Geo-dynamics GPS Service) network of GPS receivers at various locations on the Earth as references. These absolute trajectories were intended to be used for the validation of the RGPS performance and for the validation of the mathematical modelling of the GPS receiver.

According to this concept, the post-flight data processing included the following steps:

- Reconstitution of the navigation filter data flow from the recorded GPS raw data of chaser and target and chaser attitude and thrust data.
- Reconstitution of 'best estimated' *absolute* trajectories of chaser and target by DGPS processing of the outputs of the chaser and target GPS receivers with the records of the reference GPS receivers on ground.

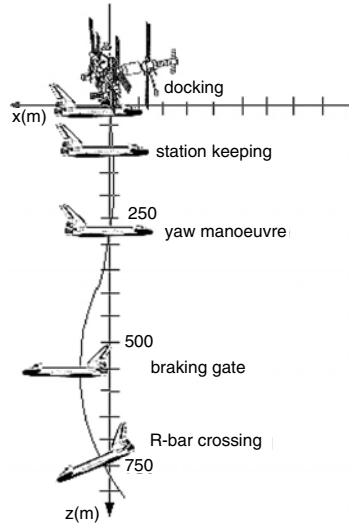

Figure 10.18. Final approach trajectory of Orbiter to Mir (courtesy ESA).

- Comparison of the relative trajectory from the output of the navigation filter with the 'best estimated' *relative* trajectory, obtained from the differences between the absolute trajectories of chaser and target obtained from the DGPS results using the IGS receivers.
- Comparison of the relative trajectory from the output of the reconstituted navigation filter with relative trajectory data from the optical sensor measurements. Optical sensor data were, however, not available for all ranges and all trajectory parts.
- Comparison of the actual absolute trajectory output of the test GPS receiver with the output of the mathematical model of the receiver, fed by the 'best estimated' absolute trajectory obtained from the DGPS results using the IGS receivers and by the GPS satellite constellation at the time of demonstration.

The results of the RGPS experiments during the two flights have been analysed in MATRA-MARCONI (1998 a,b). During only a few short parts of the approach and departure trajectories, all measurements required for the evaluation were simultaneously available. For example, during the entire first flight, no optical sensor measurements and useful GPS measurements of both receivers could be obtained at the same time. During the second flight a complete set of data could be recorded only during the departure phase. The reasons were: a partial non-availability of one receiver and a less suitable attitude or shadowing by one or both vehicles, such that the minimum of four commonly tracked GPS satellites was not achieved; or that the target reflectors were outside the FOV of the optical sensor.

The accuracy of the best estimated relative trajectories obtained from the DGPS processing with the IGS receivers was about 15–25 m in position and about 3–5 cm/s in velocity, which is about twice the required performance of RGPS ($<$10 m). Although this was not sufficient for a validation of RGPS performance, the DGPS data helped in the general assessment of results and in the detection and interpretation of disturbances. The accuracy of the best estimated absolute trajectory was, however, sufficient for the validation of the GPS receiver mathematical model. The accuracy of the relative trajectory obtained from the optical sensor measurements (TCS) of $<$1 m eventually provided the proper reference for RGPS performance validation.

The experience with this flight experiment revealed:

- the difficulties in implementing a suitable RGPS experiment setup on a mission which was not planned for this purpose;
- the problems of obtaining simultaneously suitable measurements from all necessary contributors to the demonstration experiment, during flight operations which were not designed for such a demonstration;
- the complexity of the evaluation process from indirect data concerning the performance of a sensor system as complex as relative GPS.

Shadowing and multi-path disturbances encountered during the flight experiment were found to be difficult to re-establish by simulation. This was mainly due to the high geometric complexity of the Mir Station and the Orbiter, which were difficult to represent in the multi-path model. Multi-path effects became observable at ranges below 200 m. The errors were generally below 10 m; however, short peak values of $>$100 m have also been encountered. The RGPS navigation filter was found not to be very sensitive to temporary multi-path effects. In conclusion, the flight demonstrations were successful and the results were very encouraging. They confirmed also, however, that more flight experience in an operational environment as close as possible to that of the target mission would be desirable to reduce risks of disturbances by shadowing and multi-path effects.

10.7.3 Demonstration of RV-system and operations in orbit

The objectives of an in-orbit demonstration on a systems and operations level can be:

(1) to gain general experience about a new orbital technique;

(2) to prove the readiness of systems and operations design prior to an operational rendezvous mission.

In the first case the objectives of the demonstration will be to demonstrate the general ability of performing in-orbit rendezvous and mating of two spacecraft, to build confidence in the design concept for an automated onboard rendezvous control system, and to gain experience about all issues of planning and execution of orbital operations for such

missions, including the communication and command capabilities with/from ground. One of the major interests will be to identify side effects, omissions ('not thought ofs') and any design weaknesses of any part of the space and ground systems which may have slipped through the verification exercise on ground.

In the second case, the demonstration is a final proof of operational readiness under 'real world' conditions, i.e. the final step in the validation of a complete rendezvous system, consisting of the space and ground segment functions and operations, including all infrastructure and auxiliary functions. Whereas in the first case the emphasis will be on the technical success of a new concept, in the second case the safety of the target crew (in the case of a manned mission, otherwise it will be the security of investment) during all rendezvous and capture operations is the most important feature to be demonstrated.

Example of a rendezvous and docking technology demonstration on system level

The Japanese Engineering Test Satellite ETS-VII (Kawano *et al*. 1998; Mokuno *et al.* 1999; Tsukui *et al.* 1999) is the best recent example of an RVD system technology demonstration in-orbit. The satellite system, launched in 1997, consisted of the main spacecraft, which acted during the rendezvous demonstration as the chaser, and a subsatellite, which had only attitude control capability and acted as the target (see figure 10.19). With ETS-VII, two technologies and techniques were demonstrated: rendezvous and docking and space robotics. For the purpose of this book only the rendezvous and docking part is of interest. The three major objectives of the rendezvous demonstration were:

(1) Validation of the RVD specific equipment technology, i.e. demonstration of proper functioning and performance of RGPS, of the optical rendezvous sensors and of the docking mechanism.

(2) Validation of rendezvous control technology, i.e. demonstration of proper functioning and performance of the GNC and flight management functions (the latter contains the functions called MVM and FDIR in this book).

(3) Validation of the RVD operations techniques, i.e. demonstration of supervisory control techniques of monitoring and high level controlling chaser and target during automatic rendezvous operations, demonstration of proper functioning of telecommunication techniques via relay satellite (TDRS), and demonstration of teleoperations techniques, performing trajectory control from ground.

The chaser vehicle, i.e. the main spacecraft of 2500 kg mass, had the following RVD specific equipment:

- a double-redundant onboard control computer with voting function;

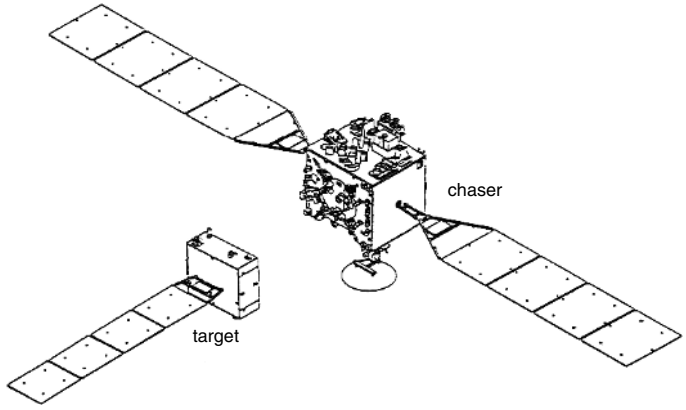

Figure 10.19. ETS-VII spacecraft for rendezvous demonstration (Kawano *et al*. 1998).

- the rendezvous control software resident in the control computer, which includes the algorithms for the GNC modes and for the flight management functions (mode sequencing, FDIR, approach abort and CAM implementation);
- a GPS receiver for absolute position measurement in all ranges and for relative position measurement between 9 km and 500 m;
- a laser radar type rendezvous sensor for relative measurement between 500 m and 2 m;
- an optical proximity sensor for relative position and relative attitude measurement between 2 m and contact;
- an unpressurised docking mechanism consisting of three latches of the type shown in figure 8.6.

Along with the other equipment necessary for the operation of a satellite, such as the reaction control system, the communication system for data exchange with the target satellite and ground (via TDRS) and attitude control sensors, such as gyros and Earth sensors, video cameras and a floodlight installation were available to observe and record the approach and docking operations.

Because of its more passive function in the rendezvous demonstration, the target vehicle had a smaller size and a mass of only 400 kg. Its GNC functions were reduced mainly to attitude control. It carried the following RVD specific equipment:

- a GPS receiver,
- the target reflectors for the laser radar rendezvous sensor,
- the target pattern for the proximity sensor,

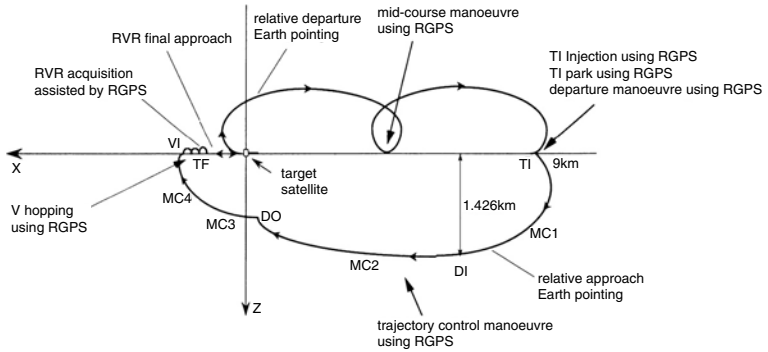

Figure 10.20. Planned trajectories of third ETS-VII RVD flight campaign (Kawano 1997).

- the handlebars for the docking latches,
- an optical target for the video camera.

Attitude control electronics, gyros and Earth sensors, a reaction control system and equipment for an inter-satellite link with the chaser vehicle enabled this sub-satellite to function as an independent spacecraft.

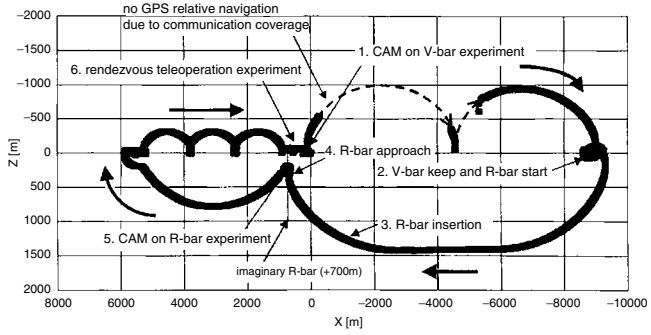

Figure 10.21. Actual trajectories of third ETS-VII RVD flight campaign (Yamanaka 2000).

The RVD demonstration was planned to be performed in several flight campaigns with trajectory strategies designed to demonstrate particular features, such as V-bar separation and docking, V-bar final approach, complete V-bar approach sequence including all ranges of relative navigation and docking, contingency operations, R-bar approach, and remotely manually controlled approach. In spite of thruster failures, all demonstration objectives could be achieved, i.e. all equipment and system functions addressed above

have been demonstrated successfully. As an example, the planned trajectories for the third flight campaign are shown in figure 10.20 (Kawano 1997). The actual strategy of the third campaign had been modified, however, to include features which were originally planned for an additional flight campaign. The flight trajectories recorded from the RGPS navigation data are shown in figure 10.21 (Yamanaka 2000).

In-flight demonstration of system readiness prior to operational use

As indicated above, the objective of such a demonstration would be to test all the systems and operations in their proper context prior to a real mission, i.e. prior to the first mating with the target spacecraft. The problem of validation of a rendezvous system is similar to the problem of validation of a launcher: the necessary confidence in proper functioning and performance can be obtained only by demonstration of systems and operations with the real vehicle. Demonstrations with other vehicles will always lead to different body and contact dynamics, which will require an adaptation of GNC and docking systems to those dynamics. Also, the infrastructure of the reaction control system, the data management system, the communications system and other subsystems will be different on another vehicles, so that, in the end, such a demonstration would be no more than the technology type of demonstration described above. The dilemma is that, when using different vehicles, the objective of proving flight readiness of the operational system cannot be achieved; on the other hand, with an unproven system, proximity operations and mating with the target form a risk, in particular if the target vehicle is manned.

Let us consider in more detail what the problems and limitations of validity are if the same or different vehicles are used:

- The target can be the real one down to a safe distance, whereas at close proximity and contact the target for the demonstration should be different for safety reasons. However, if the target is different:
  - the target attitude motion will be different, which is a drawback for the verification of the RV-control system of the chaser for the last part of final approach;
  - target mass and inertia will be different, which is a drawback for contact/ capture dynamics verification.

  The result would be, in both cases, that, even if the demonstration were successful, there would be no guarantee for success of close proximity operations and docking with the real target.

- If the chaser vehicle is different, practically the entire onboard GNC system has to be adapted to the vehicle properties of the demo vehicle – in particular the navigation filter and the control function. The demonstration would then be in essence a demonstration of the approach strategy and operations only. Except in very particular cases, where such a mission, including launch, could be implemented very

cheaply and where some particular systems or operational features are to be proven, a demonstration with a different chaser vehicle for the proof of flight readiness of the complete RVD system will probably not be worth the investment.

- If the chaser vehicle is of the same design as that for the operational mission, all GNC system and operations demo-objectives can be realised, except for the last part of final approach and contact/capture dynamics verification. The last task would, in this case, require safety-critical operation of a yet undemonstrated system with the manned space station as the target.

It appears then that the dilemma that

(a) system functions and operations for the most critical part of final approach and capture cannot satisfactorily be proven in a demonstration with a different target of opportunity, and

(b) a first time proximity operation and contact with the real target vehicle should be avoided, since it is safety-critical,

cannot be solved without taking the risks of endangering the operational target either in the demonstration mission or in the first operational mission. For this reason, the following solution has been proposed, which tries to reduce the risk to be taken to the maximum possible extent:

(1) Perform the demonstration of the RVD system and the operational approach strategy with the *real chaser* vehicle to the *real target* vehicle up to a point where the safety risk is acceptable. For vehicles visiting the International Space Station, this could be, e.g., for the approach strategies described in section 5.7, the point S3 in example 1 (figure 5.27) or the point S4 in example 2 (figure 5.28).

(2) Perform the rest of the approach in steps with additional stop points, where system and trajectory verifications can be performed and where the vehicle could be commanded to back off, if necessary.

(3) Demonstrate prior to the start of the final approach a CAM, and, during the final approach, a back-off manoeuvre, to prove commandability and proper functioning of such manoeuvres and to prove capability of ground to implement recovery operations and new flight plans.

(4) Perform the last metres of approach from a hold point, at which availability and functioning of all systems and equipment required for the docking operations have been checked.

In the previous demonstration steps, proper functioning of the onboard system and of all onboard and ground operations for the contingency case have been demonstrated.

At the last hold point, availability of sensor functions and GNC modes for the last few metres have been checked. If, at that point, all systems are functioning and no major failures have occurred before, which may have reduced redundancies, the residual risk for the last part of approach and capture should be considered bearable.

Appendix A

Motion dynamics

by

Finn Ankersen

A.1 Equations of relative motion for circular orbits

This section intends to provide the details and intermediate calculations required for the derivation of the general equations of the relative motion for circular orbits. The results of this derivation will be shown as a set of differential equations and in a closed form of the state transition matrix for the system.

A.1.1 General system of differential equations

The general assumption for this derivation is, at this point, that the motion of a body is subject to the effects of a central spherical gravity field and to forces from thruster actuation or disturbances. The spacecraft are considered as point masses for this work.

The position vectors in inertial space are defined in figure A.1 for the chaser ($\mathbf{r}_\mathrm{c}$) and target ($\mathbf{r}_\mathrm{t}$). Their relative position is denoted by $\mathbf{s}$. The equations of motion will be derived conveniently in the target local orbital frame $\boldsymbol{F}_\mathrm{lo}$. In the following, scalars will be in normal type and vectors and matrices will be in bold, and it should be clear from the context what is what. Vectors are defined as column vectors.

The general equation for motion under the influence of a central force is Newton's law of gravitation (Newton 1713); see also Eq. (3.1):

$$\mathbf{F}_\mathrm{g}(\mathbf{r}) = -G\frac{Mm}{r^2}\frac{\mathbf{r}}{r} = -\mu\frac{m}{r^3}\mathbf{r} \tag{A.1}$$

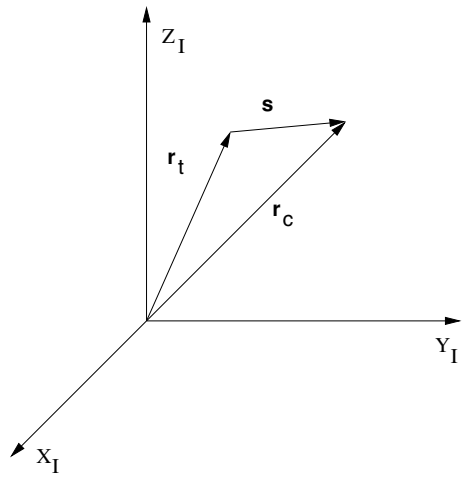

Figure A.1. Definition of the position vectors to the chaser and target as well as the relative vector in the inertial frame.

where

$\mathbf{F}_{\mathrm{g}}$	=	gravitational force
G	=	universal gravitational constant
M	=	mass of the central body (e.g. Earth)
m	=	mass of the spacecraft (second mass)
$\mathbf{r}$	=	the radius vector, $r = \lvert\mathbf{r}\rvert$
μ	=	GM

Dividing by the mass on both sides of Eq. (A.1) to normalise the equation, one obtains for the general motion:

$$\mathbf{f}_{\mathrm{g}}(\mathbf{r}) = -\mu\frac{\mathbf{r}}{r^3} \tag{A.2}$$

The target motion from Eq. (A.1) is

$$\mathbf{F}_{\mathrm{g}}(\mathbf{r}_{\mathrm{t}}) = m_{\mathrm{t}}\ddot{\mathbf{r}}_{\mathrm{t}} = -\mu\frac{m_{\mathrm{t}}}{r_{\mathrm{t}}^3}\mathbf{r}_{\mathrm{t}}$$

$$\mathbf{f}_{\mathrm{g}}(\mathbf{r}_{\mathrm{t}}) = \ddot{\mathbf{r}}_{\mathrm{t}} = -\mu\frac{\mathbf{r}_{\mathrm{t}}}{r_{\mathrm{t}}^3} \tag{A.3}$$

The chaser motion from Eq. (A.1) and from the non-gravitational force is

$$m_{\mathrm{c}}\ddot{\mathbf{r}}_{\mathrm{c}} = \mathbf{F}_{\mathrm{g}}(\mathbf{r}_{\mathrm{c}}) + \mathbf{F} = -\mu\frac{m_{\mathrm{c}}}{r_{\mathrm{c}}^3}\mathbf{r}_{\mathrm{c}} + \mathbf{F}$$

Inserting Eq. (A.2) yields

$$\ddot{\mathbf{r}}_{\mathrm{c}} = \mathbf{f}_{\mathrm{g}}(\mathbf{r}_{\mathrm{c}}) + \frac{\mathbf{F}}{m_{\mathrm{c}}} \tag{A.4}$$

The relative motion $\mathbf{s}$ is defined as follows, and the relative accelerations become directly the derivatives in inertial space:

$$\begin{aligned} \mathbf{r}_\mathrm{t} + \mathbf{s} &= \mathbf{r}_\mathrm{c} \\ \mathbf{s} &= \mathbf{r}_\mathrm{c} - \mathbf{r}_\mathrm{t} \\ \ddot{\mathbf{s}} &= \ddot{\mathbf{r}}_\mathrm{c} - \ddot{\mathbf{r}}_\mathrm{t} \end{aligned} \tag{A.5}$$

Inserting Eqs. (A.3) and (A.4) into Eq. (A.5), one obtains

$$\ddot{\mathbf{s}} = \mathbf{f}_\mathrm{g}(\mathbf{r}_\mathrm{c}) - \mathbf{f}_\mathrm{g}(\mathbf{r}_\mathrm{t}) + \frac{\mathbf{F}}{m_\mathrm{c}} \tag{A.6}$$

We will now linearise $\mathbf{f}_\mathrm{g}(\mathbf{r}_\mathrm{c})$ around the vector $\mathbf{r}_\mathrm{t}$ by means of a Taylor expansion to first order:

$$\mathbf{f}_\mathrm{g}(\mathbf{r}_\mathrm{c}) = \mathbf{f}_\mathrm{g}(\mathbf{r}_\mathrm{t}) + \left.\frac{\mathrm{d}\mathbf{f}_\mathrm{g}(\mathbf{r})}{\mathrm{d}\mathbf{r}}\right|_{\mathbf{r}=\mathbf{r}_\mathrm{t}} (\mathbf{r}_\mathrm{c} - \mathbf{r}_\mathrm{t}) \tag{A.7}$$

Since vectors are defined as column vectors, the Jacobian matrix becomes (Wie 1998)

$$\frac{\mathrm{d}\mathbf{g}(\mathbf{x})}{\mathrm{d}\mathbf{x}} = \begin{bmatrix} \frac{\partial g_1}{\partial x_1} & \cdots & \frac{\partial g_1}{\partial x_3} \\ \vdots & \ddots & \vdots \\ \frac{\partial g_3}{\partial x_1} & \cdots & \frac{\partial g_3}{\partial x_3} \end{bmatrix}$$

To obtain the elements of the Jacobian of Eq. (A.7), we will initially find the diagonal elements of the Jacobian, where we define

$$\mathbf{r} = [r_x, r_y, r_z]^T \; and \; r = |\mathbf{r}| = \sqrt{(r_x^2 + r_y^2 + r_z^2)}$$

For element (i, j), where $i = j$, and using Eq. (A.2):

$$\begin{aligned} \frac{\partial f_\mathrm{g}(r_i)}{\partial r_i} &= -\mu \left[r^{-3} + r_i\big(-\frac{3}{2}\big)(r_x^2 + r_y^2 + r_z^2)^{-\frac{5}{2}} 2r_i \right] \\ &= -\mu \left[r^{-3} - 3r^{-5} r_i^2 \right] \\ &= -\frac{\mu}{r^3}\left[1 - 3\frac{r_i^2}{r^2} \right] \end{aligned} \tag{A.8}$$

For element (i, j), where $i \neq j$ and it shall be noticed that r_i is not a function of r_j,

$$\begin{aligned} \frac{\partial f_\mathrm{g}(r_i)}{\partial r_i} &= -\mu \left[-\frac{3}{2}(r_x^2 + r_y^2 + r_z^2)^{-\frac{5}{2}} 2r_j r_i \right] \\ &= -\mu \left[-3r^{-5} r_i r_j \right] \\ &= -3\frac{\mu}{r^3}\frac{r_i r_j}{r^2} \end{aligned} \tag{A.9}$$

Rewriting Eq. (A.7) and inserting Eqs. A1.1 (A.8) and (A.9), and defining $\mathbf{r} = \mathbf{r}_\mathrm{t}$ we obtain

$$\mathbf{f}_\mathrm{g}(\mathbf{r}_\mathrm{c}) - \mathbf{f}_\mathrm{g}(\mathbf{r}_\mathrm{t}) = -\frac{\mu}{r_\mathrm{t}^3}\mathbf{M}\mathbf{s}$$

where

$$\mathbf{M} = \begin{bmatrix} 1 - 3\frac{r_x^2}{r_\mathrm{t}^2} & 3\frac{r_x r_y}{r_\mathrm{t}^2} & 3\frac{r_x r_z}{r_\mathrm{t}^2} \\ 3\frac{r_y r_x}{r_\mathrm{t}^2} & 1 - 3\frac{r_y^2}{r_\mathrm{t}^2} & 3\frac{r_y r_z}{r_\mathrm{t}^2} \\ 3\frac{r_z r_x}{r_\mathrm{t}^2} & 3\frac{r_z r_y}{r_\mathrm{t}^2} & 1 - 3\frac{r_z^2}{r_\mathrm{t}^2} \end{bmatrix}$$

and Eq. (A.6) becomes

$$\ddot{\mathbf{s}} = -\frac{\mu}{r_\mathrm{t}^3}\mathbf{M}\mathbf{s} + \frac{\mathbf{F}}{m_\mathrm{c}} \tag{A.10}$$

The objective is to represent the chaser motion in the rotating target local orbital frame $\mathbf{F}_\mathrm{lo}$, which has its origin at the COM of the target spacecraft and is defined in section 3.1.3.

From a general kinematic equation for translation and rotating systems, we can obtain the chaser acceleration in the rotating target frame. The translation is trivial and part of the equations (Symon 1979). Generally one obtains the following, where the starred frame $(*)$ is rotating with the orbital rate $\boldsymbol{\omega}$:

$$\frac{\mathrm{d}^2\mathbf{x}}{\mathrm{d}t^2} = \frac{\mathrm{d}^{*2}\mathbf{x}^*}{\mathrm{d}t^2} + \boldsymbol{\omega} \times (\boldsymbol{\omega} \times \mathbf{x}^*) + 2\boldsymbol{\omega} \times \frac{\mathrm{d}^*\mathbf{x}^*}{\mathrm{d}t} + \frac{\mathrm{d}\boldsymbol{\omega}}{\mathrm{d}t} \times \mathbf{x}^* \tag{A.11}$$

We now define $\mathbf{s} = \mathbf{x}$ and $\mathbf{s}^* = [x, y, z]^\mathrm{T}$ in the rotating starred system, and inserting Eq. (A.10) yields

$$\frac{\mathrm{d}^{*2}\mathbf{s}^*}{\mathrm{d}t^2} + \boldsymbol{\omega} \times (\boldsymbol{\omega} \times \mathbf{s}^*) + 2\boldsymbol{\omega} \times \frac{\mathrm{d}^*\mathbf{s}^*}{\mathrm{d}t} + \frac{\mathrm{d}\boldsymbol{\omega}}{\mathrm{d}t} \times \mathbf{s}^* + \frac{\mu}{r_\mathrm{t}^3}\mathbf{M}\mathbf{s}^* = \frac{\mathbf{F}}{m_\mathrm{c}} \tag{A.12}$$

Expressed in the target frame, we obtain for $\mathbf{r}_\mathrm{t}$ and $\boldsymbol{\omega}$

$$\mathbf{r}_\mathrm{t} = \begin{bmatrix} 0 \\ 0 \\ -r \end{bmatrix} \quad \text{and} \quad \boldsymbol{\omega} = \begin{bmatrix} 0 \\ -\omega \\ 0 \end{bmatrix}$$

The terms of Eq. (A.12) become

$$\boldsymbol{\omega} \times \mathbf{s}^* = \begin{bmatrix} -\omega z \\ 0 \\ \omega x \end{bmatrix}$$

$$\boldsymbol{\omega} \times (\boldsymbol{\omega} \times \mathbf{s}^*) = \begin{bmatrix} -\omega^2 x \\ 0 \\ -\omega^2 z \end{bmatrix}$$

$$\boldsymbol{\omega} \times \frac{\mathrm{d}^* \mathbf{s}^*}{\mathrm{d}t} = \begin{bmatrix} -\omega \dot{z} \\ 0 \\ \omega \dot{x} \end{bmatrix}$$

$$\frac{\mathrm{d}\boldsymbol{\omega}}{\mathrm{d}t} \times \mathbf{s}^* = \begin{bmatrix} -\dot{\omega} z \\ 0 \\ \dot{\omega} x \end{bmatrix}$$

$$\mathbf{M}\mathbf{s}^* = \begin{bmatrix} 1 & 0 & 0 \\ 0 & 1 & 0 \\ 0 & 0 & -2 \end{bmatrix} \mathbf{s}^* = \begin{bmatrix} x \\ y \\ -2z \end{bmatrix}$$

As the angular momentum $\mathbf{L}$ is constant for fixed elliptical orbits and, for the special case of circular orbits the angular rate ω is also constant, it can be expressed as

$$\omega^2 = \frac{\mu}{r_{\mathrm{t}}^3} \tag{A.13}$$

From Eq. (A.13) we see that $\mathrm{d}\omega/\mathrm{d}t = 0$. We will now insert Eq. (A.13) and the terms for Eq. (A.12) into Eq. (A.12) to obtain the general linear equations for the relative motion, Known as Hill's equations (Hill 1878); see also section 3.21:

$$\begin{aligned} \ddot{x} - 2\omega\dot{z} &= \frac{1}{m_{\mathrm{c}}} F_x \\ \ddot{y} + \omega^2 y &= \frac{1}{m_{\mathrm{c}}} F_y \\ \ddot{z} + 2\omega\dot{x} - 3\omega^2 z &= \frac{1}{m_{\mathrm{c}}} F_z \end{aligned} \tag{A.14}$$

It shall be noted that the system of linear time varying differential equations in Eqs. (A.14) is the general system valid for an arbitrary relative trajectory between a chaser spacecraft and a target spacecraft, where the latter moves under the influence of a central gravity field only. Hence the validity of Eq. (A.14) for the target spacecraft.

For convenience we will now represent Eq. (A.14) in state space form. In order to reduce the size of the matrices it is convenient to have two systems: one for the out-of-plane and one for the in-plane dynamics. The general form is

$$\dot{\mathbf{x}} = \mathbf{A}\mathbf{x} + \mathbf{B}\mathbf{u} \tag{A.15}$$

where $\mathbf{x}$ is the state vector, $\mathbf{u}$ is the input vector, $\mathbf{A}$ is the transition matrix and $\mathbf{B}$ is the input matrix with matching dimensions.

For in-plane motion, the coupled dynamics from Eq. (A.14) is as follows, with the state vector $\mathbf{x} = [x, z, \dot{x}, \dot{z}]^{\mathrm{T}}$:

$$\begin{bmatrix} \dot{x}(t) \\ \dot{z}(t) \\ \ddot{x}(t) \\ \ddot{z}(t) \end{bmatrix} = \begin{bmatrix} 0 & 0 & 1 & 0 \\ 0 & 0 & 0 & 1 \\ 0 & 0 & 0 & 2\omega \\ 0 & 3\omega^2 & -2\omega & 0 \end{bmatrix} \begin{bmatrix} x(t) \\ z(t) \\ \dot{x}(t) \\ \dot{z}(t) \end{bmatrix} + \begin{bmatrix} 0 & 0 \\ 0 & 0 \\ \frac{1}{m_{\mathrm{c}}} & 0 \\ 0 & \frac{1}{m_{\mathrm{c}}} \end{bmatrix} \begin{bmatrix} F_x \\ F_z \end{bmatrix} \tag{A.16}$$

The out-of-plane dynamics from Eq. (A.14) is as follows, with the state vector $\mathbf{x}_o = [y, \dot{y}]^{\mathrm{T}}$:

$$\begin{bmatrix} \dot{y}(t) \\ \ddot{y}(t) \end{bmatrix} = \begin{bmatrix} 0 & 1 \\ \omega^2 & 0 \end{bmatrix} \begin{bmatrix} y(t) \\ \dot{y}(t) \end{bmatrix} + \begin{bmatrix} 0 \\ \frac{1}{m_c} \end{bmatrix} \begin{bmatrix} F_y \end{bmatrix} \tag{A.17}$$

The equation system described in Eqs. (A.16) and (A.17) is known as Hill's equations (Hill 1878). In the literature, these equations are sometimes also referred to as the Clohessy–Wiltshire (CW) equations, though the CW equations are here presented in Eq. (A.22).

A.1.2 Homogeneous solution

In practice, the forces on the right hand side of Eq. (A.14) are not regular well-behaved functions of time, and therefore it is complex to find a general particular solution to Eq. (A.14), if possible at all in the general case. In this section we will instead concentrate on arriving at an analytical homogeneous solution which will give a good insight into the behaviour of the relative trajectories when treated as an initial value problem.

A Laplace transformation method will be used to find the solution, recalling that the transformation of a derivative in the initial value case is

$$\mathcal{L}(f'(t)) = sF(s) - f(0_+) \tag{A.18}$$

and

$$\mathcal{L}(f''(t)) = s^2F(s) - sf(0_+) - f'(0_+) \tag{A.19}$$

Applying Eqs. (A.18) and (A.19) to Eq. (A.14), we obtain the following expressions in the Laplace domain:

$$\begin{aligned} s^2X(s) - sx_0 - \dot{x}_0 - 2\omega sZ(s) + 2\omega z_0 &= 0 \\ s^2Y(s) - sy_0 - \dot{y}_0 + \omega^2Y(s) &= 0 \\ s^2Z(s) - sz_0 - \dot{z}_0 + 2\omega sX(s) - 2\omega x_0 - 3\omega^2Z(s) &= 0 \end{aligned} \tag{A.20}$$

Solving for $X(s)$ and $Z(s)$ in Eq. (A.20) and re-arranging, the Laplace transformation of the components can be written as

$$\begin{aligned} X(s) &= x_0\frac{1}{s} + (\dot{x}_0 - 2\omega z_0)\frac{1}{s^2} + 2\omega z_0\frac{1}{s^2+\omega^2} + 2\omega\dot{z}_0\frac{1}{s(s^2+\omega^2)} \\ &\quad + 2\omega(4\omega^2 z_0 - 2\omega\dot{x}_0)\frac{1}{s^2(s^2+\omega^2)} \\ Y(s) &= y_0\frac{s}{s^2+\omega^2} + \dot{y}_0\frac{1}{s^2+\omega^2} \\ Z(s) &= z_0\frac{s}{s^2+\omega^2} + \dot{z}_0\frac{1}{s^2+\omega^2} + (4\omega^2 z_0 - 2\omega\dot{x}_0)\frac{1}{s(s^2+\omega^2)} \end{aligned} \tag{A.21}$$

The inverse Laplace transformation is performed to obtain the time domain solution. Taking the inverse Laplace transformation of each term in Eqs. (A.21) and collecting terms, the final homogeneous solution can be found to be, where the initial time is t_0 and $\tau = t - t_0$:

$$\begin{aligned} x(t) &= \left(\frac{4\dot{x}_0}{\omega} - 6z_0\right)\sin(\omega\tau) - \frac{2\dot{z}_0}{\omega}\cos(\omega\tau) + (6\omega z_0 - 3\dot{x}_0)\tau + \left(x_0 + \frac{2\dot{z}_0}{\omega}\right) \\ y(t) &= y_0\cos(\omega\tau) + \frac{\dot{y}_0}{\omega}\sin(\omega\tau) \\ z(t) &= \left(\frac{2\dot{x}_0}{\omega} - 3z_0\right)\cos(\omega\tau) + \frac{\dot{z}_0}{\omega}\sin(\omega\tau) + \left(4z_0 - \frac{2\dot{x}_0}{\omega}\right) \end{aligned} \tag{A.22}$$

From Eqs. (A.22) one sees that $y(t)$ and $z(t)$ are oscillating, whereas $x(t)$ progresses with time t. The equations in (A.22) are the CW equations (Clohessy & Wiltshire 1960) without input forces.

As for the differential equations in (A.16) and (A.17), we will find a state space representation of the solution to the equations. First we will find the Laplace transformation of Eq. (A.15) which becomes:

$$s\mathbf{x}(s) - \mathbf{x}(0_+) = \mathbf{A}\mathbf{x}(s) + \mathbf{B}\mathbf{u}(s) \tag{A.23}$$

Re-arranging Eq. (A.23) gives

$$(s\mathbf{I} - \mathbf{A})\mathbf{x}(s) = \mathbf{x}(0_+) + \mathbf{B}\mathbf{u}(s) \tag{A.24}$$

and the resolvant matrix is defined as

$$\mathbf{\Phi}(s) = (s\mathbf{I} - \mathbf{A})^{-1} \tag{A.25}$$

Re-arranging Eq. (A.24) and inserting Eq. (A.25), we obtain the frequency domain solution as

$$\mathbf{x}(s) = \mathbf{\Phi}(s)[\mathbf{x}(0_+) + \mathbf{B}\mathbf{u}(s)] \tag{A.26}$$

From Eq. (A.26) it is easy to obtain the solution in the time domain:

$$\mathbf{x}(t) = \underbrace{\mathcal{L}^{-1}[\mathbf{\Phi}(s)\mathbf{x}(0_+)]}_{\text{zero input component}} + \underbrace{\mathcal{L}^{-1}[\mathbf{\Phi}(s)\mathbf{B}\mathbf{u}(s)]}_{\text{zero state component}} \tag{A.27}$$

Equation (A.27) gives the desired solution. The first component depends only on the initial state $\mathbf{x}(0_+)$, and the second component depends only on the input. The first term of Eq. (A.27) is actually equivalent to the equation set in Eqs. (A.22), but in matrix notation.

Another form of the general solution to the state space system in Eq. (A.15) is

$$\mathbf{x}(t) = \boldsymbol{\phi}(t, t_0)\mathbf{x}(t_0) + \mathbf{x}_\mathrm{p} \tag{A.28}$$

where $\mathbf{x}_\mathrm{p}$ is the particular solution and $\boldsymbol{\phi}(t, t_0)$ is the transition matrix which maps the initial state vector to the final state vector at time t. The general form of the particular solution is

$$\mathbf{x}_\mathrm{p} = \int_{t_0}^{t} \boldsymbol{\phi}(t, a)\mathbf{B}\mathbf{u}(a)\mathrm{d}a \tag{A.29}$$

There exist several methods of obtaining the transition matrix in Eq. (A.28). The easiest method in this case, as we already have the general solution in Eqs. (A.22), is to find the derivatives and re-arrange with respect to the initial values. A more formal methodology is to calculate it according to Eq. (A.30), which describes the general way of calculating the transition matrix for state space systems:

$$\boldsymbol{\phi}(t, t_0) = \mathrm{e}^{\mathbf{A}(t-t_0)} = \mathrm{e}^{\mathbf{A}(\tau)} \tag{A.30}$$

From Eqs. (A.27) and (A.28), we see the equivalence of the matrices:

$$\phi(\tau) \leftrightarrow \boldsymbol{\Phi}(s) \tag{A.31}$$

The transition matrix in terms of τ now follows for the in-plane and the out-of-plane motion, respectively. For in-plane motion,

$$\phi(\tau) = \begin{bmatrix} 1 & 6(\omega\tau - \sin(\omega\tau)) & \frac{4}{\omega}\sin(\omega\tau) - 3\tau & \frac{2}{\omega}(1 - \cos(\omega\tau)) \\ 0 & 4 - 3\cos(\omega\tau) & \frac{2}{\omega}(\cos(\omega\tau) - 1) & \frac{1}{\omega}\sin(\omega\tau) \\ 0 & 6\omega(1 - \cos(\omega\tau)) & 4\cos(\omega\tau) - 3 & 2\sin(\omega\tau) \\ 0 & 3\omega\sin(\omega\tau) & -2\sin(\omega\tau) & \cos(\omega\tau) \end{bmatrix} \tag{A.32}$$

And for out-of-plane:

$$\phi_o(\tau) = \begin{bmatrix} \cos(\omega\tau) & \frac{1}{\omega}\sin(\omega\tau) \\ -\omega\sin(\omega\tau) & \cos(\omega\tau) \end{bmatrix} \tag{A.33}$$

A.1.3 Particular solution

In this section we will find an analytical solution for $\mathbf{x}_\mathrm{p}$ in Eq. (A.28). We will consider the special case where the input $\mathbf{u}(t)$ is a super-position of step functions, and the resulting pulses are assumed to be of constant amplitude. This is the solution for a special case, but is nevertheless of interest since the actuators for trajectory manoeuvres provide forces as pulses.

For the development of a solution, we will consider only a single principal pulse, which will later be generalised for an arbitrary number of pulses. The input function is defined as follows:

$$f(t) \triangleq k u_{t_1}(t) - k u_{t_2}(t) \tag{A.34}$$

where k is the amplitude of the pulse and $u_a(t)$ is the unit step function defined as

$$u_a(t) = \begin{cases} 1 & \text{for} \quad t \geq a \\ 0 & \text{for} \quad t < a \end{cases} \tag{A.35}$$

For Eq. (A.34) the following inequality must be fulfilled, where t_0 is the initial time:

$$t_0 \leq t_1 < t_2 \tag{A.36}$$

In order to find the zero state component in Eq. (A.27), we will now find the Laplace transformation of Eq. (A.34), yielding

$$\mathcal{L}(f(t)) = F(s) = \frac{k}{s}(\mathrm{e}^{-t_1 s} - \mathrm{e}^{-t_2 s}) \tag{A.37}$$

The product $\mathbf{\Phi}(s)\mathbf{B}$ in Eq. (A.27) consists only of the last two columns of $\mathbf{\Phi}(s)$ as the first two rows of $\mathbf{B}$ in Eq. (A.16) are zero. For the out-of-plane equation it concerns only the last row using Eq. (A.17).

The principles of this particular solution will be based on the in-plane equation, which will be similar for the out-of-plane solution except the dimensions are smaller. From Eq. (A.16) we find the product $\mathbf{BF}(s)$, yielding

$$\mathbf{BF}(s) = \frac{1}{m_\mathrm{c}} \begin{bmatrix} 0 \\ 0 \\ F_x(s) \\ F_z(s) \end{bmatrix} \tag{A.38}$$

What we seek is the zero state component of Eq. (A.27) and, using Eq. (A.38), we can write the form of that term for the in-plane motion as

$$\mathcal{L}^{-1}[\mathbf{\Phi}(s)\mathbf{Bu}(s)] = \frac{1}{m_\mathrm{c}}\mathcal{L}^{-1} \begin{bmatrix} \Phi_{1,3}(s)F_x(s) + \Phi_{1,4}(s)F_z(s) \\ \Phi_{2,3}(s)F_x(s) + \Phi_{2,4}(s)F_z(s) \\ \Phi_{3,3}(s)F_x(s) + \Phi_{3,4}(s)F_z(s) \\ \Phi_{4,3}(s)F_x(s) + \Phi_{4,4}(s)F_z(s) \end{bmatrix} \tag{A.39}$$

The Laplace transformation of the transition matrix can be found from Eq. (A.32). We will not calculate all the elements in detail, but we will look at the first non-zero one, which is element $\Phi(s)_{1,3}$ multiplied by the third element of Eq. (A.38):

$$\Phi_{1,3}(s)F_x(s) = \frac{1}{m_\mathrm{c}} \left[\frac{4}{s^2 + \omega^2} - \frac{3}{s^2} \right] \frac{k}{s}(\mathrm{e}^{-t_1 s} - \mathrm{e}^{-t_2 s}) \tag{A.40}$$

and on re-arranging terms, it yields

$$\Phi_{1,3}(s)F_x(s) = \frac{k}{m_\mathrm{c}} \left[\frac{4}{s(s^2 + \omega^2)} - \frac{3}{s^3} \right] (\mathrm{e}^{-t_1 s} - \mathrm{e}^{-t_2 s}) \tag{A.41}$$

The inverse Laplace transformation of Eq. (A.41) yields

$$\frac{k}{m_{\mathrm{c}}}\left[\frac{4}{\omega^2}[\cos(\omega(t-t_2))-\cos(\omega(t-t_1))]+\frac{3}{2}[(t-t_2)^2-(t-t_1)^2]\right] \tag{A.42}$$

The procedure is the same for the other elements for both in-plane and out-of-plane equations. Considering *one* pulse only, we can formulate the particular solution $\mathbf{x}_{\mathrm{p}}$ as

$$\mathbf{x}_{\mathrm{p_{one}}}=\frac{1}{m_{\mathrm{c}}}\mathbf{H}\mathbf{u} \tag{A.43}$$

where $\mathbf{H}$ is a 4×2 matrix for the in-plane motion and a 2×1 matrix for the out-of-plane motion, both consisting of the terms in Eq. (A.39) and illustrated in Eq. (A.41). The mass m_{c} is kept separate in Eq. (A.43) and the input vector $\mathbf{u}$ is re-defined to contain only the amplitude of the pulses applied, being 2×1 for the in-plane and a scalar for the out-of-plane.

To write this in a more compact form, we will now separate out the columns of Eq. (A.39) as follows:

$$\mathbf{H}=[\mathbf{h}_1\ \mathbf{h}_3] \tag{A.44}$$

for the in-plane motion and directly one column $\mathbf{h}_2$ for the out-of-plane motion.

We are now in a position to find all the elements of the column vectors for the particular solution; this yields

$$\mathbf{h}_1=\begin{bmatrix} \frac{4}{\omega^2}\left[\cos(\omega(t-t_2))-\cos(\omega(t-t_1))\right]+\frac{3}{2}\left[(t-t_2)^2-(t-t_1)^2\right] \\ \frac{2}{\omega^2}\left[\sin(\omega(t-t_1))-\sin(\omega(t-t_2))+\omega(t_1-t_2)\right] \\ \frac{4}{\omega}\left[\sin(\omega(t-t_1))-\sin(\omega(t-t_2))\right]+3(t_1-t_2) \\ \frac{2}{\omega}\left[\cos(\omega(t-t_1)-\cos(\omega(t-t_2))\right] \end{bmatrix} \tag{A.45}$$

$$\mathbf{h}_2=\begin{bmatrix} \frac{1}{\omega^2}\left[\cos(\omega(t-t_2))-\cos(\omega(t-t_1))\right] \\ \frac{1}{\omega}\left[\sin(\omega(t-t_1))-\sin(\omega(t-t_2))\right] \end{bmatrix} \tag{A.46}$$

and

$$\mathbf{h}_3=\begin{bmatrix} \frac{2}{\omega^2}\left[\sin(\omega(t-t_2))-\sin(\omega(t-t_1))+\omega(t_2-t_1)\right] \\ \frac{1}{\omega^2}\left[\cos(\omega(t-t_2))-\cos(\omega(t-t_1))\right] \\ \frac{2}{\omega}\left[\cos(\omega(t-t_2)-\cos(\omega(t-t_1))\right] \\ \frac{1}{\omega}\left[\sin(\omega(t-t_1))-\sin(\omega(t-t_2))\right] \end{bmatrix} \tag{A.47}$$

We recall that the result in Eqs. (A.45), (A.46) and (A.47) is for one single pulse. This result can now be generalised for an arbitrary number of pulses, by making a summation of particular solutions, where the corresponding start time t_1 and finish time t_2 must be inserted for each pulse. We can now write the general expressions.

For the in-plane expression, there is a summation where index i and k refer to the x-axis and the z-axis, respectively:

$$\mathbf{x}_{\mathrm{p}} = \frac{1}{m_{\mathrm{c}}} \sum_{i} \sum_{k} \left[(\mathbf{h}_1 u_1)_i + (\mathbf{h}_3 u_3)_k \right] \tag{A.48}$$

For the out-of-plane expression, there is a summation index j which refers to the y-axis:

$$\mathbf{x}_{\mathrm{p_o}} = \frac{1}{m_{\mathrm{c}}} \sum_{j} \left[(\mathbf{h}_2 u_2)_j \right] \tag{A.49}$$

Equations (A.48) and (A.49) describe the general form of the particular solutions, whether it is a series of pulses or a constant thrust. Cases with simple initial conditions are presented in section 3.3.3.

A.1.4 Discrete time state space system

For the design of controllers in continuous time, the models in Eqs. (A.16) and (A.17) are convenient, but discrete time controllers are most convenient and efficient when designed directly in the discrete time domain. For that purpose a discrete time model is required.

To obtain the discrete model we use a step invariant Z-transformation, where the input signal is considered constant during the sample time T. This fits very well with this type of system, where the inputs are pulses of constant amplitude. The time t is now considered as the discrete time, and time $t + 1$ means the current time plus the sampling time T. The state space model is defined as

$$\mathbf{x}(t+1) = \mathbf{F}\mathbf{x}(t) + \mathbf{G}\mathbf{u}(t) \tag{A.50}$$

The coefficient matrix $\mathbf{F}$ can be found from Eq. (A.32) for the in-plane motion and from Eq. (A.33) for the out-of-plane motion by replacing the independent variable τ with the sampling time T, and formally computed as

$$\mathbf{F} = \mathrm{e}^{\mathbf{A}T} = \phi(T) \tag{A.51}$$

The input matrix in Eq. (A.50), $\mathbf{G}$, is defined as follows:

$$\mathbf{G} = \int_0^T \mathrm{e}^{\mathbf{A}t} \mathbf{B} \, \mathrm{d}t \tag{A.52}$$

The product $\mathrm{e}^{\mathbf{A}t}\mathbf{B}$ can be found from Eqs. (A.32) and (A.33) for the in- and out-of-plane motion, respectively. From Eqs. (A.16) and (A.17), it can be seen that it gives the last two, respectively one, columns of Eqs. (A.32) and (A.33) divided by the mass.

These elements are then integrated according to Eq. (A.52) from zero to the sampling time, with the following result for in-plane motion:

$$\mathbf{G} = \frac{1}{m_c}\begin{bmatrix} \frac{4}{\omega^2}(1-\cos(\omega T)) - \frac{3}{2}T^2 & \frac{2}{\omega^2}(\omega T - \sin(\omega T)) \\ \frac{2}{\omega^2}(\sin(\omega T) - \omega T) & \frac{1}{\omega^2}(1-\cos(\omega T)) \\ \frac{4}{\omega}\sin(\omega T) - 3T & \frac{2}{\omega}(1-\cos(\omega T)) \\ \frac{2}{\omega}(\cos(\omega T) - 1) & \frac{1}{\omega}\sin(\omega T) \end{bmatrix} \tag{A.53}$$

And for the out-of-plane motion,

$$\mathbf{G}_o = \frac{1}{m_c}\begin{bmatrix} \frac{1}{\omega^2}(1-\cos(\omega T)) \\ \frac{1}{\omega}\sin(\omega T) \end{bmatrix} \tag{A.54}$$

It should be recalled that the discrete state space model is not an approximation of the continuous model, but gives the exact values at the sampling times. For designs where the implementation is in discrete time, meaning a computer controlled system, the direct design in discrete time should always be performed. It ensures a better design with larger stability margins for the same sampling time. The sampling time should be selected such that it is seven to ten times faster than the fastest mode in the closed loop system.

A.1.5 Travelling ellipse formulation

This formulation will only be for the in-plane motion, where a cycloid motion exists. The out-of-plane motion is a pure oscillator and is decoupled, as we know from previous sections. The motivation for this formulation is that it is easier to work with than Eq. (A.22) because the cycloid centre coordinates are expressed explicitly and the influence of velocities appears clearer.

The formulation of the solution to the CW equations in Eqs. (A.22) and (A.28) may take several forms. Here we consider an elliptic formulation, chosen because it is very practical for analytical work with the in-plane guidance and calculation of ΔV manoeuvres.

The form of a general ellipse can be formulated as

$$\begin{Bmatrix} x \\ z \end{Bmatrix} = \begin{Bmatrix} x_c \\ z_c \end{Bmatrix} + \begin{Bmatrix} a\cos(\theta) \\ b\sin(\theta) \end{Bmatrix} \tag{A.55}$$

Equation (A.55) is the parametric equation for a general ellipse with the centre at (x_c, y_c), and with semi major axis a and semi minor axis b. The period of the ellipse is in this case the orbital period, and the θ in Eq. (A.55) is equivalent to the eccentric anomaly. We will now rewrite Eqs. (A.22) as follows:

$$\begin{aligned} x(t) &= 2[A\sin(\omega t) - B\cos(\omega t)] + (6\omega z_0 - 3\dot{x}_0)t + (x_0 + \tfrac{2\dot{z}_0}{\omega}) \\ z(t) &= A\cos(\omega t) + B\sin(\omega t) + (4z_0 - \tfrac{2\dot{x}_0}{\omega}) \end{aligned} \tag{A.56}$$

In Eqs. (A.56) we recognise the vertical component of the centre to be

$$z_{\mathrm{c}} = 4z_0 - \frac{2\dot{x}_0}{\omega} \tag{A.57}$$

From Eqs. (A.56) and (A.57) the horizontal component of the centre of the ellipse yields

$$x_{\mathrm{c}} = x_0 + \frac{2\dot{z}_0}{\omega} + \frac{3}{2}\omega\left(4z_0 - \frac{2\dot{x}_0}{\omega}\right)t \tag{A.58}$$

$$x_{\mathrm{c}} = x_0 + \frac{2\dot{z}_0}{\omega} + \frac{3}{2}z_{\mathrm{c}}\omega t \tag{A.59}$$

From Eqs. (A.22) the semi minor axis can be expressed as

$$b = \sqrt{A^2 + B^2} = \sqrt{\left(\frac{2\dot{x}_0}{\omega} - 3z_0\right)^2 + \left(\frac{\dot{z}_0}{\omega}\right)^2} \tag{A.60}$$

and on adding and subtracting z_0 to A we obtain a more compact form:

$$b = \sqrt{\left(\frac{2\dot{x}_0}{\omega} - 4z_0 + z_0\right)^2 + \left(\frac{\dot{z}_0}{\omega}\right)^2} \tag{A.61}$$

$$b = \sqrt{(z_0 - z_c)^2 + \left(\frac{\dot{z}_0}{\omega}\right)^2} \tag{A.62}$$

From Eqs. (A.56) we recognise that the semi major axis is twice the size of the semi minor axis, leading to

$$a = 2b \tag{A.63}$$

As the coefficients for the trigonometric functions in Eqs. (A.56) are opposite in x and z, and with opposite sign for the cosine function, the same phase angle will be obtained in θ, where

$$\theta = \omega t + \varphi \tag{A.64}$$

and

$$\varphi = \arctan\left(\frac{A}{B}\right) \tag{A.65}$$

$$\varphi = \arctan\left(\frac{\frac{2\dot{x}_0}{\omega} - 3z_0}{\frac{\dot{z}_0}{\omega}}\right) \tag{A.66}$$

$$\varphi = \arctan\left(\frac{z_0 - z_c}{\frac{\dot{z}_0}{\omega}}\right) \tag{A.67}$$

$$\varphi = \arctan\left(\frac{\omega}{\dot{z}_0}(z_0 - z_{\mathrm{c}})\right) \tag{A.68}$$

The correct quadrant has to be taken care of by performing the inverse trigonometric function in Eq. (A.65). Summarising the results for the in-plane motion in parameterised elliptic form yields

$$x(t) = x_{\mathrm{c}}(t) + 2b\cos(\omega t + \varphi) \tag{A.69}$$

$$z(t) = z_{\mathrm{c}} + b\sin(\omega t + \varphi) \tag{A.70}$$

where

$$x_{\mathrm{c}}(t) = x_0 + 2\frac{\dot{z}_0}{\omega} + \frac{3}{2}z_{\mathrm{c}}\omega t \tag{A.71}$$

$$z_{\mathrm{c}} = 4z_0 - 2\frac{\dot{x}_0}{\omega} \tag{A.72}$$

$$b = \sqrt{(z_0 - z_c)^2 + \left(\frac{\dot{z}_0}{\omega}\right)^2} \tag{A.73}$$

$$\varphi = \arctan\left(\frac{\omega}{\dot{z}_0}(z_0 - z_{\mathrm{c}})\right) \tag{A.74}$$

It is seen from Eq. (A.71) that the centre of the ellipse travels with a constant velocity $\dot{x}_{\mathrm{c}}$ proportional to the altitude of the centre of the ellipse z_{c}. If z_{c} is zero and no disturbances are present, it is theoretically possible to station keep without any expenditure of fuel.

An important consideration in the guidance for controlling the in-plane motion is that of minimising the performance index for fuel expenditure, which consists of the sum of ΔV pulses. From Eq. (A.72) it is seen that a change in altitude is only affected by x-axis velocity corrections. Similarly in Eq. (A.71) it is seen that $x_{\mathrm{c}}(t)$ is affected only by z-axis velocity corrections. It is therefore clear that, in order to control the drift of the ellipse, it will be sufficient to apply forces only in the vertical direction.

A.2 Attitude dynamics and kinematics

In this section, the details and intermediate calculations required for the derivation of the general equations of the attitude dynamics and kinematics are provided.

A.2.1 Direction cosine matrix (DCM)

This section summarises the direction cosine matrix (DCM) for an Euler (3,2,1) rotation, as the individual matrices will be needed. Recall that 1 is x-axis, 2 is y-axis and 3 is z-axis. The rotation is from a frame a to a frame b, such that

$$\mathbf{v}_b = \mathbf{R}_{ba}\mathbf{v}_a \tag{A.75}$$

where $\mathbf{v}_a$ is a vector projected on the axes of the a frame and $\mathbf{v}_b$ is the same vector projected on the axes of the b frame. The DCM is derived by a rotation around the

third axis of a followed by rotations around the second and first axes of the resulting intermediate frames. We can therefore write the three individual matrices as follows:

$$\mathbf{R}_{ba}(\boldsymbol{\theta}) = \mathbf{R}_1(\theta_1)\mathbf{R}_2(\theta_2)\mathbf{R}_3(\theta_3) \tag{A.76}$$

$$\mathbf{R}_{ba}(\boldsymbol{\theta}) = \begin{bmatrix} 1 & 0 & 0 \\ 0 & \cos(\theta_1) & \sin(\theta_1) \\ 0 & -\sin(\theta_1) & \cos(\theta_1) \end{bmatrix} \begin{bmatrix} \cos(\theta_2) & 0 & -\sin(\theta_2) \\ 0 & 1 & 0 \\ \sin(\theta_2) & 0 & \cos(\theta_2) \end{bmatrix} \begin{bmatrix} \cos(\theta_3) & \sin(\theta_3) & 0 \\ -\sin(\theta_3) & \cos(\theta_3) & 0 \\ 0 & 0 & 1 \end{bmatrix} \tag{A.77}$$

$$\mathbf{R}_{ba}(\boldsymbol{\theta}) = \begin{bmatrix} c(\theta_3)c(\theta_2) & c(\theta_2)s(\theta_3) & -s(\theta_2) \\ s(\theta_1)s(\theta_2)c(\theta_3) - c(\theta_1)s(\theta_3) & s(\theta_1)s(\theta_2)s(\theta_3) + c(\theta_1)c(\theta_3) & s(\theta_1)c(\theta_2) \\ c(\theta_1)s(\theta_2)c(\theta_3) + s(\theta_1)s(\theta_3) & c(\theta_1)s(\theta_2)s(\theta_3) - s(\theta_1)c(\theta_3) & c(\theta_1)c(\theta_2) \end{bmatrix} \tag{A.78}$$

where $c(\theta_i) = \cos(\theta_i)$ and $s(\theta_i) = \sin(\theta_i)$, and where $\boldsymbol{\theta} = [\theta_1, \theta_2, \theta_3]^{\mathrm{T}}$ is the rotation angle about the respective axis. The inverse rotation is found from the transpose of the orthonormal matrix $\mathbf{R}_{ba}$ such that $\mathbf{R}_{ab} = \mathbf{R}_{ba}^{\mathrm{T}}$.

A.2.2 Nonlinear dynamics

We can write the angular momentum of a rigid body as

$$\mathbf{L} = \mathbf{I}\boldsymbol{\omega} \tag{A.79}$$

where $\mathbf{I}$ is the inertia matrix and $\boldsymbol{\omega}$ is the inertial angular velocity vector. The torque vector $\mathbf{N}$ can be expressed as (Symon 1979)

$$\frac{\mathrm{d}\mathbf{L}}{\mathrm{d}t} = \mathbf{N} \tag{A.80}$$

Expressing a vector in a rotating (starred) system we get for Eq. (A.79)

$$\frac{\mathrm{d}\mathbf{L}}{\mathrm{d}t} = \frac{\mathrm{d}^*\mathbf{L}^*}{\mathrm{d}t} + \boldsymbol{\omega} \times \mathbf{L}^* \tag{A.81}$$

$$\mathbf{N} = \frac{\mathrm{d}^*(\mathbf{I}\boldsymbol{\omega}^*)}{\mathrm{d}t} + \boldsymbol{\omega} \times \mathbf{I}\boldsymbol{\omega}^* \tag{A.82}$$

and as $\boldsymbol{\omega}$ is also the angular velocity of the rotating frame, $\boldsymbol{\omega}^* = \boldsymbol{\omega}$. If we also consider the rotating frame fixed to the body, the inertia matrix is constant, and we can express Eq. (A.82) in the body frame as

$$\boxed{\mathbf{I}\dot{\boldsymbol{\omega}} + \boldsymbol{\omega} \times \mathbf{I}\boldsymbol{\omega} = \mathbf{N}} \tag{A.83}$$

In the special case of the body axes being along the principal axes of inertia, the inertia matrix $\mathbf{I}$ is diagonal and Eq. (A.83) becomes

$$\begin{aligned} I_x\dot{\omega}_x + (I_z - I_y)\omega_z\omega_y &= N_x \\ I_y\dot{\omega}_y + (I_x - I_z)\omega_x\omega_z &= N_y \\ I_z\dot{\omega}_z + (I_y - I_x)\omega_y\omega_x &= N_z \end{aligned} \tag{A.84}$$

From Eqs. (A.84) we see that a body cannot spin with constant angular velocity $\boldsymbol{\omega}$, except about a principal axis, unless external torques are applied. If $\dot{\boldsymbol{\omega}} = \mathbf{0}$, Eq. (A.83) becomes $\boldsymbol{\omega} \times \mathbf{I}\boldsymbol{\omega} = \mathbf{N}$, and the left hand side is zero only if $\mathbf{I}\boldsymbol{\omega}$ is parallel to $\boldsymbol{\omega}$, that is, if $\boldsymbol{\omega}$ is along a principal axis of the body.

A.2.3 Nonlinear kinematics

For the kinematics we seek the differential equations of the motion of the body frame $\mathbf{F}_a$ with respect to the reference frame $\mathbf{F}_{\mathrm{lo}}$, relating the Euler (3,2,1) angles with the angular velocity vector $\boldsymbol{\omega}_{a\mathrm{lo}}$.

The $\boldsymbol{\omega}_{a\mathrm{lo}}$ between the frames is the sum of the individual rotation rates, referred to and added in the final frame. Using the individual rotation matrices from the Euler (3,2,1) rotation in Eq. (A.76) we can write

$$\boldsymbol{\omega}_{a\mathrm{lo}} = \begin{bmatrix} \dot{\theta}_x \\ 0 \\ 0 \end{bmatrix} + \mathbf{R}_1(\theta_x) \begin{bmatrix} 0 \\ \dot{\theta}_y \\ 0 \end{bmatrix} + \mathbf{R}_1(\theta_x)\mathbf{R}_2(\theta_y) \begin{bmatrix} 0 \\ 0 \\ \dot{\theta}_z \end{bmatrix} \tag{A.85}$$

Multiplying the matrices $\mathbf{R}_1(\theta_x)$ and $\mathbf{R}_2(\theta_y)$ from section A.2.1 and collecting terms, Eq. (A.85) becomes

$$\boldsymbol{\omega}_{a\mathrm{lo}} = \begin{bmatrix} 1 & 0 & -\sin(\theta_y) \\ 0 & \cos(\theta_x) & \sin(\theta_x)\cos(\theta_y) \\ 0 & -\sin(\theta_x) & \cos(\theta_x)\cos(\theta_y) \end{bmatrix} \begin{bmatrix} \dot{\theta}_x \\ \dot{\theta}_y \\ \dot{\theta}_z \end{bmatrix} \tag{A.86}$$

We need the inverse relationship of Eq. (A.86), and it shall be noted that the matrix is not a DCM and is not orthonormal, so we need to find the inverse matrix. The determinant becomes $\cos(\theta_y)$ and the inverse can be written as follows in the body frame:

$$\begin{bmatrix} \dot{\theta}_x \\ \dot{\theta}_y \\ \dot{\theta}_z \end{bmatrix} = \frac{1}{\cos(\theta_y)} \begin{bmatrix} \cos(\theta_y) & 0 & 0 \\ \sin(\theta_x)\sin(\theta_y) & \cos(\theta_x)\cos(\theta_y) & \sin(\theta_x) \\ \cos(\theta_x)\sin(\theta_y) & -\sin(\theta_x)\cos(\theta_y) & \cos(\theta_x) \end{bmatrix} \boldsymbol{\omega}_{a\mathrm{lo}} \tag{A.87}$$

A.2.4 Linear kinematics and dynamics attitude model

We will now develop the main steps taken in arriving at a combined linear model for dynamics and kinematics for the attitude motion of a spacecraft from the models in Eqs. (A.83) and (A.87), respectively.

The linearisation will be a general Taylor series expansion around a working point as both the kinematics and the dynamics models are functions of two variables. For a general function $f(x, u)$ we obtain to first order

$$f(x,u) = f(x_0,u_0) + \left.\frac{\partial f(x,u)}{\partial x}\right|_{x_0,u_0} (x - x_0) + \left.\frac{\partial f(x,u)}{\partial u}\right|_{x_0,u_0} (u - u_0) \tag{A.88}$$

where the subscript 0 denotes the operating point.

We can write Eq. (A.83) for the dynamics as $\mathbf{I}\dot{\boldsymbol{\omega}} = f(\boldsymbol{\omega}, \mathbf{N})$, where the operating point for the torque is $\mathbf{N}_0 = \mathbf{0}$ and the operating point for the angular rate is the angular rate of the orbital frame $\boldsymbol{\omega}_0 = [0, -\omega_0, 0]^{\mathrm{T}}$.

We can write Eq. (A.87) for the kinematics as $\boldsymbol{\theta} = g(\boldsymbol{\theta}, \boldsymbol{\omega}_{a\mathrm{lo}})$, where the operating point for the attitude angles is $\boldsymbol{\theta}_0 = \mathbf{0}$ and the operating point for the angular rate to the body frame is $\boldsymbol{\omega}_{a\mathrm{lo}_0} = \mathbf{0}$.

We will not go through all the trivial derivations of the partial derivatives. We proceed to the combined linear model, defining the state vector as $\mathbf{x} = [\theta_x, \theta_y, \theta_z, \omega_{a\mathrm{lo}_x}, \omega_{a\mathrm{lo}_y}, \omega_{a\mathrm{lo}_z}]^{\mathrm{T}}$ yielding

$$\boxed{\dot{\mathbf{x}} = \mathbf{A}\mathbf{x} + \mathbf{B}\mathbf{N}} \tag{A.89}$$

where the system matrix $\mathbf{A}$ becomes

$$\mathbf{A} = \begin{bmatrix} 0 & 0 & \omega_0 & 1 & 0 & & 0 & \\ 0 & 0 & 0 & 0 & 1 & & 0 & \\ -\omega_0 & 0 & 0 & 0 & 0 & & 1 & \\ & \mathbf{0}_{3\times 3} & & \omega_0\mathbf{I}^{-1} & & \begin{bmatrix} I_{31} & 2I_{32} & I_{33}-I_{22} \\ -I_{32} & 0 & I_{12} \\ I_{22}-I_{11} & -2I_{12} & -I_{13} \end{bmatrix}_{3\times 3} & \end{bmatrix} \tag{A.90}$$

and the input matrix $\mathbf{B}$ becomes

$$\mathbf{B} = \begin{bmatrix} \mathbf{0}_{3\times 3} \\ \mathbf{I}^{-1}_{3\times 3} \end{bmatrix} \tag{A.91}$$

In the case where the inertia matrix $\mathbf{I}$ is diagonal, meaning that the body axes coincide with the principal axes, the linear attitude dynamics can be simplified to

$$\dot{\mathbf{x}} = \begin{bmatrix} 0 & 0 & \omega_0 & 1 & 0 & 0 \\ 0 & 0 & 0 & 0 & 1 & 0 \\ -\omega_0 & 0 & 0 & 0 & 0 & 1 \\ 0 & 0 & 0 & 0 & 0 & \omega_0\frac{I_{33}-I_{22}}{I_{11}} \\ 0 & 0 & 0 & 0 & 0 & 0 \\ 0 & 0 & 0 & \omega_0\frac{I_{22}-I_{11}}{I_{33}} & 0 & 0 \end{bmatrix}\mathbf{x} + \begin{bmatrix} 0 & 0 & 0 \\ 0 & 0 & 0 \\ 0 & 0 & 0 \\ \frac{1}{I_{11}} & 0 & 0 \\ 0 & \frac{1}{I_{22}} & 0 \\ 0 & 0 & \frac{1}{I_{33}} \end{bmatrix}\mathbf{N} \tag{A.92}$$

Appendix B

Rendezvous strategies of existing vehicles

B.1 Space Shuttle Orbiter

The description of the rendezvous strategy of the US Space Shuttle Orbiter is based on information obtained by the author and his colleagues during various meetings with NASA on the rendezvous sensor demonstration missions on the Shuttle flights STS-80, STS-84 and STS-86 to the Mir Space Station (see also section 10.7.2). Additional information has been obtained from NASA documentation on these missions (NASA 1996, NASA 1997) and from corresponding information by RSC Energia. A further source was NASA's *Rendezvous/Proximity Operations Crew Training Handbook* (NASA 1989).

The phasing strategy of the Space Shuttle consists of a number of standard manoeuvres, which aim to achieve a viable phasing orbit, to adjust the orbit plane to that of the target and to arrive at an initial aim point Ti at a fixed distance from the target and at a particular time. The various manoeuvres shown in figure B.1 have the following purposes:

- *OMS2*. Boost manoeuvre executed by the 'Orbital Maneuvering System' to raise the perigee and achieve viable phasing orbit.

- *NC*. Series of in-plane manoeuvres to support phasing, to adjust perigee and correct thrust errors from the previous manoeuvres. NC manoeuvres are usually performed at the end of a crew working period and prior to sleep.

- *NH*. Larger height adjustment manoeuvre. The necessity of such larger in-plane manoeuvres will depend on the launch injection conditions and on the target position.

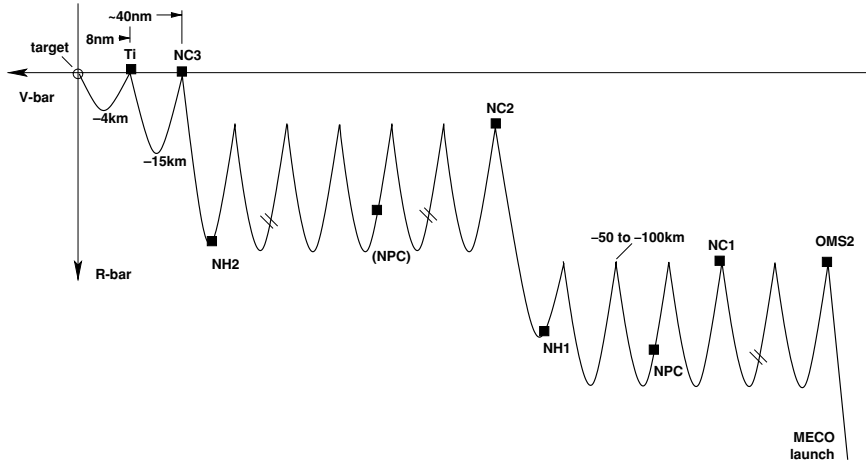

Figure B.1. Example of phasing and far range rendezvous strategy of the Space Shuttle. Note: nm = nautical miles.

- *NPC*. Orbit plane correction manoeuvre. This lateral manoeuvre may be executed at a convenient point of the phasing trajectories to correct RAAN and inclination errors.

All manoeuvres up to the last NC (NC3 in figure B.1) are controlled from ground. The subsequent manoeuvres are controlled autonomously by the onboard GNC system based on star tracker and rendezvous radar measurements. Along the transfer trajectories, the cargo bay of the Shuttle points towards the target. The navigation filter processes all inputs of star tracker, rendezvous radar, inertial measurement unit, thrust commands and the inputs of initial conditions by ground. It propagates the state vector of the vehicle as described in section 6.2.1 above.

- *NCC*. First manoeuvre controlled by the onboard system using filter information updated by star tracker measurements of two previous orbital arcs. The manoeuvre will have in- and out-of-plane components to arrive at Ti in-plane and with the required accuracy.

- *Ti*. Terminal phase initiation manoeuvre. This manoeuvre is executed at a fixed point of 8 nautical miles (14.8 km) behind and 1200 ft (355 m) above the target. All previous manoeuvres are calculated to meet this initial aim point.

- *MC*. Mid-course correction manoeuvre, correcting thrust dispersions of the Ti manoeuvre, measurement errors, residual out-of-plane components, etc., based on Lambert targeting.

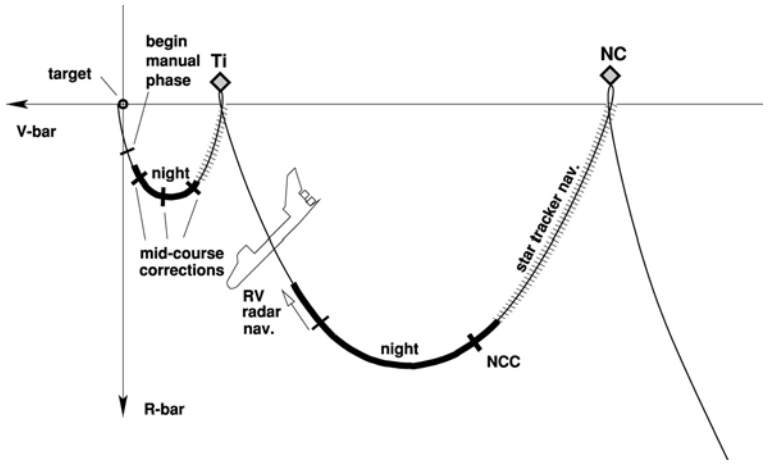

Figure B.2. Typical far range rendezvous profile of the Space Shuttle.

During the last arc, shortly before crossing R-bar, the manually controlled phase commences. Sensors that are available to the crew to increase navigation accuracy, in addition to the rendezvous radar, are:

(1) Crew Optical Alignment Sight (COAS), a passive optical instrument aligned with the x-axis of the Orbiter;

(2) Closed Circuit Television System (CCTV), a system of two cameras, mounted at the front and aft ends of the cargo bay, measuring the angle between the x-axis and the target;

(3) Trajectory Control Sensor (TCS), a laser range finder type of sensor (see section 7.4.1), capable of measuring range and LOS angles.

Nominal approaches of the Space Shuttle are on the $+$V-bar and $+$R-bar sides. Depending on whether a V-bar or R-bar approach is planned, manoeuvres after V-bar crossing will differ.

In a *V-bar approach*, the trajectory is targeted at a point approximately 150 m in front of the target, where a stop pulse is applied. Inside a range of 300 m, the Orbiter has to maintain a velocity profile of range/1000 s. The final approach starts with a velocity toward the target and continues with hops, where a ΔV in the z-direction is applied each time the vehicle crosses V-bar (see figure B.3; see also figure 3.24 for a straight line V-bar approach).

In an *R-bar approach*, an impulse in the $-x$-direction is given at R-bar crossing to reduce the forward velocity. Thereafter, an impulse is applied in the $-z$-direction to compensate for the natural orbital motion, which would have resulted in a $-x$- and $+z$-direction of the trajectory. Each time the vehicle crosses R-bar, a ΔV is applied in

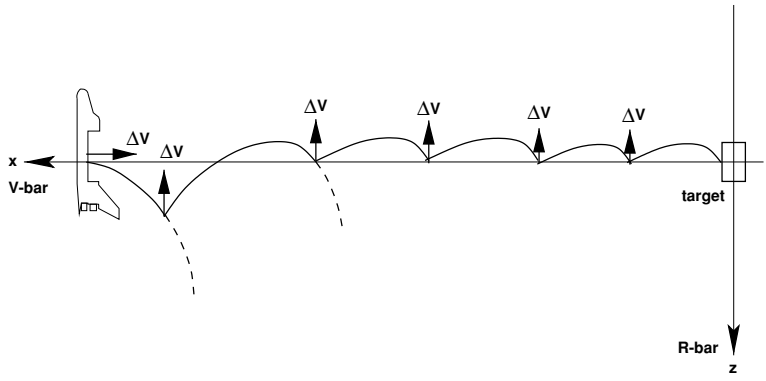

Figure B.3. V-bar approach of the Space Shuttle.

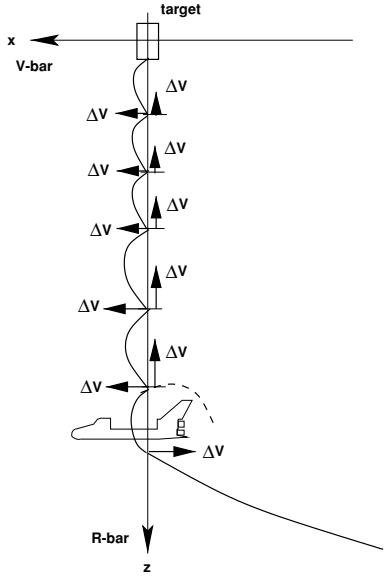

Figure B.4. R-bar approach of the Space Shuttle.

the $-z$-direction, and the vehicle moves in hops along R-bar toward the target (see figure B.4; see also figure 3.25 for a straight line R-bar approach).

A decrease in the approach velocity is achieved in the V-bar approach by reduction in the thrust applied at V-bar crossing (cf. Eq. (3.47) for a straight line approach). In the R-bar approach, the thrusts to be applied are a combination of a ΔV in the $-x$-direction and a ΔV in the $-z$-direction. As shown in figure 3.25, for a constant approach velocity the ΔVs in the $-z$-direction decrease with decreasing altitude difference to the target. The same occurs in an approach where the thrusts occur at discrete points in time instead of continuously. If a velocity profile has to be implemented in an R-bar approach, both ΔV_x and ΔV_z will have to be modified accordingly (cf. Eqs. (3.52) for a straight line approach).

In figure B.2, it is shown that the trajectory crosses R-bar shortly after orbital night. In a V-bar approach, the Orbiter arrives at V-bar approximately at orbital noon. The final approach up to capture will then take place during the second half of the illuminated part of the orbit (see also figure 5.17), with the Sun above and behind the target. In an R-bar approach, the final approach starts directly after R-bar crossing, so that it can take place in the first half of the orbital day. In both cases the Sun will be in front of the approaching vehicle, which may be a disturbance to the pilot. Hold points can be included, on V-bar at any position, and on R-bar at a close distance to the target to save propellant or to wait for more suitable illumination conditions. In the approach from the +R-bar side, the Sun will never illuminate the target docking port side. In this case artificial illumination has to be used for the black and white target pattern used to guide the last part of the approach up to contact.

B.2 Soyuz/Progress

The description of the Soyuz and Progress rendezvous strategy is based mainly on information obtained by the author and his colleagues during various meetings with RSC Energia in the context of the work on ATV. Further sources included a report by the Russian organisation TsNII Mash 1993, prepared in support of the European Hermes project (TsNII-Mash 1992), and a report by CNES 1998 after a meeting with specialists of the Russian mission control centre (TSUP) (Labourdette & Martin 1998).

In contrast to the Space Shuttle, the phasing strategy of the Soyuz and Progress vehicles is based on near circular orbits. This makes the planning of manoeuvres and the time schedule easier. The standard phasing manoeuvres are executed in three sets of one to three boosts (see figure B.5). The strategy takes into account the location and occurrence of communication visibility windows.

(1) The objective of the first set of boosts is to transfer the vehicle to the correct phasing altitude; they are calculated according to the phase angle after launch, according to the altitude of the station, and to the intended time of arrival, to meet proper docking conditions. The manoeuvre set is a Hohmann type transfer, combined

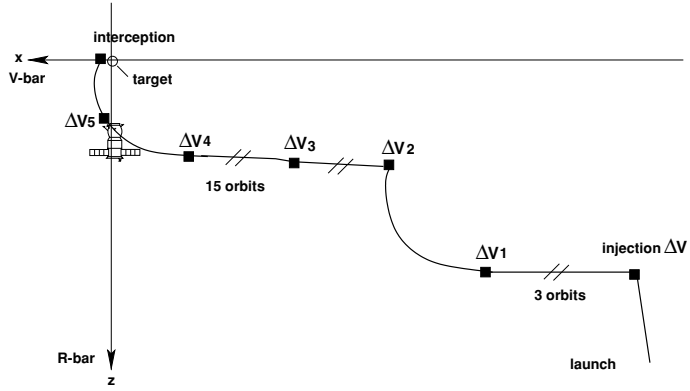

Figure B.5. Phasing strategy of the Soyuz and Progress vehicles.

with orbit plane corrections, and will be executed during the fourth to fifth orbital revolution after launch.

(2) The next manoeuvre will be performed during the 17th orbital revolution. Its purpose is to correct trajectory errors arising after the first set of manoeuvres.

(3) The third set of manoeuvres consists of three boosts, the first two of which, M4 and M5, are calculated to ensure interception of the target orbit precisely at the aim point. The final manoeuvre would inject the chaser vehicle into the target orbit in front of the target, at a distance of approximately 1.5 km. The implementation of this manoeuvre is described in more detail below. The boosts of the third set are performed during the 32nd and 33rd orbital revolutions.

Phasing manoeuvres are executed by the main engines, basically as tangential boosts. Lateral thrust components are obtained by the according attitude angles of the vehicle, e.g. out-of-plane components by yaw angles, in-plane radial components by pitch angles. Whereas the first two sets of manoeuvres are controlled from ground, the last set is implemented automatically by the onboard control system, using, for the calculation of manoeuvres M5 and M6, the measurements of the Kurs rendezvous sensor system (see section 7.2.5). Manoeuvre M4 is calculated and executed by the onboard system based on orbital parameters and conditions loaded into the onboard computer during the previous phase. Preliminary values for manoeuvre M5 and for the injection manoeuvre M6 at the aim point are calculated prior to M4 as a solution to the three-impulse-transfer problem. The preliminary results for $\Delta V6$ obtained in this way are kept as reference by the onboard system.

Shortly after M4, the trajectory enters into the operational range of the Kurs system. The control system will then calculate, based on the relative state vector established by Kurs, an update of the time at which M5 should be executed, an update of the values

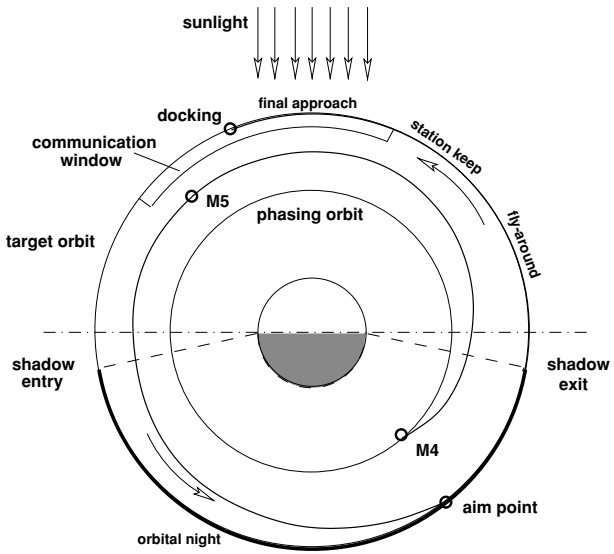

Figure B.6. Rendezvous phase of the Soyuz and Progress vehicles.

of the thrust components of M5 in three directions and of the expected relative velocity at the aim point. To attain a smooth braking velocity profile when arriving at the target orbit, the necessary braking impulse is actually implemented in three manoeuvres (M6–M8), where the first (M6) is applied about 1 km below the target orbit. This first manoeuvre is executed by the main engines, the other two by the attitude control thrusters. Except for the boost with the main engines, the spacecraft points along the approach trajectory toward the target.

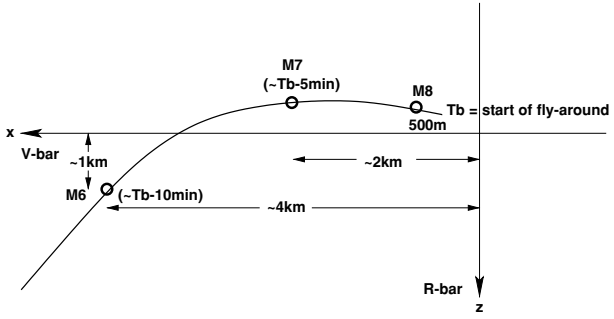

Figure B.7. Soyuz/Progress manoeuvres at V-bar arrival.

An important requirement for the final approach and docking is the illumination of the target docking port. For monitoring reasons, the target should be illuminated by the Sun

with an angle between 30 and 60 deg w.r.t. the docking axis (see also section 5.4.1). For this purpose the Sun must be behind the chaser, which is the case for a $+$V-bar approach in the first half of the orbital day, for a $-$V-bar approach in the second half and for a $-$R-bar approach in the two sectors before and after orbital noon. As we have seen in the previous section, there will be no such condition for the $+$R-bar approach, as the Sun will always be in the hemisphere behind the target. A further constraint which had to be taken into account for the design of the Soyuz/Progress approach strategy, was the fact that the target station (Mir) could have both LVLH and inertial (Sun-pointing) attitude for power reasons.

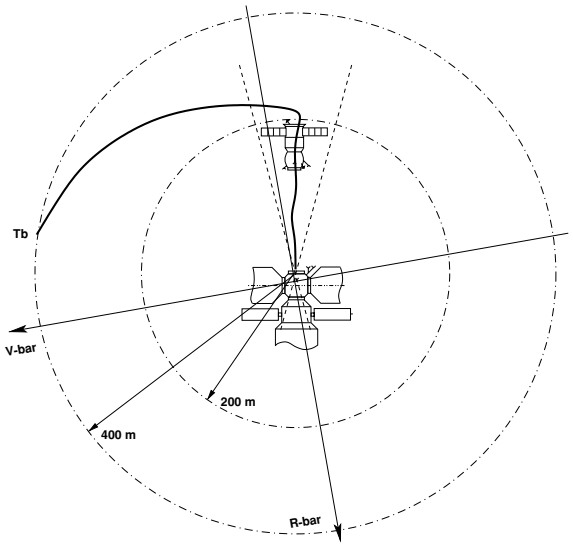

Figure B.8. Soyuz/Progress fly-around and final approach.

At the end of the standard for range approach (M8), the envisaged target docking port may point in a direction not aligned with the approach direction followed so far. In order to achieve alignment with the target docking axis, a fly-around is performed at a range between 400 m and 200 m, which will transfer the chaser to the required approach line for target docking ports on $+$V-bar, $-$R-bar or $-$V-bar, or to that of an inertially pointing port. This fly-around is a two-pulse transfer with components in radial and out-of-plane directions (see also figures 3.14, 3.17 and 3.18), depending on the direction of the docking axis. Considering the fact that both radial and out-of-plane transfers are cyclic motions, returning to the point of departure after one orbit, the impulsive fly-around has the important positive features of safety, repeatability and quasi-constant illumination conditions.

The latter feature can easily be understood considering the following example: starting an impulsive radial transfer with a ΔV at orbital dawn at the $+$V-bar side, the Sun

will be behind the chaser vehicle, illuminating the target. This will continue along the trajectory until the chaser is at the −V-bar side and the Sun enters the shadow of the Earth. This behaviour does not change when an additional out-of-plane component is applied. The fly-around can be stopped at any time, whilst maintaining the same illumination conditions, which means that the docking port can be at any angle in the upper hemisphere.

After the fly-around, the vehicle will perform station keeping, whilst waiting for the go-ahead from the MCC; this waiting time will be utilised for the synchronisation of the final approach with the communication windows and the final adjustment of the illumination conditions. The final approach is a straight line closed loop controlled trajectory with a velocity profile of approximately 1 m/s at its start (150–200 m), which will be reduced to 0.1–0.3 m/s at contact.

Appendix C

Rendezvous vehicles of the ISS scenario

The objective of this appendix is to provide an overview of the vehicles which perform rendezvous and capture in the ISS scenario. Of interest are the features of these vehicles which are most important for the implementation of the rendezvous trajectories and for the mating process. These are:

- masses and inertias of the vehicles;
- actuation means and force/torque capabilities;
- location of thrust engines;
- features of the vehicle geometry related to rendezvous and capture issues, such as size and shape of main body and appendages;
- type and location of mating devices;
- type of rendezvous sensors;

It is not the intention to give here a detailed and exhaustive description of all these vehicles, which may anyway undergo changes in the course of their development.

General information on the various vehicles can be obtained from the NASA, NASDA and ESA web-sites. Detailed information on design and history of the Russian vehicles can be obtained from NASAs 'Mir hardware heritage' (Portree 1995). Information on all aspects of space stations can be found in Messerschmid & Bertrand (1999). Some information contained in this appendix has been extracted from technical reports and specifications of the International Space Station Programme for the Station and its visiting vehicles (NASA 1999), and some has been obtained by verbal communication from specialists involved in the development of the various spacecraft.

In the first two sections of this appendix, the target vehicles ISS and Mir are discussed, in the following sections the chaser vehicles of the ISS scenario are considered.

C.1 International Space Station

At the time of writing, the International Space Station is the target vehicle for the majority of all rendezvous and docking/berthing operations. In the 'assembly complete' state, the ISS will be the largest spacecraft ever built and for its assembly in orbit more than 20 launches will be necessary. Some of the modules are self-navigating, arriving at, and docking to, the station automatically, whereas other modules and assemblies are delivered to the station by the Space Shuttle. The first module of the ISS, the FGB, was launched in November 1998. Figure C.1 shows the 'assembly-complete' configuration, which, at the time of writing, was planed for 2004.

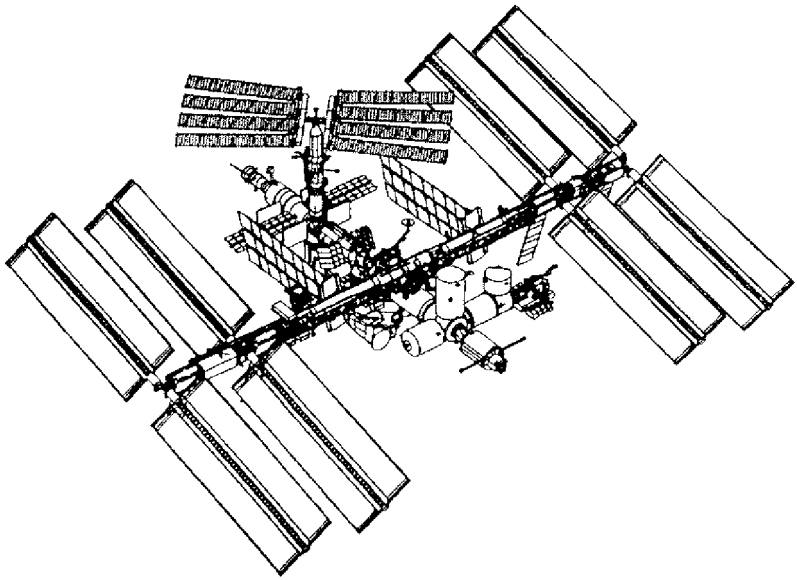

Figure C.1. International Space Station ISS (courtesy NASA).

Design features

The elements of the ISS the 'assembly-complete' configuration are shown in figure C.2 (obtained from NASA (1998c)). In this configuration the ISS will include the following major modules:

- Russian built FGB (the first module of the ISS in orbit);

- Russian Service Module (SM);
- Node 1 (with mating adapters for connection to FGB and for connection of other modules);
- US HAB module (pointing down with the docking port in the R-bar direction);
- US LAB module (in a longitudinal direction);
- Node 2 (pointing with the docking port in V-bar direction);
- Japanese Experiment Module (JEM) (on right side, when looking in flight direction);
- European Laboratory (on left side, when looking in flight direction);
- Centrifuge Module (pointing up);
- Italian Mini Pressurised Module (MPLM) pointing down (this module is not permanently attached, but is transported up and down by the Shuttle);
- Russian Science Power Platform (SPP) (attached to the inter-connecting element of the Service Module);
- second FGB with interconnecting element (attached to the interconnecting element of the Service Module);
- several Russian Research-, Docking- and Storage Modules attached at various places on the Russian side of the ISS.

The dimensions, mass and inertia of the ISS depend on the assembly status and on the number and type of servicing vehicles/modules attached to it. The values given in table C.1 refer to the 'assembly-complete' status, without other vehicles attached. They are estimates, based on the design status before the year 2001.

Orbit parameters

- altitude: 350–460 km;
- inclination: 51.6 deg.

Location and type of docking/berthing ports

The ISS has several ports facilitating the attachment of vehicles and modules. The main type of mating is docking, but due to its manipulator system the ISS has also the capability to attach vehicles or modules by berthing. Berthing techniques will be used, e.g., for the mating of the HTV and for unloading of the payload from the cargo bay of the Space Shuttle Orbiter. The following ports are available:

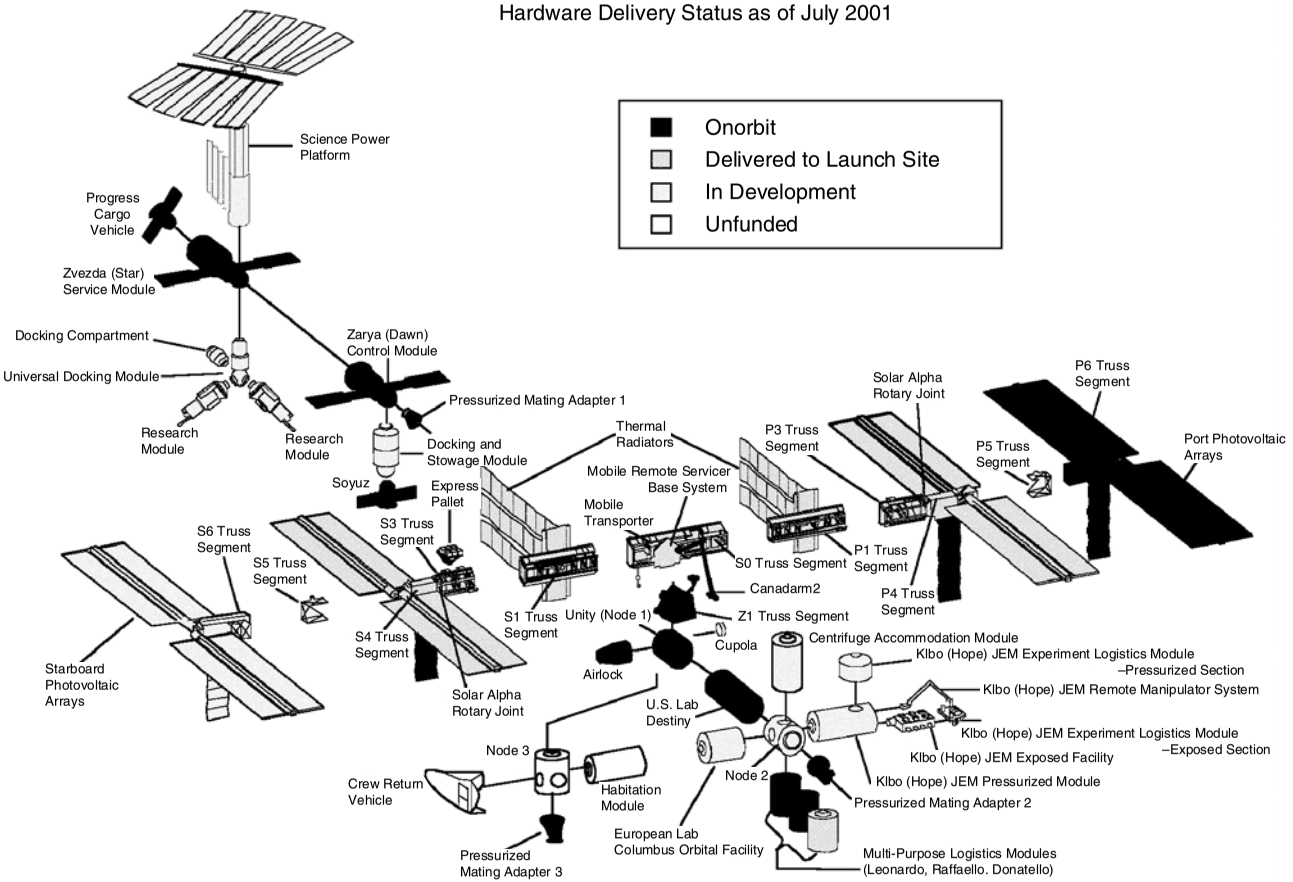

Figure C.2. Modules of the International Space Station, ISS (courtesy NASA).

(1) +V-bar port for docking of the Space Shuttle Orbiter in front of Node 1, APDS-type docking mechanism (see figure 8.10);

(2) R-bar port for docking of the Space Shuttle Orbiter below the US HAB Module, APDS-type docking mechanism (see figure 8.10);

(3) R-bar berthing port for MPLM and HTV at the nadir pointing side of Node 1, CBM type of berthing mechanism (see figure 8.13);

(4) −V-bar docking port for Soyuz, Progress and ATV vehicles aft of the Service Module, probe/drogue type docking mechanism (see figure 8.8);

(5) R-bar docking port for Soyuz and Progress vehicles on the nadir pointing side of the second FGB, probe/drogue type docking mechanism (see figure 8.8);

(6) R-bar docking port for Soyuz and Progress vehicles on the nadir pointing side of the Docking and Storage Module, probe/drogue type docking mechanism (see figure 8.8).

The main ports for visiting vehicles are the +V-bar and −V-bar docking ports at the forward and aft ends of the Station and the R-bar berthing port on Node 1.

Visiting vehicles

It is planned that the ISS will be serviced by the following vehicles:

- the US Space Shuttle (crew and cargo);
- the Russian Soyuz (crew);
- the Russian Progress (cargo, refuelling and re-boost);
- the European ATV (cargo and re-boost);
- the Japanese HTV (cargo).

Additionally there may be a re-boost module delivered by the Space Shuttle for orbit maintenance of the Station.

Rendezvous sensor systems used

The interfaces of the rendezvous sensors of the visiting vehicles and the corresponding functions on the target station are not standardised on the ISS, but are specific to each of the visiting vehicles. For vehicles using optical rendezvous sensors, their according interfaces formed by reflector arrangements are accommodated near to the docking port or berthing box specific for this vehicle. The equipment on the Space Station (transponder) for the Russian Kurs system has been described in section 7.2.5. For RGPS, raw data will be used from one of the GPS receivers on the Station. The sensor systems used are identified below in the sections on the visiting vehicles.

Table C.1. Dimensions, mass and moments of inertia of ISS.

Dimensions	$x = 67.5$ m $y = 108.48$ m $z = 44.98$ m rotational envelope of solar arrays $d = 72.93$ m
Mass	$m = 470\,000$ kg, depending on payload
Principal moments of inertia	$I_{xx} \approx 128\,000\,000$ kg m^2 $I_{yy} \approx 107\,000\,000$ kg m^2 $I_{zz} \approx 201\,000\,000$ kg m^2

Actuators

Rotating actuators Four control moment gyroscopes (CMGs) with a two DOF gimbal system, providing a maximum torque of about 250 N m. The CMGs are mounted on the truss. Attitude control will be performed mainly by control moment gyros.

Thrusters RCS thrust engines will be used, mainly for CMG de-saturation, but also for slew manoeuvres and for control of position. For pitch and yaw control the thrust engines of the Service Module will be used, if no visiting supply vehicle (Progress, ATV) is attached to its docking port. It is a requirement of the ISS that visiting vehicles docked to the Service Module will provide thrust support for attitude control. For roll control, to provide sufficient lever arm, thrusters attached to the Science Power Platform (SPP) were planned. In the case of a configuration of the Station without the SPP, the thrusters of a vehicle (e.g. Soyuz or Progress), attached to the inter-connecting element of the second FGB, could be used.

Re-boost manoeuvres for orbit maintenance will be performed mainly by visiting vehicles, i.e. Progress and ATV, and possibly by the above-mentioned re-boost module. If no visiting vehicle is attached, the main thrusters of the Service Module can be used for re-boost of the Station.

The thrust levels (of thrusters on the Service Module) are as follows:

- 32 bi-propellant attitude control thrusters, thrust level: 130 N;
- two re-boost thrusters, thrust level: 3070 N;

The locations of the thrusters on the Service Module are as follows:

- attitude control thrusters: in four groups on the cylindrical surface at the aft of the SM;

- re-boost thrusters on the aft plane of the SM.

The thrusters of the visiting vehicles used for attitude control and re-boost are addressed in the respective sections below.

C.2 Russian Space Station 'Mir'

The Russian space station Mir played a significant role in the preparation phase of the International Space Station Programme. A large number of international crew members obtained operational experience aboard the Mir station. The US Space Shuttle visited Mir ten times within the context of this preparation programme. During the first visit the Shuttle performed rendezvous only down to a distance of 12.2 m without docking. Mir is described here as a second reference example of a target station in the rendezvous process because it has been involved in the largest number of rendezvous and docking operations of all spacecraft so far, and will be used as reference in many years to come. Mir was de-orbited on 23 March 2001.

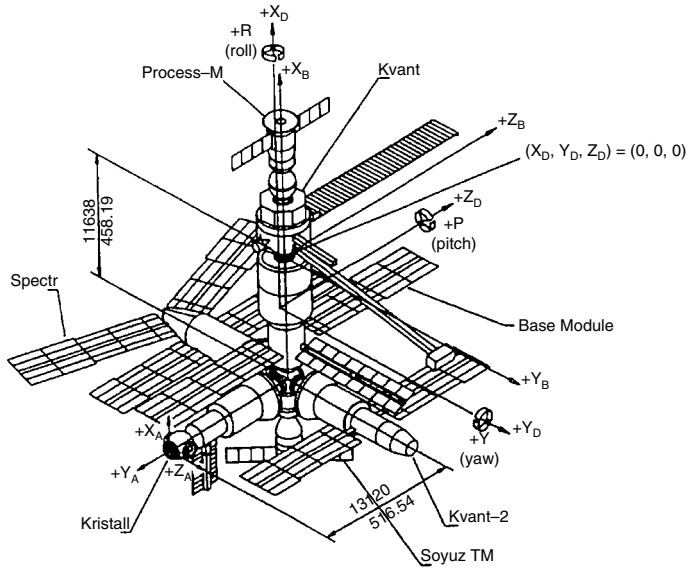

Figure C.3. Russian space station Mir (courtesy RSC Energia).

Design features

The first module of Mir, the Base Block, was launched in 1986. The Base Block had an aft docking port and an inter-connecting element with five ports at its forward end. The size of the station was increased and its configuration was modified by adding further modules:

- the Kvant Module in 1987;
- the Kvant-2 Module in 1989;
- the Kristall Module in 1990;
- the Spektr Module in 1995;
- the Docking Module for Space Shuttle dockings in 1995;
- the last addition, the Priroda Module in 1996.

The first Kvant was attached to the aft port of the Base Block; the other modules, except for the Docking Module, were attached to the inter-connecting element of the Base Block. The Docking Module was attached to the Kristall Module. A manipulator arm was available to re-configure the station by moving a module to a different port. The mating process used for all vehicles with Mir was docking.

The dimensions, mass and moments of inertia of Mir were dependent on the configuration and were therefore increasing with the attachment of each new module. Typical values for the configuration prior to attachment of the Priroda Module are shown in table C.2.

Table C.2. Dimensions, mass and moments of inertia of Mir.

Dimensions	$x = 33.14$ m (Base Block and Kvant plus one Soyuz and one Progress vehicle attached) $y = 27.35$ m (body length of Kvant 2 + inter-connecting element + Spektr) $z = 29.67$ m (span of solar arrays of Base Block)
Mass	$m = 111\,600$ kg
Principal moments of inertia	$I_{xx} \approx 3\,600\,000$ kg m^2 $I_{yy} \approx 7\,000\,000$ kg m^2 $I_{zz} \approx 8\,100\,000$ kg m^2

Module properties

- Base Block: mass 20.4 ton, length 13.13 m, max. diameter 4.15 m;
- Kvant: mass 11.5 ton, length 5.8 m, max. diameter 4.15 m;
- Kvant-2: mass 19.6 ton, length 13.73 m, diameter 4.35 m;

- Kristall: mass 19.64 ton, length 13.73 m, diameter 4.35 m (including inter-connecting element with two APAS docking ports);
- Spektr: mass 19.5 ton, length 12 m, diameter 4.4 m;
- Priroda: mass 19 ton, length 13 m, diameter 4.3 m.

The configuration shown in figure C.3 is the one prior to arrival of the Spektr Module in 1995.

Orbit parameters

- altitude: 330–390 km;
- inclination: 51.6 deg.

Location and type of docking ports

- Two probe/drogue type docking mechanisms (see figure 8.8) along the x-axis of the complex, on the aft of the Kvant module and on the opposite side on the inter-connecting element of the base block.
- Two APDS-type docking mechanisms (see figure 8.10) on the inter-connecting element of the Kristall module and on the docking module for the Space Shuttle, which was attached to one of the APDS ports of Kristall in 1995.

Visiting vehicles

Mir was serviced/visited by

- the Russian Soyuz (crew);
- the Russian Progress (cargo, re-fuelling and re-boost);
- the US Space Shuttle (crew and cargo).

Rendezvous sensor systems

In the first years of the Mir station the older IGLA system (also an RF-sensor system) was used. The Kurs system was installed in 1989 (see section 7.2.5).

Actuators

Rotating actuators

- Up to 12 control moment gyros (called ‘gyrodynes’), located in the various modules.

Thrusters The thrust levels were:

- Base Block, Kvant, Progress: 135 N;
- Kvant2, Spektr: 390 N.

The thruster locations were as follows:

- Each of the Mir modules had its own set of thrusters. Additionally the thrusters of the attached Progress vehicle were used for attitude and trajectory control and for orbit maintenance.

C.3 Space Shuttle Orbiter

Mission objectives

The US Space Shuttle is the largest transport vehicle in the ISS scenario. It can transport up to seven crew and of the order of 15 000 kg of payload to the ISS orbit (depending on station altitude and payload geometry). With its 60 ft long and 15 ft diameter payload bay (the space necessary for the docking mechanism and its substructure has to deducted), the Space Shuttle is capable of transporting the largest Modules to the ISS.

Design features

Body features of the Space Shuttle Orbiter in terms of dimensions, mass and moments of inertia are indicated in table C.3.

Table C.3. Dimensions, mass and moments of inertia of the Shuttle Orbiter.

Dimensions	$x = 37.24$ m (12.17 ft)
	$y = 23.79$ m (78.06 ft)
	$z = 17.25$ m (56.58 ft)
Mass[a]	$m = 90\,700$–$104\,330$ kg (200 000–230 000 lb)
Principal moments	$I_{xx} \approx 1\,310\,000$ kg m^2
of inertia[b]	$I_{yy} \approx 10\,220\,000$ kg m^2
	$I_{zz} \approx 10\,650\,000$ kg m^2

[a] At landing, depending on mission. The rendezvous mass will be nearer to the larger value.
[b] Typical values, depending on mission and payload.

Launcher

The Space Shuttle is an integrated launch system using solid fuel strap-on engines plus an external liquid fuel tank and the main engines of the Orbiter for the launch boost.

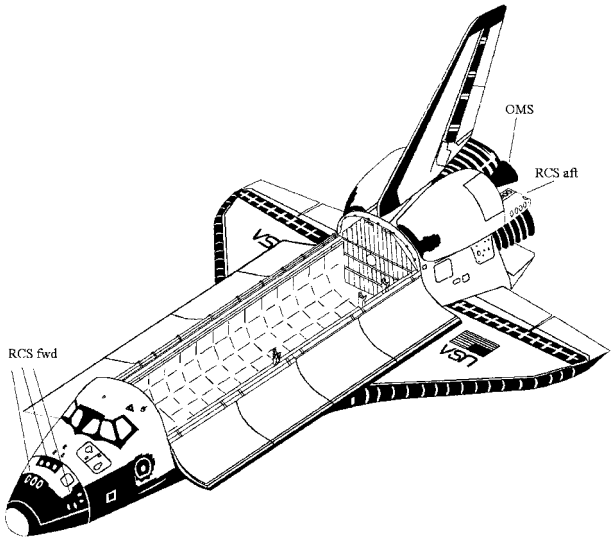

Figure C.4. Space Shuttle Orbiter (courtesy NASA).

Mating system

This is an APDS-type docking mechanism (see figure 8.10) .

The docking system is mounted on a bridge on the forward end of the cargo bay. The Orbiter attaches itself to the Station by docking. The nominal contact velocity is <0.05 m/s. The payload is transferred and attached to the Station by a manipulator in a berthing type of process.

Rendezvous sensor systems

These comprice star tracker, rendezvous radar, Crew Alignment Sight (COAS) and Trajectory Control Sensor (TCS) (see section B.1 and figure B.2).

Thrusters

(a) Orbital Maneuvering system (OMS): two bi-propellant rocket engines for major orbit changes.

(b) Reaction control system (RCS): 44 bi-propellant engines for attitude- and trajectory control.

Thrust level

(a) Orbital manoeuvring system (OMS): 26 700 N (6000 lb) each.

(b) Reaction control system (RCS): 3871 N (870 lb) primary engines; 107 N (24 lb) vernier engines.

Location

(a) Orbital manoeuvring system (OMS): on both sides at the base of the vertical tail.

(b) Reaction control system (RCS):

- two aft RCS groups, one at each side of the aft fuselage pod near the OMS engines: there are 12 primary and two vernier engines in each group;
- forward RCS group: 14 primary and two vernier on both sides and on top of the Orbiter nose.

C.4 Soyuz

The Russian Soyuz vehicle has a long design heritage: the original concept dates from 1963, the first flight of an unmanned Soyuz vehicle took place in 1966, and the first manned mission was in 1967. The design of the vehicle has been improved over the years and has been adapted according to the needs of the particular mission scenario, i.e. the various Salyut space stations, the Apollo–Soyuz Test Program (ASTP), Mir and eventually the ISS. The data given below are valid for the Soyuz–TM configuration, which has been in use since the emergence of the Mir Station.

Detailed information on the design and history of Soyuz can be obtained from NASA web sites and from Portree (1995).

Design features

The vehicle is composed of three modules: the Orbital Module, the Descent Module and the Service Module. The first carries the crew to the target station and has a docking mechanism located at its front end. The second is the re-entry vehicle for return to ground. The last third of the Soyuz vehicle is formed by the so-called Instrument Service Module, which contains all functions necessary for the operation of the spacecraft, i.e. propulsion, avionics, communications, power and thermal control functions. The physical properties of Soyuz in terms of dimensions, mass and moments of inertia are shown in table C.4.

Table C.4. Dimensions, mass and moments of inertia of Soyuz-TM.

Dimensions	length = 7.5 m
	diameter = 2.7 m (without appendages)
	solar arrays: span 10.6 m, area 10 m^2
Mass	$m \approx 6850$ kg at mating
	CoM location ≈ 3.8 m from docking plane
Principal moments of inertia[a]	$I_{xx} \approx 5300$ kg m^2
	$I_{yy} \approx 33000$ kg m^2
	$I_{zz} \approx 33000$ kg m^2

[a] Depending on payload.

Mission objectives

- Transfer of up to three crew to and from the target space station.
- Transfer of a small amount of payload to the target station (200–250 kg) and back to ground (70–90 kg).

Launcher

The Soyuz spacecraft is launched by the Russian Soyuz launcher.

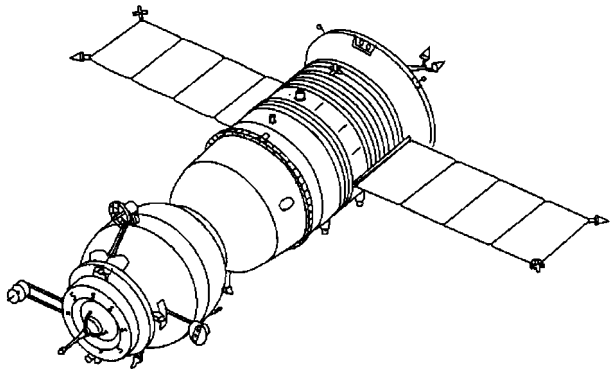

Figure C.5. Soyuz crew transport vehicle (development RSC Energia).

Mating system

A probe/drogue type docking mechanism (see figure 8.8) is mounted on the forward end of the vehicle. The acceptable range of contact velocities is 0.1–0.35 m/s.

Rendezvous sensor system

The Kurs sensor system (see section 7.2.5) is used.

Thrusters

Thrust level

- 1×3000 N main engine;
- 14×130 N translation control;
- 12×26 N attitude control;

Location The main engine is located in the centre of the aft plane, the force is in the $+x$-direction. The trajectory and attitude control engines are located at the rim of the aft plane and on a ring at the interface between the Service Module and the Descent Module.

C.5 Progress

The Russian Progress vehicle has been developed as an unmanned cargo carrying version of Soyuz, and its first flight took place in 1975. Progress was built primarily for the re-supply of the Salyut stations. Its design has continually been updated, according to the needs of the various mission scenarios. The data given below are valid for the Progress-M configuration in use since its first launch in 1989.

Design features

The vehicle is composed, similar to the design of Soyuz, of three modules: the Cargo Module, the Re-fuelling Module and the Service Module. The first carries the pressurised cargo to the target station and has a docking mechanism located at its front end. The second contains propellant tanks for re-fuelling and re-boosting of the station. The third module is, as in the case of the Soyuz vehicle, the so-called Instrument Service Module. It contains all the functions necessary for the operation of the spacecraft, i.e. propulsion, avionics, communications, power and thermal control functions. The body features of Progress in terms of dimensions, mass and moments of inertia are indicated in table C.5.

Table C.5. Dimensions, mass and moments of inertia of Progress.

Dimensions	length = 7.23 m diameter = 2.72 m (without appendages) solar arrays: span 10.6 m, area 10 m^2
Mass	$m \approx 7130$ kg (at launch)
Principal moments of inertia[a]	$I_{xx} \approx 5100$ kg m^2 $I_{yy} \approx 31000$ kg m^2 $I_{zz} \approx 31000$ kg m^2

[a] Depending on payload.

Mission objectives

- Transfer of a maximum of 2600 kg of combined dry, liquid and gaseous cargo to the target space station for logistics re-supply and experiments.
- Transfer of approximately the same amount of waste at re-entry back into the atmosphere for burning up.
- Orbit maintenance of the target station using the main engine.

Launcher

The Progress spacecraft is launched by the Russian Soyuz launcher.

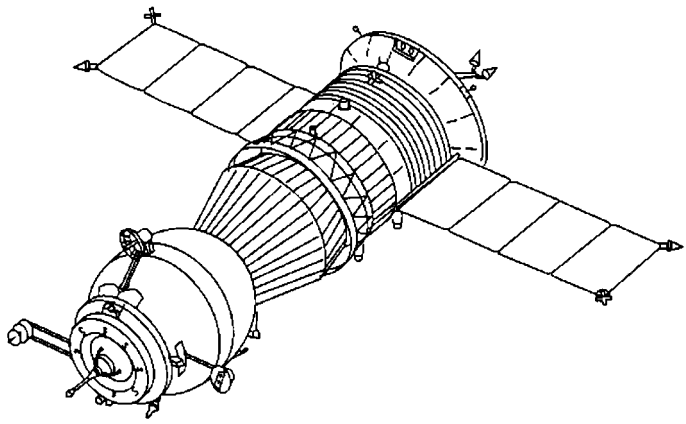

Figure C.6. Progress cargo transport vehicle (development RSC Energia).

Mating system

A probe/drogue type docking mechanism (see figure 8.8) is mounted on the forward end of the vehicle. The acceptable range of contact velocities is 0.1–0.35 m/s.

Rendezvous sensor system

The Kurs sensor system (see section 7.2.5) is used.

Thrusters

Thrust level

- 1×3000 N main engine;
- 28×130 N translation and attitude control.

Location The main engine is located in the centre of the aft plane, the force is in the $+x$-direction. The trajectory and attitude control engines are located at the outer diameter of the aft plane and on a ring at the interface between the Service Module and the Descent Module.

C.6 ATV

Design features

The European ATV is developed specifically for the ISS scenario. The vehicle consists of two modules: a Spacecraft Function Module and a Payload Carrier. The vehicle has a payload carrying capability into the ISS orbit of up to 6900 kg including propellant for re-boost of the Station. The dimensions, ranges of mass and moments of inertia of the ATV are indicated in table C.6.

Mission objectives

- To transport to the ISS dry pressurised cargo for crew supply, experiments and logistics.
- To transport to the ISS water and gases.
- To re-fuel the ISS with fuel and oxidiser.
- To provide propellant for re-boost of the Station to a higher orbit.
- To remove waste for burning up at re-entry.

Table C.6. Dimensions, mass and moments of inertia of the ATV.

Dimensions	length = 9.03 m diameter = 4.48 m (without appendages) solar arrays: span 22.28 m, area 4×8.4 m^2
Mass[ab]	$m \approx 13\,000$–$19\,600$ kg at docking
Principal moments of inertia[a]	$I_{xx} \approx 41\,000$–$59\,000$ kg m^2 $I_{yy} \approx 82\,000$–$138\,000$ kg m^2 $I_{zz} \approx 82\,000$–$138\,000$ kg m^2

[a] Values at docking depend on the payload.
[b] COM location: 2.5–4.25 m from origin of reference system at Ariane interface plane

Launcher

The ATV is launched by the European Ariane V launcher.

Mating system

A Russian probe/drogue type docking mechanism (see figure 8.8). is used. The ATV will dock to the −V-bar port on the Service Module of the ISS. The nominal contact velocity is 0.05–0.10 m/s.

Rendezvous sensors

- >30 km: absolute GPS;
- 30 km–500 m: RGPS (see section 7.3.3);
- <500 m: scanning laser range finder type of optical sensor (see section 7.4.1);
- <20 m: camera type of optical sensor (see section 7.4.2).

Thrusters

There are four main engines and 28 RCS engines.

Thrust level

- Main engines 490 N;
- RCS thrusters 220 N.

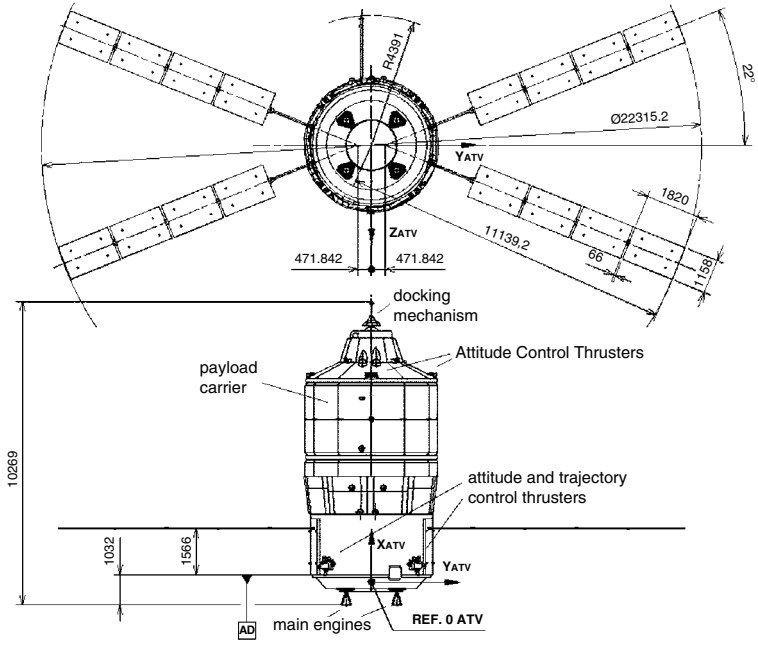

Figure C.7. Automated Transfer Vehicle ATV (courtesy ESA).

Location

- The main engines are at the aft plane of the ATV.
- The RCS engines in four groups of five thrusters each on the Propulsion Module at the aft of the vehicle and four groups of two thrusters each at the forward end of the cylindrical part of the payload carrier.

C.7 HTV

Design features

The Japanese HTV is also specifically developed for the ISS scenario. The spacecraft consists of three modules: a Propulsion Module, an Avionics Module and a Logistics Carrier (see figure C.8). The Logistics Carrier comes in two versions: a pressurised carrier and a mixed carrier with a section for pressurised cargo and an unpressurised section. Figure C.8 shows the mixed carrier version. The payload carrying capability to the ISS orbit is 6000 kg for the mixed version and 7000 kg for the pressurised version. The HTV has solar panels surrounding its body. It receives its power supply from both solar panels and batteries. Typical values for the body features of the HTV in terms of dimensions, mass and moments of inertia are indicated in table C.7.

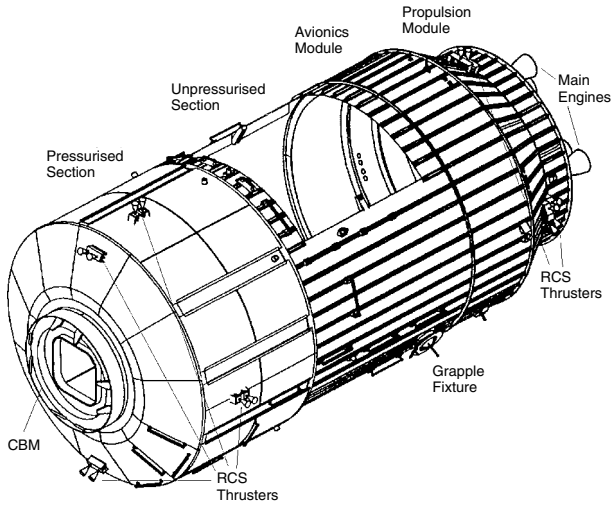

Figure C.8. H-II Transfer Vehicle, HTV (courtesy NASDA).

Mission objectives

- The transportation of experiments and re-supply cargo to the pressurised modules of the ISS.
- The transportation of experiments and equipment for outside accommodation on the ISS (e.g. on ISS Truss, or the platform of the JEM).
- The removal of waste for burning up at re-entry.

Launcher

The HTV is launched by the Japanese H-IIA launcher.

Mating system

- Capture: grapple fixture for manipulator end effector (see figure 8.28). The HTV is captured by the Remote Manipulator System of the ISS in a berthing box below the Japanese Experiment Module. The nominal relative velocity at capture is zero.
- Attachment: CBM type of berthing mechanism (see figure 8.13). The HTV is berthed to the nadir port of Node 2.

Rendezvous sensors

- $>$23 km: absolute GPS;

Table C.7. Dimensions, mass and moments of inertia of the HTV.

Dimensions	length = 7.4 m (pressurised logistics carrier), length = 9.2 m (mixed logistics carrier) diameter = 4.4 m
Mass[a]	$m \approx 15$ ton (launch mass)
Principal moments of inertia[a]	$I_{xx} \approx 41200$ kg m^2 $I_{yy} \approx 128500$ kg m^2 $I_{zz} \approx 128500$ kg m^2

[a] Values depend on the payload.

- 23 km–500 m: RGPS (see section 7.3.3);
- <500 m: optical laser range finder type rendezvous sensor (see section 7.4.1).

Thrusters

There are four Main engines and 28 RCS thrusters.

Thrust level

- 500 N main engine;
- 120 N RCS thruster.

Location

- The main engines are at the aft plane of the HTV.
- The RCS engines are in four groups of four around the Propulsion Module, in four groups of two around the forward part of the Payload Carrier, and in two groups of two on the front side of the vehicle.

Glossary

Abbreviations and acronyms

AE Approach Ellipsoid (ISS traffic control and safety zone).

ATV Automated Transfer Vehicle: cargo transport vehicle, to be launched by the European launcher Ariane V and docking to the ISS, European contribution, for servicing the ISS.

CAM collision avoidance manoeuvre: fixed boost manoeuvre moving the chaser for all approach conditions safely out of the vicinity of the target. To be initiated in case of danger of collision.

CC control centre.

CCD charge coupled device.

CCSDS Consultative Committee for Space Data Systems.

CoM centre of mass.

CRV Crew Return Vehicle.

CTRL control function.

CW Clohessy–Wiltshire.

DCM direction cosine matrix.

DGPS Differential Global Positioning System.

DOF degrees of freedom.

DRS data relay satellite.

EPOS European Proximity Operations Simulator: stimulation facility for optical rendezvous sensors.

ESA European Space Agency.

ESTEC European Space Research and Technology Centre (ESA establishment).

ETS-VII Engineering Test Satellite no. 7: developed and launched 1997 by Japan. Performed a rendezvous and docking demonstration with a sub-satellite.

EURECA European Retrievable Carrier: spacecraft developed by ESA, brought into orbit in 1992 and retrieved from orbit in 1993 by the US Space Shuttle. EURECA was developed for multiple use, but has been flown only once.

EVA extra-vehicular activity.

FDIR failure detection, isolation and recovery.

FDI failure detection and isolation.

FOV field of view: extension of measurement range in directions normal to the line of sight.

GDOP geometric dilution of precision: quality criterion for the geometrical constellation of four navigation satellites selected for measurement.

GEO geostationary orbit.

GLONASS Global Orbiting Navigation Satellite System.

GNC guidance, navigation and control: automatic process of determining the present and implementing the desired position, attitude and rates.

GPS global positioning system: satellite navigation system based on orbit and time information broadcast by Navstar satellites.

GUI guidance function.

Hermes Project for a European spaceplane to carry crew and cargo to and from the Columbus Man-Tended Free-Flyer. Abandoned in 1993.

HTV H-II Transfer Vehicle: cargo transport vehicle, to be launched by the Japanese launcher H-II and to be berthed to the ISS by the ISS manipulator arm; Japanese contribution for servicing the ISS.

H/W hardware.

ISS International Space Station: permanent orbital station with components provided by the USA, Russia, Europe, Japan and Canada. First module launched November 1998, 'assembly complete' configuration planned for 2004.

IVA intra-vehicular activity.

KOZ Keep Out Zone (ISS traffic and safety control zone).

Kurs Russian navigation system for rendezvous and proximity operations.

LEO low Earth orbit.

LOS line of sight.

LVLH local vertical/local horizontal.

MIB minimum impulse bit.

MIMO multiple-input–mutiple-output.

MMI man–machine interface.

Mir Russian (Soviet) permanent orbital station: first modules launched in 1986, decay and burn-up in the atmosphere in 2001.

MTFF Man-Tended Free-Flyer: European project for a man-visited space station abandoned in 1992, also known under the name Columbus Free-Flyer.

MVM mission and vehicle management.

NASA National Aeronautics and Space Administration (USA).

NASDA National Space Development Agency (Japan).

NAV navigation function.

Progress Russian cargo transport vehicle, launched by the Russian Soyuz launcher and docking to the Mir Space Station. Also used for servicing the ISS.

PRN pseudo-random number.

RA relative attitude.

RAAN right ascension of ascending node: angle measured in the equatorial plane from the line of the vernal equinox to the line of the ascending node of the orbit.

RF radio-frequency.

RGPS Relative Global Positioning System using the differences of GPS raw data measured on chaser and target to obtain relative position with improved accuracy.

RSC Energia Rocket Space Corporation 'Energia': Russian space company, responsible for the development of the Mir Space Station, of the Russian part of the ISS and of the Soyuz and Progress vehicles.

RV rendezvous.

RVD rendezvous and docking: process of approach and attachment of a chaser vehicle to a target vehicle.

RVD/B rendezvous and docking or berthing: general term to cover the approach and both types of mating processes, i.e. docking and berthing.

RVS rendezvous sensor.

SA selective availability: process of degradation of GPS data for non-military use.

S/C spacecraft.

S/W software.

SISO single-input – single-output.

Soyuz Russian crew transport vehicle launched by the Soyuz launcher and used to transport crew to and from the Mir Space Station. Also planned for crew transport to and from the ISS.

SPAS Shuttle Pallet Satellite: family of spacecraft developed by MBB (DASA) and brought into and retrieved from orbit several times by the US Space Shuttle.

TBD to be determined.

TC telecommand: command sent from a remote control station via radio link to the spacecraft.

TDRSS Tracking and Data Relay Satellite System.

TEA torque equilibrium attitude.

TM telemetry: data sent by the spacecraft via radio link to a remote control station.

w.r.t. with respect to.

Terminology

apogee highest point of an orbit around the Earth.

approach corridor safe corridor in the vicinity of a target vehicle, which the approaching vehicle must not exceed.

ballistic coefficient ratio of mass to drag coefficient, indicating the sensitivity of a vehicle to the effects of the residual atmosphere.

berthing attachment in space of one vehicle or module to another one, effected by a manipulator arm. The berthing process includes the capture of one vehicle by the manipulator of the other one, the transfer from the capture position to the berthing port, the insertion into the berthing mechanism interfaces and the structural connection.

berthing box virtual volume in space, in which the capture of the according interfaces (*see* grapple fixture) on one vehicle by the manipulator on the other vehicle takes place. The manipulator transfers the captured vehicle from the berthing box to the berthing port (berthing mechanism interface).

berthing mechanism mechanism providing mechanical guidance, structural interface and latching functions for the attachment of one vehicle or module to another by aid of a manipulator arm.

capture first connection of two bodies, preventing subsequent escape.

capture range range of approach velocities, lateral and angular misalignment and rates for which capture is assured by the mechanism.

chaser active vehicle in the rendezvous process, approaching the target vehicle.

close range rendezvous part of the rendezvous process, which includes the transfer to and acquisition of the docking axis, or to the berthing box approach line, and the final transfer to the docking port or berthing box.

closing possible trajectory elements within the close range rendezvous to reduce the distance to the target.

control process deriving and producing the actuation commands, which shall change the actual state of a vehicle to comply with the required nominal one.

de-berthing process of disengagement of the physical interfaces between two berthed vehicles, i.e. the release of utility connections, structural and capture latches, and the removal by a manipulator arm from the berthing location to a departure location.

delta-V (ΔV) velocity increment added to the present state of a vehicle in orbit in order to change the trajectory.

departure manoeuvre(s), moving the departing vehicle (chaser) out of the vicinity of the staying vehicle (target station).

departure corridor safe corridor in the vicinity of a target vehicle, which the departing vehicle must not exceed.

docking attachment in space of one vehicle to another, effected by one vehicle's reaction control system, guided and controlled by the onboard GNC system or remotely by human operators.

docking mechanism mechanism providing mechanical guidance, capture, attenuation of impact energy, structural interface and latching functions for the attachment of one vehicle to another, effected by the reaction control system of one of the vehicles.

docking/berthing mechanism mechanism providing mechanical guidance, capture, attenuation of impact energy, structural interface and latching functions for the attachment of one vehicle or module to another by both methods, i.e. effected either by the reaction control system of one of the vehicles or by a manipulator arm.

far range rendezvous part of the rendezvous process which brings the approaching vehicle from the end point of phasing (first aim point) to a point much closer to the target, from where the close range rendezvous process with a fixed sequence of manoeuvres can commence. The major function of the far range rendezvous is to reduce the position and velocity dispersions commensurate with the decrease of distance to the target.

final approach final translation on the docking axis or approach line to docking port or berthing box.

first aim point end point of phasing, usually acquired by an open loop manoeuvre. The first aim point is, in most rendezvous strategies, located a few kilometres below and a few tens of kilometres behind the target.

grapple fixture mechanical interface for capture by the end effector of a manipulator arm for berthing (note: the grapple fixture is not part of the berthing mechanism).

guidance process defining the nominal state of a vehicle over time, i.e. the present and future nominal positions, velocities, attitude angles and angular rates to be assumed by a vehicle.

H-bar coordinate in the direction of the angular momentum vector of the orbit.

Hohmann transfer transfer from a lower to a higher circular orbit or vice versa by two tangential boosts, separated by half an orbital revolution.

hold point point where the velocities w.r.t. the target are nominally zero. For a longer duration and without excessive propellant consumption, such a point needs to be located on the target orbit.

J_2-effect effect of the oblateness of the Earth on the orbital evolution.

mating general term describing the process of attachment of one vehicle or module to another, whether performed by docking or by berthing.

navigation process determining the actual state vector of a vehicle by measurements and the expected future state by propagation of the actual state.

node intersection of an orbit with the equatorial plane. The ascending node is the one where a satellite crosses the equator in the northern direction.

perigee lowest point of an orbit around the Earth.

phasing first part of the rendezvous strategy after launch, in which the chaser reduces the phase angle to the target (catches up) and arrives at an orbital altitude close to it.

plume volume of exhaust gases of a thruster in action.

port location on a vehicle providing mechanical, sensor and utility interfaces for connection of another vehicle or module.

qualification the sum of all verification and validation efforts in terms of analysis, simulation, physical testing and comparison with already flown or qualified designs, to ensure flight worthiness of an item or system.

R-bar coordinate in the direction of the radius vector toward the centre of the Earth.

reception range range of approach velocities, lateral and angular misalignment and rates for which the mechanical guidance and capture functions of the mechanism are designed (*see* capture range).

rendezvous general term describing the process of bringing one spacecraft into the close vicinity of another spacecraft or a celestial body.

RV-control system the hardware and software items forming the onboard system responsible for the implementation of the automatic rendezvous approach up to mating.

separation process of achieving a physical distance between two vehicles or modules after undocking or de-berthing.

state vector set of values describing the kinematic condition of a body w.r.t. a particular coordinate system. The state vector typically contains the values for position and attitude and for translational and rotational velocities.

target passive vehicle in the rendezvous process: it does not perform position changing manoeuvres to facilitate the rendezvous.

trajectory gate the margins in position and velocities at a particular point of the trajectory, e.g. at a particular distance from the target. A trajectory gate can be used, e.g., as a criterion for success probability of the further approach evolution up to mating.

undocking process of disengagement of the physical interfaces between two docked vehicles, i.e. the release of utility connections, structural and capture latches.

V-bar coordinate in direction of the orbital velocity vector (circular orbits).

References

Ackroyd, N. & Lorimer, R. (1990). *Global Navigation – A GPS Users Guide*. Lloyd of London Press, London.

AIAA (1993). 'Guide for servicable spacecraft grasping/berthing/docking interfaces', Technical Report AIAA G-056-1992.

Anand, D. K. (1984). *Introduction to Control Systems*. Pergamon Press,

Arguello, L. & Miro, J. (2000). Distributed interactive simulation for space projects. *ESA Bulletin*, **102**.

ARINC (1999). 'Navstar GPS space segment/navigation user interfaces, Rev. C', Technical Report ICD-GPS-200C.

Bielski, P. (1998). 'Determination of berthing volumes for ISS visiting vehicles', Technical note prepared for NASA JSC, preliminary issue, unpublished.

Bloom, K. & Campbell, G. (1970), 'The Apollo docking system', *Proceedings of the Fifth Aerospace Mechanisms Symposium*, p. 3–8.

Bomer, T. & Tulet, M. (1990). 'CCD rendezvous sensor proposed for Hermes spaceplane and Columbus MTFF providing nominal performances with the Sun in its field of view'. *Signal and Image Processing System Performance Evaluation*, *SPIE*, **1310**, pp. 207–214.

Brondino, G., Marshal, P., Grimbert, D. & Noirault, P. (1990), 'A dynamic motion simulator for future European docking systems', 24th Aerospace Mechanism Symposium, Kennedy Space Center, Florida, NASA Conference Publication 3062, pp. 75–88.

Brown, R. & Hwang, Y. (1992). *Introduction to Random Signals and Applied Kalman Filtering*. Wiley and Sons, New York.

Carrou, J.-P., editor (1995). *Spaceflight Dynamics*. Cepadues-Editions, Toulouse.

Carter, T.E. (1998), 'State transition matrices for terminal rendezvous studies: brief survey and new example', *J. Guidance, Control & Dynamics*, **21,** (1), 148–155.

CCSDS (1987a). 'Telecommand, summary of concept and rationale', Technical Report CCSDS 200.0-G-6.

(1987b). 'Telemetry, summary of concept and rationale', Technical Report CCSDS 100.0-G-1.

(1997). 'Radiofrequency and Modulation Systems, Part 1, Earth Stations', Technical Report 411.0-G-3.

Cislaghi, M., Fehse, W., Paris, D., & Ankersen, F. (1999), The 'ATV Rendezvous Pre-Development Programme (ARP)', *Proceedings of the 22nd AAS Guidance and Control Conference*, Beckenridge, Colorado.

Clohessy, W. & Wiltshire, R. (1960). 'Terminal guidance system for satellite rendezvous'. *Aerospace Sci. J.* **27** (9).

Cornier, D. *et al.* (1999). 'The Automated Transfer Vehicle (ATV) Mission to the International Space Station (ISS)', *Proceedings of the AIAA International Space Station Service Vehicle Conference*, Houston, Texas.

Data Book: Service Module (2000), Technical Report SFOC-FL2212, NASA/United Space Alliance, unpublished.

Data Book: Soyus/Progress (2000), Technical Report SFOC-FL2721, NASA/United Space Alliance, unpublished.

D'Azzo, J. J. (1995), *Linear Control System Analysis and Design*, McGraw-Hill, New York.

Desplats, E. (1988), 'Description of the refined plume impingement model, WP241 of ESA Contract RVD-GSP', Technical Report MATRA S295/NT/39.88, unpublished.

Dye, S. & Baylin, F. (1997), *The GPS Manual*, Baylin Publications, Boulder, CO.

Ehling, E. H. (1967), *Range Instrumentation*, Prentice-Hall, Inc, Englewood Cliffs, NJ.

Fabrega, J., Frezet, M., & Gonnaud, J. (1996), 'ATV GNC during rendezvous', *Proceedings of the Third ESA International Conference on Spacecraft Guidance*, Navigation and Control Systems, ESA SP-381, pp. 85–93.

Fehse, W. & Ortega, G. (1998), 'Operator monitoring and support system for rendezvous and docking', Paper ID: 2a004, *SpaceOps98: Proceedings, Fifth International Symposium on Space Mission Operations and Ground Data Systems*.

Franklin, G. & Emami-Naeini, A. (1990), *Digital Control of Dynamic Systems*, Addison-Wesley Publishing Company, Reading, MA.

Franklin, G., Powell, J., & Workman, M. (1998), *Digital Control of Dynamic Systems,* 3rd edn, Addison-Wesley, Menlo Park, CA.

Franklin, G. *et al*. (1994), *Feedback Control of Dynamic Systems*, Addison-Wesley Publishing Company, Reading, MA.

GMV (1997), 'Use of GPS for rendezvous operations', Technical Report GMVSA 464/97, ESA contract, unpublished.

Gonzales-Vallejo, J., Fehse, W., & Tobias, A. (1992), 'A multipurpose model of Hermes-Columbus Docking Mechanism', *Proceedings of the 26th Aerospace Mechanisms Symposium*.

Gonzales-Vallejo, J., Tobias, A., and Hayden, P. (1993), 'European docking system: 10 years of development, ready for demonstration in orbit', *Third European In-Orbit Operations Technology Symposium*.

Grimbert, D. & Marshal, P. (1987), 'Dynamic testing of a docking system', *First European In-Orbit Operations Technology Symposium*, Darmstatdt, ESA SP-272, pp. 281–288.

Hartl, P. (1977), *Fernwirktechnik in der Raumfahrt*, Springer-Verlag, Berlin.

Hedin, A. (1986), 'MSIS-86 thermospheric model, *J. Geophys. Res.*, **92**, 4649–4662.

Heimbold, G., Prins, J., & Fehse, W. (1987), 'EPOS – European Proximity Operations Simulation', *First In-Orbit Operations Technology Symposium*, ESA SP-272.

Heimbold, G. & Zunker, H. (1996), 'EPOS simulator H/W control. Key element for a safe test bed Operation', *4th Workshop on Simulators for European Space Programmes*, ESA.

Hill, G. (1878), 'Researches in the Lunar Theory', *Am. J. Math.* **1** (1).

Hinkel, H., Park, Y.-W., & Fehse, W. (1995), 'Realtime GPS relative navigation flight experiment', *Procedings of the National Technical ION Meeting*, ION, pp. 593–601.

Hohmann, W. (1925), *Die Erreichbarkeit der Himmelskoerper*, Oldenbourg Verlag, Munich; 3rd edn, 1994.

Howard, R. *et al*. (1997), 'Active sensor system for automatic rendezvous and docking', In *Laser Radar Technology and Applications*, SPIE, pp. 175–184.

Howard, R. *et al*. (1999), 'The video guidance sensor: a flight proven technology, In *Guidance and Control 1999*, vol. 101, AAS, pp. 281–298.

Shin-ichiro Ichikawa S. *et al*. (1993), 'Development of docking systems and its test facilities', *Proceedings of the 3rd European In-Orbit Operations Symposium*.

Illi, E. (1992), 'Space station freedom berthing mechanism', *Proceedings of the 26th Aerospace Mechanism Symposium*.

Inoue, M. (1991), 'Development of a hybrid docking dynamics simulator, *First ESA International Conference on Spacecraft Guidance Navigation and Control System*, Noordwijk, ESA SP-323, pp. 601–606.

Issermann, R. (1981), *Digital Control Systems*, Springer-Verlag, Berlin.

Jacchia, L. G. (1977), 'Thermospheric temperature, density and composition: new models', *Smth. Astrophys. Obs. Spec.*, Rep-375-1977.

Jenkins, H. H. (1991), *Small-Aperture Direction Finding*, Artech House, Norwood, MA.

Kalman, R. (1960), 'A new approach to linear filtering and prediction problems', *J. Basic Eng.*, **82**, 95–108.

Kaplan, E. D. (1996), *Understanding GPS, Principles and Applications*, Artech House, Boston.

Kaplan, M. (1976), *Modern Spacecraft Dynamics and Control*, Wiley and Sons, New York.

Kawano, I. (1997), 'ETS-VII rendezvous docking system and flight demonstration', Viewgraph Presentation by the National Space Development Agency of Japan to the ISS Program Team at NASA JSC, unpublished.

Kawano, I., Mokuno, M., Oda, M. & Anegewa, H. (1998), 'First results of autonomous rendezvous docking technology experiments on NASDA's ETS-VII satellite', *49th International Astronautical Congress*, Melbourne.

Kawasaki, O. *et al*. (2000), 'The on-orbit demonstration and operations plan of the H-2 Transfer Vehicle (HTV)', *IAF 51st International Astronautical Congress*, Rio de Janeiro.

Kayton, M. & Fried, W. R. (1997), *Avionics Navigation Systems*, John Wiley & Sons, Inc., New York.

Kendal, B. (1987), *Manual of Avionics, An Introduction to the Electronics of Civil Aviation*, BSP Professional Books, Oxford.

Kolk, K.-H. & Moebius, B. (2000), 'Rendezvous sensor for automatic guidance of transfer vehicles to the International Space Station', *Photonics for Space Environment VII*, SPIE, pp. 290–297.

Labourdette, P. & Martin, T. (1998), 'Operations de rendez-vous Soyouz TM-28/Mir', Technical Report DTS/MPI/MS/MN/98-077, CNES, unpublished.

Larson, W. & Wertz, J., editors (1992), *Space Mission Analysis and Design*, 2nd edn, Microcosm and Kluwer Academic Publishers, Dordrecht.

Lewis, J. & Carroll, M. B. (1999), 'Prototype low impact docking system, *AIAA International Space Station Service Vehicle Conference*.

Lupo, P. (1995), 'Revised berthing box analysis for ATV', Technical Note by NASA JSC addressed to the author, unpublished.

Luther, J. & Meissner, D. (2000), 'Laser range finder of the rendezvous sensor for ATV and HTV', *Photonics for Space Environment VII*, SPIE, pp. 310–321.

MATRA (1993), 'Rendezvous & docking pre-development programme, final report', Book 1, vol. 2, part II, Technical Report, ESA Contract 8369/89/NL, unpublished.

(1994), 'Summary on the LISAR rendezvous sensor', Technical Report 447/JFS/ES/94/333, unpublished.

MATRA-MARCONI (1998a), 'FD2 RGPS post-flight analysis', Technical Report ARPK-RP-SYS-4393-MMT, ESA contract, unpublished.

(1998b), 'FD3 RGPS post-flight analysis', Technical Report ARPK-RP-SYS-4587-MMT, ESA contract, unpublished.

MBB (1988), 'Optische Sensoren fuer Rendezvous und Docking', Technical Report FKZ: 01 QV 8730, unpublished.

Messerschmid, E. & Bertrand, R. (1999), *Space Stations, Systems and Utilization*, Springer-Verlag, Berlin.

Miro, J., Arguello, L., Fehse, W., Vankov, A. & Chliaev, P. (1998), 'HLA based distributed simulation for International Space Station operation', *SpaceOps98, 5th International Symposium on Space Mission Operations and Ground Data Systems*, Tokyo.

Moebius, B., Kolk, K.-H. & Manhart, S. (1997), 'Development and application of a rendezvous and docking sensor "RVS"', *International Conference on Space Optics*, CNES.

Mokuno, M., Kawano, I. & Kasai, T. (1999), 'Experimental results of autonomous rendezvous and docking on Japanese ETS-VII satellite', Guidance and Control 1999, *Proceedings of the Annual AAS Rocky Mountain Guidance and Control Conference*, vol. 101, pp. 221–238.

Morga, W. & Gordon, G. (1989), *Communications Satellite Handbook*, John Wiley & Sons, New York.

NASA (1989), *Rendezvous/Proximity Operations Crew Training Handbook*.

(1992), *Program Requirements Document for the Trajectory Control Sensor, JSC-25175*, NASA JSC, unpublished.

(1994), *International Space Station Concept of Operations and Utilization, SSP 50011, Rev. B*, International Space Station Program, NASA JSC, Houston.

(1996), 'Rendezvous STS-84', Technical Report JSC-48072-84, NASA-JSC, Mission Operations Directorate.

(1997), 'Flight Plan STS-84', Technical Report JSC-48000-84, NASA-JSC, Mission Operations Directorate.

(1998a), 'International Space Station familiarization', Technical Report at td9702A.pdf, http://www.isc.nasa.gov/er/seh/spaceid.htm

(1998b), *System Specification for the International Space Station, SSP 41000*, International Space Station Program, NASA JSC, Houston.

(1999), *On-Orbit Assembly, Modelling, and Mass Properties Data Book*, Technical Report JSC 26557, Rev.J, Vol.1, International Space Station Program, NASA JSC, Houston.

(2001), *A Key to Discovery, The International Space Station Fact Book*, Technical Report, http://www.isc.nasa.gov/er/seh/spaceid.htm

Newton, I. (1713), *Mathematical Principles of Natural Philosophy*.

Noges, E. & Frank, P. (1975), *Pulsfrequenzmodulierte Regelungssysteme*, Oldenbourg Verlag, Munchen.

Ortega, G. (1999), 'Linux for the International Space Station Program', *Linux J*.

Ortega, G. & Alvarez, L. (1998), 'GOAS: a cybertool for spacecraft rendezvous', *IEEE International Conference on Systems, Man and Cybernetics*.

Ortega, G., Mora, E., & Carracossa, C. (1998), 'GPS multipath effects during the shuttle to Mir rendezvous for the STS-84 Flight Atlantis', *ION GPS-98 11th International Technical Meeting of the Satellite Division of the Institute of Navigation*, Nashville, Tenessee.

Pairot, J., Fehse, W. & Getzschmann, A. (1992), 'Development of an autonomous onboard control system for rendezvous and docking', *Automatic Control in Aerospace 1992*, vol. 12, pp. 331–338.

Park, Y., Brazzel, J., Carpenter, R., Hinkel, H. & Newman, J. (1996), 'Flight test results from realtime relative GPS flight experiment on STS-69', *AAS Guidance and Control Conference 1996*, AAS 96–182.

Portree, D. S. (1995), 'Mir Hardware Heritage', Technical Report NASA RP 1357, NASA-JSC.

Press, W. H., Teukolsky, S. A., Vetterling, W. T. & Flannery, B. P. (1992), *Numerical Recipes – The Art of Scientific Comuting*, Cambridge University Press.

RDOTS (1997), 'Rendezvous and docking operations test system', leaflet by the National Space Development Agency of Japan.

Renner, U., Nauck, J. & Balteas, N. (1988), *Satelliten-Technik*, Springer-Verlag, Berlin.

Retali, O. (1990), 'Plume impingement', Technical Report RVDB/DBCA/SYS/MATRA/TN6.1, ESA contract, unpublished.

Roy, A. (1988), *Orbital Motion*, Hilger.

Sarlo, L., Barrera, M. & Ortega, G. (1998), 'On-line simulation systems: support to in-orbit infrastructure operations', *SESP: 5th International Workshop on Simulation for European Space Programmes*.

Sarlo, L., Barrera, M., Ortega, G. & Franco, R. (1999), 'On-line simulation enabling technologies, innovation paradigms and perspectives, IAF-99-T.3.07', IAF-99, Amsterdam.

Pace, S. (1995), *The Global Positioning System: Assessing National Policies*, United States Office of Science and Technology, RAND, Santa Monica, CA.

Semyachkin, V. (2001), 'Modifications of the Kurs system', letter to the author, unpublished.

Sidi, M. (1997), *Spacecraft Dynamics and Control*, Cambridge University Press.

Strietzel, R. (1999), 'A rendezvous and docking sensor with CCD camera', *European Control Conference ECC'99*, Karrlsruhe, pp. 782–788.

Suslennikov, V. (1993), 'Radio system for automatic rendezvous and docking of Soyuz/Progress spacecraft and Mir Station, *Third European In-Orbit Operations Technology Symposium*, number ESA WPP-059. ESTEC, Noordwijk, The Netherlands.

Swan, W. (1976), 'Apollo–Soyuz', *Proceedings of the Tenth Aerospace Mechanism Sysmposium*.

Symon, K. R. (1979), *Mechanics*, Addison-Wesley, Reading, MA.

Syromiatnikov, V. S. (1971), 'Docking devices for the Soyuz-type spacecraft', *Proceedings of the Sixth Aerospace Mechanism Symposium*, pp. 143–150.

(1990), *Spacecraft Docking Devices*, Moscow, Mashinostroenie, 1984 (translation into English: Space Study Institute, Soviet Technical Paper Number SSI VSS-1, Princeton, New Jersey).

Taniguchi, Y. *et al*. (1991), 'The development of rendezvous and docking technology for Japanese future space systems', *42nd Congress of the International Astronautical Federation*, Montreal.

Tobbe, P. & Naumann, C. (1992), 'Automated rendezvous and capture at NASA/MSFC', *AIAA Space Programs and Technologies Conference*.

Tobias, A., Venditti, F. & Cable, N. (1989), 'Docking Berthing Systems', *Proceedings of the 2nd European In-Orbit Operations Symposium*, pp. 259–270.

TsNII-Mash (1992), 'Study on Hermes system aspects', W.P.2 Space Dynamics Engineering, Technical Report 92.390.11, unpublished.

Tsukui, J. *et al*. (1999), 'Rendezvous and docking demonstration by engineering test satellite VII', *AIAA International Space Station Service Vehicles Conference, Houston, Texas*.

Ussher, T. & Doetsch, K. (1983), 'An overview of the Shuttle remote manipulator system', *Space Shuttle Technical Conference*, JSC Houston, Texas, pp. 892–903.

Vankov, A. & Arguello, L. (1998), 'Distributed interactive simulation in support to the ISS', *SESP'98: 5th Workshop on Simulation for European Space Programmes.*

Vankov, A. *et al*. (1996), 'Remote intervention in automatic onboard GNC systems', *Third ESA International Conference on Spacecraft Guidance Navigation and Control'*, ESA/ESTEC, pp. 109–118.

Vreeburg, J. (1999a), 'Acceleration measurement on Sloshsat FLEVO for liquid force and location determination', *4th ESA International Conference on Spacecraft Guidance Navigation and Control Systems*, ESA, pp. 579–585.

(1999b), 'Diagnosis of water motion in the Sloshsat FLEVO tank', *5th International Astronautical Congress*, Amsterdam, IAF.

Wertz, J. & Larson, W., eds. (1991), *Space Mission Analysis and Design*, Microcosm and Kluwer Academic Publishers, Dordrecht.

Wie, B. (1998), *Space Vehicle Dynamics and Control*, American Institute of Aeronautics and Astronautics.

Wilde, D. & Sytin, O. (1999), 'The X-Mir Inspector Mission', *Proceedings of Space Flight Dynamics Symposium*, Toulouse, pp. 63–73.

Wolfsberger, W., Weiss, J. & Rangnitt, D. (1983), 'Strategies and schemes for rendezvous in geostationary transfer orbit', *Acta Astronautica*, **10,** (8), 527–538.

Yamanaka, K. (2000), 'ETS-VII rendezvous experiment', Viewgraph presentation to ESA/ESTEC, unpublished.

Yamanaka, K. & Ankersen, F. (2002), 'New state transfer matrix for relative motion on an arbitrary elliptical orbit', *J. Guidance, Control & Dynamics*, **25**, (1), 60–66.

Index